The Molecular Correlates of Sleep and Sleep Deprivation *in vivo* and *in vitro*

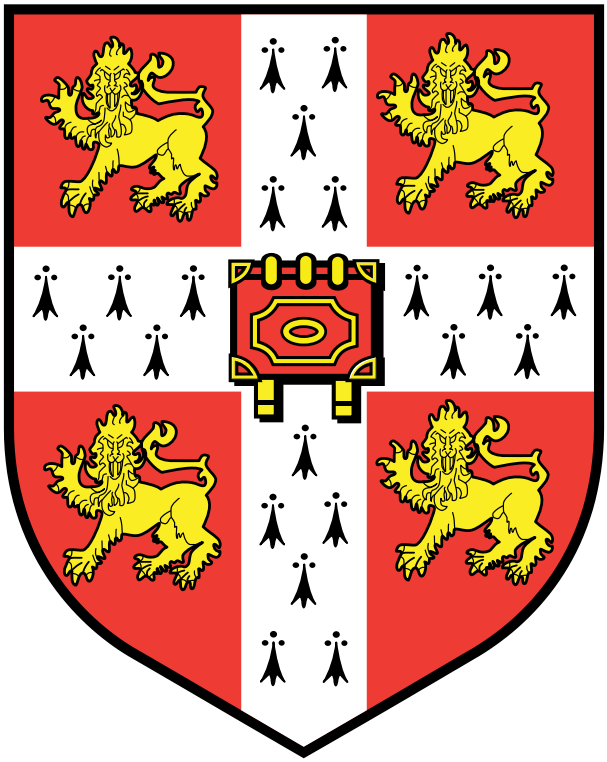

William Gee

Selwyn College

This dissertation is submitted for the degree of Doctor of Philosophy

October 2018

The Molecular Correlates of Sleep and Sleep Deprivation *in vivo* and *in vitro*

William Gee

Summary

This thesis describes the use of *in vivo* and *in vitro* models to better understand the molecular correlates of sleep and sleep deprivation. Unlike previous studies, we utilise a timecourse based experimental design throughout, which has the advantage of identifying how the abundance of molecules return to baseline following sleep deprivation. Chapter 3 outlines the transcriptome of mouse cortex collected over 54 hours from mice subjected to varied durations of sleep deprivation. The timecourse experimental design aids in the identification of genes that are induced during both spontaneous and enforced wakefulness, and facilitates the dissociation of genes whose expression is tightly linked to the current wake state of the animal from those whose expression is linked to the total amount of wakefulness recently experienced by the animal. Like previous studies, we identify several genes involved in the unfolded protein response and synaptic function that are upregulated by sleep deprivation. We also find that increasing durations of sleep deprivation progressively reduces the total number of rhythmically expressed genes in mouse cortex, with only a handful of transcripts identified as diurnal following 12 hour sleep deprivation.

Chapter 4 outlines the proteomic and metabolomic effects of 12 hour sleep deprivation. Proteomic analyses indicate that the abundance of ribosomal and nucleosomal proteins is suppressed for at least 24 hours following sleep deprivation, whilst the abundance of several phosphodiesterases are acutely increased following sleep deprivation. Metabolomic analyses of sleep deprived mouse cortex identified 3 molecular species whose abundance profile implicate them as sleep homeostats.

Finally, we also set out to develop an *in vitro* model of sleep deprivation based on the optogenetic activation of a neuroblastoma cell line, which is outlined in Chapter 5. Following several rounds of optimisation, the stable expression of an opsin was found to induce intracellular calcium spikes and immediate early gene expression during illumination. Transcriptomic profiling of illuminated SH-SY5Y cells induced large scale transcriptomic changes, and modulated the expression of genes involved in synapses, cholesterol synthesis, the molecular clock and the unfolded protein response. Although these functional classes are reminiscent of those modulated by *in vivo* sleep deprivation, there was only a slight enrichment of individual genes modulated by *in vivo* sleep deprivation amongst the blue light sensitive genes, indicating further work is required to more closely model *in vivo* sleep deprivation.

Declaration

This dissertation is the result of my own work and includes nothing which is the outcome of work done in collaboration except as declared in the Preface and specified in the text.

It is not substantially the same as any that I have submitted, or, is being concurrently submitted for a degree or diploma or other qualification at the University of Cambridge or any other University or similar institution except as declared in the Preface and specified in the text. I further state that no substantial part of my dissertation has already been submitted, or, is being concurrently submitted for any such degree, diploma or other qualification at the University of Cambridge or any other University or similar institution except as declared in the Preface and specified in the text.

It does not exceed the prescribed word limit for the relevant Degree Committee.

Signed: _____ (William Gee)

Acknowledgements

First and foremost, I would like to thank Ak Reddy for giving me the opportunity to carry out a PhD in his lab. Very few students have simultaneously had the opportunity to carry out large scale studies and had the opportunity to use many recent innovations during their PhD, and so I'd like to thank Ak further for his technologically minded approach to research.

I would like to thank all of the Reddy Lab members, past and present, who helped me with my project. Particular thanks is due to Laura Bollepalli and David Pritchett, who helped me extensively with the basic handling, set up of experiments and even sleep deprivations involved in the *in vivo* work presented here. Alessandra Stangherlin, the cloning queen, taught me as many cloning and cell culture tricks as I could learn, which were invaluable for the *in vitro* work presented here. Whenever I had a question on how to handle data, I could always count on Guillaume Rey and Utham Valekunja for sound advice. I'd like to thank Sandipan Ray for his help with my proteomics project. I'd also like to thank all the members of the Reddy lab for the day to day discussions and jokes that made the workday more enjoyable.

I'd like to thank Greg Strachan for his confocal microscopy training, ordering and interesting lunchtime discussions about new techniques. At CBS, which at times felt like my home away from home, I'm indebted to Ian Purvis, John Mcquillan, and especially Charley Beresford and Laura McKinven for all their help with preparation of rooms, cabinet checks and general husbandry, without which I would have only seen dim red light for several months straight!

Away from work, I'm tremendously grateful to my friends Claire Bromley, Nick Jamieson and Christopher Lim, who, through their own experiences of PhDs, all shared the highs and pointed out the silver linings of the lows.

The final thanks must go to my partner, and now wife, Rachel. Her indomitable happiness and support has been the biggest constant throughout my studies, maintaining a good outlook on things, whatever the problem I was facing. Although I suspect she wasn't particularly happy when I started my PhD, I'm certain she'll be overjoyed when I hand it in, and, as such, it is dedicated to her.

Contents

List of Figures

List of Tables

Abbreviations

µg	Microgram
µl	Microlitre
2D	Two-dimensional
3'	3-prime (of nucleic acids)
3D	Three-dimensional
5'	5-prime (of nucleic acids)
5-HT	5-hydroxytryptamine, serotonin
AC	Adenylate Cyclase
aCSF	Artificial Cerebral Spinal Fluid
AMP	Adenosine Monophosphate
AMPA	α-amino-3-hydroxy-5-methyl-4-isoxazolepropionic acid
AMPK	Adenosine Monophosphate-activated Protein Kinase
ANOVA	Analysis of Variance
ARAS	Ascending Reticular Activating System
ATP	Adenosine triphosphate
BCA	Bicinchoninic Acid
BDNF	Brain Derived Neurotrophic Factor
BL	Blue Light
bp	Base Pair
bPAC	Bacterial Photoactivated Adenylyl Cyclase
cAMP	Cyclic Adenosine Monophosphate

CCD	Charge Coupled Device
cDNA	Complementary DNA
cGPDE	cGMP Phosphodiesterase
CHALIP	ChR2(C128T)-2A-Halorhodopsin-IRES-PuroR
CHES	Cyclohexyl-2-aminoethanesulfonic acid
ChIP-Seq	Chromatin Immunoprecipitation- Sequencing
ChR2	Channelrhodopsin 2
CLOCK	Circadian Locomotor Output Cycles Kaput
cm	centimetre
CMV	Cytomegalovirus
CO_2	Carbon Dioxide
CoA	Coenzyme A
CRF	Corticotropin Releasing Factor
CRIP	ChR2(C128T)-RCAMP-IRES-PuroR
CRY	Cryptochrome
CSF	Cerebral Spinal Fluid
DMEM	Dulbecco's Modified Eagle's Medium
DMH	Dorsomedial Hypothalamus
DNA	Deoxyribonucleic Acid
DREADD	Designer Receptor Exclusively Activated by Designer Drugs
DRN	Dorsal Raphe Nucleus
dscDNA	Double-stranded Complementary DNA
EDTA	EthyleneDiamine Tetraacetic Acid
EEG	Electroencephalography

EGFP	Enhanced Green Fluorescent Protein
EMG	Electromyography
eNpHR	Enhanced Natronomonas Halorhodopsin
EOG	Electro-Oculography
ER	Endoplasmic Reticulum
EVH1	Enabled/Vasodilator-stimulated phosphoprotein Homology 1
FBS	Foetal Bovine Serum
FDR	False Discovery Rate
FRAP	Fluorescence Recovery after Photobleaching
GABA	gamma-Aminobutyric acid
GAPDH	Glyceraldehyde 3-Phosphate Dehydrogenase
GPCR	G-Protein Coupled Receptor
GTP	Guanosine Triphosphate
HEK	Human Embryonic Kidney
HEPES	4-(2-hydroxyethyl)-1-piperazineethanesulfonic acid
IP3	Inositol triphosphate
IRES	Internal Ribosome Entry Site
LB	Luria-Bertani
LC	Liquid Chromatography
LC-MS	Liquid Chromatography Mass Spectrometry
LDT	Laterodorsal Tegmental nucleus
LED	Light Emitting Diode
LHA	Lateral Hypothalamus Area
LTP	Long Term Potentiation

MEM	Minimal Eagle's Medium
mm	millimetre
MnPO	Median Preoptic Nucleus
MOPS	(3-(N-morpholino)propanesulfonic acid)
MOSFET	Metal-Oxide-Semiconductor Field-Effect Transistor
mRNA	Messenger Ribonucleic Acid
ms	millisecond
mW	milliwatt
mW/cm2	milliwatt per square centimetre
NADH	Nicotinamide Adenine Dinucleotide
NADPH	Nicotinamide Adenine Dinucleotide Phosphate
NEB	New England Biolabs
nm	nanometre
NMDA	N-methyl-D-aspartate
NP40	Nonionic Polyoxyethylene-40
NREM	Non Rapid Eye Movement
NSAID	Non-Steroidal Anti-Inflammatory Drug
NTRK2	Neurotrophic Tyrosine Receptor Kinase 2
PCR	Polymerase Chain Reaction
PDE	Phosphodiesterase
PEG	Polyethylene Glycol
PEI	Polyethylene Imine
PGD2	Prostaglandin D2
PGH2	Prostaglandin H2

PLC	Phospholipase C
PPT	Pedunculopontine Tegmentum
PuroR	Puromycin Resistance
qPCR	Quantitative Polymerase Chain Reaction
REM	Rapid Eye Movement
RIP	RCAMP-IRES-PuroR
RNA	Ribonucleic Acid
RNA-Seq	Ribonucleic Acid Sequencing
SCN	Suprachiasmic Nucleus
SD	Sleep Deprivation
SLC	Solute Carrier Family
SREBP	Sterol regulatory element-binding protein
SV40	Simian Virus 40
SWS	Slow Wave Sleep
TAPSO	N-[Tris(hydroxymethyl)methyl]-3-amino-2-hydroxypropanesulfonic acid
TBP	TATA-Box Binding Protein
TCEP	Tris(2-Carboxyethyl)Phosphine
TEAB	Triethylammonium Bicarbonate
TMN	Tuberomammillary Nucleus
TMT	Tandem Mass Tag
TNF-α	Tumour Necrosis Factor Alpha
UPL	Universal Probe Library
UPR	Unfolded Protein Response
VEGF	Vascular Endothelial Growth Factor

VLPO	Ventrolateral Preoptic Hypothalamus
WLL	White Light Laser
Xbp1	X-Box Binding Protein 1

1. General Introduction

This section summarises the current understanding of the function and control of sleep, the molecular signatures of wakefulness, and the experimental models and tools available to researchers. This chapter concludes with an outline of the aim and approach of this thesis.

1.1. What is Sleep?

1.1.1. Behavioural Definition of Sleep

We spend approximately one third of our lives asleep, and we intuitively know that it is a prolonged period of night-time rest during which we become much less aware of the environment. Common experience also teaches us that we will wake if there is a particularly loud noise, and that a poor night's sleep will usually lead to sleeping longer the next evening. Together, these simple observations form the basis of the formal definition of sleep across the animal kingdom.

Sleep is thus generally defined as a rapidly reversible state of immobility and reduced responsiveness to external stimuli, into which the animal enters during specific times of the day in a characteristic posture, and the duration of which is under homeostatic control (Foster & Lockley 2012). Of these criteria, reduced responsiveness, the rapid reversibility of the state (which differentiates sleep from hibernation or coma), and the presence of homeostatic control are considered to be the core behavioural characteristics of sleep.

1.1.2. Electroencephalographic Definition of Sleep

In animals with well-developed brains, electroencephalography (EEG) measurements can be used to more precisely define sleep in real time. EEG uses electrodes, implanted either onto the scalp or directly into the brain, to monitor voltage fluctuations due to ion flux associated with neuronal activity in the cortex. EEG can be complemented with electromyography (EMG), which uses electrodes to monitor muscle tone, or electrooculography (EOG), which monitors eye movement.

EEG studies during the 1950s showed that as mammals fall asleep, the EEG measurements gradually change from the high frequency (>12Hz), low amplitude pattern characteristic of wakefulness to a low frequency (<5Hz), high amplitude pattern, termed delta waves, characteristic of deep, slow wave sleep (SWS) (Hess *et al.* 1953). Concomitant with the reduced frequency pattern, there is a decrease in muscle tone as measured by EMG. In humans, after approximately 70 minutes, the EEG profile returns to a pattern characteristic of wakefulness, despite the person still being asleep. This stage of sleep is accompanied by rapid eye movements, and so is known as Rapid Eye Movement (REM) Sleep (Dement & Kleitman 1957). Although EEG measurements struggle to differentiate between wakefulness and REM sleep, the rapid eye movement and complete lack of muscle tone associated with REM sleep can be detected by EOG and EMG, respectively. After the initial bout of REM sleep, the person returns to non-REM (NREM) sleep which gradually deepens to SWS. This cycle of NREM to REM sleep happens every 90 minutes throughout the night, punctuated by occasional awakenings (Foster & Lockley 2012). Over the course of the night, the proportion of SWS decreases, whereas the proportion of REM sleep increases. The daily duration and architecture of sleep varies across species, with mammals subject to

predation and those with small brains relative to body size demonstrating a lower abundance of REM sleep (Lesku *et al.* 2006).

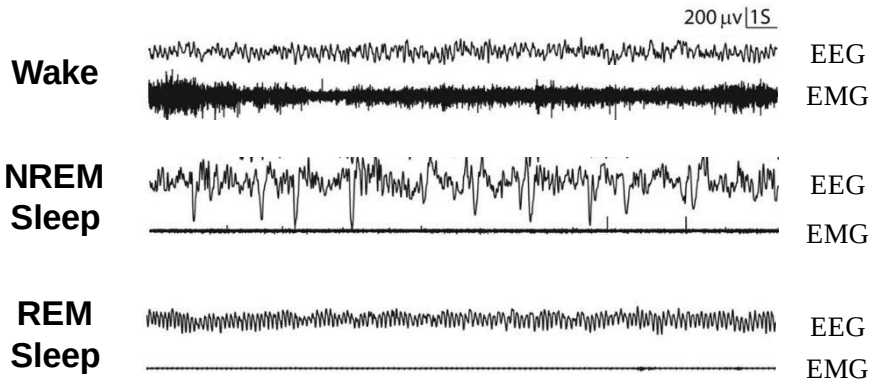

Figure 1.1. Representative EEG and EMG Spectra of Wake and Sleep in Mice: Sleep can be tracked in real time using electroencephalography (EEG) which tracks cortical voltage fluctuations. The EEG spectrum of an awake mouse is characterised by small amplitude high frequency oscillations, as is the EEG spectrum of a mouse in rapid eye movement (REM) sleep. In contrast the EEG spectrum of mice in non-REM (NREM) sleep is characterised by high amplitude low frequency oscillations. Electromyography (EMG), which monitors muscle tone, can be used to complement EEG sleep scoring. The EMG spectrum of an awake mouse exhibits significant fluctuations, whereas mice in NREM, and especially REM sleep, exhibit almost static EMG spectra.

Figure modified, with permission, from one provided by D.Pritchett.

The power of delta waves in an EEG spectrum is negatively correlated with the amount of sleep previously obtained. For example, the proportion of time spent in SWS is highest at the beginning of normal sleep (Feinberg *et al.* 1967), and is increased following sleep deprivation (Borbély *et al.* 1981) but decreased by daytime naps (Feinberg *et al.* 1985). Therefore the delta power is considered an indicator of the need for sleep, or "sleep debt" (Feinberg 1974).

1.2. Functions of Sleep

1.2.1. The Cost of Sleep

"If sleep doesn't serve an absolutely vital function, it is the greatest mistake evolution ever made."

This quote by sleep research pioneer Allan Rechtschaffen succinctly identifies that there are great costs attached to sleep that are presumably offset by some fundamental purpose. All animals studied to date display a sleep like state, characterised by prolonged inactivity with a reversibly increased arousal threshold and a requirement for additional recovery sleep following sleep deprivation. During this period, animals are unable to forage, search for mates and are vulnerable to predators, and yet some animals, like the brown bat, spend as much as 80% of their life asleep (Campbell & Tobler 1984). Although animals can postpone sleep in response to a threat, the homeostatic drive to recuperate sleep later leaves them vulnerable. Severe evolutionary pressure has even failed to eliminate sleep in dolphins and other marine mammals, which have instead evolved a uni-hemispheric sleep pattern to allow them to continuously surface for air (Mukhametov 1987; Mukhametov *et al.* 1977, 1985). However, despite the costs of sleep being clear, why sleep exists at all remains enigmatic.

1.2.2. The Necessity of Sleep

To date, the function of sleep has been mostly investigated experimentally by studying the effects of sleep deprivation. Early studies found that rats can survive an average of 19 days of total sleep deprivation, approximately the same period as they can survive total starvation (Everson *et al.* 1989). No common cause of death is associated with total sleep deprivation. Instead, rats show oedema, skin lesions, impaired immune responses and metabolic abnormalities, indicating the collapse of multiple systems. For example, Koban *et al.* found that persistently sleep deprived rats had double the caloric intake of control rats, yet were still in negative energy balance due to massive energy expenditure (Koban *et al.* 2008; Koban & Swinson 2005), whilst Everson found opportunistic invasion of the bloodstream by normally harmless bacteria without a febrile response (Everson 1993). Remarkably, allowing rats to sleep usually reverses most of the adverse effects of prolonged sleep deprivation within two days.

Although sleep deprivation has also been shown to induce death in cats after two weeks (McGinty & Sterman 1968), and even within twelve hours in *Drosophila* cyc^{01} mutants (Shaw *et al.* 2002), whether sleep deprivation is lethal to humans is unknown. In 1965, Randy Gardner voluntarily stayed awake for 11 consecutive days without any apparent long-term damage. However, both acute and chronic sleep loss have been linked to several disorders in humans (Colten *et al.* 2006).

1.2.3. Central Effects of Sleep Deprivation

The most obvious immediate effects of sleep loss include cognitive defects and reduced reaction speed. For example, decision making during a market based game was severely compromised after one night's sleep deprivation (Harrison & Horne 1999), whilst reaction speeds in psychomotor vigilance tests are also reduced (Christie *et al.* 2008; Roca *et al.* 2012; Rupp 2013). Outside of the laboratory, these deficiencies can have significant effects: the rate of clinical mistakes has been correlated to sleep loss (Philibert 2005; Ruggiero *et al.* 2012), and even 20 hours of prolonged wakefulness has the same effect on reaction time as consuming the legal alcohol limit for driving (Williamson & Feyer 2000), and is associated with an increased risk of car accidents (Garbarino *et al.* 2004; Liu *et al.* 2003; Maycock 1997).

In addition to reducing cognitive performance, sleep deprivation also impairs memory formation and consolidation. In humans, sleep has been shown to be beneficial for declarative memory (i.e. recalling facts and events) (Gais & Born 2004), procedural memory (i.e. learning tasks) (Backhaus & Junghanns 2006; Plihal & Born 1997), and emotional memory (Groch *et al.* 2013). Even six-minute naps were found to be sufficient to increase the recall of word lists 60 minutes after learning them (Lahl *et al.* 2008). Decreased learning has also been shown in both mice and rats after acute and chronic partial sleep deprivation, and flies fail to associate an odour with an aversive outcome after sleep deprivation (Li *et al.* 2009). Therefore, memory consolidation has been proposed as a fundamental function of sleep conserved across species.

Sleep has also been proposed to have evolved to facilitate central metabolic homeostasis. The metabolic theory of sleep was first based on the concept that during wakefulness the brain operates in a way that is not sustainable over long periods, and must eventually rest in a manner analogous to muscles after strenuous exercise, in order to clear waste products and prepare for the next session of activity. Consistent with this theory, early studies showed that brain glycogen content is depleted by prolonged wakefulness in rats and flies (Kong *et al.* 2002; Zimmerman *et al.* 2004) and is increased after sleep onset and during anaesthesia (Karnovsky *et al.* 1983), with lactate showing the opposite pattern (Naylor *et al.* 2012). AMPK activity is increased by sleep deprivation, indicating an increased demand for ATP during wakefulness (Chikahisa *et al.* 2009), whilst there is a large increase in ATP following sleep onset, which is independent of the time of day (Dworak *et al.* 2010). More recent studies have shown through two-photon *in vivo* microscopy that flow through the brain's "glymphatic" system greatly increases during sleep and anaesthesia in mice, contributing to the clearance of waste metabolites and β-amyloid protein (Xie *et al.* 2013).

Sleep deprivation also induces the Unfolded Protein Response (UPR) and endoplasmic reticulum (ER) stress response in the brain, characterised by the upregulation of several heat-shock chaperone proteins (Maret *et al.* 2007; Terao *et al.* 2003). The induction of ER stress and the UPR by sleep deprivation has been directly linked to reduced protein synthesis in sleep deprived mouse cortex (Naidoo *et al.* 2005), which appears to have a protective role. Indeed increasing the temperature, which induces heat-shock proteins independently of sleep, protects *Drosophila* from the lethal effects of sleep deprivation (Shaw *et al.* 2002). In summary, at the cellular level it appears that prolonged wakefulness is characterised by increased energy expenditure, and decreased synthesis of proteins. In contrast, sleep is associated with the upregulation of multiple anabolic pathways, including haem and porphyrin synthesis, translation and cholesterol biosynthesis (Mackiewicz *et al.* 2007). Therefore at the cellular level, falling asleep appears to correspond to a shift from the catabolic state of wakefulness to an anabolic state of sleep.

1.2.4. System-wide Effects of Sleep Deprivation

Cognitive performance, memory consolidation, central metabolism and cellular housekeeping are all dependent on sleep, indicating that sleep plays a large part in the function of the brain. However, more subtle purposes of sleep have been proposed based on changes that occur during sleep deprivation and affect the entire body. Interplay between sleep and the immune system has been inferred from the tendency for infections and toxins to increase sleep duration, and because prolonged sleep deprivation of rats can lead to opportunistic bacterial infections (Everson 1993). Since then, the effectiveness of Influenza, Hepatitis A and Hepatitis B vaccinations has been shown to be reduced by sleep restriction (Lange *et al.* 2003; Prather *et al.* 2012; Spiegel *et al.* 2002). Similarly, 48 hours of sleep deprivation was shown to reduce the phytohemagglutinin induced activation of human lymphocytes for five days after sleep loss (Palmblad *et al.* 1979). Accordingly, prolonged wakefulness has been shown to induce the expression of several cytokines within the brain, which appear to decrease neuronal activity (Besedovsky *et al.* 2012). The use of common signalling molecules by both immune cells and sleep deprived brain tissue may provide a mechanistic insight into the crosstalk between immune function and sleep.

Sleep has also been tightly linked to whole body metabolic homeostasis in humans. Several epidemiological studies have found sleep duration to be inversely linked to BMI in both adults (Ko *et al.* 2007; Kripke *et al.* 2002; Moreno *et al.* 2006) and children (Padez *et al.* 2005; Reilly *et al.* 2005; von Kries *et al.* 2002). A meta-analysis using data from a total of 630,000 participants found that the Odds Ratio for short sleep duration and obesity for children was 1.89, and 1.55 for adults (Cappuccio *et al.* 2008). Remarkably, other studies have found a U-shaped relationship between weight and sleep

duration, with those sleeping fewer than 7 hours, or more than 9 hours a day, having an increased risk of obesity (Gottlieb *et al.* 2006; Patel *et al.* 2006). Consistent with epidemiological studies, acute sleep deprivation in human volunteers has been shown to increase food intake (Brondel *et al.* 2010; Markwald *et al.* 2013), with a change in preference toward more energy dense foods, and decreased glucose tolerance (Beebe *et al.* 2013; Benedict *et al.* 2012; Greer *et al.* 2013). Although there are conflicting reports on whether activity is increased (Jung *et al.* 2011) or decreased (Benedict *et al.* 2011) after sleep loss, those studies that find increased activity usually report that food intake is still in excess of energy expenditure (Spaeth *et al.* 2013; St-Onge *et al.* 2011).

1.2.5. Societal Costs of Poor Sleep

With the advent of electrical lighting and increased caffeine availability, the average duration of daily sleep of both adults and children has potentially been decreasing in the past century (Depner *et al.* 2014; Matricciani *et al.* 2012). A population wide chronic sleep restriction may have significant implications for the health of modern day societies. Whilst chronic sleep restriction has been linked to reduced immune function and increased incidence of diabetes and obesity, acute sleep deprivation is linked to an increased prevalence of car accidents and clinical mistakes. The burden of poor sleep on the healthcare system could be reduced by an increased understanding of the mechanisms through which sleep maintains overall health. Understanding sleep at the molecular level may be especially promising, since that would reveal targets amenable to rational drug design that may provide novel treatments for sleep associated disorders.

Table 1: Phenotypes of Sleep Deprivation

	Phenotype	References
Central Phenotype of Sleep Deprivation	Cognitive and Memory Deficits Impaired Reaction Speed Impaired β-amyloid clearance	(Backhaus & Junghanns 2006; Gais & Born 2004; Groch *et al.* 2013; Harrison & Horne 1999; Li *et al.* 2009; Plihal & Born 1997) (Christie *et al.* 2008; Roca *et al.* 2012; Rupp 2013) (Di Meco *et al.* 2014; Xie *et al.* 2013)

Whole Animal Phenotypes of Sleep Deprivation	Impaired Immune Function Impaired Metabolic Homeostasis	(Everson 1993; Lange *et al.* 2003; Palmblad *et al.* 1979; Prather *et al.* 2012; Spiegel *et al.* 2002) (Cappuccio *et al.* 2008; Gottlieb *et al.* 2006; Ko *et al.* 2007; Kripke *et al.* 2002; Moreno *et al.* 2006; Padez *et al.* 2005; Patel *et al.* 2006; Reilly *et al.* 2005; von Kries *et al.* 2002)
Societal Costs of Sleep Deprivation.	Increased Incidence of Clinical Errors Increased Incidence of Car Accidents	(Philibert 2005; Ruggiero *et al.* 2012) (Garbarino *et al.* 2004; Liu *et al.* 2003; Maycock 1997; Williamson & Feyer 2000)

1.3. The Neurological Control of Sleep

1.3.1. Overall Output of Sleep Circuitry

The regulation of sleep can be well described by the two-process regulation model, proposed by Borbély (Borbély 1982). This model proposes that there are two separate processes that affect sleep timing and duration: Process S, the homeostatic drive to sleep, and Process C, the circadian drive to sleep. The homeostatic need for sleep increases with prolonged wakefulness and is dissipated by sleep, whilst the circadian sleep drive oscillates during the day. In humans, the two processes work together to maintain sleep pressure below a threshold throughout the day and promote a consolidated bout of sleep through the night (see Fig 1.2.).

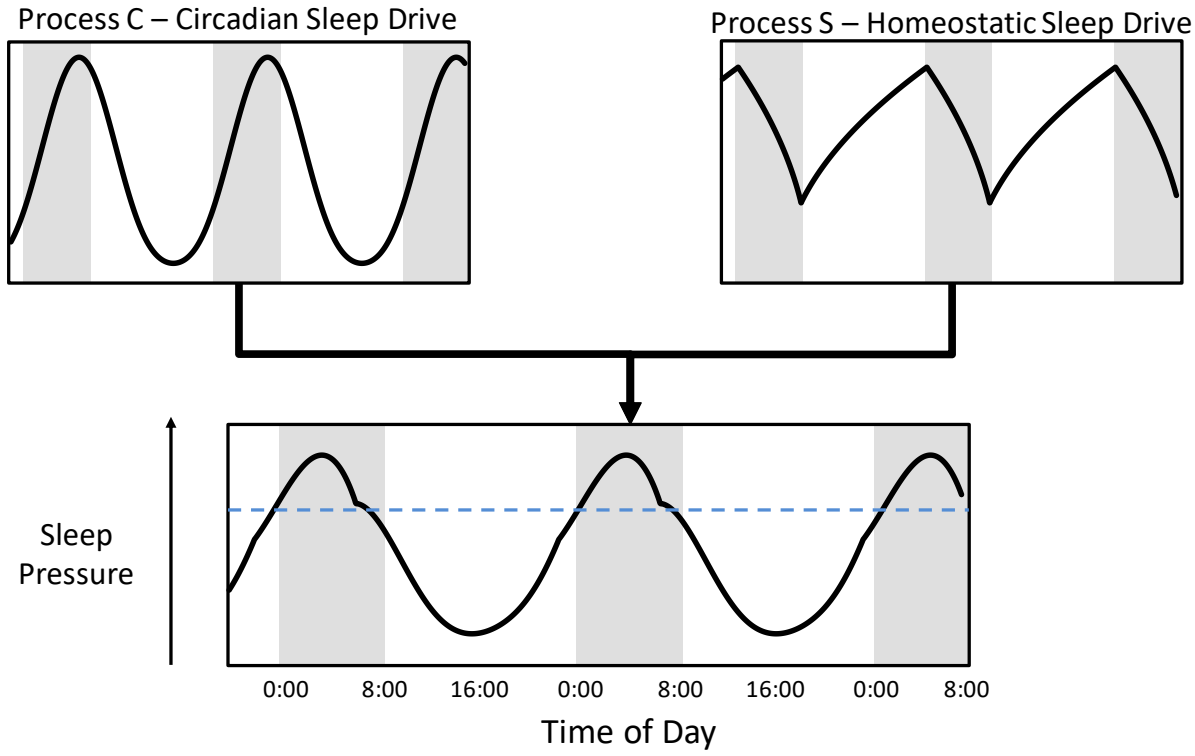

Figure 1.2. The Two Process Model proposes an Interaction between a Circadian and Homeostatic Drive for Sleep: This schematic represents an idealised two process model for a human, who is only awake between 8am until midnight each day. Process S, the homeostatic drive for sleep, progressively increases during continued wakefulness, and decreases during subsequent sleep. In contrast, Process C, the circadian sleep drive, oscillates over a 24-hour period, peaking just before habitual wake time and reaching its minimum a few hours before habitual sleep time. The two processes interact, and the net effect is that sleep pressure is maintained below a theoretical threshold (blue line) during the day, and above that threshold during the night. Therefore, the processes interact to generate consolidated periods of wake and sleep, despite mounting and dissipating sleep pressure, respectively.

1.3.2. Circuitry that Controls Sleep

Wakefulness and sleep are coordinated by several excitatory and inhibitory neural networks that extend throughout the brain. Regions of the brain responsible for sleep were first identified in the 1920s by autopsies of encephalitis sufferers exhibiting sleep disorders (Von Economo 1930). Patients who had suffered from excess sleep (hypersomnia) often had lesions in the brainstem and posterior hypothalamus, whilst those suffering from insomnia typically had lesions in the anterior hypothalamus. Since then, the projections and neurotransmitter profile of these regions have been characterised.

Several of the wake-promoting centres are part of the ascending reticular activating system, including the noradrenergic locus ceruleus (LC), the serotonin (5-HT) producing dorsal raphe nucleus (DRN), histaminergic neurons of the tuberomammillary nucleus (TMN), and the cholinergic neurons of the pedunculopontine tegmental (PPT) and lateral dorsal tegmental (LDT) nuclei (Moruzzi & Magoun 1949). The ascending reticular system projects from these centres in the brainstem and posterior hypothalamus to the hypothalamus, thalamus, basal forebrain and the cortex (see Fig 1.3.). Accordingly, lesioning several of the nuclei induces hypersomnia, as does histamine or 5-HT blockade (Landolt *et al.* 1999; Monti *et al.* 1991), whilst optogenetic activation of the LC is sufficient to induce awakening (Carter *et al.* 2010). Further wake promoting neurons are found in the basal forebrain, where the optogenetic activation of glutamatergic and cholinergic signalling has been shown to induce wakefulness (Xu *et al.* 2015).

The firing of the individual wake-promoting nuclei is coordinated by a cluster of excitatory neurons in the lateral hypothalamic area (LHA), promoting prolonged sessions of wakefulness. The neurones release orexin (also known as hypocretin), a neuropeptide first named for its induction of feeding following intracerebroventricular injection (Sakurai *et al.* 1998). Later, however, it was found that orexin overexpression induces fragmented sleep, whilst orexin deficiency is linked to narcolepsy and cataplexy in humans, mice and dogs (Chemelli *et al.* 1999; Hara *et al.* 2001; Lin *et al.* 1999; Peyron *et al.* 2000; Thannickal *et al.* 2000). As well as projecting to the DRN, LC, TMN, LDT and PPT (Bayer *et al.* 2001; Horvath *et al.* 1999; Liu *et al.* 2002; Yamanaka *et al.* 2003b), orexinergic neurons also extend throughout the forebrain, including to the feeding and reward centres of the hypothalamus (Nakamura *et al.* 2000; Yamanaka *et al.* 2000). In mice, overexpression of orexin protects against diet induced obesity and hyperglycaemia (Funato *et al.* 2009), whilst orexin antagonism decreases self-administration of cocaine, ethanol and high fat food (Harris *et al.* 2005; Moorman & Aston-Jones 2009; Valdivia *et al.* 2014). Therefore, orexinergic neurons both directly and indirectly regulate several aspects of complex behaviours in addition to the sleep-wake cycle.

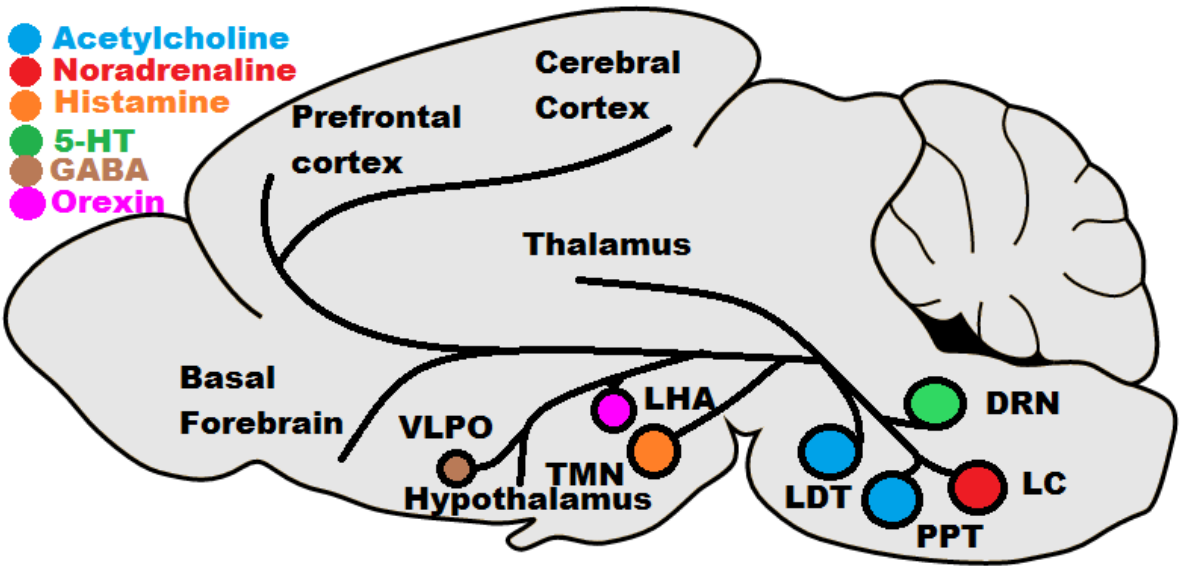

Figure 1.3. Sleep and Wake Circuitry of the Mammalian Brain: The wake promoting ascending reticular activating system includes noradrenergic locus coeruleus (LC), the serotonergic (5-HT) dorsal raphe nucleus (DRN), histaminergic tuberomammillary nucleus (TMN), and the cholinergic pedunculopontine tegmental (PPT) and lateral dorsal tegmental (LDT). It extends throughout the brain, directly activating the cortex and thalamus, and inhibiting the sleep promoting, GABA-ergic ventrolateral preoptic nucleus (VLPO). The sleep promoting nuclei are activated by orexin expressing neurons of the lateral hypothalamus (LHA), and inhibited by the VLPO.

Opposing the wake-promoting system of the ascending reticular activating system and orexinergic systems are a population of wake inactive, sleep active GABAergic and galaninergic neurons in the median preoptic (MnPO) and ventrolateral preoptic (VLPO) areas of the hypothalamus (Gaus *et al.* 2002; Sherin *et al.* 1996). Interestingly, neurons in the VLPO are also activated by several anaesthetics (Moore *et al.* 2012), further suggesting a role in sleep promotion. The preoptic hypothalamus extends inhibitory projections to the wake-promoting centres of the brainstem (Uschakov *et al.* 2007) and lateral and posterior hypothalamus (Saito *et al.* 2013; Sherin *et al.* 1998), and so induce sleep by inhibiting several wake-promoting pathways simultaneously. Severe lesioning of the VLPO in cats and rats causes over 50% reduction in NREM sleep time (McGinty & Sterman 1968; Szymusiak & McGinty 1986), with the number of sleep active neurons remaining after lesioning correlating with sleep time (Lu *et al.* 2000). Furthermore, the ability of the VLPO to rapidly induce sleep has recently been shown by DREADD (Designer Receptors Exclusively Activated by Designer Drugs) and optogenetic based approaches (Chung *et al.* 2017; Zhang *et al.* 2015).

Conversely, the wake-promoting centres extend inhibitory projections to the VLPO (Chou *et al.* 2002; Deurveilher *et al.* 2002; Gallopin *et al.* 2000). The mutual inhibition of the wake and sleep-promoting

centres acts as a "Flip-Flop Switch" to ensure stability of wakefulness and sleep, as well as facilitating rapid state transitions between the two states, which can occur within 1 second (Takahashi *et al.* 2010). The extensive communication between the centres also facilitates the integration of the signals that determine whether an animal is awake or asleep.

1.3.3. Circadian Inputs to the Sleep Circuitry

The probability of an animal being awake is affected by the time of day - Process C in the two-process model- and the amount of time spent awake- Process S. In humans, circadian drive to sleep decreases during the day, offsetting an increasing homeostatic drive to maintain nearly constant alertness. Shortly before habitual sleep time, the circadian drive begins to increase, normally resulting in sleep, which in turn decreases the homeostatic drive. However, if wakefulness is prolonged, the drive to sleep increases rapidly due to the combination of ever increasing circadian and homeostatic sleep pressure. The circadian component of sleep timing has been well demonstrated in humans, where total sleep deprivation is characterised by a drastic and progressive decrease in alertness and cognitive performance until the habitual waking time, followed by a partial recovery of alertness the next morning when the circadian component again begins to favour wakefulness (see Fig 1.4.) (Dijk *et al.* 1992). However, alertness and performance are still reduced compared to the day before sleep deprivation, reflecting an increased homeostatic drive for sleep.

Information about the time of day is relayed to the rest of the body from the suprachiasmatic nucleus (SCN) of the hypothalamus (Moore & Eichler 1972). The circadian oscillation of SCN activity acts as a master pacemaker that synchronises the internal clock of peripheral cells (Buijs *et al.* 1999; Cailotto *et al.* 2009). The activity of neurons in the SCN is dependent on their own cellular clock, which is sensitive to several environmental stimuli, most notably light (Do & Yau 2010). Although the SCN only has sparse direct innervations of the sleep circuitry, circadian input is relayed to the sleep circuitry via the dorsomedial hypothalamus (DMH), which in turn extends GABAergic projections to the VLPO, and excitatory glutamatergic projections to orexinergic neurons of the lateral hypothalamus (Chou *et al.* 2003). Indeed, blinding rats or maintaining them in constant light gradually dampens rhythms in sleep (Eastman & Rechtschaffen 1983; Ibuka & Kawamura 1975), whereas lesioning the DMH or the SCN in rats causes sleep to permanently become evenly distributed across the light-dark cycle (Chou *et al.* 2003; Eastman *et al.* 1984; Ibuka & Kawamura 1975). Although lesioning the SCN in squirrel monkeys also results in a marked increase in daily sleep duration (Edgar *et al.* 1993), total sleep duration in rats is not significantly affected by lesioning of the SCN or DMH. Ablation in mice has been shown to both increase (Easton *et al.* 2004) and to have no effect on (Ibuka *et al.* 1980) sleep duration, which may be linked to strain differences.

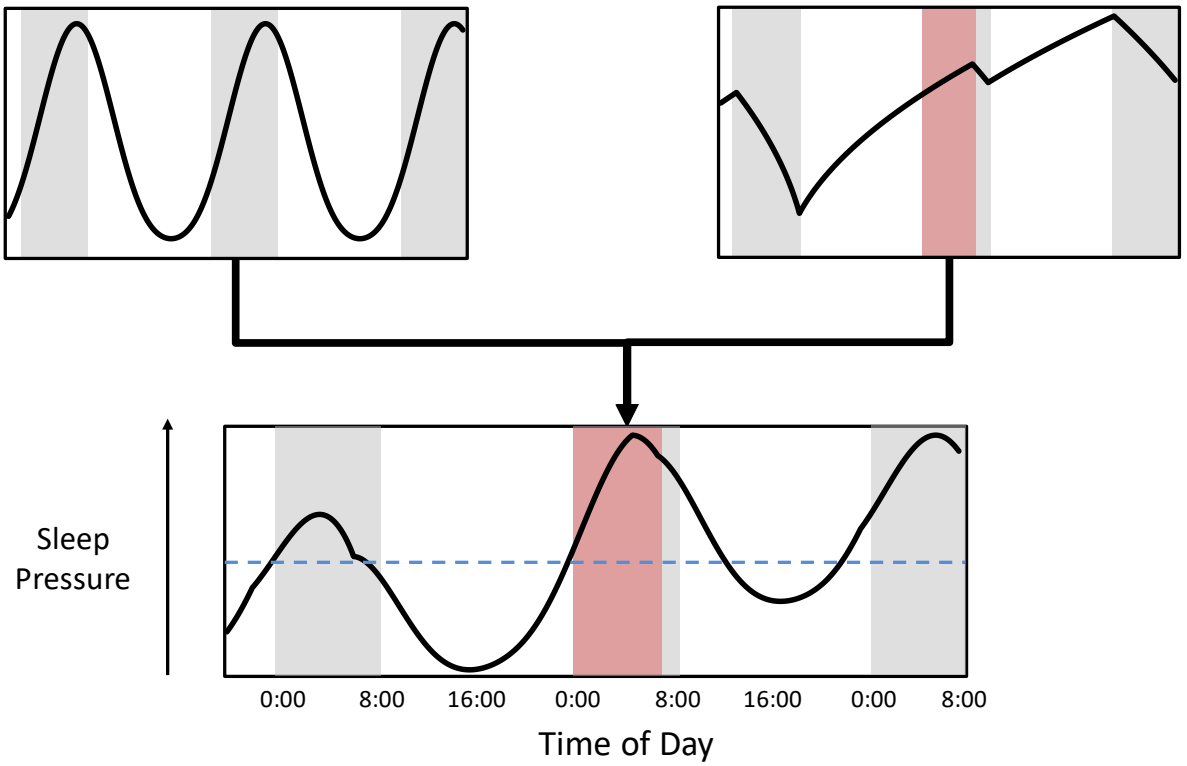

Figure 1.4. The Two Process Model predicts that Sleep Deprivation Increases Sleep Drive the following Day: This schematic represents an idealised two process model for a human, who is normally only awake between 8am until midnight each day, but is subjected to 6 hour additional sleep deprivation (red bar) before waking at 8am. Process S, the homeostatic drive for sleep, progressively increases during the day and continues to rise during the sleep deprivation. During the two hour sleep opportunity, Process S decreases, but then rises again following waking at 8am. Compared to the day before, the homeostatic drive is much higher following sleep deprivation. In contrast, Process C is here modelled as being unaffected by sleep deprivation. Interaction of the two processes indicates that if able the person would have remained asleep past 8am or gone to sleep earlier than midnight following sleep deprivation, because the theoretical threshold had been surpassed. However, the model also predicts that the person would struggle to fall asleep around 4pm, despite exceptionally high homeostatic sleep pressure.

Similar to the ablation of the SCN, transgenic mice lacking core circadian genes such as *Bmal1* or both *Cry1* and *Cry2* have less rhythmic sleep patterns (Laposky *et al.* 2005; Wisor *et al.* 2002). However, genetic disruption of the clock also significantly affects total sleep duration, with the *Bmal1*$^{-/-}$ and *cry1*$^{-/-}$/*cry2*$^{-/-}$ mice sleeping 90 and 110 minutes longer per day than wild-type controls, respectively, even under rhythmic light dark cycles. EEG analysis showed that the increased sleep duration of these clock mutants is associated with an increased NREM delta power, indicative of an elevated requirement for sleep despite sleeping longer than wild type controls. In contrast, knockout of *Clock* in mice results in a 2 hour reduction of daily sleep time with reduced daily delta energy compared to wild-type controls (Naylor *et al.* 2000), indicating an reduced intrinsic requirement for sleep. Although

the effect of SCN ablation on sleep duration in mice is unclear, the observation that the global knockout of core clock genes can have opposing effects on sleep duration indicates that these genes can modulate sleep timing and duration through a mechanism distinct from a non-functional SCN.

1.3.4. Homeostatic Inputs to Timing of Sleep

The timing and duration of sleep is also under homeostatic control (Process S), with the propensity to sleep being dependent on the total duration of recent wakefulness. This central feature of sleep remains much less understood than the circadian control of sleep. The presence of homeostatic control necessitates a mechanism by which animals can assess the length of sleep and wakefulness. Unlike the circadian input, which is associated with a well-defined group of neurons that rhythmically signals to sleep and wake controlling centres, there does not seem to be an analogous group of neurons whose activity is directly related to the proportion of time spent awake. Another possibility may be the coupling of excitatory wake-promoting signals with a slow, long-term inhibitory signal. Indeed, both cholinergic neurons of the basal forebrain (Saunders *et al.* 2015) and histaminergic neurons of the TMN have been shown to co-transmit GABA, with genetic knockdown of GABA function in TMN neurons decreasing sleep time in mice (Yu *et al.* 2015). Recently, sleep-active cortical interneurons expressing nitric oxide synthase have been suggested to be homeostatic neurons, based on the observation that their firing appears to positively correlate to NREM delta power, a measure of sleep debt (Gerashchenko *et al.* 2008; Zielinski *et al.* 2013). However, the activity of these neurons is strongly suppressed during wake, even after 6 hours of sleep deprivation, indicating that these neurons do not signal homeostatic sleep pressure in the awake animal (Morairty *et al.* 2013).

An alternative to a cluster of specialised neurons being responsible for the homeostatic sleep drive is a molecular homeostat, the abundance of which is linked to the sleep-wake cycle. Indeed, evidence for endogenous, sleep-deprivation induced molecules was first found over a century ago (Kubota 1989). The ideal homeostat would either promote sleep, accumulate during wakefulness and be removed during sleep; or show the inverse pattern and inhibit sleep. Indeed, it is clear that several metabolites and signal molecules which may act as potential homeostats accumulate during prolonged wakefulness in the extracellular space in the brain (see Section 1.4.) (Krueger & Obal 2003). The best characterised of these molecules is adenosine, the concentration of which increases during wakefulness and decreases during sleep (Porkka-Heiskanen *et al.* 1997). Adenosine was first implicated as important for sleep induction when the stimulant effects of caffeine and other methylxanthines was attributed to the antagonism of adenosine receptors (Landolt *et al.* 1995; Schwierin *et al.* 1996), a trait that is conserved from humans to flies (Shaw *et al.* 2000). Conversely, adenosine receptor agonists promote sleep with an EEG pattern resembling the deep sleep that follows sleep deprivation (Benington *et al.* 1995). The most widespread adenosine receptor (A_1)

couples to G_{i3} which inhibits adenylate cyclase, leading to the silencing of the neuron (Dunwiddie & Fredholm 1989; LaMonica *et al.* 1985). The less ubiquitous excitatory A_{2A} receptor is expressed in sleep active neurons of the preoptic area of the hypothalamus (Scammell *et al.* 2001). Therefore, much of the sleep-inducing effect of adenosine has been attributed to the A_1 receptor repression of wake-promoting neurons, and the A_{2a} receptor mediated activation of sleep-promoting centres (Porkka-Heiskanen *et al.* 2000).

1.3.5. The Timing of Sleep is Sensitive to Environmental Cues

The two-process model is an idealised representation of sleep regulation; however the *in vivo* control of sleep transitions is not rigid, but instead flexible and sensitive to the environment. Hunger, thirst and the possibility of a threat are all stressors able to increase wakefulness, despite mounting sleep pressure. For example, male rats placed in a cage previously occupied by another male for 1 week show reduced total sleep and higher sleep fragmentation in the following 6 hours compared to control rats transferred to clean cages (Cano *et al.* 2008; Revel *et al.* 2009), whilst rats subjected to total starvation progressively decrease daily sleep time, and have almost no sleep at all in the final 24 hours before death (Jacobs & McGinty 1971). Similarly, introducing a novel object or tapping on a cage can induce transient wakefulness in mice. At the neuronal level, these stressors appear to be integrated into the sleep-wake cycle by orexin neurons. The lateral hypothalamus receives projections from the amygdala, which activates orexin neurons in response to fear stimuli such as foot shock (Winsky-Sommerer *et al.* 2004). Orexin neurons are also directly activated by ghrelin, a gut hormone which signals hunger, and inhibited by leptin, an adipokine which signals a positive energy balance (Yamanaka *et al.* 2003a). Therefore, the timing of sleep is also dependent on environmental cues, allowing animals to postpone sleep to better cope with threats and opportunities.

1.4. The Molecular and Cellular Basis of Sleep and Sleep Homeostasis

In contrast to the well understood neural pathways involved in the control of wakefulness, the molecular and cellular changes that occur during sleep and wakefulness are poorly understood. Several molecules accumulate during prolonged wakefulness, and some (e.g. adenosine) appear to be involved in sleep induction and homeostasis. Other molecules are elevated during wakefulness compared to sleep, but, rather than acting as a signal, appear to have a functional role in meeting the demands of the awake state. Conversely, some molecules elevated during sleep appear to have roles that hint at the function of sleep. Finally, there are a group of molecules modulated by sleep that appear to mediate the pathophysiological effects of acute and chronic sleep loss.

1.4.1. Small Molecule Changes that Accompany Sleep and Sleep Deprivation

Adenosine is the best characterised of the small molecules that accumulate during sleep, yet even its functions are unclear. A major obstacle to identifying its involvement in sleep is that the adenosine moiety is a component of several essential cofactors (e.g. ATP, NADH, Coenzyme A), and so can be produced and consumed by several independent pathways. During wakefulness, extracellular adenosine is increased by both neuronal and glial contributions (Schmitt *et al.* 2012). Neuronal ATP is packaged into vesicles and released with several neurotransmitters (Burnstock 1999; Richardson & Brown 1987), whilst the glial ATP containing vesicles released by glutamate stimulation do not appear to contain other transmitters (Newman 2003). Once in the extracellular space, ATP is rapidly degraded by progressive dephosphorylation to adenosine (Dunwiddie *et al.* 1997). Intracellular adenosine can cross the membrane through channels, and during periods of metabolic stress, intracellular conversion of ATP to adenosine has been hypothesised to increase extracellular adenosine (Brundege & Dunwiddie 1998). Consistent with this, infusion of the mitochondrial uncoupler dinitrophenol into the brain has been shown to increase extracellular adenosine (Kalinchuk *et al.* 2003), whereas supplementing the diet of rats with creatine attenuates sleep deprivation induced adenosine accumulation (Dworak *et al.* 2017).

The rate of adenosine released increases with the duration of previous activity, with brain slices prepared from sleep deprived animals releasing more adenosine in response to glutamatergic stimulation (Sims *et al.* 2013). Removal of extracellular adenosine is mediated by both adenosine deaminase, which converts adenosine to inosine, and astrocytic adenosine kinase, which produces AMP (Porkka-Heiskanen *et al.* 2002). During prolonged activity, adenosine accumulates more quickly than it is cleared, whilst inactivity favours clearance of adenosine.

Extracellular adenosine activates four known G-protein coupled receptors (GPCR), which utilise cAMP as a secondary messenger. Inhibitory A_1 and A_3 receptors decrease cAMP levels, whereas excitatory A_{2a} and A_{2b} receptors increase intracellular cAMP (Haas & Selbach 2000). A1 agonism has also been shown to activate inwardly rectifying potassium channels, providing a second inhibitory mechanism (Andoh *et al.* 2006; Kirsch *et al.* 1990). The most widespread receptor is the inhibitory A_1 receptor, whereas excitatory A_{2a} receptors are present in sleep promoting regions of the preoptic area of the hypothalamus. Therefore, adenosine mediated activation and inhibition of sleep- and wake-promoting centres, respectively, is a plausible mechanism by which sleep pressure is induced by prolonged wakefulness. Remarkably, however, genetic knockout of the A_1 receptor is not only viable, but also has no significant effect on sleep duration or homeostasis, indicating that other mechanisms exist for sleep induction and homeostasis (Stenberg *et al.* 2003).

Adenosine and synaptic activity also locally stimulate the release of tumour necrosis factor-alpha (TNF-α) and other cytokines from glia (Hide *et al.* 2000), which have been shown to modulate neuronal activity, increase local blood flow and induce sleep (Imeri & Opp 2009). Therefore, release of adenosine from cells appears to signal prolonged activity and the possibility of metabolic stress, and acts to reduce activity, boost cell survival and increase phagocytosis and waste clearance. Consistent with a neuroprotective role of adenosine, inhibition or knockout of A_1 receptors exacerbates the excitatory neurotoxicity of kainic acid (Matsuoka *et al.* 1999).

Untargeted metabolomic studies have since shown that several other small molecules increase during sleep deprivation, although several of these have examined serum or urine, and so whether these changes reflect those occuring in the brain is unclear. Plasma metabolites most affected by sleep deprivation are typically lipids, acylcarnitines and amino acids (Bell *et al.* 2013; Davies *et al.* 2014; Weljie *et al.* 2015). Serum phenylalanine and tryptophan, which are precursors to several neurotransmitters, and urine indoxyl-sulfate are all increased following sleep deprivation (Giskeødegård *et al.* 2015), which may indicate an increased rate of central neurotransmitter turnover. The changes in lipid concentrations are more difficult to interpret, as lipids act as both an energy source and as signalling molecules. Elevated acylcarnitines suggests a role of lipid breakdown in sleep deprivation, whereas elevated lysophospholipids may point toward prostaglandin synthesis. Indeed, the abundance of prostaglandins D_2 and E_2 in rat cerebral spinal fluid is progressively increased by sleep deprivation, where they promote sleep (Ram *et al.* 1997).

Recently, a role of simple metal cations in the control of wakefulness states has been identified (Ding *et al.* 2016). The concentration of potassium ions rapidly increases in the CSF of mice at the transition from sleep to wakefulness, accompanied by a slower decrease in magnesium and calcium ion

concentrations. At the onset of spontaneous sleep and isoflurane induced anaesthesia, the opposite pattern is observed. Manipulation of these cations through infusion of modified aCSF into the cisterna magna is sufficient to trigger state changes in both spontaneously awake and asleep mice. Remarkably, local administration of sleep inducing aCSF to the left hemisphere of awake mice induces increases in delta power in the left hemisphere comparable to that seen in asleep mice, without causing a concominant change in the right hemisphere. Conversely, the reverse pattern was also shown in asleep mice with local application of wake inducing aCSF.

In contrast to the activity induced inhibition mediated by adenosine and prostaglandins, however, it appears that the activity of extracellular cations should form a positive feedback cycle. Neural activity elevates extracellular potassium, partially depolarising nearby neurons, whereas reduced magnesium during wake lessens the magnesium lock on NMDA receptors, further promoting excitatory glutamatergic signalling. Furthermore, *in vivo* extracellular cation concentrations are relatively stable except at state transitions, indicating that their concentration carries little information about how long the animal has recently spent in either state. Therefore, it appears that the changing ion concentrations may mechanistically induce and maintain state transitions, but not provide the homeostatic drive for sleep.

1.4.2. Macromolecule Abundance Changes that Accompany Sleep and Sleep Deprivation

The transcriptomic effects of sleep deprivation on mouse and rat cortex and whole brain have been investigated through microarray based studies, which have identified several transcripts that are upregulated following sleep deprivation (Cirelli *et al.* 2004; Mackiewicz *et al.* 2007; Maret *et al.* 2007). A group of these genes, including *Arc* and *Homer1a,* had previously been characterised as immediate early genes and are expressed in neurons in response to recent activity (Lyford *et al.* 1995; Sato *et al.* 2001), indicating that sleep deprivation is associated with increased neural activity in the cortex. *Arc* mRNA and protein is localised to dendrites of neurons, where it promotes internalisation of AMPA glutamate receptors (Chowdhury *et al.* 2006). Primary neurons either lacking *Arc* or constitutively overexpressing *Arc* indicate that the proportion of AMPA receptors on the cell surface negatively correlates with the abundance of Arc protein (Shepherd *et al.* 2006), suggesting that *Arc* is involved in activity induced inhibition of neuronal activity.

Homer1a is an activity induced splice variant of the constitutively expressed long form Homer1. Long form Homer1 is a tetrameric scaffold protein that contains an EVH1 domain, which binds cell surface metabotropic glutamate receptors and endoplasmic reticulum IP3 receptors. As metabotropic glutamate receptors induce the production of IP3, Homer1 facilitates glutamate induced calcium release from intracellular stores. Homer1a contains the same EVH1 domain, but lacks the coiled coil

domain responsible for oligomerisation, reducing the proportion of metabotropic glutamate receptors involved in a functional scaffold (Tu *et al.* 1998). It therefore appears that Homer1a, like Arc, is involved in activity induced attenuation of excitatory signals. Unexpectedly, mice specifically lacking the Homer1a variant exhibit increased daily sleep time that is more fragmented than wild type controls and have an intact homeostatic response to sleep deprivation (Naidoo *et al.* 2012).

Brain-derived neurotrophic factor (BDNF) and its receptor, NTRK2, are also transcriptionally upregulated by sleep deprivation (Cirelli & Tononi 2000). BDNF decreases the intrinsic excitability of cortical neurons (Desai *et al.* 1999), whereas central injection of BDNF in rats induces a 15% increase in sleep time over the following day (Kushikata *et al.* 1999) and TrkB antagonism decreases sleep duration (Faraguna *et al.* 2008), indicating that BDNF may act as a molecular homeostat. However, BDNF, together with Arc, is also extensively involved in synaptic plasticity and homeostatic scaling of synapses. During wake, long-term potentiation (LTP) of individual synapses within the brain is linked with learning and the formation of memories. Left unchecked however, net increases in synaptic strength would increase global firing rates, not only increasing the metabolic demands of the brain, but also decreasing the signal-to-noise ratio of firing patterns within neural networks. The "Synaptic Homeostasis Hypothesis" postulates that a function of sleep is to allow a balancing homeostatic net decrease in synaptic strength to occur (Tononi & Cirelli 2003). This hypothesis is consistent with apparent increases in central energy demand during wakefulness and the disruption of learning caused by sleep deprivation.

Microarray studies of sleep deprived mouse and rat brain have identified several genes involved in oxidative phosphorylation, most notably subunits of NADH dehydrogenase, cytochrome-C oxidase and ATP synthase, are upregulated at the mRNA level after only three hours of sleep deprivation, consistent with an increased demand for ATP (Cirelli & Tononi 1998, 1999; Nikonova *et al.* 2010). Conversely, one study showed that sleep deprivation decreases the mRNA expression of haem and porphyrin synthesis, translation and cholesterol biosynthesis (Mackiewicz *et al.* 2007). In addition to revealing an increase in catabolic gene expression, studies have also shown that the unfolded protein response (UPR) and endoplasmic reticulum (ER) stress response is induced by sleep deprivation, characterised by the upregulation of several heat-shock proteins and X-box binding protein-1 (Xbp1) (Maret *et al.* 2007; Terao *et al.* 2003). Unfolded protein and ER stress responses reduce the translation of protein, whereas NREM sleep is associated with centrally increased incorporation of isotopic leucine into protein, suggesting that sleep is associated with an upregulation protein synthesis (Ramm & Smith 1990). Therefore, at the transcript level and protein level, sleep is associated with anabolic processes whilst wake is associated with catabolic pathways.

Although most studies have focussed on global transcript changes within the brain, Bellesi et *al.* interrogated how sleep deprivation alters the glial transcriptome (or more specifically, the glial mRNA undergoing translation), by precipitating RNA associated with genetically tagged ribosomes (Bellesi *et al.* 2015). Amongst the genes most upregulated by sleep deprivation were several cytoskeletal and extracellular matrix proteins, suggesting astrocytic changes in shape in response to neuronal activity.

In contrast to the well-studied transcriptional correlates of sleep and wake, changes in protein levels between wake and sleep are comparatively poorly characterised, reflecting the technological limitations of proteomic analysis. Early studies used 2D gel electrophoresis to identify spots that change following sleep deprivation, coupled with mass-spectrometry based identification of the proteins in those spots. The utility of 2D gel based proteomics is limited by the low proportion of spots being identified, and also by post-translational modifications affecting migration within the gel, such that phosphorylation of a protein may be misinterpreted as a global decrease in its abundance, as both events would decrease the parent spot intensity. However, based on 2D gel studies, authors concluded that the abundance of proteins involved in mitochondrial energy production is modulated by sleep deprivation (Pawlyk *et al.* 2007), a finding that has recently been supported by a small scale mass-spectrometry based study (Ren *et al.* 2016).

1.4.3. Evidence of Localised Sleep

The link between neuronal activity and local release of sleep inducing molecules, and the direct activity of those molecules on neurons, present an interesting question: can individual regions of the brain "sleep" independently of other regions? Although counterintuitive, sleepwalking and other parasomnias could be described as some regions of the brain being "awake" despite other regions being "asleep" (Mahowald & Schenck 2005). This is shown, for example, by the ability to avoid objects or to open doors, despite the absence of consciousness. In humans, the low frequency waves characteristic of SWS predominate in the frontal cortex before more posterior regions, and similarly, blood flow during sleep is not the same across the brain, but instead shows regional dependence (Braun *et al.* 1997; Maquet 2001; Werth *et al.* 1997). Therefore behavioural, electrical and blood flow markers of sleep throughout the brain appear to be location dependent.

The cortex of the brain is organised into columns, with individual layers of the column involved in their own function, such as input or output (Krueger *et al.* 2008). In the organisation of the cortex, the different layers of a column are thought to represent a basic unit, responsible for a specific process, like responding to stimulation of a whisker. Local field potentials from individual columns can be measured, and show different patterns during whole animal wake and sleep (Rector *et al.* 2005). Periods of sleep-like local field potentials in a cortical column can also appear during whole animal

wakefulness. Remarkably, rats trained to respond to the stimulation of a specific whisker show a greater incidence of error of when the local field potential of the cortical column receiving the input from that whisker is in a sleep like state. Consistent with the possibility of local activity dependent regulation of sleep, the rate of whisker stimulation was positively associated with the probability of the corresponding column entering a sleep like state (Krueger *et al.* 2008).

1.4.4. Implications of Local Sleep

If individual collections of cells are able to sleep independently of other cells in the same animal, the sleep and wake-promoting nuclei may have evolved not to induce sleep itself, but instead to coordinate the rest phase of different neuronal assemblies across the brain. This effect would be analogous to the SCN acting as a master-pacemaker, synchronising otherwise cell-autonomous circadian rhythms. By synchronising the sleep states of the brain, the sleep controlling networks may maximise the regions of brain in an awake state during the active phase of the animal, facilitating the interaction of multiple regions required for higher level tasks and processing. Cognitive defects during sleep deprivation may therefore be mechanistically linked to several regions of the cortex entering into a sleep-like state, despite the animal remaining awake (Vyazovskiy *et al.* 2011). Indeed, fluoro-deoxyglucose uptake in the cortex of awake humans previously subjected to 24-hour sleep deprivation is reduced compared to rested awake controls, indicating wake-induced local inactivation of networks (Thomas *et al.* 2000).

The ability of individual regions to enter a sleep-like state, despite the action of wake promoting centres and other nearby regions remaining in an awake state, indicates the presence of highly-localised state-controlling signals, with important practical implications for investigating the molecular and cellular aspects of sleep function and homeostasis. Homeostatic signals may not diffuse as far as wake-controlling centres, and may even remain within the cell and exclusively act in an autocrine manner. Removing the obligation for homeostats to diffuse long distances within the brain, or even leave the cell, extends the list of possible molecular homeostats to include the abundance, or even localisation, of proteins, transcripts, ions and other small molecules. Indeed, almost any aspect of cellular composition or architecture may be co-opted to record the duration of recent activity.

The phenomenon of local sleep may also allow sleep to be modelled *ex vivo*, separate from wake and sleep promoting centres. Indeed, transcriptomic analysis of primary mouse neurones stimulated with a cocktail of excitatory and wake associated neurotransmitters induces similar changes at the transcript level as found in mouse cortex after six hours of sleep deprivation (Hinard *et al.* 2012). An *ex vivo* model could ultimately allow a reductionist approach to sleep research. Although the *in vivo*

validity of conclusions based on *in vitro* data is often questionable, an *in vitro* model of sleep would allow the rapid and cost-effective screening of pharmacological or genetic interventions designed to perturb molecular correlates of sleep.

1.5. Models to Investigate Sleep at the Molecular and Cellular Level

The molecular study of sleep is hindered by the absence of a good model. Although behavioural aspects of sleep can be investigated well using human volunteers, collecting samples, other than blood and urine, for molecular analysis is not usually possible in human studies. Therefore, alternative systems must be used to model human sleep, each with their own advantages and disadvantages.

1.5.1. Rodent Models of Sleep

The molecular study of sleep has been based almost entirely on *in vivo* rat and mouse models. There are several benefits of mammalian *in vivo* models. Mammals have a clear readout for sleep and wakefulness (EEG), exhibit both REM and NREM sleep stages, and have similar brain architecture and neurochemistry to humans. More generally, working with animals also allows interactions between different tissues to be interrogated. Drugs and other interventions, such as lesions or varied light cycles, can be introduced in the adult or developing animal. Rodents, especially mice, are also genetically tractable, and several knock-in and knock-out mice as well as viral vectors are available, facilitating the interrogation of individual gene functions. More recently, genetically encoded fluorescent reporters allow for the non-destructive, *in vivo* real-time readout of calcium spikes and other cellular events. Finally, being a well-established model, a wealth of knowledge surrounding sleep in rodents already exists, which facilitates experiment design and formation of further conclusions.

There are, however, several biological differences between human and rodent sleep patterns. Sleep is far less consolidated in rodents than in humans, with sleep bouts averaging only a few minutes in duration, and unlike humans they spend around a third of their active phase asleep (Franken *et al.* 1999). Rats and mice are both nocturnal, which may complicate interpretations about the interaction between the homeostatic and circadian drive for sleep.

Rodents such as *Arvicanthis ansorgei* have recently been introduced as a diurnal model for sleep research. However, despite being more active during the day than night, the sleep patterns of *Arvicanthis* follow a crepuscular pattern, with wake predominating at dawn and dusk, and sleep periods being evenly distributed across the light and dark phases (Hubbard *et al.* 2015). As the

Arvicanthis model is still being developed, it lacks the availability of previous studies, transgenic lines or whole genome sequences that are available in other rodent models.

There are also experimental difficulties in using rodents to model human sleep. Unlike human sleep deprivation studies, where the subjects can be asked to remain awake, animals must be kept awake by constant stimulation, which can be stressful. Initial total sleep deprivation protocols were based on the "disk over water technique", where a rat is placed onto a rotating platform surrounded by water (Rechtschaffen & Bergmann 1995). When the rat falls asleep, the platform begins to rotate, and forces the rat to either move to counteract the rotation, or be carried into the water. This technique can be used to impose wakefulness for up to 30 days in rats, but is associated with a massive increase in corticosteroid levels, indicating the rats are highly stressed (Everson *et al.* 1989). Although the animal is nevertheless still sleep deprived, the stress associated with the induction of sleep deprivation may significantly affect its subsequent response to the increased sleep drive. Indeed, the stress associated with single housing mice appears sufficient to fragment recovery sleep after sleep deprivation. The disk over water technique has also been proposed to induce "learned helplessness", which can induce several systemic symptoms (Rial *et al.* 2007). These significant confounders reduce the reliability of results obtained by this protocol.

To reduce the stressfulness of sleep deprivation, the "gentle handling" protocol has been employed (Franken *et al.* 1991). Gentle handling involves continuously introducing novel stimuli, tapping the cage or handling the mice to maintain wakefulness. Compared to the disk over water technique, corticosteroid levels remain low. However, gentle handling requires many researchers to maintain prolonged wakefulness in even a few mice, and is only effective for approximately 8 hours. Therefore, gentle handling protocols have the disadvantage of being highly laborious, leading to underpowered studies.

1.5.2. Fly Models of Sleep

Drosophila melanogaster has become a useful model organism for investigating several aspects of sleep, especially at the cellular level. The night-time consolidated rest period of flies has several parallels with mammalian sleep (Cirelli & Bushey 2008), including a reversibly increased arousal threshold, a requirement for additional recovery sleep following sleep deprivation (Shaw *et al.* 2000), and similar changes in gene expression profiles induced by sleep deprivation (Cirelli *et al.* 2005). *Drosophila* are readily manipulated genetically (Elliott & Brand 2008), are low cost, and procedures on flies are unregulated. Combined with highly accurate activity based readouts of wakefulness,

Drosophila allow for a high throughput analysis of sleep through environmental, genetic and pharmacological interventions.

However, differences in brain structure, intercellular signalling pathways and gene homology between flies and humans reduce the relevance of findings in flies to that of human sleep (Sehgal *et al.* 2007). Pharmacological interventions are usually carried out by addition of drugs to the food, severely limiting temporal resolution and obligating the exposure of peripheral tissue to the drug. Dosage of drugs is difficult to control, especially if the drug is susceptible to degradation in the food or is not absorbed well, and any drug that induces sleep will also reduce its own dosage by reducing available feeding time. Although flies facilitate high-powered, high throughput behavioural experiments, the amount of tissue available from each individual fly is comparatively very low compared to mammalian models. Therefore collecting sufficient tissue for molecular analyses is very laborious, especially if the brain is dissected from the rest of the fly head, leading to underpowered molecular studies.

1.5.3. *In vitro* Models of Sleep

Cell lines, primary cell cultures and tissue explants have been used to model the molecular aspects of several diseases, including diabetes, cancer and Alzheimer's disease. Nevertheless, *in vitro* models have yet to be extensively employed in sleep research, presumably because it is unclear what the behaviour based definitions of sleep and wakefulness actually correlate to at the cellular level. However, the observation that sleep deprivation modifies transcription shows that cells within the cortex have signalling pathways that link wakefulness with intracellular changes. If these same pathways can be modulated pharmacologically or genetically, then it may be possible to model molecular changes associated with wake and sleep *in vitro*.

Tissue explants maintained *ex vivo* sever long range neuronal connections whilst preserving local cellular connections and organisation. Organotypic brain slices have been used to experimentally demonstrate cellular changes in neuronal activity following *in vivo* sleep deprivation (Campbell *et al.* 2002; Liu *et al.* 2010), and to investigate whether sleep associated observations are conserved *ex vivo* (Ding *et al.* 2016; Han *et al.* 2014; Hu *et al.* 2010; Sims *et al.* 2013). Unlike slice cultures, preparation of primary neurons involves the disruption of intercellular connections followed by the selection of neuronal cells. Although new connections form between cultured primary neurons, the networks formed will not be identical to those found *in vivo*. Hinard *et al.* showed that primary cortical neurons treated with a cocktail of wake associated neurotransmitters show changes at the transcriptomic level that are very similar to those induced in mouse brain by six hours of sleep deprivation in mice (Hinard *et al.* 2012), indicating that sleep and wakefulness can be modelled *in vitro,* despite the reduced number of glial cells and native neuronal networks.

Slice cultures and primary neurons allow the researcher to control the extracellular environment of mature neurons. Slices and primary neurons are both genetically tractable, either by the use of transgenic mouse lines or viral vectors. However, organotypic slice cultures and primary neurons are laborious and costly to prepare and maintain, and can introduce variability between experiments. Therefore, a neuronal cell line based model would be a promising addition to sleep research. Cell lines allow for a high throughput, low variability approach to research, and also enable samples of human origin to be generated. Cell lines stably expressing transgenes can readily be generated, which not only allows the manipulation of cell dynamics, but also facilitates the real time monitoring of cellular parameters through fluorescent or bioluminescent based reporters.

1.6. Tools to Interrogate Molecular Changes Associated with Sleep and Sleep Deprivation

The availability of multiple systems to model sleep is complemented by recent technological advances that facilitate the molecular interrogation of samples. Advantages of newer techniques include higher accuracy, reproducibility, throughput and cost-effectiveness. However, many have yet to be applied to sleep research.

1.6.1. Next Generation Sequencing of DNA

Perhaps the most drastic advance has been in the field of sequencing small sections of DNA, which, driven by innovations associated with the Human Genome Project, has now become much more high-throughput and cost effective. Several approaches to sequencing have been developed, but one of the most commonly used is Illumina sequencing. The library preparation for sequencing includes a fragmentation step that results in approximately 200bp lengths of DNA. The DNA fragments produced are subsequently fused to short adaptors, which are then used to prime the sequencing reaction. During the sequencing reaction, nucleotides with a fluorophore fused to the 3’ hydroxyl group are used, with a different fluorophore for each nucleotide. Sequencing is achieved by stepwise template directed synthesis to add a single nucleotide at a time, followed by fluorescent microscopy to determine which fluorophore, and hence nucleotide, had been added. After imaging, the 3’ hydroxyl group is restored by cleavage of the fluorophore, allowing the next nucleotide to be added. Illumina platforms allow for the parallel sequencing of approximately 2 billion 100bp DNA sequences at a time, which can then be compiled to form a genome, or aligned to a reference genome in order to quantify how many reads from each region are present in the sample.

Compared to microarrays, next generation sequencing technology offers several advantages. Although microarrays may have several thousand probes, each probe is designed based on expected

sequences, excluding the possibility of discovering novel exon junctions and splice variants. Sequencing of DNA is better able to distinguish between similar sequences that may both hybridise with the same bait molecules in a microarray, improving specificity and sensitivity to less abundant reads. In turn, sequencing offers a greater dynamic range of detection, as there is no background signal nor upper saturation limit.

By varying the original source for the DNA fragments being sequenced, multiple common uses for next generation sequencing have been developed, including exome-sequencing, the quantitative characterisation of protein DNA binding patterns through chromatin immunoprecipitation (ChIP-Seq) and the transcriptome wide quantification of gene expression (RNA-Seq). Genomic sequencing of patients or animals with specific phenotypes is able to link individual point mutations to pathologies. Regions of the genome that are bound by specific transcription factors or histones can be enriched by co-immunoprecipitation with that factor before sequencing in order to characterise the binding pattern of that factor. Alternatively, RNA-Seq involves the production of DNA fragments from the reverse-transcription of RNA, which are then prepared for sequencing.

Sequencing DNA fragments originating from mouse genomic DNA, coupled with phenotypic characterisation of ethylnitrosourea mutated mice, has been used in sleep research to identify mutations associated with altered sleep duration (Funato *et al.* 2016). RNA-Seq can be used to identify differences in gene expression or splicing associated with a treatment, such as sleep-deprivation, whereas ChIP-Seq can be used to link expression patterns to histone modifications or the activity of specific transcription factor binding sites. However, to date, there is very little RNA-Seq or ChIP-Seq based data available relating to sleep.

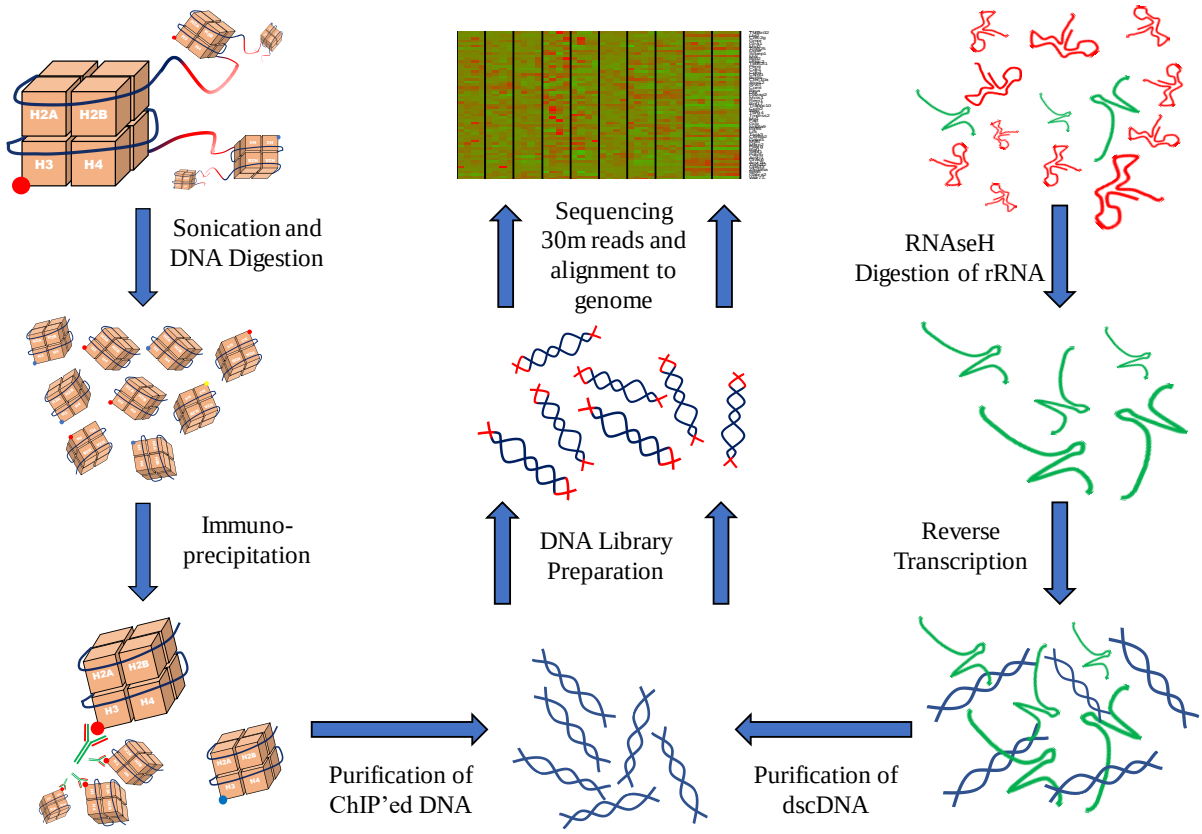

Figure 1.5. Next Generation Sequencing Pipeline: Next generation sequencing (NGS) allows for the sequencing of hundreds of millions of small (25-200bp) DNA fragments. These sequences can then be aligned to a genome to identify point mutations. Alternatively, the number of fragments originating from every known coding or promotor region within that genome can be quantified, and the abundance compared between samples. By using chromatin immunoprecipitation (ChIP), the abundance of specific chromatin marks at promotors can be inferred. By using RNA as a source for double stranded cDNA (dscDNA) fragments, the abundance of several thousand known transcripts can be inferred.

1.6.2. Tandem Mass Tag based Proteomics

Similar in concept to Next Generation Sequencing, Tandem Mass Tag (TMT) Mass Spectrometry quantifies proteins by fusing short peptide fragments, produced by enzymatic digestion of proteins, to small molecular tags. Each tag is composed of a reporter region, a cleavable linker region, a mass normalisation region and a protein reactive region. Using isotopic nitrogen and carbon, the mass of the reporter region of different tags is varied, offset by an equivalent change in mass in the mass normalisation region. Therefore, the total mass and chemical structure of each tag is identical, only the distribution of mass across the reporter and normalisation regions vary between tags. Therefore, these tags allow up to eleven samples to be multiplexed and analysed at the same time during liquid chromatography and subsequent mass spectrometry, greatly reducing the technical variation between samples.

The precise mass of peptides is determined using mass spectrometry and then the possible amino acid compositions that match that molecular weight are compared to proteomic or genomic references and assigned to a specific protein. The abundance of the peptide in each sample is inferred from the relative amounts of the different reporter regions, which is cleaved from the rest of the tag during ionisation. Similar to ChIP-Seq, the pool of proteins examined by mass-spectrometry can first be filtered on the basis of phosphorylation status, subcellular localisation or binding partners by techniques such as titanium dioxide columns, subcellular fractionation or co-immunoprecipitation, respectively (Possemato *et al.* 2017; Schwertman *et al.* 2013; Simor *et al.* 2017).

1.6.3. Genetically Encoded Real Time Molecular Reporters

One pitfall of the destructive sampling techniques used for the molecular characterisation of sleep is that treatment groups within most experiments are made up of distinct individuals, and therefore treatment effects may be confounded by individual biological variation. Although blood may be taken from the same person for RNA-Seq or proteomic analyses before and after sleep deprivation, the same cannot be done with mouse cortex. Similarly, destructive techniques place practical limits on the sampling frequency that is possible during lengthy treatments such as sleep deprivation and sleep recovery, which in turn reduces the temporal resolution of experiments.

In contrast, non-destructive techniques such as video tracking or EEG analysis allow the same individual animal to be monitored repeatedly and continuously. By non-destructively monitoring the same individual, baseline values can be generated for each individual before treatment. Therefore non-destructive techniques allow individuals to act as their own control, increasing the power of the experiment. The temporal resolution of continuous recordings also tends to be very high- video tracking based behavioural experiments may collect data at 50 frames per second- allowing short lived or specifically timed events to be detected.

Some molecular events can be directly and non-destructively monitored. For example, one study monitored the autofluorescence of the brain across the sleep wake cycle, from which the authors concluded that central NADH levels are state dependent (Mottin *et al.* 1997). Other events can be monitored by taking advantage of small molecules whose fluorescence depends on their molecular interactions. For example, using the calcium sensitive BAPTA dye, one study found that cortical intracellular calcium waves of newly born mouse pups were more prevalent *in vivo* during the rest phase than the active phase (Adelsberger *et al.* 2005).

As an alternative to small molecule sensors, the genetic introduction of the calcium binding calmodulin to green-fluorescent protein (GFP) has enabled a genetically modified protein to be used whose fluorescence is dependent on the local calcium concentration (Nakai *et al.* 2001). Since then,

genetically encoded fluorescent sensors have been developed that are sensitive to several molecular parameters, such as NADPH concentration (Tao *et al.* 2017), reactive oxygen species (Bilan *et al.* 2013), pH (Tantama *et al.* 2011), and membrane potential (St-Pierre *et al.* 2014). Further developments have allowed fluorescent imaging at red-shifted wavelengths, enabling simultaneous monitoring of two separate sensors within the same cell (Akerboom *et al.* 2013). The localisation of the sensor can be genetically controlled, either by the addition of a short signal peptide to direct the sensor to specific organelles within the cell, or by using a promotor to limit expression of the construct to a specific cell type. The use of circadian promotors, such as *Bmal* or *Per2* promotors, to drive fluorescent or bioluminescent constructs has been extensively used as a readout of the cellular clock (Noguchi *et al.* 2010), facilitating high-throughput drug screens (Lee *et al.* 2016). The combinatorial use of promotors, subcellular localisation signals and multicolour sensors therefore offers a very powerful toolbox for the investigation of sleep at the molecular level.

1.7. Aims and Approach of this PhD Project

The aim of this PhD project is to better understand the fundamental changes that occur at the molecular and cellular level during sleep and wakefulness, and specifically to address the absence of data about the abundance of sleep dependent molecules during recovery from sleep deprivation. In the first two bodies of work presented in this thesis, we take advantage of recent technological advances in automated sleep deprivation and molecular analytical methods to identify the transcriptomic, proteomic and metabolic correlates of sleep deprivation and recovery sleep in mouse cortex. In the final set of experiments presented in this thesis, we attempt to create an *in vitro* model of sleep deprivation using a human neuroblastoma cell line and optogenetic tools, and discuss to what extent the transcriptional correlates are conserved between the two models. Within the lab, but not discussed in this thesis, these findings are compared to data generated using *Drosophila* by other members in the lab. By using several models, each with their own advantages and confounders, we hope to identify fundamental functions of sleep and the molecular mechanisms of sleep homeostasis.

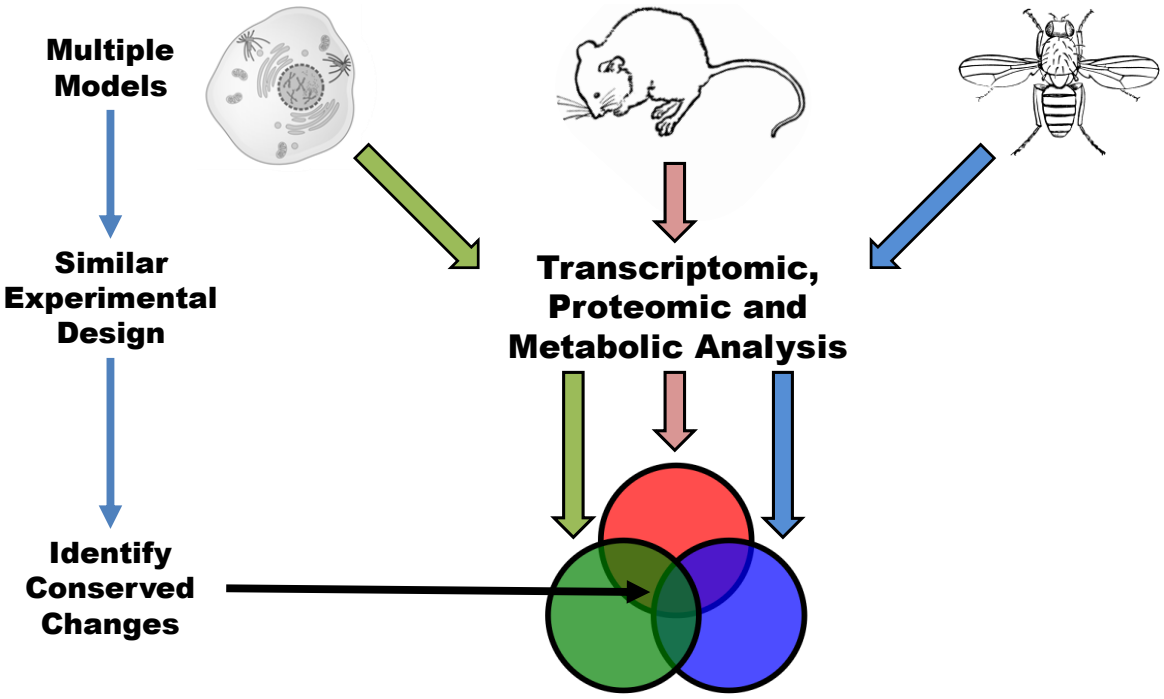

Figure 1.6. Experimental Approach within the Lab: Although sleep is conserved across species, the duration, timing and architecture of sleep bouts vary significantly. Our hypothesis is that sleep is conserved across species due to a fundamental function that is also conserved. Using any single model in isolation to understand sleep risks confounding fundamental functions of sleep with species specific changes. By using similar experimental designs to characterise molecular changes in *in vitro*, mouse and fly models of sleep deprivation, we hope to identify conserved and presumably fundamental molecular signatures of sleep and wakefulness. In this thesis, data from the mouse and *in vitro* models are presented and compared. Work relating to the *Drosophila* model was carried out exclusively by other members of the lab, and so will not be discussed in this thesis.

The experiments upon which this thesis is based contribute novel data. Although numerous studies have previously characterised transcriptomic and proteomic changes associated with sleep deprivation, the vast majority have used now outdated technology and have been limited in scope to a handful of timepoints. In this thesis, we collect tissue at ten timepoints distributed across a total of 54 hours, and used next-generation sequencing based transcriptomics to characterise the effects of 3,6 and 12 hours sleep deprivation. The timecourse style experiment places sleep dependent changes into a circadian perspective and allows the kinetics of recovery to be inferred. We complement these transcriptomic analyses with similar proteomic and metabolomic timecourses. Although other groups have attempted to model sleep *in vitro*, previous studies have pharmacologically activated tissue explants or primary neurons. Here we present our work in generating a cell-line model of sleep deprivation that can be optogenetically stimulated in a large scale and easily controlled manner.

The overall emphasis of this thesis is on the molecular rather than anatomical or behavioural aspects of sleep deprivation. An improved understanding of sleep at a basic molecular level may ultimately facilitate the discovery of pharmacological interventions to alter sleep patterns and treat sleep related pathologies.

2. General Methods

This section details the experimental procedures used to gather data for this thesis.

2.1. Mice Used

Wild type, male C57/Bl6J mice were purchased from Charles River Laboratories and allowed to acclimatise in the new institute for at least 2 weeks after arrival. During acclimatisation, mice were group housed in individually ventilated cages, with *ad libitum* access to standard chow and water and a 12h light, 12h dark cycle (lights on at 06:00). Mice were all aged 9-10 weeks at the time of experiments.

2.2. Sleep Deprivation Protocol

Sleep deprivation was applied using sleep fragmentation chambers (Campden Instruments, Model 80391), which have been previously demonstrated to effectively deprive mice (Kaushal *et al.* 2012). The chambers resemble a typical laboratory mouse cage, except that there is a movable "L" shaped bar descending from the cage lid, the horizontal section of which spans the width of the cage. The bar couples to a frame containing a worm gear motor, which causes the bar to sweep across the cage every 7.5 seconds. When the bar reaches one edge of the cage, the direction of the motor is reversed and the bar sweeps back again. Although the speed of the motor is fixed, it is possible to delay the switching of the motor direction, such that the bar pauses at one edge of the cage. During this time, mice still have access to food and water.

The chambers allowed *ad libitum* access to food and water, and the chambers placed inside a customised cabinet with a controlled light cycle (12h light, 12h dark, lights on at 06:00). The chambers had woodchipping, but did not have nesting material or environmental enrichments such as chew toys, as these block the movement of the bar.

Mice were transferred into sleep fragmentation chambers at 15:00, Day 0. Mice used for transcriptomic and proteomic analyses were pair housed, whilst those used for metabolomic analyses were trio housed. Sleep deprivation was initiated at lights on (06:00) on Day 2, by switching on the motors. The motors were set to pause for 120 seconds between sweeps for the first 30 minutes of sleep deprivation, and the duration of the pause was gradually decreased (through pauses of 60s, 30s and 15s duration) to 0s during the first 90 minutes of sleep deprivation, such that by 07:30, the bar was moving continuously. During this time, the novelty of the moving bar was sufficient to maintain constant activity of the mice, despite the bar only moving a fraction of the time. The mice were continuously monitored during the first 2 hours of sleep deprivation to ensure the mice were avoiding the bar, and to remove anything blocking movement of the bar (e.g. food pellets, piles of woodchipping).

During 12 hour sleep deprivation protocols, wakefulness was maintained between 12:00-18:00 by occasional tapping on the cage, moving the cage or gentle touches with a brush, in addition to the

sweeping bar. At the end of sleep deprivation, motors were switched off when the sweeping bar was at the edge of the cage furthest from the food hopper and water bottle.

2.3. Timecourse Tissue Sampling Protocol

All tissue sampling timecourses had 10 timepoints, spaced 6 hours apart, beginning 12 hours before sleep deprivation and ending 42 hours after the start of sleep deprivation (see Fig 3.6.). The capacity of the cabinet was limited to 8 cages, and therefore to generate the number of samples required, multiple rounds of tissue collections were pooled to generate an entire timecourse.

For transcriptomic and proteomic analyses, mice were pair housed, and 2 cages were taken per timepoint (to give a final n=4). Therefore, each individual treatment group was composed of 3 separate tissue collection timecourses. For metabolomic analyses, mice were trio housed, and 1 cage was taken per timepoint (to give a final n=3). Therefore, each individual treatment group was composed of 2 separate tissue collection timecourses.

For transcriptomic and proteomic analyses, pair-housed mice were simultaneously sacrificed using a rising CO_2 concentration. Whole brains were quickly removed from each animal and frozen on dry ice. After both brains had been removed, both livers were removed, before other peripheral tissues (heart, kidney, epidydimal fat and femoral muscle) were harvested and frozen on dry ice. For metabolomic analyses, mice from one cage were sequentially sacrificed by cervical dislocation and their brain and liver harvested. Cerebral cortex was isolated from the rest of the brain using a flat blunt instrument before freezing on dry ice. Tissues were then transferred to long term storage at -80^{o}C.

2.4. Preparation of Libraries for RNA-Seq Analysis

For RNA-Seq analysis of mouse cortex, a 3mm thick section of cortex was isolated from the left side of the frozen brains, spanning between 0.5mm anterior to bregma to 2.5mm posterior to bregma (see Fig 2.1.). This region samples cingulate, motor, somatosensory, parietal, auditory and visual regions of the cortex. The dissection was carried out on dry ice to maintain RNA quality by preventing the tissue from thawing. The frozen sections were returned to the freezer. To extract RNA, 700µl of TRIzol® was added to the tissue chunk and the tissue homogenised using a disposable pestle. 700µl of ethanol was then added, and RNA extracted using Direct-zol™ RNA MiniPrep Kit (Zymo Research), following the manufacturer's instructions.

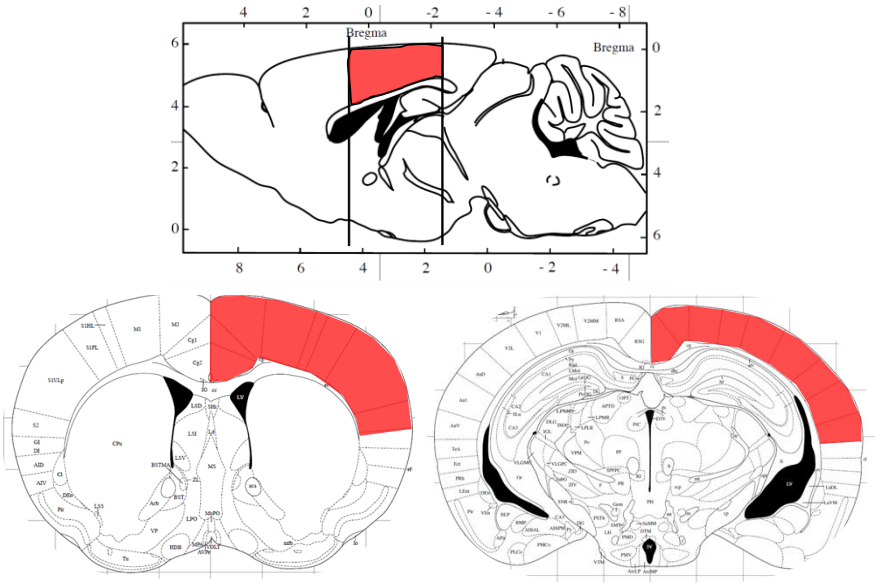

Figure 2.1. RNA for RNA-Seq was extracted from the left cortex between 0.5mm anterior to 2.5mm posterior to Bregma: The cortex sample collected for RNA-Seq is highlighted in red, from a sagittal perspective (upper tile) and coronal perspective (lower tiles)

The integrity of the extracted RNA was confirmed using a QIAxcel system (QIAGEN), before total RNA libraries were prepped for sequencing using the KAPA-RiboErase Hyper Prep, using manufacturer's instructions. Briefly, the library prep was carried out on 1µg total RNA. Ribosomal RNA (rRNA) was depleted using DNA oligomers that are complementary to rRNA and subsequent RNAse H degradation of rRNA-rDNA hybrids. The rDNA oligomers were subsequently degraded by DNAse treatment. rRNA depleted RNA was then fragmented to approximately 200bp sized fragments by incubation at 94°C for 6 minutes in 1x KAPA Fragment, Prime and Elute Buffer. This RNA was then used as a template for double stranded DNA synthesis, before adaptors were ligated onto the 5' end of the fragments. The library was then amplified by PCR, but to minimise the effect of PCR bias on subsequent sequencing, the rounds of PCR were kept to a minimum (3-5 rounds).

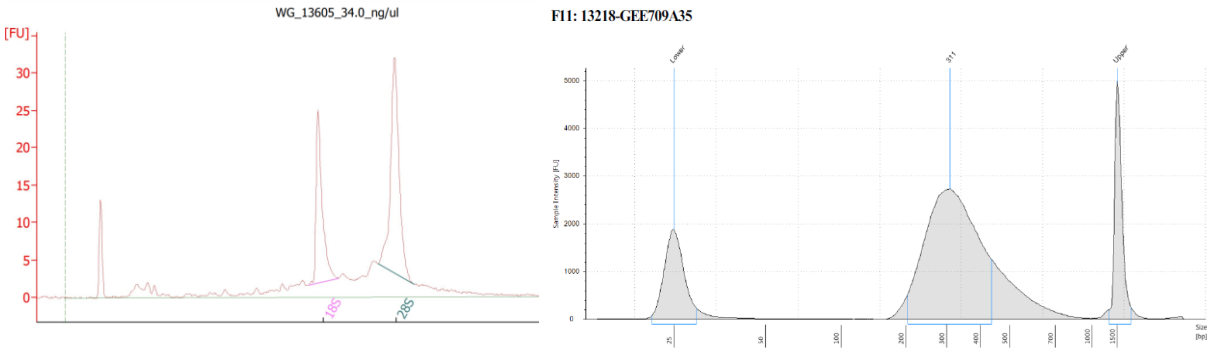

Figure 2.2. Typical Input RNA and Final Library Electropherogram: RNA integrity is estimated on the basis of electrophoresis (left panel). The relative abundance of 28S and 18S peaks, centred at 4.7kb and 1.9kb, respectively, is used as an indicator of quality. During library preparation, RNA is fragmented to approximately 200bp fragments. The average size of fragments is increased to approximately 300bp following ligation of adapters (see right panel).

After each step of the protocol, a bead based clean-up was carried out using KAPA Pure Beads to remove reagents from the previous step. Briefly, KAPA Pure Beads is a suspension of magnetic nucleic acid binding beads in a solution containing sodium chloride and polyethylene glycol (PEG). The higher the concentration of PEG and NaCl, the higher the proportion of nucleic acid bound to the beads, and so addition of the suspension to RNA or DNA containing solutions results in the nucleic acid binding to the beads. The solution, containing reagents, was removed from the beads using a magnetic stand, and the beads twice washed in 80% ethanol to remove any residual solution. When the beads are resuspended in an aqueous solution without high PEG and salt conditions, the nucleic acids elute from the beads and can be used for the next step of the protocol.

2.5. Analysis of RNA-Seq Data

Libraries were sequenced using an Illumina HiSeq 2500 or HiSeq 4000, generating approximately 30 million 100bp pair-ended reads per sample. Reads were aligned using the Tophat Cufflinks pipeline, described below. Reads were initially trimmed on the basis of their sequencing quality score using Trimmomatic, such that any 4 nucleotide region with an average Phred score of less than 15 (equating to a predicted sequencing accuracy of 97%) was removed from that read. Any pair of reads where one of the reads were trimmed to a length shorter than 36nt was discarded (see Fig 2.3., line 13). Trimmed paired-end reads were then aligned to the appropriate genome (GRCm38/mm10 and GRCh38/hg38 for mouse and human RNA sources, respectively) using TopHat2, using the “no-novel-juncs” option to instruct TopHat2 to only consider previously identified exon junctions (see Fig 2.3., line 20). Alignment for RNA-Seq using TopHat2 was typically 85%. Samtools was then used to discard any reads aligning to multiple loci in the genome and sort the remainder by chromosome coordinate (see Fig 2.3., line 22).

```
1  #!/bin/bash
2  # Simple SLURM sbatch example
3  #SBATCH --job-name=gee
4  #SBATCH --ntasks=1
5  #SBATCH --time=60:00:00
6  #SBATCH --mem-per-cpu=128G
7  #SBATCH --partition=compute
8
9
10
11 ml Trimmomatic/0.36-Java-1.7.0_80
12
13 java -jar $EBROOTTRIMMOMATIC/trimmomatic-0.36.jar PE -phred33 INPUT_FILE_1.fastq.gz INPUT_FILE_2.fastq.gz
   EXP_ID_R1_trim.fastq.gz waste_EXP_ID_R1.fastq.gz EXP_ID_R2_trim.fastq.gz waste_EXP_ID_R2.fastq.gz LEADING:3 TRAILING:3
    SLIDINGWINDOW:4:15 MINLEN:36
14
15
16 ml Bowtie2/2.2.9-foss-2016b
17 ml TopHat/2.1.1-foss-2016b
18 ml SAMtools/1.3.1-foss-2016b
19
20 tophat2 -p 32 -o EXP_ID -G Mus_musculus.GRCm38.84.chr.gtf --no-novel-juncs Mus_musculus.GRCm38 EXP_ID_R1_trim.fastq.gz
    EXP_ID_R2_trim.fastq.gz
21
22 samtools sort EXP_ID/accepted_hits.bam -m 128G | samtools view - | grep -e "^@" -e "XM:i:[012][^0-9]" | grep -v
   "XS:i:" > /EXP_ID/deduplicated.sam
23
24 ml Cufflinks/2.2.1-foss-2016b
25 cuffquant -p 16 -o /EXP_ID -M mm10_rRNA_only.gtf Mus_musculus.GRCm38.84.chr.gtf /EXP_ID/deduplicated.sam
```

Figure 2.3. Tophat Pipeline Example: Above is a representative example of a cuffdiff command submission script. Lines 1-7 outlines parameters about the job, such as memory to be allocated, whereas lines 11,16,17 and 18 specify which software packages are required. Paired end sequencing files (INPUT_FILE_1 and INPUT_FILE_2) are first trimmed based on sequencing quality using Trimmomatic. The trimmed reads are then used as an input for tophat2, which exports aligned reads to accepted_hits.bam. Samtools uses this file as an input and is used to sort the reads and remove multiply aligned reads. The sorted, filtered reads are then used as an input to cuffquant, which quantifies the abundance of each individual transcript.

The number of reads aligning to each transcript was then determined using the Cuffquant command of the Cufflinks package (see Fig 2.3., line 25), and then all the Cuffquant outputs were subsequently compared in the same cuffdiff command. Cuffdiff normalises the number of reads per transcript on the basis of the size of that transcript followed by the number of reads in that library to produce a value quoted in fragments per kilobase per million fragments (FPKM). Cuffdiff was run using the geometric library normalisation method (which normalises across libraries based on the number of reads of the median expressed gene in each library rather than total number of reads), and to account for variable rRNA depletion during library preparation, was instructed not to consider any reads aligning to rRNA genes (see Fig 2.4., line 13 and 14).

```
#!/bin/bash
# Simple SLURM sbatch example
#SBATCH --job-name=gee
#SBATCH --ntasks=1
#SBATCH --time=250:00:00
#SBATCH --mem-per-cpu=256G
#SBATCH --partition=hmem

ml Bowtie2/2.2.9-foss-2016b
ml TopHat/2.1.1-foss-2016b
ml Cufflinks/2.2.1-foss-2016b

cuffdiff -p 16 -o Cuffdiff_geo -library-norm-method geometric -L C_01,C_02,...,SD12_10
-M mm10_rRNA_only.gtf Mus_musculus.GRCm38.84.chr.gtf
./C_01_A/abundances.cxb,./C_01_B/abundances.cxb,./C_01_C/abundances.cxb,./C_01_D/abundances.cxb \
./C_02_A/abundances.cxb,./C_02_B/abundances.cxb,./C_02_C/abundances.cxb,./C_02_D/abundances.cxb \
..... \
./SD12 10 A/abundances.cxb,./SD12 10 B/abundances.cxb,./SD12 10 C/abundances.cxb,./SD12 10 D/abundances.cxb
```

Figure 2.4. Cuffdiff Command Example: Above is a representative example of a cuffdiff command submission script. Lines 1-7 outlines parameters about the job, such as memory to be allocated, whereas lines 9-11 specify which software packages are required, whilst a representative cuffdiff command is outlined on lines 13-18.

Differential expression analysis between single timepoints is carried out within cuffdiff, and the statistical values for isoform and gene differential analysis extracted from isoform_exp.diff and gene_exp.diff, respectively, whilst the FPKM values of individual biological replicates were extracted from isoform.read_group_tracking and genes.read_group_tracking and analysed using R to identify genes with a rhythmic and sleep deprivation dependent expression profile.

2.6. Proteomics Analyses

For Proteomic analysis, a separate 2mm section of cortex was taken from both the left and right side of the brain, spanning from approximately 2.5mm anterior to bregma to 0.5mm anterior to bregma (see Fig 2.5.). This region therefore encompasses cingulate, motor, somatosensory, orbital and insular agranular regions of the cortex. The tissue was chopped on dry ice to prevent thawing, before being homogenised by a mini-pestle in protein lysis buffer (9M Urea, 0.5% NP40, 50mM HEPES pH=8.5), containing 0.25µg/ml benzonase nuclease, 1x Halt™ Protease and Phosphatase Inhibitors (ThermoScientific #78429 and ThermoScientific #78420). Proteins were prepared for proteomic quantification using the TMT10plex™ Isobaric Label Reagent Set (ThermoScientific #90110), which allows for the simultaneous quantification of proteins from up to 10 samples during the same mass spectrometry run. 4 ten-plex experiments were carried out: one pair of ten-plex experiments was carried out on the control and the sleep deprived mice, using protein pooled from 4 biological replicates at each time point, such that each TMT-label was associated protein from a different timepoint. A second pair of tenplex experiments was carried out using unpooled protein from 3 individual biological replicates collected at the end of the light phase the day before and after sleep deprivation and a further 4 biological replicates collected immediately following 12 hour sleep deprivation.

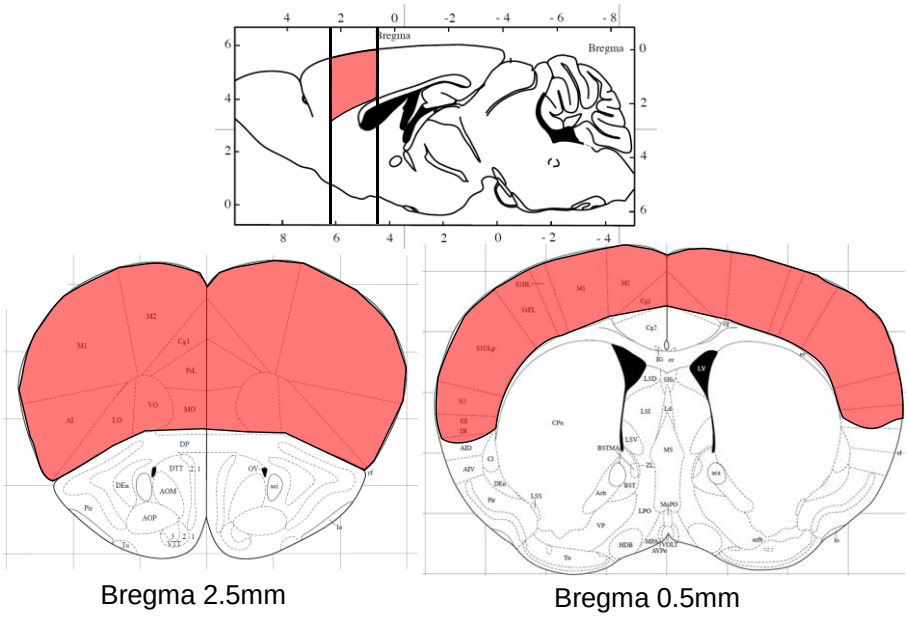

Figure 2.5. Protein for TMT-based Proteomics was extracted from the cortex between 2.5mm to 0.5mm anterior to Bregma: The cortex sample collected for proteomic analysis is highlighted in red, from a sagittal perspective (upper tile) and coronal perspective (lower tiles)

Briefly, protein was precipitated by the addition of 6 volumes of ice cold acetone followed by overnight incubation at 4°C. The supernatant was discarded and the pellet resuspended by sonication in 100mM Triethylammonium bicarbonate (TEAB) buffer (SIGMA #T7408), and quantified using a bicinchoninic acid (BCA) assay kit (ThermoScientific #23225). A total of 100µg protein in 100µl 100mM TEAB buffer was reduced by incubation with 5µl of 200mM tris(2-carboxyethyl)phosphine (TCEP) solution at 55°C for 60 minutes. The sample was then incubated with 5µl of 375mM iodoacetamide at room temperature for 30 minutes, to alkylate thiol groups that would otherwise react with the TMT-labels. The reduced, alkylated protein was then digested by overnight incubation at 37°C with 2.5µg trypsin. The next day, the ten TMT Label Reagents were resuspended in 40µl acetonitrile and added to the protein digest fragments, such that different samples ultimately run in the same tenplex are labelled with different reagents. Following one-hour incubation, the labelling reaction was quenched by addition of 8µL of 5% hydroxylamine. The labelled fragments originating from different samples were then pooled in equimolar amounts, and subjected to mass spectrometry analysis. Peptide and parent protein identification and quantification was carried out using MaxQuant and statistical analysis was performed using R. Maxquant based identification and quantification was carried out by another member of the lab (Dr S. Ray), but subsequent R based analyses was carried out by the author of this thesis.

2.7. Metabolomic Analyses

For Metabolomic analyses, the left side of the whole mouse cortex was lyophilised overnight using a freeze-drier. The dried tissue was then finely ground using an apothecary's pestle and mortar, its dry weight measured and was then placed into a 2ml Eppendorf microfuge tube and returned to a -80^{o}C freezer.

Once all the samples had been ground, 400µl HPLC grade Chloroform (Sigma, 650498-1L) and 200µl LC-MS grade Methanol (Sigma, 000000001060351000) was added to each tube and the samples vortexed to suspend the dried tissue. The samples were incubated at 4^{o}C for 60 minutes, during which time they were subjected to 3x8minute sonication in a water bath sonicator. The samples were then centrifuged at 0^{o}C at 16,000g for 10 minutes, and the supernatant removed into a new Eppendorf tube. 400µl Methanol and 200µl LC-MS grade water (Sigma, 000000001153331000) containing 3 nmol $^{13}C_{5,}{}^{15}N_{1}$-valine was added to each sample, and the samples vortexed to resuspend the pellet. The tubes were then incubated at 4^{o}C for 60 minutes, during which time they were subjected to another 3x8minute sonication in a water bath sonicator. After sonication, the samples were centrifuged at 0^{o}C at 16,000g for 10 minutes and the supernatant added to the previously removed supernatant. The isolated supernatants were then dried in a speed vac and resuspended into 50µl chloroform, 150µl methanol and 150µl water. This solvent mixture partitions into two phases: the upper aqueous layer contains polar metabolites, the lower apolar phase contains apolar metabolites, whilst cell debris and proteins accumulate at the interphase.

The equivalent of 1mg of dried tissue of the polar phase from each sample was subjected to liquid chromatography mass spectrometry (LC-MS), in addition to a pooled sample that was run multiple times. The LC-MS spectra were analysed using both a targeted and untargeted approach. All identified peaks were quantified using Progenesis QI, and the identities of peaks of interest were predicted using the ChemSpider database. Any peaks whose size exhibited a coefficient of variance of greater than 0.3 between the repeated sampling of the pooled sample were removed from downstream analysis. Additionally, the abundance of specific compounds was determined through a targeted approach. Solutions containing individual compounds of interest purchased from Sigma were subjected to LC-MS, to identify precise elution windows, mass-to-charge ratio and fragmentation pattern returned by the same machine as used for cortex samples. Fragmentation of ions from the pooled sample matching the mass and elution time of target compounds was used to further confirm that the peak corresponds to the compound of interest, and that the compound of interest was extracted in detectable quantities from the cortex. The area of these peaks were then quantified using TraceFinder, and the data exported for statistical analysis in R.

2.8. Statistical Analysis of Datasets

Omic datasets were analysed through a combination of Cuffdiff, JTK analyses, Analysis of variance (ANOVA) and Student t-tests. The resulting p-values were then corrected for multiple testing to produce q-values using the "p.adjust" function in R, using the Benjamini-Hochberg method (Benjamini & Hochberg 1995). Tests returning q-values lower than 0.05 were considered for further analysis.

RNA-Seq data alignment and quantification utilised the Cufflinks pipeline, the final stage of which, Cuffdiff, performs statistical analysis of differential gene expression for each gene in each sample pair based on raw reads.

The final output values for each replicate (FPKM normalised RNA expression, protein abundance, metabolite peak area) were also subjected to JTK analysis for the identification of rhythmic molecules (Hughes *et al.* 2010), setting the number of replicates to 4, time between timepoints as 6 hours and the cycle period to 24 hours. For metabolomic and proteomic and the cellular RNA-Seq timecourses, all the timepoints were considered in JTK analysis. For the RNA-Seq of mouse cortex, only timepoints 1-8 were considered, due to timepoints 9 and 10 of the control and SD6 groups suffering from batch effects. Notably, inclusion of the additional timepoints in JTK analysis does not alter the ultimate conclusions about the global effect of sleep deprivation on rhythmic genes.

Identification of sleep dependent genes was performed between pairs of conditions (e.g. Control vs SD6) using ANOVA analysis using the "aov" function in R, with the format aov(value ~ Group * Time, data=(Control&SD6)). This function produces 3 p-values, indicating the significance of the effects of Group, Timepoint and whether there is an interaction between the two (i.e. a differently shaped abundance profile). Only timepoints 3-8 were considered in the ANOVA analysis, with the interaction p-value being exported for further use.

Two-tailed, unpaired student t-tests were used to compare differential metabolite and protein abundances at specific timepoints, and for comparing qPCR expression data.

2.9. Media used for Cell Experiments

Table 2: Media Compositions used for *in vitro* Experiments

Name	Use	Cell Lines	Contents
Normal Base	General Growth and Culture of Cell lines	U20S, HEK293T	Dulbecco's Modified Eagle's Medium (DMEM) (Sigma Aldrich D5671), Supplemented with 10% FBS (HyClone, SV30180.03), 1% Glutamax (Gibco, 35050-038), 1% Non-Essential Amino Acid Mixture (Sigma, M7145), 1% Penicillin / Streptomycin mixture (Sigma, P0781), 0.2% Mycozap Plus (Lonza, VZA-2022)
OptiSHY	General Growth and Culture of Cell lines	SH-SY5Y	50% OptiMEM (Gibco, 31985-047), 50% F12 Ham Mixture (Sigma, N6658), Supplemented with 12% FBS, 1% Glutamax 1% Non-Essential Amino Acid Mixture, 1% Penicillin / Streptomycin mixture,0.2% Mycozap
AIR Medium	Assays in atmospheric CO_2	U20S, HEK293T, SH-SY5Y	DMEM Powder (without $NaHCO_3$ or Phenol Red) (Sigma D5030), Reconstituted with 10% FBS, 1% Glutamax, 1% Non-Essential Amino Acid Mixture, 1% Penicillin / Streptomycin mixture, 0.2% Mycozap, 5g/L glucose, 40mM MOPS (Sigma, M3183) or HEPES (Sigma, H4034).

2.10. Cell Maintenance

Cells were maintained in Corning T75 flasks, and were passaged when they were approximately 70-90% confluent. The medium was aspirated, the cells washed with 10ml pre-warmed phosphate buffered saline (PBS), and then 3ml of trypsin-EDTA solution added. The cells remained in the trypsin solution with gentle tapping until almost all of the cells had detached, before the trypsin was neutralised by addition of 10ml of medium. A proportion (HEK: 5%, U20S: 10%, SH-SY5Y: 25%) of the suspension of detached cells were transferred to a new T75 flask, and medium added to make the total volume to 15ml, and the new flask returned to the incubator (37°C, 5% CO_2). The remaining cells were either discarded, or seeded into plates for transfection or assays.

2.11. Generation of Stable Cell Lines

For production of stable cell lines, cells were plated into a 6-well plate. One day after plating, cells were transfected with the relevant plasmid using 25kDa Linear Polyethyleneimine (PEI) (Alfa Aesar, #43896). The next day, cells were trypsinised and transferred to a 10cm cell culture dish, and the appropriate antibiotic (e.g. puromycin or Geneticin) added 48 hours after transfection at the lowest concentration previously determined to eliminate untransfected cells of that type (typically

2µg/ml Puromycin (Invivogen, ant-pr-1), or 100-200 µg/ml Geneticin (Gibco, 10131-035). Resistant colonies appeared on the plate after 2-6 weeks, depending on cell type and selection antibiotics. Monoclonal lines were produced by placing sterile filter paper disks soaked in trypsin solution on top of individual colonies, and transferring them to their own well in a cell culture plate. Polyclonal lines were produced by the pooling of multiple colonies.

For faster and more reliable production of polyclonal SH-SY5Y puromycin resistant stable cell lines, cells were plated into 10cm dishes and transfected using PEI when 50% confluent. 2 days later, cells were treated with puromycin for two days, and then allowed to recover in puromycin free medium for 2 days. The cycling treatment of antibiotic continued for 2 weeks, before the cells were continuously grown in puromycin containing medium.

2.12. Stimulation of Cells with Neurotransmitter Cocktail

A Neurotransmitter Cocktail containing multiple neurotransmitters associated with wakefulness was produced, based on Hinard et al. A 100x stock concentration containing 1mM carbachol (Sigma, C4382), 100 µM NMDA (Cambridge Bioscience, 14581-50 mg-CAY), 100 µM AMPA (Sigma, A0326), 100 µM kainic acid (Sigma, K0250), 100 µM ibotenic acid (Sigma, I2765), 100 µM serotonin (Sigma, H9523), 100 µM histamine (Sigma, 53300), 100 µM noradrenaline (Sigma, 74480), 100 µM dopamine (Sigma, PHR1090), and 1µM orexin (Sigma, O6012) was dissolved in water, aliquoted, and frozen. This stock concentration was added to cells and the cells returned to the incubator. After 4 hours of cocktail treatment, cells were lysed in TriReagent and the RNA purified.

2.13. Stimulation of Cells with Light

The stimulation of cells with light was developed during this project, and the outlined protocol below represents the final product of this development. In the course of the project, preliminary data were generated with similar protocols, but without some of the method refinements. Method details specific to individual experiments are listed in the appropriate section of Section 5.2..

Cells expressing opsin containing constructs were illuminated with blue light (wavelength 468.5±1.5nm), green light (523.5±1.5nm) or red light (622.5±2.5nm) using a programmable LED array, based on the NeoPixel Shield LED array (Adafruit) controlled by an Arduino Uno. Each cell containing plate was illuminated by two arrays at a distance of 3cm, held in place by a custom printed part. The maximum light intensity able to be supplied to cells at this distance was calculated to be 1.6mW/cm^2, 0.42mW/cm^2, and 0.38mW/cm^2 for the blue, green and red LEDs, respectively, and measured to be 1.2mW/cm^2, 1.0mW/cm^2 and 0.95mW/cm^2, respectively.

The Arduino is programmable in such a way that when powered up, it runs a set of commands once and then operates a command loop continuously until power is removed. The programmed single run commands consisted of a pause of 20 seconds, whilst the loop specifies which colour LEDs are activated, intensity of light emitted, number of flashes per second, duration of each flash, and how many flashes occur in a row before a pause in flashing. During the sample preparation for the transcriptomic analyses of CoChR-RCAMP expressing cells, green and blue LEDs were both active at maximum light intensity, at a frequency of 8Hz. Each flash consisted of 20ms of both blue and green light, followed by a further 5ms of green light only. After ten seconds (i.e. 80 flashes), there was a 10 second pause before the next train of flashes.

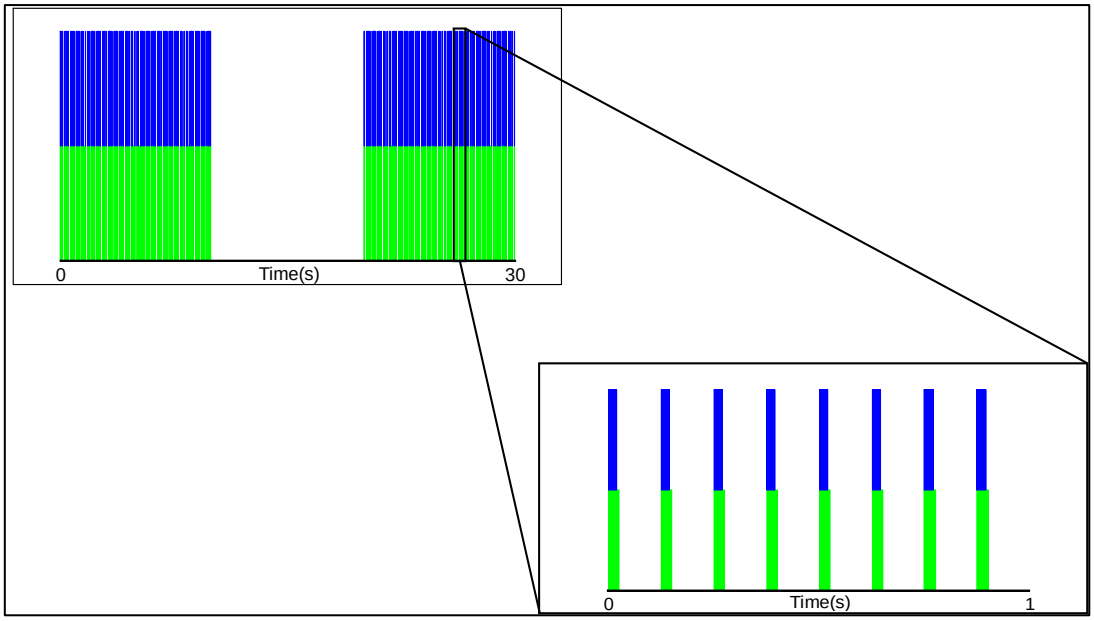

Figure 2.6. Schematic of LED Illumination Pattern: Arduino controlled LED shields containing RGB LEDs were used to illuminate cells. Each flash of light was composed of blue and green light, with simultaneous onset. The blue light flash lasts 20ms whereas the green flash lasts 25ms. 8 flashes per second took place during the on phase, which lasted 10 seconds, followed by complete darkness for 10 seconds. Every 10 minutes, the arrays were switched off for 30 seconds.

Because each plate was illuminated by two arrays controlled by separate Arduino boards, small differences in timekeeping between pairs of Arduinos caused the flashes of the arrays to become desynchronised. Therefore, to re-synchronise each individual array, the power supplies to all the Arduino boards were controlled by a master Arduino through a MOSFET module. This master Arduino was programmed to remove the power for 10 seconds every 10 minutes, causing each Arduino to restart its set of commands, thereby synchronising all of the arrays before significant drift could occur.

Illumination took place in a light tight incubator with atmospheric CO_2 at 37°C. Arrays were placed inside individual compartments of light tight boxes, such that light from an array could only reach the cells placed directly above it and not others in the same incubator. At the rear of each compartment was a 10cm diameter fan that ran continuously to reduce any local heating due to the LEDs. Cells could be placed into and removed from their compartment for sampling without exposing plates in other compartments to environmental light. Cells had their medium replaced with AIR medium (see Section 2.8.) and their plates sealed before being placed into the incubator. The cells were then maintained in darkness for 36 hours before onset of light exposure.

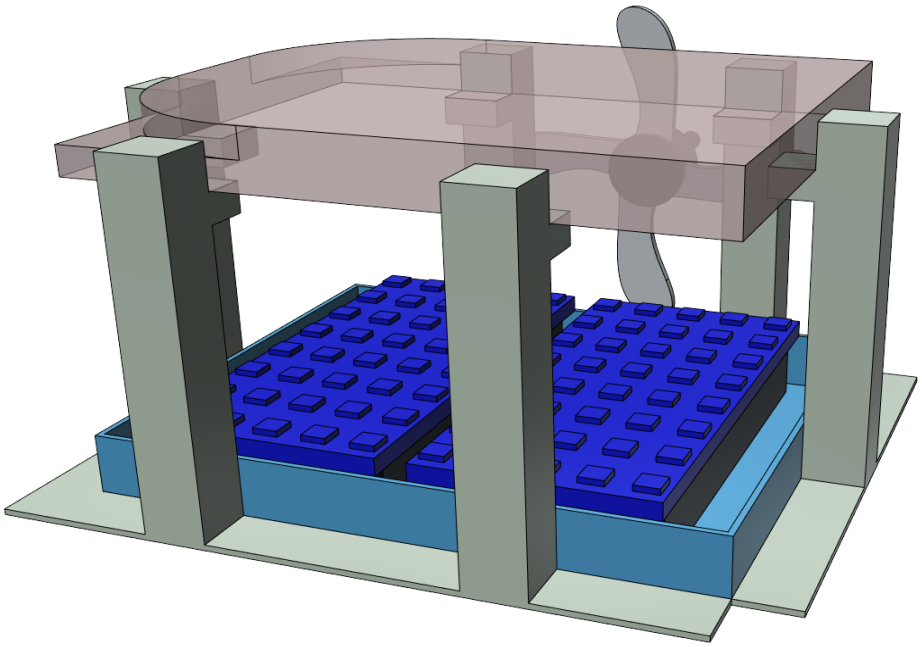

Figure 2.7. Schematic of Final LED based Illumination System: Arduino controlled LED shields containing RGB LEDs were used to illuminate cells. Cells were positioned 3cm above the light arrays using a printed scaffold. Behind each system was a 10cm fan, which was on whenever cells were in the incubator to maintain a constant temperature during illumination. The cells, LED arrays and fan were placed inside individual compartments of light tight boxes in a 37 °C incubator, such that each plate could be individually accessed without exposing nearby plates to ambient light. The LED arrays were powered through a master Arduino, which removed the power supply briefly every 10 minutes, thereby resynchronising the two individual shields of each array.

2.14. Live Cell Luminescence

U2OS cells, expressing luciferase under the control of the *Per2* promoter were transfected with the CRIP or CHALIP plasmid (see Section 2.14.), and stable expression of the construct was selected for using 2µg/ml puromycin and 200µg/ml Geneticin.

Six 96-Well Assay Plates were seeded with the channelrhodopsin-expressing U2OS luciferase cell lines produced above, and the original luciferase cell lines. The cell lines were all cultured for 1 week before this experiment in Normal Base Medium supplemented with 1µM retinyl acetate and 1µM all-trans retinal. The day after seeding, plates had their circadian clocks synchronised by treatment with 100nM dexamethasone for 20 minutes, before having the medium replaced with luciferin containing AIR Medium, supplemented with 1µM retinyl acetate (Sigma, R4632) and 1µM all-trans retinal (Insight Biotechnology sc-210778A) and placed into a dark incubator.

Between 12-32 hours after dexamethasone treatment, cells were illuminated with flashing blue light (Intensity = 20/255, at 20Hz, 5 seconds on, 5 seconds off) for four hours using the custom LED arrays described above. The cells were then placed into an incubator with a deep cooled CCD camera, to quantify light emission by luciferase in 30 minute bins. After 5 days, images were analysed using an ImageJ script, and the bioluminescence of each well quantified. An R script was used to plot and detrend (baseline-correct) the raw data.

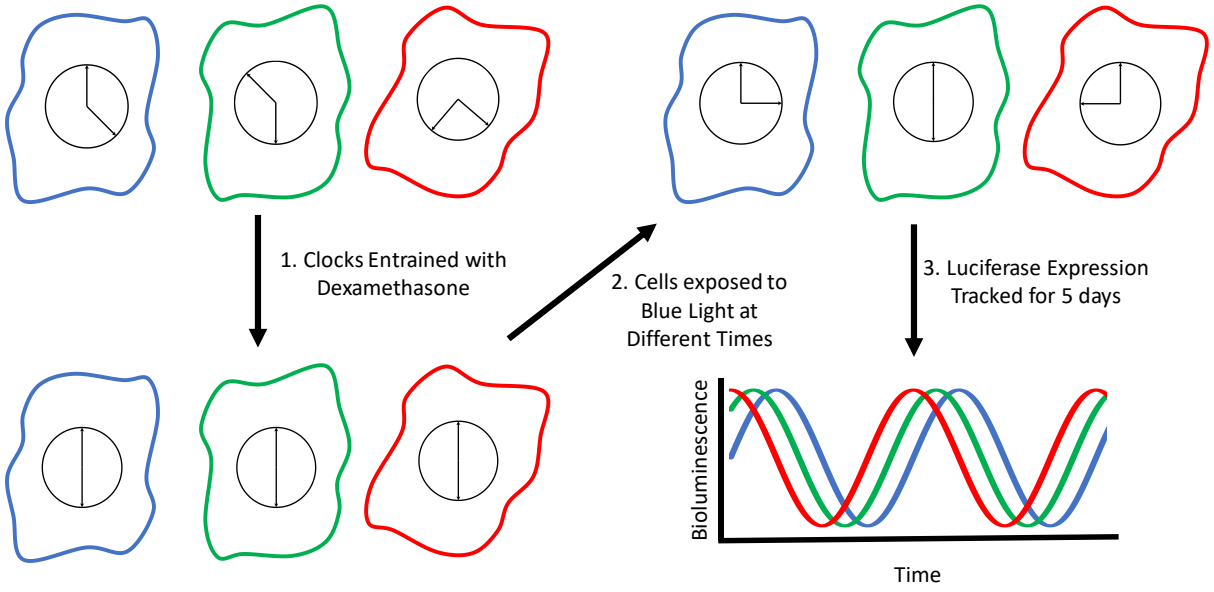

Figure 2.8. Experimental layout for U20S Light Stimulation and Luciferase based Readout of the Cellular Clock: Human Osteosarcoma cells (n=24) expressing an opsin construct and luciferase under the Per2 promotor were plated in 96 well plates and allowed to grow to confluency. Half the cells had their clocks synchronised by dexamethasone at 9am, the other half at 9pm. 12-32 hours after dexamethasone treatment, the cells were treated with flashing light for 4 hours, and then placed into a dark incubator, under a CCD camera. Photos were taken with a 25 minute exposure every 30 minute, and the luminescence of each well quantified for each timepoint using ImageJ. The data were subsequently analysed using an R script to fit sine waves to the raw data, and parameters such as phase, period and amplitude determined.

2.15. Generation of Plasmids for Stable Expression of Opsins

Plasmids to be used to generate light sensitive cells were produced by Gibson assembly, and incorporated into the pEGFP N1 plasmid backbone, to form products which lacked GFP. The pEGFP N1 plasmid contains a CMV promoter, pBR322 origin, Neomycin/Kanamycin resistance cassette, and an SV40 origin, which allows plasmid replication independent of cell division in cell lines expressing SV40 large T-antigen.

Gibson assembly involves amplifying coding regions from multiple constructs by PCR, using the high fidelity Phusion Hot Start II DNA polymerase (Thermo Scientific, F-549S). The primers are >40bp, and are designed such that the 3' end is complementary to the sequence being amplified, whilst the 5' end is complementary to the sequence to which that amplicon will be fused. The design of primers was facilitated by the NEBuilder Assembly Tool (nebuilder.neb.com). The PCR products were all mixed in stoichiometric ratios with the cleaved backbone, and NEB Gibson Master Mix (2x) (NEB, E2611S). The product of the assembly was transformed into Stbl3 competent cells (Thermoscientific, C7373-03), using manufacturer's instructions, and plated onto Kanamycin plates. Colonies were picked, amplified, plasmid DNA extracted using Qiagen MaxiPreps (#12163) and subsequently sequenced. The expression of the construct and puromycin resistance was initially checked in HEK 293T cells before stable expression in SH-SY5Y cells.

Four sets of plasmid production occurred, with some constructs from the first two batches being used as templates for later rounds of cloning. The first two plasmids created were ChR2(C128T)-RCAMP-IRES-PuroR (CRIP) and ChR2(C128T)-2A-eNpHR2.0-IRES-PuroR.

The ChR2(C128T) coding sequence was amplified from Addgene Plasmid 20295, deposited by Karl Deisseroth. RCAMP1h was amplified from Addgene Plasmid 42874, deposited by Loren Looger. The IRES-Puro sequence was amplified from Addgene plasmid 30205, deposited by Darrell Kotton. The 2A sequence-N-terminus of eNpHR2.0 was amplified from Addgene Plasmid 22047, deposited by Edward Boyden, whilst the C-terminal of eNpHR2.0 was amplified from Addgene Plasmid 26966, deposited by Karl Deisseroth. The plasmid backbone was produced by gel purification of the restriction digestion products of Addgene Plasmid 22047 by enzymes EcoRI, KpnI and EcoRV.

Table 3: Primers used for the Gibson Assembly of Plasmids CRIP and CHALIP

Plasmid being Assembled	Fragment Being Generated	Primer 1	Primer 2	Donor Plasmid
CHALIP	ChR2 (C128T)	ACCGGTGCCACCATGGGTACCATGG ACTATGGCGGCGCTTTG	CAATTTTCTGTTTGCTCACCATGGT GGCGGC	(Addgene # 20295)
CHALIP	2A-eNpHR (N-terminus)	CATGGTGAGCAAACAGAAAATTGTG GCAC	CGACAGGCACCAGAATTGTGCTCAC TGC	(Addgene # 22047)
CHALIP	eNpHR2.0 (C-terminus)	CACAATTCTGGTGCCTGTCGTCAGC ATTG	TAGGGGGGGGGGTTACACCACGTTG ATGTCGATC	(Addgene # 26966)
CHALIP	IRES-PuroR	CAACGTGGTGTAACCCCCCCCCCTA ACGTTAC	TCGCGGCCGCTCAACATGTGAATTC TTAGGCACCGGGCTTGCG	(Addgene # 30205)
CRIP	ChR2 (C128T)	ACCGGTGCCACCATGGGTACCATGG ACTATGGCGGCGCTTTG	GATGAGAACCGCTCACCATGGTGGC GGC	(Addgene # 20295)
CRIP	RCAMP1h	CATGGTGAGCGGTTCTCATCATCAT CATCATC	TTAGGGGGGGGGGTTACTTCGCTGT CATCATTTG	(Addgene # 42874)
CRIP	IRES-PuroR	AGCGAAGTAACCCCCCCCCCTAACG TTAC	TCGCGGCCGCTCAACATGTGAATTC TTAGGCACCGGGCTTGCG	(Addgene # 30205)

A second batch of plasmids were created which substituted the ChR(C128T) opsin of CRIP for one of ChRonos, CoChR or CHIEF (E162A/T198C). The ChRonos fragment was amplified from Addgene Plasmid 62726, deposited by Edward Boyden. The CoChR fragment was amplified from Addgene Plasmid 59070, deposited by Edward Boyden, whilst the CHIEF (E162A/T198C) fragment was amplified from Addgene Plasmid 51095, deposited by Jonathan Ting. These fragments were fused to RCAMP-IRES-PuroR, amplified from CRIP. The plasmid backbone was produced by gel purification of the restriction digestion products of Addgene Plasmid 22047 by enzymes EcoRI, KpnI and EcoRV.

Table 4: Primers used for the Gibson Assembly of Plasmids Chronos-, CoChR-, and CHIEF-RIP

Plasmid being Assembled	Fragment Being Generated	Primer 1	Primer 2	Donor Plasmid
Chronos-RIP	Chronos Opsin	ACCGGTGCCACCATGGGTACGGA AACAGCCGCCACAAT	TAGCCATACCCGCCACTCCTCCCTCCT C	(Addgene # 62726)
Chronos-RIP	RCAMP-IRES-PuroR	AGGAGTGGCGGGTATGGCTAGCA TGACTG	TCGCGGCCGCTCAACATGTGAATTCTT AGGCACCGGGCTTGCG	CRIP
CoChR-RIP	CoChR Opsin	ACCGGTGCCACCATGGGTACGCT GGGAAACGGCAGCGC	TAGCCATACCTGCTACTACCGGTGCCG CC	(Addgene # 59070)
CoChR-RIP	RCAMP-IRES-PuroR	GGTAGTAGCAGGTATGGCTAGCA TGACTG	TCGCGGCCGCTCAACATGTGAATTCTT AGGCACCGGGCTTGCG	CRIP
CHIEF-RIP	CHIEF (E162A/T198C)	ACCGGTGCCACCATGGGTACGTC GCGGAGGCCATGGCT	TAGCCATACCGGCTCCGCTTCCGTTAA CG	(Addgene # 51095)
CHIEF-RIP	RCAMP-IRES-PuroR	AAGCGGAGCCGGTATGGCTAGCA TGACTG	TCGCGGCCGCTCAACATGTGAATTCTT AGGCACCGGGCTTGCG	CRIP

Constructed plasmids from Gibson assembly were amplified by transforming competent *E. coli* cells (New England Biolabs, #C2527I) with the Gibson assembly reaction products, following manufacturer's instructions, followed by plating onto agar plates containing 50 µg/g kanamycin. Following overnight incubation at 37^{o}C, colonies were picked with a sterile tip. A portion of the colony was transferred into sterile a 96-well plate, containing Luria-Bertani (LB) broth, containing 50 µg/ml kanamycin, whilst the remainder was transferred into a PCR reaction tube containing Taq Polymerase master-mix (NEB, #M0270L), and primers flanking the whole insert. Following PCR amplification, following manufacturer's instructions, the PCR products were subjected to gel electrophoresis in a 1% agarose gel containing SyberSafe, and imaged. Colonies which resulted in amplification of the correct sized fragments were amplified overnight in LB-broth, and the plasmids purified using the Qiagen Maxiprep protocol. All plasmids were sequenced to ensure no errors had been incorporated, which was carried out by Source Bioscience.

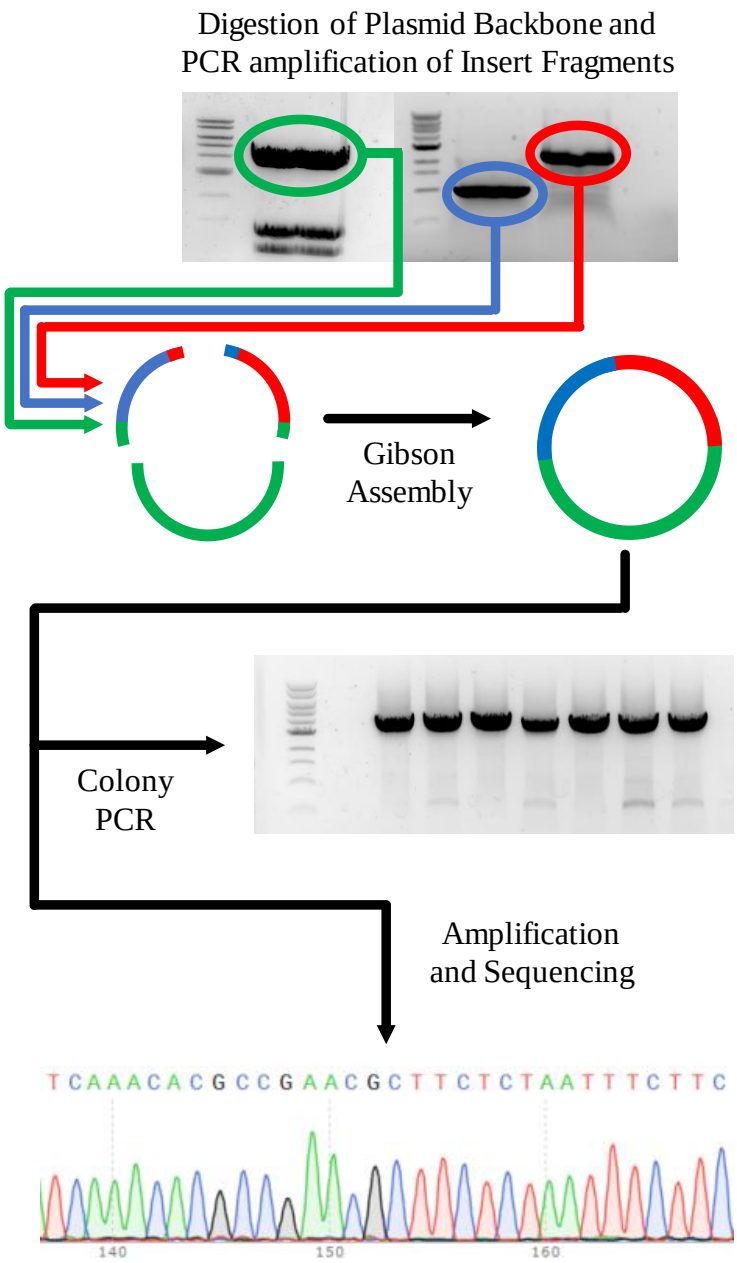

Figure 2.9. Experimental layout for Gibson Assembly of Plasmids: Primers were designed whose 3' end was complementary to the fragment being amplified, whilst the 5' end was complementary to the 5' adjacent fragment of the final plasmid. PCR using these primers and suitable donor plasmids yielded fragments flanked by regions complementary to the flanks of other fragments. The backbone was produced by enzymatic digestion of a donor plasmid. The fragments and cleaved backbone were gel purified and subsequently mixed and incubated together in the presence of Gibson Assembly Master Mix.

The final reaction mixture was used to transform competent *E. coli* which were then plated onto antibiotic containing agar plates. Colonies were picked the next morning. Some of the colony was used to inoculate LB broth, the rest of the colony was placed into a PCR reaction mixture containing primers flanking the full expected insert. PCR was carried out, and the products subjected to gel electrophoresis. Colonies yielding fragments of the expected size were amplified and the plasmids purified. Finally, the plasmids were sequenced to ensure no mutations or errors had occurred during the cloning process.

2.16. Quantitative Real Time PCR (qPCR)

For quantification of expression of genes of interest, cells were lysed in TRI Reagent (Zymo, R2050), and RNA Extraction was performed using the Zymo RNA extraction kit (R2052), or Zymo 96 well RNA extraction kit (R2054), using the manufacturer's instructions, including the DNase digestion step. The isolated RNA had its concentration determined using a NanoDrop 1000 Spectrophotometer machine (Thermo Scientific). 1µg per sample of extracted RNA was Reverse Transcribed using the RT High Capacity Kit (Life Technologies, 4368814), following manufacturer's instructions, in a total reaction volume of 20µl. Following inactivation of the Reverse Transcriptase, the solution was diluted by addition of 80µl water. 2µl of the cDNA solution was used per reaction for quantitative PCR, using the Universal Probe Library (UPL) Technique (Roche).

Expression of genes was quantified from ct values using the delta CT method. The quantity of RNA of a given gene in a sample was expressed relative to the expression of a housekeeping gene (GAPDH, for SH-SY5Y and TBP for mouse derived samples) in the same sample, using *Equation 1*.

Equation 1.

$$E_{G_i} = n \times 2^{-(CT_i - CT_{hk})}$$

$E_{G_i} -$ *Expression of Gene* $\quad$ $n -$ *Any constant number*

$CT_i -$ *CT value of Gene* $\quad$ $CT_{hk} -$ *CT Value of Housekeeping Gene*

Table 5: Primers and Probe Combinations used in qPCR

Gene Name	Primer 1	Primer 2	UPL Probe
Arc	CTCCCAGGGGAGAGTAGAAGTC	GAAGCACCGGGACATCAG	84
Dusp1	TGGGTACATCAAGTCCATCTG	GCAAAAAGAAACCGGATCAC	29
Dusp4	TGCATCCCAGTGGAAGATAA	GCAGTCCTTCACGGCATC	17
Fos	ACTACCACTCACCCGCAGAC	CCAGGTCCGTGCAGAAGT	67
GAPDH	AGCCACATCGCTCAGACAC	AATACGACCAAATCCGTTGACT	60
Homer1a	TTTGGTTGCTCGCTCCAC	TAAGGCTGCGGGTTCAAA	22
Npas4	GCACTCGTGCAAGCACAC	AGAGACGCTACGTTCCTTTCC	8
Nr4a1	TCCTGGTGTAAGCTTTGGTAT	GGATCCCTGCCCTCTAACAG	49
Nr4a3	TGCCTGTATTTATTGCAAGAC	GTCACTGTGAACACCCCATTTA	17
P4HA1	AAGATCTAACAGGACTAGATGTTTCCA	TCCTCCAACTCCATAATTTGC	6
Xbp1	GGAGTTAAGACAGCGCTTGG	CACTGGCCTCACTTCATTCC	37

2.17. Live Cell Microscopy of RCAMP Expressing Cells

Live cells expressing RCAMP containing constructs were imaged using a Leica SP8 confocal microscope. Cells in AIR medium were imaged at 37ºC under atmospheric CO_2 every 200ms using the White Light Laser (WLL) for excitement of the RCAMP fluorophore at 570nm, whilst emission was monitored between 580-620nm using a hybrid detector. Drugs and salts were added by addition of between 2-20µl of a stock solution. Cells were imaged during blue light treatment using the FRAP (fluorescence recovery after photobleaching) module. Whilst constantly imaging RCAMP at 570nm using low level WLL light, cells were exposed to high levels of blue light for 400ms using the 488nm and 476nm argon laser lines. The frames imaged during exposure to argon laser light were deleted and not included in subsequent data analysis. Data from the traces were normalised using the Leica software default normalisation, which defines the highest intensity recorded as 1 and scales other frames linearly, and exported for plotting using R scripts. The half-life of decay for CoChR mediated calcium spikes was determined using an R script that isolated each individual peak from multiple FRAP traces and determined the time taken for the magnitude of the peak to halve and quarter.

3. The Effect of Wake and Sleep on the Mouse Cortex Transcriptome

This section details our transcriptomic profiling of sleep deprived mouse cortex. Using a timecourse style experimental design, we find several genes whose expression is diurnal in undisturbed animals and increases during experimentally imposed sleep deprivation, indicating that these genes are dependent on the wake state of the animal rather than time of day. Additionally, we find a group of genes whose expression is induced specifically during sleep deprivation, but do not show oscillations in control animals. By characterising the expression of genes during recovery from sleep deprivation, we speculate one whether genes may play a homeostatic function. Finally, global rhythms in transcription are progressively blunted following increasing durations of sleep deprivation, underscoring the bidirectional relationship between sleep patterns and biological rhythms.

3.1.1. Typical Sleep and Activity Patterns in Mice

Mice display several differences in key sleep parameters compared to humans, including the duration, timing and degree of consolidation of sleep. Under constant 12:12 light dark conditions, single housed lab mice sleep approximately 10.5 hours per day, with the majority of the light phase being spent asleep (Franken *et al.* 1999).

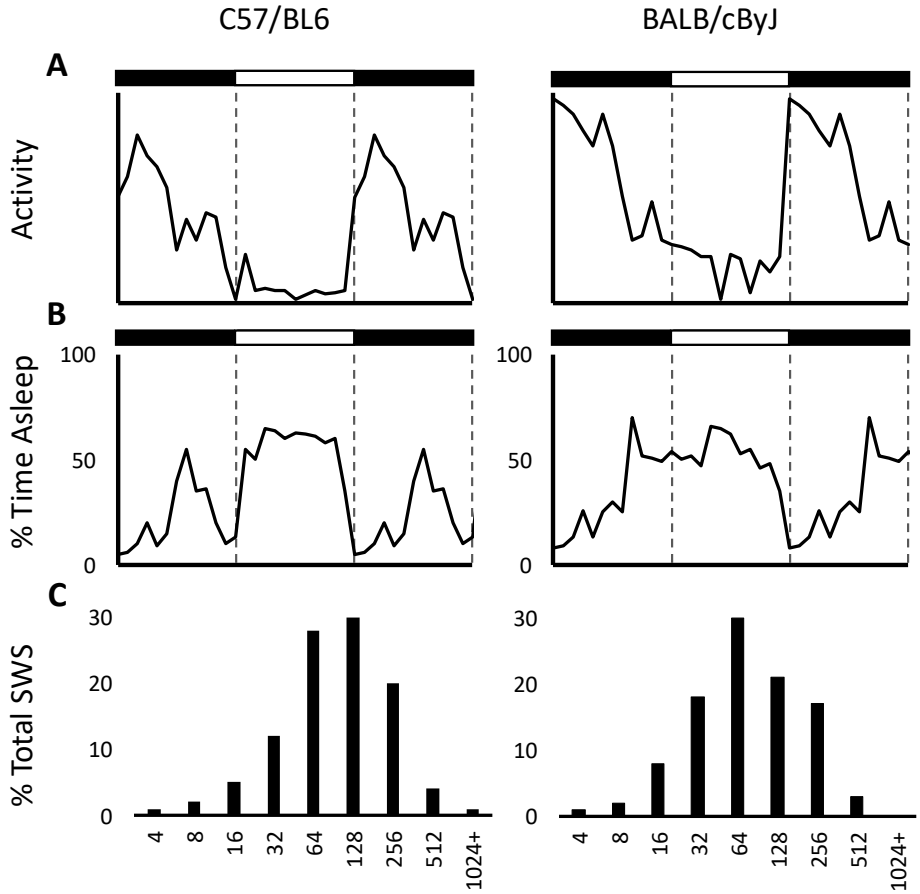

Figure 3.1. Typical Sleep and Activity Patterns of two Strains of Mice: Previously recorded locomotor activity (A) and sleep (B) patterns of C57/BL6 (left column) and BALB/cByJ mice (right column) are plotted, relative to the 12:12 light dark cycle indicated above the plots. Although both strains are predominantly active during the dark phase and register most of their sleep during the light phase, the pattern of sleep and activity plots vary. The bout distribution of slow wave sleep (SWS), expressed as a proportion of total SWS accrued in that bout length, is also plotted (C).

Locomotor activity plots (A) are plotted using data from Kopp (2001), whilst sleep and bout duration plots (B,C) are plotted using data from Franken *et al.* (1999).

Locomotor activity is greatly suppressed during the light phase, but begins to rise around the start of the dark period (Kopp 2001). Activity peaks shortly after the onset of darkness (Welsh *et al.* 1986) and remains high for the first half of the dark phase before reducing to a level significantly above daytime activity. However, despite this elevated locomotor activity, approximately 30% of the total sleep of

mice is nevertheless obtained during the dark phase (Franken *et al.* 1999). Unlike humans, mice also exhibit highly fragmented sleep patterns with over 20 episodes of wake per hour being typical. Due to the high number of wake intervals, the average bout duration of slow wave sleep (SWS) is short in mice, with the majority of SWS being achieved in bouts lasting less than 4 minutes (Franken *et al.* 1999).

Depriving mice of the opportunity to sleep after the onset of light modulates both the timing and consolidation of subsequent sleep. Sleep deprivation (SD) during the first 6 hours of the light phase, during which period mice typically sleep 200 minutes, induces C57BL/6J mice to spend a greater proportion of the subsequent 6 hours asleep compared to previous day and in more consolidated bouts (Franken *et al.* 1999). However, the additional time spent asleep during the remainder of the dark phase only totals approximately 40 minutes, indicating that the sleep deficit has not been balanced before the onset of darkness. Consistent with this expectation, the proportion of time spent asleep remains elevated compared to undisturbed controls over the following dark period, sleeping an additional 80 minutes compared to controls. Therefore, only approximately 60% of the sleep lost during SD is recouped over the following 18 hours of recovery opportunity. The incomplete recovery of total sleep time may be compensated by a twofold increase in delta power observed during the initial stages of recovery sleep, which is thought to reflect a deeper sleep and increased sleep pressure. Indeed the recovery of lost delta energy, the integral of delta power, is close to complete following 18 hours of *ad libitum* sleep (Franken *et al.* 1999).

Importantly, there are significant differences in the major sleep parameters of different strains of mice, with AKR/J mice sleeping 3 hours longer per day than DBA/2J mice (Franken *et al.* 1999). Some strains exhibit a short rest period during the dark phase, whilst the BALB/cByJ strain demonstrates an extended rest period that begins in the latter half of the dark phase and continues until the end of the light phase. The routine sleep-wake patterns of mice have important experimental implications. If sleep deprivation is experimentally imposed at the beginning of the light phase, then mice whose rest phase begins midway through the dark period will have likely already dissipated a substantial proportion of the homeostatic sleep pressure from the previous active phase before sleep deprivation is applied. In contrast, mice whose rest phase usually commences at the onset of light will enter sleep deprivation with a high homeostatic drive for sleep. At the cessation of sleep deprivation, these mice would therefore experience a homeostatic sleep pressure that is significantly higher than any sleep pressure normally experienced over the course of a day. At the molecular level, the especially high homeostatic drive may be required to trigger cellular pathways to cope with sleep deprivation.

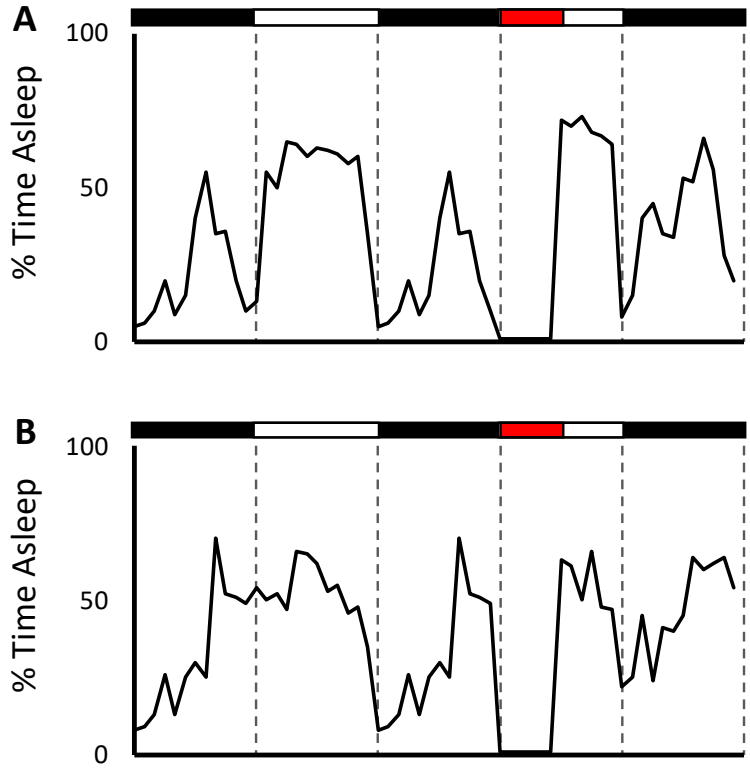

Figure 3.2. 6-Hour Sleep Deprivation of Mice Increases Sleep Duration during the subsequent Dark Phase: Previously recorded sleep patterns of C57/BL6 (A) and BALB/cByJ mice (B) following 6-hour sleep deprivation are plotted. The 12:12 light dark cycle is indicated above the plots by the white and black bars, whilst the red bar indicates sleep deprivation. Imposition of sleep deprivation almost totally removes sleep, and the lost duration of sleep is partially recovered by an increase of sleep duration over the next 24 hours

Both plots are plotted using data from Franken *et al.* (1999).

A further consideration is that any candidate gene or pathway identified as a result of sleep deprivation experiments may be further investigated by the use of transgenic mice. Because of the significant effect that genetic background can have on sleep patterns, and the considerable time and expense required for the typical 10 backcrosses to produce congenic backgrounds, performing experiments on strains of mice with several transgenic lines already available, such as C57/BL6, can greatly facilitate downstream experiments involving transgenic lines (Eisener-Dorman *et al.* 2009; Seong *et al.* 2004).

3.1.2. Methods for Sleep Restriction of Rodents

One of the defining characteristics of sleep is a reversibly reduced sensitivity to the environment. An asleep animal will typically not be aware of small variations in the environment, but will wake in response to a loud noise or sudden pain. Sleep deprivation can therefore be imposed onto animals by repeatedly introducing environmental or sensory events.

Sleep deprivation has been experimentally achieved by taking advantage of several sensory approaches, including touch, temperature, pain, smell and noise. Some approaches, such as placing a mouse into a cage containing the smell of a predator or forced immobility (Papale *et al.* 2005), rely on the induced stress to maintain wakefulness. Other techniques, such as the disk over water technique (Rechtschaffen & Bergmann 1995), introduce significant stress to the animal, as indicated by elevated corticosterone levels (Ramesh *et al.* 2008). Although stressful sleep deprivation techniques may be effective at maintaining wakefulness, stress can be a significant confounder in sleep deprivation studies, and can also disrupt subsequent recovery sleep following the cessation of imposed sleep deprivation.

Table 6: Techniques for Applying Sleep Deprivation to Rodents

Technique	Methodology	Advantages and Disadvantages	Reference
Gentle Handling	Introduction of novel stimuli, e.g. items into cage, tapping on cage, gentle touching, movement of cage.	+ Relatively Low Stress + Commonly Used Protocol + Little forced increase in activity - Laborious and Low Throughput	(Franken *et al.* 1991)
Cage Change	Mice are placed into a clean cage, or one previously occupied by another mouse or rat.	+ Simple - Can only impose sleep loss for short periods	(Febinger *et al.* 2014)

Forced Restraint	Animals are placed into a small cylinder only just big enough to fit them.	+ Simple - Locomotion, eating, drinking, socialising and grooming behaviours are severely disrupted	(Papale *et al.* 2005)
Forced Locomotion	Mice are placed onto rotating treadmills or onto one of two adjacent platforms that are alternately submerged.	+ Simple + Can maintain wakefulness for long periods - Forces large increase in activity and may disrupt other behaviours	(Borbély & Neuhaus 1979; Piérard *et al.* 2007)
Disk Over Water Technique	Mouse is placed on a platform above water and its sleep patterns monitored by EEG. When the mouse falls asleep, the platform rotates, forcing the mouse to move or be plunged into the water.	+ Can maintain wakefulness for long periods (upto 4 weeks in rats) + Not as laborious as gentle handling. - Highly stressful	(Rechtschaffen & Bergmann 1995)
Environmental Noise	Speakers are placed near the cage and loud noises (e.g. traffic, sirens, bell) played at random intervals.	+ Simple and High throughput - Only achieves partial sleep deprivation	(Mavanji *et al.* 2013; Rabat *et al.* 2005)

Lafayette Sleep Fragmentation Chamber	A motor drives the continuous sweeping of a bar along the floor of the home cage. Mice must step over the bar or be hit by it.	+ High Throughput + Low Stress - Food or bedding can block the movement of the bar, so requires supervision by the researcher.	(Ramesh *et al.* 2008)

Therefore "gentle handling" has emerged as the gold-standard of sleep deprivation. Gentle handling relies on the introduction of novel objects to the cage, small noises and gentle touches to impose wakefulness in animals. Corticosterone levels of mice sleep deprived by gentle handling are lower than those sleep deprived by techniques such as the disk over water, indicating that it imposes sleep deprivation in a less stressful manner. However, prolonged sleep deprivation is difficult to achieve with gentle handling, and its laborious nature greatly reduces the scale of experiments that can be carried out. For this reason, higher throughput sleep deprivation approaches that apply sleep deprivation in a reliable and low stress manner have been developed in recent years.

Recently, multiple automated cages have been developed which employ noise (Mavanji *et al.* 2013), airpuffs (Gross *et al.* 2015) and moving bars to maintain wakefulness (Kaushal *et al.* 2012). The Lafayette Sleep Fragmentation Chamber is similar in size to a typical cage, and multiple mice may be housed inside with *ad libitum* access to food and water. Sleep disruption is applied through an "L" shaped bar that descends from the top of the cage and spans the width of the living area. The bar connects to a worm motor driven module, which when switched on causes the bar to repeatedly sweep across the base of the living area. The mouse must climb over the bar, thus imposing sleep restriction. This chamber has been used to impose both total sleep deprivation (Kaushal *et al.* 2012) and sleep fragmentation (Nair *et al.* 2011) through continuous or intermittent sweeping of the bar, respectively. Mice subjected to 6 hours of continuous sweeping of the bar at the onset of the active phase spend 95% of that period in the wake state (Kaushal *et al.* 2012), without a significant increase in plasma corticosterone levels at the end of the procedure (Ramesh *et al.* 2008). In contrast, mice subjected to sleep deprivation through the disk-over-water technique demonstrated a two-fold increase in plasma corticosterone, indicating that this procedure is significantly more stressful (Ramesh *et al.* 2008). Some of the novel sleep deprivation protocols have already questioned some of the conclusions of more stressful sleep deprivation studies (Wang *et al.* 2013).

Other approaches to manipulating sleep patterns in rodents include lesioning sleep-promoting or inhibiting centres and genetic approaches, such as the overexpression or knockout of orexin. Although both approaches can modulate sleep duration, the pleitropic effects of orexin and the likelihood of lesions destroying long range connections and other neurons unrelated to sleep makes the interpretation of the results difficult (Revel *et al.* 2009). Recent advances in pharmacogenetics and optogenetics have now facilitated the activation and silencing of specific neurons with millisecond precision (Fenno *et al.* 2011; Urban & Roth 2015). The activation of wakefulness controlling centres has already been shown to modulate sleep duration (Carter *et al.* 2010). However, the emphasis of studies to date has been on demonstrating a neural pathway participates in sleep regulation or anaesthesia, rather than characterising the effects of sleep deprivation induced in this manner. Although more challenging, laborious and perhaps more variable than automated sleep deprivation approaches, specific activation of sleep promoting centres through optogenetic or pharmacogenetic approaches would allow the researcher to carry out sleep elongation studies (Zhang *et al.* 2015), which may yield fascinating data that complement sleep deprivation studies.

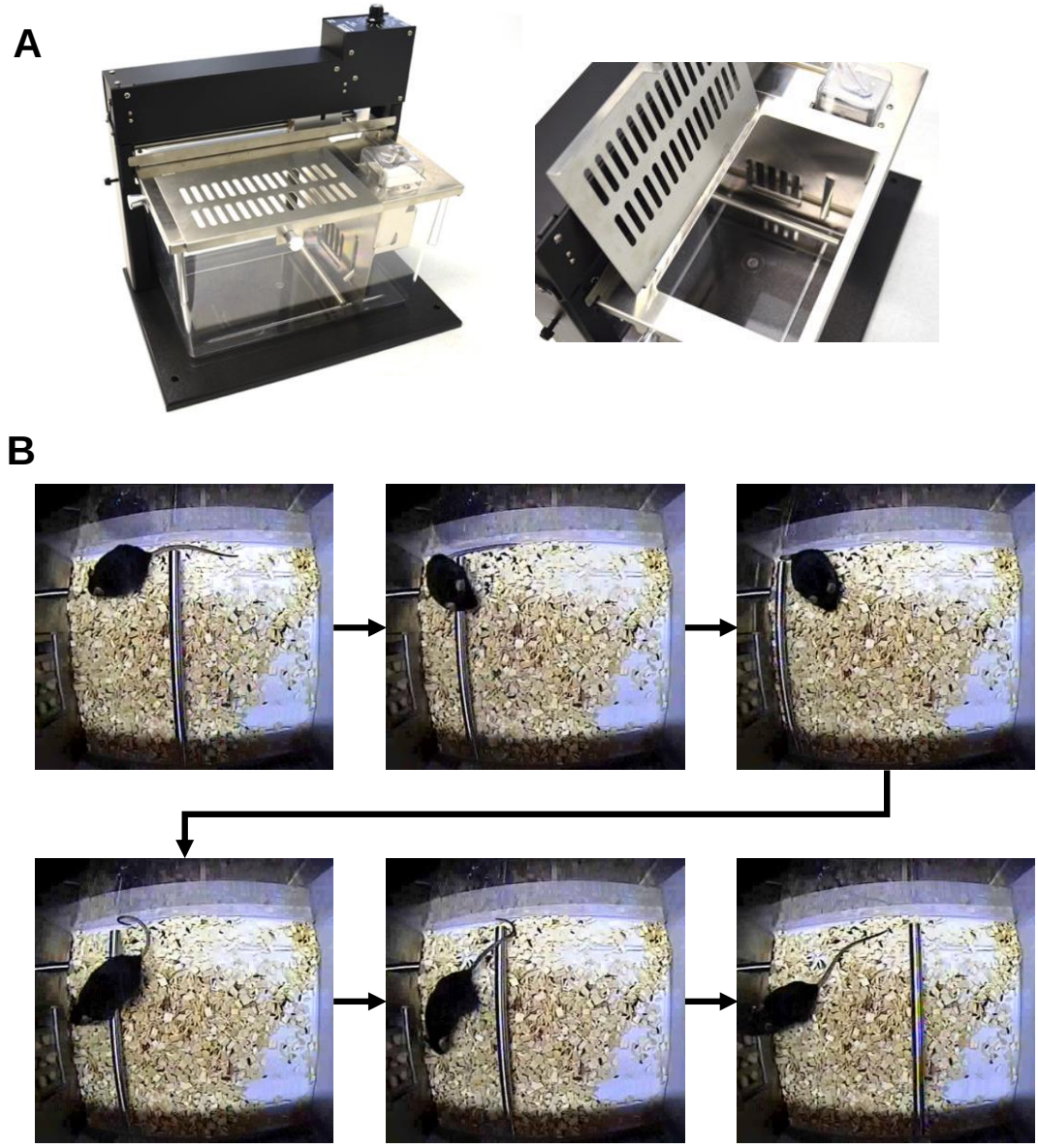

Figure 3.3. The Lafayette Sleep Fragmentation Chamber disrupts Sleep in mice using a motor driven bar: The Lafayette Sleep Fragmentation Chamber consists of a cage and stand (A). The cage contains living quarters, with access to food and water, and an "L"-shaped bar which descends from the cage top and spans the width of the cage. The stand houses a motor which, when the cage is docked to the stand, couples to the "L"-shaped bar, and therefore drives its movement. (B) shows six photos taken across a total of 10 seconds during sleep deprivation of a single mouse. As the bar approaches, the mouse must climb over it. Once the bar is at the end of the cage, the bar changes direction, and the mouse must climb over it once again after which it feeds from the food hopper. The bar makes a full circuit approximately every 15 seconds.

Photos in (A) are provided, with permission, by Lafayette Instrument Company, Inc.

3.1.3. Tissues Affected by Sleep Deprivation

It is generally assumed that sleep is a phenomenon that primarily affects the function of the brain, presumably because the most striking consequence of falling asleep is a loss of consciousness. Nevertheless, there is significant evidence that sleep affects the function of several peripheral tissues. For example, following sleep deprivation, humans have reduced glucose tolerance (Beebe *et al.* 2013; Benedict *et al.* 2012; Greer *et al.* 2013), an impaired immune response to vaccination (Lange *et al.* 2003; Prather *et al.* 2012; Spiegel *et al.* 2002) and increased blood pressure and variable heart rate (Dettoni *et al.* 2012; Sauvet *et al.* 2010). Consistent with functional disruption, sleep deprivation has also been shown to induce molecular changes in peripheral tissues. Sleep deprivation of mice modulates the expression of 500 genes in the lungs and 1000 genes in the heart (Anafi *et al.* 2013), induces the unfolded protein response in the pancreas (Naidoo *et al.* 2014) and causes oxidative damage and cell death in the intestinal lining (Everson *et al.* 2014). To what extent these peripheral phenotypes may be secondary effects of disrupted brain function, elevated corticosterone levels, or the additional activity and opportunity for food intake associated with sleep deprivation is unclear. Intriguingly, it was recently demonstrated that peripheral tissues contribute toward the control of sleep duration and timing. Genetic knockout of *Bmal1* in mice increases the daily duration of sleep by 2.5 hours and ablates circadian rhythmicity (Laposky *et al.* 2005). Restoring *Bmal1* expression specifically in the brain, but not in skeletal muscle, restores circadian locomotor rhythms (McDearmon *et al.* 2006). Remarkably, although the increase in sleep duration is not rescued by central *Bmal1* expression, expression of *Bmal1* in skeletal muscle is sufficient to restore wild type sleep duration (Ehlen *et al.* 2017). This surprising finding supports the theory that the control of sleep timing does not reside solely within the brain, and the contribution of peripheral tissue to the control of sleep suggests that sleep may play a role in the normal function of tissues outside the brain.

Whether or not peripheral tissues play a major role, it is clear that the brain is responsible for a considerable proportion of the control of sleep. Optogenetic activation of the locus coeruleus is sufficient to wake sleeping mice within one second (Carter *et al.* 2010), whereas central perfusion of adenosine agonists induces sleep (Benington *et al.* 1995). Both spontaneous and pharmacologically induced sleep is also associated with large scale and reproducible changes in EEG spectra (Dement & Kleitman 1957), extracellular fluid volume and flux (Xie *et al.* 2013), and localised neuronal activity (Moore *et al.* 2012), indicating that sleep plays a significant role in several aspects of brain physiology and function.

However, due to the heterogeneity in brain structure and function, the role and effects of sleep certainly vary across even small distances. For example, the sleep active, sleep promoting ventrolateral preoptic region of the hypothalamus is situated only 2mm from the wake promoting histaminergic tuberomammillary nucleus, whilst the lateral hypothalamus contains both wake promoting orexin expressing and wake inhibiting melanin concentrating hormone expressing neurons (Konadhode *et al.* 2013). Unsurprisingly, sleep dependent molecular changes have also been determined to be region specific. For example, glycogen and glucose content of C57/BL6 mice is modulated by 6 hours sleep deprivation in the cortex, but not the cerebellum or the brain stem (Franken *et al.* 2003). Similarly, a microarray study comparing transcription in cortex and cerebellum found that of the 220 genes identified as being modulated by sleep deprivation in either region, only 55 (25%) were differentially expressed following sleep deprivation in both cortex and cerebellum (Cirelli *et al.* 2004).

Molecular analysis of whole brain homogenate is therefore likely to reduce the apparent magnitude of molecular changes following sleep deprivation, which in turn may cause several effects to be overlooked. Instead, the majority of studies investigating the molecular correlates of sleep have to date focussed on the cerebral cortex, because the cortex generates EEG signatures that are characteristic of the current and recent wake state of the animal (Franken *et al.* 1999; Steriade & Hobson 1976), and exhibits reduced function following sleep deprivation (Vyazovskiy *et al.* 2011).

3.1.4. Research Aims

In the body of work presented below, we outline our efforts in carrying out a screen of molecular changes associated with sleep deprivation in mouse cortex. Utilising a recently developed, semi-automated sleep deprivation technique, we produced tissue samples from mice that had been sleep deprived for varying durations. Unlike previous studies, we allowed significant recovery sleep and sampled repeatedly during this period, and therefore our studies provide insight into the kinetics with which changes associated with acute sleep deprivation return to baseline levels. We couple this semi-automated sleep deprivation approach with RNA-sequencing to produce a large scale, timecourse style transcriptomic screen of sleep deprived cortex.

3.2.1. Design of Cabinets for Housing Mice for Sleep Deprivation

To generate sleep deprived tissue for molecular analyses, mice were housed inside Lafayette Sleep Fragmentation Chambers placed inside a ventilated Techniplast cabinet. The cabinets required extensive customisation in order to be suitable for automated sleep deprivation. In order to maximise the capacity of the cabinet, the rear metal panel of the cabinet was replaced by a second set of doors, which also aided vision and accessibility of the cages. Barriers were constructed and placed between cages to prevent mice seeing mice in adjacent cages. The interior lights were stripped and replaced with dimmable, cool white LED strips above each cage and a single red LED strip in the centre of the shelf. The cycle of these LEDs were controlled by a timer plug and set to a 12:12 light dark cycle.

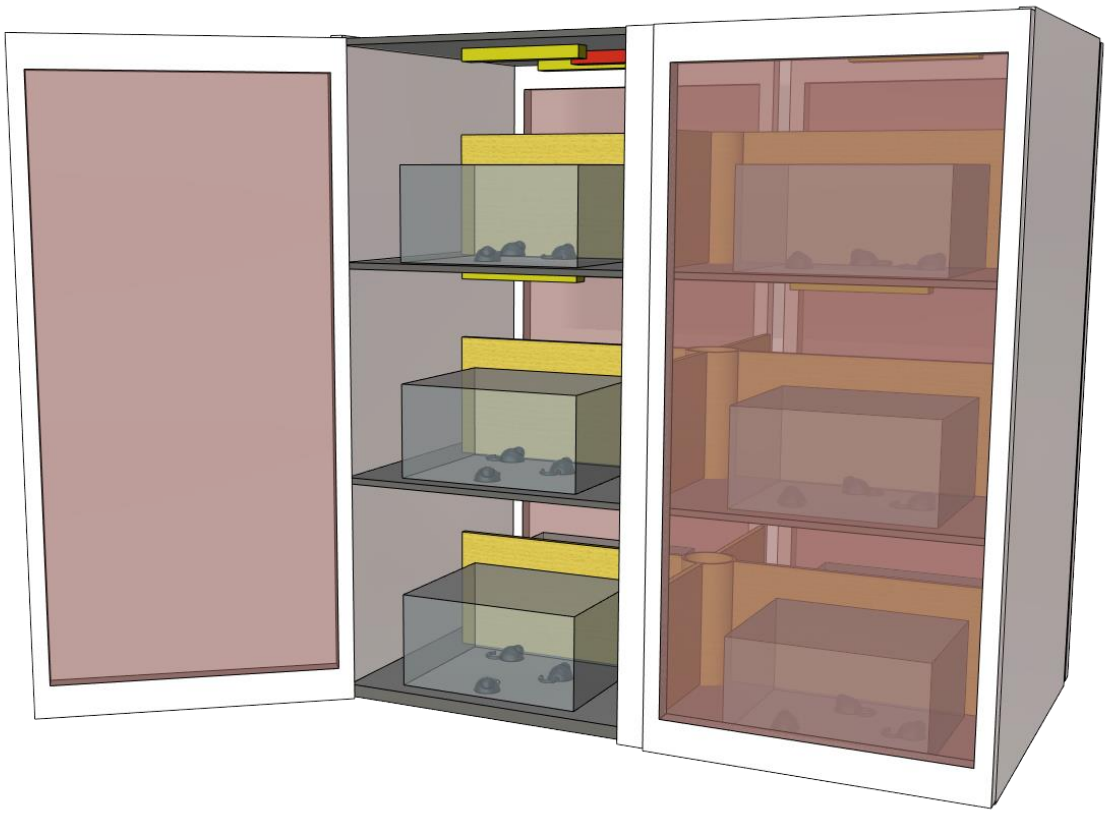

Figure 3.4. Customisation of the Sleep Deprivation Cabinet: To house the animals during sleep deprivation experiments, we customised a Techniplast Cabinet. Red tinted transparent doors were added to both sides of the cabinet to utilise the maximum space available and to facilitate access and observation of the mice. The interior lights were replaced with dimmable cool white LED strips placed above each cage and a central red LED strip, controlled by separate timer plugs. Barriers were constructed to prevent mice in one cage seeing mice in another. The cabinet itself was housed in a room illuminated only by dim red light, to minimise the impact of opening the doors during sampling.

3.2.2. Validation of Automated Sleep Deprivation

The Lafayette Sleep Fragmentation Chamber had previously been validated as an effective sleep deprivation tool in an EEG based study (Kaushal *et al.* 2012). As an initial trial experiment to determine whether the chamber was also able to induce previously reported transcriptional changes, male, young adult (8-10 weeks old) C57/Bl6 mice (n=8) were pair-housed in the sleep fragmentation chambers with access to food and water overnight. The motors were switched on intermittently (every 30 seconds) the following morning. Initially, the bar sweeping across the cage every 30s was sufficient to maintain continuous wakefulness, as mice investigated the bar during the periods when the bar was stationary. After 2 hours however, the novelty of the moving bar was insufficient to prevent the mice falling asleep, so the motor was switched on continuously. Mice quickly learnt how to climb over the bar, and did not appear to be stressed by the moving bar. Sleep deprivation was applied for a total of 8 hours, during which time the mice were monitored constantly. By the end of the procedure, mice were visibly sleep deprived and entering a sleep posture almost immediately after the bar had passed. In contrast, control mice appeared to have spent the majority of the time asleep.

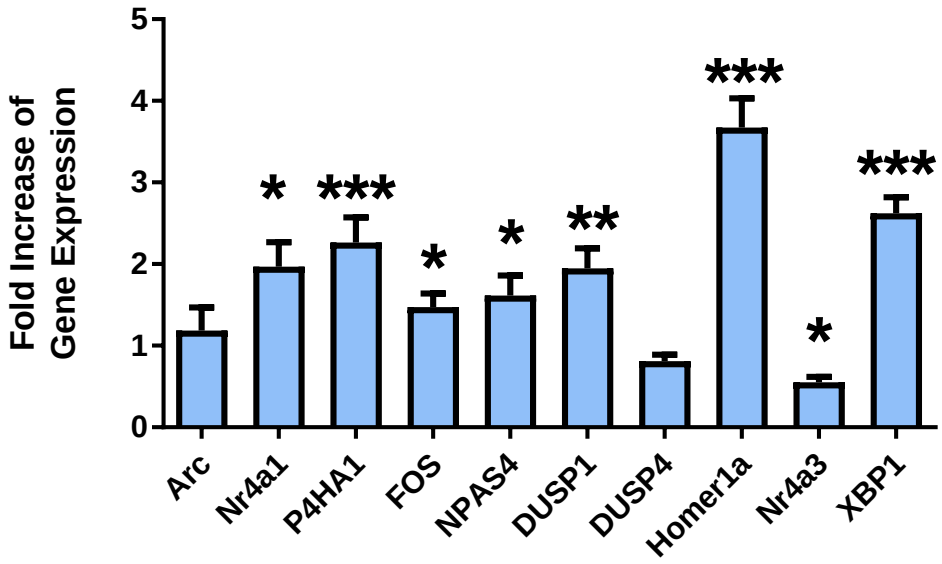

Figure 3.5. Sleep Deprivation Markers are Induced in Mouse Cortex by Automated Sleep Deprivation: Male mice aged 8-10 weeks were sleep deprived for 8 hours (data are mean ± SEM). Cortex was harvested and the expression of genes previously related to sleep deprivation quantified. The expression of genes was normalised to the housekeeping gene TATA-binding protein (TBP), and the fold change of expression compared to *ab libitum* sleep controls plotted.

p-values were determined using a Student t-test, comparing the treated to untreated group for each gene, and the p-value indicated by the number of asterisks above the relevant gene.

* - $p<0.05$, **-$p<0.01$, ***-$p<0.001$.

Immediately following sleep deprivation, the brain from each mouse was harvested and RNA extracted from the cortex. qPCR was carried out to quantify the expression of some genes previously indicated as being upregulated during sleep deprivation in rat or mouse. Several of the target genes were upregulated after the sleep deprivation, indicating that the automated system is sufficient to maintain sleep deprivation.

3.2.3. Experimental Design and Possible Molecular Profiles

Having become satisfied that the automated sleep deprivation protocol was able to maintain prolonged wakefulness in mice, we designed an experimental plan that would allow the identification of sleep related molecules and to characterise how the concentration of these molecules is dependent on the sleep wake status of the animal.

We hypothesised that during sleep deprivation the concentration of molecules would fall into one of four patterns, “independent”, “binary”, “homeostatic” or “stress response” (see Fig 3.7.). A molecule that was independent of sleep deprivation was expected to exhibit no change during or following sleep deprivation compared to control animals. Binary molecules were expected to exhibit stepwise high and low expression over the course of a normal day, linked to the sleep wake cycle, and for sleep deprivation to prolong the high level without affecting the absolute concentration. Therefore, the concentration of a binary molecule would indicate the current state of the animal but give no information about the amount of sleep in the preceding 24 hours. In contrast, homeostatic molecules were expected to oscillate over the course of a normal day with a cosine pattern, with the change in concentration of the molecule being dependent on the sleep wake cycle. Therefore, the concentration of a homeostatic molecule would not indicate the current wake state of the animal, but instead give information about the total amount of sleep in the recent past. Importantly, the concentration of these molecules is not expected to return to baseline levels until excess homeostatic sleep pressure, evidenced by the presence of recovery sleep, has been dissipated. In Figure 3.7., dissipation of excess homeostatic sleep pressure following 12 hour sleep deprivation is modelled as taking exactly 12 hours. Finally, we expected some molecules to demonstrate a stress response profile, where expression was constitutively low but strongly activated after a prolonged period of wake. These genes may exhibit a spike during the course of a normal day or only be induced following sleep deprivation. Therefore the concentration of these molecules would indicate whether or not the animal was exhibiting particularly high homeostatic sleep pressure.

To identify sleep related molecules and which pattern best characterises their expression, we designed a timecourse style experiment. Mice were placed into the sleep deprivation cabinet 3 hours before the onset of dark on Day 0 with a 12:12 light dark cycle. At the beginning of the light phase on

Day 2, mice were sleep deprived for 0, 3, 6 or 12 hours, after which time they were allowed *ad libitum* sleep. Mice were sacrificed at 10 timepoints separated by 6 hours across the course of 54 hours, with the sampling being synchronised to the beginning and middle of the light and dark phases. Sampling began 12 hours before the onset of sleep deprivation and continued as long as 39 hours following cessation of sleep deprivation. The 10-timepoint design of this experiment reflects the limit of multiplexing in TMT-based proteomics, as there were only 10 isobaric TMT tags available at that time (since then an eleventh tag has become available). For consistency of analysis and to ease comparison across different data sets, this same 10-point timecourse design was used for characterising the transcriptomic, proteomic and metabolomic associated with sleep deprivation in mouse cortex.

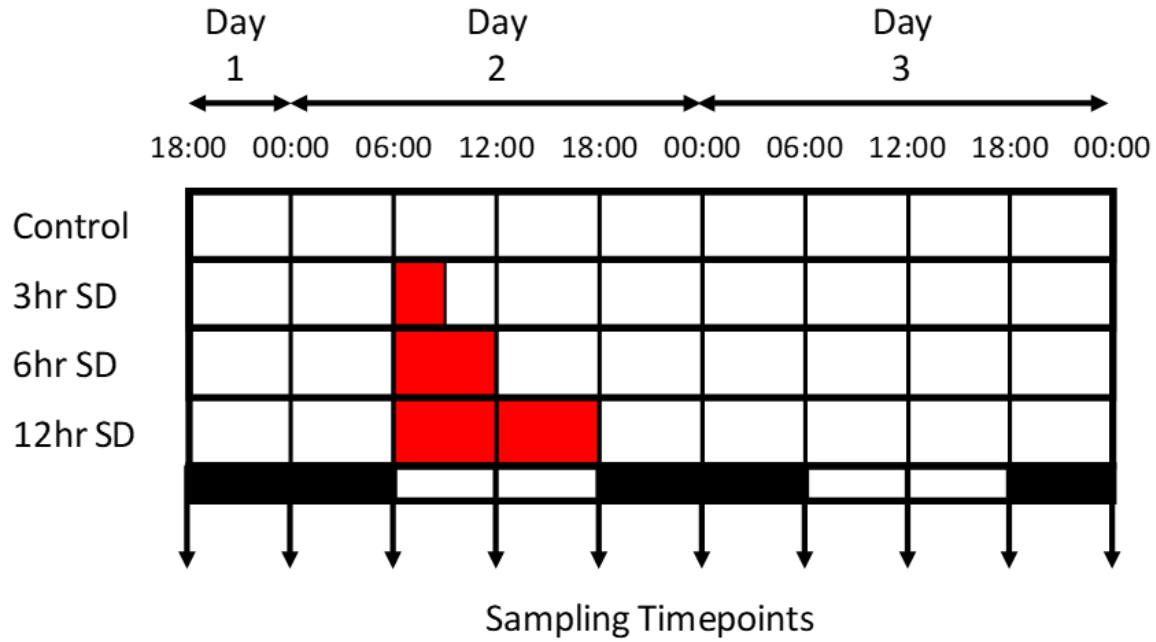

Figure 3.6. Experimental Design for Transcriptomic Characterisation of Sleep Deprivation in Mice: To identify which genes are modulated by sleep deprivation, and then to determine the rate at which their expression returns to baseline levels, we designed a timecourse style experiment. Mice were sampled every 6 hours for 54 hours, beginning at the beginning of the dark phase before sleep deprivation, and extending to the middle of the second dark phase following sleep deprivation. Sleep deprivation (in red) took place from the beginning of the light phase on Day 2, and lasted either 3, 6 or 12 hours. The black and white bar at the bottom of the figure represents the light dark cycle to which the mice were exposed. SD- Sleep Deprivation.

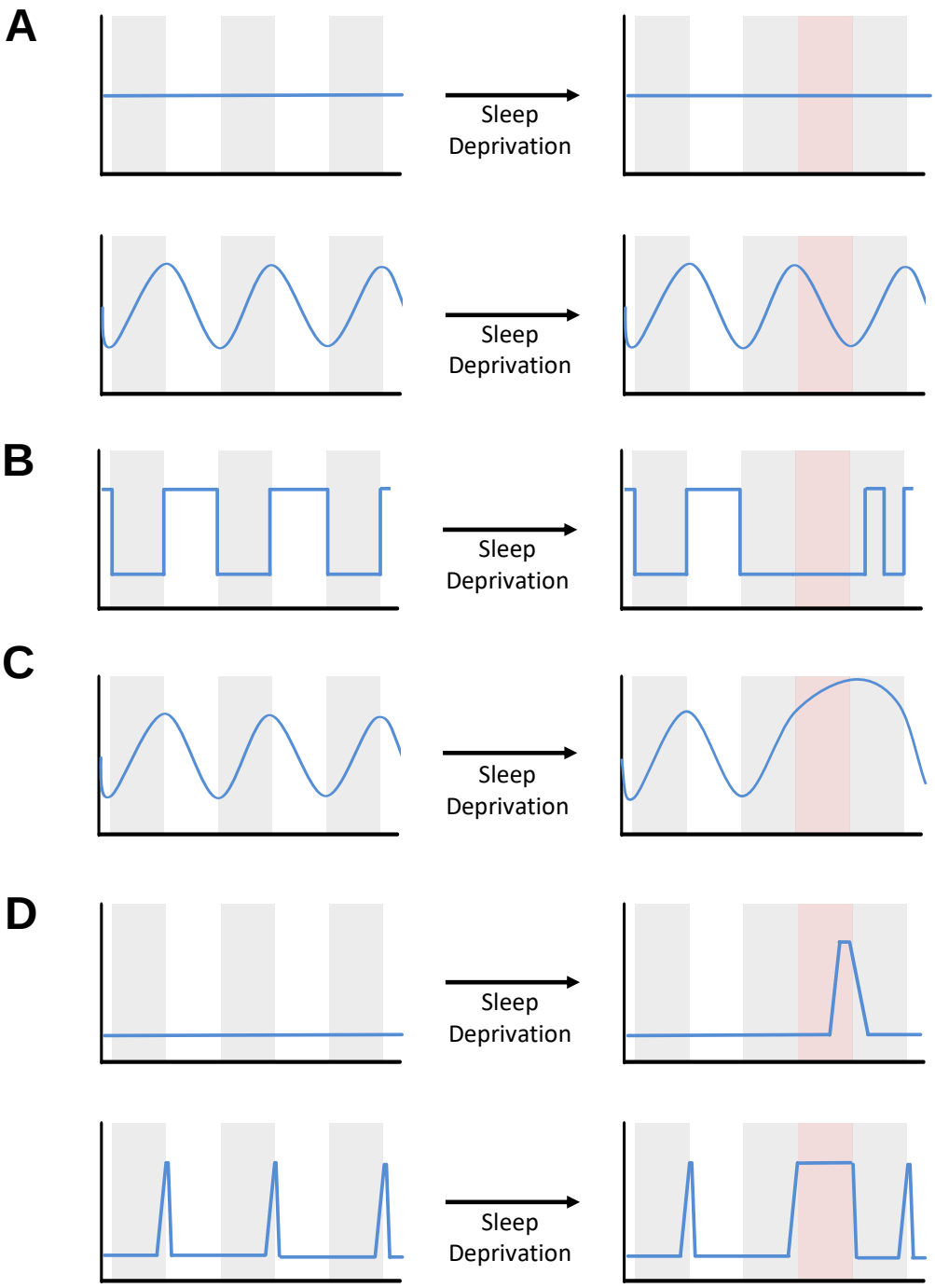

Figure 3.7. Hypothetical Effects of Sleep Deprivation on Molecular Abundance Profiles in Mouse Cortex: We hypothesised that individual molecular abundance profiles would fit into one of four broad and idealised classes. Class A is characterised by molecules with either constant or oscillatory concentration that is unaffected by sleep deprivation. Class B is characterised by molecules that rapidly change their abundance in response to state changes. Class C is characterised by molecules whose concentration is dependent on the proportion of time recently spent awake or asleep. Class D is characterised by molecules whose concentrations rapidly change in response to exceptionally high sleep pressure. The light dark cycle is indicated by the shaded grey bars, whilst sleep deprivation is indicated by the red shaded region.

3.2.4. Transcriptional Profiling of Sleep Deprived Mouse Cortex

To identify to what extent sleep deprivation affects the transcriptomic profile of mouse cortex, we carried out the timecourse described in Section 3.2.3.. 9-10 week old, male, C57/Bl6J mice were pairhoused and subjected to sleep deprivation. Four animals were sacrificed, and the cortex collected every 6 hours for 54 hours. Therefore each group required a total of 40 animals and the whole experiment made use of tissue from a total of 160 animals. Total RNA was collected from the cortex and each replicate was individually subjected to RNA-Seq analysis. Due to the size of the experiment, the samples were interrogated in two separate batches; the first containing the Control and 6 hour SD groups, the second containing the 3 hour and 12 hour SD groups. Following alignment, data were analysed both through the Cufflinks package differential expression function, to compare a treated group at an individual timepoint to the control group at that same timepoint.

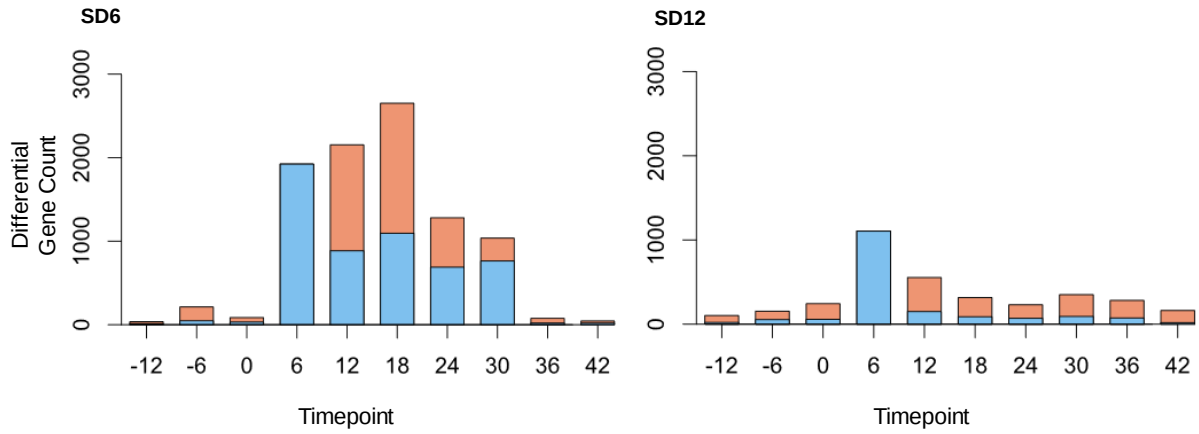

Figure 3.8. Sleep Deprivation Induces changes in the Abundance of Thousands of Genes in Mouse Cortex: RNA from mouse cortex was collected at timepoints separated by 6 hours over the course of 54 hours. Control mice were allowed *ad libitum* sleep, whereas the sleep deprived groups were subjected to 3, 6 or 12-hour sleep deprivation beginning at the onset of the light phase on Day 2. Plotted above are the number of genes differentially expressed between 6-hour sleep deprived and control mice (SD6), and the number of genes differentially expressed between mice subjected to 3 hours and 12 hour sleep deprivation (SD12). The total height of the bar indicates the total number of differentially expressed genes, whilst the blue portion indicates the number of genes differentially expressed at that timepoint that are also differentially expressed in that timecourse after 6 hours sleep deprivation.

Following 6 hours of sleep deprivation, approximately two thousand genes were significantly modulated compared to control mice with uninterrupted sleep. The number of significantly modulated genes remained high for approximately 24 hours following sleep deprivation before returning to baseline levels. Of the 1499 genes that were significantly increased following 6 hours sleep deprivation, there was an enrichment in genes coding for ribosomal proteins, oxidative

phosphorylation, mRNA splicing, GTP binding proteins, the endoplasmic reticulum, nucleosome assembly and cell-cell adherens junctions. Following 6 hours recovery, genes coding for ribosomal proteins remained enriched amongst upregulated genes, as did genes associated with oxidative phosphorylation, nucleosome assembly and cell-cell adherens junctions. Additionally, genes associated with the proteasome complex, translation elongation factors and antioxidant proteins were enriched. Similar gene functions were enriched among upregulated genes following up to 24 hours recovery from sleep deprivation.

Table 7: Gene Classes Upregulated in Mouse Cortex following 6-hour Sleep Deprivation Compared to non-sleep deprived mice sacrificed at the same timepoint.

Timepoint	Functional Cluster	q-value
12:00, Day 2 6 Hour Sleep Deprivation	Ribosomal Proteins	1.0×10^{-39}
	Oxidative Phosphorylation	5.7×10^{-13}
	mRNA Splicing	4.1×10^{-10}
	GTP Binding Proteins	2.5×10^{-2}
	Endoplasmic Reticulum	3.9×10^{-3}
	Nucleosome Assembly	2.0×10^{-2}
	Cell-cell Adherens Junction Genes	3.6×10^{-2}
18:00, Day 2 6 Hour Sleep Deprivation, 6 Hour Recovery	Ribosomal Proteins	2.9×10^{-67}
	Oxidative Phosphorylation	5.1×10^{-36}
	Nucleosome Assembly	1.5×10^{-6}
	Cell-cell Adherens Junction Genes	4.8×10^{-3}
	Proteasome Complex	1.6×10^{-7}
	Translation Elongation Factors	9.8×10^{-4}
	Antioxidant Genes	2.7×10^{-3}
00:00, Day 3 6 Hour Sleep Deprivation, 12 Hour Recovery	Ribosomal Proteins	2.3×10^{-46}
	Oxidative Phosphorylation	2.7×10^{-25}
	Proteasome Complex	3.4×10^{-7}
	Endoplasmic Reticulum	2.1×10^{-5}
	Antioxidant Genes	2.4×10^{-2}

06:00, Day 3 6 Hour Sleep Deprivation, 18 Hour Recovery	Ribosomal Proteins Oxidative Phosphorylation Nucleosome Assembly Proteasome Complex Cell-cell Adherens Junction Genes	$5.5x10^{-57}$ $4.8x10^{-34}$ $1.2x10^{-6}$ $5.8x10^{-3}$ $1.4x10^{-2}$
12:00, Day 3 6 Hour Sleep Deprivation, 24 Hour Recovery	Ribosomal Proteins Oxidative Phosphorylation Nucleosome Assembly Proteasome Complex	$2.9x10^{-47}$ $8.2x10^{-19}$ $3.0x10^{-6}$ $3.3x10^{-2}$

In contrast to upregulated genes, far fewer genes were statistically downregulated following sleep deprivation. 524 genes were significantly downregulated immediately following 6 hour sleep deprivation, but these genes were not statistically enriched in any ontology group following adjustment for multiple testing other than membrane proteins. Following 6 hours recovery from sleep deprivation, 485 genes were significantly reduced compared to mice that had not been sleep deprived, which were enriched in genes relating to ion transport, including calcium ion transport, postsynaptic density genes, and plexin genes. Similar groups were enriched amongst downregulated genes following a total of 12 hours recovery, however there was little functional enrichment amongst downregulated genes following more than 12 hour recovery from sleep deprivation.

Table 8: Gene Classes Downregulated in Mouse Cortex following 6-hour Sleep Deprivation Compared to non-sleep deprived mice sacrificed at the same timepoint.

Timepoint	Functional Cluster	q-value
12:00, Day 2 6 Hour Sleep Deprivation	Membrane Proteins Glycoproteins	$8.0x10^{-6}$ $6.1x10^{-4}$
18:00, Day 2 6 Hour Sleep Deprivation, 6 Hour Recovery	Ion Transport Calcium Transport Postsynaptic Density Plexin Genes	$8.4x10^{-4}$ $4.4x10^{-2}$ $6.3x10^{-5}$ $2.4x10^{-2}$
00:00, Day 3 6 Hour Sleep Deprivation, 12 Hour Recovery	Postsynaptic Density Ion Transport Calcium Transport cAMP Signalling Pathways	$1.0x10^{-9}$ $7.5x10^{-5}$ $1.7x10^{-3}$ $9.5x10^{-3}$

After 6 hours sleep deprivation was found to induce the differential expression of thousands of genes, we repeated the timecourse with mice sleep deprived for 3 or 12 hours to determine to what extent the change in expression of wake related genes was dependent on the duration of sleep deprivation. However, comparison between the two pairs of timecourses identified several thousand genes as differentially expressed at pre-sleep deprivation timepoints, indicating that technical variation between the two batches would hinder comparison of samples between batches. Therefore, for the purposes of differential expression analyses, mice that had been sleep deprived for 12 hours were compared to mice that had been sleep deprived for 3 hours rather than *ab libitum* sleep controls.

Following the first 6 hours of sleep deprivation, compared to mice that had only been sleep deprived for 3 hours (and so had already had 3 hours of recovery sleep opportunity), 402 genes were significantly upregulated in mouse cortex. These genes were enriched in ribosomal protein genes, chaperone genes, dual specificity phosphatases and genes associated with oxidative phosphorylation. Remarkably, fewer genes were significantly increased following 12 hour sleep deprivation, and amongst the 353 genes that were upregulated, there was surprisingly little functional enrichment. Upregulated genes were enriched in genes associated with the extracellular matrix, positive regulation of transcription and developmental proteins. In contrast, genes associated with synapses and neurogenesis were decreased immediately following 6 hours sleep deprivation, whereas glycoprotein genes were downregulated following 12 hour sleep deprivation.

Genes that were significantly upregulated in both pairs of timecourses immediately following sleep deprivation were enriched in genes coding for ribosomal proteins and genes associated with oxidative phosphorylation, whereas genes that were significantly decreased immediately following sleep deprivation were enriched in genes associated with glycoproteins, the postsynaptic membrane and kinases.

Transcriptomic data were also analysed through a custom R script that carries out JTK and ANOVA analyses on the entire timecourse, to identify genes that have circadian and statistically different expression patterns. Following alignment, a total of 17875 transcripts were identified as being expressed in the cortex, on the basis of having an average abundance greater than 0.5 FPKM and being detectable in every sample. The expression of 16% (2914) of these expressed transcripts was identified through JTK analysis as rhythmic with a period of 24 hours in animals not subjected to any sleep deprivation. It is noteworthy that genes cycling with a 24-hour rhythm cannot firmly be identified as circadian on the basis of this experiment, due to the 12:12 light dark cycle imposed on these animals. Strictly, circadian genes are those that show oscillations in abundance even in the absence of

environmental cues. With this experimental design, it is impossible to determine whether a given gene is “anticipating” or “responding to” the environment.

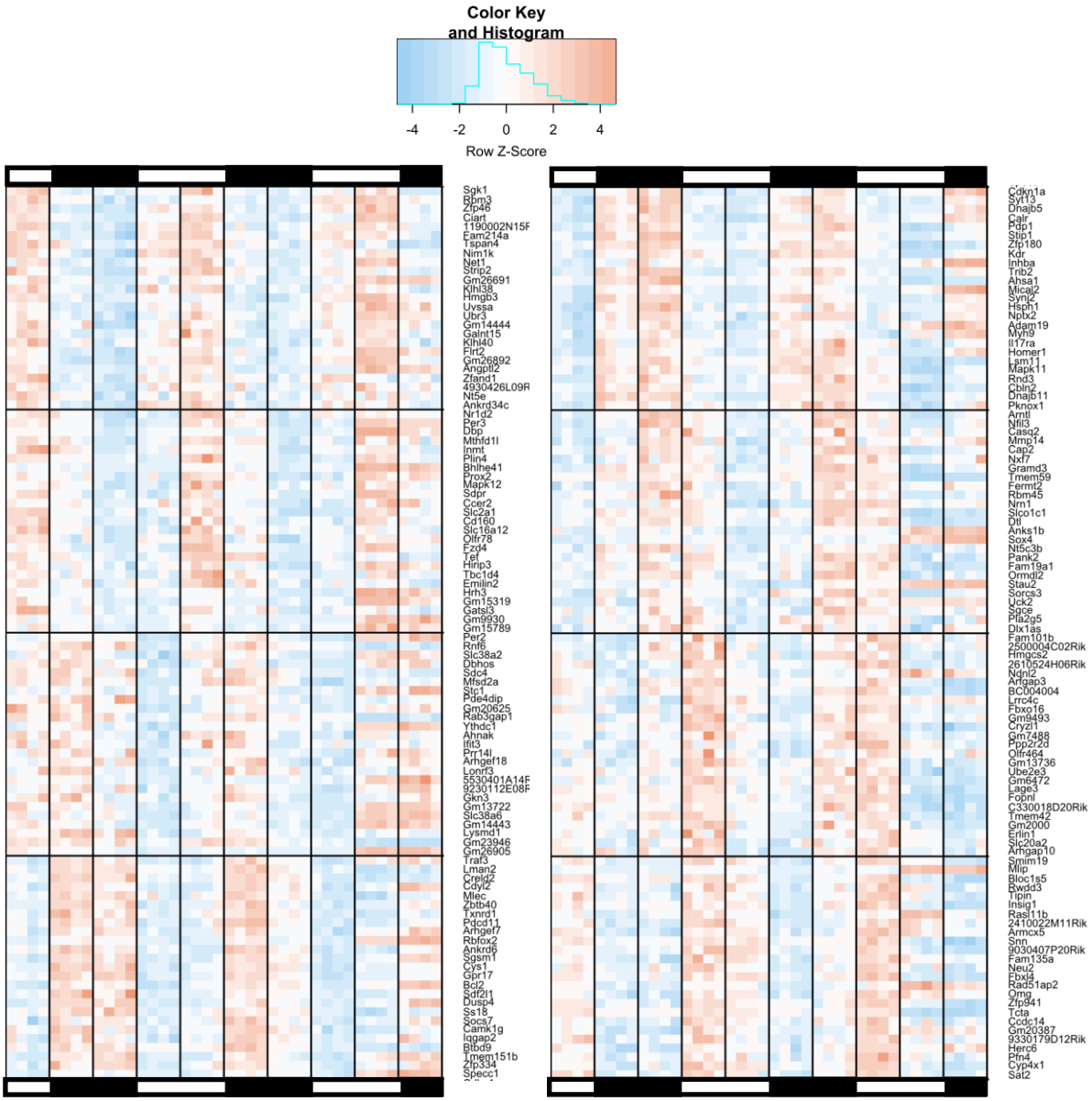

Figure 3.9. 16% of Expressed Cortical Transcripts in non-Sleep Deprived Mice Exhibited Significant 24 hour Oscillations during the Timecourse: RNA collected from individual biological replicates was subjected to RNA-Seq analyses. Genes with 24 hour cycles of expression were identified using JTK analysis. The expression of 25 genes from each of the 8 identified phases (timing of peak) are plotted, with red cells representing high expression and blue cells representing low expression.

Genes identified as rhythmic were enriched in genes associated with a broad array of processes, including Biological Rhythms, the regulation of transcription, Synapses, DNA damage, Kinases, the ER, Chaperones, Ubiquitin conjugation and AMPK signalling. 38% (1120) of rhythmic genes were identified as peaking within 3 hours of the end of the dark phase, and were enriched in genes related to

chaperone function, synapses, and biological rhythms. In contrast, genes that peak at the end of the light phase were enriched in genes relating DNA damage repair and ubiquitin conjugation.

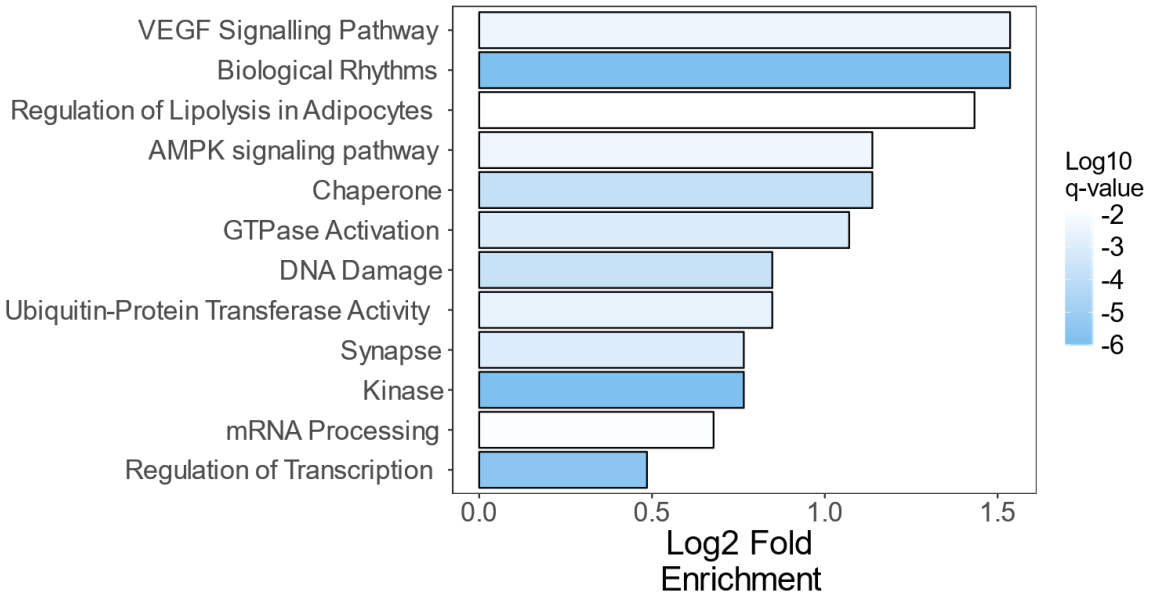

Figure 3.10. Enriched Gene Classes amongst Diurnal Genes: Genes whose expression in mouse cortex oscillated with a 24-hour rhythm were subjected to functional annotation, and enriched gene classes displayed above. The enrichment of genes is indicated by the width of each bar, whilst the q-value is indicated by the colour of the bar.

To identify which genes are affected by sleep deprivation, we carried out ANOVA analyses followed by FDR based correction for multiple testing to determine the genes whose abundance show an interaction between time and sleep deprivation duration. Of the 2914 genes oscillating with a 24 hour rhythm in control mice, 505 genes (17%) exhibited a significantly different pattern of expression in both mice that had been sleep deprived for 6 and 12 hours. These genes were enriched in genes relating to synapses, including cholinergic synapses, protein processing in the endoplasmic reticulum, biological rhythms and chaperone functions. Of these 505 genes, 176 also demonstrated a significantly different expression pattern between mice subjected to 3 hour or 12 hour sleep deprivation. These genes were enriched in synapse proteins.

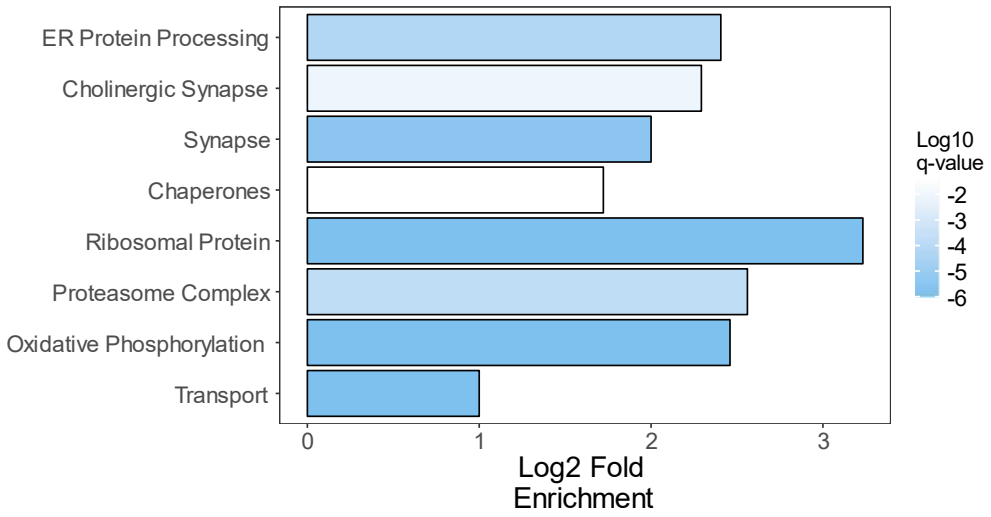

Figure 3.11. Enriched Gene Classes amongst Sleep Deprivation Dependent Genes: Genes whose expression profile in mouse cortex was modulated by sleep deprivation were subjected to functional annotation, and enriched gene classes displayed above. The enrichment of genes is indicated by the width of each bar, whilst the q-value is indicated by the colour of the bar.

In contrast, only 5% of non-circadian genes (790 genes) showed a significantly different pattern between control mice and both mice that had been sleep deprived for 6 or 12 hours. The functional classes enriched amongst these genes were ribosomal proteins, transport, oxidative phosphorylation, the proteasome complex and glycolysis. Of these, only 6% (47 genes) showed a significantly different expression pattern between mice subjected to 3 hour or 12 hour sleep deprivation.

To determine which genes show a homeostatic gene profile (see Fig 3.7.C.) genes were filtered to identify those which were rhythmic and peaked at the end of the dark (active) phase in control mice, showed a consistently significantly different expression profile, and whose abundance remained elevated during 6 and 12 hour sleep deprivation. 17 genes were identified whose expression matched this homeostatic profile, and a further 3 genes matched the reverse pattern (i.e. have their minimum daily expression at the onset of the rest phase and remain suppressed during sleep deprivation).

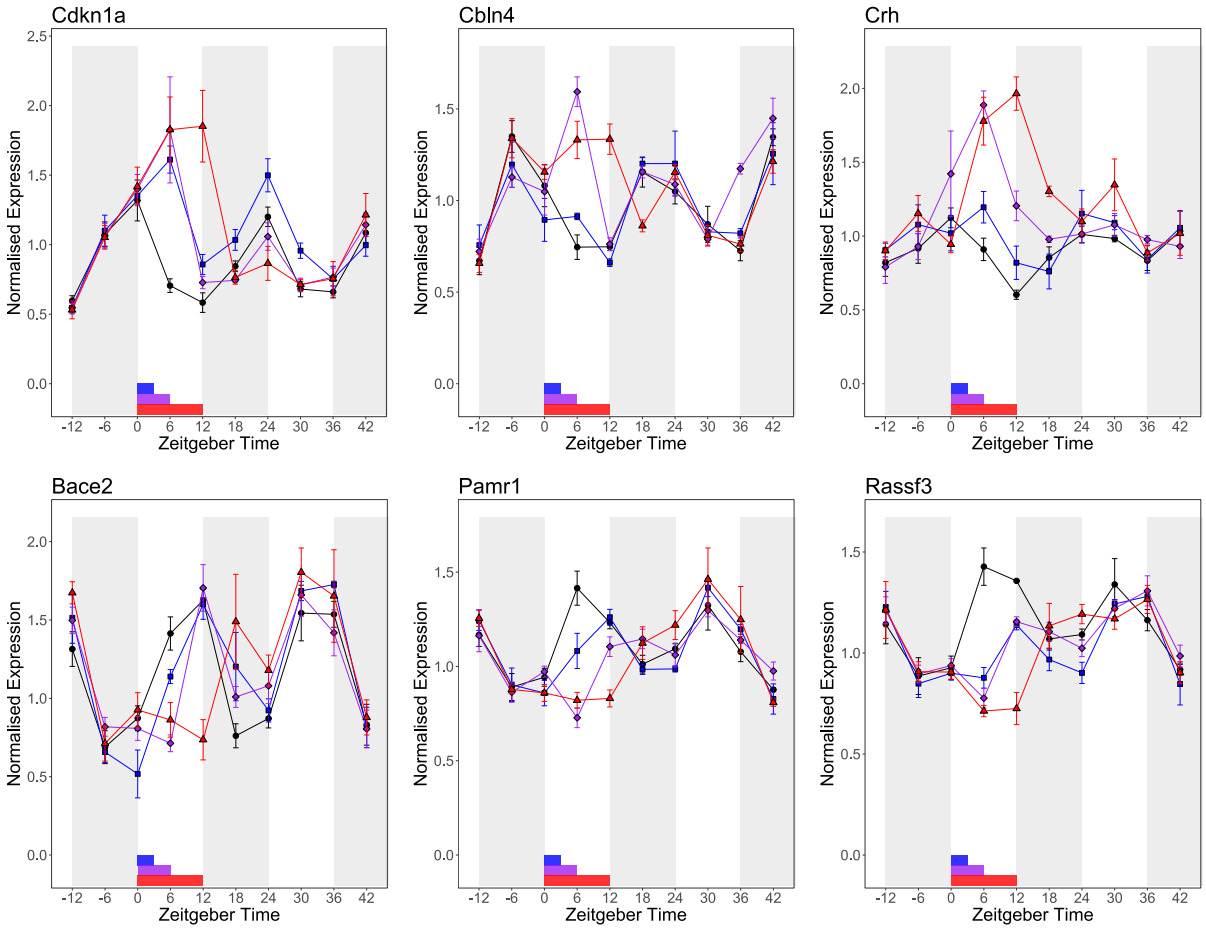

Figure 3.12. 17 Genes Matching the Hypothetical Homeostatic Profile were Identified: The expression profiles of genes were filtered to identify rhythmic genes that peaked at the end of the active phase and remained elevated during sleep deprivation but not during sleep, or showing the opposite pattern. Plotted on the same axes is the expression data from individual timecourses, normalised to the average of the first 3 (pre-treatment) timepoints, with error bars indicating SEM. The black line represents expression data from mice with uninterrupted sleep, whilst the blue, purple and red lines represent the data from mice subjected to 3, 6 and 12-hour sleep deprivation, respectively. The vertical grey bars indicate the timing of the dark phase, whereas the horizontal blue, purple and red bars situated between Zeitgeber time 0-12 represents the duration of 3, 6 and 12- hour sleep deprivation, respectively.

To identify genes that may match the stress gene profile, genes were filtered to identify those which were not rhythmic in control mice, or were rhythmic but whose peaks were not synchronised with the onset of the rest phase, but nevertheless showed a consistently elevated expression during sleep deprivation. A total of 15 genes were identified, made up of 10 genes which were identified as exhibiting rhythmic oscillations and 5 genes that did not exhibit oscillations in control mice.

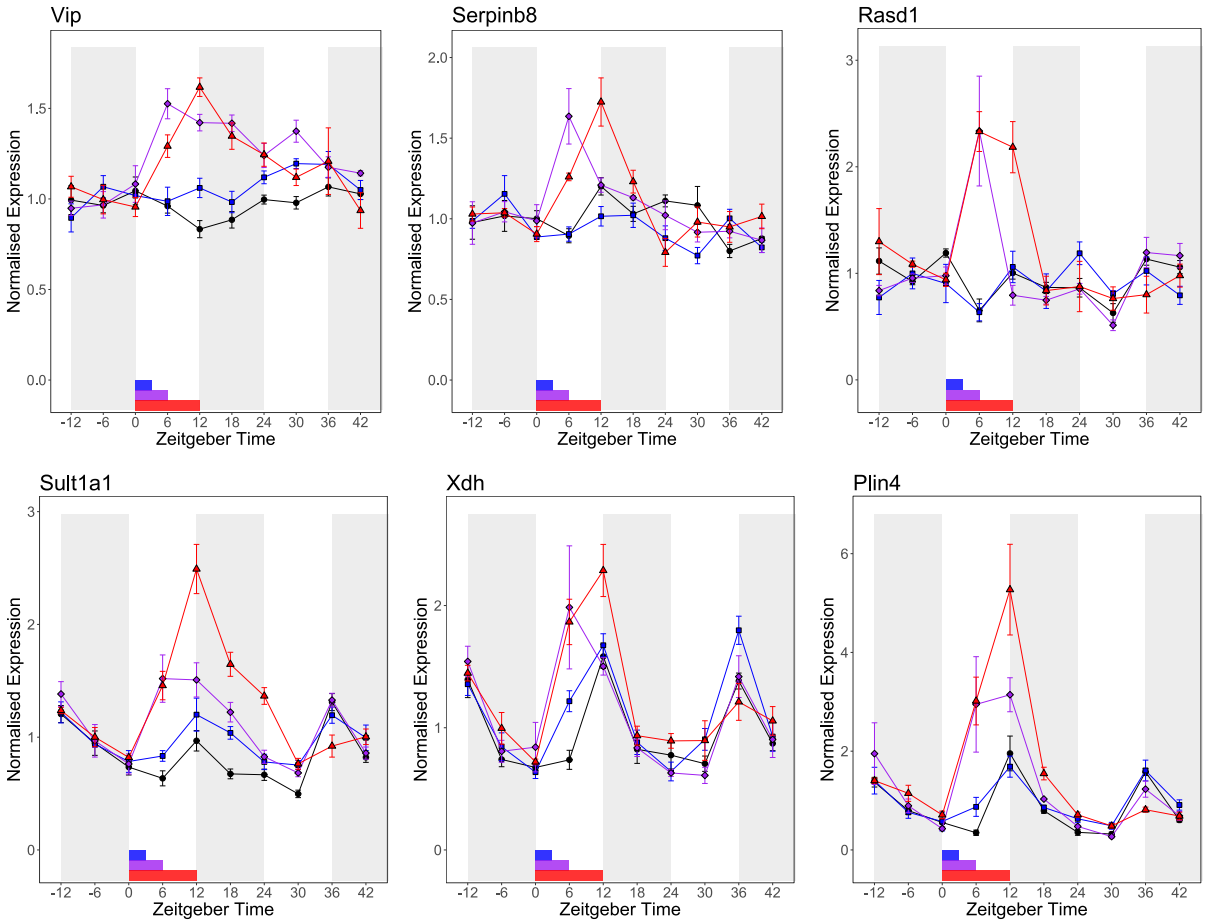

Figure 3.12. 15 Genes Matching the Hypothetical Stress Gene Profile were Identified: The expression profiles of genes were filtered to identify genes that were elevated during sleep deprivation, but whose expression is not synced to the sleep-wake cycle in control animals. Plotted on the same axes is the expression data from individual timecourses, normalised to the average of the first 3 (pre-treatment) timepoints, with error bars indicating SEM. The black line represents expression data from mice with uninterrupted sleep, whilst the blue, purple and red lines represent the data from mice subjected to 3, 6 and 12-hour sleep deprivation, respectively. The vertical grey bars indicate the timing of the dark phase, whereas the horizontal blue, purple and red bars situated between Zeitgeber time 0-12 represents the duration of 3, 6 and 12- hour sleep deprivation, respectively.

RNA-sequencing data can also be used to estimate the abundance of a specific isoform of a gene, rather than the sum abundance of all the isoforms of that gene. Splice variants of the same gene can have dramatically different functions and expression patterns. For example, the isoform Homer1a competes for binding partners with full length scaffold protein Homer1, and so acts to uncouple excitatory signalling in neurones. In line with previous studies, we found that the expression of Homer1a, but not the total expression of all isoforms of Homer1, was significantly upregulated following 12-hour sleep deprivation.

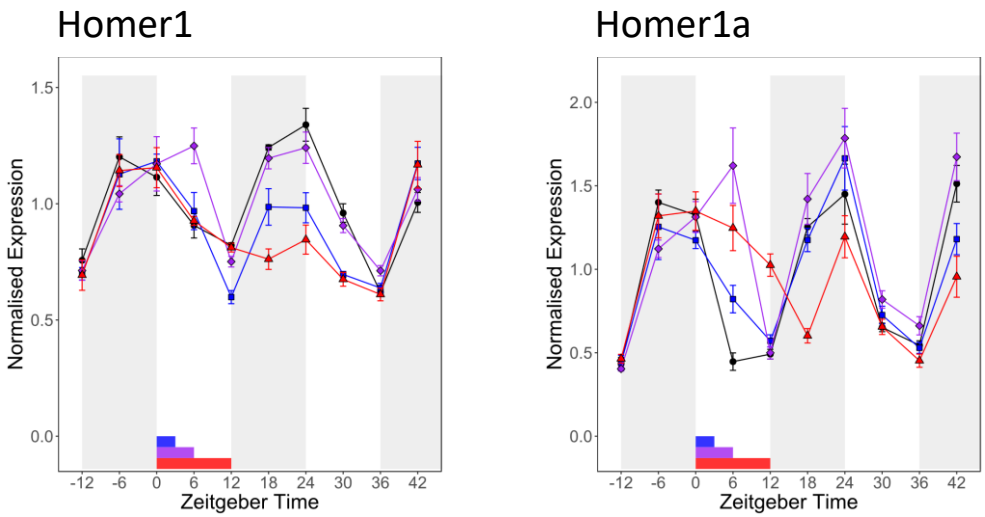

Figure 3.13. Homer1a demonstrates a different Expression Pattern to the total Homer1 in Response to Sleep Deprivation: The expression profiles of Homer1 and Homer1a are plotted to demonstrate how isoform expression can vary from whole gene expression.

The output from Cuffdiff based quantification of isoform expression, which only considers genes with at least two known isoforms, revealed that rhythmically expressed isoforms were enriched in transcripts relating to biological rhythms, mRNA processing, the regulation of transcription, Synapses, ubiquitin conjugation, the cell cycle and lipid biosynthesis. Isoforms peaking at the end of the dark phase were enriched in transcripts relating to synapses, unfolded protein binding and biological rhythms, whilst transcripts peaking at the end of the light phase were enriched in transcripts relating to mRNA processing, transcription regulation, DNA replication and lipid metabolism. 426 of these circadian isoforms had statistically different expression profiles following 6 and 12 hour sleep deprivation, compared to undisturbed mice, which were enriched in transcripts relating to chaperones, synapses, biological rhythms. Of these, 171 genes also showed a different expression pattern between mice subjected to 3 and 12 hour sleep deprivation, which were enriched in transcripts relating to kinases and synapses. A further 84 non-rhythmic isoforms were identified as exhibiting a dose dependent change in expression profile in response to sleep deprivation, which were enriched in transcripts relating to the cytosolic large ribosomal subunit and mitochondrial function.

To determine which genes show a homeostatic gene profile, isoforms were filtered to identify those which were rhythmic and peaked at the end of the dark (active) phase in control mice, showed a consistently significantly different expression profile, and whose abundance remained elevated during 6 and 12 hour sleep deprivation. 17 transcripts were identified whose expression matched this homeostatic profile, and a further 4 transcripts matched the reverse pattern. Isoform analysis identified some homeostatic isoforms that were previously identified at the whole gene level, but

also identified isoforms of Homer1, Wisp1, Mical2, Ezr, Pdzd2, Syne1 and Rasgef1b as exhibiting homeostatic expression profiles.

A total of 21 transcripts were identified that matched the stress gene profile, made up of 12 transcripts which were identified as exhibiting rhythmic oscillations and 9 transcripts that did not exhibit oscillations in control mice. Again, there was significant overlap with stress genes identified at the whole gene level, but also include Hif3a, Sgk1 and Fkbp5.

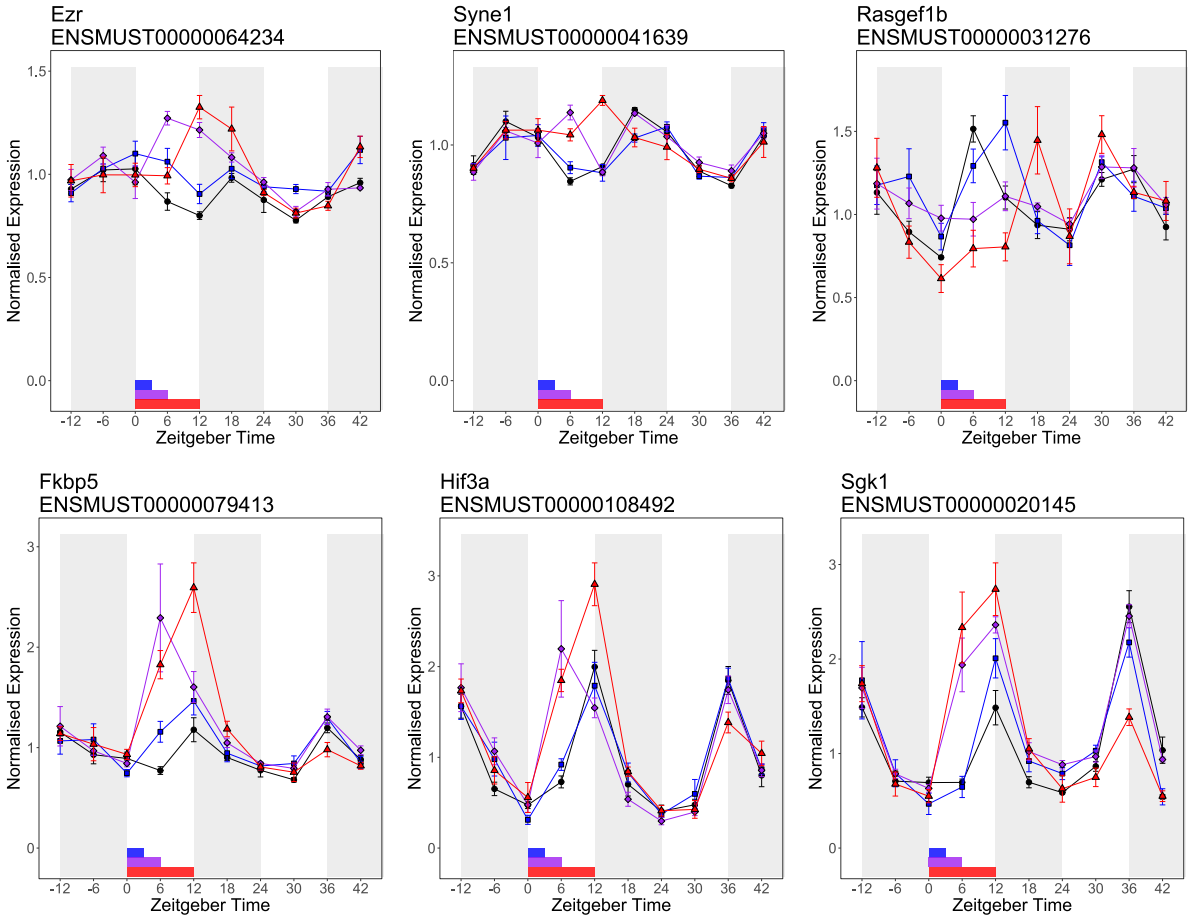

Figure 3.14. 17 Isoforms Matching the Hypothetical Homeostatic Profile and 21 Matching the Stress Profile were Identified: The expression profiles of isoforms were filtered to identify homeostatic and stress expression profile isoforms, as outlined above. Plotted on the same axes is the expression data from individual timecourses, normalised to the average of the first 3 (pre-treatment) timepoints, with error bars indicating SEM. The black line represents expression data from mice with uninterrupted sleep, whilst the blue, purple and red lines represent the data from mice subjected to 3, 6 and 12-hour sleep deprivation, respectively. The vertical grey bars indicate the timing of the dark phase, whereas the horizontal blue, purple and red bars situated between Zeitgeber time 0-12 represents the duration of 3, 6 and 12- hour sleep deprivation, respectively

3.3.1. Comparison to Previous Studies

The transcriptomic effects of sleep deprivation have previously been examined using microarray technology in rats (Cirelli *et al.* 2004), mice (Mackiewicz *et al.* 2007; Maret *et al.* 2007), sparrows (Jones *et al.* 2008), fish (Sigurgeirsson *et al.* 2013) and flies (Cirelli *et al.* 2005; Zimmerman *et al.* 2006). This work is the first large scale sequencing-based profiling of sleep deprived mammalian cortex that we are aware of. Because of the timecourse style experimental design and biological replication, we have been able to carry out statistical tests not only comparing individual timepoints, but the expression profile as a whole. Previous studies have implicated a broad range of genes as being subject to regulation by wakefulness, and several studies have concluded that wake modulated genes fall into one of three broad functional groups: response to cellular stress, synaptic plasticity, and metabolism (Mackiewicz *et al.* 2009). To what extent do the data presented here overlap with previously published data?

3.3.2. Heatshock proteins

Previous studies have repeatedly identified the induction of heatshock proteins and genes involved in the unfolded protein response as a molecular correlate of sleep deprivation across several species. Although body temperature is elevated during wakefulness, the induction of heat shock proteins through cellular stress pathways is thought to represent a mechanism by which protein synthesis is reduced during prolonged wakefulness. A previous microarray study in mice identified 8 heatshock genes as being upregulated during sleep deprivation (Mackiewicz *et al.* 2007). Of the 7 detected in this study (Hsp105 did not reach the expression threshold to be considered for analysis), 3 had significantly different expression profiles following 6 hour sleep deprivation compared to non-sleep deprived mice, whilst Hspa5 trended toward significance. Consistent with these genes performing a function during spontaneous wakefulness, rather than only being induced during particularly high homeostatic sleep pressure, all 7 genes exhibited 24-hour rhythms in expression in control animals.

Table 9: Previously Implicated Chaperone Gene Expression Data

Gene	Rhythmic q-value	Fold Change 6hr SD	Fold Change 12hr SD	SD6 ANOVA q-value
Dnajb11	1.72×10^{-4}	1.24 *	1.08	7.21×10^{-3}
Dnajb5	7.80×10^{-6}	1.16	1.24	3.50×10^{-1}
Dnajc1	1.16×10^{-2}	1.22	1.19	2.97×10^{-3}
Dnajc3	5.24×10^{-4}	1.46 *	1.1	1.22×10^{-3}
Hspa1a	1.16×10^{-2}	1.21	0.99	1.18×10^{-1}
Hspa1b	1.06×10^{-2}	1.96*	1.09	1.42×10^{-1}
Hspa5	1.27×10^{-3}	1.55 *	1.28 *	6.45×10^{-2}

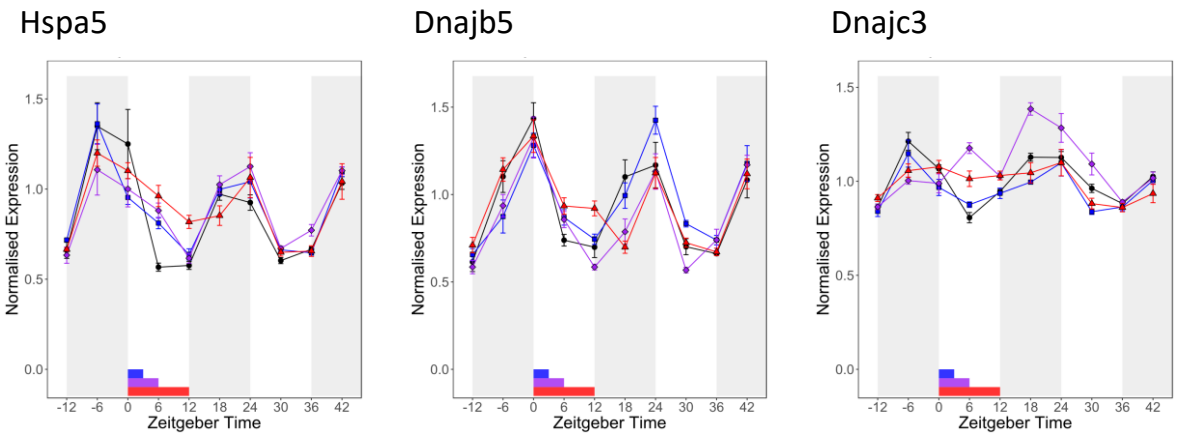

Figure 3.15. Chaperone Genes are Induced by both Spontaneous and Enforced Wakefulness: The cortex expression of chaperone genes previously identified as dependent on the wake state of the animal was found to be dependent on both time of day in control animals and duration of sleep deprivation. The table outlines the JTK derived q-value for rhythmic gene expression in control mice, the fold change in expression immediately following 6 hour and 12 hour sleep deprivation (compared to control animals and mice subjected to only 3 hour sleep deprivation, respectively), and the q-value comparing the expression profile of 6 hour sleep deprived mice to control mice. The asterisks in the fold change columns denote whether cuffdiff identified that comparison as significantly different (i.e. q-value < 0.05). The expression of individual genes are plotted in the graphs, where the grey bars indicate the light-dark cycle, whilst the blue, purple and red bars and lines indicate the timing and expression of 3-, 6-, and 12-hour sleep deprived mice, respectively. The expression of control animals is plotted in black.

Several other chaperones and mediators of the unfolded protein response were implicated in our transcriptomic screen. Therefore the data presented in this chapter supports the role of chaperone proteins in both the regulation of spontaneous and prolonged wakefulness.

Table 10: Further Chaperone Gene Expression Linked to Wakefulness

Gene	Rhythmic q-value	Fold Change 6hr SD	Fold Change 12hr SD	SD6 ANOVA q-value
Atf6	$5.85x10^{-1}$	1.35 *	1.14	$4.77x10^{-2}$
Calr	$1.57x10^{-5}$	1.22	1.18	$1.65x10^{-3}$
Chordc1	$4.83x10^{-3}$	1.8 *	1.22 *	$7.18x10^{-5}$
Derl1	$8.68x10^{-2}$	1.24 *	1.03	$4.32x10^{-2}$
Hsp90aa1	$1.34x10^{-1}$	1.35 *	0.99	$4.74x10^{-3}$
Hsp90b1	$3.14x10^{-4}$	1.39 *	1.09	$9.45x10^{-4}$
Hspd1	$3.70x10^{-2}$	1.39 *	1.08	$2.03x10^{-3}$
Pdcl	$3.70x10^{-2}$	1.21	1.2	$1.18x10^{-3}$
Pdia6	$2.06x10^{-3}$	1.22 *	1.14	$2.04x10^{-2}$
Stt3b	$1.45x10^{-3}$	1.25 *	1.14	$1.13x10^{-3}$
Yod1	1	1.49 *	0.99	$3.90x10^{-3}$

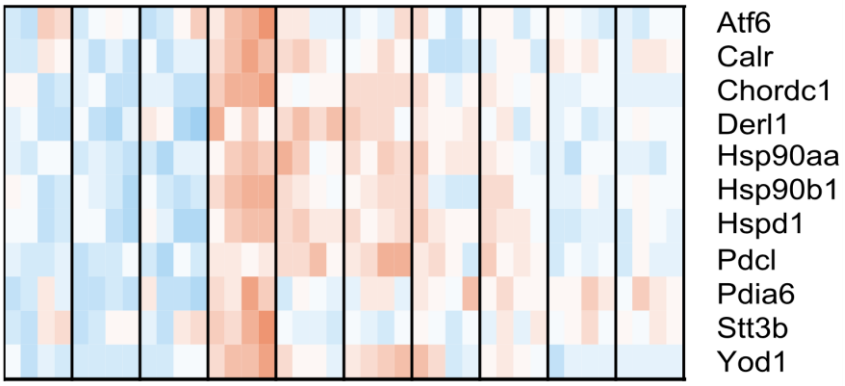

Figure 3.16. Further Chaperone Genes are Induced by both Spontaneous and Enforced Wakefulness: The cortex expression of other chaperone genes were identified as dependent on the wake state of the animal. The table outlines the JTK derived q-value for rhythmic gene expression in control mice, the fold change in expression immediately following 6 hour and 12 hour sleep deprivation (compared to control animals and mice subjected to only 3 hour sleep deprivation, respectively), and the q-value comparing the expression profile of 6 hour sleep deprived mice to control mice. The asterisks in the fold change columns denote whether cuffdiff identified that comparison as significantly different (i.e. q-value < 0.05). The heatmap indicates the z-score normalised expression of individual genes in the cortex of mice subjected to 6 hour sleep deprivation, compared to undisturbed mice at the same timepoint, where blue indicates low expression and red indicates elevated expression.

3.3.3. Cholesterol Synthesis

A microarray study published by Mackiewicz et al concluded that a key function of sleep is the biosynthesis of lipids, and identified the transcription of the majority of the cholesterol biosynthetic enzymes as sleep dependent (Mackiewicz *et al.* 2007). The authors hypothesised that cholesterol biosynthesis and uptake may play an important role in membrane homeostasis and promote the formation of lipid rafts at synapses during sleep. It is worth remarking here that that study was more powerful than previous studies, and so was able to statistically identify smaller magnitude changes in gene expression. Indeed, the authors found that the expression of many of the cholesterol biosynthetic genes was statistically downregulated by approximately 25% or less following 12 hour sleep deprivation, significantly lower than the magnitude of changes reported in immediate early genes and other gene classes. However, a later study found that cholesterol biosynthetic genes were no longer affected by sleep deprivation following adrenalectomy, indicating that their expression is under regulation by glucocorticoid signalling (Mongrain *et al.* 2010).

Our data suggests that although some cholesterol metabolising genes are affected by sleep deprivation, the expression of the pathway is not tightly linked to either the time of day or the state of wakefulness of the animal. Genes involved in general cholesterol metabolism, but not synthesis, trended toward being enriched amongst transcripts identified as oscillating with 24-hour rhythms

(q-value = 0.08 and 0.37, respectively), whilst cholesterol biosynthetic genes were not statistically overrepresented amongst genes identified as being downregulated by either 6 or 12-hour sleep deprivation. Of the 10 cholesterol biosynthesis genes identified as upregulated during sleep by Mackiewicz, we found a total of 4 were significantly downregulated immediately following either 6 or 12-hour sleep deprivation (Dhcr24, Dhcr7, Hmgcs1, Mvk), whilst the expression profile of 1 enzyme (Fdps) was statistically different following 6 hours sleep deprivation. None of these genes demonstrated rhythmic expression in control animals, which is unexpected for genes postulated to perform a key function of sleep. In the context of the modest sized changes induced by 6 and 12-hour sleep deprivation, it may be the case that the expression is indeed rhythmic, but sufficiently low amplitude to not be detected in our study. Therefore, although cholesterol biosynthesis being linked to the rest phase is an attractive conclusion that is consistent with the theoretical anabolic and membrane homeostasis roles of sleep, the transcriptomic data obtained in this work does not support cholesterol synthesis as a core function of sleep.

Table 11: Gene Expression of Genes in Cholesterol Metabolising Pathway

Gene	Rhythmic q-value	Fold Change 6hr SD	Fold Change 12hr SD	SD6 ANOVA q-value
Dhcr24	1	0.79 *	0.74 *	$5.97x10^{-2}$
Dhcr7	1	0.66 *	0.77	$1.32x10^{-1}$
Fdft1	1	1.06	0.93	$1.04x10^{-1}$
Fdps	$8.89x10^{-1}$	1.21	0.73	$2.09x10^{-2}$
Hmgcr	$7.79x10^{-1}$	1	0.97	$6.80x10^{-1}$
Hmgcs1	$8.89x10^{-1}$	1.12	0.83 *	$3.49x10^{-1}$
Lss	$7.54x10^{-2}$	0.72	0.94	$5.62x10^{-1}$
Mvd	1	0.76	0.57	$7.37x10^{-2}$
Mvk	1	0.86	0.73 *	$3.03x10^{-1}$
Nsdhl	$3.08x10^{-1}$	0.81	0.86	$3.14x10^{-1}$

Figure 3.17. Some Cholesterol Genes are Modulated by Sleep Deprivation, but none are Rhythmic in Undisturbed Mice: A previous study indicated that the expression of several cholesterol biosynthetic genes are downregulated in mouse cortex by sleep deprivation. This table presents data from this screen for the genes previously identified as repressed during sleep deprivation. The table outlines the JTK derived q-value for rhythmic gene expression in control mice, the fold change in expression immediately following 6 hour and 12 hour sleep deprivation (compared to control animals and mice subjected to only 3 hour sleep deprivation, respectively), and the q-value comparing the expression profile of 6 hour sleep deprived mice to control mice. The asterisks in the fold change columns denote whether that comparison was significantly different (i.e. q-value < 0.05).

3.3.4. Circadian Genes

Biological rhythms play a large role in determining both the duration and timing of sleep, with core circadian genes implicated in influencing both Process C and Process S of the Two Process Model proposed by Borbély. The interplay between circadian rhythms and the sleep wake cycle is further complicated by the presence of both local cellular clocks and a central pacemaker (the SCN), whilst experimental sleep deprivation in mice disrupts several behavioural patterns, by the introduction of stress, modulated neuronal excitability, and increased opportunity for eating, drinking and social behaviour. Since sleep deprivation induces recovery sleep during the subsequent habitual active phase, further disrupting the typical behaviour of the animal, it has previously been proposed that sleep deprivation may perturb circadian rhythms (Challet *et al.* 2001; Deboer *et al.* 2003). Indeed, expression of core clock components has previously been linked to sleep deprivation, whereas the DNA binding activity of core clock components CLOCK, Arntl and NPAS2 is reduced following sleep deprivation (Mongrain *et al.* 2011), suggesting that the expression of a considerable proportion of rhythmic transcripts is affected by sleep deprivation.

Immediately following sleep deprivation, expression changes in core clock genes were relatively modest, with a significant increase in CLOCK and Npas2, and decrease of Dbp expression being identified. Similarly, the expression profile of only a handful of core clock genes is significantly different following 6 hours of sleep deprivation, indicating that short term sleep deprivation induced disruption to the canonical transcription based molecular clock in the cortex may overall only be slight. However, during the recovery phase from 12-hour sleep deprivation, the expression of core clock genes such as Arntl, Clock and Dbp remains perturbed for 24 hours following cessation of sleep deprivation, suggesting that longer term sleep deprivation and the subsequent recovery sleep may greatly disrupt rhythmic gene expression.

Table 12: Gene Expression of Clock Machinery Genes

Gene	Rhythmic q-value	Fold Change 6hr SD	Fold Change 12hr SD	SD6 ANOVA q-value
Arntl	1.08×10^{-6}	1.08	1.18	4.34×10^{-1}
Clock	8.08×10^{-2}	1.30 *	1.22	4.79×10^{-2}
Cry1	9.52×10^{-5}	1.07	1.02	6.86×10^{-2}
Cry2	2.63×10^{-2}	0.84	1.01	1.02×10^{-1}
Dbp	1.28×10^{-5}	0.69 *	1.03	2.55×10^{-2}
Npas2	7.93×10^{-3}	0.91	1.38 *	2.52×10^{-1}
Nr1d1	5.83×10^{-3}	0.75	0.92	2.83×10^{-1}
Nr1d2	5.69×10^{-6}	1.16	0.97	9.42×10^{-3}
Per2	2.17×10^{-5}	1.29	1.21	1.60×10^{-2}
Per3	8.15×10^{-6}	0.94	1.10	7.63×10^{-2}

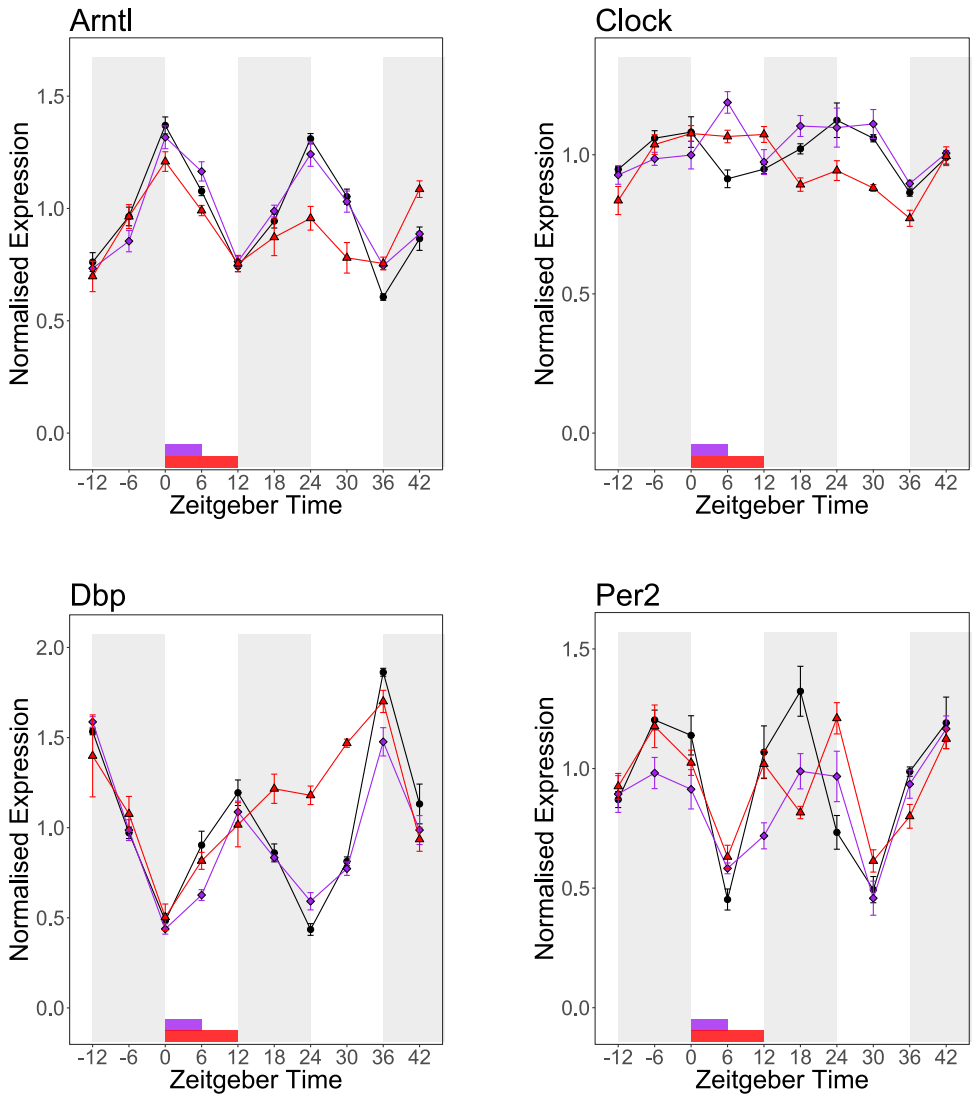

Figure 3.18. The Expression of Clock Genes is only Modestly Affected during Sleep Deprivation, but Severely Perturbed during Recovery from 12 hour Sleep Deprivation: Previous studies have indicated clock genes as involved in the response to sleep deprivation in mouse cortex. This table presents data from this screen for the a subset of core clock genes. The table outlines the JTK derived q-value for rhythmic gene expression in control mice, the fold change in expression immediately following 6 hour and 12 hour sleep deprivation (compared to control animals and mice subjected to only 3 hour sleep deprivation, respectively), and the q-value comparing the expression profile of 6 hour sleep deprived mice to control mice. The asterisks in the fold change columns denote whether that comparison was significantly different (i.e. q-value < 0.05). The expression of individual genes are plotted in the graphs, where the grey bars indicate the light-dark cycle, whilst the purple and red bars and lines indicate the timing and expression of 6-, and 12-hour sleep deprived mice, respectively. The expression of control animals is plotted in black.

Indeed, transcriptome wide analysis reveals that increasing durations of sleep deprivation progressively dampen rhythmic transcript expression in the cortex. Whereas 2917 genes were identified as rhythmic in animals with unperturbed sleep, 1248 (43%) transcripts were rhythmic following 3-hour sleep deprivation and 769 (26%) following 6 hour sleep deprivation. Remarkably, following 12 hour sleep deprivation only 63 genes (2%) were still identified as rhythmic. The dramatic reduction in rhythmic transcript number may indicate that sampling every 6 hours results in a study that is underpowered to find rhythmic transcripts following small perturbations in expression, rather than a complete ablation of the clock. However, the near absence of rhythmic transcripts following 12 hour sleep deprivation appears to indicate that almost every gene whose expression habitually oscillates with a 24 hour rhythm in the cortex is subject to modulation by the sleep wake cycle. There are several possible molecular mechanisms through which the expression of individual rhythmic genes could be disrupted, including through altered homeostatic sleep pressure, resetting of the molecular clock and altered glucocorticoid rhythms. Based on the data in this thesis, it is difficult to conclude which mechanism is responsible for specific gene perturbations, however on the basis of expression patterns following progressively increasing durations of sleep deprivation, it is possible to speculate and to identify possible candidates.

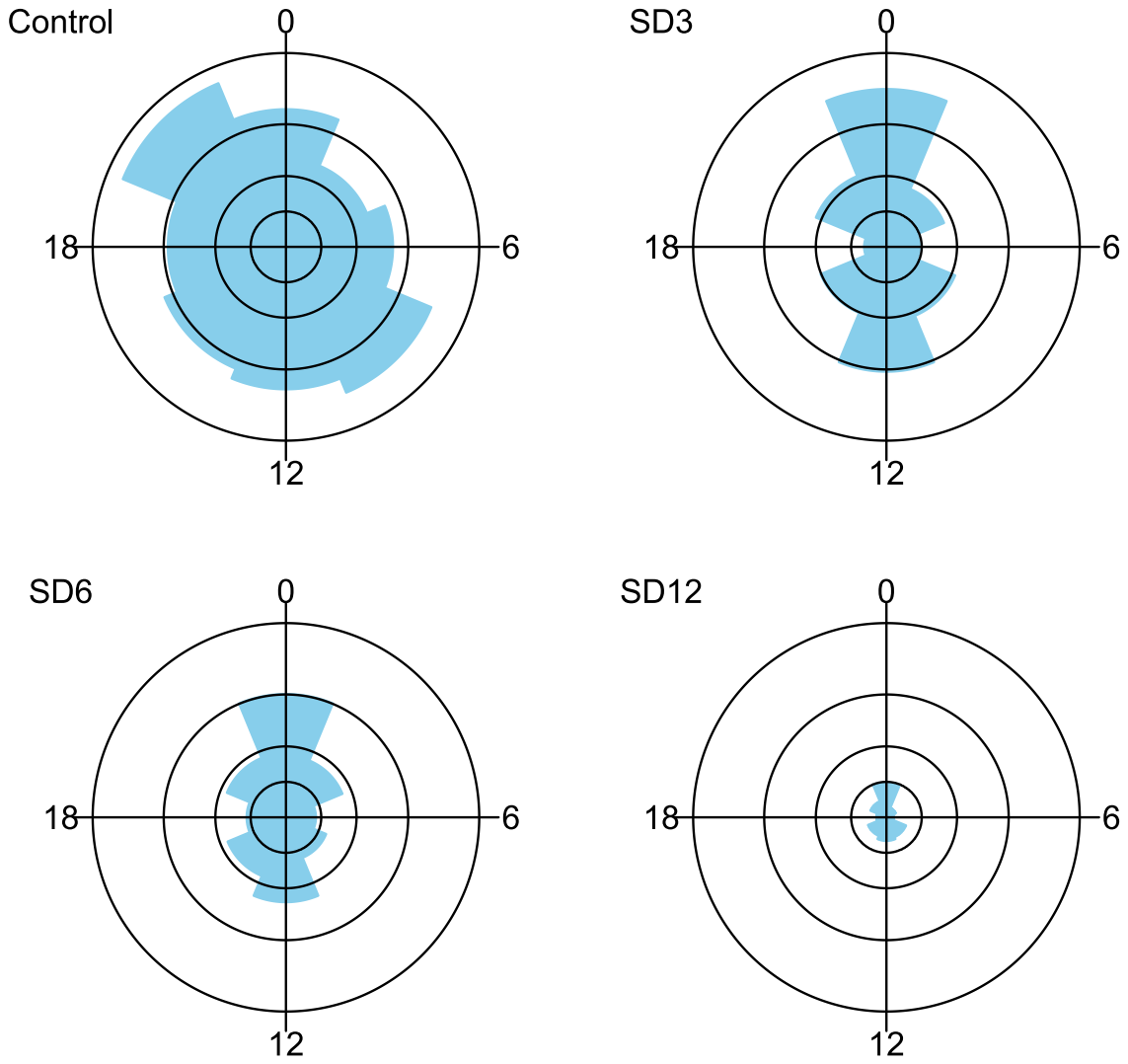

Figure 3.19. The Number of Rhythmic Transcripts in Mouse Cortex is Progressively Reduced by Increasing Duration of Sleep Deprivation: The number of rhythmic transcripts in each dataset identified by JTK analysis is indicated by the area of blue, whilst the Zeitgeber time of day that those transcripts peak is indicated by the angle from the centre (where 0 is the onset of the light phase and 12 is the onset of the dark phase). The black concentric circles are guides that indicate the total number of genes present. The total area of the circles, from inner to outer, represents 200, 800, 2400,4000 and 6000 genes. Since segments are binned into 3-hour phase intervals, a segment touching the inner circle will therefore contain 25 genes, whilst a segment touching the outermost circle will contain 750 genes.

3.3.5. Homeostatic Profile Genes

Our hypothesis before this experiment was that there is a subgroup of sleep dependent molecules that exhibit a "homeostatic profile", the abundance of which would be related to the homeostatic sleep pressure the animal was experiencing. To identify homeostatic candidates, we searched for genes demonstrating increasing abundance during the active phase and declining abundance during the rest phase in control animals, but an increased abundance following sleep deprivation in a dose dependent manner. When we applied these filters to our dataset, we found several genes previously implicated in sleep homeostasis met those criteria, and some that matched the reverse profile.

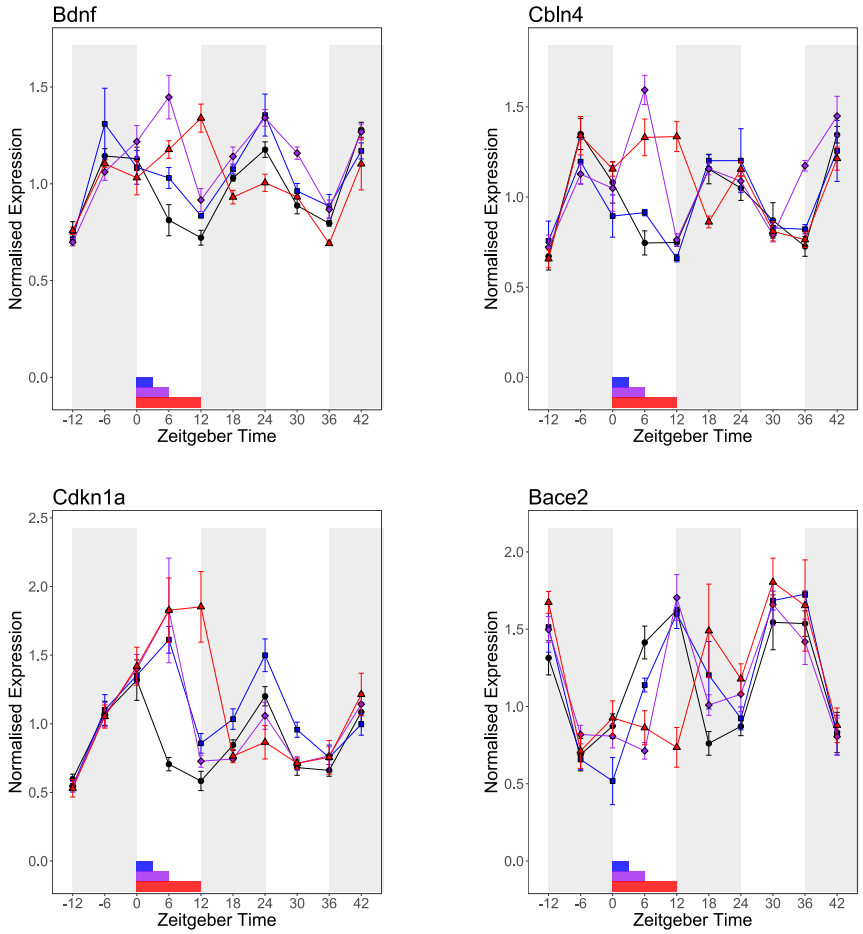

Figure 3.20. Representative Homeostatic Gene Expression Profiles: The expression pattern of genes were filtered for homeostatic genes on the basis of rhythmic expression in control mice that peaked at the end of the active phase, and were induced by sleep deprivation. Plotted here are 3 genes that demonstrate that profile, and one that demonstrates the reverse profile.

However, once plotted, it became clear that genes selected on this basis (e.g. Bdnf, Cbln4, Cdkn1a, Bace2) typically rebounded to baseline expression very quickly following 3 or 6-hour sleep deprivation, whereas following 12-hour sleep deprivation, expression was even reduced compared to non-sleep deprived controls following only 6-hour recovery sleep opportunity. These findings were unexpected for genes that are postulated to act as homeostatic markers of sleep deprivation, as we expected the abundance to remain elevated above that of control animals until the sleep deprived animal had had sufficient opportunity for recovery sleep.

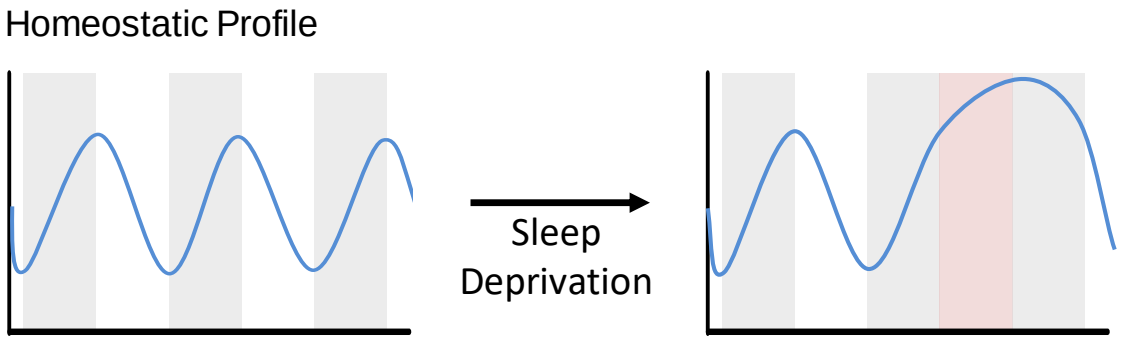

Figure 3.21. Idealised Homeostatic Gene Expression Profiles: Ideally, homeostatic genes should oscillate during the normal wake-sleep cycle but continue to increase during sleep deprivation and remain high until the animal has had sufficient time for complete recovery sleep. These idealised graphs show the expected expression of a homeostatic gene in a mouse, where the dark bars represent the habitual active phase of the mouse, and the pink section represents enforced wakefulness.

Instead, the expression profile of these genes appears to be more consistent with a "binary gene", i.e. a gene whose expression is tightly linked to the very recent wake state of the animal, but carries little information about historic sleep deprivation or the homeostatic sleep pressure the animal is currently experiencing. A binary gene expression would be consistent with a rapid recovery following 6-hour sleep deprivation, as both sleep deprived and control animals are predominantly asleep during this period. A binary pattern also predicts that 12-hour sleep deprivation should result in lower expression in the subsequent dark phase than control animals, because the proportion of time spent awake in this period is considerably reduced due to high homeostatic sleep pressure.

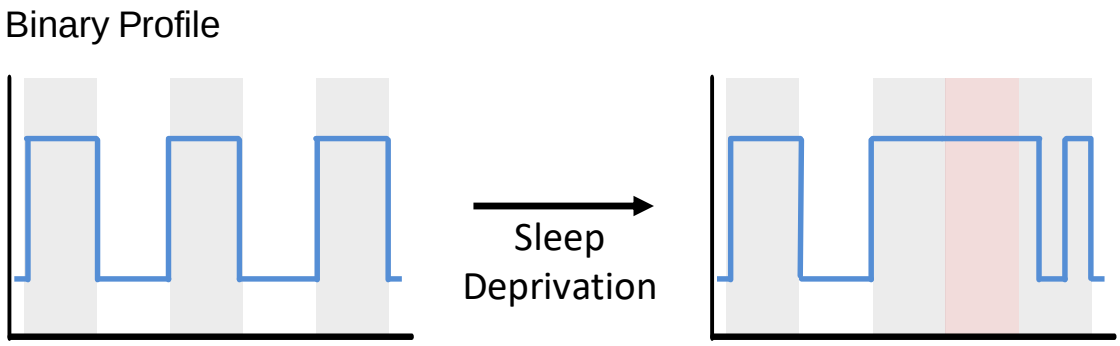

Figure 3.22. Idealised Binary Gene Expression Profiles: Ideally, the expression of "binary" genes should be high during wakefulness and low during sleep, and not be affected by the duration of prior bouts of wakefulness. These idealised graphs show the expected expression of a binary gene in a mouse, where the dark bars represent the habitual active phase of the mouse, and the pink section represents enforced wakefulness. For simplicity, the fragmented nature of rodent sleep is not reflected here, but recovery sleep during the habitual active phase of mice is indicated.

However, transcripts that demonstrate a binary expression profile should not necessarily be discarded when searching for homeostatic molecules. Indeed, it could be argued that a binary pattern would be exactly what would be expected for a transcript that ultimately codes for a protein with a homeostatic function. Assuming a similar translation efficiency of binary transcripts across the sleep-wake cycle, the rate of synthesis of the corresponding proteins would be high during wake and low during sleep. If degradation of these proteins is also unaffected by the wake status of the animal, an appropriate rate of degradation would result in the accumulation of the protein during wake and the net removal of that protein during sleep. Therefore, homeostatic sleep pressure may be signalled through the transcriptionally regulated increase of extracellular signalling proteins like BDNF, CBLN2, CBLN4, or enzymes responsible for the production of extracellular signal molecules, such as PTGS2 or DIO2, whilst proteins such as HOMER1a or CDKN1a may coordinate the intracellular response to elevated sleep drive. A reduced expression of BACE2, implicated in the removal of amyloid plaques which accumulate during sleep deprivation (Abdul-Hay *et al.* 2012; Kang *et al.* 2009; Xie *et al.* 2013), may play a role in the pathogenesis of sleep deprivation.

Do previous studies support a role of these transcripts in homeostasis? Intracerebral injection of BDNF protein increases sleep in rats (Kushikata *et al.* 1999), whilst unilateral injections of BDNF induce increases in local slow wave activity but not the contralateral hemisphere, with BDNF antagonists eliciting the reverse effect (Faraguna *et al.* 2008). In humans, a polymorphism in the coding region of BDNF has been linked to an increased time spent in deep NREM sleep in humans (Bachmann *et al.* 2012). Similarly, Ptgs2, identified in our screen, has also been implicated in control of sleep induction. Ptgs2 encodes cyclooxygenase-2, which carries out the committed step in prostaglandin synthesis, producing prostaglandin H2 (PGH2) from arachidonic acid (Tetsuya *et al.* 2005). PH2 itself acts as a

precursor for prostaglandin D2 (PGD2), which strongly induces sleep when introduced centrally in rats and monkeys (Hayaishi 1991), whilst levels of PGD2 and other products from PGH2 are elevated in rats during both spontaneous sleep and during sleep deprivation (Ram *et al.* 1997). Interesingly, prostaglandin D synthase (Ptgds) expression is also upregulated following both 6- and 12-hour sleep deprivation. The increased expression of Ptgs2 and Ptgds may induce an increase in PGD2 levels through an increase in the availability of PGH2 precursor and prostaglandin D synthase activity. Consistent with a sleep inducing role of prostaglandin synthesis pathways, inhibition of cyclooxygenase-2 through the consumption of non-steroidal anti-inflammatory drugs (NSAID) at night time disrupts sleep in humans (Murphy *et al.* 1994), whilst intracerebroventricular injection of specific cyclooxygenase-2 inhibitors reduces both spontaneous and TNF-α induced sleep duration in rats (Terao *et al.* 1998; Yoshida *et al.* 2003).

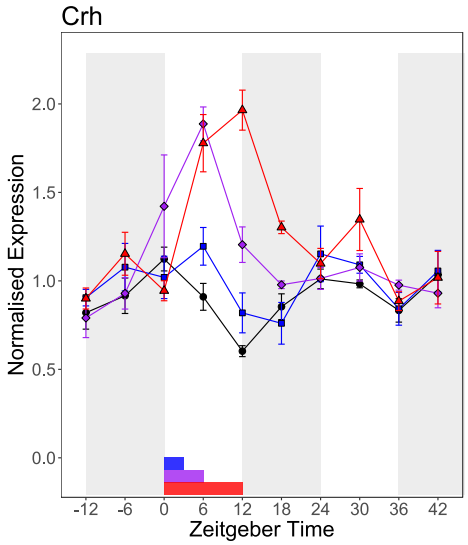

Figure 3.23. The Expression of *Crh* Reflects an Idealised Homeostatic Gene Profile: The expression profile of Corticotropin Releasing Hormone (Crh) is of special interest because it matches the idealised homeostatic gene expression profile.

One transcript, Crh, did demonstrate a homeostatic expression pattern, whereby expression remained high during the initial portion of the recovery phase and did not fall below the expression seen in control animals during recovery. The half-life of Crh mRNA has been previously identified as being short ($t_{½}$ < 15 minutes) (Ma *et al.* 2001), and therefore the elevated levels during the recovery phase are not due to a slow degradation of the mRNA. A homeostatic profile for Crh mRNA may reflect that its protein product, corticotropin releasing factor (CRF), also has a short half-life (Schulte *et al.* 1982; Schürmeyer *et al.* 1984) and therefore requires a sustained elevation of synthesis to maintain a high abundance. Therefore the upstream signalling pathways inducing Crh expression in response to sleep loss may be distinct from those involved in the control of seemingly current state dependent genes.

Crh, which codes for corticotropin releasing factor (CRF), appears to play a different role in the control of sleep. Although CRF is strongly linked to stress induction, and therefore may appear to be a technical artefact of experimental sleep deprivation, its rhythmic expression which peaks at the end of the active phase in control animals suggests that it may also be involved in the homeostasis of spontaneous wake and sleep. However, intracerebral injection of CRF in mice appears to increase wakefulness and decrease both NREM and REM sleep, which is unexpected for a molecule signalling high homeostatic sleep pressure (Sanford *et al.* 2008). The effect on wakefulness and NREM sleep appears to be mediated through Crh receptors expressed in the brain, as central knockout of Crhr1 abrogates the Crh mediated decrease in NREM sleep duration, despite the corticosterone induction remaining intact (Romanowski *et al.* 2010). The induction of Crh may therefore be a stress induced consequence of experimental sleep deprivation, or a molecular mechanism through which wakefulness is maintained, despite rising homeostatic and circadian sleep pressure. However, it is important to remember that this experiment isolated RNA from the cortex, whilst the stress related functions of Crh are typically associated with the hypothalamus (Füzesi *et al.* 2016). Crh signalling in the cortex may therefore serve a function distinct from the stress response.

3.3.6. Stress Profile Genes

We also predicted that there may be a subset of genes that demonstrate "stress" expression profiles, which would be switched on during periods of particularly high homeostatic sleep pressure to either induce sleep or cope with the demands of extended wakefulness. We hypothesised that such genes would be upregulated during sleep deprivation, but either not be rhythmic in control animals, or show a peak just before habitual sleep time.

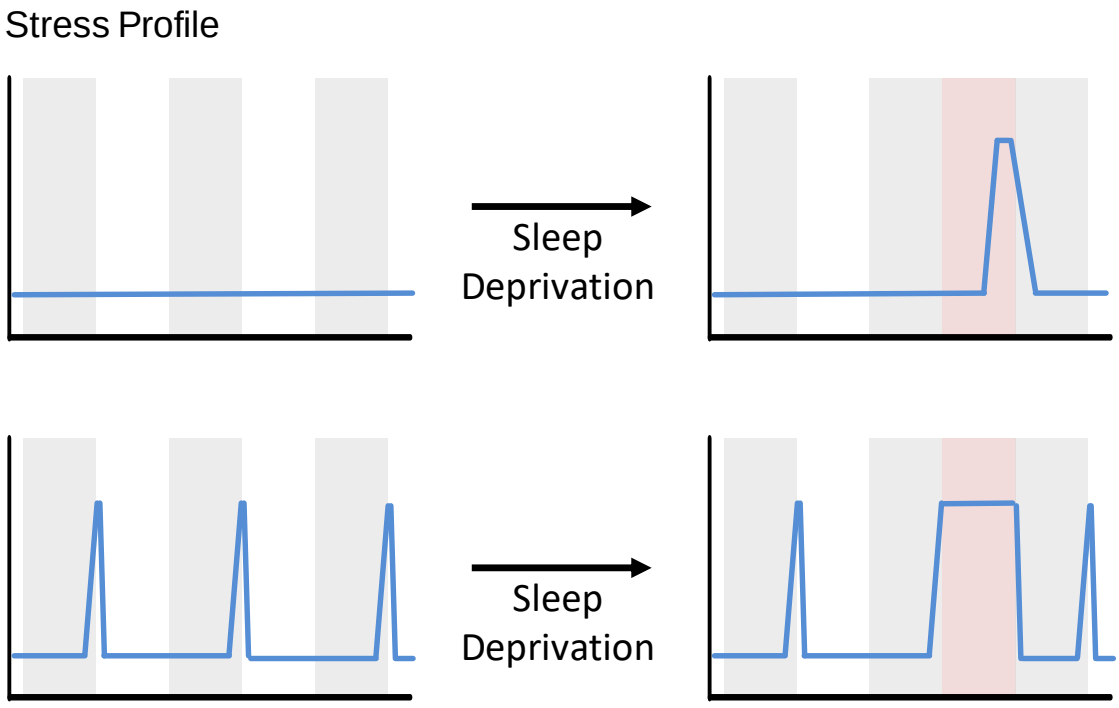

Figure 3.24. Idealised Stress Gene Expression Profiles: Ideally, the expression of "stress" genes should be induced during particularly high sleep pressure. The expression of these genes may therefore be triggered only following sleep deprivation, or may be triggered at the end of the habitual wake phase. These idealised graphs show the expected expression of a stress gene in a mouse, where the dark bars represent the habitual active phase of the mouse, and the pink section represents enforced wakefulness.

Amongst the genes identified as exhibiting a "stress" expression pattern were Rasd1 and Vip. Rasd1, also known as ras-related dexamethasone induced or Dexras1, has previously been identified as a sleep deprivation dependent transcript in mouse (Thompson *et al.* 2010) and playing a role in circadian entrainment to light (Cheng *et al.* 2004), whilst a SNP near Rasd1 is associated with habitual wake time in humans (Hu *et al.* 2016). At the molecular level, Rasd1 is a monomeric G-protein that is activated by NMDA-receptor activity and nitric oxide (Fang *et al.* 2000). Activation of Rasd1 is associated with

efflux of iron from lysosomes, which in turn leads to the inhibition of neuronal firing (White *et al.* 2016). Therefore Rasd1 may act in a negative feedback loop, which limits neuronal firing in response to neuronal activity.

Intriguingly, Vip, which codes for vasoactive intestinal peptide, also demonstrates a non-rhythmic expression pattern in control animals and is activated following sleep deprivation, but does not return to baseline levels within 6 hours of recovery sleep opportunity like Rasd1. Vip has previously been associated with sleep and sleep deprivation studies, with VIP abundance increasing in cerebral spinal fluid during sleep deprivation, whilst intracerebral injection of VIP promotes sleep (Bourgin *et al.* 1997; Jime´nez-Anguiano *et al.* 1993; Prospe´ro-Garcia *et al.* 1986). Conversely, knockout of Vip in mice results in reduced sleep duration, altered distribution of sleep across the day and a blunted rebound in response to sleep deprivation (Hu *et al.* 2011). Interestingly, these sleep effects of VIP appear to predominantly be associated with REM sleep rather than NREM sleep, as VIP knockout and injection induce greater changes to REM sleep duration, whilst specifically depriving REM sleep is also sufficient to induce Vip expression. Therefore, based on previous studies, it appears as though VIP may play a role in sleep homeostasis, specifically REM sleep homeostasis. An elevated expression for several hours following the cessation of sleep deprivation is consistent with a homeostatic transcript, however it is unexpected that the expression of Vip does not oscillate during the day in control animals.

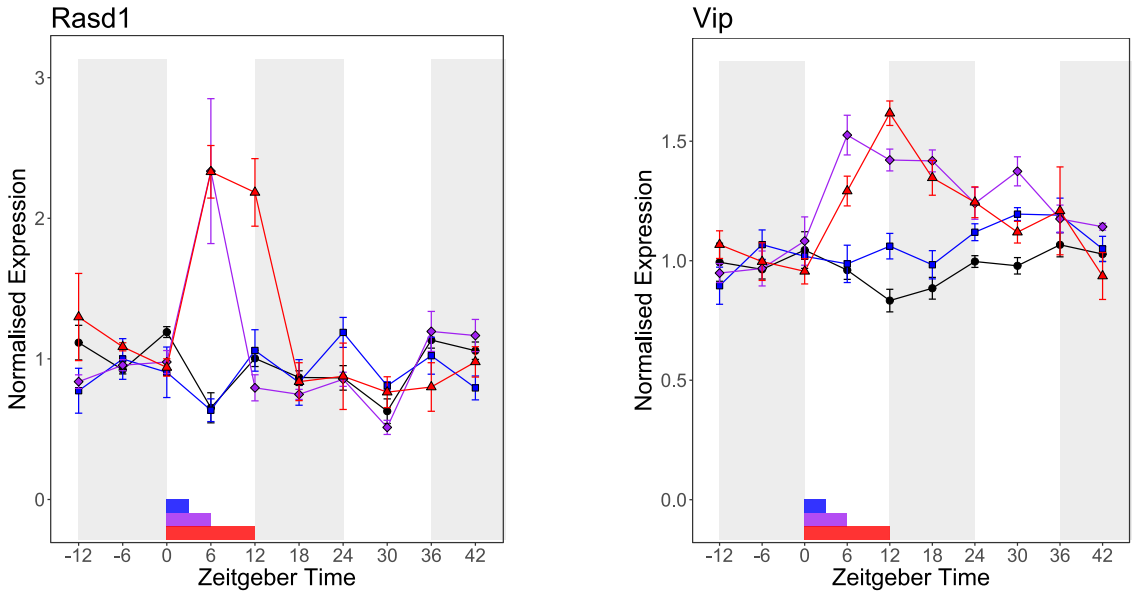

Figure 3.25. Rasd1 and Vip Expression Fit Different Stress Gene Profiles: Rasd1 and Vip expression is induced during sleep deprivation, but does not display rhythmic expression in control animals, suggesting that their induction is specifically linked to prolonged wakefulness. Whereas Rasd1 expression rapidly returns to baseline following cessation of sleep deprivation, Vip expression remains elevated for prolonged periods.

When we expanded our criteria of stress genes to include genes that are ordinarily rhythmic in control animals, but do not peak during spontaneous waking, we identified some genes that are strongly induced by sleep deprivation but typically peak at the end of the rest phase in control animals (e.g. Xdh, Plin4, Tsc22d3). It is difficult to immediately reconcile in terms of sleep homeostasis how genes that normally have highest expression at the end of the rest phase can be strongly induced by sleep deprivation. Instead it seems more plausible that these genes are induced not by sleep deprivation but by an increase in corticosterone associated with sleep deprivation. Plasma corticosterone levels in the mouse usually oscillate during the day, with the peak abundance occurring near the end of the light phase (Ottenweller *et al.* 1979; Yoshida *et al.* 2005), whereas experimental sleep deprivation may induce plasma corticosterone increases. Genes induced by corticosterone would therefore be expected to usually demonstrate a peak at the end of the rest phase (coinciding with the peak of plasma corticosterone), and possibly demonstrate an elevated expression following 6 hour sleep deprivation. Consistent with this finding, Plin4 and Tsc22d3 have previously been shown to be induced in the brain by dexamethasone (Juszczak & Stankiewicz 2018), whilst the sleep deprivation mediated induction of Xdh and Tsc22d3 was absent in mice which had undergone adrenalectomy (Mongrain *et al.* 2010).

Therefore, genes with a "stress" expression pattern may truly be induced by a stress associated increase in corticosterone during experimental sleep deprivation. However, it is difficult to determine whether the induction of corticosteroids is a physiological signalling pathway utilised in response to extended wakefulness, or an experimental confounder of imposing sleep deprivation. Surgical removal of the adrenal glands may help delineate the individual contributions of stress and sleep deprivation: indeed intact adrenal glands are required for the induction of an estimated 70% of wake dependent transcripts in response to sleep deprivation (Mongrain *et al.* 2010). However, adrenalectomy also disrupts feedback pathways between corticosteroids and Crh, a wake promoting transcript, perhaps introducing further confounding effects (Ma *et al.* 2001).

Utilising different model systems or sleep deprivation techniques may indicate to what extent corticosteroid modulated gene expression is an artefact of experimental sleep deprivation. (Friess *et al.* 2004). Administration of wake promoting stimulants, including caffeine, methamphetamine and methylphenidate, raises plasma corticosterone in rodents (L. *et al.* 2006; Petit *et al.* 2010; Spindel & Wurtman 1984). Sleep deprivation in humans has been demonstrated to induce increases in plasma cortisol (Spiegel *et al.* 1999), which in turn has been demonstrated to influence sleep architecture and increase delta power. Therefore, corticosteroid induction may be tightly linked with prolonged wakefulness, rather than an experimental artefact.

3.3.7. Attributes of this Experimental Design

In addition to the use of next-generation sequencing technology, the timecourse style of our experiment, coupled with varied durations of sleep deprivation is what is novel about the data presented in this chapter. This approach has the advantage that it can identify not only the acute gene expression changes occurring during sleep deprivation, but also the rate at which these genes return to baseline levels and how this recovery depends on the amount of sleep debt accrued. To illustrate the value of such timecourse datasets, data and expression profiles are presented below of 4 genes identified in previous studies as increasing during sleep deprivation. In our study, the expression of all of them are identified as increasing at least twofold following 6 hour sleep deprivation compared to non-sleep deprived mice, however data from the additional timepoints reveal marked differences in habitual expression in undisturbed mice as well as differences in recovery from sleep deprivation.

3 of the genes show significant 24 hour rhythms in undisturbed mice, with the expression of Rasd1 being approximately flat during the day. Of the 3 rhythmic genes, Sult1a1 peaks at the beginning of the habitual active phase, whereas Arc and Cdkn1a both peak just before the end of the active phase. Whereas 6 hour sleep deprivation increases the expression of Cdkn1a, Sult1a1 and Rasd1 to levels higher than occurring during the course of the normal day, sleep deprivation appears only to lessen the reduction in Arc expression. Compared to 6 hours, 12 hour sleep deprivation further increases the expression of Sult1a1, in contrast to the expression of Cdkn1a and Rasd1 which appear to reach a plateau. Finally, following cessation of sleep deprivation, the expression of Arc, Cdkn1a and Rasd1 quickly rebound to baseline levels, whilst the expression of Sult1a1 remains high for at least 12 hours.

Table 13: Gene Expression of Arc, Cdkn1a, Sult1a1 and Rasd1

Gene	Rhythmic q-value	Fold Change 6hr SD	Fold Change 12hr SD	SD6 ANOVA q-value
Arc	9.54E-03	2.05 *	1.63 *	5.99E-01
Cdkn1a	7.80E-06	2.59 *	2.16 *	5.31E-03
Sult1a1	3.70E-02	2.39 *	2.08 *	9.47E-03
Rasd1	3.87E-01	3.58 *	2.06 *	2.62E-04

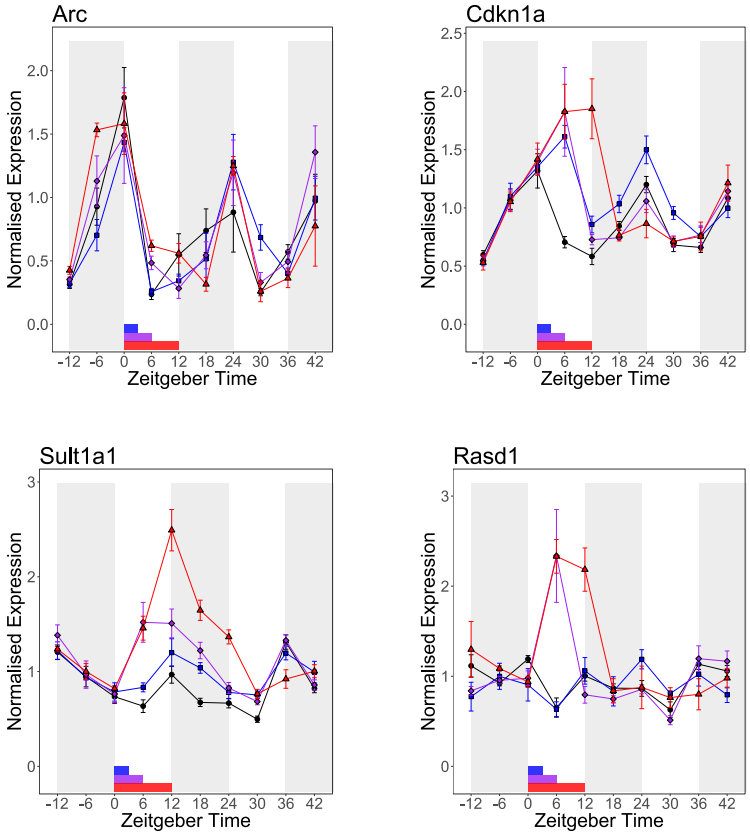

Figure 3.26. Genes Previously Identified as Induced by Sleep Deprivation have Markedly different Expression Profiles during Spontaneous Wake Cycles and during Recovery Sleep: The expression of Arc, Cdkna1, Sult1a1 and Rasd1 have all been previously identified as strongly induced during sleep deprivation. However, previous studies did not indicate that the expression of each of these genes demonstrate distinct expression patterns during spontaneous wake, sleep deprivation and recovery, emphasising the power of a timecourse style experimental design. The table outlines the JTK derived q-value for rhythmic gene expression in control mice, the fold change in expression immediately following 6 hour and 12 hour sleep deprivation (compared to control animals and mice subjected to only 3 hour sleep deprivation, respectively), and the q-value comparing the expression profile of 6 hour sleep deprived mice to control mice. The asterisks in the fold change columns denote whether that comparison was significantly different (i.e. q-value < 0.05). The expression of individual genes are plotted in the graphs, where the grey bars indicate the light-dark cycle, whilst the blue, purple and red bars and lines indicate the timing and expression of 3-, 6-, and 12-hour sleep deprived mice, respectively. The expression of control animals is plotted in black.

Naturally, the power of this experiment to determine the kinetics of recovery could have been greatly increased by decreasing the time between timepoints. However, increasing the resolution necessarily results in either an increase in total samples, or reduction in total timecourse duration or replicates, and therefore we sought to strike a balance between these factors. One option may have been to include additional sampling timepoints during the 12 hour sleep deprivation period, whilst maintaining a 6 hour resolution between other timepoints. In this way, the acute effects of short term sleep deprivation as well as the rate of recovery could be better characterised.

The biggest practical problem encountered during this project was the number of sleep deprived mice that were necessary. Due to the costs involved in both the generation of tissue and subsequent transcriptomic analyses, samples were generated and processed in two batches, the first containing the control and 6 hour sleep deprived mice, and the second containing the 3 and 12 hour sleep deprived mice. This introduced an undesirable batch effect which complicated downstream data analyses- whilst the overall shape of the expression profiles were similar between batches, direct comparison of absolute expression values between batches was problematic. Therefore, we found ourselves in the unenviable position of comparing the 12 hour deprivation group to the 3 hour sleep deprivation group for absolute gene expression. Even in hindsight, it is difficult to conclude whether it would have been better to process all the samples simultaneously to aid the subsequent data analysis, or to have progressed with caution as we chose.

3.3.8. Comparison to Adrenalectomized Mice

Mongrain *et al* previously showed that a significant proportion of the transcriptional response to sleep deprivation in the cortex is in part coordinated by glucocorticoid signalling (Mongrain *et al.* 2010). By observing the effects of sleep deprivation on transcription in adrenalectomized mice, they identified a core subset of genes whose expression in the cortex is linked to sleep deprivation independent of glucocorticoid induction, which may be an experimental confounder or true physiological response.

Comparing the work presented here with a list of 78 genes identified by Mongrain *et al* as being modulated by sleep deprivation and time of day, we find that 65% of those genes are also modulated by sleep deprivation in our study, whilst 89% of those genes showed a diurnal rhythm in expression in control animals (Fig 3.27.A.). Interestingly, 6 hour sleep deprivation induced only a transient change in expression of these genes (Fig 3.27.B.), indicating that these core genes typically demonstrate a binary expression profile. Since sleep homeostasis appears unaffected following adrenalectomy in mice, sleep homeostasis may be encoded by the expression of binary genes. It is noteworthy, however, that the elicited delta power increase in different strains following sleep deprivation is positively correlated with the magnitude of glucocorticoid induction. Whether this link is due to an important signalling role of glucocorticoids during sleep deprivation or due to the extra interaction required to maintain wakefulness at higher sleep pressure is still unclear, however.

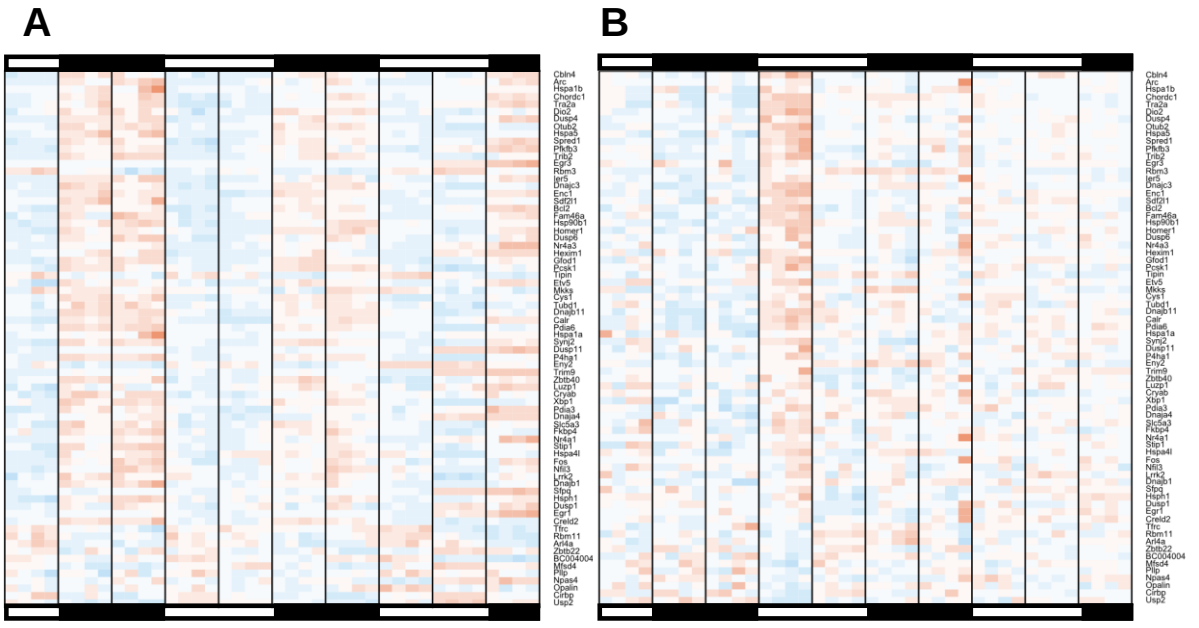

Figure 3.27. Genes Previously Identified as Modulated by Sleep Deprivation in Adrenalectomized mice demonstrate Diurnal Expression and an acute response to Sleep Deprivation: The cortex expression of glucocorticoid independent genes identified by Mongrain *et al* are plotted here. The heatmaps indicate the z-score normalised expression of individual genes in the cortex of mice in undisturbed mice (A) and those subjected to 6 hour sleep deprivation, compared to undisturbed mice at the same timepoint (B), where blue indicates low expression and red indicates elevated expression.

3.3.9. Suggested Subsequent Experiments

Several downstream studies are possible following this transcriptomic screen. Perhaps the most pressing is the EEG-characterisation of sleep patterns during and following sleep deprivation. Although 6 hour sleep deprivation in C57/Bl6 mice is well characterised (Franken *et al.* 1999), the sleep rebound following 12 hour sleep deprivation is less understood. Similarly, although 6 hour sleep deprivation using the automated system that we used has been previously validated (Kaushal *et al.* 2012), sleep deprivation was difficult to maintain during the subsequent 6 hours, and was therefore applied through a mixture of gentle handling and automated sleep deprivation. Although supervision of the mice ensured that they were deprived of sleep, we have no quantitative estimate of the proportion of time spent asleep by the mice. Confirmation of the efficacy of sleep deprivation, as well as the time required for the sleep patterns of mice to recover to baseline levels, would inform the analysis of the transcriptomic dataset.

This experiment extracted total RNA from homogenised mouse cortex, and so the RNA interrogated included contributions from different cell types and different cellular localisations. Therefore, any cell or location specific changes in RNA abundance are overlooked by this experimental approach. Local translation of mRNA occurs at dendrites and axons, and is thought to be important in axonal maintenance and synaptic potentiation (Verma *et al.* 2005; Zhang & Poo 2002). Therefore, it would be interesting to understand which RNA molecules accumulate specifically near synapses and in the soma, or in specific cell types. However, the presence of mRNA at a location does not necessarily show that that gene is undergoing translation. Indeed, recently it was shown that Arc mRNA is encapsulated in viral like particles, and released by donor neurons for translation in recipient neurons (Pastuzyn *et al.* 2018). Isolating RNA that is being actively translated in a given cell type can be achieved through a translating-ribosome affinity-purification approach (Heiman *et al.* 2014), which has previously been performed to characterise the effect of sleep deprivation on oligodendrocytes (Bellesi *et al.* 2013). Combining this technique with subcellular fractionation may reveal synaptic specific translation changes.

During the tissue collection for this timecourse, peripheral tissues were also collected. Since the brain has been the major focus of studies investigating the molecular consequences of sleep deprivation, a similar transcriptomic screen of these peripheral tissues would provide entirely novel data. Previous studies indicate that gene expression in peripheral tissues is modulated by sleep deprivation (Anafi *et al.* 2013; Maret *et al.* 2007), whilst muscle has recently been implicated in the control of sleep duration (Ehlen *et al.* 2017). Understanding which pathways are activated during sleep deprivation in these tissues may therefore provide clues about the extent the periphery controls sleep timing and duration,

and possibly identify pathological pathways that are activated during sleep deprivation. Whether peripheral tissues experience similar disruption to rhythmic expression as found in the cortex may be particularly interesting. Tissues exhibit different rates of recovery from jetlag (Yamazaki *et al.* 2000), and so sleep deprivation may also induce the desynchrony that is thought to underlie the negative effects of jetlag (Vosko *et al.* 2010).

The different shaped expression profiles of wake dependent genes surely reflect differences in control of transcription and degradation. Having identified genes with a homeostatic and binary expression profile, one particularly interesting downstream experiment may be to investigate what transcription factors bind to the promotor regions of those genes, and whether a handful of transcription factors are enriched amongst those that bind those sites. The involvement of those transcription factors during sleep deprivation could be confirmed through either identifying their localisation or phosphorylation status through immunofluorescence or western blotting, or by directly quantifying the DNA-binding patterns through chromatin immunoprecipitation sequencing (ChIP-Seq). Any transcription factor implicated as binding in response to sleep deprivation could be further investigated by characterising the effect on sleep of the conditional knockout or the overexpression of a constitutively active form of that factor.

The intuitive experiment to follow transcriptomic profiling, however, is the proteomic profiling of similar samples. Because the most apparent function of mRNA molecules is to code for the corresponding protein, it could be argued that changes occurring at the protein level are far more relevant to the ultimate cellular processes occurring within the cell.

4. The Proteomic and Metabolomic Impact of Sleep Deprivation on Mouse Cortex

This section details our experiments to better understand the proteomic and metabolomic effects of sleep deprivation in mouse cortex. Using a similar experimental design as our transcriptomic experiments, we find that the abundance of hundreds of proteins is modulated by 12-hour sleep deprivation, including several synaptic proteins. We also find a prolonged decrease in abundance of many ribosomal protein subunits, suggesting global protein synthesis may be depressed following sleep deprivation. In contrast, we identify relatively few metabolites whose abundance are dependent on time of day or sleep deprivation.

4.1. Proteomic Profiling of Sleep Deprived Mouse Cortex

To identify to what extent transcriptomic changes are reflected at the protein level, we carried out TMT-based proteomic analysis of cortex from mice that had been sleep-deprived for 12 hours. At the time of running the experiment, 10 TMT tags were available, and therefore the maximum number of samples able to be compared within one multiplex was 10. Due to the technical difficulties of comparing between different ten-plex experiments, four separate ten-plex experiments were carried out. The first involved comparing individual biological replicates, using 3 replicates from 12 hours before the onset of sleep-deprivation, 4 replicates from immediately after 12 hours sleep deprivation, and 3 replicates from 24 hours after the cessation of sleep deprivation. These three timepoints were separated by 24 hours (Fig 4.1.A). The same ten-plex was carried out on non-sleep deprived animals. A second pair of ten-plex experiments was carried out where protein from 4 individual biological replicates at 10 timepoints spaced 6 hours apart was pooled to a single technical replicate (Fig 4.1.B).

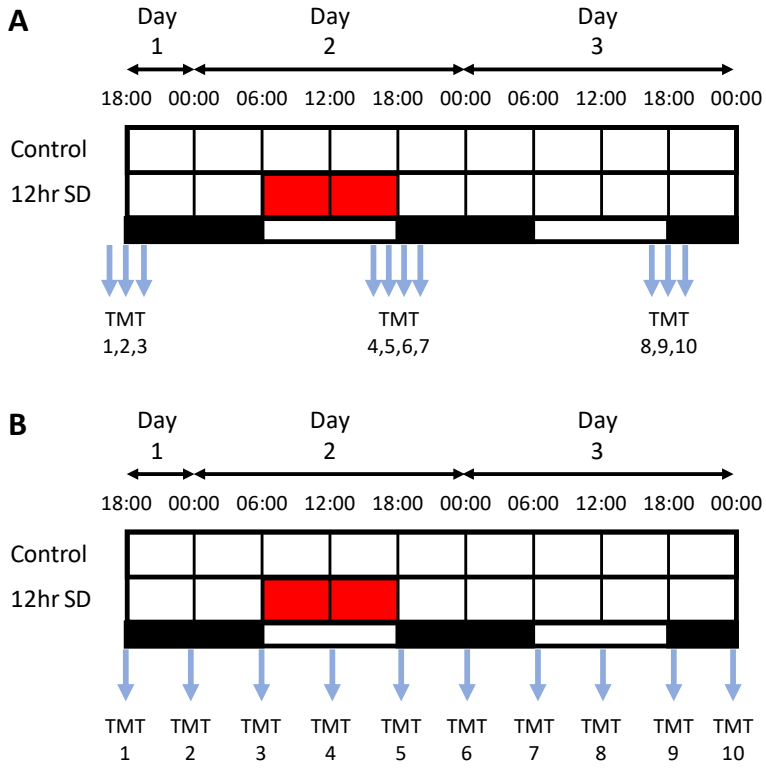

Figure 4.1. Experimental Design for Proteomic Characterisation of Sleep Deprivation in Mice: Protein from individual timepoints were subjected to proteomic based analyses. In one pair of experiments, protein from tissue collected at 18:00 on Day 1, Day 2 or Day 3 formed the ten-plex. In a second pair of experiments, protein was pooled from biological replicates at each of the 10 timepoints, spaced 6 hours apart. The red section represents sleep deprivation, whilst the black and white bar represents the light-dark cycle imposed on the mice.

5357 proteins were identified in mice with uninterrupted sleep from the ten-plex designed as Figure 4.1.A. There were relatively few proteins that were statistically differentially expressed between the samples collected at the onset of the dark phase on Day 1, Day 2 and Day 3. Pairwise comparison between Day 1 and Day 2, Day 1 and Day 3, and Day 2 and Day 3 revealed a total of 27, 0 and 6 proteins, respectively, were statistically differentially expressed. 7 of the 9 proteins whose abundance was significantly higher in samples collected on Day 2 than Day 1 were serum proteins (bikunin, Complement C3, haptoglobin, hemopexin, inter alpha-trypsin inhibitor, orosomucoid 1, serum amyloid A), indicating that the samples collected on Day 2 had more blood contamination than those collected on Day 1. Consistent with this conclusion, the 5 proteins whose abundance was higher on Day 2 compared to Day 3 were all serum proteins (Complement C3, fibrinogen alpha, fibrinogen beta, hemopexin and orosomucoid 1).

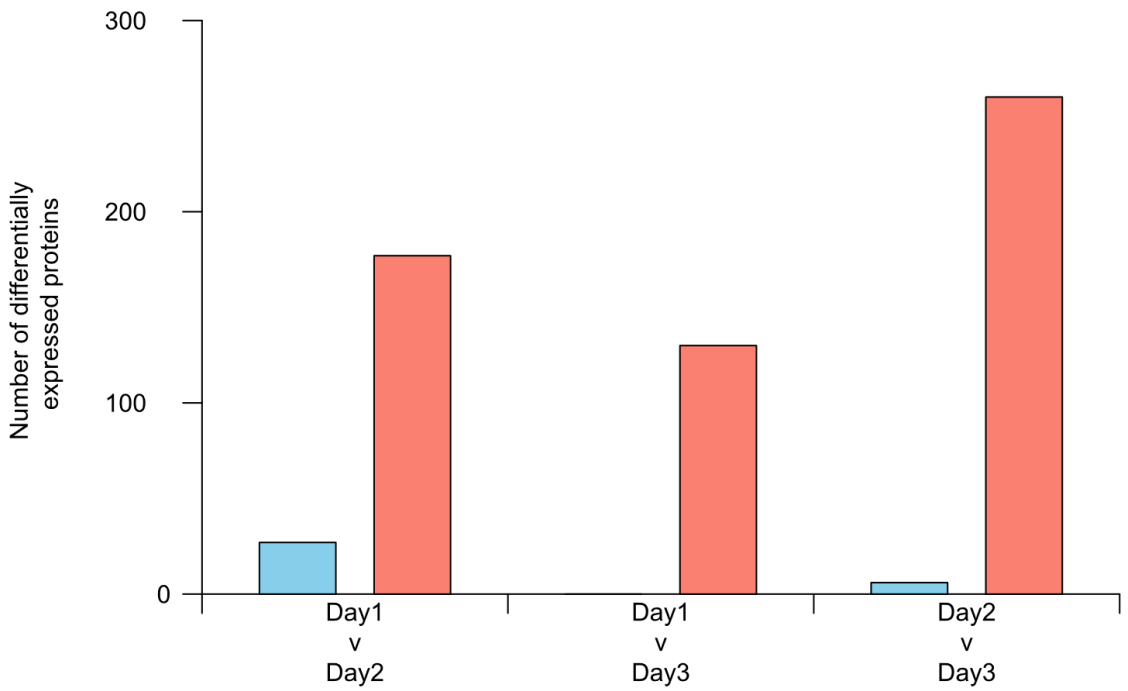

Figure 4.2. 12-hour Sleep Deprivation Induces changes in the Abundance of Hundreds of Proteins in Mouse Cortex: Protein from mouse cortex was collected at the end of the light phase over 3 days and subjected to TMT-based proteomic analyses. Control mice were allowed *ad libitum* sleep, whereas the sleep deprived group were subjected to 12-hour sleep deprivation during the entirety of the light phase on Day 2. FDR adjusted student t-tests between groups identified proteins whose abundance significantly changed. The blue bars plotted above represent the number of proteins that significantly differed in the control group in the respective comparison, whereas the red bars represent the number of proteins that differed in the 12-hour sleep deprived group.

In contrast to non-sleep deprived samples, of the 5600 proteins identified, the abundance of a total of 177, 130 and 260 proteins was statistically different between cortex samples collected from sleep deprived mice on Day 1 and Day 2, Day 1 and Day 3, and Day 2 and Day 3, respectively. Among the total of 425 proteins that exhibited a significant change in abundance across at least one of these three comparisons, there was an enrichment in proteins involved with synapses, the cytosolic large ribosomal subunit, microtubules, the mitochondrial inner membrane, motor proteins, symport, phosphodiesterase function, proteins with C2 domains or EF-hand domains, and complement and coagulation cascades.

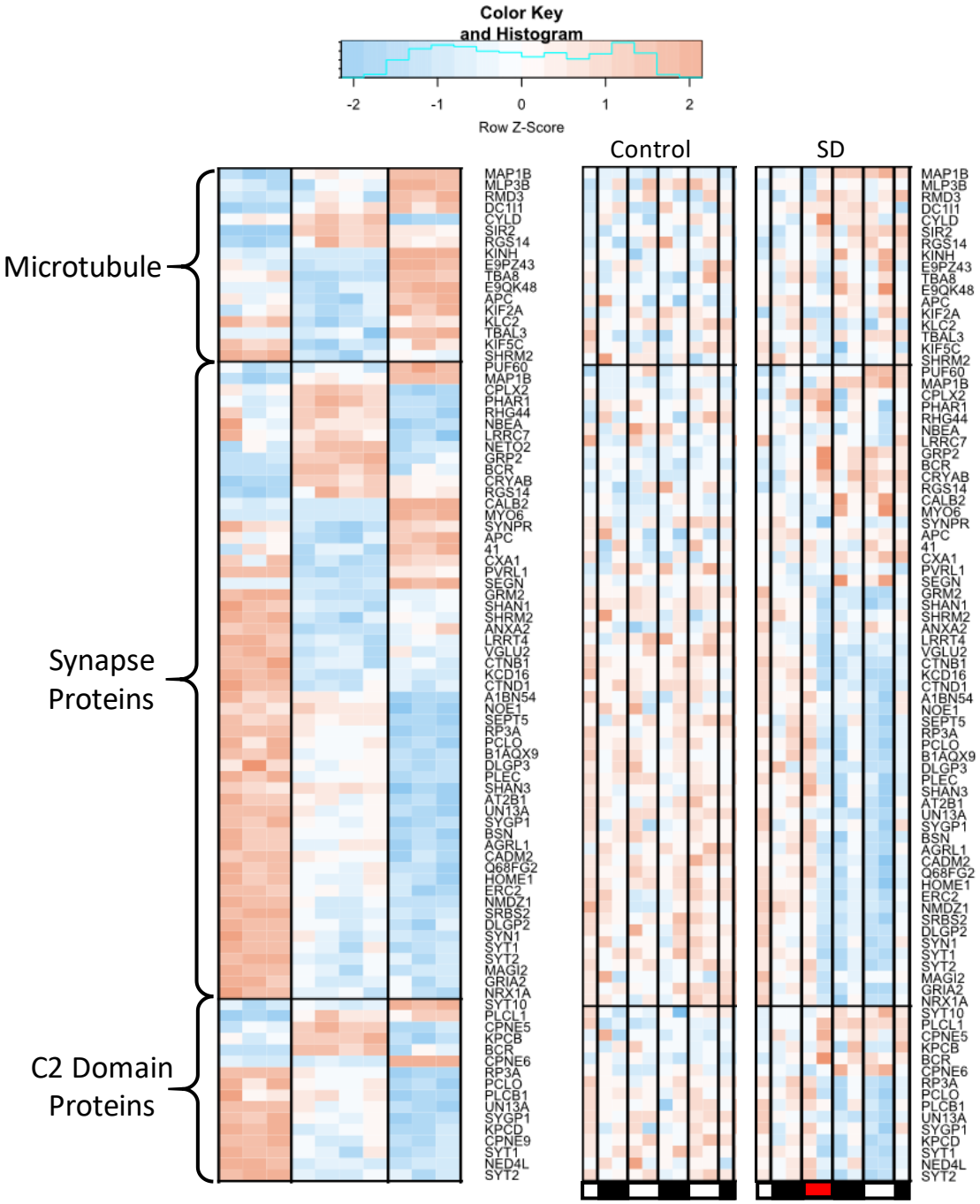

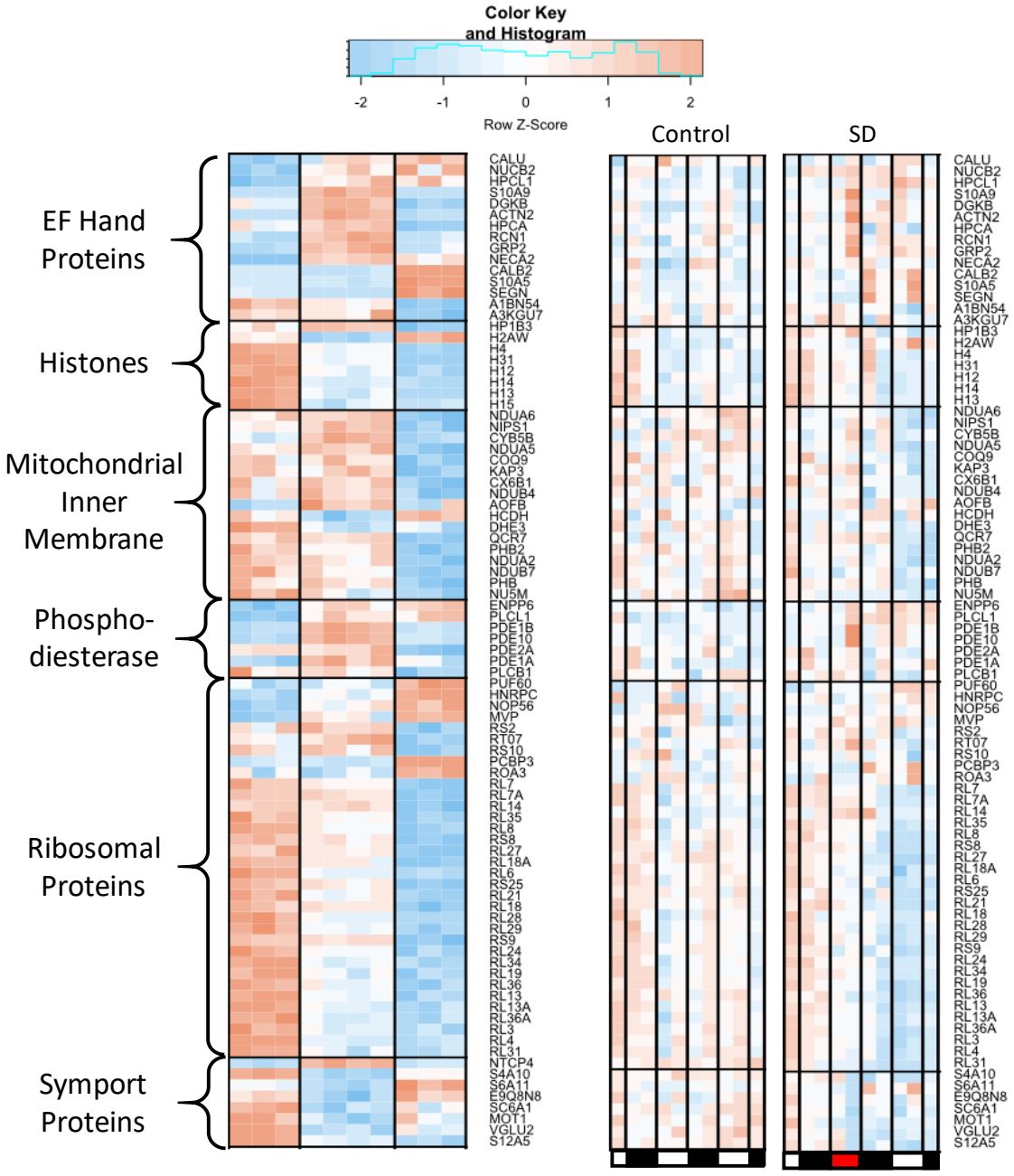

Figure 4.3. TMT-based Proteomics reveals Abundance Changes in Proteins relating to Microtubules, Synapses, Calcium Binding Proteins, Histones, Mitochondrial Function, Phosphodiesterases, Ribosomes and Transport : Protein from mouse cortex was collected at the end of the light phase over 3 days and subjected to TMT-based proteomic analyses. Control mice were allowed *ad libitum* sleep, whereas the sleep deprived group were subjected to 12-hour sleep deprivation during the entirety of the light phase on Day 2. FDR adjusted student t-tests between groups identified proteins whose abundance significantly changed, and enriched functional groups identified using DAVID functional annotation. Functional clusters are plotted above, with the functional group indicated. The Z-score normalised abundance of a protein in individual biological replicates is indicated by the colour, where red indicates a high abundance and blue indicates a low abundance. The left heatmap shows replicate data from 3 timepoints. The leftmost section indicates samples collected Day 1 (no

sleep deprivation), the middle section indicates samples collected Day 2 (immediately following 12-hour sleep deprivation), and the rightmost section indicates samples collected Day 3 (following 12-hour sleep deprivation and 24 hour recovery). The right heatmaps show pooled data from the control and sleep deprived timecourses. The black and white bars represent the light dark cycle, whilst the red bar indicates the timing of sleep deprivation. Proteins that fall into multiple group are re-plotted in each group. Note that not all proteins detected in the replicate dataset were detected in the timecourse datasets.

Of the 66 proteins upregulated following 12 hours sleep deprivation, there was a statistical enrichment of proteins involved containing the calcium binding EFh domain, proteins associated with phosphodiesterase activity and proteins associated with dopaminergic synapses. In contrast, the 110 proteins that were downregulated following 12 hour sleep deprivation were enriched in synapse proteins, cytosolic large ribosomal subunits, and proteins associated with symport and nucleosomes. The abundance of proteins associated with blood microparticles was also significantly reduced, indicating that the samples collected on Day 1 had more blood contamination than those collected immediately following sleep deprivation.

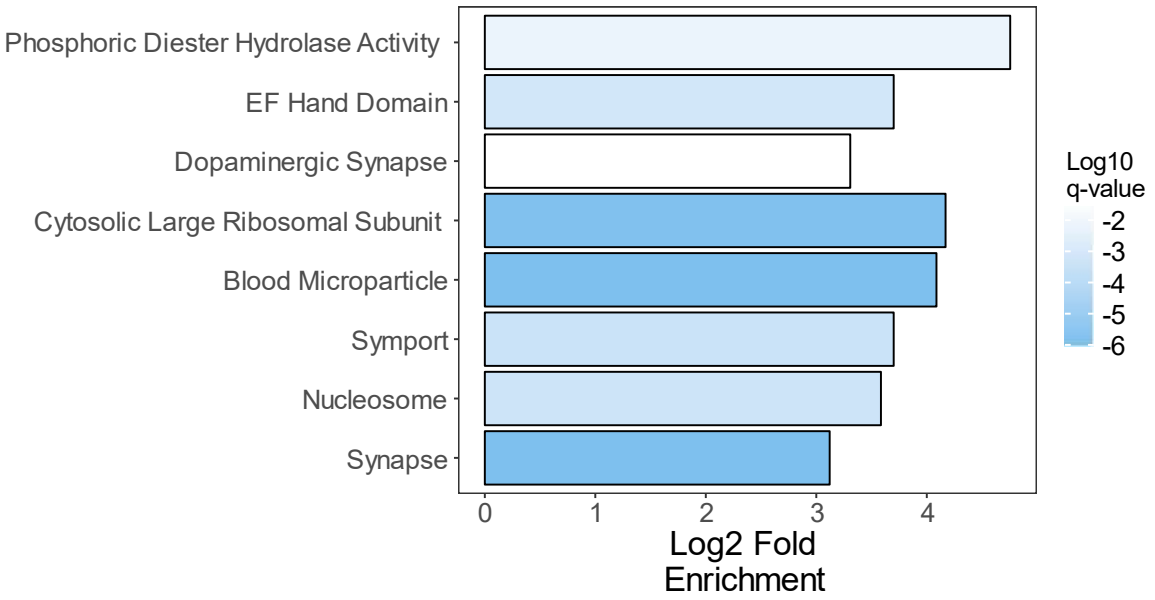

Figure 4.4. Protein Classes Differentially Expressed in Mouse Cortex following 12-hour Sleep Deprivation Compared to Mice Sacrificed without Sleep Deprivation: Proteins identified as modulated immediately following 12 hour sleep deprivation compared to non-sleep deprived mice were subjected to functional annotation, and enriched gene classes displayed above. The enrichment of genes is indicated by the width of each bar, whilst the q-value is indicated by the colour of the bar.

The 140 proteins that exhibited significantly lower abundance following 24 hours recovery from sleep deprivation were enriched in proteins associated with proteins with EF hand domains, phosphodiesterase activity, and those associated with dopaminergic synapses. Therefore it appears that those classes that had been upregulated during sleep deprivation reduced toward baseline levels during subsequent recovery. Remarkably, following 24-hour recovery, downregulated proteins are enriched with ribosomal proteins, including the cytosolic large ribosomal subunit proteins. Proteins that were downregulated following 24 hours recovery were also enriched in mitochondrial inner membrane proteins, including Complex I subunits and ATP Synthase components. Proteins upregulated following 24-hour recovery were enriched in proteins associated with blood, indicating that there was more blood contamination in the samples collected following 24-hour recovery than after 12-hour sleep deprivation.

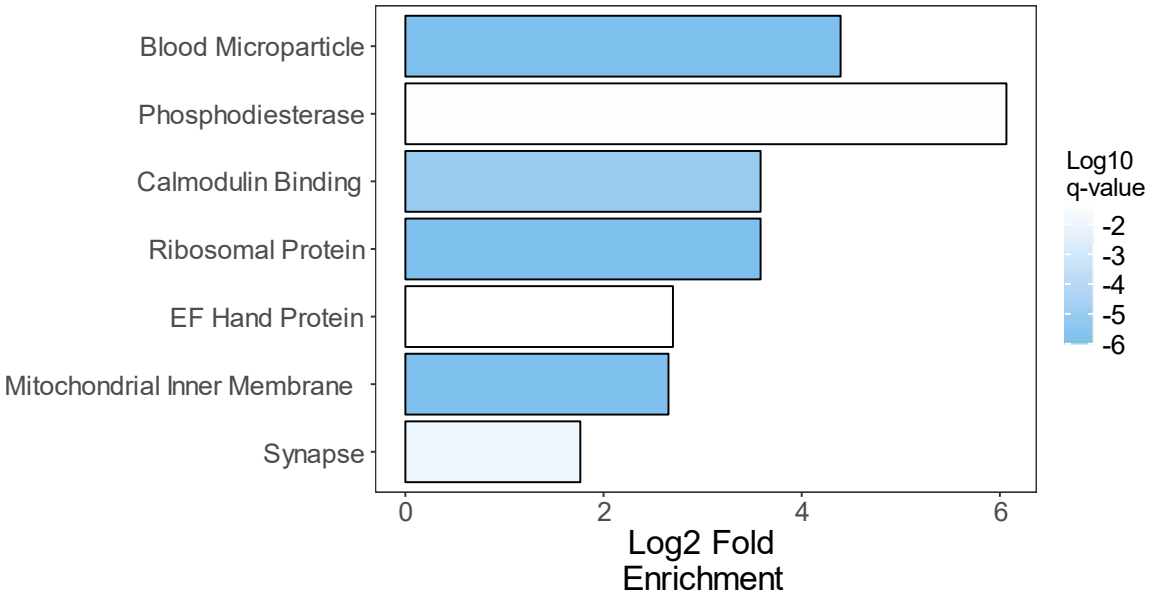

Figure 4.5. Protein Classes Differentially Expressed in Mouse Cortex following 12-hour Sleep Deprivation Compared to Mice Sacrificed following 24 hour Recovery from 12-hour Sleep Deprivation: Proteins identified as modulated immediately following 12 hour sleep deprivation compared to mice allowed 24 hours recovery were subjected to functional annotation, and enriched gene classes displayed above. The enrichment of genes is indicated by the width of each bar, whilst the q-value is indicated by the colour of the bar.

Comparison between mice sacrificed on Day 1 and those that had been sacrificed on Day 3 revealed that 73 proteins exhibit reduced abundance following 12-hour sleep deprivation and 24-hour recovery. The downregulated proteins were enriched in ribosomal proteins, especially those associated with the large ribosomal subunit; synapse proteins, including those associated with excitatory synapses, and genes associated with nucleosome function. The 57 proteins whose

abundance was increased following 12 hour sleep deprivation and 24 hour recovery compared to pre-sleep deprivation mice were enriched only in proteins associated with the cytoskeleton.

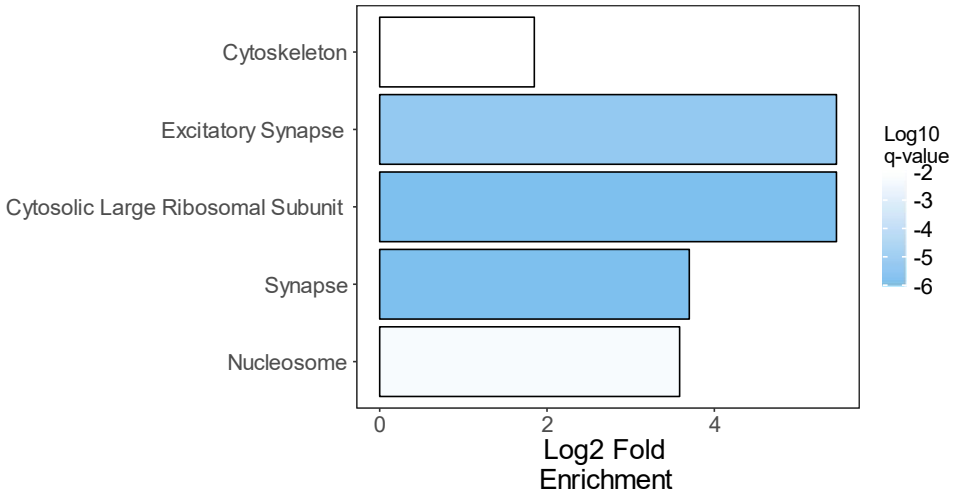

Figure 4.6. Protein Classes Differentially Expressed in Mouse Cortex following 12-hour Sleep Deprivation and 24-hour Recovery Compared to Mice Sacrificed without Sleep Deprivation: Proteins identified as modulated following 24 hour recovery from 12 hour sleep deprivation compared to non-sleep deprived mice were subjected to functional annotation, and enriched gene classes displayed above. The enrichment of genes is indicated by the width of each bar, whilst the q-value is indicated by the colour of the bar.

To determine to what extent changes at the transcript level are reflected by changes in protein abundance, the abundance of proteins encoded by genes identified as exhibiting a homeostatic or stress profile were plotted. Approximately 40% of the proteins encoded by the transcripts of interested were detected in our proteomics screen. Of the 9 proteins detected from homeostatic transcripts, only Homer1 showed a significant difference in abundance following sleep deprivation, specifically between the pre-sleep deprivation timepoint and following 24 hour recovery (q-value = 0.047). Remarkably, despite the Homer1a transcript increasing during sleep deprivation and recovering to baseline within 24 hours, Homer1 protein abundance trends downward immediately following sleep deprivation (q-value = 0.07) and remains lower over the following 24 hours. A similar abundance profile is suggested by the circadian ten-plex. Of the stress profile genes, only LSAMP protein was significantly different following sleep deprivation, which showed a significant decrease on Day 3 as compared to Day 2 (q-value=0.029).

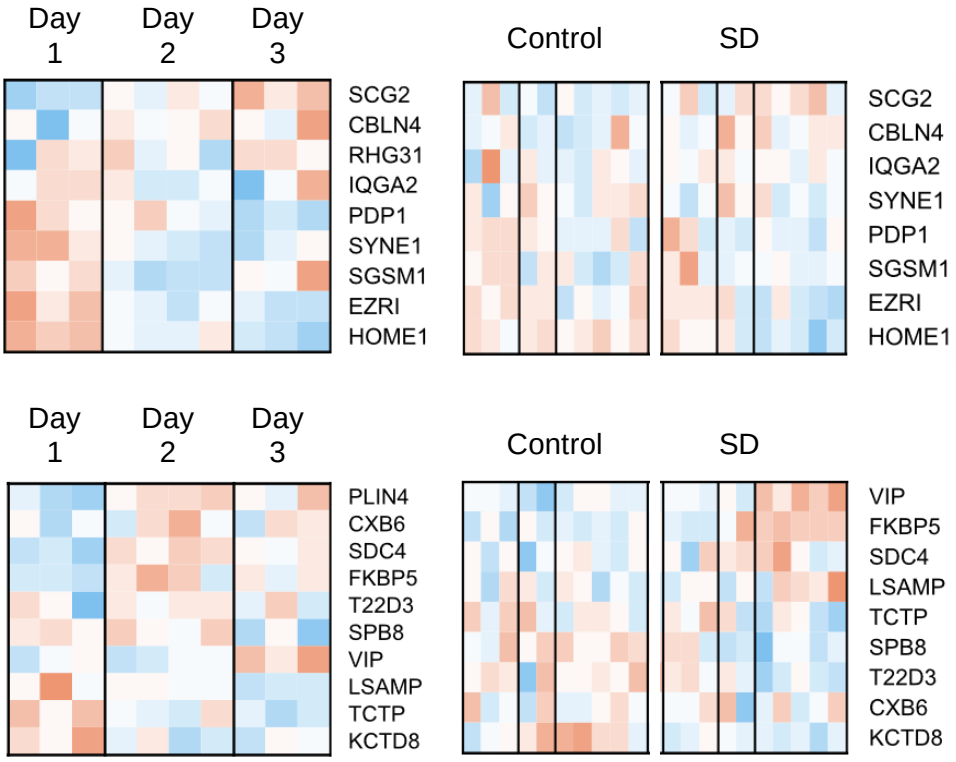

Figure 4.7. Heatmap of Proteins whose Transcript was Identified as Exhibiting a Homeostatic or Stress Profile: The abundance of detected proteins coded for by sleep dependent transcripts are plotted above, with homeostatic genes plotted in the upper set of heatmaps, and stress profile genes plotted in the lower set. The Z-score normalised abundance of protein is indicated by the colour, where red indicates a high abundance and blue indicates a low abundance. The leftmost tiles represent protein replicate data, taken from mice on Day 1 at 18:00 (no sleep deprivation), Day 2 (immediately following 12-hour sleep deprivation), and Day 3 (following 12-hour sleep deprivation). The rightmost maps show protein abundance from Control and Sleep Deprived mice collected 6 hours apart, where sleep deprivation takes place immediately following the third timepoint and ends immediately following the fifth timepoint.

4.2. Proteomic Changes consistent with Reduced Neuronal Excitability following Long Term Sleep Deprivation

Previous publications have extensively investigated the transcriptomic changes associated with sleep deprivation. In contrast, the proteomic changes associated with the state of wakefulness of animals is very poorly characterised. In this work we present two sets of TMT-based proteomic experiments: one set examined only three timepoints with biological replicates, whilst the second generated a timecourse style dataset, with only single replicate data. In this way we were able to statistically identify proteins whose abundance was affected by sleep deprivation, and then to qualitatively understand how their abundance profile changes over time.

The proteins whose abundance was significantly increased immediately following sleep deprivation were enriched in proteins whose function with phosphodiesterase function, whilst a reduced abundance of several synaptic proteins was also observed. An increased activity of phosphodiesterases such as PDE1a, PDE1b, PDE2a and PDE10a would be expected to reduce the intracellular abundance of cAMP and cGMP, dampening excitatory signalling pathways. Synaptic proteins downregulated included subunits of the NMDA (Gria2), AMPA (Grin1) and metabotropic glutamate receptor (Grm2) classes, the scaffold protein Homer1, as well as subunits of GABA symporters (SLC6A1, SLC6A11). Gria2 and Grin1 function in excitatory ionotropic glutamate signalling, whereas Homer1 promotes the release of intracellular calcium stores in response to metabotropic glutamate receptor activation. In contrast, GABA symporters act to rapidly reduce the concentration of extracellular GABA, leading to the cessation of inhibitory signalling. Therefore, immediately following sleep deprivation, it appears that the abundance changes of several proteins would be expected to dampen excitatory signalling pathways and enhance inhibitory pathways in the cortex.

Although these protein changes appear consistent with the concept of local sleep and activity induced inhibition of neuronal signalling, sleep deprivation followed by subsequent experimental measurement of cortical excitability in humans and rats indicate that neurones become more excitable following sleep deprivation, not less (Huber *et al.* 2013; Vyazovskiy *et al.* 2009; Yan *et al.* 2011). One possible explanation for this apparent contradiction is that changes in localisation or phosphorylation status of excitatory pathway constituents may offset the increase in abundance of inhibitory proteins. Another explanation may account the differences to differing experimental design, and that short-term sleep deprivation (e.g. 4 hours) has markedly different consequences for neuronal excitability than the longer term 12-hour sleep deprivation applied here. Consistent with this concept, spontaneous wakefulness in flies leads to increased neuronal activity, whilst prolonged sleep deprivation (29 hours wakefulness) eventually reduces neuronal activity and responsiveness (Bushey *et al.* 2015).

4.3. Proteomic Changes Consistent with Reduced Protein Synthesis and Cell Replication following Sleep Deprivation

As well as proteins related to neuronal firing being modulated by sleep deprivation, histones and protein ribosomal subunits are downregulated immediately following 12 hour sleep deprivation. Reduced histone abundance may indicate a reduction in cell division following sleep deprivation, which has previously been reported for cells in the hippocampus and cortical oligodendrocytes (Bellesi *et al.* 2013; Guzmán-Marín *et al.* 2003; Murata *et al.* 2017). Reduced ribosomal protein abundance may indicate a general suppression in protein synthesis, consistent with the hypothesis that sleep promotes anabolic pathways within the brain. Indeed, sleep deprivation has previously been shown to inhibit central protein synthesis in rodents (Naidoo *et al.* 2005; Ramm & Smith 1990; Tudor *et al.* 2016).

Intriguingly, the abundance of ribosomal and nucleosomal proteins remains reduced even following 24 hours recovery sleep opportunity, whilst the timecourse style dataset indicates that the abundance of these proteins remains lower than that of non-sleep deprived animals at all timepoints sampled following sleep deprivation. Therefore, total sleep deprivation may impair protein synthesis and cell division for up to two days or more, which may in turn have consequences for plasticity and learning.

4.4. Poor Overlap Between Proteomic and Transcriptomic Changes

Because we had access to a transcriptomic dataset of similar experimental design, we were able compare the abundance profile of detected proteins to the expression of the associated transcript. However, of the detected proteins identified as exhibiting a homeostatic or stress profile at the transcript level, only two (Homer1 and LSAMP) exhibited significantly different protein abundance following sleep deprivation. Remarkably, although sleep deprivation induces both Homer1a and LSAMP transcript expression, the abundance of the corresponding proteins appears to fall following sleep deprivation. In the case of Homer1, this may be driven by a decrease in the full length Homer1 protein, whose transcript abundance is comparatively unaffected by sleep deprivation. Overall therefore, the correlation between protein abundance and transcript profile is poor. The general lack of strong correlation between transcriptomic and proteomic responses has been previously reported (Ghazalpour *et al.* 2011), and may implicate post-transcriptional processes as an important regulator of protein abundance. Similarly, in the context of reduced ribosomal protein availability, an increase in transcript abundance may be required to maintain a constant level of short half-life proteins.

4.5. Suggested Further Experiments to Interrogate the Proteomic Effect of Sleep Deprivation

There is currently a relative absence of published proteomic studies investigating the effects of sleep deprivation in mammalian brain, and so there are several avenues for future research. Proteins are subject to several post-translational modifications, which can drastically change their function, localisation or target them for degradation. Because the synthesis of new proteins is suppressed during wakefulness compared to sleep (Naidoo *et al.* 2005), modulating the activity of proteins already present in the cell through phosphorylation may be the major pathway through which cells adapt to sleep deprivation. A phosphoproteomic screen of sleep deprived mouse brain, which can be achieved through the titanium dioxide enrichment of phosphopeptides before TMT-tag labelling (Possemato *et al.* 2017), may therefore provide insight into which signalling pathways are activated during prolonged wakefulness. Immunoaffinity based approaches can similarly be used to enrich proteins tagged with ubiquitin prior to mass-spectrometry based quantification (Schwertman *et al.* 2013), which may indicate proteins targeted for degradation during sleep deprivation. Local accumulation or depletion of proteins may play an important role in the regulation of sleep-wake cycles, yet be overlooked by global proteomics approaches. Subcellular fractionation of tissue homogenate, followed by proteomic interrogation could reveal important cellular events such as translocation of transcription factors to the nucleus, release of neuropeptides or neurotrophic factors into the extracellular space, or translocation of receptors to synapses.

4.6. Metabolomic Profiling of Sleep Deprived Mouse Cortex

The diverse transcriptomic and proteomic changes induced during sleep deprivation included several synaptic genes and proteins, indicating that cell-to-cell communication is modulated by sleep deprivation. We therefore hypothesised that the abundance of small molecule messengers released at synapses, such as glutamate, acetylcholine and histamine, may too be modified by sleep deprivation. Similarly, both transcriptomic and proteomic profiling of sleep deprived mice indicated an effect of sleep deprivation on ribosomes and mitochondrial oxidative phosphorylation, which is consistent with the hypothesis that the sleep-wake cycle may represent different stages of anabolism and catabolism within the brain. We therefore hypothesised that the abundance of molecules relating to energy production and macromolecule synthesis would be modulated by sleep deprivation and give insight into the metabolic state of the cell during wakefulness and sleep deprivation. We therefore carried out metabolomic analyses of sleep deprived mouse cortex using liquid-chromatography mass spectrometry (LC-MS). Using this technology, we were able to characterise the abundance of polar molecules, but not hydrophobic molecules such as long chain fatty acids. To also characterise the effects of recovery, we carried out a timecourse to collect tissue from mice that had been sleep deprived for 12 hours, with tissue from 3 mice being collected at each timepoint.

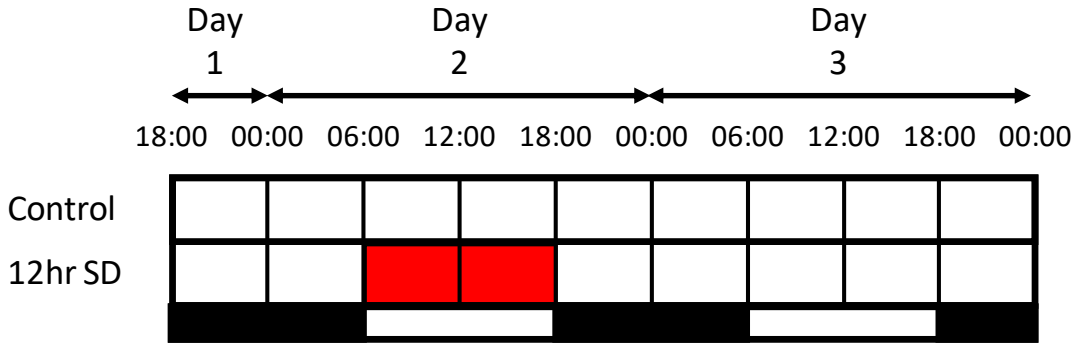

Figure 4.8. Experimental Design for Metabolic Characterisation of Sleep Deprivation in Mice: Cortex was collected from two groups of mice every 6 hours for a total of 54 hours. One group of mice had *ad libitum* sleep, whilst the other group was sleep deprived during the entire light phase of Day 2 (indicated by red boxes). Mice were trio housed and a single cage taken per timepoint to provide n=3 per timepoint. Whole cortex was removed whilst fresh, frozen on dry ice, and subsequently polar molecules were extracted and quantified.

Initially we carried out targeted metabolomic analysis to quantify the abundance of approximately 60 specific molecules in mouse cortex, however we were only able to identify and quantify 47 of these metabolites. Amongst the metabolites that we could not reliably quantify in our targeted analyses were neurotransmitters (e.g. dopamine, histamine) and pentose-phosphate pathway intermediates (e.g. ribulose 5-phosphate, ribose 5-phosphate). The abundance of molecules involved in glucose metabolism (e.g. glycolytic, pentose phosphate pathway and citric acid cycle intermediates), carnitine

conjugates and amino acids were quantified in order to identify whether there were changes in glucose utilisation, fatty acid oxidation or protein synthesis, respectively. ANOVA analysis was carried out on the abundance profile of molecules, and student t-tests were performed to compare individual timepoints between treatment groups. Remarkably however, no molecule exhibited statistically significant differences (i.e. adjusted p value < 0.05) in abundance as a result of 12-hour sleep deprivation, following correction for multiple testing.

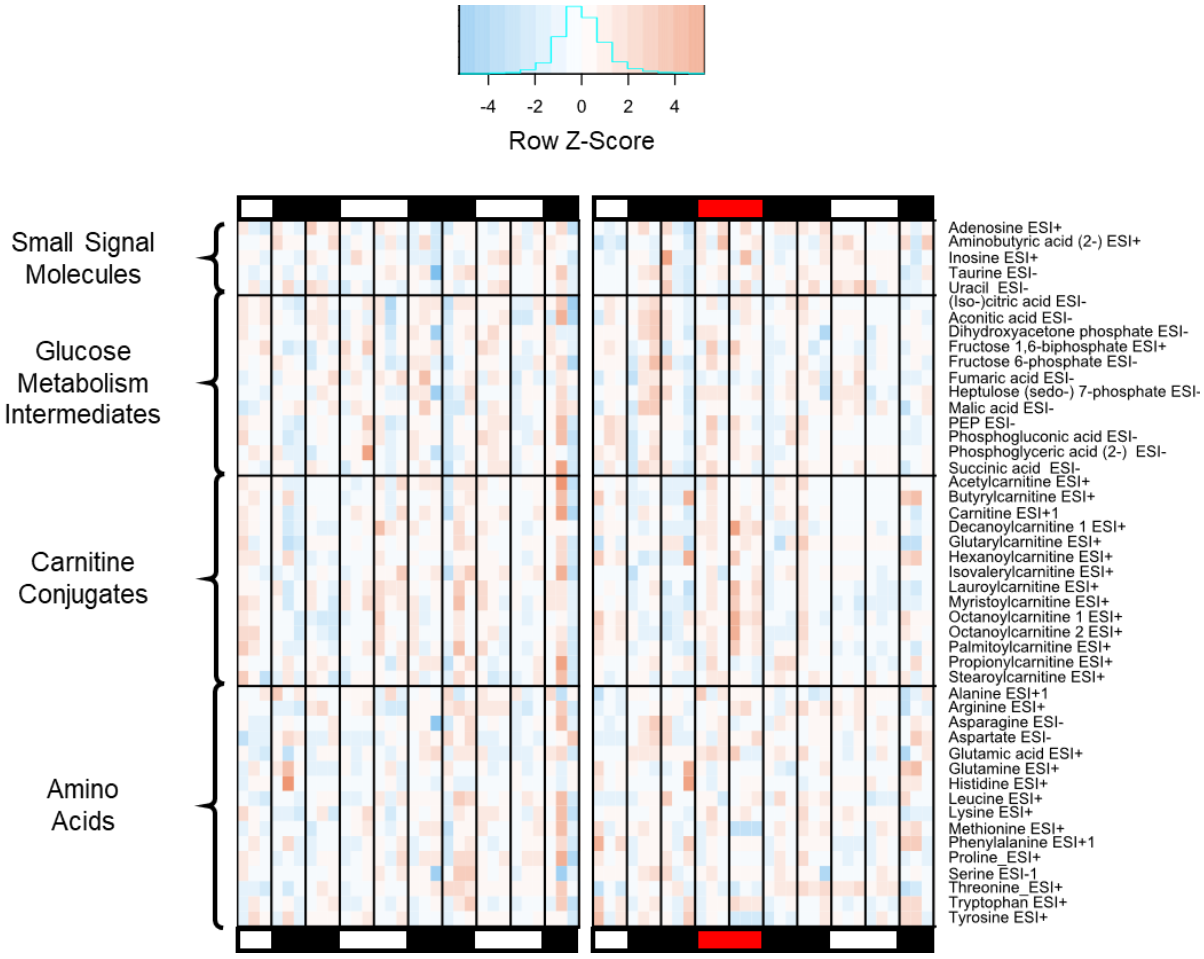

Figure 4.9. No Statistical Change in Metabolite Abundance was Identified through Targeted Metabolite Analysis: Cortex was collected from two groups of mice every 6 hours for a total of 54 hours. The black and white bars represent the light dark cycle. One group of mice had *ad libitum* sleep, whilst the other group was sleep deprived during the entire light phase of Day 2 (indicated by red boxes). Polar molecules were extracted and quantified through liquid chromatography-mass spectrometry, normalised to the number of ions detected from that sample, and the Z-score normalised replicates plotted above, where red indicates high abundance and blue represents low abundance. Control mice are plotted on the left plot, whilst mice subjected to sleep deprivation are plotted on the right plot. Molecules are grouped by their functional class and then alphabetically. Metabolite names are indicated to the right of the figure, whilst ESI (electrospray ionisation) indicates whether the detected ion was positively or negatively charged.

Aspartate was visually identified as a molecule fitting the idealised homeostatic profile, as it appeared to peak at the end of the dark phase in control mice, but continued to rise during sleep deprivation (see Fig 4.10.). Similarly, some other amino acids (arginine, methionine, tryptophan and tyrosine) appeared to show relatively large changes following 12 hour sleep deprivation, but were not statistically significant following correction for multiple testing. Similarly, adenosine did not show a statistical difference in expression profile or abundance following 12 hour sleep deprivation. Overall, visual inspection of individual molecular abundance profiles appeared to indicate that the variation in abundance of molecules between timepoints and treatment groups was usually low, which combined with a small replicate number (n=3) and multiple testing, likely severely limited the ability of this experiment to identify molecules whose abundance was dependent on the sleep wake cycle.

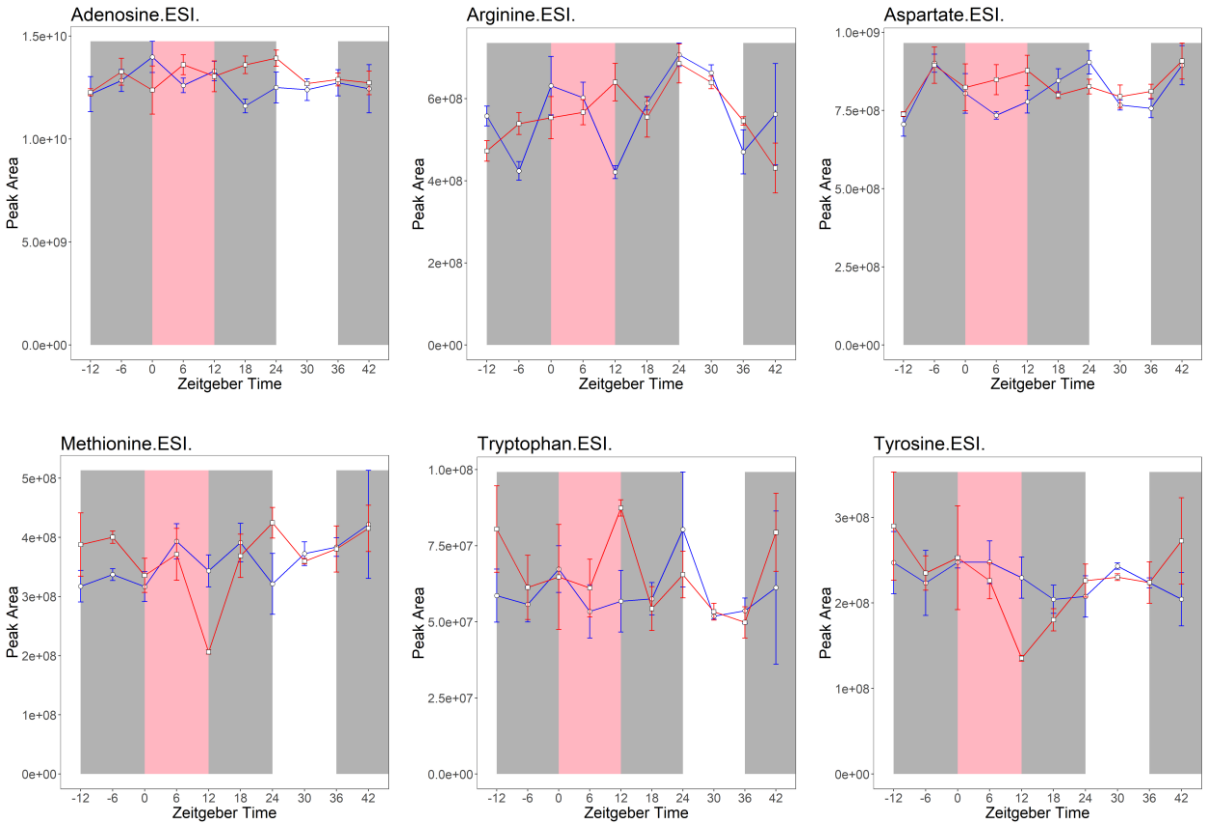

Figure 4.10. Individual Abundance Plots of Adenosine, Arginine, Aspartate, Methionine, Tryptophan and Tyrosine: The abundance of adenosine, arginine, aspartate, methionine, tryptophan and tyrosine in samples extracted from mouse cortex are plotted above. Data from mice with access to ad libitum sleep are plotted in blue, whilst those subjected to sleep deprivation are plotted in red. The grey bars represent the dark phase, whilst the pink section indicates the sleep deprivation period.

We also carried out untargeted analyses, whereby individual peaks corresponding to different ions are quantified in each sample, allowing a hypothesis free approach. Following quantification of peaks, identification of the molecules that those peaks correspond to can be attempted based on the molecular mass and charge of the ion. Of the 624 peaks that were assigned at least one molecular identity and was found in each sample, JTK analysis identified 3 peaks whose abundance oscillated with a 24-hour rhythm. A total of 8 peaks were identified as having a significantly different abundance profile following adjustment for multiple tests, including all 3 of the rhythmic peaks. Identification of the peaks indicated that the rhythmic molecules were possibly nicotinic acid derivatives and inosine monophosphate (IMP).

Table 14: Predicted Molecular Identities of Peaks Modified by Sleep Deprivation

Peak m/z Ratio	Rhythmic q-value	ANOVA q-value	Possible Molecular Identities
153.066	0.017	0.0048	N-methyl-pyridone-carboxamide, N-(Hydroxymethyl)nicotinamide
154.050	0.00049	0.028	Amino-hydroxybenzoic acid, Hydroxy-methylnicotinic acid, 3-Hydroxyanthranilic acid
347.039	0.024	0.028	Inosinic acid (IMP), 5-Formamidoimidazole-4-carboxamide ribotide (FAICAR), Mannopyranosyloxy-phosphonooxy-propanoic acid
141.066	0.72	0.024	Isonicotinic acid, Imidazolepropionic acid, Methylimidazoleacetic acid, 1,3-dimethyluracil, Niacin, Picolinic Acid
148.044	1.0	0.044	Methionine
165.077	1.0	0.0037	Deoxy -mannitol
169.062	1.0	0.031	Glycyl-4-hydroxyproline, N-Acetylglutamine
296.082	0.96	0.0080	Methylthioadenosine

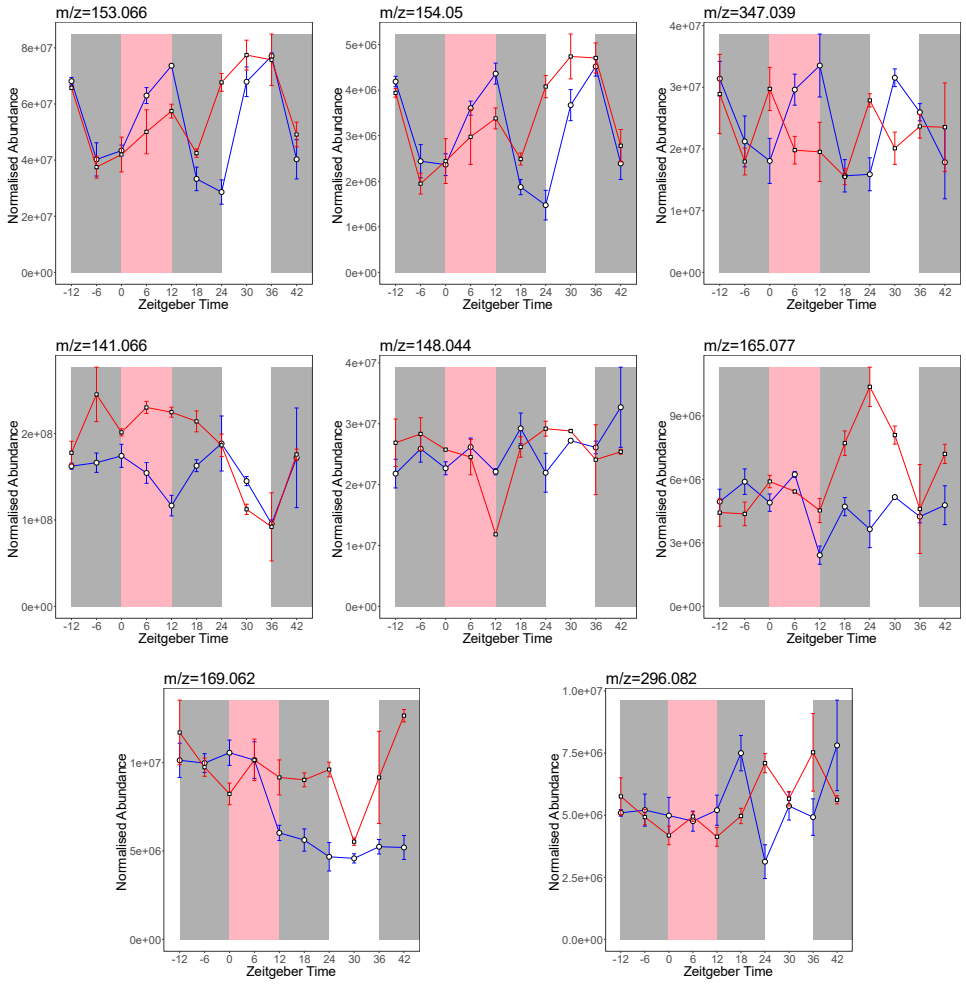

Figure 4.11. Individual Abundance Plots of Peaks Identified as Sleep-Wake dependent: The abundance of peaks identified as significantly disrupted by sleep deprivation by ANOVA analysis of untargeted metabolomic profiling of mouse cortex are plotted above. Data from mice with access to ad libitum sleep are plotted in blue, whilst those subjected to sleep deprivation are plotted in red. The grey bars represent the dark phase, whilst the pink section indicates the sleep deprivation period.

4.7. Metabolomic Profiling Implicates 3 Molecular Peaks as Potential Homeostats

Our metabolomic analyses of polar molecules within the cortex identified a total of 8 molecular peaks whose abundance profile was significantly affected by 12-hour sleep deprivation. Remarkably, the mass to charge ratio of three of these peaks match the expected masses of different nicotinamide molecules. Furthermore, the abundance of the molecules tentatively identified as hydroxymethyl-nicotinamide and hydroxymethyl-nicotinic acid demonstrated significant 24 hour oscillations in control animals, peaking at the end of the rest phase. In contrast, sleep deprived mice demonstrate a blunted increase of these same molecules during sleep deprivation, followed by an increase, rather than decrease, in abundance during the second half of the subsequent dark phase. Therefore, these molecules appear to demonstrate an abundance profile expected from a homeostatic molecule. Intriguingly, the molecule assigned as nicotinic acid demonstrates an approximately opposite pattern. Although the abundance of the molecule was not statistically rhythmic in control mice, visually the abundance appears to be rhythmic which peaks at the end of the active phase. Remarkably, the abundance of this molecule remains elevated during sleep deprivation, and so would appear to also demonstrate a homeostatic profile, but one which mirrors the profile of the hydroxymethyl-nicotinamide derivatives.

Table 15: Predicted Molecular Identities of Potential Small Molecule Homeostats

Peak m/z Ratio	Rhythmic q-value	ANOVA q-value	Possible Molecular Identities
141.066	0.72	0.024	Isonicotinic acid, Methylimidazoleacetic acid, Imidazolepropionic acid, 1,3-dimethyluracil, Niacin, Picolinic Acid
153.066	0.017	0.0048	N-methyl-pyridone-carboxamide, N-(Hydroxymethyl)nicotinamide
154.050	0.00049	0.028	Amino-hydroxybenzoic acid, Hydroxy-methylnicotinic acid, 3-Hydroxyanthranilic acid

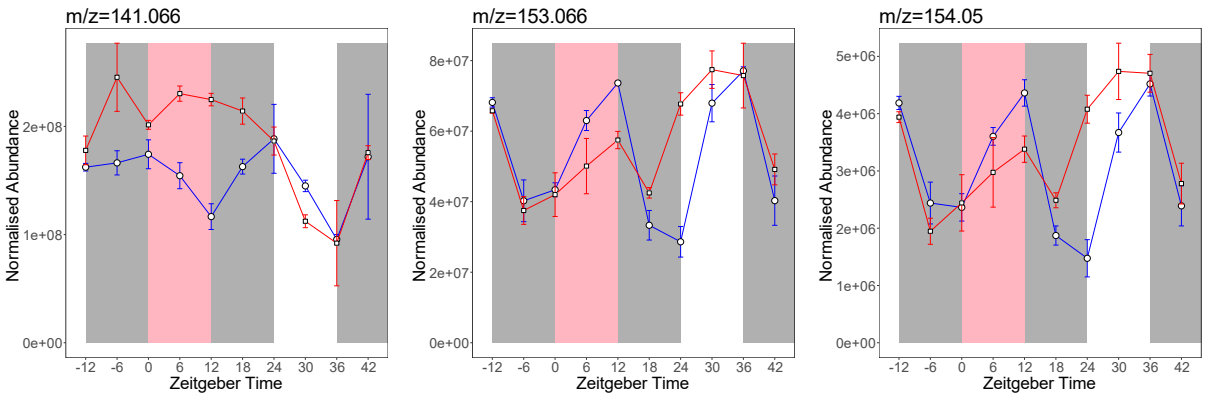

Figure 4.12. Individual Abundance Plots of Peaks Resembling a Homeostatic Abundance Profile: The abundance of 3 peaks appearing rhythmic in control animals and significantly disrupted by sleep deprivation are plotted above. Data from mice with access to ad libitum sleep are plotted in blue, whilst those subjected to sleep deprivation are plotted in red. The grey bars represent the dark phase, whilst the pink section indicates the sleep deprivation period. Information about their mass to charge (m/z) ratio, whether the abundance oscillates with a 24 hour rhythm in control mice and possible molecular identities, are outlined in the table.

Since methyl-pyridone-carboxamides are breakdown products of nicotinic acid, one interpretation of these mirrored profiles may be that the degradation of nicotinic acid is linked to sleep, and is inhibited during normal wake and sleep deprivation. However, the biological implications of this would be unclear, because nicotinic acid derivatives include both nicotinamide adenine dinucleotide (NAD) and nicotinamide adenine dinucleotide-phosphate (NADPH). Whilst NADH is involved in a range of catabolic processes (e.g. glycolysis, citric acid cycle, β-oxidation of fatty acids), the NADPH pool is typically participates in anabolic pathways and other pathways requiring strong reducing equivalents (e.g. fatty acid synthesis, reduction of glutathione).

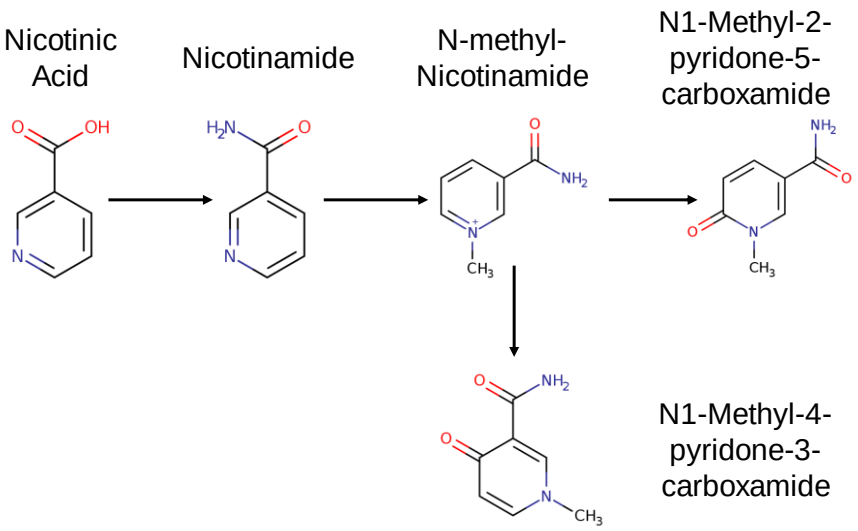

Figure 4.13. Sleep Deprivation may Reduce the Breakdown of Nicotinic Acid: Molecules whose abundance demonstrated a homeostatic profile may be involved in the breakdown of nicotinic acid. One possible identification for the peak at m/z=141.066 is nicotinic acid, which is high during the habitual active phase, low during the habitual rest phase, and elevated during sleep deprivation. Intriguingly, one possible identification of the peak at m/z=153.066 is N-methyl-pyridone-carboxamide, which is a breakdown product of nicotinic acid.

However, it is important to recall that these molecular assignments have been performed on the basis of the mass to charge ratio only, and therefore several chemical isomers are equally valid assignments. Indeed, the peak tentatively assigned as nicotinic acid may instead be methylimidazoleacetate, imidazolepropionate, dimethyluracil or picolinic acid, the products of histamine, histidine, methylxanthine and tryptophan breakdown, respectively. Similarly, the peak at (m/z=154.050) may equally be assigned as 3-hydroxyanthranilic acid, another product of tryptophan breakdown, and a precursor to picolinic acid. Therefore, another equally valid interpretation of the mirrored peak abundance profiles may be that the kynurenine pathway, through which both 3-hydroxyanthranilic acid and picolinic acid are produced, is dependent on the sleep-wake cycle. This possibility is intriguing, not least because another product of the kynurenine pathway is the potent NMDA-receptor agonist, quinolinic acid, which has previously been linked to sleep and to reduce sleep duration following intracerebroventricular injection (Cho *et al.* 2018; Milaśius *et al.* 1990). Further work is therefore required to determine which molecular assignments, if any, are correct.

4.8. The Global Effect of Sleep Deprivation on Cortex Metabolites appears modest

Overall however, the number of molecules demonstrating significant oscillations in control animals or that were identified as dependent on the wake state of the animal was low, especially when compared to the transcriptomic and proteomic datasets presented in this thesis. One possible explanation is simply that these findings reflect the biological reality, and that the abundance of only a handful of polar metabolites show variations large enough to be statistically identified with three replicates, following correction for multiple testing. A second possibility is that an artefact of the experimental design masked real changes occurring at the metabolite level. For example, animals are inevitably awake during the period leading up to tissue collection, independent of the time of day or previous sleep deprivation, due to the transfer and handling of them and their cagemates. Therefore, any molecule whose abundance rapidly changes in response to the current sleep-wake state of the animal would likely not be identified as wake dependent, because at the time of sacrifice those molecules would all be in their "wake" concentration.

Comparison of previous work to the data presented here is hindered by the almost complete absence of published metabolomic data originating from sleep deprived brain tissue. The lack of published studies may be consistent with attempted studies yielding no positive results. The only metabolomic data of 6 hour sleep deprived mouse cortex we are aware of is presented in Hinard *et al* (Hinard *et al.* 2012). In this publication, the authors conclude a role for sleep is membrane homeostasis, because the majority of the handful of metabolites identified as increased during sleep deprivation were lysolipids. However, because our approach only quantified polar metabolites, we were unable to determine the abundance of the hydrophobic lysolipids. Of the polar molecules detected, Hinard *et al* found increases in alanine and lactate, aspartate, methylimidazoleacetate and 4-hydroxybutyrate, and decreases in the abundance of methylthioadenosine and pantothenate, although the fold-changes observed was not reported. Our targeted metabolomics quantified alanine, but found very little variation between time points or sleep deprivation, whilst we were unable to quantify lactate through targeted metabolomics. Intriguingly, our targeted approach identified aspartate as trending toward a wake dependent abundance profile, whereas methylimidazoleacetate is a potential identity of the wake dependent peak at m/z=141.066. Methylthioadenosine was also statistically implicated as a potential wake dependent metabolite in this study, however the abundance profile in control animals is unusual, with great variation between timepoints in the latter half of the timecourse but almost none in first half.

Adenosine is perhaps the best characterised small molecule somnogen, and infusion of adenosine receptor agonists and antagonists into wake controlling centres has previously been shown to induce

and reduce sleep, respectively (Porkka-Heiskanen *et al.* 1997; Scammell *et al.* 2001; Schwierin *et al.* 1996; Zong-Yuan *et al.* 2005). Release of adenosine in an activity dependent manner has been reported from *in vitro* studies (J. & Nicholas 2007), whilst a microdialysis study carried out on cats indicated that extracellular adenosine in the cortex increases by approximately 20% during sleep deprivation (Porkka-Heiskanen *et al.* 2000). Our experiments indicate that adenosine levels show relatively little variation with time or sleep deprivation. Similarly, adenosine is not identified as a sleep dependent molecule by Hinard *et al* (Hinard *et al.* 2012). This discrepancy may reflect biological variation between rodents and cats. Another possibility is that whilst microdialysis based studies strictly measure the abundance of extracellular metabolites, mass spectrometry based analysis of tissue homogenate measures the combined abundance of both intracellular and extracellular metabolites. Therefore, discrepancies between microdialysis and mass spectrometry based studies may reflect changes in the localisation rather than the abundance of metabolites.

4.9. Further Experiments to Understand the Metabolomic Impact of Sleep Deprivation

Further metabolomic studies include confirming the identification of these molecules through the targeted tandem mass spectrometry of these peaks and comparison of the molecular fragments with the fragmentation spectrum derived from purchased standards. Following a firm identification of a sleep related molecule, that molecule could be intracerebrally injected and its effects on sleep determined through EEG analyses. Alternatively, the effect of the infusion of inhibitors of the relevant pathway could be determined.

An alternative approach to determining what aspects of metabolism are important in the regulation of sleep is to screen the effect of several small molecule inhibitors of metabolic pathways for a sleep phenotype. Having identified a small molecule inhibitor that affects sleep duration or timing, the implicated pathway could then be investigated. Although an untargeted screen is possible in mice, the cost of housing, EEG implantation and surgery required for infusion of small molecules would hinder the discovery of sleep modulating drugs. One possibility is to perform a drug screen in Drosophila by introducing drugs into their food, however controlling the precise timing of ingestion and the dosage of drug is difficult. Ideally, a large scale drugs screen would involve the use of a mammalian cell line model, because cell lines not only offer a mammalian system whose environment is easily controlled, but also are far less costly and more easily scaled than mouse colonies. However, no widely available cell line based model of sleep deprivation currently exists.

5. Modelling Sleep Deprivation *in vitro*

This section details our efforts to create an *in vitro* model of sleep deprivation using a human derived neuroblastoma cell line. *In vitro* models are often lower cost, higher throughput and less regulated than mammalian models, facilitating high-throughput studies or small molecule screens. We first recreate experiments carried out on primary neurones, and find that neuroblastoma cell lines retain a transcriptional response to excitatory neurotransmitters. We then use optogenetic tools to create cell lines that can be subjected to the high throughput and straightforward application and withdrawal of stimulation. Ultimately, we perform a timecourse style experiment to identify the transcriptomic effects of 12 hour activation of this cell line. We find several functional gene groups that have previously been associated with sleep deprivation are upregulated following the prolonged activation of SH-SY5Y cells, indicating that it is possible to model sleep deprivation *in vitro* in a high throughput manner.

5.1.1. Previous use of *in vitro* models in sleep research

Sleep deprivation driven changes in transcription and intracellular protein expression indicate that cells are sensitive to the wake state of the animal. Furthermore, the observation that regions of the cortex can enter a sleep like state despite the animal remaining awake (Vyazovskiy *et al.* 2011) suggests that groups of neurons may possess an intrinsic ability and drive for sleep. In trying to understand what is the minimum assembly that exhibits sleep like behaviour, researchers have turned to *in vitro* studies, predominantly using tissue explants and primary neuron cultures.

In a seminal paper linking the *in vitro* properties of neurons to the *in vivo* effects of sleep deprivation, Hinard et *al.* identified that dissociated cortical neurons treated with a cocktail of excitatory drugs exhibit changes that closely resemble those induced by wakefulness *in vivo* (Hinard *et al.* 2012). After 7 days in culture, primary mouse neurons developed synchronous, low frequency firing patterns, similar to those of sleeping mice. Exposure to excitatory neurotransmitters caused a dose dependent decrease in synchrony, similar to that seen in waking mice. Excitatory stimulation of primary neurons also induced similar transcriptomic changes as seen in sleep deprived mice, and both the cocktail and sleep deprivation led to a reversible phosphorylation of metabotropic glutamate receptors. Stimulation of primary neurons also led to a 40% increase in oxygen consumption and the production of several lysolipids, which are elevated in the serum of sleep deprived humans (Davies *et al.* 2014). Therefore, Hinard et al. demonstrated several molecular correlates of sleep and wake are preserved in primary neuron cultures, introducing the possibility of a reductionist approach to understanding sleep.

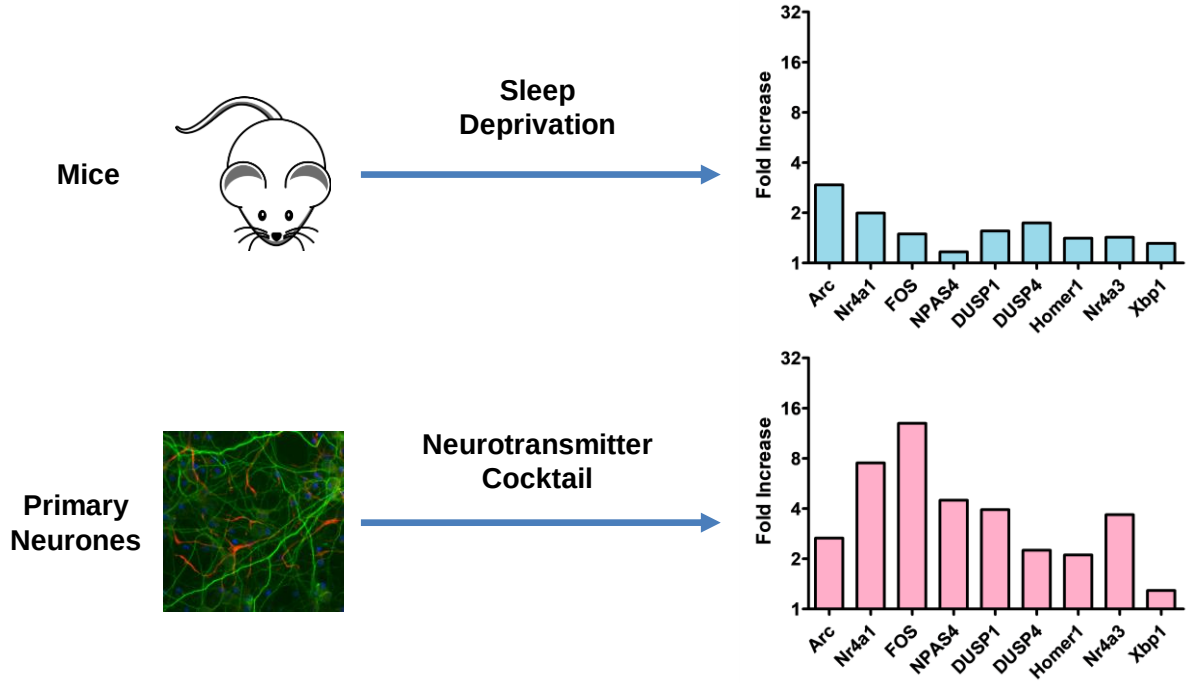

Figure 5.1. Genes Induced by Sleep Deprivation are Induced in Primary Neurones Treated with an Excitatory Cocktail: Hinard *et al* showed that primary mouse neurones treated with a cocktail of excitatory neurotransmitters induces several genes also induced in mouse cortex during sleep deprivation. Data for these plots is taken from Hinard *et al*, and represents the expression of genes relative to unperturbed mice or cells.

5.1.2. SH-SY5Y cells provide a source of Human derived Neuronal like cells

A reductionist approach to understanding sleep would carry several experimental benefits. Being able to control the environment that cells are exposed to much more precisely than *in vivo* allows the researcher to more easily characterise the effects of small molecules on cell biology. The comparatively low cost of *in vitro* systems also facilitates high throughput studies, whilst having a homogenous cell population *in vitro* removes uncertainty surrounding which cells in a tissue sample are responsible for the molecular changes identified. However, the choice of which cell type to use as a model for *in vitro* studies is crucial for the validity and potential uses of that model. Organotypic brain slices or primary neurones derived from animals represent one approach to culture cells with a neuronal phenotype, but suffer from being laborious to generate and being derived from rodents. Alternatively, human stem cell culture offers the possibility of generating human neurones for *in vitro* studies, but is very expensive and laborious, limiting its use in high-throughput studies. In contrast, transformed cell lines offer a comparatively inexpensive approach to readily generate large numbers of human derived samples. A fundamental limitation of cell lines in research, however, is the uncertainty surrounding how closely transformed cells recapitulate the functions and phenotypes

demonstrated *in vivo*. Therefore, the choice of cell line is an important consideration that determines the ultimate validity and limitations of the final model.

Several human neuronal model cell lines have been generated, but one of the most commonly used and best characterised are SH-SY5Y cells. SH-SY5Y cells are of neuroblastoma origin isolated from a bone marrow metastasis (Biedler *et al.* 1978) and is a thrice subcloned semi-adherent derivative of the human SK-S-SH neuroblastoma cell line, selected for on the basis of neuroblast morphology. SH-SY5Y cells were originally shown to synthesise acetylcholine, dopamine and GABA (Biedler *et al.* 1978), and since have also been shown to produce norepinephrine through dopamine hydroxylase (Kume *et al.* 2008). The dopaminergic phenotype of the SH-SY5Y cell line has led to its widespread use as a Parkinson's Disease model and also in general neurotoxicity research, leading to its in-depth characterisation.

Typical for a cancer derived cell line, SH-SY5Y cells exhibit genetic abnormalities compared to healthy human cells, including a complete trisomy of chromosome 7. However a whole exome sequencing study suggested that the genetic defects seen in SH-SY5Y cells are expected to only have a small effect on Parkinson's disease and Huntington's disease related pathways (Krishna *et al.* 2014), indicating that genetic abnormalities of this cell line does not preclude SH-SY5Y cells from modelling some aspects of neuronal biology.

Several differentiation protocols have been developed for SH-SY5Y cells, with the aim of creating a phenotype that more closely resembles mature neurons. Differentiation is characterised by the withdrawal from the cell cycle, the extension of long neurite structures and the expression of mature neuronal markers (Lopes *et al.* 2010). Retinoic acid is the most commonly used differentiation agent for SH-SY5Y cells (Påhlman *et al.* 1984), but other approaches use phorbol esters (Påhlman *et al.* 1981), dibutyryl cAMP (Kume *et al.* 2008) or serum deprivation (Shipley *et al.* 2016). Some studies further supplement the differentiation medium with cholesterol (Sarkanen *et al.* 2007), brain derived neurotrophic factor (BDNF) (Encinas *et al.* 2000) or Vitamin D (Celli *et al.* 1999), and the length of published differentiation protocols range from 24 hours to three weeks. The variety of differentiation protocols can make findings from separate studies using SH-SY5Y cell culture difficult to reconcile. Indeed, the precise method of differentiation can drive SH-SY5Y cells toward distinct neuronal phenotypes. For example, phorbol ester treated SH-SY5Y cells produce 50 fold higher levels of norepinephrine compared to retinoic acid treated cells (Påhlman *et al.* 1984), whereas retinoic acid treatment drives higher levels of muscarinic receptor and acetylcholine synthesis (Adem *et al.* 1987). Therefore the differentiation protocol used in experiments, if any, has to be carefully chosen.

Previous studies have shown that SH-SY5Y cells resemble neurons in several aspects, including neurotransmitter synthesis and synaptic packaging (Sarkanen *et al.* 2007), having an electrically active membrane (Forsythe *et al.* 1992), and expression of neuron specific markers, such as NeuN (Agholme *et al.* 2010). SH-SY5Y cells have also been shown to exhibit neuronal characteristics linked to sleep, such as sensitivity to anaesthetic (Zhang *et al.* 2009) and induction of cytokines following intense stimulation, which remarkably is attenuated by treatment with the sleep associated melatonin (Parameyong *et al.* 2013). Therefore, SH-SY5Y cells may prove a useful system to model molecular and cellular aspects of wake and sleep.

5.1.3. Optogenetic Tools Available to Researchers

In recent years, light sensitive proteins have been exploited by researchers to trigger cellular signalling pathways with extraordinary temporal precision. Like neurotransmitter receptors, the detection of light is typically coupled to the production of secondary signalling molecules or the movement of ions across cellular membranes. Different domains of life have independently evolved sensors that incorporate retinoid cofactors, however functional and mechanistic differences between prokaryotic and eukaryotic sensors introduce important practical considerations.

5.1.3.1. Rhodopsin Based Light Sensors

Rhodopsin is the G-protein coupled receptor (GPCR) protein responsible for light detection within rod cells of mammalian eyes. Rhodopsin is structurally similar to ligand gated GPCRs, but is instead sensitive to light. Light absorption by its 11-cis retinal cofactor moiety induces a change in configuration to all-trans retinal, in turn inducing conformational changes within rhodopsin that activates its associated G-protein. The all-trans retinal cofactor is then removed from the protein and replaced with a new 11-cis cofactor, restoring light sensitivity, whilst the all-trans retinal is recycled by nearby cells. Rhodopsin activates a G-protein which stimulates cGMP hydrolysis and subsequent hyperpolarisation of the neuron. However chimeric receptors have been engineered that combine the light sensitivity of rhodopsin and the protein-protein interaction partners of adrenergic receptors (Airan *et al.* 2009; Kim *et al.* 2005), adenosine 2A receptor (Li *et al.* 2015) and mu opioid receptor (Siuda *et al.* 2015). These engineered opsins can be used not only to interrogate intracellular signalling pathways of specific receptors, but also as a tool to trigger a variety of intracellular signalling pathways in response to light.

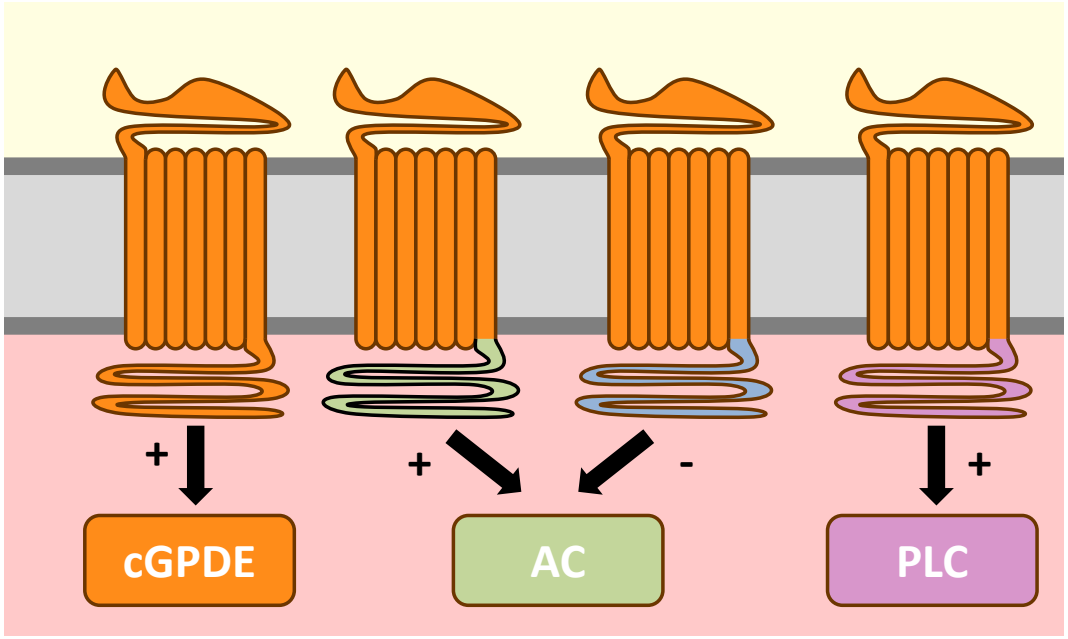

Figure 5.2. Rhodopsin based Optogenetic tools operate through Secondary Signal Molecules: Mammalian rhodopsin actvates cGMP phosphodiesterases (cGPDE) in response to light. Chimeric receptors combining rhodopsin with the intracellular domains of other receptors create light sensitive tools that activate distinct signalling pathways. A rhodopsin A2A receptor chimera activates adenylate cyclase (AC) in response to light, leading to an increase in cyclic AMP, whereas a mu opiod receptor chimera inactivates AC. Similarly, a beta-adrenergic receptor based chimera stimulates phospholipase C (PLC) in response to light, inducing inositol triphosphate and diacylglycerol based signalling cascades.

5.1.3.2. Microbial Opsins

In contrast to the secondary signalling molecule mediated activation or inhibition of neurons triggered by light sensitive rhodopsin based tools, microbial retinal based receptors are typically ionotropic. The best characterised microbial opsin is Channelrhodopsin 2 (ChR2), a blue light sensitive proton and cation channel isolated from the alga *C. reinhardtii* (Nagel *et al.* 2003). Expression of ChR2 in HEK293 cells, Xenopus oocytes and mouse neurons is sufficient to generate light dependent currents across the membrane and trigger neuronal firing *in vivo* (Boyden *et al.* 2005). Like rhodopsin, light absorption drives conformational changes in ChR2 through a change in configuration of a retinal cofactor. However, unlike rhodopsin, the dark acclimatised ChR2 contains all-trans retinal, and the 13-cis retinal produced upon light exposure spontaneously returns to an all-trans configuration *in situ*.

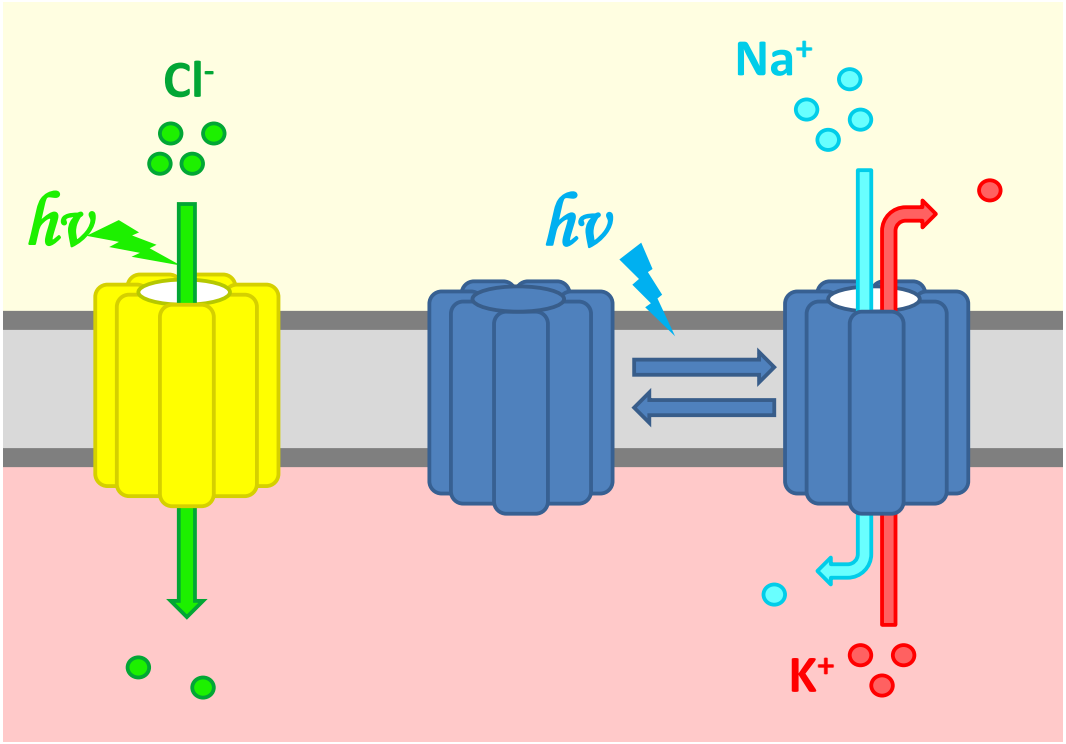

Figure 5.3. Microbial Opsins are Ionophoric: In contrast to mammalian rhodopsin, microbial opsins directly mediate the movement of ions. Halorhodopsin couples light absorption to the inward pumping of chloride ions, hyperpolarising the membrane. Channelrhodopsin 2 is a light gated channel, which once opened in the presence of light facilitates the passive diffusion of protons and cations across the membrane.

Exposure to blue light induces ChR2 mediated currents to start within 2ms, which reduce with a half-life of 14ms after cessation of light exposure (Lin *et al.* 2009). Because of the almost instantaneous induction of electrical activity within neurons, ChR2 expression in neurons can drive rapid and extraordinary changes in behaviour. For example, optogenetic activation of neurons controlling aggression in mice is sufficient to switch males from attacking to grooming pups (Wu *et al.* 2014). The clear potential of ChR2 as a tool in neuroscience has motivated several studies that examine the biophysical characteristics of ChR2, in turn facilitating the optimisation of ChR2 through mutagenesis.

ChR2 is 50% activated by 470nm wavelength light at an intensity of 1mW/mm^2, which is significantly higher than the intensity of direct sunlight (Benedetti *et al.* 2001). Once opened, ChR2 facilitates the passive diffusion of protons and cations across the membrane, showing the highest conductivity for protons, followed by sodium, potassium and calcium. Therefore, under physiological conditions, photocurrents elicited by ChR2 expressed in neurons are dominated by comparably sized sodium and proton currents (Schneider *et al.* 2013). Initial studies of ChR2 photocurrents revealed that its photocycle is not a simple binary switch between open and closed. Instead, at the beginning of a flash, the elicited photocurrent transiently peaks (I_0) before decaying to a stationary conductance (I_S) for the remainder of the flash. This process is termed desensitisation. For wild-type ChR2, the peak

photocurrent is approximately fivefold higher than its stationary photocurrent (Nagel *et al.* 2003). Recent exposure to light reduces the peak photocurrent elicited by subsequent flashes, in a process termed inactivation, reducing the probability of triggering an action potential. ChR2 requires approximately 30 seconds of darkness to recover from inactivation, which can be accelerated by exposure to 570nm light (Lin *et al.* 2009). The large decrease in conductivity following previous light exposure and relatively slow recovery presents practical problems for researchers wishing to drive repeated or rapid depolarisation within the same cells.

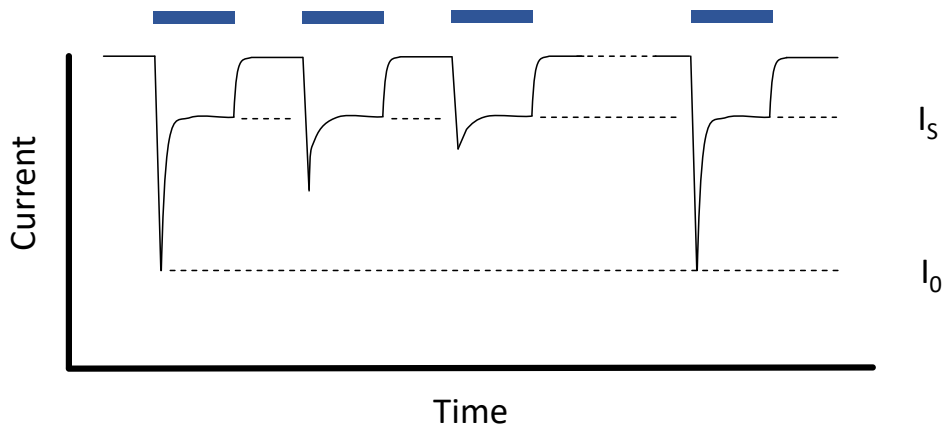

Figure 5.4. Repeated Stimulation reduces Channelrhodopsin 2 mediated Photocurrents: Channelrhodopsin 2 (ChR2) opens in response to blue light (represented by the blue rectangles above the plot), however the current elicited is not constant. After illumination, a peak current (I_0) is achieved that rapidly decays to a much reduced stationary current (I_s). The difference between I_0 and I_s is a measure of the desensitisation of ChR2. Repeated flashes also reduce the elicited I_0, in a process termed inactivation. However, ChR2 gradually recovers from inactivation in darkness, with I_0 being almost fully restored after 30 seconds of darkness.

5.1.3.3. Refinement of Channelrhodopsin as an Optogenetic Tool

The clear potential but practical limitations of wild type channelrhodopsin inspired the search for better performing opsins through mutagenesis and genome mining. Today there is an extensive toolbox of microbial opsins, and there is no longer any scenario where wild-type ChR2 is the best suited experimental tool available (Klapoetke *et al.* 2014).

ChR2 (H134R) was identified based on the homology of Channelrhodopsin with the well characterised Bacteriorhodopsin, and exhibits increased photocurrents but slower kinetics (Nagel *et al.* 2005). Similarly, ChR2 (T159C) was found to produce even greater photocurrents with even slower closing kinetics (Berndt *et al.* 2011). Conversely, ChR2 (E123T) produces much faster kinetics and is able to drive a much higher frequency of action potentials *in vivo*, but suffers from reduced photocurrents

(Gunaydin *et al.* 2010), reflecting that high photocurrents are associated with slow kinetics (Mattis *et al.* 2012). Step function opsins are produced by the mutation of C128, characterised by a channel closing rate orders of magnitude greater than wild type ChR2 (Berndt *et al.* 2009). The slow closing rate of step function opsins has the effect of increasing apparent light sensitivity by a few orders of magnitude. However, the maximum photocurrent and the associated change in membrane potential is significantly reduced.

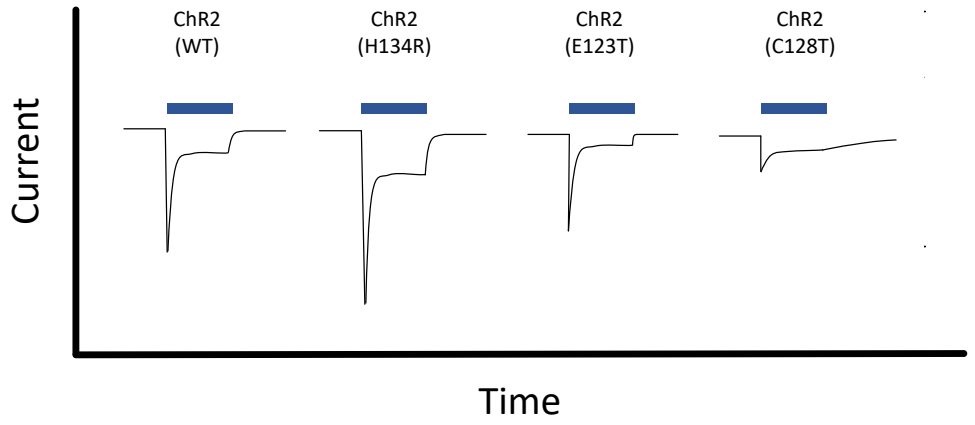

Figure 5.5. Point Mutations Alter the Magnitude and Kinetics of Photocurrents: Mutation of H134 or T159 increases the photocurrent of Channelrhodopsin 2, but also results in slower kinetics. In contrast, E123 mutants generate smaller photocurrents but faster kinetics. Mutation of C128 greatly reduces the peak photocurrent and channel closing rate, conferring an apparent increase in light sensitivity.

A second strategy employed to improve ChR2 as an optogenetic tool has been to engineer a chimera channel by combining ChR2 with ChR1, a second opsin isolated from *C. reinhardtii* (Sineshchekov *et al.* 2002). Unlike ChR2, ChR1 produces very small photocurrents when expressed *in vivo*, however does not appear to have significant desensitisation. Lin et *al.* reasoned that combining regions of ChR1 and ChR2 may produce a chimera with sizeable photocurrents but with reduced desensitisation. Indeed the chimeric opsin produced, termed ChIEF, has similar kinetics and similar peak photocurrent as ChR2, however displays only 20% desensitisation, and therefore has stationary photocurrents approximately fourfold higher than wild-type ChR2 (Lin *et al.* 2009), allowing ChIEF to drive more rapid chains of action potentials *in vivo*.

More recently, genome mining has uncovered 61 ChR2 related opsins in microbial algae (Klapoetke *et al.* 2014). Three opsins in particular were found to have characteristics that make them attractive for use as an optogenetic tool. The opsin Chrimson exhibits a greatly red-shifted absorbance spectrum,

with a peak absorbance of 600nm. Its red shifted spectrum allows the independent activation of distinct neural populations in close proximity, by expressing Chrimson in one population and a blue light sensitive opsin in the other. However, the kinetics and photocurrents of Chrimson are otherwise comparable to ChR2, limiting its use outside of multiwavelength control of neuronal activity. In contrast, the slightly green-shifted Chronos exhibits very fast kinetics and is able to drive action potentials at rates exceeding 50 Hz, but nevertheless exhibits much larger photocurrents than ChR2 with reduced desensitisation and is able to drive action potentials at much lower light intensity. Therefore, the generally superior parameters of Chronos compared to ChR2 make Chronos an attractive tool for optogenetic activation of cells in a wide variety of experimental designs. Finally, the opsin CoChR has the largest photocurrent generated by any identified microbial opsin by blue or green light, due to a combination of very high single channel conductance and excellent trafficking to the cell membrane. Coupled with its low desensitisation and rapid recovery from inactivation, CoChR can drive repeated activation of neurons at low light levels (Schild & Glauser 2015). However, CoChR does exhibit slightly slower closing kinetics than ChR2, which may limit its general use.

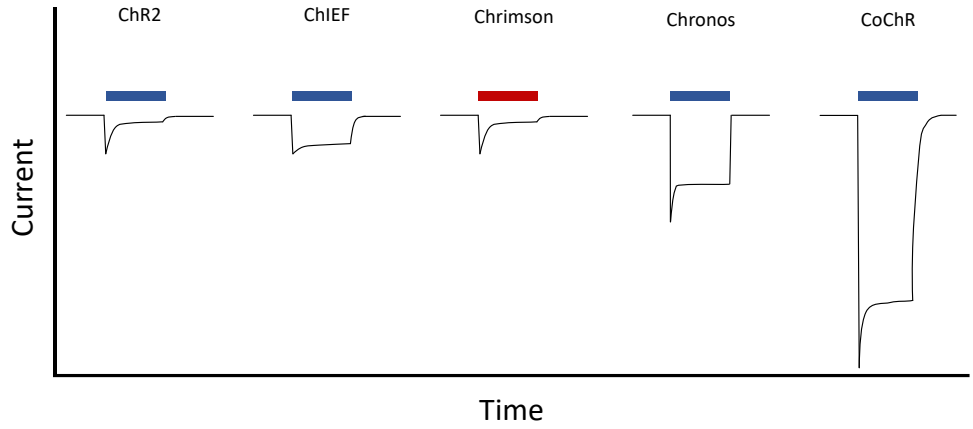

Figure 5.6. Genome Mining and Chimeric Opsins provide Superior Optogenetic Tools: ChIEF, an engineered chimera of Channelrhodopsin 1 and Channelrhodopsin 2 (ChR2), shows similar peak photocurrents as ChR2, but significantly reduced desensitisation and inactivation. Chrimson is a naturally occurring red light sensitive opsin, with comparable kinetics and photocurrent as ChR2. Chronos has rapid kinetics and sizeable photocurrents, whereas CoChR has very large photocurrents and demonstrates excellent trafficking to the cellular membrane in mammalian cells.

5.1.3.4. Inhibitory Microbial Opsins

Complementary to microbial light-gated cation channels are a group of microbial light driven pumps that hyperpolarise cells. The first of these pumps to be expressed *in vivo* was the chloride pumping halorhodopsin isolated from *N. pharaonis* (Schobert & Lanyi 1982), which couples absorption of yellow light to the inward movement of chloride ions, thereby hyperpolarising and silencing neurons (Gradinaru *et al.* 2008). The distinct absorption spectra and functions of ChR2 and halorhodopsin made it an attractive tool for the bidirectional control of the same cell (Han *et al.* 2009). However, halorhodopsin has a tendency to aggregate in the endoplasmic reticulum when expressed at high levels, and even when fused with motifs to enhance trafficking can fail to entirely silence neurons. In contrast, the light driven proton pump archaerhodopsin, isolated from *H. sodomense,* was found to almost totally silence neurons in response to light (Chow *et al.* 2010; Han *et al.* 2011). However, the comparatively high light intensity required for pumps and the use of protons to carry charge across the membrane may result in local heat and pH changes following long term light exposure.

Microbial light-gated anion channels provide an alternative to pump based inhibition of neurons. Through the mutagenesis of pore residues of ChR2, the normally excitatory cation conducting opsin can be converted to an inhibitory chloride permeable channel, allowing the temporally precise silencing of neurons *in vivo* (Berndt *et al.* 2014; Wietek *et al.* 2014, 2015). Similarly, genome mining has uncovered naturally occurring microbial anion channels in *Guillardia theta*, which causes rapid silencing of primary neurons at lower light levels than anion permeable ChR2 variants (Govorunova *et al.* 2015).

5.1.3.5. Comparison of Eukaryotic and Prokaryotic Optogenetic Tools

The optogenetic toolbox available to researchers wishing to control neuronal activity includes both ion mediated tools derived from prokaryotes and secondary signalling molecule mediated tools, largely derived from eukaryotes. The most appropriate tool depends on several aspects of the experimental design, including the system, duration of stimulation and the temporal resolution required. Whilst microbial opsins offer extremely precise control of action potential firing, driving inappropriate firing patterns *in vivo* may induce a supraphysiological response and result in unusual behavioural outputs. Under these circumstances, the activation of cAMP signalling pathways by rhodopsin based tools to generally elevate neuronal activity may produce more physiologically relevant results. In contrast, modified rhodopsin based tools are susceptible to arrestin mediated inhibition and require recycling of the retinal cofactor. Therefore microbial opsins may be better suited for repeated stimulation or in systems where the cofactor may not be effectively recycled.

5.1.4. *In vitro* Research Aims

In the body of work presented below, we outline our efforts to generate an *in vitro* model of sleep deprivation using SH-SY5Y cells and optogenetic tools. The development of the model is guided by transcriptomic correlates of sleep deprivation in mice. Although primary neurons have previously been identified as a promising system with which to study molecular aspects of sleep, extraction and culture of primary neurons is laborious, and do not allow many advantages over established *in vivo* models for large scale studies. In contrast, a cell line based model may provide a useful system in which preliminary drug screens could be carried out in a high throughput manner.

5.2.1. Excitation of SH-SY5Y Cells Stimulates Gene Expression

Hinard *et al.* (2012) showed that treating primary mouse neurones with a cocktail of wake associated neurotransmitters for six hours causes changes at the transcriptomic level that resemble changes that occur after *in vivo* sleep deprivation in mouse brain. As the first stage in determining whether cell lines could be used as an appropriate model for sleep deprivation, we treated human neuroblastoma SH-SY5Y cells with a cocktail of wake-associated neurotransmitters, (containing noradrenalin, histamine, carbachol, dopamine, serotonin, kainic acid, ibotenic acid, AMPA and orexin) for 4 hours, and quantified the gene expression of 9 genes previously associated with sleep deprivation. We found that, normalised to GAPDH expression, 8 of the 9 target genes significantly increased after treatment with the cocktail (Fig 5.7.).

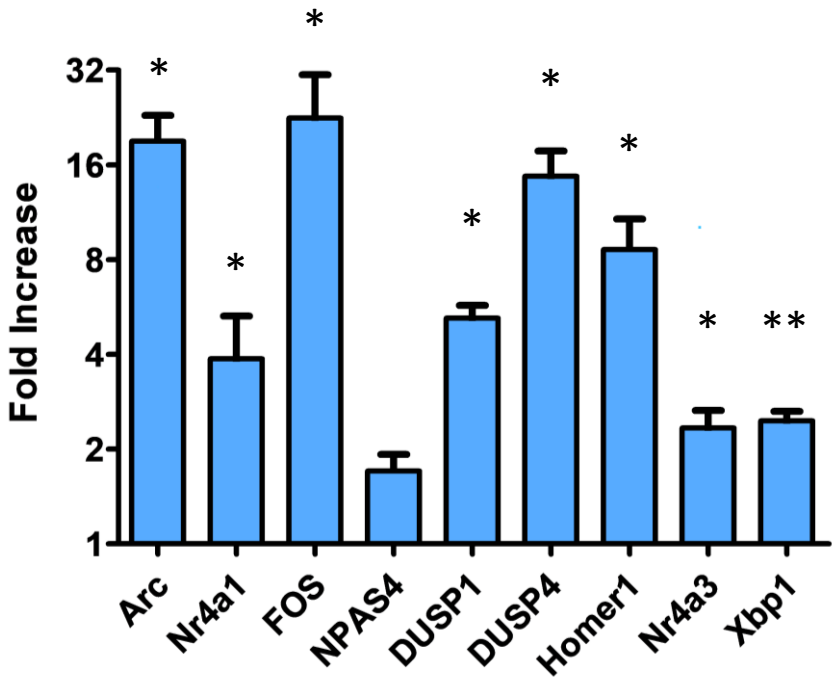

Figure 5.7. Sleep Deprivation Markers are Induced by Excitatory Neurotransmitters in SH-SY5Y Cells: Human Neuroblastoma cells (n=6) were treated with a cocktail of waking neurotransmitters for 4 hours. The expression of several sleep deprivation associated transcription factors was quantified relative to GAPDH by qPCR, and plotted relative to untreated controls (data are mean ± SEM).

p-values were determined using a Student t-test, comparing the treated to untreated group for each gene, and the p-value indicated by the number of asterisks above the relevant gene.

* - $p<0.05$, **-$p<0.01$

5.2.2. Activation of Channelrhodopsin Stimulates Gene Expression in SH-SY5Y Cells

The upregulation of sleep deprivation markers in SH-SY5Y cells after neurotransmitter cocktail treatment indicated that SH-SY5Y cells retain the cellular machinery required to respond to excitatory signals at the molecular level. We therefore decided that these cells could be used to model transcription and other molecular changes that occur during sleep deprivation.

There are, however, three major disadvantages of using a stimulatory cocktail to model sleep deprivation. Firstly, during long term activation, as the neurotransmitters are degraded and their receptors are attenuated through arrestin mediated pathways, the stimulatory effect of the cocktail will vary significantly over time. Secondly, modelling recovery after prolonged activity necessitates a medium change to remove the excitatory neurotransmitters. A medium change would also remove any molecules released into the extracellular space during activity, which may otherwise play a role in the subsequent recovery phase, thereby confounding experiments attempting to model recovery sleep in this model. Thirdly, repeated medium changes would ultimately limit the use of the final model in high-throughput screens of drugs that modulate the molecular response to sleep deprivation.

We reasoned, however, that optogenetic tools, which have been used *in vivo* to activate and silence neuronal activity with very precise temporal resolution, might offer several advantages over the neurotransmitter cocktail. By using light as a stimulus, channelrhodopsin would not only activate the cells in a convenient and high-throughput manner, but also allow rapid withdrawal of stimulation. In this way, we hoped to be able to model the molecular changes associated with prolonged neuronal firing and subsequent recovery. Since the ultimate end goal of modelling sleep deprivation in cells was using -omics tools to generate a full picture of the molecular intracellular changes during wakefulness, stable cell lines were produced, to eliminate the effects of variable construct expression, membrane instability and cell death that accompany transient transfection.

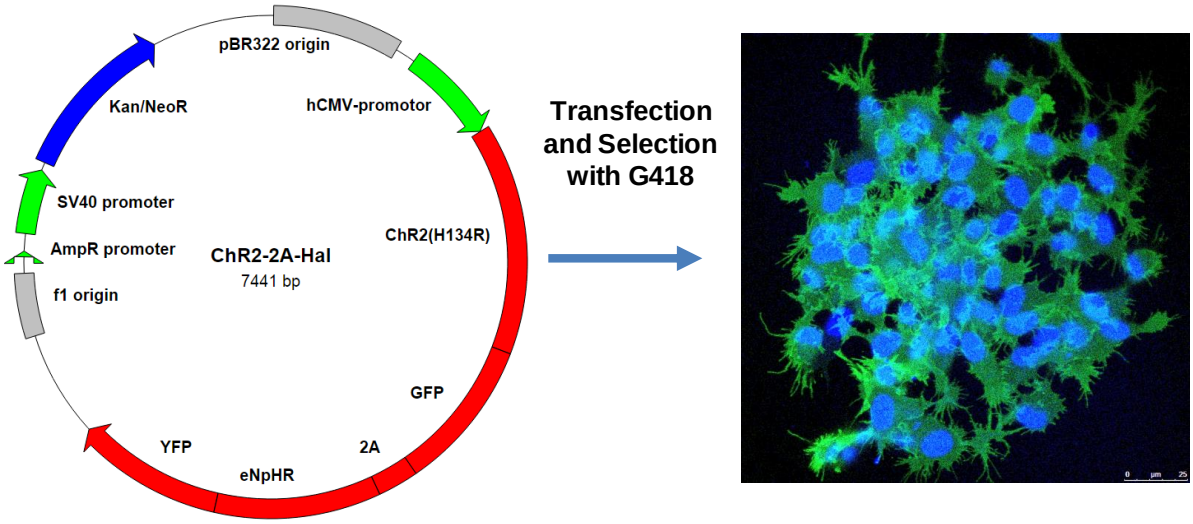

Figure 5.8. Production of Light Sensitive Cells: Monoclonal Human Neuroblastoma cells stably expressing Channelrhodopsin and Halorhodopsin were produced by selection of G418 resistant GFP expressing cells.

SH-SY5Y cells were transfected with ChR2-GFP-2A-Hal-YFP, a plasmid that utilises a viral 2A sequence that induces ribosomal skipping to induce approximately 1:1 expression of Channelrhodopsin 2 and Halorhodopsin. Stable insertion of the plasmid was selected for using G418, and GFP labelled colonies chosen to generate monoclonal cell lines (Fig 5.8.). Generation of SH-SY5Y cell lines stably expressing the transgene was complicated by the high tendency of SH-SY5Y cells to senesce at low confluency, however eventually stable clones were produced after approximately 90 days.

SH-SY5Y cells stably expressing channelrhodopsin were exposed to flashing blue light, using a custom programmable LED array. Cells were exposed to 20 flashes of blue light a second, each lasting 20ms, at an intensity of 0.5mW/cm^2 in a cycle of 5 seconds on and then 5 seconds of darkness for 4 hours. RNA was harvested and the expression of the target genes examined in Section 3.2.1. determined. Compared to light exposed wild type cells and ChR2 expressing cells maintained in the dark, expression of the target genes were increased, but not by the same magnitude as seen with the neurotransmitter cocktail (Fig 5.9.).

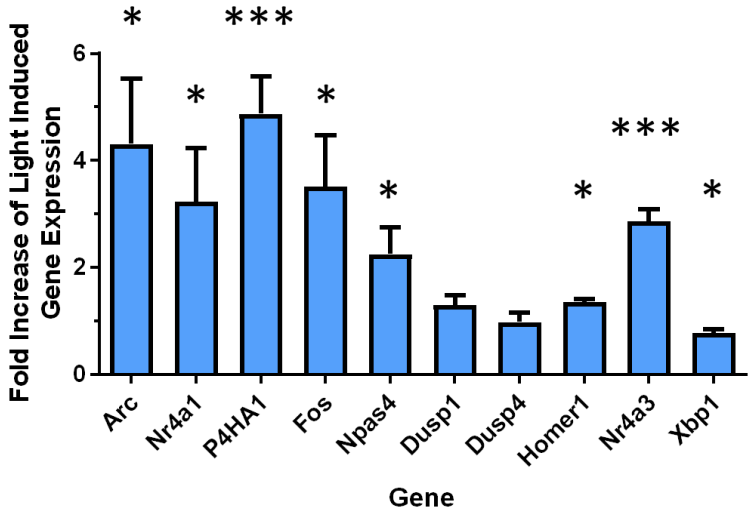

Figure 5.9. Sleep Deprivation Markers Induced by Light Exposure in SH-SY5Y cells: Human Neuroblastoma cells (n=6) stably expressing [ChR2-2A-Hal] were exposed to flashing blue light for 4 hours at an intensity of 0.5mW/cm^2. The expression of sleep deprivation associated genes was determined relative to GAPDH expression and plotted with plotted relative to controls maintained in darkness (data are mean ± SEM).
* - p<0.05, **-p<0.01, ***-p<0.001

5.2.3. Blue Light Activation of SH-SY5Y Cells *in vitro* Induces Global Transcription Changes Similar to Sleep Deprivation *in vivo*

Having determined that SH SY5Y cells respond to an optogenetic stimulus at the transcriptional level, we wished to determine to what extent the change in transcription resembles that seen *in vivo*. In particular, we were interested in potential homeostatic genes. Homeostatic genes are expected to either increase during prolonged wakefulness and then decline during subsequent sleep, or show the inverse pattern. To identify transcripts that fit either pattern, wild type SH-SY5Y cells and those expressing ChR2-2A-Hal were treated with blue light for 6 hours, and then allowed to recover in

darkness for 3 hours. Cells were lysed at 3-hour intervals, and RNA extracted and prepared for RNA-Seq analysis.

Transcripts were filtered to identify those modulated by blue light in Channelrhodopsin expressing cells but unaffected in wild-type SH-SY5Y cells. Because this experiment was carried out without replicates, a gene was identified as being of interest if its expression in ChR2 expressing cells a) was similar at baseline conditions between the two genotypes, and b) changed by at least a factor of 2 after 6 hours of illumination, and c) differed by at least 4 standard deviations from the mean expression of that gene in the control group after 6 hours illumination, but not in wild type cells. In this way, a total of 464 genes were identified as having their expression modulated during illumination.

285 genes were identified as increasing during blue light in ChR2 expressing but not wild-type cells, of which 265 recovered toward baseline levels during the subsequent recovery dark phase. Conversely, the expression of a further 179 genes decreased during blue light of which 176 rebounded during subsequent darkness. The genes that increased during illumination were enriched in genes relating to the regulation of transcription, chaperone function, and biological rhythms (Benjamini corrected q-values = 3.5×10^{-7}, 1.9×10^{-3} and 6.1×10^{-3}, respectively), whilst genes that decreased during illumination were enriched in genes relating to DNA replication (q-value = 3.1×10^{-3}).

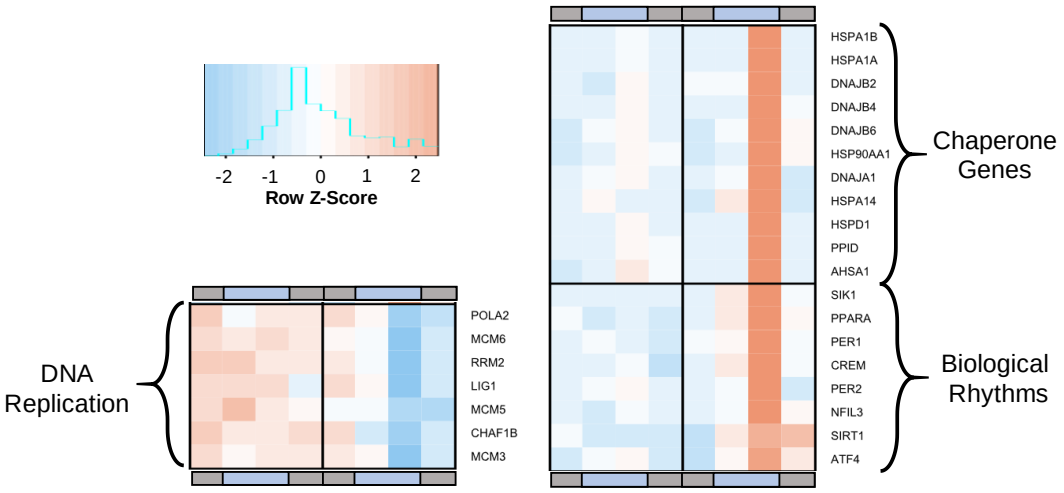

Figure 5.10. Blue Light Exposure Modulates the Expression of Chaperone, Biological Rhythm and DNA Replication Genes: Human Neuroblastoma cells stably expressing [ChR2-2A-Hal] were exposed to flashing blue light for 6 hours at an intensity of 0.5mW/cm^2 and allowed to recover for 3 hours. Cells were sampled every 3 hours, and subjected to RNA-Seq analysis in single replicates. Gene clusters significantly modulated included Chaperone, Biological Rhythm and DNA replication genes. Plotted above are heatmaps of the Z-score normalised expression of genes within these clusters, where blue indicate low expression and red indicates high expression. The blue and grey bars represent the blue light exposure periods.

The expression data from this experiment was compared to the 72 genes from Hinard et al. that were identified as changing both during *in vivo* sleep deprivation and by treatment of primary neurones with an excitatory neurotransmitter cocktail. Of these 72 genes, 56 were expressed in SH-SY5Y cells, 9 of which were "significantly" changed in SH-SY5Y cells, based on the criteria laid out above. However, plotting the remaining 47 genes indicated a good overlap between light stimulation and previous data collected by Hinard *et al*., as several genes appeared to fit the pattern, but did not reach our criteria because of differences in baseline gene expression or variation within the control group.

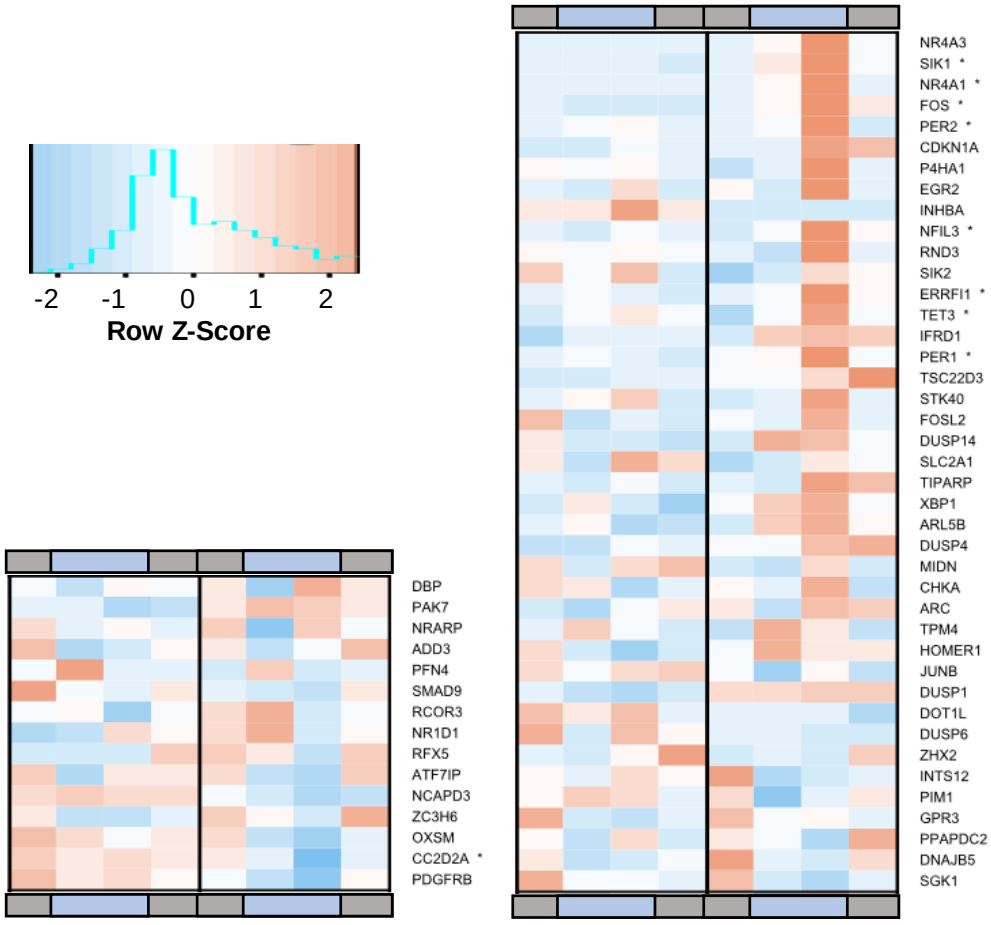

Figure 5.11. Optogenetic Activation of SH-SY5Y Cells produces a similar Expression Trend as that previously observed following the Pharmacological Activation of Primary Neurones: Human Neuroblastoma cells stably expressing [ChR2-2A-Hal] were exposed to flashing blue light for 6 hours at an intensity of 0.5mW/cm^2 and allowed to recover for 3 hours. Cells were sampled every 3 hours and subjected to RNA-Seq analysis in single replicates. The Z-score normalised expression of genes previously indicated as conserved between *in vivo* sleep deprivation and *in vitro* activation of primary neurons are plotted above, where blue represents low expression and red indicates high expression. Genes that met our significance criteria are annotated with an asterisk following their name. The blue and grey bars represent the blue light exposure periods.

5.2.4. Refinement of the Optogenetic Protocol

RNA-seq analysis revealed several transcripts associated with neuronal firing and sleep deprivation were upregulated in SH-SY5Y cells following exposure to light. Heat shock proteins (HSP) were amongst the genes most upregulated, and although several HSPs are induced by sleep deprivation *in vivo*, they are also upregulated by heat and free radical production. Indeed, during illumination, the temperature of the plates increased to 39-40°C.

We therefore introduced physical approaches to reduce increases in temperature associated with illumination. Cells were raised above the LED arrays by 3cm using custom printed parts. Additionally, a fan was placed behind each array, such that there was a constant air flow through the light tight compartment that each array was placed into. These measures had the combined effect of reducing increases in temperature to less than 0.3°C during illumination.

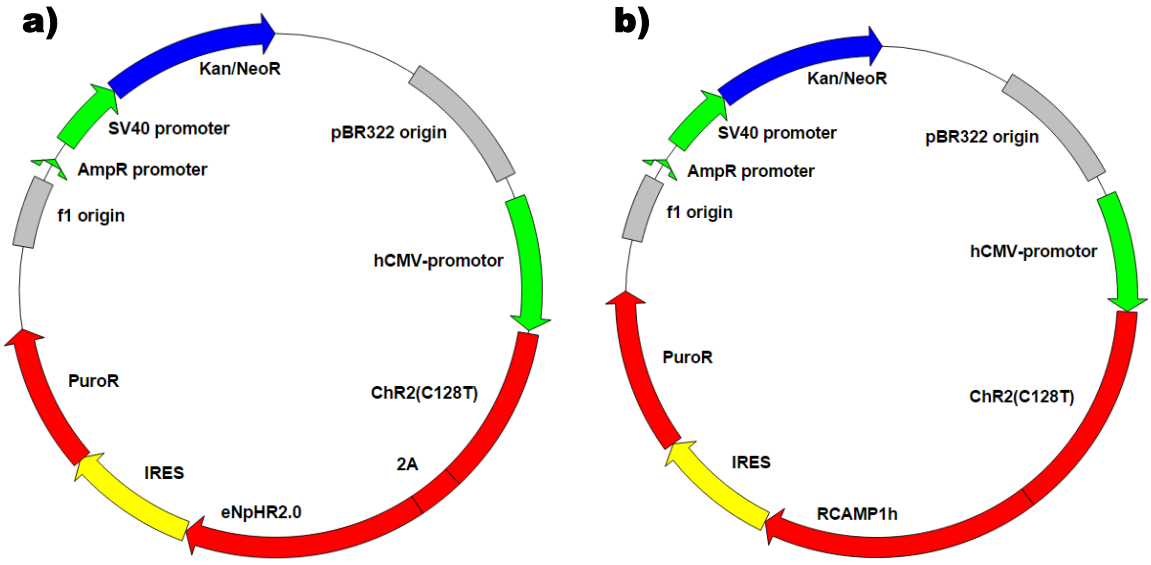

Figure 5.12. Refined Optogenetic Plasmids: CHalIP (a) and CRIP (b) plasmids were produced by Gibson Assembly to improve light sensitivity, remove blue light sensitive fluorescent tags, and directly couple antibiotic resistance to construct expression. CHalIP allows bidirectional optogenetic control, whilst CRIP allows for Calcium imaging at wavelengths independent of Channelrhodopsin2.

We also redesigned the plasmids to encode for optogenetic constructs better suited for long term light exposure. To reduce heat and phototoxicity, we wanted to reduce the amount of light that the cells were exposed to. We therefore replaced the ChR2 (H134R) variant with ChR2(C128T). This "Step Function Opsin" has a greatly reduced channel closing time compared to ChR2 (H134R) (t_{off} = 2s vs 25ms), previously shown to increase light sensitivity at a population level by an order of magnitude. To reduce GFP mediated ROS production, we replaced fluorescent protein tags with an IRES-PuroR cassette, which directly couples antibiotic resistance to the expression of the construct. For

bidirectional optogenetic control, we fused 2A-eNpHR2.0 to the C-terminus of ChR2 (C128T) in one construct. In another construct, we fused the red shifted calcium sensor RCAMP1h to the C-terminus of ChR2 (C128T). The RCAMP1h fusion not only acts as a red shifted fluorescent tag to the opsin, but also allows calcium monitoring at wavelengths outside of the absorbance spectrum of Channelrhodopsin.

SH-SY5Y cells stably expressing the constructs were produced. Both constructs were able to drive larger increases in Fos expression in response to a fivefold lower light intensity (0.1mW/cm^2) than the previous construct (Fig 5.13.).

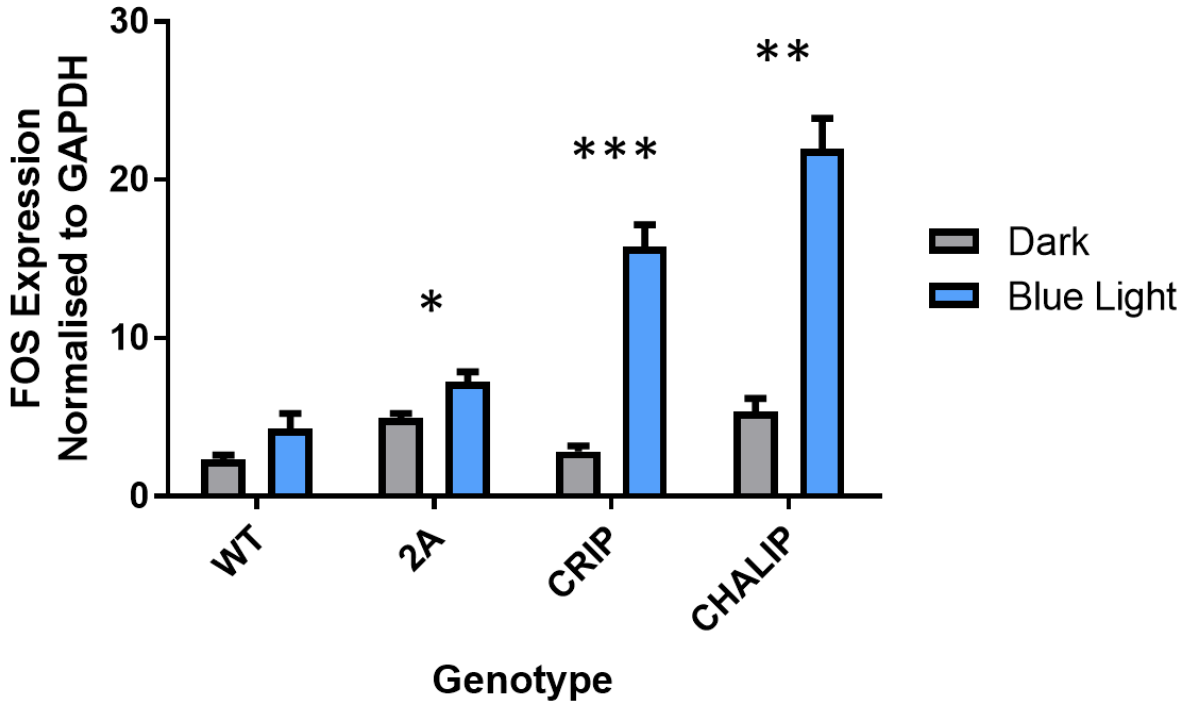

Figure 5.13. Refined Optogenetic Plasmids Induce Fos Expression at Low Light Levels: SH-SY5Y cells, stably expressing CRIP, CHALIP or the original ChR2-2A-Hal construct (2A), were exposed to flashing blue light at intensity 0.1mW/cm^2 for 6 hours, and the expression of Fos determined by qPCR (n=6). Fos expression is plotted relative to GAPDH expression (data are mean ±SEM).
p-values were determined using a Student t-test, comparing the light exposed group to the dark treated cells of the same genotype, and the p-value indicated by the number of asterisks above the column. * - $p<0.05$, **-$p<0.01$, ***-$p<0.001$

Having established that the step-function opsins could drive Fos expression in response to lower levels of light than the ChR2(H134R) variant, we next wanted to know whether red light activation of halorhodopsin could prevent ChR2 mediated Fos expression in SH-SY5Y cells. We therefore exposed cells stably expressing the ChR2(C128T)-2A-eNpHR2.0 construct to both blue and red light and quantified expression of Fos through qPCR. Red light was unable to significantly reduce Fos induction by blue light, and alone was sufficient to induce a small but significant increase in Fos expression. We consequently discarded the concept of using halorhodopsin to hyperpolarise SH-SY5Y cells in our model.

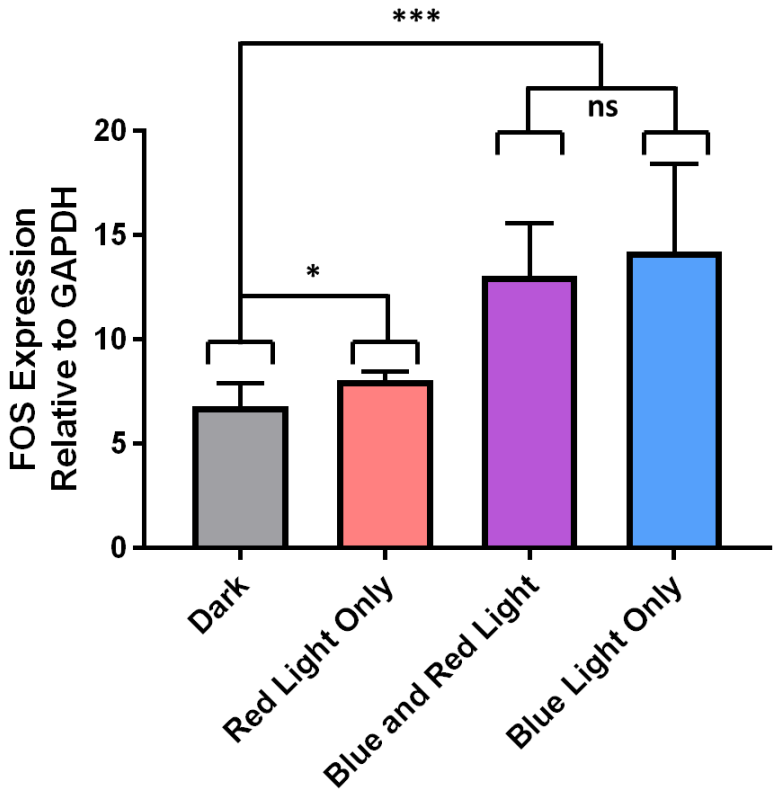

Figure 5.14. Halorhodopsin Activation is not Sufficient to Prevent Channelrhodopsin Mediated Fos Expression: SH-SY5Y cells stably expressing CHALIP were exposed to flashing blue light at intensity 0.1mW/cm^2 with or without constant red light at intensity 0.2mW/cm^2 for 6 hours, and the expression of Fos determined by qPCR (n=6). Fos expression is plotted relative to GAPDH expression (data are mean ±SEM).

p-values were determined using a Student t-test, comparing the light exposed groups to the dark treated cells, and the p-value indicated by the number of asterisks above the column.
ns- $p > 0.05$, * - $p<0.05$, ***-$p<0.001$

5.2.5. Opsin Activation Modulates the Molecular Clock

RNA-Seq revealed that the expression of core circadian clock genes was modulated by blue light exposure and recovery. To test the hypothesis that photocurrents through Channelrhodopsin affects the cellular clock, stable U20S cell lines were produced that express both luciferase under the control of the Per2 promoter, and either the CRIP or CHALIP construct. U20S cells were chosen as they are an established cellular model of circadian rhythms, and U20S cells stably expressing luciferase under the Per2 promotor present an easily accessible readout of the cellular clock.

Cells had their internal circadian clocks synchronised, and were subsequently exposed to flashing blue light in HEPES buffered AIR medium between 12-32 hours after synchronisation. The bioluminescence of each well was tracked for over 4 days, plotted and detrended to determine the period and phase of their oscillations. The phase of U20S cells not expressing Optogenetic constructs was not greatly affected (<1 hour) by blue light treatment, although one-way analysis of variance (ANOVA) did reveal a statistical dependence of time of treatment. In contrast, the expression of the CHalIP or CRIP constructs leads to the phase of the cellular clock being much more sensitive to the timing of blue light exposure, indicated by a highly significant interaction of genotype and response to the timing of light treatment ($p<0.0001$), as shown by two-way ANOVA.

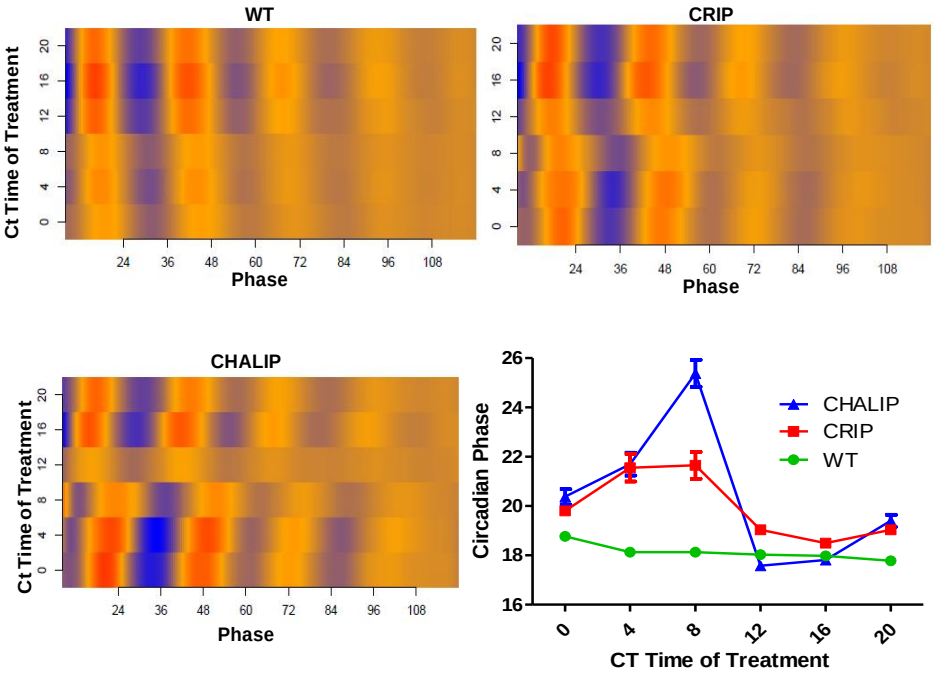

Figure 5.15. Circadian Effects of Photocurrents in U20S Osteosarcoma Cells: CHalIP or CRIP was stably expressed in U20S cells expressing luciferase under the control of the *Per2* promoter. After the cellular clocks were synchronised, cells were exposed to flashing blue light for 4 hours, starting at cell time (CT) 0, 4, 8, 12, 16 or 20. The bioluminescence was tracked over several days, detrended and the data plotted as a heatmap. Blue represents a local minimum in luciferase activity, whilst red represents a maximum. Data are also plotted as Mean ±SEM in the adjacent scatter plot.

5.2.6. c-Fos Activation by Channelrhodopsin is Highly Sensitive to Medium Components and Conditions

Prior to the luciferase experiments outlined in Section 5.2.5., all the characterisations of opsin expressing cells had been performed in bicarbonate buffered medium. However, exposure to light took place at atmospheric CO_2 levels, and therefore the bicarbonate-based buffering had been ineffective. Indeed, the presence of bicarbonate at atmospheric CO_2 caused the pH of the medium to increase to pH 9 within 1 hour of transfer. Despite this pH rise not appearing to cause any cell death or detachment of cells, we decided that the dramatic change in pH toward alkaline conditions was wholly unphysiological and would likely be a major confounder in our experiment. We therefore carried out further experiments in AIR Medium (see Section 2.8.), which replaced the sodium bicarbonate buffering system with HEPES.

The first experiment carried out in HEPES buffered medium aimed to titrate light intensity against FOS expression in CRIP expressing SH-SY5Y cells, to minimise light exposure in future experiments. Previous experiments had indicated that flashes at 0.1mW/cm^2 were sufficient to induce FOS expression in bicarbonate buffered medium under atmospheric CO_2, however in HEPES buffered medium FOS induction by blue light was eliminated, even at higher light intensities (Fig 5.16).

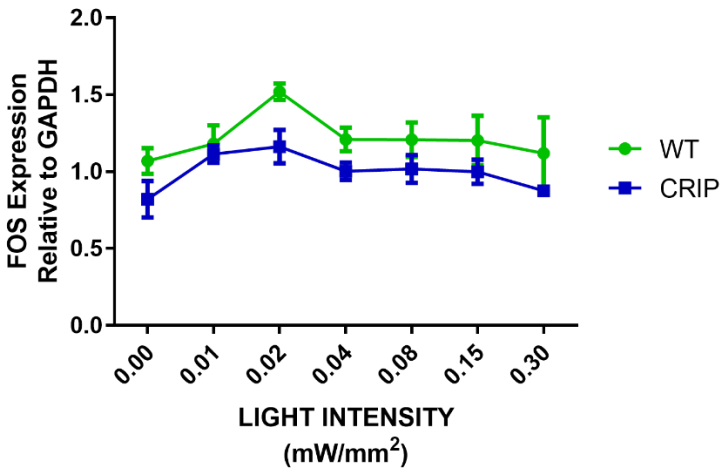

Figure 5.16. HEPES Buffered Medium Removes Sensitivity of Cells to Blue Light: Wild type SH-SY5Y cells and those stably expressing CRIP were exposed to flashing blue light at intensities ranging from 0.0-0.3mW/cm^2 for 6 hours, and the expression of Fos determined by qPCR (n=3). Fos expression is plotted relative to GAPDH expression (data are mean ±SEM).

HEPES has previously been demonstrated to cause phototoxicity in the presence of other medium components, and so we hypothesised that the response to light could be restored by replacing HEPES with another appropriate buffer, such as MOPS or TAPSO. Whereas TAPSO buffered medium was statistically associated with a decrease in FOS expression during exposure to blue light, expression of FOS in MOPS based medium had no dependence on blue light. In contrast, cells expressing opsins in bicarbonate containing medium showed induction of FOS in response to blue light (Fig 5.17.). Cells in bicarbonate containing medium also had an increased level of basal FOS expression compared to cells in HEPES, MOPS or TAPSO buffered media.

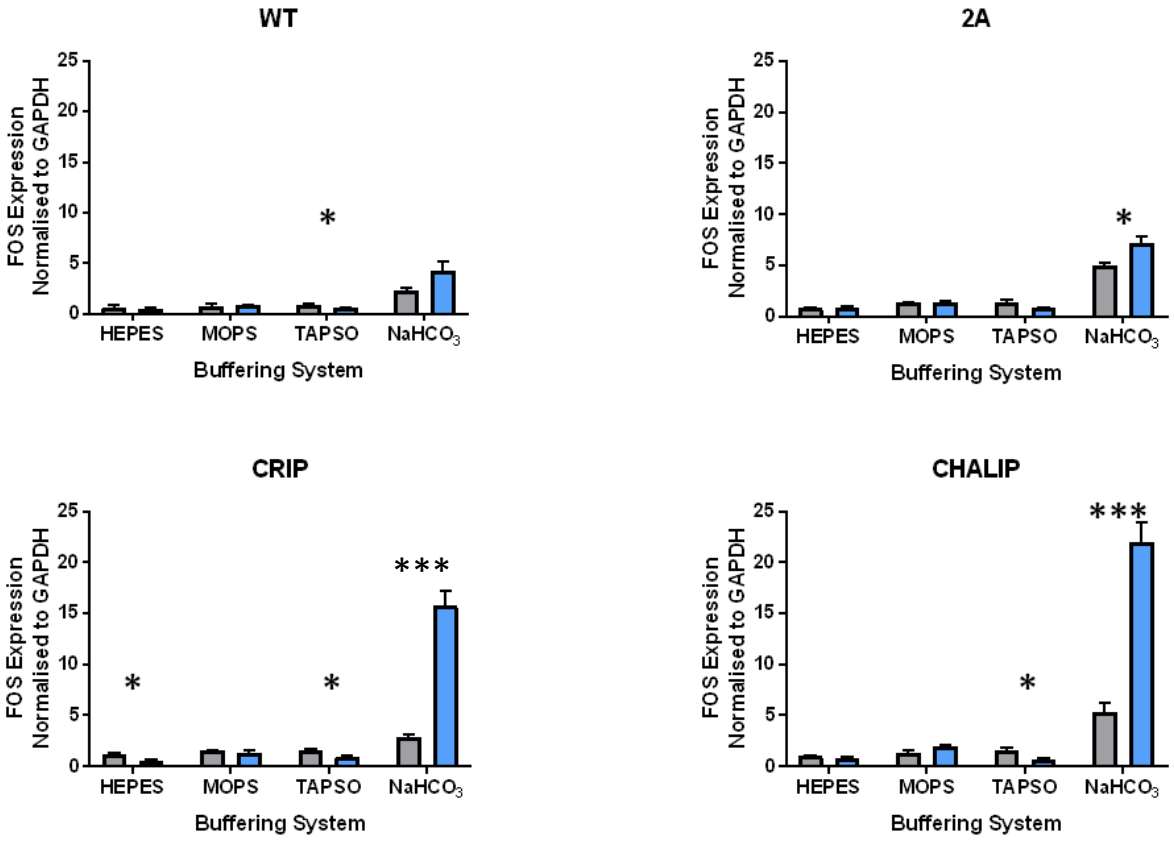

Figure 5.17. Medium Buffered at Neutral pH Removes Sensitivity of Cells to Blue Light: SH-SY5Y cells, stably expressing CRIP, CHALIP or the original ChR2-2A-Hal construct (2A), were exposed to flashing blue light at intensity 0.1mW/cm^2 for 6 hours in the presence of either HEPES, MOPS, TAPSO or bicarbonate ($NaHCO_3$) buffered media at atmospheric CO_2, and the expression of Fos determined by qPCR (n=3). Black bars represent dark treated controls, Blue bars represent blue light treated cells
* - p<0.05, **-p<0.01, ***-p<0.001

We next determined that FOS induction in bicarbonate buffered medium was dependent on exposure to atmospheric CO_2, as sealing the plates to prevent gas exchange prevented blue light induced FOS induction in bicarbonate containing medium. We therefore hypothesised that high pH, rather than specific medium components, was required for the opsin conferred light sensitivity. To test this hypothesis, we exposed cells expressing CRIP to blue light, having changed their media 18 hours prior to light exposure to media buffered either with 40mM MOPS at pH 7 or 8, or buffered with 40mM CHES at pH 9 or 10. Cells maintained at pH 10 died overnight, whereas those buffered at pH 7-9 showed no sensitivity to blue light (Fig 5.18.).

Our next hypothesis was that the change in pH was relevant, rather than the pH value itself. At the molecular level, we considered the possibility that alkaline conditions caused the non-enzymatic hydrolysis of glutamine present in the media to glutamate, which in turn may activate glutamatergic receptors on the surface of SH-SY5Y cells, with which channelrhodopsin activation was synergistic. This would explain the increase of Fos expression in the absence of light, as well as the light mediated increase in Fos expression. In contrast, after prolonged high pH, the rate of glutamate formation may have decreased, and extracellular glutamate become depleted through uptake mechanisms. We therefore tested the possibility that non-hydrolysable drugs added to the medium the day before light exposure may exhibit the same synergism with blue light. Cells expressing CRIP were exposed to blue light in medium buffered with MOPS at pH 7.4, containing the cocktail used in Section 5.2.1. at a concentration ranging from 10^{-6} - 1X. However, drug addition failed to produce any response to blue light (Fig 5.18.).

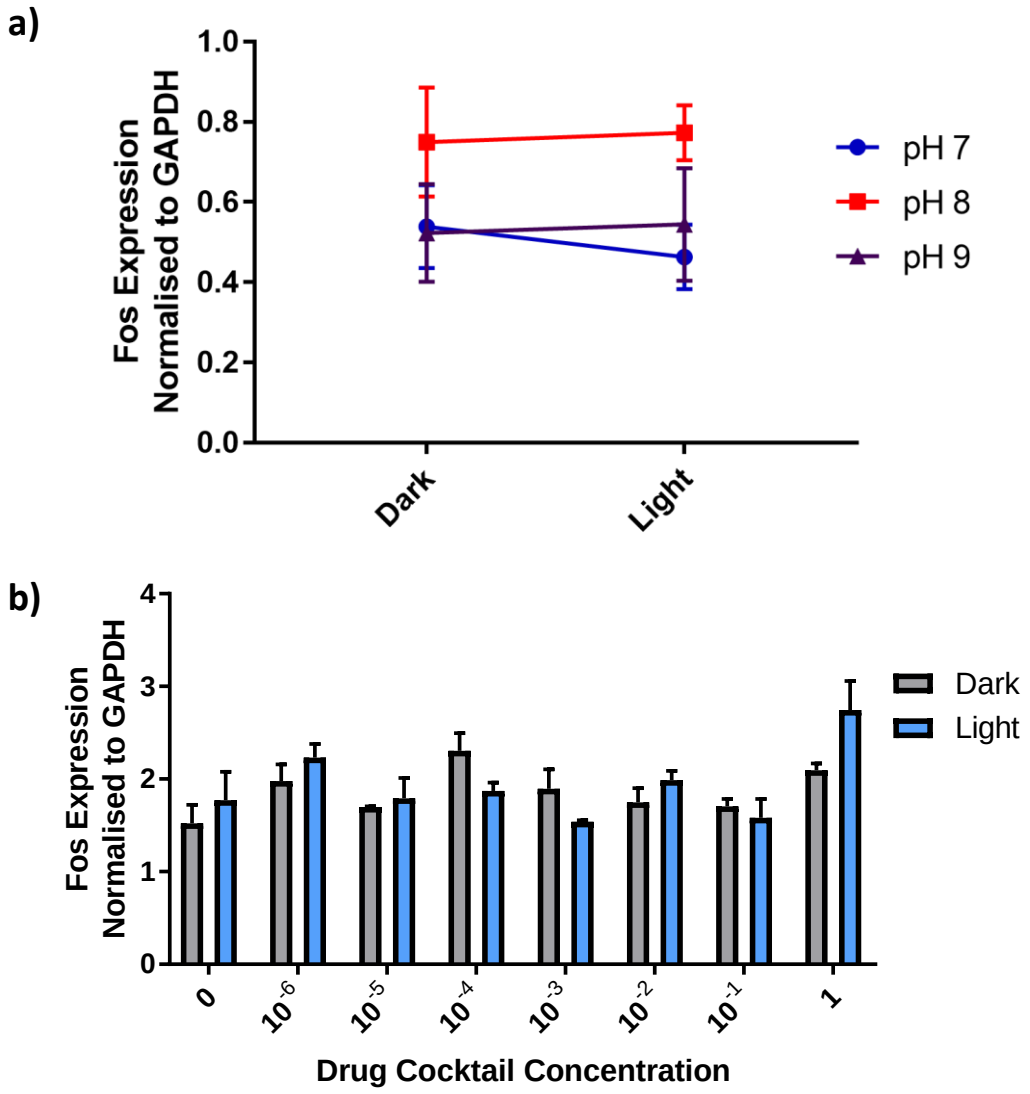

Figure 5.18. Varying pH or Introducing Excitatory Drugs to the Medium Fails to Restore Sensitivity of Cells to Blue Light:

a) SH-SY5Y stably expressing CRIP were exposed to flashing blue light at 0.1mW/cm^2 for 6 hours, in medium buffered at pH 7,8 or 9, and the expression of Fos determined by qPCR (n=3). Fos expression is plotted relative to GAPDH expression (data are mean ±SEM).

b) SH-SY5Y stably expressing CRIP were exposed to flashing blue light at 0.1mW/cm^2 for 6 hours, in medium containing a range of concentration of excitatory neurotransmitter cocktail at pH 7.4, and the expression of Fos determined by qPCR (n=3). Fos expression is plotted relative to GAPDH expression (data are mean ±SEM).

5.2.7. Expression of a High Conductivity Opsin Confers Sensitivity to Light at Neutral pH

Having ruled out several pH mediated effects on the cells and media composition, we then considered the effect of high pH on channelrhodopsin itself. Previous studies had shown that the kinetics, conductivity and ion selectivity of channelrhodopsin is highly dependent on pH. Although the majority of data available relates to neutral and acidic conditions, we speculated that the shift to basic conditions changed some basic parameters of channelrhodopsin to make it more favourable for activation of SH-SY5Y cells. There were three parameters of channelrhodopsin we thought important: the size of photocurrent, its photocycle kinetics, and the inactivation kinetics, relating to the decrease in photocurrent following repeated light exposure. We therefore chose to create new stable cell lines, expressing recently discovered or engineered opsins found to have improved conductivity and kinetics.

CoChR is a naturally occurring green shifted algal opsin, found to have much higher conductivity and expression levels than wild type ChR2 with comparable photocycle kinetics and greatly reduced inactivation. CHIEF (E162A/T198C) is a synthetic chimera opsin with very fast kinetics and greatly reduced inactivation, whereas Chronos is a naturally occurring opsin with generally superior photocycle and inactivation kinetics, light sensitivity and conductivity.

Plasmids encoding for the stable expression of Chronos, CoChR or CHIEF (E162A/T198C) fused to RCAMP were produced. Despite stably expressing in HEK 293T cells, expression of CHIEF (E162A/T198C) containing constructs was lethal in SH-SY5Y cells, and no puromycin resistant cells survived after transfection with CHIEF (E162A/T198C)-RCAMP. However, both Chronos-RCAMP and CoChR-RCAMP constructs were stably expressed. As an initial experiment, cells were exposed to between 2-32 pulses of light per second, with each pulse lasting 25ms and consisting of both blue and green light at a total light intensity of 2mW/cm^2 in medium buffered at pH 7.4 with 40mM MOPS. After six hours of illumination, cells were lysed and the expression of Fos determined (see Fig 5.19.).

Expression of Fos was statistically upregulated following light exposure to CoChR expressing cells at pulse frequencies of 8Hz and higher, whereas Chronos expressing cells only had a statistical increase in Fos expression at a pulse frequency of 32Hz. We therefore chose to pursue the use of CoChR to activate SH-SY5Y cells. Initially, the degree of Fos induction was found to be inconsistent and sensitive to several experimental design parameters, most notably days in culture, confluency and the presence of supplemental retinoids. However, guided in part by microscopy experiments outlined in Section 3.2.8., we eventually standardised light exposure to occur 7 days after plating at high confluency in the absence of supplementary retinoids. Under these conditions, we were able to

reliably induce a large (30-100X) increase in Fos expression by exposure to light, which rapidly recovers toward baseline levels after cessation of illumination (see Figure 3.19.).

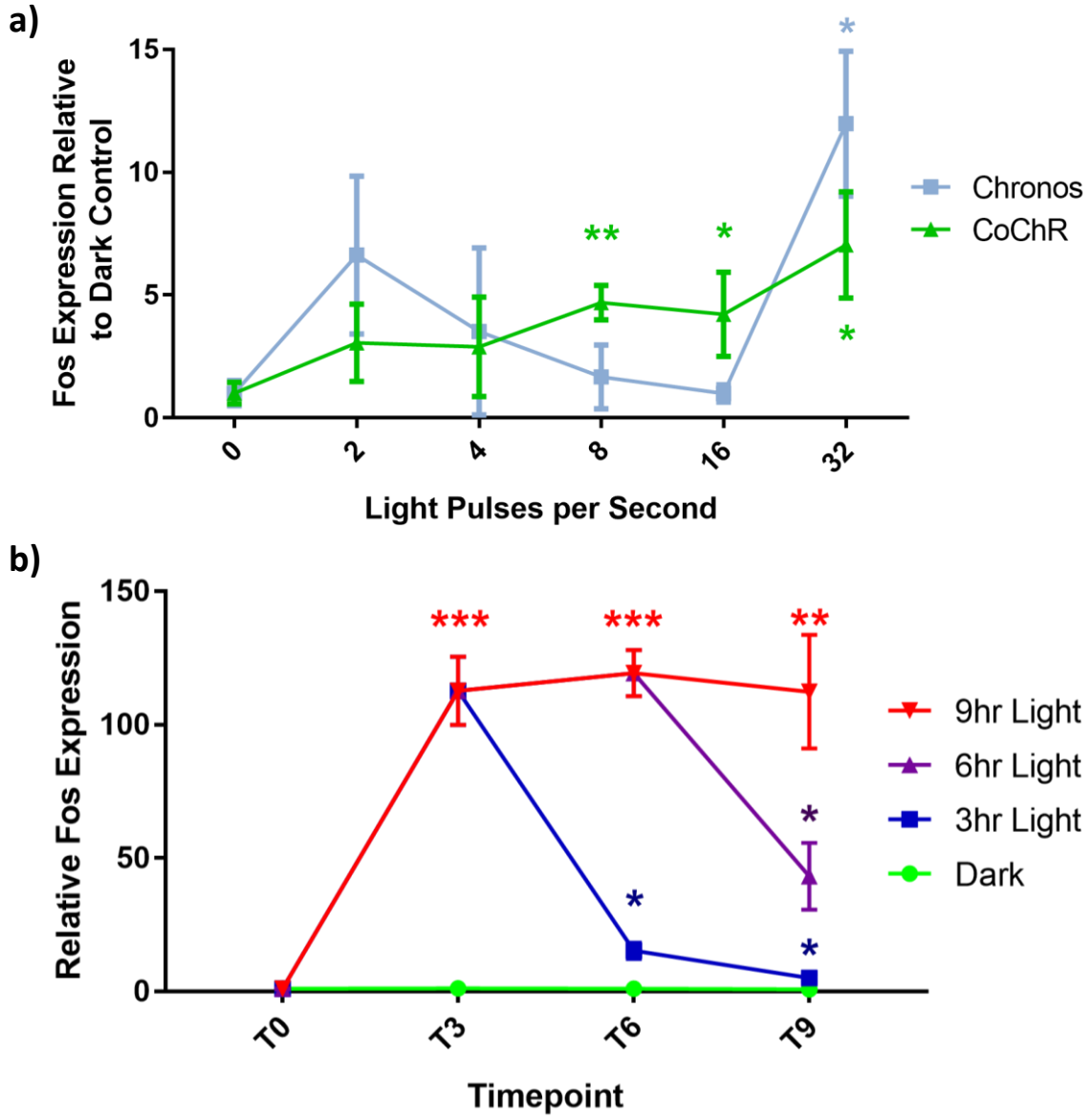

Figure 5.19. Expression of CoChR Confers Light Sensitivity to SH-SY5Y cells at Neutral pH:
a) SH-SY5Y cells, stably expressing Chronos or CoChR supplemented with 1µM retinal were exposed to flashing blue and green light at a total intensity of 2mW/cm^2 for 6 hours at pH 7.4 and the expression of Fos determined by qPCR and plotted relative to the expression of untreated cells of the same genotype (n=3). Asterisks indicate the statistical significance of a flash frequency compared to untreated cells of the same genotype.
b) Undifferentiated SH-SY5Y cells stably expressing CoChR were exposed to 8 flashes of blue and green light per second at a total intensity of 2mW/cm^2 for 3,6 or 9 hours at pH 7.4 without supplemental retinoids, and the expression of Fos determined by qPCR (n=4) and normalised to the first timepoint of the dark treated control. For clarity, recovery timepoints are joined by lines to their final illumination timepoint, but that illumination timepoint has not been repeated multiple times. Asterisks indicate the statistical significance of a treated timepoint compared to untreated cells at the same timepoint.
* - p<0.05, **-p<0.01, ***-p<0.001

5.2.8. Fluorescent Calcium Imaging Reveals Intracellular Calcium Increases in Response to Stimulation with Light

We took advantage of the RCAMP moiety fused to opsins to image intracellular calcium at red-shifted wavelengths whilst simultaneously stimulating cells with either ions, drugs or blue light activation of the opsin.

Surprisingly, in the absence of any external stimulation, no spontaneous calcium signals were ever detected (Fig 5.20.), but intracellular calcium readily responded to addition of potassium to the medium. Intracellular calcium also increased in response to the neurotransmitter cocktail used in section 5.2.1., showing responses individually to dopamine, histamine, and carbachol (Fig 5.21.).

In contrast to cells expressing ChR2(C128T) or Chronos, cells expressing CoChR showed transient calcium spikes in response to pulses of light, the magnitude of which was sensitive to light intensity and extracellular calcium levels (Fig 5.22.). The half life of the peaks was determined to be approximately 1 second, considerably larger than the 200ms t_{off} previously measured for CoChR.

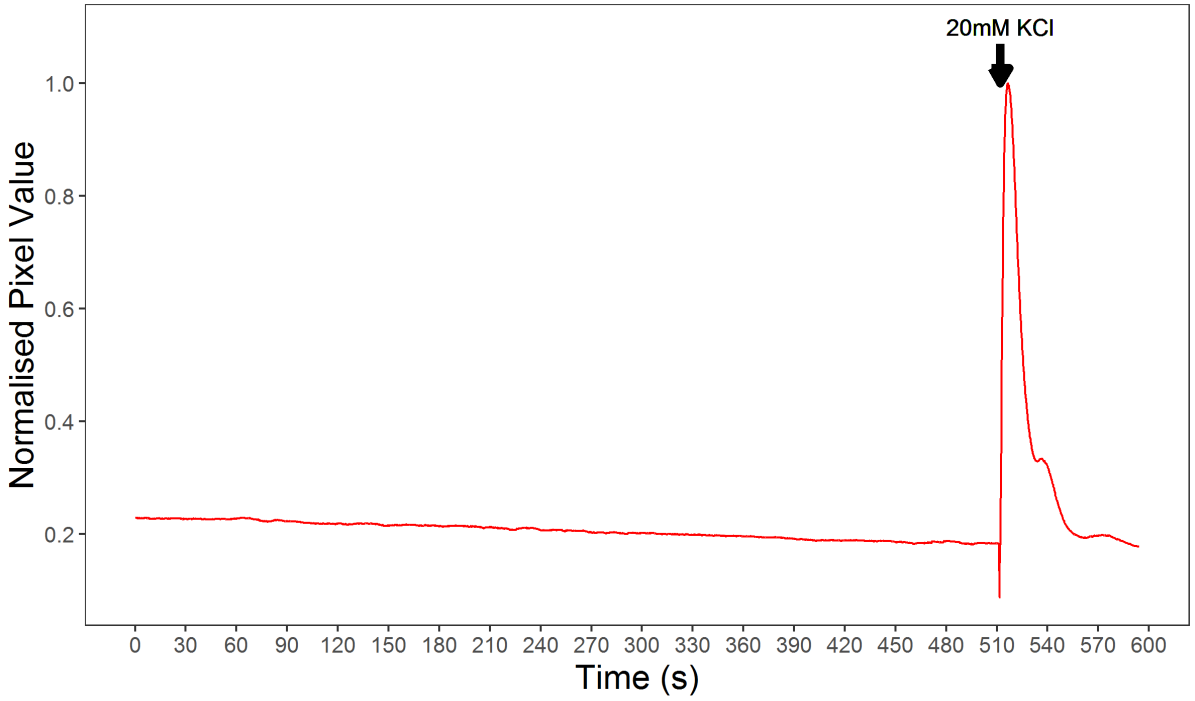

Figure 5.20. SH-SY5Y Cells do not Exhibit Spontaneous Calcium Spikes: Live SH-SY5Y cells, stably expressing CoChR-RCAMP were imaged 5 times per second at 570nm to excite the calcium sensitive RCAMP fluorophore. No spontaneous changes in RCAMP fluorescence were detected, however addition of 20mM KCl induces a rise in intracellular calcium. Pixel values were normalised by defining the maximum intensity recorded in the recording as 1 and linearly scaling all other images, and no smoothing was applied.

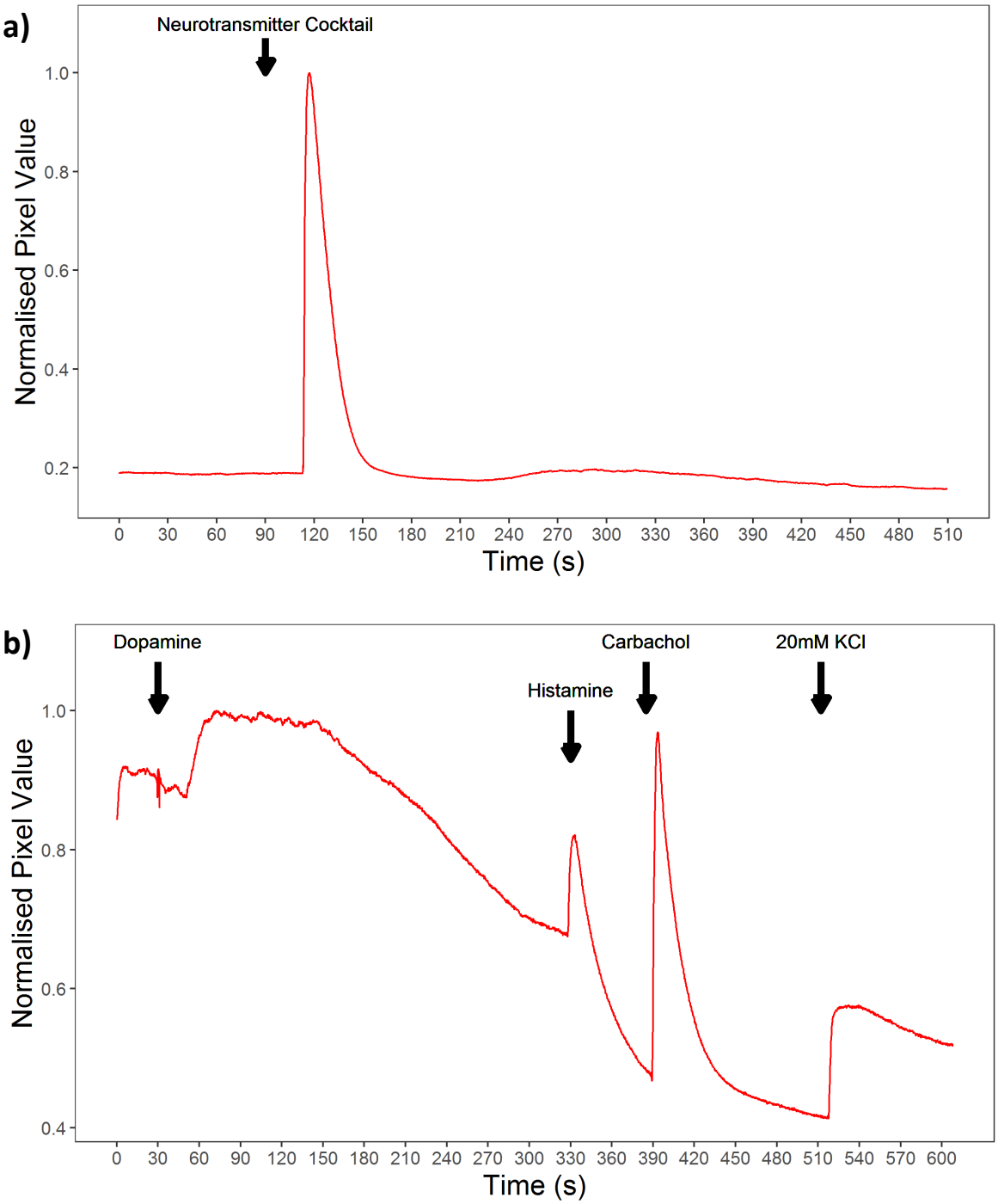

Figure 5.21. Excitatory Drugs Induces Intracellular Increases in Calcium in SH-SY5Y Cells: Live undifferentiated SH-SY5Y cells stably expressing CoChR-RCAMP were imaged at 570nm to excite the calcium sensitive RCAMP fluorophore. Pixel values were normalised by defining the maximum intensity recorded in the timecourse as 1 and linearly scaling all other images, and were not subjected to any smoothing. **a)** After 90 seconds, a cocktail of excitatory drugs was added to the cells at a final concentration of 10µM carbachol, 1µM NMDA, 1µM AMPA, 1µM kainic acid, 1µM ibotenic acid, 1µM serotonin, 1µM histamine, 1µM noradrenaline, 1µM dopamine and 10nM orexin. **b)** After 30 seconds, Dopamine was added to a final concentration of 5µM. After 330 seconds, Histamine was added to a final concentration of 5µM, and after 390 seconds, Carbachol was added to a final concentration of 50µM.

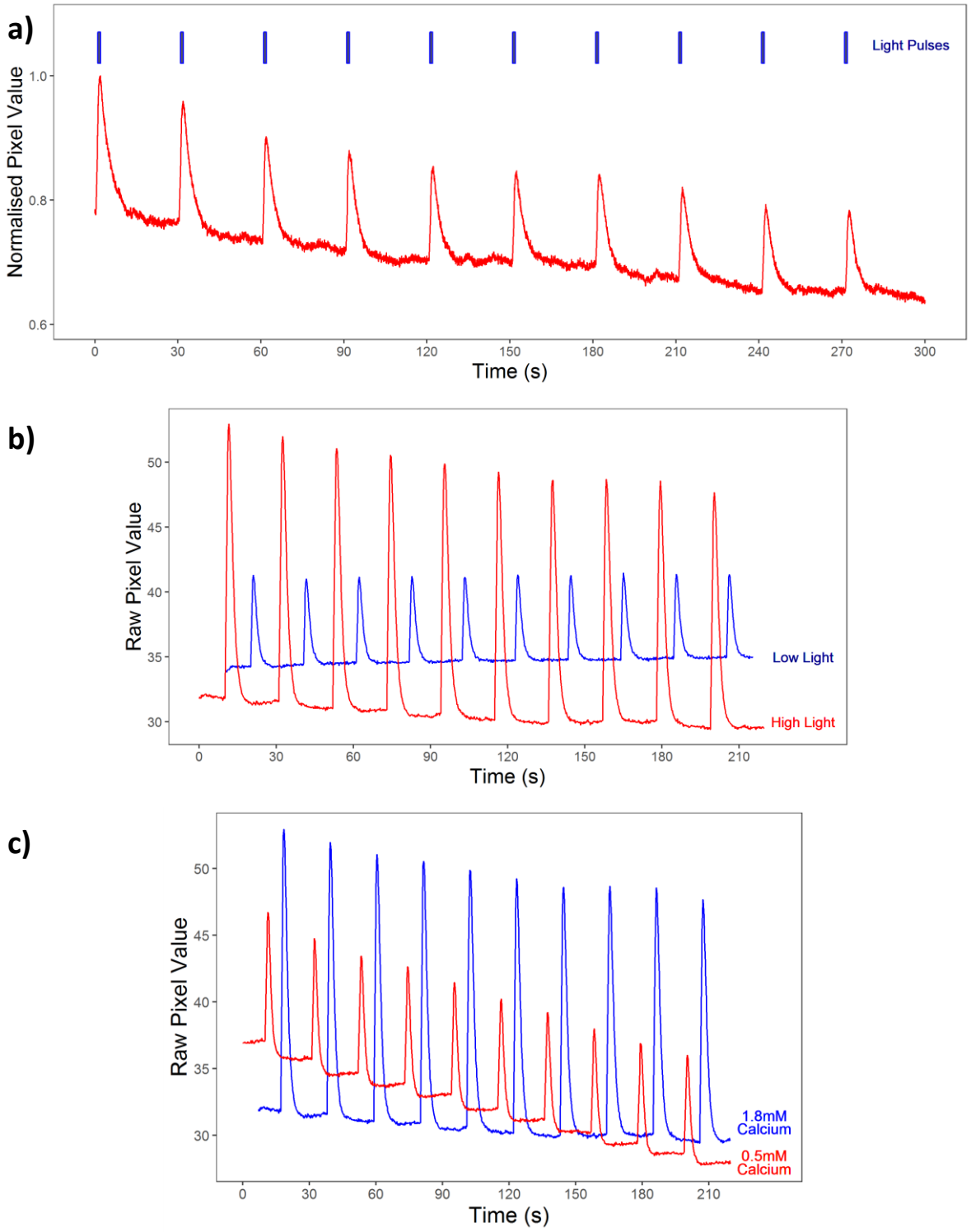

Figure 5.22. Stimulation with Blue Light Increases Intracellular Calcium in SH-SY5Y Cells Stably Expressing CoChR in an Intensity and Extracellular Calcium Dependent Manner: Live undifferentiated SH-SY5Y cells, stably expressing CoChR-RCAMP were imaged every 200ms in AIR medium at 570nm, and **a)** simultaneously excited using an argon laser at 488nm for 200ms every 30 seconds, or **b)** stimulated with either low or high light intensities (10% 488nm or 50% 476nm + 50% 488nm laser power, respectively) every 20 seconds, or **c)** stimulated at high light intensity every 20 seconds in medium containing either 0.5mM or 1.8mM calcium. Frames captured during blue light stimulation were discarded from subsequent data analysis, and lines were not subjected to any smoothing.

The fluorescent imaging of RCAMP therefore confirmed in real time that treatment with drugs and CoChR mediated light stimulation induced intracellular calcium responses in undifferentiated SH-SY5Y cells. In contrast, retinoic acid differentiated cells showed severely dampened responses to drugs and light and revealed considerable variation between the calcium responses of adjacent cells. The desensitising effect of retinoic acid was not rescued by prolonging the length of differentiation up to six weeks, nor was the expression of the construct abrogated by differentiation. Therefore, despite retinoic acid inducing morphological changes that cause SH-SY5Y cells to more closely resemble mature neurons, retinoic acid differentiation appeared to reduce the molecular response to excitatory signals.

Remarkably, supplementing the medium with retinal or retinyl acetate was not necessary for light induced calcium responses, presumably because the serum component contains sufficient levels of retinoids. Indeed, supplementation with retinoids actually reduced the magnitude and reproducibility of the observed calcium responses, resembling the effect of retinoic acid. Removal of supplemental retinal from the medium of SH-SY5Y cells also led to an increased and reproducible level of light mediated Fos induction, as assayed by qPCR, consistent with a greater proportion of cells responding to light stimulation. SH-SY5Y cells have previously been shown to convert retinol and retinal to retinoic acid, and chronic exposure to low levels of retinyl acetate has been shown to induce a partial differentiation of SH-SY5Y cells. Although treatment with retinal does not induce the rapid extension of processes characteristic of retinoic acid differentiation, it appears that supplementation with retinal triggers a cellular response that leads to a dampened response to excitatory stimulation.

5.2.9. Transcriptomic Analyses Reveals an Acute Response to CoChR Activation in SH-SY5Y Cells

To determine to what extent light activated SH-SY5Y cells recapitulate the transcriptomic changes observed during *in vivo* sleep deprivation, we carried out a timecourse experiment to produce samples for RNA-Seq. Undifferentiated, high confluency SH-SY5Y cells were exposed to flashing blue light for 12 hours, and lysed every 6 hours. Sampling began 12 hours before the onset of blue light and finished 24 hours following the end of stimulation. Therefore the timecourse spanned a total of 48 hours. A second set of SH-SY5Y cells expressing CoChR were maintained in the dark and sampled at the same timepoints to act as the control group.

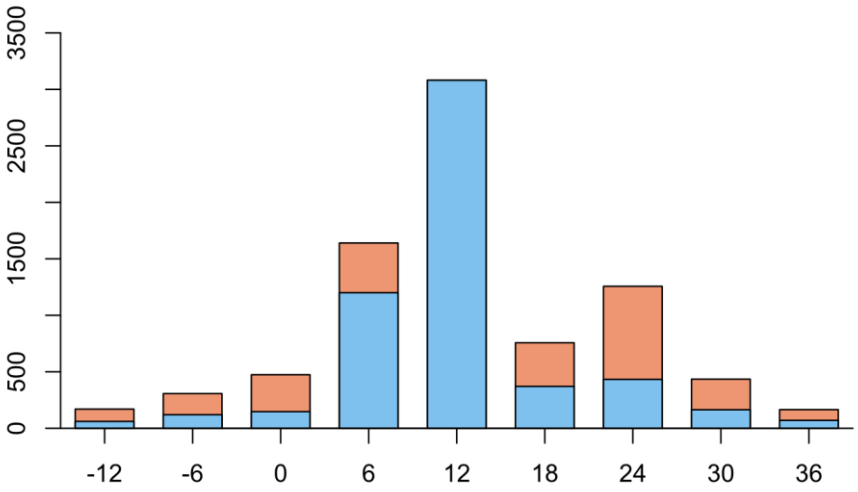

Figure 5.23. Blue Light Stimulation of SH-SY5Y cells expressing CoChR induces the Differential Expression of more than 3000 Transcripts: Live undifferentiated SH-SY5Y cells, stably expressing CoChR-RCAMP were exposed to flashing blue light for 12 hours, beginning at 0 hours, and allowed to recover for up to 24 hours. Cells were sampled in triplicate every 6 hours and subjected to sequencing based transcriptomic analyses and subsequent Cufflinks based differential expression analysis. The total height of each bar represents the number of genes differentially expressed in light exposed cells compared to cells maintained in darkness at that timepoint. The blue portion of each bar indicates the number of genes that are also differentially expressed following 12 hours exposure to blue light.

Differential expression analysis revealed 3082 transcripts were significantly differentially expressed immediately following 12 hour exposure to blue light (Fig 5.23.). Of these, 30% were also differentially expressed following only 6 hours blue light exposure. Remarkably, the expression of 85% of the transcripts differentially expressed following 12 hours blue light rebound to baseline levels following only 6 hours recovery.

The 1740 transcripts significantly upregulated by 12 hours blue light exposure were statistically enriched in genes relating to the regulation of transcription, chaperone function, the endoplasmic reticulum, the cell cycle, mRNA splicing, and sterol biosynthesis. Genes relating to the regulation of transcription, chaperone function, the endoplasmic reticulum, the cell cycle and sterol biosynthesis were also significantly upregulated following only 6 hours blue light exposure. In contrast, none of these functional gene groups are statistically enriched amongst upregulated genes during the recovery phase, indicating that the expression of these genes is tightly linked to activity. Instead, genes upregulated during the recovery phase are enriched in membrane proteins and genes associated with Golgi transport following 6 hours recovery, and glycolysis and microtubule function following 12 hours recovery.

Table 16: Genes Upregulated following Blue Light Exposure

Timepoint	Functional Cluster	q-value
6hr BL	Regulation of Transcription	$3x10^{-16}$
	Chaperones	$4x10^{-9}$
	Endoplasmic Reticulum	$5x10^{-6}$
	Cell Cycle	$9x10^{-4}$
	Sterol Biosynthesis	$2x10^{-8}$
12hr BL	Regulation of Transcription	$2x10^{-21}$
	Chaperones	$8x10^{-11}$
	Endoplasmic Reticulum	$2x10^{-10}$
	Cell Cycle	$1x10^{-8}$
	mRNA Processing	$3x10^{-7}$
	Sterol Biosynthesis	$8x10^{-6}$
12hr BL, 6hr R	Membrane Proteins	$1x10^{-6}$
	Golgi Trafficking	$6x10^{-3}$
12hr BL, 12hr R	Glycolysis	$3x10^{-7}$
	Microtubule	$1x10^{-3}$

Despite a similar number of transcripts being downregulated as upregulated following 12 hours blue light exposure, there was remarkably little functional enrichment observed in downregulated genes. Genes involved in cell junctions and mitochondrial function were statistically downregulated, following 12 hours blue light, whilst genes relating to mitochondrial function were also downregulated

following only 6 hours of blue light. Following 6 hours recovery, downregulated transcripts were enriched in histones and synapse, and following 12 hours recovery, the expression of histones, DNA replication genes, respiratory chain genes, and ribosomal proteins are repressed.

Table 17: Genes Downregulated following Blue Light Exposure

Timepoint	Functional Cluster	q-value
6hr BL	Mitochondria	$3x10^{-2}$
12hr BL	Cell Junction	$3x10^{-2}$
	Mitochondria	$4x10^{-2}$
12hr BL, 6hr R	Histones	$4x10^{-16}$
	Synapse	$2x10^{-4}$
12hr BL, 12hr R	Histones	$2x10^{-36}$
	DNA Replication	$3x10^{-9}$
	Respiratory Chain	$1x10^{-8}$
	Ribosomal Protein	$1x10^{-7}$

JTK analysis was carried out to identify which genes exhibit circadian oscillations in expression. Remarkably, no transcripts were identified as exhibiting statistically significant rhythmic expression in cells maintained in darkness. 37 transcripts were identified as rhythmic in the light treated group, however these transcripts may be false positives due to a modulation of expression induced by blue light. The absence of rhythmic transcripts indicates that the individual cellular clocks of the cell population were not synchronised. Therefore the criteria used in Section 3.2.3. to identify homeostatic genes *in vivo* (genes with a rhythmic expression under control conditions, whose expression is modulated by sleep deprivation in a dose dependent manner) cannot be applied in this *in vitro* experiment.

ANOVA analyses identified that the expression of 373 genes increased at least 2 fold following 12 hours illumination and had a significant interaction between treatment group and timepoint. The genes that increased were enriched in genes relating to the endoplasmic reticulum, cholesterol synthesis, chaperones and circadian regulators. In contrast, the 394 genes whose expression reduced by at least 50% and was identified as having a significant interaction between timepoint and treatment were significantly enriched only in postsynaptic genes, specifically cholinergic receptor subunits.

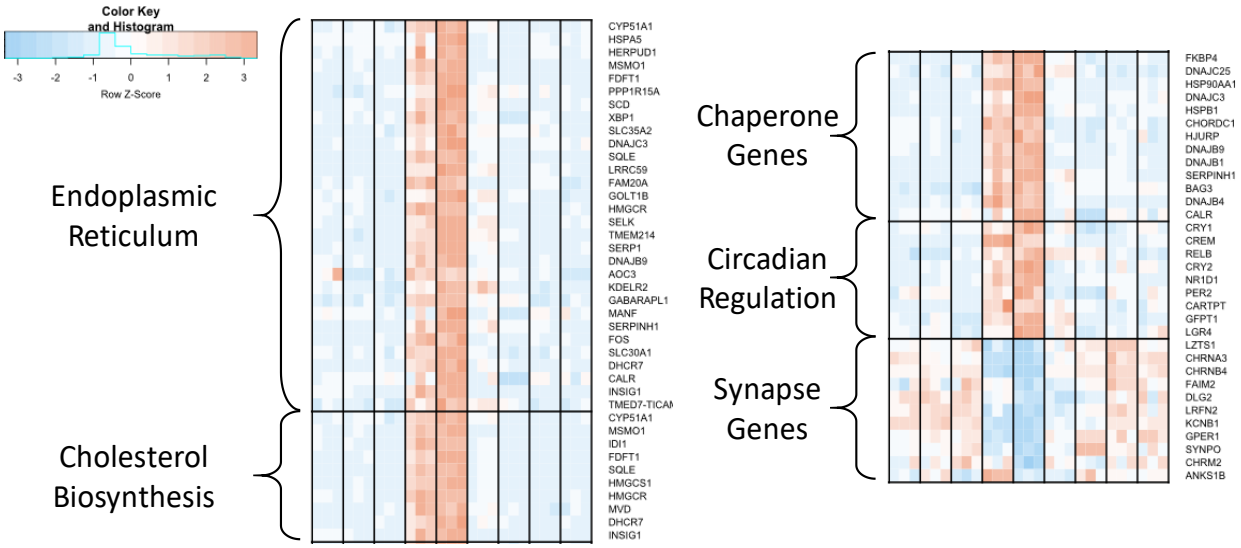

Figure 5.24. Blue Light Illumination Modulates the Expression of Genes Related to Specific Functions: The transcripts modulated by blue light were enriched in genes related to the endoplasmic reticulum, cholesterol biosynthesis, chaperone proteins, circadian regulation and synapse genes. Genes that appear in multiple clusters are plotted in each individual region.

5.3. Light Activation of SH-SY5Y cells induces similar functional Gene Groups, but not the same genes, as *in vivo* Sleep Deprivation

To what extent do the changes identified following blue light exposure of SH-SY5Y cells compare to those seen following sleep deprivation of mice? We can assess the similarity by determining the overlap of individual genes modulated following treatment and the overlap of overrepresented functional gene groups affected by treatment.

5.3.1. Direct gene comparison

At the level of individual gene comparison between mouse cortex and human SH-SY5Y cells, approximately 60-65% of genes identified as expressed in one model were also expressed in the other. Unlike mouse cortex, no genes were identified as undergoing rhythmic expression in untreated cells, and the rhythmic expression of no transcript was conserved across models. Of the 10148 genes expressed in both mouse cortex and SH-SY5Y cells, 1282 (13%) were identified as being modulated following 12-hour blue light exposure. Of the genes identified as rhythmic in mouse cortex, 17% were modulated by blue light, whilst 16% of genes modulated by sleep deprivation in mouse cortex were also modulated following opsin mediated activation of SH-SY5Y cells. Therefore, the enrichment of sleep deprivation associated genes amongst those modulated by blue light appears slight, suggesting that blue light activation of SH-SY5Y cells does not faithfully recapitulate the same gene expression changes induced in mouse cortex during sleep deprivation.

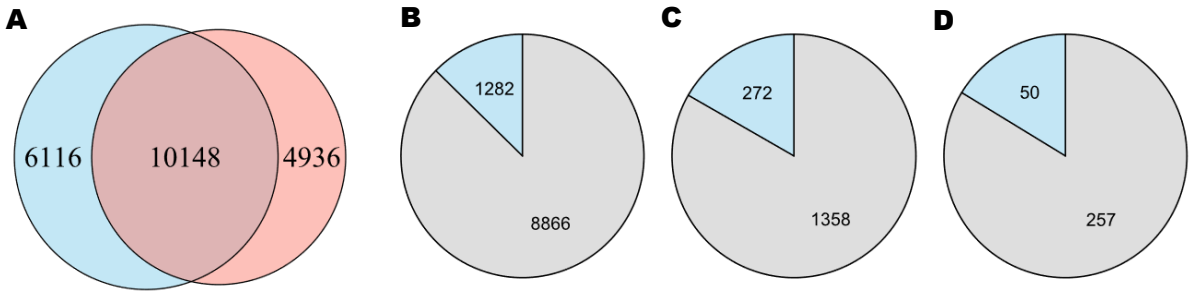

Figure 5.25. Limited Overlap of Blue Light Inducible and Sleep Associated Mouse Genes: Panel (A) demonstrates the overlap of total gene expression between the two models. 10148 genes were expressed in both mouse cortex (blue circle) and SH-SY5Y cells (red cirlce). Panel (B) shows the proportion of commonly expressed genes modified by blue light. Panel (C) shows the proportion of commonly expressed genes identified as rhythmic in mouse cortex modified by blue light, whilst Panel (D) shows the proportion of commonly expressed genes identified as sleep deprivation dependent in mouse cortex that are modified by blue light. In Panels (B-D), the blue section represents the number of genes modulated by blue light, whilst the grey section represents the number of genes in that category unaffected by blue light exposure.

In contrast, the enrichment amongst blue light sensitive transcripts of genes associated with the endoplasmic reticulum and synapse, chaperone function and circadian regulation is similar to the functional clusters identified in mouse cortex following sleep deprivation, whilst the enrichment of genes associated with cholesterol biosynthesis is reminiscent of sleep deprivation data published by other groups (Mackiewicz *et al.* 2007).

5.3.2. Cholesterol Biosynthesis is Induced in SH-SY5Y Cells, but not Sleep Deprivation

Previous studies have linked cholesterol synthesis to sleep in mouse brain, but specifically those studies found that sleep deprivation leads to a slight downregulation in cholesterol biosynthetic gene expression. In contrast, blue light activation of SH-SY5Y cells induces a marked upregulation of the pathway. Several fatty acid biosynthetic genes are also upregulated, indicative of sterol regulatory element-binding protein (SREBP) controlled transcription (Brown & Goldstein 1997).

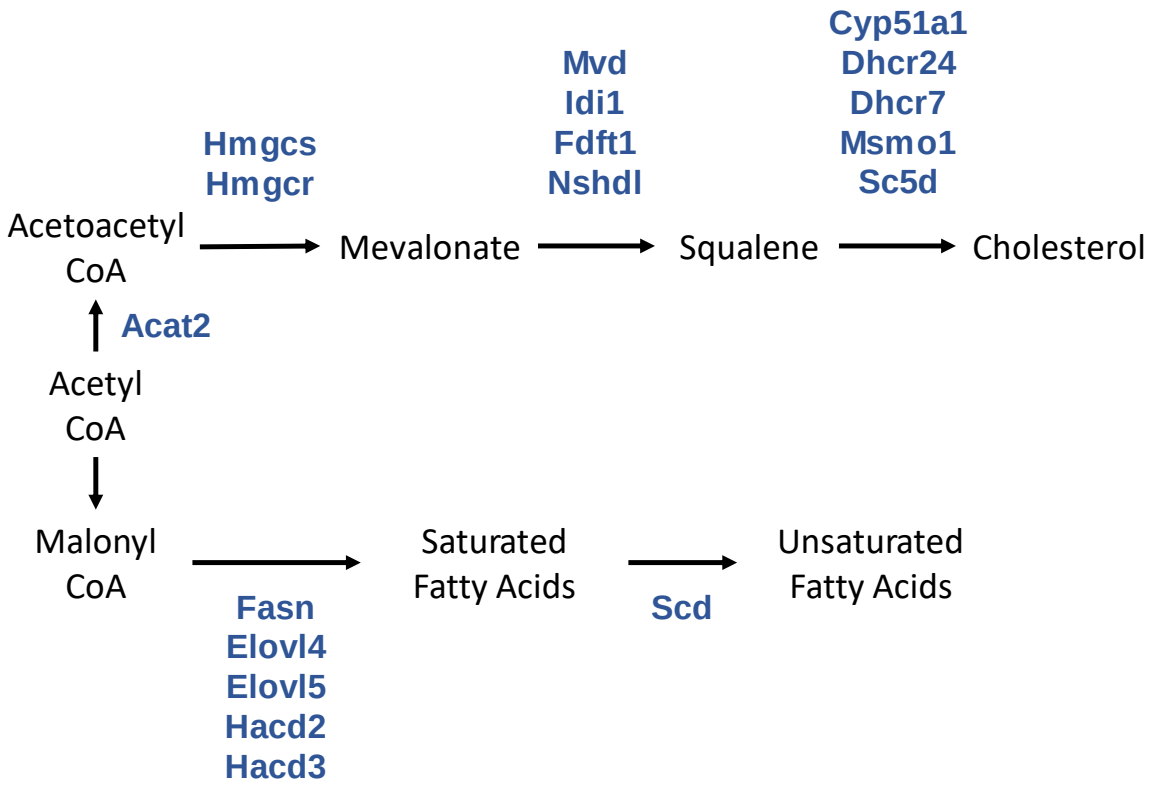

Figure 5.26. Blue Light Activation of SH-SY5Y Cells Induces the Expression of Cholesterol and Fatty Acid Synthetic Pathways: Selected metabolic intermediates in the cholesterol and fatty acid biosynthetic pathways are displayed in black. Displayed in blue are enzymes responsible for the catalysis of intermediate steps that were found to be upregulated at the transcript level in opsin expressing SH-SY5Y cells following blue light exposure.

Brain cholesterol is almost exclusively synthesised locally, and so net synthesis of cholesterol rich components such as myelin sheaths or lipid rafts requires the local induction of cholesterol synthesis (Helga & Pierre 2002; Jurevics *et al.* 1997). SREBP signalling is dependent on several cellular systems, including the molecular clock (Gilardi *et al.* 2014) and receptor tyrosine kinase or NMDA-receptor signalling pathways (Porstmann *et al.* 2005; Taghibiglou *et al.* 2009). The activation of cholesterol synthesis in response to excitatory NMDA-signalling is consistent with the induction seen in response to opsin mediated activation of cells. Cholesterol has previously been shown to influence neuronal activity and dendrite growth (Bukiya *et al.* 2017; Moutinho *et al.* 2016), whilst BDNF induces the *de novo* synthesis of cholesterol in cortical neurones, which is subsequently deposited in lipid rafts (Suzuki *et al.* 2007). The strong induction of cholesterol synthesis in response to activity in SH-SY5Y cells may therefore indicate the production of lipid rafts and the induction of synaptic homeostasis. Since BDNF is induced in response to sleep deprivation *in vivo*, it's remarkable that cholesterol synthesis is either unaffected or downregulated by sleep deprivation. The contrasting response of SH-SY5Y cells may reflect a very low spontaneous electrical activity of the cell-line prior to optical stimulation, which may greatly decrease baseline expression of activity related genes, resulting in an inflated fold change of these genes following stimulation. Similarly, if cholesterol synthesis is activity dependent, the available pool of cholesterol in cells prior to blue light exposure may be very low, and so the production of lipid rafts would oblige *de novo* cholesterol synthesis.

5.3.3. Clock Genes are Modulated in SH-SY5Y Cells and by Sleep Deprivation

A major conclusion of the transcriptomic profiling of mouse cortex was that rhythmic expression of transcripts is progressively reduced with increasing durations of sleep deprivation, with 12-hour sleep deprivation reducing the number of rhythmic transcripts by 98%. The absence of any rhythmic transcription under control conditions in this SH-SY5Y dataset excludes the possibility of a similar comparison being made here. However, it is noteworthy that genes involved in circadian regulation were an overrepresented class amongst genes that were strongly induced by blue light exposure. Previous studies have demonstrated that the expression of clock genes in mammalian cell lines can be induced by raising intracellular calcium or cAMP (Balsalobre *et al.* 2000), resulting in subsequent rhythmic gene expression. Similarly, Per2 induction by neuronal activity has been shown both *in vitro* and *in vivo,* and is linked to the presence of cAMP/Ca^{2+} response elements in the promoter region of Per2 (Balsalobre *et al.* 2000; Koyanagi *et al.* 2011; Yan & Okamura 2002). Following cessation of illumination however, the expression of core clockwork genes returns to baseline within 6 hours, and moreover does not oscillate in the following 24 hours. Therefore, the elevated expression of clock

genes appears to be tightly linked to blue-light activation and does not appear sufficient to entrain the cellular clock of SH-SY5Y cells.

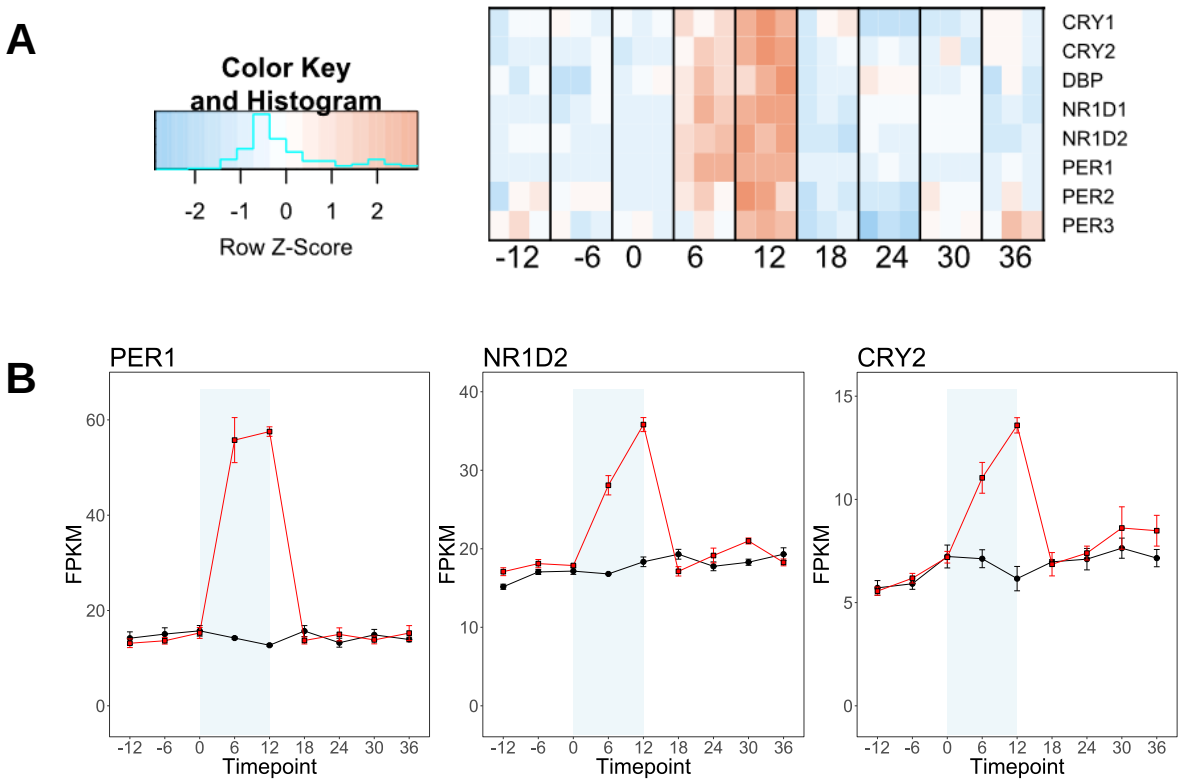

Figure 5.27. The Expression of Core Clockwork Genes is Transiently Induced by Blue Light, but does not Oscillate in Untreated Cells: Core clockwork genes are induced by blue light exposure compared to untreated controls but rapidly return to baseline following cessation of light exposure. The heatmap plots the z-score normalised expression of genes compared to untreated controls, with red indicating higher expression and blue indicating lower expression. The timepoint is indicated below, with blue light exposure occurring between 0-12 hours (A). Individual gene expression profiles are plotted in black for untreated cells, and in red for treated cells. The blue bar represents the timing of blue light exposure. Expression is plotted in FPKM (fragments per kilobase per million reads).

5.3.4. Chaperone Genes are Induced in both SH-SY5Y cells by Sleep Deprivation

Similar to in vivo sleep deprivation, several chaperone genes are induced following blue light illumination of opsin expressing SH-SY5Y cells. Genes induced compared to dark-maintained cells include CHORDC1, DNAJC3, HSP90AA1 and HSPA5, all of which are similarly upregulated in mouse cortex during sleep deprivation. Like the overwhelming majority of blue-light modulated genes, the induction of chaperone genes is limited to within the illumination period and rapidly return to baseline expression levels in darkness.

Several chaperone genes are named heat shock proteins due to their involvement with the cellular response to elevated temperature (Richter *et al.* 2010). One unavoidable consequence of illuminating cells is that absorption of light by the cell medium or any part of the dish will result in a local temperature increase. Because elevated temperatures quickly induce chaperone expression, it is appropriate to be cautious before concluding that light exposure induces chaperone expression through a photocurrent induced increase in activity, rather than through an unwanted heating effect. However, introducing distance between the light source and cells, placement of fans and pauses between cycles of illumination reduced temperature increases during illumination to approximately 0.3^{o}C, which is comparable to the variation of temperature measured at different levels within the incubator. Conversely, our preliminary transcriptomic analysis of SH-SY5Y cells found that chaperone genes were induced particularly in opsin expressing cells. Although conditions varied greatly between the two experiments, it is noteworthy that cells involved in preliminary experiment underwent a tenfold greater increase in temperature than those in the final transcriptomic timecourse experiment, and yet the expression of chaperone genes in wild type cells was largely unaffected. Whilst it is possible that the expression of opsin containing constructs sensitises cells to heat stress, this data is consistent with the expression of chaperone proteins being linked to neuronal activity. Indeed, exposure of primary neurones to glutamate induces HSPA5 expression in the absence of a temperature increase, and is associated with the local activation of the unfolded protein response at postsynaptic dendrites (Atsushi *et al.* 2017).

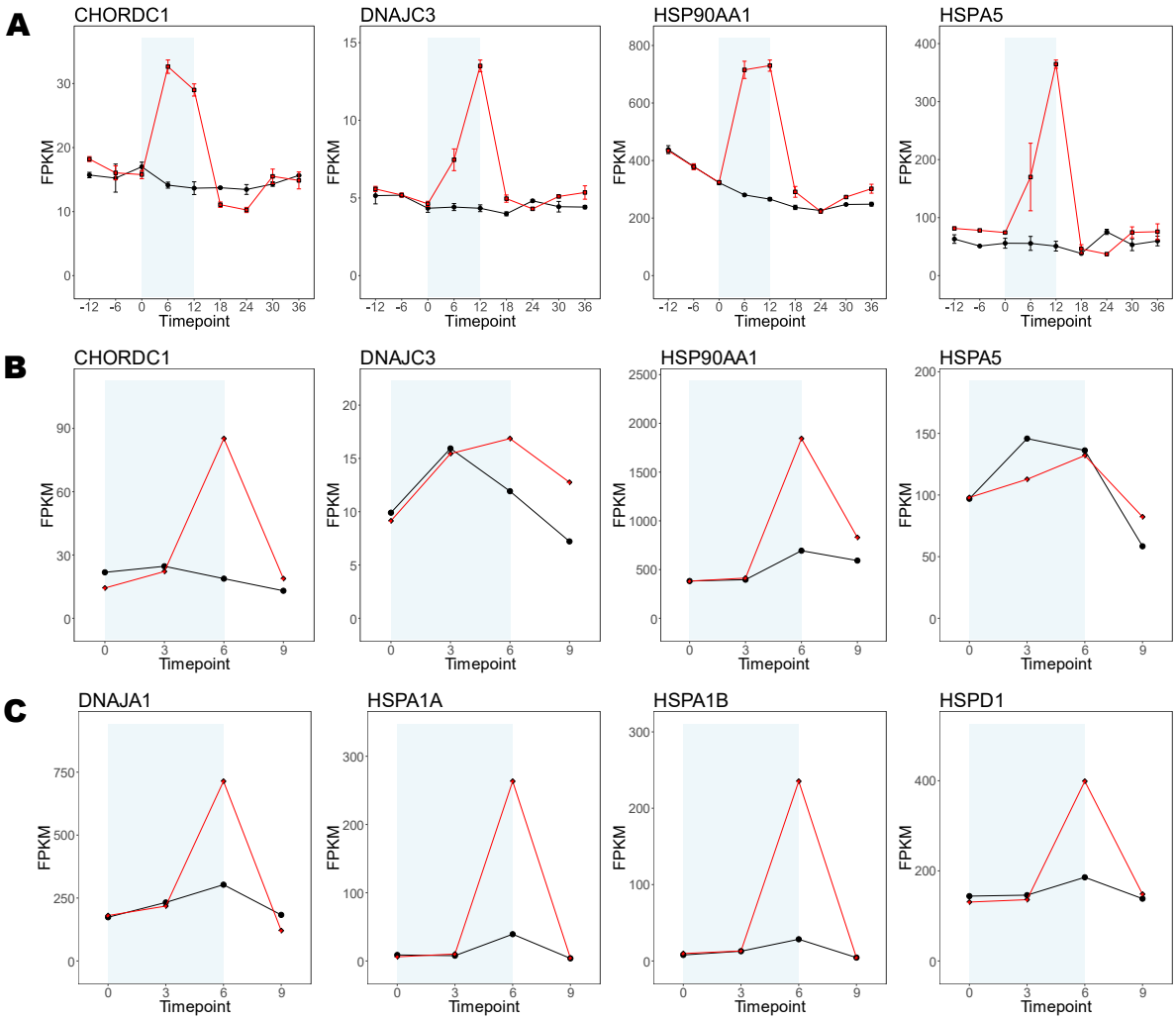

Figure 5.28. The Expression of Chaperone Genes is Induced only in Illuminated Opsin Expressing SH-SY5Y cells: Panel A shows the expression of sleep deprivation induced chaperone genes during 12 hour illumination in CoChR expressing SH-SY5Y cells (red line), compared to dark maintained CoChR expressing cells (black line). Panels B and C shows the expression of genes during 6 hour illumination in ChR2-2A-Hal expressing SH-SY5Y cells (red line), compared to illuminated wild-type cells (black line). Note that timepoints are spaced by 6 hours in Panel A and by 3 hours in Panel B. Illumination of opsin expressing cells induces chaperone expression, but opsin expression or illumination alone does not. The timing of blue light exposure is indicated by the blue shading.

The expression of chaperone genes has previously been linked to sleep deprivation in both flies (Shaw *et al.* 2000) and rodents, including following adrenalectomy (Maret *et al.* 2007; Mongrain *et al.* 2010; Terao *et al.* 2003). It appears that chaperone induction has a protective function, with temperature mediated increases in chaperone expression protecting against the lethality of subsequent sleep deprivation in flies and glutamate excitotoxicity in primary neurones (Rordorf *et al.* 1991; Shaw *et al.* 2002). Since chaperone proteins are conserved across kingdoms, they may be a conserved feature of sleep deprivation across species and might hint at some of the fundamental functions of sleep. It is also intriguing to note that chaperone genes are induced in peripheral tissues such as the liver during

sleep deprivation, and so their sleep-related function may not be limited to only within the brain. Moreover, our study found that chaperone expression is associated with both spontaneous and enforced wakefulness, indicating that they play a role in physiological wakefulness, rather than responding only to a stress specifically associated with exceptionally prolonged periods of waking.

Although mammalian body temperature is closely linked with the state of wakefulness, it is likely that chaperones perform a temperature-independent function during sleep deprivation. The commonly proposed function of chaperone protein induction during sleep deprivation is to reduce translation of proteins, which is expected to decrease additional cellular stress (Harding *et al.* 2000). Indeed, ageing reduces the induction of chaperone proteins and increases the abundance of pro-apoptotic markers in mouse cortex following sleep deprivation (Naidoo *et al.* 2008). Since protein synthesis is energetically costly, the induction of chaperones may act to limit the anabolic load occurring during wakefulness.

5.3.5. SH-SY5Y Transcriptomic Response may be Orchestrated by Creb 3

Intriguingly, cholesterol biosynthetic enzymes and the unfolded protein response are both induced by the transcription factor Creb3, also known as Luman (Ying *et al.* 2015). Luman mRNA is locally translated at sites of axonal damage and is subsequently transported to the nucleus where it stimulates transcription (Ying *et al.* 2014). Luman mRNA knockdown disrupts axonal regeneration in response to injury, whilst previously it has been shown that components of the unfolded protein response are involved in BDNF neurite outgrowth (Hayashi *et al.* 2007). Therefore both chaperone and cholesterol biosynthesis induction during blue light exposure may support neurite outgrowth in SH-SY5Y cells. Consistent with this, Luman expression is elevated in SH-SY5Y cells following 12 hour blue light exposure. Although our *in vivo* transcriptomic screen did not find Luman to be regulated by sleep deprivation, a previous study found that Luman demonstrated markedly increased DNA-hydroxymethylation in mouse cortex following 6 hour sleep deprivation (Massart *et al.* 2014), indicating that Luman may play a role in sleep *in vivo*.

5.3.6. Experimental Design Considerations

The ultimate aim of this project was to produce a low cost, human derived *in vitro* model of sleep and sleep deprivation. Outlined in the results section is our approach and experimental findings whilst we were developing this model. The expression of light-gated channels in SH-SY5Y cells was used to promote membrane depolarisation in response to light, and therefore treated cells were actually subjected to two interventions: expression of an opsin and exposure to light. Exposure to high light levels likely has opsin-independent effects on the transcriptome of cells, but similarly, the expression of the opsin itself almost certainly has profound effects, including on the growth rate of the cells. The two intuitive controls used to determine the effects of blue light exposure on opsin expressing SH-SY5Y cells were either cells of the same genotype maintained in darkness, or cells of a different genotype maintained in the same light routine. Ideally, both sets of controls would be carried out in each experiment, but this would not only impose considerable additional cost, but also complicate the design and execution of the experiment. During the development and characterisation of this model, the control group chosen to compare the treated group against was therefore an important consideration, and the best choice of control groups varied between experiments.

Initially it was important to determine whether the opsin was functionally able to modify transcription, and because cells were subjected to significant heating during preliminary experiments we were also expecting large scale changes in expression during illumination through opsin-independent mechanisms. In the early stages of the development of the model, the control group was therefore chosen to be wild-type cells treated with the same light exposure as opsin expressing cells. In this way, the effect of the opsin itself was identified, allowing us to choose a suitable opsin to activate SH-SY5Y cells with.

However, following the introduction of physical refinements such as the elevation of the cells above the light source and the installation of fans to reduce heating and promote cooling during illumination, our concerns about the heating effects of illumination were reduced. Subsequently, we had also confirmed through microscopy and qPCR that CoChR was active in SH-SY5Y cells and able to trigger intracellular events in response to light. We had also found that the response to light was modulated by several environmental cues, including cell density, time between plating and light exposure, and pH. Therefore, in later experiments we were less concerned about the effects of heating (because the increase in temperature during illumination had been decreased by 90%), and more concerned about other aspects of the environment that cells were exposed to during illumination. We noticed that SH-SY5Y lines expressing different opsins demonstrated differences in growth rate. Opsin expressing cells demonstrated longer doubling time in culture compared to wild-type cells,

presumably due to the presence of puromycin in the growth medium and the burden imposed by the high expression of the opsin and antibiotic resistance genes. Therefore, during preparation for experiments, it was difficult to match cell density between different genotypes, which also led to different rates of acidification of the medium following plating out the cells. These secondary effects of differing genotypes, coupled with the expected changes in gene expression in response to the highly expressed opsin construct and the presence of antibiotic, would possibly change the baseline expression of several genes and also introduce variation between experiments. Therefore, for later experiments, we opted for dark maintained, opsin expressing cells as a control for light exposed cells.

A third possible control group would have been a cell line expressing a non-functional opsin which is then exposed to the same light regime as CoChR expressing cells. We explored this possibility but could not identify a suitable non-functional construct. Introduction of the R120A and E107A mutations has previously been shown to reduce channelrhodopsin photocurrents by up to 90% (Kato *et al.* 2012), but whether the corresponding mutations in CoChR would be sufficient to remove all opsin mediated effects was unknown, and a partial effect of the opsin would greatly complicate subsequent data analysis.

It should also be noted that the possible experimental designs for downstream experiments are limited if the chosen control group cannot respond to light through opsin mediated pathways. Ultimately, our transcriptomic profiling experimental design only exposed cells to light for 12 hours, whilst control cells were maintained in constant darkness. Since RCAMP recording of cells did not identify any spontaneous intracellular calcium events, it could be argued that the default state of cells is a low activity state. Given the complete absence of identified rhythmic genes in the dark maintained cells, it appears this default state does not rhythmically transition into a more active state that may reflect the sleep-wake cycle. Therefore, this experiment might not have modelled sleep deprivation *per se*, but instead a single period of waking, the duration of which is less than the typical wake bout for humans. In hindsight, another experimental design may have been to expose cells to a series of 12 hour light-dark cycles before the start of the experiment, to recreate a normal sleep-wake cycle. Sleep deprivation could then be modelled by extending the illumination whilst the controls would be exposed to darkness. Importantly, a prerequisite for such experimental designs is that both the control and “sleep deprivation” group respond to blue light in the same manner during the acclimatisation period that mimics the normal day.

5.3.7. Perspectives on Future Cell Studies

We have undertaken a reductionist approach to investigating sleep by characterising the effect of prolonged activity on SH-SY5Y neuroblastoma cells. Reductionist approaches have been extensively used to model intracellular changes in complex processes, such as diabetes, but have yet to be widely used in the sleep field. The premise for this model is based on the work of Hinard *et al*, who showed that the transcriptional effects of sleep deprivation can be recapitulated *in vitro* by pharmacological activation of primary neurons derived from mouse cortex (Hinard *et al.* 2012). As a trial, we treated SH-SY5Y cells with the same cocktail and showed that they still respond at the transcript level to pharmacological activation. However, the temporal precision of optogenetic tools allows the rapid and complete removal of stimulus, offering the possibility of modelling the subsequent recovery phase or inducing intermittent activity. Stable expression of opsin based constructs in neuroblastoma cells has provided access to an effectively unlimited quantity of low cost, low variability neuron like cells whose activity can be easily manipulated. These characteristics are some of the primary advantages of taking a reductionist, *in vitro* approach.

A key consideration for future *in vitro* experiments is whether to continue using SH-SY5Y cells as a model system or to use another cell line, primary neuron or explant-based culture. Primary neuron or brain explant-based approaches would facilitate the comparison with *in vivo* mouse data, and so would be especially useful in determining which molecules modulated by sleep deprivation are dependent on local neuronal activity, rather than associated with wake controlling nuclei within the brain or circulating hormones such as corticosterone. However, such an approach would not be likely to offer any more insight than *in vivo* studies into human specific sleep modulated molecules, nor would it facilitate a low cost, high-throughput screening platform for potential wake modulating compounds.

Stem cell culture offers an intermediate solution, whereby human cells very closely matching a neuronal phenotype, or even organoids closely matching brain tissue (Lancaster & Knoblich 2014), can be produced. Indeed, opsin mediated activity was recently demonstrated in human stem cell-derived neurones (Klapper *et al.* 2017). Modulating the activity of human derived cerebral organoid cultures could provide an extraordinary level of insight into the molecular effects of sleep deprivation in humans. However, the high cost and labour intensity of stem cell culture would hinder the development of a stem cell-based model and its eventual use as a drug screening platform.

The low cost and scalability of cell lines makes them the most suitable model for high-throughput screens. However, the fundamental disadvantage of cell line based approaches is the question of their validity; specifically whether an immortalised adrenal neuroblastoma cell line can be used to model

senescent, long lived neurons in the brain. Although several previous studies had outlined similarities between SH-SY5Y cells and neurones, those studies used a range of differentiation protocols, which appeared to interfere with opsin mediated gene expression. Replacing SH-SY5Y cells with another cell line is one option for future experiments. NG108-15 cells, which are known to have an entrainable cellular clock (Hampp *et al.* 2008), had been considered for this project, but were rejected because they are rat-mouse hybridoma cell line, which was expected to complicate sequencing based transcriptomic experiments. Other cell lines commonly used to model neurons include the human derived Ntera2 cells (Pleasure & Lee 1993), rat derived PC12 cells (Greene & Tischler 1976) and mouse derived Neuro 2a cells (Tremblay *et al.* 2010). Although these cell lines may resemble mature neurons in several aspects, whether they would provide more suitable sleep-deprivation models than SH-SY5Y cells is unclear.

Model System	Cost and Labour Intensity	Validity as Neuronal Model	Insight into Human Biology	Use in Drug Screens
In vivo Sleep Deprivation	+++	++++	+	++
Primary Neurons and Explant Culture	+++	+++	+	+
Stem Cell derived Neuronal Culture	++++	+++	+++	+
Immortalised Cell Line	+	+	++	++++

Figure 5.29. Comparison of Neuronal Model Systems: Several model systems are available to researchers investigating neuronal biology. The choice of which system to use depends on the ultimate end goal of the experiment, as well as the available resources.

5.3.8. Future *in vitro* experiments

Further characterisation of the opsin expressing cells is required for SH-SY5Y cells to continue to be used as an *in vitro* model of sleep deprivation. Electrophysiological characterisation of the SH-SY5Y cells used in this experiment would quantify the electrical activity of the cells more directly than the RCAMP-based calcium imaging experiments performed in this thesis. Combining electrophysiological measurements with specific inhibitors of ion channels would also identify which ion channels are operating during illumination, and also whether prolonged illumination modulates the activity of specific ion channels. To some extent, these experiments could be carried out using genetically encoded fluorescent voltage sensors (Perron *et al.* 2009), however bleaching of the sensors during

opsin activation may complicate the precise quantification of membrane electrical gradients in this manner.

A major failing of the experimental design used in this study is the lack of 24 hour rhythms exhibited in the transcriptome of control cells. Efforts to entrain the molecular clock of SH-SY5Y cells using serum shock failed, whilst pre-treatment of SH-SY5Y cells with dexamethasone, which is routinely used to synchronise the cellular clocks of other cell lines (Rey *et al.* 2016), abrogated subsequent c-FOS induction in response to blue light. However, a cell line with a functional molecular clock may not actually be desirable. Core clock genes were robustly induced by illumination in SH-SY5Y cells, whilst opsin expressing U20S cells demonstrated a phase shift following illumination, indicating that the resetting of the molecular clock would confound transcriptomic studies in cells with functional rhythms.

One approach to recreate rhythmic expression in SH-SY5Y cells may be to subject both the control and "sleep deprived" cells to 12:12 light-dark cycles prior to the beginning of the timecourse. The control group would continue on this 12:12 cycle throughout the time course, whilst the treated group would have the illumination extended into the habitual rest phase. However, how to suitably model the subsequent recovery phase following sleep deprivation is not readily apparent. One option would be to continue the light dark cycles, such that the treated group would be exposed to 36 hour continuous illumination. This may be appropriate if we were trying to model the effects of 36 hour enforced wakefulness, but is flawed when comparing to mice that have the opportunity to sleep during their habitual active phase following sleep deprivation. A second, more novel option is to model the illumination pattern during the recovery phase, or perhaps even the entire experimental design, on EEG determined wake-sleep patterns of mice. Indeed, one experimental advantage of optogenetic tools over pharmacological agents is that stimuli can be introduced and withdrawn with millisecond precision, and so even the fragmented sleep-wake patterns of rodents could be closely mimicked with illumination patterns. Basing the illumination pattern on EEG data of undisturbed and sleep deprived mice might aid in directly comparing the subsequent cell-line expression data to that found *in vivo*.

If SH-SY5Y cells are capable of accumulating homeostatic sleep pressure, it is feasible that the cells would release a somnogenic signal molecule into the extracellular space during illumination. The release of signal molecules could be investigated using a perfusion system to continuously sample cell medium during constant illumination, and the molecules identified using mass spectrometry based proteomic or metabolomic approaches. Any molecules identified in this screen could be intracranially perfused into mice, and the *in vivo* effect on sleep-wake cycles monitored either through electro-encephalography or video tracking. Whether SH-SY5Y cells release any neuroactive compounds during

illumination could be more directly tested *in vitro*. The cell medium of light treated cells could be transferred to a second well containing SH-SY5Y cells, primary neurones or an explant culture. Whether the donor medium is sufficient to modulate neuronal activity in the recipient cell culture can be determined by electrophysiological parameters, fluorescent reporter intensity or c-Fos expression.

It is worth remarking that prolonged wakefulness *in vivo* eventually leads to the failure of neurones to electrically respond to stimuli (Bushey *et al.* 2015; Vyazovskiy *et al.* 2011). In contrast, CoChR directly and reliably depolarises the membrane, even following repeated stimulation (Klapoetke *et al.* 2014). Because CoChR is a microbial opsin, it is likely insensitive to mammalian pathways, such as the arrestin pathway, that limit the activity of receptor signalling. Therefore the expression and activation of CoChR in a neuronal cell may drive a supraphysiological duration of activity that bypasses the mechanisms through which neurons would usually enter an activity induced sleep-like state. Experimentally, this may be beneficial and aid in the identification of stress responses. However, enforcing activity in neurons past the physiological limits may induce non-physiological pathways or even cell death. Depending on the aims of the experiment therefore, the use of a step-function-opsin may be more appropriate to modulate activity of *in vitro* cells. The low conductivity and slow kinetics of step-function opsins promote a sustained subthreshold increase in excitability of neurons (Berndt *et al.* 2009). Therefore step-function opsins increases the spontaneous electrical activity of neurons without directly invoking action potentials, and so may be more suitable for experiments that aim to preserve the entry of neurons into a sleep-like state.

6. General Discussion

6.1. What is Sleep Deprivation?

This thesis aimed to outline the changes that occur at the molecular level during wake, sleep and sleep deprivation. The importance of the homeostatic and circadian control of sleep timing encouraged us to carry out a timecourse style experiment throughout, with tissue production being facilitated by a semi-automated sleep deprivation approach. We then characterised the effects of sleep deprivation at a system-wide level using omics approaches. The abundance of molecules during the course of a normal day and during sleep deprivation and subsequent recovery then allowed us to speculate on the involvement of these molecules in the response to sleep deprivation.

Therefore, this thesis centred on the effect of two separate variables on the molecular biology of the brain: time and sleep deprivation. But what sleep deprivation represents is not straightforward, nor is deciding what is desirable from experimentally imposed sleep deprivation. In addition to prolonged wakefulness, sleep deprivation also represents a period of increased opportunity for eating, activity, social behaviour and light exposure. Since the experiments presented in this thesis then consider later timepoints, during which period mice are undergoing recovery sleep, the effect of these confounders is later reversed. However, it is important to recall that mice have fragmented sleep and spend about 30% of their rest phase awake, and so already have opportunity for these activities throughout the day in between bouts of sleep. Perhaps larger confounders are that experimental sleep deprivation also incorporates a potential stress response, which may drive gene expression changes through glucocorticoid induction (Mongrain *et al.* 2010), and a learning or exploratory response, which itself has been shown to induce sleep deprivation related genes such as Homer1a and Arc (Vazdarjanova *et al.* 2002).

During experimental design, the researcher is able to tailor conditions to precisely identify the effect of the exact variable that he is interested in. Experimentally, the confounders listed above, except the learning response to the application of sleep deprivation itself, could potentially be controlled. For example, mice can be adrenalectomized and single housed in darkness without access to food. Arguably, if the researcher is solely interested in the homeostatic drive for sleep, the experiment could also be performed on mice whose circadian rhythms have been ablated through either constant light exposure, genetic disruption of the molecular clock, or ablation of the SCN. Under such conditions, any changes seen could be reliably attributed to prolonged wakefulness, rather than a confounder of experimental sleep deprivation.

However, applying all of these interventions before sleep deprivation not only imposes significant labour and ethical constraints on the experiment, but also drastically changes the model from which the data are gathered. Although this model may more precisely identify wake dependent genes, and so may be interesting from a basic science perspective, the model is several steps further removed from humans, limiting the translational uses of the data. Furthermore, in trying to remove confounders during an experiment examining the homeostatic response to sleep deprivation, a researcher may unwittingly begin to unpick important components of the homeostatic machinery itself. Therefore, by imposing several experimental interventions to generate a better controlled experiment, the resulting data may indicate wholly unphysiological responses. Based on this reasoning, the experiments in this thesis involved sleep deprivation that was performed on wild type mice under conventional housing conditions, resulting in potentially more confounded data but from a more biologically relevant source.

6.2. What is the Aim of Sleep Deprivation?

Considering what is the most desirable outcome from sleep deprivation is often overlooked. Generally it seems 100% wakefulness is the aim of sleep deprivation protocols, with total sleep deprivation being obtainable for the initial stages and then ranging from 80-95% wakefulness during longer term sleep deprivations. Total sleep deprivation has the advantage of being a clearly defined behavioural state, however, as well as being impracticable, is again unphysiological for mice. Perhaps, sleep deprivation should instead aim to achieve 75% wakefulness, similar to the proportion of time spent awake by mice during their active phase. However, any stress profile molecules that are suddenly induced during particularly high homeostatic pressure to immediately induce sleep may be overlooked by less severe sleep deprivation protocols. On balance therefore, it may be best to aim for total sleep deprivation but not be concerned if mice nevertheless spend about 10% of the time asleep.

However, the practical difficulties surrounding applying 100% sleep deprivation introduces a further confounder that may vary between protocols and experimenters. During manual sleep deprivation, a mouse may be asleep for a couple of minutes whilst the experimenter is engaged with other cages. Because of the preceding sleep deprivation, that mouse will have accrued significant sleep pressure and therefore have a deeper sleep during this period, characterised by increased delta power and periods of slow wave sleep. Therefore, this mouse, over a period of 12 hours, will have prolonged periods of wake followed by prolonged periods of deep sleep, and so experience a more consolidated wake-sleep pattern. In contrast, a mouse undergoing automated sleep deprivation, such as that used in this thesis, may have a markedly different sleep pattern, despite spending a similar period of time

asleep. Once acclimatised to the movement of the bar, it was observed that mice typically gravitated to one corner of the cage and remained there for extended periods of time. Whilst in that corner, mice would have to only interact with the bar every 15 seconds, and so may have been able to sleep whilst the bar moved to the other end of the cage and returned back again. These mice therefore would never have a sleep opportunity longer than 15 seconds, but that opportunity would occur four times every minute. Entering into this experiment, the author of this thesis was uneasy that, depending on how long an individual mouse required to fall asleep, the total proportion of time spent awake during automated sleep deprivation could vary drastically. It was for this reason that manual sleep deprivation was applied in addition to the automated bar for the second half of 12 hour sleep deprivations performed in this thesis. Any sleep achieved by the mouse during automated sleep deprivation would be expected to be limited to light stage 1 sleep, with a near complete absence of deeper slow wave sleep or REM sleep. Therefore, even though gentle handling and automated sleep deprivation may achieve similar sleep deprivation efficiency in terms of duration of wakefulness, the stages of sleep achieved and the distribution of those stages may vary drastically with difficult to foresee effects. The existence and poorly understood effects of localised sleep further complicates differences between protocols. Total sleep deprivation, if achievable, may result in an increased incidence of local sleep, whilst consolidated opportunities for sleep may lower the occurrence of local sleep. Since the effects of altered sleep architectures is still poorly understood, the only practical solution may be to publish as much information about sleep architecture alongside molecular data, such that data from different deprivation techniques can be retrospectively reconciled.

6.3. Sleep Architecture during Automated Sleep Deprivation.

The architecture of sleep during sleep deprivation is therefore a significant experimental design feature, and so a noticeable omission from this thesis is the measurement of sleep and sleep architecture, including under typical conditions, during sleep deprivation and during subsequent recovery sleep. Steps were taken before submission of this thesis to quantify sleep patterns of mice subjected to our experimental sleep deprivation protocol, which centred on EEG and video tracking based methods. EEG is the gold standard of sleep quantification, and also has the distinction of being able to define different sleep stages in mice. However, the requirement for the surgical implantation of electrodes imposes ethical and training limitations that caused significant delays in generating this data. In contrast, video tracking represents a non-invasive approach to quantify sleep, using prolonged lack of movement as a proxy for sleep. Although not described in this thesis, video tracking was performed on single housed mice subjected to sleep deprivation, but the subsequent data proved

difficult to analyse and limited in its applicability. Significant video editing was required to account for the background movement of the woodchippings and to remove unequal light densities that interfered strongly with tracking software, and several assumptions were imposed when the mouse disappeared from view (usually due to climbing the sleep deprivation bar). Because tracking uses prolonged inactivity as a proxy for sleep, sleep during the movement of the bar was inevitably "quantified" as totally absent. Video tracking of the dark phase indicated that mice had been successfully sleep restricted, evidenced by an increase of inactivity, but without any indication of the architecture during recovery sleep or the percentage wakefulness during sleep deprivation. Due to the practical difficulties, the data yielded from this experiment was qualitative at best and offered no more insight than the experimenter's observations, and as such was omitted from this thesis.

Because of this, EEG experiments remained planned. During the corrections of this thesis, preliminary EEG data from the protocol used here was generated on single housed males. In line with the author's expectations, sleep deprivation during the first 3 hours was total. Around 4 hours into sleep deprivation, an unusual pattern emerged, whereby mice would experience one epoch (4 seconds) of stage 1 sleep every 4 epochs. These sleep bouts were concentrated into small bursts, whereby mice would sleep 4 seconds every 16 seconds for approximately 20 minutes before exhibiting 20 minutes of total wakefulness. This pattern was extended throughout the remainder of the 12-hour automated sleep deprivation protocol, with total wakefulness averaging approximately 90%, despite the lack of additional manual sleep deprivation in this protocol. Importantly, there was not a single epoch of REM sleep, which may indicate why the expression of the REM sleep related VIP transcript was affected during sleep deprivation but was flat during the course of a normal day.

6.4. Limitations of the Techniques Used in this Thesis

Transcriptomic profiling of sleep deprived mouse cortex identified several genes previously implicated in sleep deprivation, and provided novel data tracking their recovery over the following 36 hours. Particularly striking was the observation that several genes previously implicated as demonstrating a homeostatic profile actually appeared to be dependent on the current state of the animal, rather than the total duration of recent wakefulness, with only Crh resembling the ideal homeostatic profile. Other genes (e.g. Gjb6, Mfsd2a, Sdc4, Sult1a1 and Vip) were induced in a seemingly dose-dependent manner for extended periods following sleep deprivation, and yet the expression of these genes does not appear to be associated with homeostatic sleep pressure in non-sleep deprived controls. Finally, the rhythmic amplitude of global transcription was found to be progressively dampened following increasing durations of sleep deprivation.

The large scale nature of this experiment was greatly facilitated by the comparable robustness and reproducibility of RNA-extraction, library preparation, sequencing and bioinformatic pipelines associated with RNA-Seq based transcriptomics. The limited technical variability, coupled with the large fold-changes in transcript expression that can be elicited by sleep deprivation or blue-light illumination of cells, allowed the author of this thesis to identify several sleep dependent genes with high confidence. However, multiple approaches are used to make alignment computationally less demanding, and during quantification of reads, several assumptions and approximations are built into software packages about how to normalise libraries, deal with duplicate reads and reads that align to multiple regions in the transcriptome. Different pipelines may deal with these problems in markedly different ways, whilst the researcher may impose further choices. Therefore, using different settings or pipelines to analyse the same raw transcriptomic dataset may yield different conclusions. In some respects, this observation emphasises the importance that different research groups perform similar experiments. Through the course of previous microarray studies, some sleep deprivation related genes have been repeatedly identified, whilst others are unique to specific screens. It is only through repeated experimentation that the "core" sleep deprivation genes are converged upon.

However, the major drawback of transcriptomic studies is not their reliability, but their utility. Knowing that a transcript is upregulated during sleep deprivation is initially only of limited use for translational research. Indeed, a recently published study examining the effect of mouse strain on the transcriptomic correlates of sleep deprivation found that some wake dependent genes are not even conserved to other strains of mouse (Diessler *et al.* 2018)! Although the expression of that gene can be experimentally modified in rodents through the use of transgenic lines or viral vectors, the therapeutic use of viral vectors in the human brain is a very invasive tool with which to treat sleep related disorders. Potentially, if the RNA codes for an extracellular signalling protein, infusion of the protein product or a peptide mimetic may play a therapeutic role. However, in the future, as the transcriptomic effects of ever more interventions are characterised, it may be possible to mine the available datasets and identify an intervention that induces a transcriptional response that mirrors that of sleep deprivation. This approach may identify novel treatments that counteract the effects of sleep deprivation.

The rational design of drugs would perhaps be most greatly facilitated by understanding which proteins and especially which metabolites play a role in the biological response to sleep deprivation. The enzymatic activity or binding interactions of proteins can be disrupted or enhanced by small molecules, which if able to cross the blood-brain barrier may ultimately provide an orally available drug to combat sleep related disorders. Indeed, phosphodiesterase inhibitors have previously been identified as a potential therapeutic tool to combat the cognitive defects associated with restricted

sleep (Guo *et al.* 2016; Vecsey *et al.* 2009). An even more direct approach would be to create mimetics of endogenous somnogenic small molecules to modulate sleep, similar to how caffeine interferes with the sleep-promoting effects of endogenous adenosine. Therefore, following the characterisation of the transcriptomic effects of sleep deprivation, we then sought to characterise the proteomic and metabolomic effects.

Our proteomics dataset demonstrated that hundreds of proteins are affected by sleep deprivation, whilst very few were statistically altered in undisturbed animals. However, the overlap between the proteomic and transcriptomic datasets was disappointingly small, a surprisingly common observation (Maier *et al.* 2009). Recently, a phosphoproteomic screen following 6 hour sleep deprivation indicated that there are large scale phosphorylation events following sleep deprivation (Wang *et al.* 2018). That same study identified only a handful of proteins whose abundance were significantly changed following sleep deprivation, indicating that the proteomic effect of short term sleep deprivation may be very small. This general trend is consistent with the concept that anabolism predominates during sleep, and therefore during wake, post-translationally modifying existing proteins rather than *de novo* synthesis may the mechanism through which protein activities are modulated in response to prolonged wakefulness. It may be intriguing to perform sleep elongation studies to determine whether the effects of excessive sleep are also mediated through modifications or through additional protein synthesis.

Although the abundance of proteins from different samples within the same multiplexed experiment can be compared with high precision, normalisation and comparison between different multiplexes is very difficult. Because there were only 10 isobaric tags available at the time of experiment, simultaneously interrogating the effects of different treatments at multiple timepoints was not technically feasible. In contrast, our metabolomic approach was able to simultaneously compare several timepoints in replicate. However, the precision of the metabolomic approach was not great enough to identify small fold changes in metabolite abundance. In hindsight, perhaps we should have instead examined a lower number of timepoints with many more replicates, in order to maximise our statistical power to identify sleep dependent molecules.

6.5. Value of Global Omic Approaches

The major advantages of examining biological processes at the system wide level are the possibilities to identify previously unimplicated pathways and the value of raw data for retrospective analysis, either by other groups with interests in different pathways, or by the same researcher following some further experimentation. With the ever decreasing cost of sequencing, transcriptome level profiling is

becoming a financially viable alternative to performing multiple quantitative PCRs, and as more transcriptomic datasets are accumulated and made publicly available, unexpected parallels may be drawn between seemingly very different conditions, potentially revealing novel treatment strategies.

A major downside of bulk sequencing, proteomics and liquid-chromatography mass-spectrometry is that information is lost regarding which cells or tissue regions are responsible for the observed changes. Potentially, a gene may be upregulated in every single cell during sleep deprivation, but a more likely scenario would be that each gene is upregulated in specific subsets of cells. One solution may be to compare genes of interest with the Allen Brain Atlas (Lein *et al.* 2006) or the recently published single cell sequencing based Tabula Muris tool (Schaum *et al.* 2018). However, these atlases are typically performed on mice under standard conditions, and so a gene whose expression is acutely induced at a specific time of day or by a treatment may be absent from these references. Potentially, a treatment may induce genes specifically in cell types that otherwise do not express that gene, and as such the atlas may be completely misleading. Under these circumstances, performing fluorescence *in situ* hybrisation (FISH) following transcriptomic studies may yield useful spatial data, and has previously been performed on sleep deprived mouse brain (Thompson *et al.* 2010). Equivalent reference atlases for proteomic and metabolomic studies would be very valuable tools

However, whilst studying heterogenous tissue or cell types, such as neurones, important molecules may be overlooked by bulk omic approaches. For example, if a small number of cortical neurons were entirely responsible for the homeostatic sleep drive, which they signalled through expression of a single gene, bulk sequencing would likely fail to identify this gene. If the gene is unique to that cell type, the resultant low number of reads may not reach the expression cut-off value necessary to be considered. Conversely, if that gene were expressed by all cell types and undergoes a tenfold increase in only a single cell type during sleep deprivation, that fold increase is greatly diluted by contributions from other cell types and likely not reach statistical significance.

Ideally, information about which cells are responsible for gene expression changes would therefore be preserved during transcriptomic experiments. Single cell sequencing technology now makes this possible, with cell transcriptomes subsequently being clustered. This approach not only allows the researcher to directly determine which cells are responsible for changes in specific gene expression and to identify expression changes in unique markers, but also allows the researcher to determine which genes are co-expressed. The transcriptomic response to sleep deprivation may be coordinated by a handful of transcription factors and so single cell sequencing may identify a transcriptional program in specific cell-subsets that is indicative of a specific transcription factor.

However, it is worth considering that preparation of samples for single cell sequencing requires dissociation and isolation of live cells immediately following tissue collection. Whilst carrying out a timecourse style experiment, especially one that is preceded by a protracted technique such as 12-hour sleep deprivation, reliably performing an involved protocol can be technically very challenging. Therefore, single cell-sequencing may not have been feasible for this experimental design.

6.6. Perspectives on the Molecular Study of Sleep

A major limitation of researching the molecular effects of sleep deprivation is that isolating cortex RNA or cellular protein necessarily involves the sacrifice of the subject. Therefore, unlike EEG or video-based assays, timecourse experiments require distinct individuals for each timepoint. This requirement slows the collection of samples by imposing the necessity to sleep deprive multiple animals, as well as by reducing the statistical power of the experiment through the introduction of biological variation between conditions. An *in vitro* model would therefore be a valuable tool for the investigation of molecular changes occurring during sleep deprivation, as it would simultaneously reduce biological variation between samples and allow the rapid production of large numbers of samples. Preferably, the *in vitro* assay for whether a drug may affect sleep patterns would not rely on the direct quantification of transcript abundance (which would involve RNA-extraction and subsequent qPCR). Instead, fluorometric assays of adenosine concentration, or ideally a live cell bioluminescence-based assay of gene expression or cellular parameter, would minimise the time and cost required to quantify the effects of drugs. Once optimised, several molecules can be screened in a low-cost, high throughput fashion, with promising candidates progressing to *in vivo* trials.

A particularly interesting aspect of *in vitro* models is the absence of wake coordinating centres, such as the VLPO or the orexinergic system, and so they have the potential to specifically reveal the mechanisms through which neuronal assemblies enter into local sleep. Understanding which molecules are involved in this transition may inform our understanding of the fundamental roles of sleep and its control. Small molecules that override the entry into local sleep, although they may be useful in combating the cognitive deficits associated with sleep deprivation, may ultimately prove to be unsafe. Speculatively, the activity dependent entry of networks into a sleep-like state may be a protective measure to prevent neuronal death, and so disrupting that process may cause sleep deprivation mediated cell death.

Perhaps the most exciting characteristic of *in vitro* models however is the potential to use human samples in research. Although EEG spectra and behavioural assays, or the molecular quantification of

hormones and metabolites in plasma and urine can be performed using humans, the quantification of gene expression or protein abundance from cortex following sleep deprivation is only possible on rodents or other lab animals. Differences in human and mouse physiologies complicate the general translation of rodent studies to humans. Similarly, the use of SH-SY5Y cells in this thesis replaces the question as to what extent mouse and human responses are similar with the question as to what extent a transformed neuroblastoma cell line resembles brain tissue. Clearly, neither mouse cortex nor SH-SY5Y cells are an ideal model with which to model the molecular changes occurring in the human brain during sleep deprivation. However, with great strides being taken in improving stem-cell technology, both in the creation of stem cells from adult humans and the differentiation protocols, it is easy to imagine that there will soon be powerful *in vitro* models based on stem cells created from naturally short- and long- sleepers. Such an approach would simultaneously remove the species and cell type differences between the experimental model and humans, maximising the translational impact of any findings.

References

Abdul-Hay, S. O., Sahara, T., McBride, M., Kang, D., & Leissring, M. A. (2012). Identification of BACE2 as an avid ß-amyloid-degrading protease. *Molecular Neurodegeneration*, **7**(1), 46.

Adelsberger, H., Garaschuk, O., & Konnerth, A. (2005). Cortical calcium waves in resting newborn mice. *Nat Neurosci*, **8**(8), 988–990.

Adem, A., Mattsson, M. E. K., Nordberg, A., & Påhlman, S. (1987). Muscarinic receptors in human SH-SY5Y neuroblastoma cell line: regulation by phorbol ester and retinoic acid-induced differentiation. *Developmental Brain Research*, **33**(2), 235–242.

Agholme, L., Lindström, T., Kgedal, K., Marcusson, J., & Hallbeck, M. (2010). An in vitro model for neuroscience: Differentiation of SH-SY5Y cells into cells with morphological and biochemical characteristics of mature neurons. *Journal of Alzheimer's Disease*, **20**, 1069–1082.

Airan, R. D., Thompson, K. R., Fenno, L. E., Bernstein, H., & Deisseroth, K. (2009). Temporally precise in vivo control of intracellular signalling. *Nature*, **458**(7241), 1025–1029.

Akerboom, J., Carreras Calderón, N., Tian, L., Wabnig, S., Prigge, M., Tolö, J., Gordus, A., Orger, M., Severi, K., Macklin, J., Patel, R., Pulver, S., Wardill, T., Fischer, E., Schüler, C., Chen, T.-W., Sarkisyan, K., Marvin, J., Bargmann, C., et al. (2013). Genetically encoded calcium indicators for multi-color neural activity imaging and combination with optogenetics . *Frontiers in Molecular Neuroscience* , p. 2.

Anafi, R. C., Pellegrino, R., Shockley, K. R., Romer, M., Tufik, S., & Pack, A. I. (2013). Sleep is not just for the brain: transcriptional responses to sleep in peripheral tissues. *BMC Genomics*, **14**, 362.

Andoh, T., Ishiwa, D., Kamiya, Y., Echigo, N., Goto, T., & Yamada, Y. (2006). A1 adenosine receptor-mediated modulation of neuronal ATP-sensitive K channels in rat substantia nigra. *Brain Research*, **1124**, 55–61.

Atsushi, S., Longjie, C., Koji, M., Yosuke, O., Masayuki, K., Soshi, K., Rie, A., & Kazunori, I. (2017). Neuronal activity-dependent local activation of dendritic unfolded protein response promotes expression of brain-derived neurotrophic factor in cell soma. *Journal of Neurochemistry*, **144**(1), 35–49.

Bachmann, V., Klein, C., Bodenmann, S., Schäfer, N., Berger, W., Brugger, P., & Landolt, H.-P. (2012). The BDNF Val66Met Polymorphism Modulates Sleep Intensity: EEG Frequency- and State-Specificity.

Sleep, **35**(3), 335–344.

Backhaus, J., & Junghanns, K. (2006). Daytime naps improve procedural motor memory. *Sleep Medicine*, **7**, 508–512.

Balsalobre, A., Marcacci, L., & Schibler, U. (2000). Multiple signaling pathways elicit circadian gene expression in cultured Rat-1 fibroblasts. *Current Biology : CB*, **10**(20), 1291–1294.

Bayer, L., Eggermann, E., Serafin, M., Saint-Mleux, B., Machard, D., Jones, B., & Mühlethaler, M. (2001). Orexins (hypocretins) directly excite tuberomammillary neurons. *European Journal of Neuroscience*, **14**, 1571–1575.

Beebe, D. W., Simon, S., Summer, S., Hemmer, S., Strotman, D., & Dolan, L. M. (2013). Dietary intake following experimentally restricted sleep in adolescents. *Sleep*, **36**, 827–34.

Bell, L. N., Kilkus, J. M., Booth, J. N., Bromley, L. E., Imperial, J. G., & Penev, P. D. (2013). Effects of sleep restriction on the human plasma metabolome. *Physiology and Behavior*, **122**, 25–31.

Bellesi, M., de Vivo, L., Tononi, G., & Cirelli, C. (2015). Effects of sleep and wake on astrocytes: clues from molecular and ultrastructural studies. *BMC Biology*, **13**(1), 66.

Bellesi, M., Pfister-Genskow, M., Maret, S., Keles, S., Tononi, G., & Cirelli, C. (2013). Effects of Sleep and Wake on Oligodendrocytes and Their Precursors. *The Journal of Neuroscience*, **33**(36), 14288 LP-14300.

Benedetti, F., Colombo, C., Barbini, B., Campori, E., & Smeraldi, E. (2001). Morning sunlight reduces length of hospitalization in bipolar depression. *Journal of Affective Disorders*, **62**(3), 221–223.

Benedict, C., Brooks, S. J., O'Daly, O. G., Almèn, M. S., Morell, A., Åberg, K., Gingnell, M., Schultes, B., Hallschmid, M., Broman, J.-E., Larsson, E.-M., & Schiöth, H. B. (2012). Acute sleep deprivation enhances the brain's response to hedonic food stimuli: an fMRI study. *The Journal of Clinical Endocrinology and Metabolism*, **97**, E443-7.

Benedict, C., Hallschmid, M., Lassen, A., Mahnke, C., Schultes, B., Schiöth, H. B., Born, J., & Lange, T. (2011). Acute sleep deprivation reduces energy expenditure in healthy men. *The American Journal of Clinical Nutrition*, **93**, 1229–1236.

Benington, J. H., Kodali, S. K., & Heller, H. C. (1995). Stimulation of A1 adenosine receptors mimics the electroencephalographic effects of sleep deprivation. *Brain Research*, **692**, 79–85.

Benjamini, Y., & Hochberg, Y. (1995). Controlling the False Discovery Rate: A Practical and Powerful Approach to Multiple Testing. *Journal of the Royal Statistical Society. Series B (Methodological)*, **57**(1),

289–300.

Berndt, A., Lee, S. Y., Ramakrishnan, C., & Deisseroth, K. (2014). Structure-Guided Transformation of Channelrhodopsin into a Light-Activated Chloride Channel. *Science*, **344**(6182), 420 LP-424.

Berndt, A., Schoenenberger, P., Mattis, J., Tye, K. M., Deisseroth, K., Hegemann, P., & Oertner, T. G. (2011). High-efficiency channelrhodopsins for fast neuronal stimulation at low light levels. *Proceedings of the National Academy of Sciences of the United States of America*, **108**, 7595–7600.

Berndt, A., Yizhar, O., Gunaydin, L. A., Hegemann, P., & Deisseroth, K. (2009). Bi-stable neural state switches. *Nat Neurosci*, **12**(2), 229–234.

Besedovsky, L., Lange, T., & Born, J. (2012). Sleep and immune function. *Pflügers Archiv - European Journal of Physiology*, **463**(1), 121–137.

Biedler, J. L., Roffler-tarlov, S., Schachner, M., & Freedman, L. S. (1978). Multiple Neurotransmitter Synthesis by Human Neuroblastoma Cell Lines and Clones Multiple Neurotransmitter Synthesis by Human Neuroblastoma Cell Lines and Clones. *Cancer Research*, 3751–3757.

Bilan, D. S., Pase, L., Joosen, L., Gorokhovatsky, A. Y., Ermakova, Y. G., Gadella, T. W. J., Grabher, C., Schultz, C., Lukyanov, S., & Belousov, V. V. (2013). HyPer-3: A Genetically Encoded H2O2 Probe with Improved Performance for Ratiometric and Fluorescence Lifetime Imaging. *ACS Chemical Biology*, **8**(3), 535–542.

Borbély, A. A. (1982). A two process model of sleep regulation. *Human Neurobiology*, **1**, 195–204.

Borbély, A. A., Baumann, F., Brandeis, D., Strauch, I., & Lehmann, D. (1981). Sleep deprivation: Effect on sleep stages and EEG power density in man. *Electroencephalography and Clinical Neurophysiology*, **51**(5), 483–493.

Borbély, A. A., & Neuhaus, H. U. (1979). Sleep-deprivation: Effects on sleep and EEG in the rat. *Journal of Comparative Physiology*, **133**(1), 71–87.

Bourgin, P., Lebrand, C., Escourrou, P., Gaultier, C., Franc, B., Hamon, M., & Adrien, J. (1997). Vasoactive Intestinal Polypeptide Microinjections into the Oral Pontine Tegmentum Enhance Rapid Eye Movement Sleep in the Rat. *Neuroscience*, **77**(2), 351–360.

Boyden, E. S., Zhang, F., Bamberg, E., Nagel, G., & Deisseroth, K. (2005). Millisecond-timescale, genetically targeted optical control of neural activity. *Nat Neurosci*, **8**(9), 1263–1268.

Braun, A. R., Balkin, T. J., Wesenten, N. J., Carson, R. E., Varga, M., Baldwin, P., Selbie, S., Belenky, G., & Herscovitch, P. (1997). Regional cerebral blood flow throughout the sleep-wake cycle. An H2 (15) O

PET study. *Brain*, **120**, 1173.

Brondel, L., Romer, M. A., Nougues, P. M., Touyarou, P., & Davenne, D. (2010). Acute partial sleep deprivation increases food intake in healthy men. *The American Journal of Clinical Nutrition*, **91**, 1550–1559.

Brown, M. S., & Goldstein, J. L. (1997). The SREBP pathway: Regulation of cholesterol metabolism by proteolysis of a membrane-bound transcription factor. *Cell*, **89**(3), 331–340.

Brundege, J. M., & Dunwiddie, T. V. (1998). Metabolic regulation of endogenous adenosine release from single neurons. *NeuroReport*, **9**, 3007–3011.

Buijs, R. M., Wortel, J., Van Heerikhuize, J. J., Feenstra, M. G., Ter Horst, G. J., Romijn, H. J., & Kalsbeek, A. (1999). Anatomical and functional demonstration of a multisynaptic suprachiasmatic nucleus adrenal (cortex) pathway. *The European Journal of Neuroscience*, **11**, 1535–1544.

Bukiya, A. N., Durdagi, S., Noskov, S., & Rosenhouse-Dantsker, A. (2017). Cholesterol up-regulates neuronal G protein-gated inwardly rectifying potassium (GIRK) channel activity in the hippocampus. *Journal of Biological Chemistry* , **292**(15), 6135–6147.

Burnstock, G. (1999). Purinergic cotransmission. *Brain Research Bulletin*, **50**, 355–357.

Bushey, D., Tononi, G., & Cirelli, C. (2015). Sleep- and wake-dependent changes in neuronal activity and reactivity demonstrated in fly neurons using in vivo calcium imaging. *Proceedings of the National Academy of Sciences*, **112**(15), 4785 LP-4790.

Cailotto, C., Lei, J., van der Vliet, J., van Heijningen, C., van Eden, C. G., Kalsbeek, A., Pévet, P., & Buijs, R. M. (2009). Effects of nocturnal light on (clock) gene expression in peripheral organs: a role for the autonomic innervation of the liver. *PloS One*, **4**, e5650.

Campbell, I. G., Guinan, M. J., & Horowitz, J. M. (2002). Sleep deprivation impairs long-term potentiation in rat hippocampal slices. *Journal of Neurophysiology*, **88**(2), 1073–1076.

Campbell, S. S., & Tobler, I. (1984). Animal sleep: a review of sleep duration across phylogeny. *Neuroscience and Biobehavioral Reviews*, **8**, 269–300.

Cano, G., Mochizuki, T., & Saper, C. B. (2008). Neural circuitry of stress-induced insomnia in rats. *The Journal of Neuroscience : The Official Journal of the Society for Neuroscience*, **28**, 10167–10184.

Cappuccio, F. P., Taggart, F. M., Kandala, N.-B., Currie, A., Peile, E., Stranges, S., & Miller, M. A. (2008). Meta-analysis of short sleep duration and obesity in children and adults. *Sleep*, **31**, 619–626.

Carter, M. E., Yizhar, O., Chikahisa, S., Nguyen, H., Adamantidis, A., Nishino, S., Deisseroth, K., & de Lecea, L. (2010). Tuning arousal with optogenetic modulation of locus coeruleus neurons. *Nature Neuroscience*, **13**, 1526–1533.

Celli, A., Treves, C., & Stio, M. (1999). Vitamin D receptor in SH-SY5Y human neuroblastoma cells and effect of 1,25-dihydroxyvitamin D3 on cellular proliferation. *Neurochemistry International*, **34**(2), 117–124.

Challet, E., Turek, F. W., Laute, M.-A., & Van Reeth, O. (2001). Sleep deprivation decreases phase-shift responses of circadian rhythms to light in the mouse: role of serotonergic and metabolic signals. *Brain Research*, **909**(1), 81–91.

Chemelli, R. M., Willie, J. T., Sinton, C. M., Elmquist, J. K., Scammell, T., Lee, C., Richardson, J. A., Williams, S. C., Xiong, Y., Kisanuki, Y., Fitch, T. E., Nakazato, M., Hammer, R. E., Saper, C. B., & Yanagisawa, M. (1999). Narcolepsy in orexin Knockout Mice. *Cell*, **98**, 437–451.

Cheng, H. Y. M., Obrietan, K., Cain, S. W., Lee, B. Y., Agostino, P. V., Joza, N. A., Harrington, M. E., Ralph, M. R., & Penninger, J. M. (2004). Dexras1 potentiates photic and suppresses nonphotic responses of the circadian clock. *Neuron*, **43**(5), 715–728.

Chikahisa, S., Fujiki, N., Kitaoka, K., Shimizu, N., & S??i, H. (2009). Central AMPK contributes to sleep homeostasis in mice. *Neuropharmacology*, **57**, 369–374.

Cho, H. J., Savitz, J., Dantzer, R., Teague, T. K., Drevets, W. C., & Irwin, M. R. (2018). Sleep disturbance and kynurenine metabolism in depression. *Journal of Psychosomatic Research*, **99**, 1–7.

Chou, T. C., Bjorkum, A. a, Gaus, S. E., Lu, J., Scammell, T. E., & Saper, C. B. (2002). Afferents to the ventrolateral preoptic nucleus. *The Journal of Neuroscience : The Official Journal of the Society for Neuroscience*, **22**, 977–990.

Chou, T. C., Scammell, T. E., Gooley, J. J., Gaus, S. E., Saper, C. B., & Lu, J. (2003). Critical role of dorsomedial hypothalamic nucleus in a wide range of behavioral circadian rhythms. *The Journal of Neuroscience : The Official Journal of the Society for Neuroscience*, **23**, 10691–702.

Chow, B. Y., Han, X., Dobry, A. S., Qian, X., Chuong, A. S., Li, M., Henninger, M. A., Belfort, G. M., Lin, Y., Monahan, P. E., & Boyden, E. S. (2010). High-performance genetically targetable optical neural silencing by light-driven proton pumps. *Nature*, **463**(7277), 98–102.

Chowdhury, S., Shepherd, J. D., Okuno, H., Lyford, G., Petralia, R. S., Plath, N., Kuhl, D., Huganir, R. L., & Worley, P. F. (2006). Arc/Arg3.1 Interacts with the Endocytic Machinery to Regulate AMPA Receptor Trafficking. *Neuron*, **52**(3), 445–459.

Christie, M. A., McKenna, J. T., Connolly, N. P., McCarley, R. W., & Strecker, R. E. (2008). 24 hours of sleep deprivation in the rat increases sleepiness and decreases vigilance: introduction of the rat-psychomotor vigilance task. *Journal of Sleep Research*, **17**, 376–84.

Chung, S., Weber, F., Zhong, P., Tan, C. L., Nguyen, T. N., Beier, K. T., Hörmann, N., Chang, W.-C., Zhang, Z., Do, J. P., Yao, S., Krashes, M. J., Tasic, B., Cetin, A., Zeng, H., Knight, Z. A., Luo, L., & Dan, Y. (2017). Identification of preoptic sleep neurons using retrograde labelling and gene profiling. *Nature*, **545**(7655), 477–481.

Cirelli, C., & Bushey, D. (2008). Sleep and wakefulness in Drosophila melanogaster. In *Annals of the New York Academy of Sciences*, Vol. 1129, pp. 323–329.

Cirelli, C., Gutierrez, C. M., & Tononi, G. (2004). Extensive and Divergent Effects of Sleep and Wakefulness on Brain Gene Expression. *Neuron*, **41**(1), 35–43.

Cirelli, C., LaVaute, T. M., & Tononi, G. (2005). Sleep and wakefulness modulate gene expression in Drosophila. *Journal of Neurochemistry*, **94**, 1411–1419.

Cirelli, C., & Tononi, G. (1998). Differences in gene expression between sleep and waking as revealed by mRNA differential display. *Molecular Brain Research*, **56**, 293–305.

Cirelli, C., & Tononi, G. (1999). Differences in gene expression during sleep and wakefulness. *Annals of Medicine*, **31**, 117–24.

Cirelli, C., & Tononi, G. (2000). Differential Expression of Plasticity-Related Genes in Waking and Sleep and Their Regulation by the Noradrenergic System. *The Journal of Neuroscience*, **20**(24), 9187 LP-9194.

Colten, H., Altevogt, B. B. M., & Colten., H. (2006). *Sleep Disorders and Sleep Deprivation: An Unmet Public Health Problem*. *Committee on Sleep Medicine and Research*. doi:10.1097/01.CHI.0000270812.55636.3b

Davies, S. K., Ang, J. E., Revell, V. L., Holmes, B., Mann, A., Robertson, F. P., Cui, N., Middleton, B., Ackermann, K., Kayser, M., Thumser, A. E., Raynaud, F. I., & Skene, D. J. (2014). Effect of sleep deprivation on the human metabolome. *Proceedings of the National Academy of Sciences* , **111**(29), 10761–10766.

Deboer, T., Vansteensel, M. J., Détári, L., & Meijer, J. H. (2003). Sleep states alter activity of suprachiasmatic nucleus neurons. *Nature Neuroscience*, **6**, 1086.

Dement, W., & Kleitman, N. (1957). Cyclic variations in EEG during sleep and their relation to eye movements, body motility, and dreaming. *Electroencephalography and Clinical Neurophysiology*, **9**,

673–690.

Depner, C. M., Stothard, E. R., & Wright, K. P. (2014). Metabolic consequences of sleep and circadian disorders. *Current Diabetes Reports*, **14**(7), 507.

Desai, N. S., Rutherford, L. C., & Turrigiano, G. G. (1999). BDNF Regulates the Intrinsic Excitability of Cortical Neurons. *Learning & Memory*, **6**(3), 284–291.

Dettoni, J. L., Consolim-Colombo, F. M., Drager, L. F., Rubira, M. C., Cavasin de Souza, S. B. P., Irigoyen, M. C., Mostarda, C., Borile, S., Krieger, E. M., Moreno, H., & Lorenzi-Filho, G. (2012). Cardiovascular effects of partial sleep deprivation in healthy volunteers. *Journal of Applied Physiology*, **113**(2), 232 LP-236.

Deurveilher, S., Burns, J., & Semba, K. (2002). Indirect projections from the suprachiasmatic nucleus to the ventrolateral preoptic nucleus: a dual tract-tracing study in rat. *European Journal of Neuroscience*, **16**, 1195–1213.

Di Meco, A., Joshi, Y. B., & Praticò, D. (2014). Sleep deprivation impairs memory, tau metabolism, and synaptic integrity of a mouse model of Alzheimer's disease with plaques and tangles. *Neurobiology of Aging*, **35**(8), 1813–1820.

Diessler, S., Jan, M., Emmenegger, Y., Guex, N., Middleton, B., Skene, D. J., Ibberson, M., Burdet, F., Götz, L., Pagni, M., Sankar, M., Liechti, R., Hor, C. N., Xenarios, I., & Franken, P. (2018). A systems genetics resource and analysis of sleep regulation in the mouse. *PLOS Biology*, **16**(8), e2005750.

Dijk, D. -J, Duffy, J. F., & Czeisler, C. A. (1992). Circadian and sleep/wake dependent aspects of subjective alertness and cognitive performance. *Journal of Sleep Research*, **1**(2), 112–117.

Ding, F., O'Donnell, J., Xu, Q., Kang, N., Goldman, N., & Nedergaard, M. (2016). Changes in the composition of brain interstitial ions control the sleep-wake cycle. *Science*, **352**(6285), 550 LP-555.

Do, M. T. H., & Yau, K.-W. (2010). Intrinsically photosensitive retinal ganglion cells. *Physiological Reviews*, **90**, 1547–1581.

Dunwiddie, T. V, Diao, L., & Proctor, W. R. (1997). Adenine nucleotides undergo rapid, quantitative conversion to adenosine in the extracellular space in rat hippocampus. *The Journal of Neuroscience : The Official Journal of the Society for Neuroscience*, **17**, 7673–7682.

Dunwiddie, T. V, & Fredholm, B. B. (1989). Adenosine A1 receptors inhibit adenylate cyclase activity and neurotransmitter release and hyperpolarize pyramidal neurons in rat hippocampus. *The Journal of Pharmacology and Experimental Therapeutics*, **249**, 31–37.

Dworak, M., Kim, T., Mccarley, R. W., & Basheer, R. (2017). Creatine supplementation reduces sleep need and homeostatic sleep pressure in rats. *Journal of Sleep Research*, **26**(3), 377–385.

Dworak, M., McCarley, R. W., Kim, T., Kalinchuk, A. V, & Basheer, R. (2010). Sleep and brain energy levels: ATP changes during sleep. *The Journal of Neuroscience : The Official Journal of the Society for Neuroscience*, **30**, 9007–9016.

Eastman, C. I., Mistlberger, R. E., & Rechtschaffen, A. (1984). Suprachiasmatic nuclei lesions eliminate circadian temperature and sleep rhythms in the rat. *Physiology & Behavior*, **32**(3), 357–368.

Eastman, C., & Rechtschaffen, A. (1983). Circadian temperature and wake rhythms of rats exposed to prolonged continuous illumination. *Physiology & Behavior*, **31**(4), 417–427.

Easton, A., Meerlo, P., Bergmann, B., & Turek, F. W. (2004). The suprachiasmatic nucleus regulates sleep timing and amount in mice. *Sleep*, **27**(7), 1307–1318.

Edgar, D. M., Dement, W. C., & Fuller, C. A. (1993). Effect of SCN lesions on sleep in squirrel monkeys: evidence for opponent processes in sleep-wake regulation. *The Journal of Neuroscience*, **13**(3), 1065 LP-1079.

Ehlen, J. C., Brager, A. J., Baggs, J., Pinckney, L., Gray, C. L., DeBruyne, J. P., Esser, K. A., Takahashi, J. S., & Paul, K. N. (2017). Bmal1 function in skeletal muscle regulates sleep. *eLife*, **6**, e26557.

Eisener-Dorman, A. F., Lawrence, D. A., & Bolivar, V. J. (2009). Cautionary insights on knockout mouse studies: The gene or not the gene? *Brain, Behavior, and Immunity*, **23**(3), 318–324.

Elliott, D. A., & Brand, A. H. (2008). The GAL4 system : a versatile system for the expression of genes. *Methods in Molecular Biology (Clifton, N.J.)*, **420**, 79–95.

Encinas, M., Iglesias, M., Liu, Y., Wang, H., Muhaisen, A., Ceña, V., Gallego, C., & Comella, J. X. (2000). Sequential Treatment of SH-SY5Y Cells with Retinoic Acid and Brain-Derived Neurotrophic Factor Gives Rise to Fully Differentiated, Neurotrophic Factor-Dependent, Human Neuron-Like Cells. *Journal of Neurochemistry*, **75**(3), 991–1003.

Everson, C. a. (1993). Sustained sleep deprivation impairs host defense. *The American Journal of Physiology*, **265**, R1148–R1154.

Everson, C. A., Bergmann, B. M., & Rechtschaffen, A. (1989). Sleep deprivation in the rat: III. Total sleep deprivation. *Sleep*, **12**, 13–21.

Everson, C. A., Henchen, C. J., Szabo, A., & Hogg, N. (2014). Cell Injury and Repair Resulting from Sleep Loss and Sleep Recovery in Laboratory Rats. *Sleep*, **37**(12), 1929–1940.

Fang, M., Jaffrey, S. R., Sawa, A., Ye, K., Luo, X., & Snyder, S. H. (2000). Dexras1: A G protein specifically coupled to neuronal nitric oxide synthase via CAPON. *Neuron*, **28**(1), 183–193.

Faraguna, U., Vyazovskiy, V. V, Nelson, A. B., Tononi, G., & Cirelli, C. (2008). A Causal Role for Brain-Derived Neurotrophic Factor in the Homeostatic Regulation of Sleep. *The Journal of Neuroscience*, **28**(15), 4088 LP-4095.

Febinger, H. Y., George, A., Priestley, J., Toth, L. A., & Opp, M. R. (2014). Effects of Housing Condition and Cage Change on Characteristics of Sleep in Mice. *Journal of the American Association for Laboratory Animal Science : JAALAS*, **53**(1), 29–37.

Feinberg, I. (1974). Changes in sleep cycle patterns with age. *Journal of Psychiatric Research*, **10**(3), 283–306.

Feinberg, I., Koresko, R. L., & Heller, N. (1967). EEG sleep patterns as a function of normal and pathological aging in man. *Journal of Psychiatric Research*, **5**(2), 107–144.

Feinberg, I., March, J. D., Floyd, T. C., Jimison, R., Bossom-Demitrack, L., & Katz, P. H. (1985). Homeostatic changes during post-nap sleep maintain baseline levels of delta EEG. *Electroencephalography and Clinical Neurophysiology*, **61**(2), 134–137.

Fenno, L., Yizhar, O., & Deisseroth, K. (2011). The development and application of optogenetics. *Annual Review of Neuroscience*, **34**, 389–412.

Forsythe, I. D., Lambert, D. G., Nahorski, S. R., & Linsdell, P. (1992). Elevation of cytosolic calcium by cholinoceptor agonists in SH-SY5Y human neuroblastoma cells: estimation of the contribution of voltage-dependent currents. *British Journal of Pharmacology*, **107**(1), 207–214.

Foster, R., & Lockley, S. (2012). *Sleep: A Very Short Introduction (Very Short Introductions)*, Oxford University. doi:March 2012

Franken, P., Dijk, D. J., Tobler, I., & Borbely, A. A. (1991). Sleep deprivation in rats: effects on EEG power spectra, vigilance states, and cortical temperature. *American Journal of Physiology - Regulatory, Integrative and Comparative Physiology*, **261**(1), R198–R208.

Franken, P., Gip, P., Hagiwara, G., Ruby, N. F., & Heller, H. C. (2003). Changes in brain glycogen after sleep deprivation vary with genotype. *American Journal of Physiology - Regulatory, Integrative and Comparative Physiology*, **285**(2), R413 LP-R419.

Franken, P., Malafosse, A., & Tafti, M. (1999). *Genetic determinants of sleep regulation in inbred mice. Sleep*, Vol. 22.

Friess, E., Tagaya, H., Grethe, C., Trachsel, L., & Holsboer, F. (2004). Acute cortisol administration promotes sleep intensity in man. *Neuropsychopharmacology*, **29**(3), 598–604.

Funato, H., Miyoshi, C., Fujiyama, T., Kanda, T., Sato, M., Wang, Z., Ma, J., Nakane, S., Tomita, J., Ikkyu, A., Kakizaki, M., Hotta-Hirashima, N., Kanno, S., Komiya, H., Asano, F., Honda, T., Kim, S. J., Harano, K., Muramoto, H., et al. (2016). Forward-genetics analysis of sleep in randomly mutagenized mice. *Nature*, **539**(7629), 378–383.

Funato, H., Tsai, A. L., Willie, J. T., Kisanuki, Y., Williams, S. C., Sakurai, T., & Yanagisawa, M. (2009). Enhanced Orexin Receptor-2 Signaling Prevents Diet-Induced Obesity and Improves Leptin Sensitivity. *Cell Metabolism*, **9**, 64–76.

Füzesi, T., Daviu, N., Wamsteeker Cusulin, J. I., Bonin, R. P., & Bains, J. S. (2016). Hypothalamic CRH neurons orchestrate complex behaviours after stress. *Nature Communications*, **7**, 11937.

Gais, S., & Born, J. (2004). Declarative memory consolidation: Mechanisms acting during human sleep. *Learning & Memory*, **11**, 679–685.

Gallopin, T., Fort, P., Eggermann, E., Cauli, B., Luppi, P. H., Rossier, J., Audinat, E., Mühlethaler, M., & Serafin, M. (2000). Identification of sleep-promoting neurons in vitro. *Nature*, **404**, 992–995.

Garbarino, S., Mascialino, B., Penco, M. A., Squarcia, S., De Carli, F., Nobili, L., Beelke, M., Cuomo, G., & Ferrillo, F. (2004). Professional shift-work drivers who adopt prophylactic naps can reduce the risk of car accidents during night work. *Sleep*, **27**, 1295–1302.

Gaus, S. E., Strecker, R. E., Tate, B. a., Parker, R. a., & Saper, C. B. (2002). Ventrolateral preoptic nucleus contains sleep-active, galaninergic neurons in multiple mammalian species. *Neuroscience*, **115**, 285–294.

Gerashchenko, D., Wisor, J. P., Burns, D., Reh, R. K., Shiromani, P. J., Sakurai, T., de la Iglesia, H. O., & Kilduff, T. S. (2008). Identification of a population of sleep-active cerebral cortex neurons. *Proceedings of the National Academy of Sciences* , **105**(29), 10227–10232.

Ghazalpour, A., Bennett, B., Petyuk, V. A., Orozco, L., Hagopian, R., Mungrue, I. N., Farber, C. R., Sinsheimer, J., Kang, H. M., Furlotte, N., Park, C. C., Wen, P. Z., Brewer, H., Weitz, K., Camp, D. G., Pan, C., Yordanova, R., Neuhaus, I., Tilford, C., et al. (2011). Comparative analysis of proteome and transcriptome variation in mouse. *PLoS Genetics*, **7**(6). doi:10.1371/journal.pgen.1001393

Gilardi, F., Migliavacca, E., Naldi, A., Baruchet, M., Canella, D., Le Martelot, G., Guex, N., Desvergne, B., & Consortium, the C. (2014). Genome-Wide Analysis of SREBP1 Activity around the Clock Reveals Its Combined Dependency on Nutrient and Circadian Signals. *PLOS Genetics*, **10**(3), e1004155.

Giskeødegård, G. F., Davies, S. K., Revell, V. L., Keun, H., & Skene, D. J. (2015). Diurnal rhythms in the human urine metabolome during sleep and total sleep deprivation. *Scientific Reports*, **5**, 14843.

Gottlieb, D. J., Redline, S., Nieto, F. J., Baldwin, C. M., Newman, A. B., Resnick, H. E., & Punjabi, N. M. (2006). Association of usual sleep duration with hypertension: the Sleep Heart Health Study. *Sleep*, **29**, 1009–1014.

Govorunova, E. G., Sineshchekov, O. A., Janz, R., Liu, X., & Spudich, J. L. (2015). Natural light-gated anion channels: A family of microbial rhodopsins for advanced optogenetics. *Science (New York, N.Y.)*, **349**(6248), 647–650.

Gradinaru, V., Thompson, K. R., & Deisseroth, K. (2008). eNpHR: a Natronomonas halorhodopsin enhanced for optogenetic applications. *Brain Cell Biology*, **36**, 129–39.

Greene, L. A., & Tischler, A. S. (1976). Establishment of a noradrenergic clonal line of rat adrenal pheochromocytoma cells which respond to nerve growth factor. *Proceedings of the National Academy of Sciences*, **73**(7), 2424 LP-2428.

Greer, S. M., Goldstein, A. N., & Walker, M. P. (2013). The impact of sleep deprivation on food desire in the human brain. *Nature Communications*, **4**, 2259.

Groch, S., Wilhelm, I., Diekelmann, S., & Born, J. (2013). The role of REM sleep in the processing of emotional memories: Evidence from behavior and event-related potentials. *Neurobiology of Learning and Memory*, **99**, 1–9.

Gross, B. a., Vanderheyden, W. M., Urpa, L. M., Davis, D. E., Fitzpatrick, C. J., Prabhu, K., & Poe, G. R. (2015). Stress-free automatic sleep deprivation using air puffs. *Journal of Neuroscience Methods*, **251**, 83–91.

Gunaydin, L. A., Yizhar, O., Berndt, A., Sohal, V. S., Deisseroth, K., & Hegemann, P. (2010). Ultrafast optogenetic control. *Nat Neurosci*, **13**(3), 387–392.

Guo, L., Guo, Z., Luo, X., Liang, R., Yang, S., Ren, H., Wang, G., & Zhen, X. (2016). Phosphodiesterase 10A inhibition attenuates sleep deprivation-induced deficits in long-term fear memory. *Neuroscience Letters*, **635**, 44–50.

Guzmán-Marín, R., Suntsova, N., Stewart, D. R., Gong, H., Szymusiak, R., & McGinty, D. (2003). Sleep deprivation reduces proliferation of cells in the dentate gyrus of the hippocampus in rats. *The Journal of Physiology*, **549**(Pt 2), 563–571.

Haas, H. L., & Selbach, O. (2000). Functions of neuronal adenosine receptors. *NaunynSchmiedebergs*

Archives of Pharmacology, **362**, 375–381.

Hampp, G., Ripperger, J. A., Houben, T., Schmutz, I., Blex, C., Perreau-Lenz, S., Brunk, I., Spanagel, R., Ahnert-Hilger, G., Meijer, J. H., & Albrecht, U. (2008). Regulation of Monoamine Oxidase A by Circadian-Clock Components Implies Clock Influence on Mood. *Current Biology*, **18**(9), 678–683.

Han, B., McCarren, H. S., O'Neill, D., & Kelz, M. B. (2014). Distinctive recruitment of endogenous sleep-promoting neurons by volatile anesthetics and a nonimmobilizer. *Anesthesiology*, **121**(5), 999–1009.

Han, X., Chow, B., Zhou, H., Klapoetke, N., Chuong, A., Rajimehr, R., Yang, A., Baratta, M., Winkle, J., Desimone, R., & Boyden, E. (2011). A High-Light Sensitivity Optical Neural Silencer: Development and Application to Optogenetic Control of Non-Human Primate Cortex . *Frontiers in Systems Neuroscience* , p. 18.

Han, X., Qian, X., Stern, P., Chuong, A., & Boyden, E. (2009). Informational lesions: optical perturbation of spike timing and neural synchrony via microbial opsin gene fusions . *Frontiers in Molecular Neuroscience* , p. 12.

Hara, J., Beuckmann, C. T., Nambu, T., Willie, J. T., Chemelli, R. M., Sinton, C. M., Sugiyama, F., Yagami, K. I., Goto, K., Yanagisawa, M., & Sakurai, T. (2001). Genetic ablation of orexin neurons in mice results in narcolepsy, hypophagia, and obesity. *Neuron*, **30**, 345–354.

Harding, H. P., Zhang, Y., Bertolotti, A., Zeng, H., & Ron, D. (2000). Perk Is Essential for Translational Regulation and Cell Survival during the Unfolded Protein Response. *Molecular Cell*, **5**(5), 897–904.

Harris, G. C., Wimmer, M., & Aston-Jones, G. (2005). A role for lateral hypothalamic orexin neurons in reward seeking. *Nature*, **437**, 556–559.

Harrison, Y., & Horne, J. a. (1999). One night of sleep loss impairs innovative thinking and flexible decision making. *Organizational Behavior and Human Decision Processes*, **78**, 128–145.

Hayaishi, O. (1991). Molecular mechanisms of sleep-wake regulation: roles of prostaglandins D2 and E2. *The FASEB Journal*, **5**(11), 2575–2581.

Hayashi, A., Kasahara, T., Iwamoto, K., Ishiwata, M., Kametani, M., Kakiuchi, C., Furuichi, T., & Kato, T. (2007). The Role of Brain-derived Neurotrophic Factor (BDNF)-induced XBP1 Splicing during Brain Development. *Journal of Biological Chemistry* , **282**(47), 34525–34534.

Heiman, M., Kulicke, R., Fenster, R. J., Greengard, P., & Heintz, N. (2014). Cell type–specific mRNA purification by translating ribosome affinity purification (TRAP). *Nature Protocols*, **9**, 1282.

Helga, J., & Pierre, M. (2002). Cholesterol for Synthesis of Myelin Is Made Locally, Not Imported into

Brain. *Journal of Neurochemistry*, **64**(2), 895–901.

Hess, R., Koella, W. P., & Akert, K. (1953). Cortical and subcortical recordings in natural and artificially induced sleep in cats. *Electroencephalography and Clinical Neurophysiology*, **5**(1), 75–90.

Hide, I., Tanaka, M., Inoue, a, Nakajima, K., Kohsaka, S., Inoue, K., & Nakata, Y. (2000). Extracellular ATP triggers tumor necrosis factor-alpha release from rat microglia. *Journal of Neurochemistry*, **75**, 965–972.

Hinard, V., Mikhail, C., Pradervand, S., Curie, T., Houtkooper, R. H., Auwerx, J., Franken, P., & Tafti, M. (2012). Key Electrophysiological, Molecular, and Metabolic Signatures of Sleep and Wakefulness Revealed in Primary Cortical Cultures. *Journal of Neuroscience*, **32**, 12506–12517.

Horvath, T. L., Peyron, C., Diano, S., Ivanov, A., Aston-Jones, G., Kilduff, T. S., & Van Den Pol, A. N. (1999). Hypocretin (orexin) activation and synaptic innervation of the locus coeruleus noradrenergic system. *Journal of Comparative Neurology*, **415**, 145–159.

Hu, J.-H., Park, J. M., Park, S., Xiao, B., Dehoff, M. H., Kim, S., Hayashi, T., Schwarz, M. K., Huganir, R. L., Seeburg, P. H., Linden, D. J., & Worley, P. F. (2010). Homeostatic Scaling requires Group I mGluR activation mediated by Homer1a. *Neuron*, **68**(6), 1128–1142.

Hu, W.-P., Li, J.-D., Colwell, C. S., & Zhou, Q.-Y. (2011). Decreased REM sleep and altered circadian sleep regulation in mice lacking vasoactive intestinal polypeptide. *Sleep*, **34**(1), 49–56.

Hu, Y., Shmygelska, A., Tran, D., Eriksson, N., Tung, J. Y., & Hinds, D. A. (2016). GWAS of 89,283 individuals identifies genetic variants associated with self-reporting of being a morning person. *Nature Communications*, **7**, 10448.

Hubbard, J., Ruppert, E., Calvel, L., Robin-Choteau, L., Gropp, C.-M., Allemann, C., Reibel, S., Sage-Ciocca, D., & Bourgin, P. (2015). Arvicanthis ansorgei, a novel model for the study of sleep and waking in diurnal rodents. *Sleep: Journal of Sleep and Sleep Disorders Research*, **38**(6), 979–988.

Huber, R., Mäki, H., Rosanova, M., Casarotto, S., Canali, P., Casali, A. G., Tononi, G., & Massimini, M. (2013). Human Cortical Excitability Increases with Time Awake. *Cerebral Cortex*, **23**(2), 1–7.

Hughes, M. E., Hogenesch, J. B., & Kornacker, K. (2010). JTK_CYCLE: An Efficient Nonparametric Algorithm for Detecting Rhythmic Components in Genome-Scale Data Sets. *Journal of Biological Rhythms*, **25**(5), 372–380.

Ibuka, N., & Kawamura, H. (1975). Loss of circadian rhythm in sleep-wakefulness cycle in the rat by suprachiasmatic nucleus lesions. *Brain Research*, **96**(1), 76–81.

Ibuka, N., Nihonmatsu, I., & Sekiguchi, S. (1980). Sleep--wakefulness rhythms in mice after suprachiasmatic nucleus lesions. *Waking & Sleeping*.

Imeri, L., & Opp, M. R. (2009). How (and why) the immune system makes us sleep. *Nature Reviews. Neuroscience*, **10**, 199–210.

J., W. M., & Nicholas, D. (2007). Auto-inhibition of rat parallel fibre–Purkinje cell synapses by activity-dependent adenosine release. *The Journal of Physiology*, **581**(2), 553–565.

Jacobs, B. L., & McGinty, D. J. (1971). Effects of food deprivation on sleep and wakefulness in the rat. *Experimental Neurology*, **30**, 212–222.

Jime´nez-Anguiano, A., Ba´ez-Saldan˜a, A., & Drucker-Coli´n, R. (1993). Cerebrospinal fluid (CSF) extracted immediately after REM sleep deprivation prevents REM rebound and contains vasoactive intestinal peptide (VIP). *Brain Research*, **631**(2), 345–348.

Jones, S., Pfister-Genskow, M., Benca, R. M., & Cirelli, C. (2008). Molecular correlates of sleep and wakefulness in the brain of the white-crowned sparrow. *Journal of Neurochemistry*, **105**(1), 46–62.

Jung, C. M., Melanson, E. L., Frydendall, E. J., Perreault, L., Eckel, R. H., & Wright, K. P. (2011). Energy expenditure during sleep, sleep deprivation and sleep following sleep deprivation in adult humans. *The Journal of Physiology*, **589**, 235–244.

Jurevics, H. A., Kidwai, F. Z., & Morell, P. (1997). Sources of cholesterol during development of the rat fetus and fetal organs. *Journal of Lipid Research* , **38**(4), 723–733.

Juszczak, G. R., & Stankiewicz, A. M. (2018). Glucocorticoids, genes and brain function. *Progress in Neuro-Psychopharmacology and Biological Psychiatry*, **82**, 136–168.

Kalinchuk, A. V., Urrila, A. S., Alanko, L., Heiskanen, S., Wigren, H. K., Suomela, M., Stenberg, D., & Porkka-Heiskanen, T. (2003). Local energy depletion in the basal forebrain increases sleep. *European Journal of Neuroscience*, **17**, 863–869.

Kang, J.-E., Lim, M. M., Bateman, R. J., Lee, J. J., Smyth, L. P., Cirrito, J. R., Fujiki, N., Nishino, S., & Holtzman, D. M. (2009). Amyloid-β Dynamics Are Regulated by Orexin and the Sleep-Wake Cycle. *Science*, **326**(5955), 1005 LP-1007.

Karnovsky, M. L., Reich, P., Anchors, J. M., & Burrows, B. L. (1983). Changes in brain glycogen during slow-wave sleep in the rat. *Journal of Neurochemistry*, **41**, 1498–501.

Kato, H. E., Zhang, F., Yizhar, O., Ramakrishnan, C., Nishizawa, T., Hirata, K., Ito, J., Aita, Y., Tsukazaki, T., Hayashi, S., Hegemann, P., Maturana, A. D., Ishitani, R., Deisseroth, K., & Nureki, O. (2012). Crystal

structure of the channelrhodopsin light-gated cation channel. *Nature*, **482**, 369.

Kaushal, N., Nair, D., Gozal, D., & Ramesh, V. (2012). Socially Isolated Mice Exhibit a Blunted Homeostatic Sleep Response to Acute Sleep Deprivation Compared to Socially Paired Mice. *Brain Research*, **1454**, 65–79.

Kim, J.-M., Hwa, J., Garriga, P., Reeves, P. J., RajBhandary, U. L., & Khorana, H. G. (2005). Light-Driven Activation of β2-Adrenergic Receptor Signaling by a Chimeric Rhodopsin Containing the β2-Adrenergic Receptor Cytoplasmic Loops. *Biochemistry*, **44**(7), 2284–2292.

Kirsch, G. E., Codina, J., Birnbaumer, L., & Brown, a M. (1990). Coupling of ATP-sensitive K+ channels to A1 receptors by G proteins in rat ventricular myocytes. *The American Journal of Physiology*, **259**, H820–H826.

Klapoetke, N. C., Murata, Y., Kim, S. S., Pulver, S. R., Birdsey-Benson, A., Cho, Y. K., Morimoto, T. K., Chuong, A. S., Carpenter, E. J., Tian, Z., Wang, J., Xie, Y., Yan, Z., Zhang, Y., Chow, B. Y., Surek, B., Melkonian, M., Jayaraman, V., Constantine-Paton, M., et al. (2014). Independent optical excitation of distinct neural populations. *Nat Meth*, **11**(3), 338–346.

Klapper, S. D., Sauter, E. J., Swiersy, A., Hyman, M. A. E., Bamann, C., Bamberg, E., & Busskamp, V. (2017). On-demand optogenetic activation of human stem-cell-derived neurons. *Scientific Reports*, **7**(1), 14450.

Ko, G. T. C., Chan, J. C. N., Chan, A. W. Y., Wong, P. T. S., Hui, S. S. C., Tong, S. D. Y., Ng, S.-M., Chow, F., & Chan, C. L. W. (2007). Association between sleeping hours, working hours and obesity in Hong Kong Chinese: the “better health for better Hong Kong” health promotion campaign. *International Journal of Obesity (2005)*, **31**, 254–260.

Koban, M., Sita, L. V, Le, W. W., & Hoffman, G. E. (2008). Sleep deprivation of rats: the hyperphagic response is real. *Sleep*, **31**, 927–933.

Koban, M., & Swinson, K. L. (2005). Chronic REM-sleep deprivation of rats elevates metabolic rate and increases UCP1 gene expression in brown adipose tissue. *American Journal of Physiology. Endocrinology and Metabolism*, **289**, E68–E74.

Konadhode, R. R., Pelluru, D., Blanco-Centurion, C., Zayachkivsky, A., Liu, M., Uhde, T., Glen, W. B., van den Pol, A. N., Mulholland, P. J., & Shiromani, P. J. (2013). Optogenetic Stimulation of MCH Neurons Increases Sleep. *The Journal of Neuroscience*, **33**(25), 10257 LP-10263.

Kong, J., Shepel, P. N., Holden, C. P., Mackiewicz, M., Pack, A. I., & Geiger, J. D. (2002). Brain glycogen decreases with increased periods of wakefulness: implications for homeostatic drive to sleep. *The*

Journal of Neuroscience : The Official Journal of the Society for Neuroscience, **22**, 5581–5587.

Kopp, C. (2001). Locomotor activity rhythm in inbred strains of mice: implications for behavioural studies. *Behavioural Brain Research*, **125**(1), 93–96.

Koyanagi, S., Hamdan, A. M., Horiguchi, M., Kusunose, N., Okamoto, A., Matsunaga, N., & Ohdo, S. (2011). cAMP-response element (CRE)-mediated transcription by activating transcription factor-4 (ATF4) is essential for circadian expression of the Period2 gene. *The Journal of Biological Chemistry*, **286**, 32416–23.

Kripke, D. F., Garfinkel, L., Wingard, D. L., Klauber, M. R., & Marler, M. R. (2002). Mortality associated with sleep duration and insomnia. *Archives of General Psychiatry*, **59**, 131–136.

Krishna, A., Biryukov, M., Trefois, C., Antony, P. M. A., Hussong, R., Lin, J., Heinäniemi, M., Glusman, G., Köglsberger, S., Boyd, O., van den Berg, B. H. J., Linke, D., Huang, D., Wang, K., Hood, L., Tholey, A., Schneider, R., Galas, D. J., Balling, R., et al. (2014). Systems genomics evaluation of the SH-SY5Y neuroblastoma cell line as a model for Parkinson's disease. *BMC Genomics*, **15**(1), 1154.

Krueger, J. M., & Obal, F. (2003). Sleep function. *Frontiers in Bioscience : A Journal and Virtual Library*, **8**, d511-9.

Krueger, J. M., Rector, D. M., Roy, S., Van Dongen, H. P. A., Belenky, G., & Panksepp, J. (2008). Sleep as a fundamental property of neuronal assemblies. *Nature Reviews. Neuroscience*, **9**, 910–9.

Kubota, K. (1989). Kuniomi Ishimori and the first discovery of sleep-inducing substances in the brain. *Neuroscience Research*, **6**(6), 497–518.

Kume, T., Kawato, Y., Osakada, F., Izumi, Y., Katsuki, H., Nakagawa, T., Kaneko, S., Niidome, T., Takada-Takatori, Y., & Akaike, A. (2008). Dibutyryl cyclic AMP induces differentiation of human neuroblastoma SH-SY5Y cells into a noradrenergic phenotype. *Neuroscience Letters*, **443**(3), 199–203.

Kushikata, T., Fang, J., & Krueger, J. M. (1999). Brain-derived neurotrophic factor enhances spontaneous sleep in rats and rabbits. *American Journal of Physiology - Regulatory, Integrative and Comparative Physiology*, **276**(5), R1334 LP-R1338.

L., S. T., A., E. L., A., G. G., V., V. C., & T., W. M. (2006). Comparison of monoamine and corticosterone levels 24 h following (+)methamphetamine, (+/–)3,4-methylenedioxymethamphetamine, cocaine, (+)fenfluramine or (+/–)methylphenidate administration in the neonatal rat. *Journal of Neurochemistry*, **98**(5), 1369–1378.

Lahl, O., Wispel, C., Willigens, B., & Pietrowsky, R. (2008). An ultra short episode of sleep is sufficient

to promote declarative memory performance. *Journal of Sleep Research*, **17**, 3–10.

LaMonica, D. a, Frohloff, N., & Dobson, J. G. (1985). Adenosine inhibition of catecholamine-stimulated cardiac membrane adenylate cyclase. *The American Journal of Physiology*, **248**, H737-44.

Lancaster, M. A., & Knoblich, J. A. (2014). Generation of cerebral organoids from human pluripotent stem cells. *Nature Protocols*, **9**, 2329.

Landolt, H. P., Dijk, D. J., Gaus, S. E., & Borbély, A. a. (1995). Caffeine reduces low-frequency delta activity in the human sleep EEG. *Neuropsychopharmacology*, **12**, 229–238.

Landolt, H. P., Meier, V., Burgess, H. J., Finelli, L. a, Cattelin, F., Achermann, P., & Borbély, a a. (1999). Serotonin-2 receptors and human sleep: effect of a selective antagonist on EEG power spectra. *Neuropsychopharmacology : Official Publication of the American College of Neuropsychopharmacology*, **21**, 455–66.

Lange, T., Perras, B., Fehm, H. L., & Born, J. (2003). Sleep Enhances the Human Antibody Response to Hepatitis A Vaccination. *Psychosomatic Medicine*, **65**(5). Retrieved from http://journals.lww.com/psychosomaticmedicine/Fulltext/2003/09000/Sleep_Enhances_the_Human_Antibody_Response_to.17.aspx

Laposky, A., Easton, A., Dugovic, C., Walisser, J., Bradfield, C., & Turek, F. (2005). *Deletion of the Mammalian Circadian Clock Gene BMAL1/Mop3 Alters Baseline Sleep Architecture and the Response to Sleep Deprivation*. *Sleep*, Vol. 28. doi:10.1093/sleep/28.4.395

Lee, J., Lee, S., Chung, S., Park, N., Son, G. H., An, H., Jang, J., Chang, D.-J., Suh, Y.-G., & Kim, K. (2016). Identification of a novel circadian clock modulator controlling BMAL1 expression through a ROR/REV-ERB-response element-dependent mechanism. *Biochemical and Biophysical Research Communications*, **469**(3), 580–586.

Lein, E. S., Hawrylycz, M. J., Ao, N., Ayres, M., Bensinger, A., Bernard, A., Boe, A. F., Boguski, M. S., Brockway, K. S., Byrnes, E. J., Chen, L., Chen, L., Chen, T.-M., Chi Chin, M., Chong, J., Crook, B. E., Czaplinska, A., Dang, C. N., Datta, S., et al. (2006). Genome-wide atlas of gene expression in the adult mouse brain. *Nature*, **445**, 168.

Lesku, J. A., Roth II, T. C., Amlaner, C. J., & Lima, S. L. (2006). A Phylogenetic Analysis of Sleep Architecture in Mammals: The Integration of Anatomy, Physiology, and Ecology. *The American Naturalist*, **168**(4), 441–453.

Li, P., Rial, D., Canas, P. M., Yoo, J.-H., Li, W., Zhou, X., Wang, Y., van Westen, G. J. P., Payen, M.-P., Augusto, E., Goncalves, N., Tome, A. R., Li, Z., Wu, Z., Hou, X., Zhou, Y., PIJzerman, A., Boyden, E. S.,

Cunha, R. A., et al. (2015). Optogenetic activation of intracellular adenosine A2A receptor signaling in the hippocampus is sufficient to trigger CREB phosphorylation and impair memory. *Mol Psychiatry*, **20**(11), 1339–1349.

Li, X., Yu, F., & Guo, A. (2009). Sleep deprivation specifically impairs short-term olfactory memory in Drosophila. *Sleep*, **32**, 1417–1424.

Lin, J. Y., Lin, M. Z., Steinbach, P., & Tsien, R. Y. (2009). Characterization of Engineered Channelrhodopsin Variants with Improved Properties and Kinetics. *Biophysical Journal*, **96**(5), 1803–1814.

Lin, L., Faraco, J., Li, R., Kadotani, H., Rogers, W., Lin, X., Qiu, X., De Jong, P. J., Nishino, S., & Mignot, E. (1999). The sleep disorder canine narcolepsy is caused by a mutation in the hypocretin (orexin) receptor 2 gene. *Cell*, **98**, 365–376.

Liu, G. F., Han, S., Liang, D. H., Wang, F. Z., Shi, X. Z., Yu, J., & Wu, Z. L. (2003). Driver sleepiness and risk of car crashes in Shenyang, a Chinese northeastern city: population-based case-control study. *Biomed Environ Sci*, **16**, 219–226.

Liu, R.-J., van den Pol, A. N., & Aghajanian, G. K. (2002). Hypocretins (orexins) regulate serotonin neurons in the dorsal raphe nucleus by excitatory direct and inhibitory indirect actions. *The Journal of Neuroscience : The Official Journal of the Society for Neuroscience*, **22**, 9453–64.

Liu, Z.-W., Faraguna, U., Cirelli, C., Tononi, G., & Gao, X.-B. (2010). Direct Evidence for Wake-Related Increases and Sleep-Related Decreases in Synaptic Strength in Rodent Cortex. *Journal of Neuroscience*, **30**(25), 8671–8675.

Lopes, F. M., Schröder, R., Júnior, M. L. C. da F., Zanotto-Filho, A., Müller, C. B., Pires, A. S., Meurer, R. T., Colpo, G. D., Gelain, D. P., Kapczinski, F., Moreira, J. C. F., Fernandes, M. da C., & Klamt, F. (2010). Comparison between proliferative and neuron-like SH-SY5Y cells as an in vitro model for Parkinson disease studies. *Brain Research*, **1337**, 85–94.

Lu, J., Greco, M. A., Shiromani, P., & Saper, C. B. (2000). Effect of lesions of the ventrolateral preoptic nucleus on NREM and REM sleep. *The Journal of Neuroscience : The Official Journal of the Society for Neuroscience*, **20**, 3830–3842.

Lyford, G. L., Yamagata, K., Kaufmann, W. E., Barnes, C. A., Sanders, L. K., Copeland, N. G., Gilbert, D. J., Jenkins, N. A., Lanahan, A. A., & Worley, P. F. (1995). Arc, a growth factor and activity-regulated gene, encodes a novel cytoskeleton-associated protein that is enriched in neuronal dendrites. *Neuron*, **14**(2), 433–445.

Ma, X.-M., Camacho, C., & Aguilera, G. (2001). Regulation of Corticotropin-Releasing Hormone (CRH) Transcription and CRH mRNA Stability by Glucocorticoids. *Cellular and Molecular Neurobiology*, **21**(5), 465–475.

Mackiewicz, M., Shockley, K. R., Romer, M. a, Galante, R. J., Zimmerman, J. E., Naidoo, N., Baldwin, D. A., Jensen, S. T., Churchill, G. a, & Pack, A. I. (2007). Macromolecule biosynthesis: a key function of sleep. *Physiological Genomics*, **31**, 441–57.

Mackiewicz, M., Zimmerman, J. E., Shockley, K. R., Churchill, G. A., & Pack, A. I. (2009). What are microarrays teaching us about sleep? *Trends in Molecular Medicine*, **15**(2), 79–87.

Mahowald, M. W., & Schenck, C. H. (2005). Insights from studying human sleep disorders. *Nature*, **437**(7063), 1279–1285.

Maier, T., Güell, M., & Serrano, L. (2009). Correlation of mRNA and protein in complex biological samples. *FEBS Letters*, **583**(24), 3966–3973.

Maquet, P. (2001). The role of sleep in learning and memory. *Science (New York, NY)*, **294**, 1048–1052.

Maret, S., Dorsaz, S., Gurcel, L., Pradervand, S., Petit, B., Pfister, C., Hagenbuchle, O., O'Hara, B. F., Franken, P., & Tafti, M. (2007). Homer1a is a core brain molecular correlate of sleep loss. *Proceedings of the National Academy of Sciences of the United States of America*, **104**, 20090–5.

Markwald, R. R., Melanson, E. L., Smith, M. R., Higgins, J., Perreault, L., Eckel, R. H., & Wright, K. P. (2013). Impact of insufficient sleep on total daily energy expenditure, food intake, and weight gain. *Proceedings of the National Academy of Sciences of the United States of America*, **110**, 5695–700.

Massart, R., Freyburger, M., Suderman, M., Paquet, J., El Helou, J., Belanger-Nelson, E., Rachalski, A., Koumar, O. C., Carrier, J., Szyf, M., & Mongrain, V. (2014). The genome-wide landscape of DNA methylation and hydroxymethylation in response to sleep deprivation impacts on synaptic plasticity genes. *Translational Psychiatry*, **4**(1), e347.

Matricciani, L. a., Olds, T. S., Blunden, S., Rigney, G., & Williams, M. T. (2012). Never Enough Sleep: A Brief History of Sleep Recommendations for Children. *Pediatrics*, **129**, 548–556.

Matsuoka, Y., Okazaki, M., Takata, K., Kitamura, Y., Ohta, S., Sekino, Y., & Taniguchi, T. (1999). Endogenous adenosine protects CA1 neurons from kainic acid-induced neuronal cell loss in the rat hippocampus. *Eur J Neurosci*, **11**, 3617–3625.

Mattis, J., Tye, K. M., Ferenczi, E. A., Ramakrishnan, C., O'Shea, D. J., Prakash, R., Gunaydin, L. A., Hyun, M., Fenno, L. E., Gradinaru, V., Yizhar, O., & Deisseroth, K. (2012). Principles for applying optogenetic

tools derived from direct comparative analysis of microbial opsins. *Nat Meth*, **9**(2), 159–172.

Mavanji, V., Teske, J. A., Billington, C. J., & Kotz, C. M. (2013). Partial sleep deprivation by environmental noise increases food intake and body weight in obesity-resistant rats. *Obesity*, **21**, 1396–1405.

Maycock, G. (1997). Sleepiness and driving: The experience of U.K. car drivers. *Accident Analysis & Prevention*, **29**, 453–462.

McDearmon, E. L., Patel, K. N., Ko, C. H., Walisser, J. A., Schook, A. C., Chong, J. L., Wilsbacher, L. D., Song, E. J., Hong, H.-K., Bradfield, C. A., & Takahashi, J. S. (2006). Dissecting the Functions of the Mammalian Clock Protein BMAL1 by Tissue-Specific Rescue in Mice. *Science*, **314**(5803), 1304 LP-1308.

McGinty, D. J., & Sterman, M. B. (1968). Sleep suppression after basal forebrain lesions in the cat. *Science (New York, N.Y.)*, **160**, 1253–1255.

Milaśius, A. M., Grinevićius, K.-K. A., & Lapin, I. P. (1990). Effect of quinolinic acid on wakefulness and sleep in the rabbit. *Journal of Neural Transmission / General Section JNT*, **82**(1), 67–73.

Mongrain, V., Hernandez, S. A., Pradervand, S., Dorsaz, S., Curie, T., Hagiwara, G., Gip, P., Heller, H. C., & Franken, P. (2010). Separating the Contribution of Glucocorticoids and Wakefulness to the Molecular and Electrophysiological Correlates of Sleep Homeostasis. *Sleep*, **33**(9), 1147–1157.

Mongrain, V., La Spada, F., Curie, T., & Franken, P. (2011). Sleep Loss Reduces the DNA-Binding of BMAL1, CLOCK, and NPAS2 to Specific Clock Genes in the Mouse Cerebral Cortex. *PLOS ONE*, **6**(10), e26622.

Monti, J. M., Jantos, H., Boussard, M., Altier, H., Orellana, C., & Olivera, S. (1991). Effects of selective activation or blockade of the histamine H3 receptor on sleep and wakefulness. *Eur J Pharmacol*, **205**, 283–287.

Moore, J. T., Chen, J., Han, B., Meng, Q. C., Veasey, S. C., Beck, S. G., & Kelz, M. B. (2012). Direct activation of sleep-promoting VLPO neurons by volatile anesthetics contributes to anesthetic hypnosis. *Current Biology*, **22**, 2008–2016.

Moore, R. Y., & Eichler, V. B. (1972). Loss of a circadian adrenal corticosterone rhythm following suprachiasmatic lesions in the rat. *Brain Research*, **42**, 201–206.

Moorman, D. E., & Aston-Jones, G. (2009). Orexin-1 receptor antagonism decreases ethanol consumption and preference selectively in high-ethanol--preferring Sprague--Dawley rats. *Alcohol (Fayetteville, N.Y.)*, **43**, 379–86.

Morairty, S. R., Dittrich, L., Pasumarthi, R. K., Valladao, D., Heiss, J. E., Gerashchenko, D., & Kilduff, T. S. (2013). A role for cortical nNOS/NK1 neurons in coupling homeostatic sleep drive to EEG slow wave activity. *Proceedings of the National Academy of Sciences* , **110**(50), 20272–20277.

Moreno, C. R. C., Louzada, F. M., Teixeira, L. R., Borges, F., & Lorenzi-Filho, G. (2006). Short sleep is associated with obesity among truck drivers. *Chronobiology International*, **23**, 1295–1303.

Moruzzi, G., & Magoun, H. W. (1949). Brain stem reticular formation and activation of the EEG. *Electroencephalography and Clinical Neurophysiology*, **1**, 455–473.

Mottin, S., Laporte, P., Jouvet, M., & Cespuglio, R. (1997). Determination of NADH in the rat brain during sleep-wake states with an optic fibre sensor and time-resolved fluorescence procedures. *Neuroscience*, **79**(3), 683–693.

Moutinho, M., Nunes, M. J., Correia, J. C., Gama, M. J., Castro-Caldas, M., Cedazo-Minguez, A., Rodrigues, C. M. P., Björkhem, I., Ruas, J. L., & Rodrigues, E. (2016). Neuronal cholesterol metabolism increases dendritic outgrowth and synaptic markers via a concerted action of GGTase-I and Trk. *Scientific Reports*, **6**, 30928.

Mukhametov, L. M. (1987). Unihemispheric slow-wave sleep in the Amazonian dolphin, Inia geoffrensis. *Neuroscience Letters*, **79**, 128–132.

Mukhametov, L. M., Laymin, O. I., & Polyakova, I. G. (1985). Interhemispheric asynchrony of the sleep EEG in northern fur seals. *Experientia*, **41**, 1034–1035.

Mukhametov, L. M., Supin, a. Y., & Polyakova, I. G. (1977). Interhemispheric asymmetry of the electroencephalographic sleep patterns in dolphins. *Brain Research*, **134**, 581–584.

Murata, Y., Oka, A., Iseki, A., Mori, M., Ohe, K., Mine, K., & Enjoji, M. (2017). Prolonged sleep deprivation decreases cell proliferation and immature newborn neurons in both dorsal and ventral hippocampus of male rats. *Neuroscience Research*. doi:https://doi.org/10.1016/j.neures.2017.08.008

Murphy, P. J., Badia, P., Myers, B. L., Boecker, M. R., & Wright, K. P. (1994). Nonsteroidal anti-inflammatory drugs affect normal sleep patterns in humans. *Physiology & Behavior*, **55**(6), 1063–1066.

Nagel, G., Brauner, M., Liewald, J. F., Adeishvili, N., Bamberg, E., & Gottschalk, A. (2005). Light Activation of Channelrhodopsin-2 in Excitable Cells of Caenorhabditis elegans Triggers Rapid Behavioral Responses. *Current Biology*, **15**(24), 2279–2284.

Nagel, G., Szellas, T., Huhn, W., Kateriya, S., Adeishvili, N., Berthold, P., Ollig, D., Hegemann, P., & Bamberg, E. (2003). Channelrhodopsin-2, a directly light-gated cation-selective membrane channel.

Proceedings of the National Academy of Sciences , **100**(24), 13940–13945.

Naidoo, N., Davis, J. G., Zhu, J., Yabumoto, M., Singletary, K., Brown, M., Galante, R., Agarwal, B., & Baur, J. A. (2014). Aging and sleep deprivation induce the unfolded protein response in the pancreas: implications for metabolism. *Aging Cell*, **13**(1), 131–141.

Naidoo, N., Ferber, M., Galante, R. J., McShane, B., Hu, J. H., Zimmerman, J., Maislin, G., Cater, J., Wyner, A., Worley, P., & Pack, A. I. (2012). Role of Homer Proteins in the Maintenance of Sleep-Wake States. *PLOS ONE*, **7**(4), e35174.

Naidoo, N., Ferber, M., Master, M., Zhu, Y., & Pack, A. I. (2008). Aging impairs the unfolded protein response to sleep deprivation and leads to pro-apoptotic signaling. *The Journal of Neuroscience : The Official Journal of the Society for Neuroscience*, **28**(26), 6539–6548.

Naidoo, N., Giang, W., Galante, R. J., & Pack, A. I. (2005). Sleep deprivation induces the unfolded protein response in mouse cerebral cortex. *Journal of Neurochemistry*, **92**, 1150–1157.

Nair, D., Zhang, S. X. L., Ramesh, V., Hakim, F., Kaushal, N., Wang, Y., & Gozal, D. (2011). Sleep Fragmentation Induces Cognitive Deficits Via Nicotinamide Adenine Dinucleotide Phosphate Oxidase-dependent Pathways in Mouse. *American Journal of Respiratory and Critical Care Medicine*, pp. 1305–1312.

Nakai, J., Ohkura, M., & Imoto, K. (2001). A high signal-to-noise Ca2+ probe composed of a single green fluorescent protein. *Nat Biotech*, **19**(2), 137–141.

Nakamura, T., Uramura, K., Nambu, T., Yada, T., Goto, K., Yanagisawa, M., & Sakurai, T. (2000). Orexin-induced hyperlocomotion and stereotypy are mediated by the dopaminergic system. *Brain Research*, **873**, 181–187.

Naylor, E., Aillon, D. V, Barrett, B. S., Wilson, G. S., Johnson, D. A., Johnson, D. A., Harmon, H. P., Gabbert, S., & Petillo, P. A. (2012). Lactate as a Biomarker for Sleep. *Sleep*, **35**(9), 1209–1222.

Naylor, E., Bergmann, B. M., Krauski, K., Zee, P. C., Takahashi, J. S., Vitaterna, M. H., & Turek, F. W. (2000). The Circadian Clock Mutation Alters Sleep Homeostasis in the Mouse. *The Journal of Neuroscience*, **20**(21), 8138 LP-8143.

Newman, E. a. (2003). Glial cell inhibition of neurons by release of ATP. *The Journal of Neuroscience : The Official Journal of the Society for Neuroscience*, **23**, 1659–1666.

Nikonova, E. V, Naidoo, N., Zhang, L., Romer, M., Cater, J. R., Scharf, M. T., Galante, R. J., & Pack, A. I. (2010). Changes in components of energy regulation in mouse cortex with increases in wakefulness.

Sleep, **33**, 889–900.

Noguchi, T., Michihata, T., Nakamura, W., Takumi, T., Shimizu, R., Yamamoto, M., Ikeda, M., Ohmiya, Y., & Nakajima, Y. (2010). Dual-Color Luciferase Mouse Directly Demonstrates Coupled Expression of Two Clock Genes. *Biochemistry*, **49**(37), 8053–8061.

Ottenweller, J. E., Meier, A. H., Russo, A. C., & Frenzke, M. E. (1979). Circadian Rhythms of Plasma Corticosterone Binding Activity in the Rat and the Mouse. *Acta Endocrinologica*, **91**(1), 150–157.

Padez, C., Mourão, I., Moreira, P., & Rosado, V. (2005). Prevalence and risk factors for overweight and obesity in Portuguese children. *Acta Paediatrica*, **94**, 1550–1557.

Påhlman, S., Odelstad, L., Larsson, E., Grotte, G., & Nilsson, K. (1981). Phenotypic changes of human neuroblastoma cells in culture induced by 12-O-tetradecanoyl-phorbol-13-acetate. *International Journal of Cancer*, **28**(5), 583–589.

Påhlman, S., Ruusala, A.-I., Abrahamsson, L., Mattsson, M. E. K., & Esscher, T. (1984). Retinoic acid-induced differentiation of cultured human neuroblastoma cells: a comparison with phorbolester-induced differentiation. *Cell Differentiation*, **14**(2), 135–144.

Palmblad, J., Petrini, B., Wasserman, J., & Akerstedt, T. (1979). Lymphocyte and granulocyte reactions during sleep deprivation. *Psychosomatic Medicine*, **41**, 273–8.

Papale, L. A., Andersen, M. L., Antunes, I. B., Alvarenga, T. A. F., & Tufik, S. (2005). Sleep pattern in rats under different stress modalities. *Brain Research*, **1060**(1), 47–54.

Parameyong, A., Charngkaew, K., Govitrapong, P., & Chetsawang, B. (2013). Melatonin attenuates methamphetamine-induced disturbances in mitochondrial dynamics and degeneration in neuroblastoma SH-SY5Y cells. *Journal of Pineal Research*, **55**, 313–23.

Pastuzyn, E. D., Day, C. E., Kearns, R. B., Kyrke-Smith, M., Taibi, A. V., McCormick, J., Yoder, N., Belnap, D. M., Erlendsson, S., Morado, D. R., Briggs, J. A. G., Feschotte, C., & Shepherd, J. D. (2018). The Neuronal Gene Arc Encodes a Repurposed Retrotransposon Gag Protein that Mediates Intercellular RNA Transfer. *Cell*, **172**(1–2), 275–288.e18.

Patel, S. R., Malhotra, A., White, D. P., Gottlieb, D. J., & Hu, F. B. (2006). Association between reduced sleep and weight gain in women. *American Journal of Epidemiology*, **164**, 947–954.

Pawlyk, A. C., Ferber, M., Shah, A., Pack, A. I., & Naidoo, N. (2007). Proteomic analysis of the effects and interactions of sleep deprivation and aging in mouse cerebral cortex. *Journal of Neurochemistry*, **103**, 2301–13.

Perron, A., Mutoh, H., Launey, T., & Knöpfel, T. (2009). Red-Shifted Voltage-Sensitive Fluorescent Proteins. *Chemistry & Biology*, **16**(12), 1268–1277.

Petit, J.-M., Tobler, I., Kopp, C., Morgenthaler, F., Borbély, A. A., & Magistretti, P. J. (2010). Metabolic Response of the Cerebral Cortex Following Gentle Sleep Deprivation and Modafinil Administration. *Sleep*, **33**(7), 901–908.

Peyron, C., Faraco, J., Rogers, W., Ripley, B., Overeem, S., Charnay, Y., Nevsimalova, S., Aldrich, M., Reynolds, D., Albin, R., Li, R., Hungs, M., Pedrazzoli, M., Padigaru, M., Kucherlapati, M., Fan, J., Maki, R., Lammers, G. J., Bouras, C., et al. (2000). A mutation in a case of early onset narcolepsy and a generalized absence of hypocretin peptides in human narcoleptic brains. *Nature Medicine*, **6**, 991–997.

Philibert, I. (2005). Sleep loss and performance in residents and nonphysicians: a meta-analytic examination. *Sleep*, **28**, 1392–1402.

Piérard, C., Liscia, P., Philippin, J.-N., Mons, N., Lafon, T., Chauveau, F., Van Beers, P., Drouet, I., Serra, A., Jouanin, J.-C., & Béracochéa, D. (2007). Modafinil restores memory performance and neural activity impaired by sleep deprivation in mice. *Pharmacology Biochemistry and Behavior*, **88**(1), 55–63.

Pleasure, S. J., & Lee, V. M. . . (1993). NTera 2 Cells: A human cell line which displays characteristics expected of a human committed neuronal progenitor cell. *Journal of Neuroscience Research*, **35**(6), 585–602.

Plihal, W., & Born, J. (1997). Effects of Early and Late Nocturnal Sleep on Declarative and Procedural Memory. *Journal of Cognitive Neuroscience*, **9**, 534–547.

Porkka-Heiskanen, T., Alanko, L., Kalinchuk, A., & Stenberg, D. (2002). Adenosine and sleep. *Sleep Medicine Reviews*, **6**, 321–332.

Porkka-Heiskanen, T., Strecker, R. E., & McCarley, R. W. (2000). Brain site-specificity of extracellular adenosine concentration changes during sleep deprivation and spontaneous sleep: an in vivo microdialysis study. *Neuroscience*, **99**(3), 507–517.

Porkka-Heiskanen, T., Strecker, R. E., Thakkar, M., Bjorkum, a a, Greene, R. W., & McCarley, R. W. (1997). Adenosine: a mediator of the sleep-inducing effects of prolonged wakefulness. *Science (New York, N.Y.)*, **276**, 1265–1268.

Porstmann, T., Griffiths, B., Chung, Y.-L., Delpuech, O., Griffiths, J. R., Downward, J., & Schulze, A. (2005). PKB/Akt induces transcription of enzymes involved in cholesterol and fatty acid biosynthesis via activation of SREBP. *Oncogene*, **24**, 6465.

Possemato, A. P., Paulo, J. A., Mulhern, D., Guo, A., Gygi, S. P., & Beausoleil, S. A. (2017). Multiplexed Phosphoproteomic Profiling Using Titanium Dioxide and Immunoaffinity Enrichments Reveals Complementary Phosphorylation Events. *Journal of Proteome Research*, **16**(4), 1506–1514.

Prather, A. a., Hall, M., Fury, J. M., Ross, D. C., Muldoon, M. F., Cohen, S., & Marsland, A. L. (2012). Sleep and Antibody Response to Hepatitis B Vaccination. *Sleep*, 2–8.

Prospe´ro-Garcia, O., Morales, M., Arankowsky-Sandoval, G., & Drucker-Colin, R. (1986). Vasoactive intestinal polypeptide (VIP) and cerebrospinal fluid (CSF) of sleep-deprived cats restores REM sleep in insomniac recipients. *Brain Research*, **385**(1), 169–173.

Rabat, A., Bouyer, J. J., Aran, J. M., Le Moal, M., & Mayo, W. (2005). Chronic exposure to an environmental noise permanently disturbs sleep in rats: Inter-individual vulnerability. *Brain Research*, **1059**(1), 72–82.

Ram, A., Pandey, H. P., Matsumura, H., Kasahara-Orita, K., Nakajima, T., Takahata, R., Satoh, S., Terao, A., & Hayaishi, O. (1997). CSF levels of prostaglandins, especially the level of prostaglandin D2, are correlated with increasing propensity towards sleep in rats. *Brain Research*, **751**(1), 81–89.

Ramesh, V., Kaushal, N., & Gozal, D. (2008). *Sleep fragmentation modifies EEG delta power during slow wave sleep in socially isolated and paired mice*. *Sleep Science*, Vol. 2.

Ramm, P., & Smith, C. T. (1990). Rates of cerebral protein synthesis are linked to slow wave sleep in the rat. *Physiology & Behavior*, **48**(5), 749–753.

Rechtschaffen, A., & Bergmann, B. M. (1995). Sleep deprivation in the rat by the disk-over-water method. In *Behavioural Brain Research*, Vol. 69, pp. 55–63.

Rector, D. M., Topchiy, I. a., Carter, K. M., & Rojas, M. J. (2005). Local functional state differences between rat cortical columns. *Brain Research*, **1047**, 45–55.

Reilly, J. J., Armstrong, J., Dorosty, A. R., Emmett, P. M., Ness, A., Rogers, I., Steer, C., & Sherriff, A. (2005). Early life risk factors for obesity in childhood: cohort study. *BMJ (Clinical Research Ed.)*, **330**, 1357.

Ren, J., Zhang, M.-J., Li, T.-M., Zhang, J., Lin, R., Chen, S., Luo, M., & Dong, M.-Q. (2016). Quantitative Proteomics of Sleep-Deprived Mouse Brains Reveals Global Changes in Mitochondrial Proteins. *PLoS ONE*, **11**(9), e0163500.

Revel, F. G., Gottowik, J., Gatti, S., Wettstein, J. G., & Moreau, J.-L. (2009). Rodent models of insomnia: a review of experimental procedures that induce sleep disturbances. *Neuroscience and Biobehavioral*

Reviews, **33**, 874–899.

Rey, G., Valekunja, U. K., Feeney, K. A., Wulund, L., Milev, N. B., Stangherlin, A., Ansel-Bollepalli, L., Velagapudi, V., O'Neill, J. S., & Reddy, A. B. (2016). The Pentose Phosphate Pathway Regulates the Circadian Clock. *Cell Metabolism*, **24**(3), 462–473.

Rial, R. V., Nicolau, M. C., Gamundí, A., Akaârir, M., Aparicio, S., Garau, C., Tejada, S., Roca, C., Gené, L., Moranta, D., & others. (2007). The trivial function of sleep. *Sleep Medicine Reviews*, **11**(4), 311–325.

Richardson, P. J., & Brown, S. J. (1987). ATP release from affinity-purified rat cholinergic nerve terminals. *Journal of Neurochemistry*, **48**, 622–30.

Richter, K., Haslbeck, M., & Buchner, J. (2010). The Heat Shock Response: Life on the Verge of Death. *Molecular Cell*, **40**(2), 253–266.

Roca, J., Fuentes, L. J., Marotta, A., López-Ramón, M.-F., Castro, C., Lupiáñez, J., & Martella, D. (2012). The effects of sleep deprivation on the attentional functions and vigilance. *Acta Psychologica*, **140**, 164–76.

Romanowski, C. P. N., Fenzl, T., Flachskamm, C., Wurst, W., Holsboer, F., Deussing, J. M., & Kimura, M. (2010). Central Deficiency of Corticotropin-Releasing Hormone Receptor Type 1 (CRH-R1) Abolishes Effects of CRH on NREM But Not on REM Sleep in Mice. *Sleep*, **33**(4), 427–436.

Rordorf, G., Koroshetz, W. J., & Bonventre, J. V. (1991). Heat shock protects cultured neurons from glutamate toxicity. *Neuron*, **7**(6), 1043–1051.

Ruggiero, J. S., Redeker, N. S., Fiedler, N., Avi-Itzhak, T., & Fischetti, N. (2012). Sleep and psychomotor vigilance in female shiftworkers. *Biological Research for Nursing*, **14**, 225–35.

Rupp, T. L. (2013). *Psychomotor Vigilance Performance*. *Encyclopedia of Sleep*. doi:http://dx.doi.org/10.1016/B978-0-12-378610-4.00148-0

Saito, Y. C., Tsujino, N., Hasegawa, E., Akashi, K., Abe, M., Mieda, M., Sakimura, K., & Sakurai, T. (2013). GABAergic neurons in the preoptic area send direct inhibitory projections to orexin neurons. *Frontiers in Neural Circuits*, **7**, 192.

Sakurai, T., Amemiya, A., Ishii, M., Matsuzaki, I., Chemelli, R. M., Tanaka, H., Williams, S. C., Richardson, J. a., Kozlowski, G. P., Wilson, S., Arch, J. R. S., Buckingham, R. E., Haynes, A. C., Carr, S. a., Annan, R. S., McNulty, D. E., Liu, W. S., Terrett, J. a., Elshourbagy, N. a., et al. (1998). Orexins and orexin receptors: A family of hypothalamic neuropeptides and G protein-coupled receptors that regulate

feeding behavior. *Cell*, **92**, 573–585.

Sanford, L. D., Yang, L., Wellman, L. L., Dong, E., & Tang, X. (2008). Mouse strain differences in the effects of corticotropin releasing hormone (CRH) on sleep and wakefulness. *Brain Research*, **1190**, 94–104.

Sarkanen, J. R., Nykky, J., Siikanen, J., Selinummi, J., Ylikomi, T., & Jalonen, T. O. (2007). Cholesterol supports the retinoic acid-induced synaptic vesicle formation in differentiating human SH-SY5Y neuroblastoma cells. *Journal of Neurochemistry*, **102**, 1941–1952.

Sato, M., Suzuki, K., & Nakanishi, S. (2001). NMDA Receptor Stimulation and Brain-Derived Neurotrophic Factor Upregulate Homer 1a mRNA via the Mitogen-Activated Protein Kinase Cascade in Cultured Cerebellar Granule Cells. *The Journal of Neuroscience*, **21**(11), 3797 LP-3805.

Saunders, A., Granger, A. J., & Sabatini, B. L. (2015). Corelease of acetylcholine and GABA from cholinergic forebrain neurons. *eLife*, **4**, e06412.

Sauvet, F., Leftheriotis, G., Gomez-Merino, D., Langrume, C., Drogou, C., Van Beers, P., Bourrilhon, C., Florence, G., & Chennaoui, M. (2010). Effect of acute sleep deprivation on vascular function in healthy subjects. *Journal of Applied Physiology*, **108**(1), 68 LP-75.

Scammell, T. E., Gerashchenko, D. Y., Mochizuki, T., McCarthy, M. T., Estabrooke, I. V., Sears, C. a., Saper, C. B., Urade, Y., & Hayaishi, O. (2001). An adenosine A2a agonist increases sleep and induces Fos in ventrolateral preoptic neurons. *Neuroscience*, **107**, 653–663.

Schaum, N., Karkanias, J., Neff, N. F., May, A. P., Quake, S. R., Wyss-Coray, T., Darmanis, S., Batson, J., Botvinnik, O., Chen, M. B., Chen, S., Green, F., Jones, R. C., Maynard, A., Penland, L., Pisco, A. O., Sit, R. V, Stanley, G. M., Webber, J. T., et al. (2018). Single-cell transcriptomics of 20 mouse organs creates a Tabula Muris. *Nature*. doi:10.1038/s41586-018-0590-4

Schild, L. C., & Glauser, D. A. (2015). Dual Color Neural Activation and Behavior Control with Chrimson and CoChR in Caenorhabditis elegans *Genetics*, **200**(4), 1029 LP-1034.

Schmitt, L. I., Sims, R. E., Dale, N., & Haydon, P. G. (2012). Wakefulness affects synaptic and network activity by increasing extracellular astrocyte-derived adenosine. *The Journal of Neuroscience : The Official Journal of the Society for Neuroscience*, **32**, 4417–25.

Schneider, F., Gradmann, D., & Hegemann, P. (2013). Ion Selectivity and Competition in Channelrhodopsins. *Biophysical Journal*, **105**(1), 91–100.

Schobert, B., & Lanyi, J. K. (1982). Halorhodopsin is a light-driven chloride pump. *Journal of Biological*

Chemistry , **257**(17), 10306–10313.

Schulte, H. M., Chrousos, G. P., Gold, P. W., Oldfield, E. H., Phillips, J. M., Munson, P. J., Cutler G. B., J. R., & Loriaux, D. L. (1982). Metabolic clearance rate and plasma half-life of radioiodinated corticotropin releasing factor in a primate. *The Journal of Clinical Endocrinology & Metabolism*, **55**(5), 1023–1025.

Schürmeyer, T. H., Avgerinos, P. C., Gold, P. W., Gallucci, W. T., Tomai, T. P., Cutler G. B., J. R., Loriaux, D. L., & Chrousos, G. P. (1984). Human Corticotropin-Releasing Factor in Man: Pharmacokinetic Properties and Dose-Response of Plasma Adrenocorticotropin and Cortisol Secretion. *The Journal of Clinical Endocrinology & Metabolism*, **59**(6), 1103–1108.

Schwertman, P., Bezstarosti, K., Laffeber, C., Vermeulen, W., Demmers, J. A. A., & Marteijn, J. A. (2013). An immunoaffinity purification method for the proteomic analysis of ubiquitinated protein complexes. *Analytical Biochemistry*, **440**(2), 227–236.

Schwierin, B., Borbely, A. A., & Tobler, I. (1996). Effects of N6-cyclopentyladenosine and caffeine on sleep regulation in the rat. *European Journal of Pharmacology*, **300**, 163–171.

Sehgal, a, Joiner, W., Crocker, a, Koh, K., Sathyanarayanan, S., Fang, Y., Wu, M., Williams, J. a, & Zheng, X. (2007). Molecular analysis of sleep: wake cycles in Drosophila. *Cold Spring Harbor Symposia on Quantitative Biology*, **72**, 557–64.

Seong, E., Saunders, T. L., Stewart, C. L., & Burmeister, M. (2004). To knockout in 129 or in C57BL/6: that is the question. *Trends in Genetics*, **20**(2), 59–62.

Shaw, P. J., Cirelli, C., Greenspan, R. J., & Tononi, G. (2000). Correlates of sleep and waking in Drosophila melanogaster. *Science (New York, N.Y.)*, **287**, 1834–1837.

Shaw, P. J., Tononi, G., Greenspan, R. J., & Robinson, D. F. (2002). Stress response genes protect against lethal effects of sleep deprivation in Drosophila. *Nature*, **417**, 287–291.

Shepherd, J. D., Rumbaugh, G., Wu, J., Chowdhury, S., Plath, N., Kuhl, D., Huganir, R. L., & Worley, P. F. (2006). Arc/Arg3.1 Mediates Homeostatic Synaptic Scaling of AMPA Receptors. *Neuron*, **52**(3), 475–484.

Sherin, J. E., Elmquist, J. K., Torrealba, F., & Saper, C. B. (1998). Innervation of histaminergic tuberomammillary neurons by GABAergic and galaninergic neurons in the ventrolateral preoptic nucleus of the rat. *The Journal of Neuroscience : The Official Journal of the Society for Neuroscience*, **18**, 4705–4721.

Sherin, J. E., Shiromani, P. J., McCarley, R. W., & Saper, C. B. (1996). Activation of ventrolateral preoptic neurons during sleep. *Science (New York, N.Y.)*, **271**, 216–219.

Shipley, M. M., Mangold, C. A., & Szpara, M. L. (2016). Differentiation of the SH-SY5Y Human Neuroblastoma Cell Line. *Journal of Visualized Experiments : JoVE*, (108), 53193.

Sigurgeirsson, B., Þorsteinsson, H., Sigmundsdóttir, S., Lieder, R., Sveinsdóttir, H. S., Sigurjónsson, Ó. E., Halldórsson, B., & Karlsson, K. (2013). Sleep–wake dynamics under extended light and extended dark conditions in adult zebrafish. *Behavioural Brain Research*, **256**, 377–390.

Simor, A., Györffy, B. A., Gulyássy, P., Völgyi, K., Tóth, V., Todorov, M. I., Kis, V., Borhegyi, Z., Szabó, Z., Janáky, T., Drahos, L., Juhász, G., & Kékesi, K. A. (2017). The short- and long-term proteomic effects of sleep deprivation on the cortical and thalamic synapses. *Molecular and Cellular Neuroscience*, **79**, 64–80.

Sims, R. E., Wu, H. H. T., & Dale, N. (2013). Sleep-wake sensitive mechanisms of adenosine release in the basal forebrain of rodents: an in vitro study. *PloS One*, **8**, e53814.

Sineshchekov, O. A., Jung, K.-H., & Spudich, J. L. (2002). Two rhodopsins mediate phototaxis to low- and high-intensity light in Chlamydomonas reinhardtii. *Proceedings of the National Academy of Sciences* , **99**(13), 8689–8694.

Siuda, E. R., Copits, B. A., Schmidt, M. J., Baird, M. A., Al-Hasani, R., Planer, W. J., Funderburk, S. C., McCall, J. G., Gereau IV, R. W., & Bruchas, M. R. (2015). Spatiotemporal Control of Opioid Signaling and Behavior. *Neuron*, **86**(4), 923–935.

Spaeth, A. M., Dinges, D. F., & Goel, N. (2013). Effects of Experimental Sleep Restriction on Weight Gain, Caloric Intake, and Meal Timing in Healthy Adults. *Sleep*, **36**, 981–990.

Spiegel, K., JF, S., & E, V. C. (2002). Effect of sleep deprivation on response to immunizaton. *JAMA*, **288**(12), 1471–1472.

Spiegel, K., Leproult, R., & Van Cauter, E. (1999). Impact of sleep debt on metabolic and endocrine function. *Lancet*, **354**(9188), 1435–1439.

Spindel, E. R., & Wurtman, R. J. (1984). Neuroendocrine Effects of Caffeine in Rat and Man BT - Caffeine: Perspectives from Recent Research. In P. B. Dews, ed., , Berlin, Heidelberg: Springer Berlin Heidelberg, pp. 119–128.

St-Onge, M.-P., Roberts, A. L., Chen, J., Kelleman, M., O'Keeffe, M., RoyChoudhury, A., & Jones, P. J. H. (2011). Short sleep duration increases energy intakes but does not change energy expenditure in

normal-weight individuals. *The American Journal of Clinical Nutrition*, **94**, 410–416.

St-Pierre, F., Marshall, J. D., Yang, Y., Gong, Y., Schnitzer, M. J., & Lin, M. Z. (2014). High-fidelity optical reporting of neuronal electrical activity with an ultrafast fluorescent voltage sensor. *Nat Neurosci*, **17**(6), 884–889.

Stenberg, D., Litonius, E., Halldner, L., Johansson, B., Fredholm, B. B., & Porkka-Heiskanen, T. (2003). Sleep and its homeostatic regulation in mice lacking the adenosine A1 receptor. *Journal of Sleep Research*, **12**(4), 283–290.

Steriade, M., & Hobson, J. A. (1976). Neuronal activity during the sleep-waking cycle. *Progress in Neurobiology*, **6**(Part 3), 157–376.

Suzuki, S., Kiyosue, K., Hazama, S., Ogura, A., Kashihara, M., Hara, T., Koshimizu, H., & Kojima, M. (2007). Brain-Derived Neurotrophic Factor Regulates Cholesterol Metabolism for Synapse Development. *The Journal of Neuroscience*, **27**(24), 6417 LP-6427.

Szymusiak, R., & McGinty, D. (1986). Sleep suppression following kainic acid-induced lesions of the basal forebrain. *Experimental Neurology*, **94**, 598–614.

Taghibiglou, C., Martin, H. G. S., Lai, T. W., Cho, T., Prasad, S., Kojic, L., Lu, J., Liu, Y., Lo, E., Zhang, S., Wu, J. Z. Z., Li, Y. P., Wen, Y. H., Imm, J.-H., Cynader, M. S., & Wang, Y. T. (2009). Role of NMDA receptor–dependent activation of SREBP1 in excitotoxic and ischemic neuronal injuries. *Nature Medicine*, **15**, 1399.

Takahashi, K., Kayama, Y., Lin, J. S., & Sakai, K. (2010). Locus coeruleus neuronal activity during the sleep-waking cycle in mice. *Neuroscience*, **169**, 1115–1126.

Tantama, M., Hung, Y. P., & Yellen, G. (2011). Imaging Intracellular pH in Live Cells with a Genetically-Encoded Red Fluorescent Protein Sensor. *Journal of the American Chemical Society*, **133**(26), 10034–10037.

Tao, R., Zhao, Y., Chu, H., Wang, A., Zhu, J., Chen, X., Zou, Y., Shi, M., Liu, R., Su, N., Du, J., Zhou, H.-M., Zhu, L., Qian, X., Liu, H., Loscalzo, J., & Yang, Y. (2017). Genetically encoded fluorescent sensors reveal dynamic regulation of NADPH metabolism. *Nat Meth*, **14**(7), 720–728.

Terao, A., Matsumura, H., Yoneda, H., & Saito, M. (1998). Enhancement of slow-wave sleep by tumor necrosis factor-α is mediated by cyclooxygenase-2 in rats. *NeuroReport*, **9**(17). Retrieved from https://journals.lww.com/neuroreport/Fulltext/1998/12010/Enhancement_of_slow_wave_sleep_by_tumor_necrosis.5.aspx

Terao, a., Greco, M. a., Davis, R. W., Heller, H. C., & Kilduff, T. S. (2003). Region-specific changes in immediate early gene expression in response to sleep deprivation and recovery sleep in the mouse brain. *Neuroscience*, **120**, 1115–1124.

Tetsuya, K., Atsuro, M., Hayato, I., Shuntaro, H., Tamiko, S., Osamu, T., Ei-ichi, T., & Tadashi, T. (2005). Characterization of the human gene (PTGS2) encoding prostaglandin-endoperoxide synthase 2. *European Journal of Biochemistry*, **221**(3), 889–897.

Thannickal, T. C., Moore, R. Y., Nienhuis, R., Ramanathan, L., Gulyani, S., Aldrich, M., Cornford, M., & Siegel, J. M. (2000). Reduced number of hypocretin neurons in human narcolepsy. *Neuron*, **27**, 469–474.

Thomas, M., Sing, H., Belenky, G., Holcomb, H., Mayberg, H., Dannals, R., Wagner JR., H., Thorne, D., Popp, K., Rowland, L., Welsh, A., Balwinski, S., & Redmond, D. (2000). Neural basis of alertness and cognitive performance impairments during sleepiness. I. Effects of 24 h of sleep deprivation on waking human regional brain activity. *Journal of Sleep Research*, **9**(4), 335–352.

Thompson, C. L., Wisor, J. P., Lee, C.-K., Pathak, S. D., Gerashchenko, D., Smith, K. A., Fischer, S. R., Kuan, C. L., Sunkin, S. M., Ng, L. L., Lau, C., Hawrylycz, M., Jones, A. R., Kilduff, T. S., & Lein, E. S. (2010). Molecular and Anatomical Signatures of Sleep Deprivation in the Mouse Brain. *Frontiers in Neuroscience*, **4**, 165.

Tononi, G., & Cirelli, C. (2003). Sleep and synaptic homeostasis: a hypothesis. *Brain Research Bulletin*, **62**(2), 143–150.

Tremblay, R. G., Sikorska, M., Sandhu, J. K., Lanthier, P., Ribecco-Lutkiewicz, M., & Bani-Yaghoub, M. (2010). Differentiation of mouse Neuro 2A cells into dopamine neurons. *Journal of Neuroscience Methods*, **186**(1), 60–67.

Tu, J. C., Xiao, B., Yuan, J. P., Lanahan, A. A., Leoffert, K., Li, M., Linden, D. J., & Worley, P. F. (1998). Homer Binds a Novel Proline-Rich Motif and Links Group 1 Metabotropic Glutamate Receptors with IP3 Receptors. *Neuron*, **21**(4), 717–726.

Tudor, J. C., Davis, E. J., Peixoto, L., Wimmer, M. E., van Tilborg, E., Park, A. J., Poplawski, S. G., Chung, C. W., Havekes, R., Huang, J., Gatti, E., Pierre, P., & Abel, T. (2016). Sleep deprivation impairs memory by attenuating mTORC1-dependent protein synthesis. *Science Signaling*, **9**(425), ra41 LP-ra41.

Urban, D. J., & Roth, B. L. (2015). DREADDs (Designer Receptors Exclusively Activated by Designer Drugs): Chemogenetic Tools with Therapeutic Utility. *Annual Review of Pharmacology and Toxicology*, **55**, 399–417.

Uschakov, A., Gong, H., McGinty, D., & Szymusiak, R. (2007). Efferent projections from the median preoptic nucleus to sleep- and arousal-regulatory nuclei in the rat brain. *Neuroscience*, **150**, 104–20.

Valdivia, S., Patrone, A., Reynaldo, M., & Perello, M. (2014). Acute high fat diet consumption activates the mesolimbic circuit and requires orexin signaling in a mouse model. *PloS One*, **9**, e87478.

Vazdarjanova, A., McNaughton, B. L., Barnes, C. A., Worley, P. F., & Guzowski, J. F. (2002). Experience-Dependent Coincident Expression of the Effector Immediate-Early Genes Arc and Homer 1a in Hippocampal and Neocortical Neuronal Networks. *The Journal of Neuroscience*, **22**(23), 10067 LP-10071.

Vecsey, C. G., Baillie, G. S., Jaganath, D., Havekes, R., Daniels, A., Wimmer, M., Huang, T., Brown, K. M., Li, X.-Y., Descalzi, G., Kim, S. S., Chen, T., Shang, Y.-Z., Zhuo, M., Houslay, M. D., & Abel, T. (2009). Sleep deprivation impairs cAMP signalling in the hippocampus. *Nature*, **461**, 1122.

Verma, P., Chierzi, S., Codd, A. M., Campbell, D. S., Meyer, R. L., Holt, C. E., & Fawcett, J. W. (2005). Axonal Protein Synthesis and Degradation Are Necessary for Efficient Growth Cone Regeneration. *The Journal of Neuroscience*, **25**(2), 331 LP-342.

Von Economo, C. (1930). Sleep As a Problem of Localization. *The Journal of Nervous and Mental Disease*, **71**, 249–259.

von Kries, R., Toschke, A. M., Wurmser, H., Sauerwald, T., & Koletzko, B. (2002). Reduced risk for overweight and obesity in 5- and 6-y-old children by duration of sleep--a cross-sectional study. *International Journal of Obesity and Related Metabolic Disorders : Journal of the International Association for the Study of Obesity*, **26**, 710–716.

Vosko, A. M., Colwell, C. S., & Avidan, A. Y. (2010). Jet lag syndrome: circadian organization, pathophysiology, and management strategies. *Nature and Science of Sleep*, **2**, 187–198.

Vyazovskiy, V. V, Olcese, U., Hanlon, E. C., Nir, Y., Cirelli, C., & Tononi, G. (2011). Local sleep in awake rats. *Nature*, **472**(7344), 443–447.

Vyazovskiy, V. V, Olcese, U., Lazimy, Y. M., Faraguna, U., Esser, S. K., Williams, J. C., Cirelli, C., & Tononi, G. (2009). Cortical Firing and Sleep Homeostasis. *Neuron*, **63**(6), 865–878.

Wang, Y., Carreras, A., Lee, S., Hakim, F., Zhang, S. X., Nair, D., Ye, H., & Gozal, D. (2013). Chronic sleep fragmentation promotes obesity in young adult mice. *Obesity (Silver Spring, Md.)*, **0**, 1–5.

Wang, Z., Ma, J., Miyoshi, C., Li, Y., Sato, M., Ogawa, Y., Lou, T., Ma, C., Gao, X., Lee, C., Fujiyama, T., Yang, X., Zhou, S., Hotta-Hirashima, N., Klewe-Nebenius, D., Ikkyu, A., Kakizaki, M., Kanno, S., Cao, L.,

et al. (2018). Quantitative phosphoproteomic analysis of the molecular substrates of sleep need. *Nature*, **558**(7710), 435–439.

Weljie, A. M., Meerlo, P., Goel, N., Sengupta, A., Kayser, M. S., Abel, T., Birnbaum, M. J., Dinges, D. F., & Sehgal, A. (2015). Oxalic acid and diacylglycerol 36:3 are cross-species markers of sleep debt. *Proceedings of the National Academy of Sciences* , **112**(8), 2569–2574.

Welsh, D. K., Richardson, G. S., & Dement, W. C. (1986). Effect of Age on the Circadian Pattern of Sleep and Wakefulness in the Mouse. *Journal of Gerontology*, **41**(5), 579–586.

Werth, E., Achermann, P., Dijk, D. J., & Borbély, A. a. (1997). Spindle frequency activity in the sleep EEG: Individual differences and topographic distribution. *Electroencephalography and Clinical Neurophysiology*, **103**, 535–542.

White, R. S., Bhattacharya, A. K., Chen, Y., Byrd, M., McMullen, M. F., Siegel, S. J., Carlson, G. C., & Kim, S. F. (2016). Lysosomal iron modulates NMDA receptor-mediated excitation via small GTPase, Dexras1. *Molecular Brain*, **9**(1), 38.

Wietek, J., Beltramo, R., Scanziani, M., Hegemann, P., Oertner, T. G., & Wiegert, J. S. (2015). An improved chloride-conducting channelrhodopsin for light-induced inhibition of neuronal activity in vivo, **5**, 14807.

Wietek, J., Wiegert, J. S., Adeishvili, N., Schneider, F., Watanabe, H., Tsunoda, S. P., Vogt, A., Elstner, M., Oertner, T. G., & Hegemann, P. (2014). Conversion of channelrhodopsin into a light-gated chloride channel. *Science (New York, N.Y.)*, **344**, 409–12.

Williamson, a M., & Feyer, a M. (2000). Moderate sleep deprivation produces impairments in cognitive and motor performance equivalent to legally prescribed levels of alcohol intoxication. *Occupational and Environmental Medicine*, **57**, 649–655.

Winsky-Sommerer, R., Yamanaka, A., Diano, S., Borok, E., Roberts, A. J., Sakurai, T., Kilduff, T. S., Horvath, T. L., & de Lecea, L. (2004). Interaction between the Corticotropin-Releasing Factor System and Hypocretins (Orexins): A Novel Circuit Mediating Stress Response. *The Journal of Neuroscience*, **24**(50), 11439 LP-11448.

Wisor, J. P., O'Hara, B. F., Terao, A., Selby, C. P., Kilduff, T. S., Sancar, A., Edgar, D. M., & Franken, P. (2002). A role for cryptochromesin sleep regulation. *BMC Neuroscience*, **3**(1), 20.

Wu, Z., Autry, A. E., Bergan, J. F., Watabe-Uchida, M., & Dulac, C. G. (2014). Galanin neurons in the medial preoptic area govern parental behaviour. *Nature*, **509**, 325–30.

Xie, L., Kang, H., Xu, Q., Chen, M. J., Liao, Y., Thiyagarajan, M., O'Donnell, J., Christensen, D. J., Nicholson, C., Iliff, J. J., Takano, T., Deane, R., & Nedergaard, M. (2013). Sleep drives metabolite clearance from the adult brain. *Science (New York, N.Y.)*, **342**, 373–7.

Xu, M., Chung, S., Zhang, S., Zhong, P., Ma, C., Chang, W.-C., Weissbourd, B., Sakai, N., Luo, L., Nishino, S., & Dan, Y. (2015). Basal forebrain circuit for sleep-wake control. *Nat Neurosci*, **18**(11), 1641–1647.

Yamanaka, A., Beuckmann, C. T., Willie, J. T., Hara, J., Tsujino, N., Mieda, M., Tominaga, M., Yagami, K., Sugiyama, F., Goto, K., Yanagisawa, M., & Sakurai, T. (2003a). Hypothalamic Orexin Neurons Regulate Arousal According to Energy Balance in Mice. *Neuron*, **38**(5), 701–713.

Yamanaka, A., Muraki, Y., Tsujino, N., Goto, K., & Sakurai, T. (2003b). Regulation of orexin neurons by the monoaminergic and cholinergic systems. *Biochemical and Biophysical Research Communications*, **303**, 120–129.

Yamanaka, a, Kunii, K., Nambu, T., Tsujino, N., Sakai, a, Matsuzaki, I., Miwa, Y., Goto, K., & Sakurai, T. (2000). Orexin-induced food intake involves neuropeptide Y pathway. *Brain Research*, **859**, 404–9.

Yamazaki, S., Numano, R., Abe, M., Hida, A., Takahashi, R., Ueda, M., Block, G. D., Sakaki, Y., Menaker, M., & Tei, H. (2000). Resetting Central and Peripheral Circadian Oscillators in Transgenic Rats. *Science*, **288**(5466), 682 LP-685.

Yan, J., Li, J.-C., Xie, M.-L., Zhang, D., Qi, A.-P., Hu, B., Huang, W., Xia, J.-X., & Hu, Z.-A. (2011). Short-term sleep deprivation increases intrinsic excitability of prefrontal cortical neurons. *Brain Research*, **1401**, 52–58.

Yan, L., & Okamura, H. (2002). Gradients in the circadian expression of Per1 and Per2 genes in the rat suprachiasmatic nucleus. *The European Journal of Neuroscience*, **15**, 1153–62.

Ying, Z., Misra, V., & Verge, V. M. K. (2014). Sensing nerve injury at the axonal ER: Activated Luman/CREB3 serves as a novel axonally synthesized retrograde regeneration signal. *Proceedings of the National Academy of Sciences of the United States of America*, **111**(45), 16142–16147.

Ying, Z., Zhai, R., McLean, N. A., Johnston, J. M., Misra, V., & Verge, V. M. K. (2015). The Unfolded Protein Response and Cholesterol Biosynthesis Link Luman/CREB3 to Regenerative Axon Growth in Sensory Neurons. *The Journal of Neuroscience*, **35**(43), 14557 LP-14570.

Yoshida, H., Kubota, T., & Krueger, J. M. (2003). A cyclooxygenase-2 inhibitor attenuates spontaneous and TNF-α-induced non-rapid eye movement sleep in rabbits. *American Journal of Physiology-Regulatory, Integrative and Comparative Physiology*, **285**(1), R99–R109.

Yoshida, M., Koyanagi, S., Matsuo, A., Fujioka, T., To, H., Higuchi, S., & Ohdo, S. (2005). Glucocorticoid Hormone Regulates the Circadian Coordination of μ-Opioid Receptor Expression in Mouse Brainstem. *Journal of Pharmacology and Experimental Therapeutics*, **315**(3), 1119 LP-1124.

Yu, X., Ye, Z., Houston, C. M., Zecharia, A. Y., Ma, Y., Zhang, Z., Uygun, D. S., Parker, S., Vyssotski, A. L., Yustos, R., Franks, N. P., Brickley, S. G., & Wisden, W. (2015). Wakefulness Is Governed by GABA and Histamine Cotransmission. *Neuron*, **87**(1), 164–178.

Zhang, J., Sutachan, J.-J., Montoya-Gacharna, J., Xu, C.-F., Xu, F., Neubert, T. A., Recio-Pinto, E., & Blanck, T. J. J. (2009). Isoflurane inhibits cyclic adenosine monophosphate response element-binding protein phosphorylation and calmodulin translocation to the nucleus of SH-SY5Y cells. *Anesthesia and Analgesia*, **109**, 1127–34.

Zhang, X. H., & Poo, M. M. (2002). Localized synaptic potentiation by BDNF requires local protein synthesis in the developing axon. *Neuron*, **36**(4), 675–688.

Zhang, Z., Ferretti, V., Güntan, İ., Moro, A., Steinberg, E. A., Ye, Z., Zecharia, A. Y., Yu, X., Vyssotski, A. L., Brickley, S. G., Yustos, R., Pillidge, Z. E., Harding, E. C., Wisden, W., & Franks, N. P. (2015). Neuronal ensembles sufficient for recovery sleep and the sedative actions of α2 adrenergic agonists. *Nature Neuroscience*, **18**, 553–61.

Zielinski, M. R., Kim, Y., Karpova, S. A., Winston, S., McCarley, R. W., Strecker, R. E., & Gerashchenko, D. (2013). Sleep active cortical neurons expressing neuronal nitric oxide synthase are active after both acute sleep deprivation and chronic sleep restriction. *Neuroscience*, **247**, 35–42.

Zimmerman, J. E., Mackiewicz, M., Galante, R. J., Zhang, L., Cater, J., Zoh, C., Rizzo, W., & Pack, A. I. (2004). Glycogen in the brain of Drosophila melanogaster: diurnal rhythm and the effect of rest deprivation. *Journal of Neurochemistry*, **88**, 32–40.

Zimmerman, J. E., Rizzo, W., Shockley, K. R., Raizen, D. M., Naidoo, N., Mackiewicz, M., Churchill, G. A., & Pack, A. I. (2006). Multiple mechanisms limit the duration of wakefulness in Drosophila brain. *Physiological Genomics*, **27**(3), 337–350.

Zong-Yuan, H., Zhi-Li, H., Wei-Min, Q., Naomi, E., Yoshihiro, U., & Osamu, H. (2005). An adenosine A2A receptor agonist induces sleep by increasing GABA release in the tuberomammillary nucleus to inhibit histaminergic systems in rats. *Journal of Neurochemistry*, **92**(6), 1542–1549.

Appendix

App. Table of Contents

App.1. Genes Modulated by 6 Hour Sleep Deprivation

Genes modulated immediately following 6-hour sleep deprivation by at least 1.5 fold, compared to mice with uninterrupted sleep opportunity. Data presented is the Gene ID and name, the Log2 fold change, and the Benjamini adjusted q-value for significance. Data derived from cuffdiff command.

Ensembl_ID	Gene	Log2_FC	q_val
ENSMUSG00000065126	Snord104	6.78	0.000521
ENSMUSG00000098343	Mir6240	4.41	0.000521
ENSMUSG00000095676	Gm25099	3.82	0.000521
ENSMUSG00000064352	mt-Ts1	3.61	0.0191
ENSMUSG00000088856	Gm24727	3.52	0.044
ENSMUSG00000092805	Gm26461	3.41	0.000521
ENSMUSG00000064382	Gm26447	3.41	0.00412
ENSMUSG00000024175	Tekt4	3.38	0.0447
ENSMUSG00000065087	Snord22	3.2	0.000521
ENSMUSG00000097312	Gm26870	3.17	0.000521
ENSMUSG00000064344	mt-Tm	3.15	0.000521
ENSMUSG00000089542	Gm25835	3.15	0.00686
ENSMUSG00000064981	Snora70	3.09	0.00448
ENSMUSG00000002831	Plin4	3.08	0.000521
ENSMUSG00000080365	Gm25776	3.07	0.000521
ENSMUSG00000080465	Gm22486	3.04	0.000521
ENSMUSG00000064360	mt-Nd3	2.96	0.000521
ENSMUSG00000064941	Gm23238	2.96	0.000521
ENSMUSG00000077563	Snora68	2.93	0.000521
ENSMUSG00000065778	Gm22154	2.92	0.000521
ENSMUSG00000091957	Rps2-ps10	2.88	0.000521
ENSMUSG00000077505	Gm24233	2.85	0.0136
ENSMUSG00000064994	Gm22422	2.84	0.000521
ENSMUSG00000075015	Gm10801	2.79	0.000521
ENSMUSG00000064634	Gm22620	2.66	0.0172
ENSMUSG00000078886	Gm2026	2.65	0.000521
ENSMUSG00000062933	Gm10123	2.63	0.000521
ENSMUSG00000075014	Gm10800	2.61	0.000521
ENSMUSG00000093355	Snora26	2.5	0.000521
ENSMUSG00000088252	Snord13	2.42	0.0109
ENSMUSG00000027654	Fam83d	2.42	0.000521
ENSMUSG00000088990	Gm22767	2.4	0.000521
ENSMUSG00000056054	S100a8	2.4	0.00224
ENSMUSG00000035694	Caps2	2.37	0.000521
ENSMUSG00000065820	Gm26316	2.37	0.000521
ENSMUSG00000097052	Snhg7	2.33	0.0121
ENSMUSG00000078887	Gm6710	2.33	0.000521
ENSMUSG00000064655	Gm25788	2.3	0.000521
ENSMUSG00000064427	Gm22748	2.27	0.00878
ENSMUSG00000044285	Gm1821	2.27	0.000521
ENSMUSG00000106746	2900064F13Rik	2.27	0.000521

Ensembl_ID	Gene	Log2_FC	q_val
ENSMUSG00000064966	Snord15b	2.25	0.000521
ENSMUSG00000078898	Gm4723	2.2	0.000521
ENSMUSG00000064604	Snora44	2.17	0.00878
ENSMUSG00000105843	Gm42644	2.17	0.000521
ENSMUSG00000092819	Gm23639	2.16	0.000521
ENSMUSG00000099440	Gm29593	2.14	0.041
ENSMUSG00000065637	Gm26397	2.11	0.00339
ENSMUSG00000026822	Lcn2	2.03	0.00263
ENSMUSG00000035202	Lars2	2.03	0.000521
ENSMUSG00000064350	mt-Ty	1.99	0.0222
ENSMUSG00000044522	A730020M07Rik	1.99	0.0118
ENSMUSG00000077254	Gm26079	1.97	0.00376
ENSMUSG00000064853	Gm23442	1.95	0.000521
ENSMUSG00000086859	Snhg20	1.95	0.000521
ENSMUSG00000084421	Gm25107	1.95	0.000521
ENSMUSG00000078875	Gm14419	1.9	0.000521
ENSMUSG00000089235	Gm23119	1.86	0.0155
ENSMUSG00000070392	Gm20634	1.85	0.0167
ENSMUSG00000049892	Rasd1	1.84	0.000521
ENSMUSG00000096684	Gm25989	1.83	0.000521
ENSMUSG00000109332	RP23-189G24.4	1.83	0.000521
ENSMUSG00000098973	Mir6236	1.78	0.000521
ENSMUSG00000065226	Gm25791	1.74	0.000521
ENSMUSG00000100755	Rps23-ps1	1.72	0.0235
ENSMUSG00000080888	Gm14387	1.72	0.00224
ENSMUSG00000080538	Gm25541	1.7	0.000521
ENSMUSG00000059835	Rpl13-ps3	1.7	0.0464
ENSMUSG00000092746	Rn7s6	1.69	0.000521
ENSMUSG00000084744	Gm25291	1.69	0.000521
ENSMUSG00000084708	Gm22988	1.66	0.000521
ENSMUSG00000056071	S100a9	1.66	0.000985
ENSMUSG00000065686	Snora5c	1.65	0.0233
ENSMUSG00000071637	Cebpd	1.64	0.00376
ENSMUSG00000094655	Gm25360	1.63	0.000521
ENSMUSG00000088008	Gm25492	1.61	0.00142
ENSMUSG00000069305	Hist1h4n	1.61	0.00518
ENSMUSG00000064387	Snora73a	1.6	0.000521
ENSMUSG00000058385	Hist1h2bg	1.6	0.000521
ENSMUSG00000017778	Cox7c	1.59	0.000521
ENSMUSG00000065353	Snora73b	1.58	0.000521
ENSMUSG00000077192	Snora17	1.58	0.00586
ENSMUSG00000056313	1810011O10Rik	1.58	0.000521
ENSMUSG00000032845	Alpk2	1.58	0.000521
ENSMUSG00000074521	Gm14327	1.54	0.000521
ENSMUSG00000024778	Fas	1.54	0.000985
ENSMUSG00000069306	Hist1h4m	1.54	0.00878
ENSMUSG00000064945	Rny3	1.5	0.000521

Ensembl_ID	Gene	Log2_FC	q_val
ENSMUSG00000066315	Gm12918	1.5	0.000521
ENSMUSG00000106147	Rnu3a	1.5	0.000521
ENSMUSG00000088088	Rmrp	1.49	0.000521
ENSMUSG00000064348	mt-Tn	1.49	0.0396
ENSMUSG00000064513	Gm22457	1.48	0.000521
ENSMUSG00000042737	Dpm3	1.46	0.000521
ENSMUSG00000064347	mt-Ta	1.46	0.0403
ENSMUSG00000097551	Gm7976	1.45	0.000521
ENSMUSG00000078872	Gm14401	1.44	0.000521
ENSMUSG00000039405	Prss23	1.44	0.000521
ENSMUSG00000087057	Gm11730	1.44	0.0425
ENSMUSG00000047259	Mc4r	1.44	0.000521
ENSMUSG00000087963	Gm25394	1.43	0.000521
ENSMUSG00000074874	Ctla2b	1.43	0.00847
ENSMUSG00000065336	Snora34	1.43	0.0399
ENSMUSG00000024066	Xdh	1.43	0.000521
ENSMUSG00000107272	Gm42730	1.4	0.000521
ENSMUSG00000079641	Rpl39	1.4	0.000521
ENSMUSG00000098557	Kctd12	1.39	0.0328
ENSMUSG00000065251	Gm23971	1.39	0.000521
ENSMUSG00000090671	Gm5067	1.38	0.0103
ENSMUSG00000041957	Pkp2	1.38	0.000521
ENSMUSG00000023067	Cdkn1a	1.37	0.000521
ENSMUSG00000023232	Serinc2	1.34	0.000521
ENSMUSG00000090691	Gm3667	1.33	0.00142
ENSMUSG00000066170	E230001N04Rik	1.33	0.00142
ENSMUSG00000102426	Kantr	1.33	0.000521
ENSMUSG00000058443	Rpl10-ps3	1.32	0.000521
ENSMUSG00000065037	Rn7sk	1.31	0.000521
ENSMUSG00000034892	Rps29	1.3	0.000521
ENSMUSG00000084350	Znf41-ps	1.3	0.00263
ENSMUSG00000054944	5330416C01Rik	1.3	0.00586
ENSMUSG00000077611	Gm23946	1.3	0.0139
ENSMUSG00000086429	Gt(ROSA)26Sor	1.29	0.000521
ENSMUSG00000073877	Gm13306	1.27	0.000521
ENSMUSG00000106219	5830416I19Rik	1.27	0.00971
ENSMUSG00000097340	Gm26617	1.26	0.000521
ENSMUSG00000008822	Acyp1	1.26	0.000521
ENSMUSG00000045996	Polr2k	1.26	0.000521
ENSMUSG00000030711	Sult1a1	1.26	0.000521
ENSMUSG00000089756	Gm8898	1.25	0.000521
ENSMUSG00000101939	Gm28438	1.25	0.000521
ENSMUSG00000071796	6820431F20Rik	1.25	0.000521
ENSMUSG00000060962	Dmkn	1.24	0.00184
ENSMUSG00000090546	Cdr1	1.24	0.000521
ENSMUSG00000024222	Fkbp5	1.23	0.000521
ENSMUSG00000038059	Smim3	1.23	0.000521

Ensembl_ID	Gene	Log2_FC	q_val
ENSMUSG00000104033	Gm37773	1.22	0.00815
ENSMUSG00000106628	Gm43558	1.22	0.000521
ENSMUSG00000039634	Zfp189	1.21	0.000521
ENSMUSG00000094856	Gm21962	1.2	0.000521
ENSMUSG00000108473	RP23-32A8.10	1.2	0.000521
ENSMUSG00000031431	Tsc22d3	1.19	0.000521
ENSMUSG00000035606	Ky	1.18	0.00263
ENSMUSG00000028578	Caap1	1.18	0.000521
ENSMUSG00000072620	Slfn2	1.18	0.000521
ENSMUSG00000083111	Gm14421	1.18	0.000521
ENSMUSG00000070858	Gm1673	1.17	0.00302
ENSMUSG00000064380	Gm26448	1.17	0.0209
ENSMUSG00000038646	Fam103a1	1.17	0.000521
ENSMUSG00000073062	Zxdb	1.17	0.000521
ENSMUSG00000064899	Snord118	1.14	0.00815
ENSMUSG00000089617	Scarna10	1.14	0.000521
ENSMUSG00000048572	Tmem252	1.13	0.000521
ENSMUSG00000089281	Scarna6	1.11	0.00184
ENSMUSG00000008668	Rps18	1.1	0.000521
ENSMUSG00000078453	Abracl	1.1	0.000521
ENSMUSG00000067578	Cbln4	1.1	0.000521
ENSMUSG00000060923	Acyp2	1.09	0.000521
ENSMUSG00000065701	Rny1	1.08	0.000521
ENSMUSG00000073940	Hbb-bt	1.08	0.000521
ENSMUSG00000057863	Rpl36	1.08	0.000521
ENSMUSG00000031762	Mt2	1.08	0.000521
ENSMUSG00000010592	Dazl	1.08	0.000521
ENSMUSG00000067288	Rps28	1.05	0.000521
ENSMUSG00000097347	Gm17275	1.05	0.000521
ENSMUSG00000020424	Gatsl3	1.05	0.00653
ENSMUSG00000023004	Tuba1b	1.05	0.000521
ENSMUSG00000050856	Atp5k	1.05	0.000521
ENSMUSG00000049796	Crh	1.05	0.000521
ENSMUSG00000028648	Ndufs5	1.05	0.000521
ENSMUSG00000067212	H2-T23	1.04	0.000521
ENSMUSG00000105366	Gm43719	1.04	0.0285
ENSMUSG00000022602	Arc	1.04	0.000521
ENSMUSG00000024480	Ap3s1	1.03	0.000521
ENSMUSG00000104297	Gm38046	1.03	0.00971
ENSMUSG00000030432	Rpl28	1.02	0.00448
ENSMUSG00000079173	Zan	1.02	0.00483
ENSMUSG00000039221	Rpl22l1	1.02	0.000521
ENSMUSG00000020857	Nme2	1.02	0.00719
ENSMUSG00000078878	Gm14305	1.02	0.000521
ENSMUSG00000046727	Cystm1	1.02	0.000521
ENSMUSG00000043498	9330132A10Rik	1.01	0.000521
ENSMUSG00000074170	Plekhf1	1.01	0.000521

Ensembl_ID	Gene	Log2_FC	q_val
ENSMUSG00000087579	1500017E21Rik	1.01	0.00376
ENSMUSG00000090733	Rps27	1	0.000521
ENSMUSG00000045534	Kcna5	1	0.0136
ENSMUSG00000105186	Gm43778	1	0.0462
ENSMUSG00000094114	Gm21967	0.998	0.000521
ENSMUSG00000084911	Gm16185	0.997	0.00518
ENSMUSG00000079018	Ly6c1	0.997	0.000521
ENSMUSG00000087968	Gm25395	0.996	0.000521
ENSMUSG00000051319	1500011K16Rik	0.992	0.000521
ENSMUSG00000053475	Tnfaip6	0.99	0.000521
ENSMUSG00000038717	Atp5l	0.989	0.000521
ENSMUSG00000037185	Krt80	0.986	0.0299
ENSMUSG00000022528	Hes1	0.98	0.000521
ENSMUSG00000089951	Gm14435	0.98	0.000521
ENSMUSG00000026238	Ptma	0.971	0.000521
ENSMUSG00000090877	Hspa1b	0.971	0.000521
ENSMUSG00000024726	Carnmt1	0.964	0.000521
ENSMUSG00000039001	Rps21	0.964	0.000521
ENSMUSG00000103477	5930409G06Rik	0.964	0.000521
ENSMUSG00000078867	Gm14418	0.957	0.000521
ENSMUSG00000063316	Rpl27	0.957	0.000521
ENSMUSG00000051243	Islr2	0.954	0.000521
ENSMUSG00000073131	Vma21	0.953	0.000521
ENSMUSG00000014313	Cox6c	0.953	0.000521
ENSMUSG00000032360	Hcrtr2	0.95	0.000521
ENSMUSG00000037653	Kctd8	0.944	0.000521
ENSMUSG00000096768	Erdr1	0.943	0.000521
ENSMUSG00000109536	RP24-439I22.3	0.942	0.000521
ENSMUSG00000095590	Gm24305	0.937	0.000985
ENSMUSG00000034936	Arl4d	0.937	0.000521
ENSMUSG00000042712	Wbp5	0.933	0.000521
ENSMUSG00000099583	Hist1h3d	0.931	0.0258
ENSMUSG00000071083	Gm10311	0.92	0.00184
ENSMUSG00000108456	RP24-143K11.2	0.918	0.027
ENSMUSG00000074575	Kcng1	0.917	0.0337
ENSMUSG00000090291	Lrrc10b	0.912	0.0115
ENSMUSG00000103322	Gm37404	0.91	0.000521
ENSMUSG00000074971	Fibin	0.909	0.00302
ENSMUSG00000072704	Smim10l1	0.908	0.000521
ENSMUSG00000040113	Mettl11b	0.908	0.0141
ENSMUSG00000054091	1810037I17Rik	0.906	0.000521
ENSMUSG00000002289	Angptl4	0.904	0.00448
ENSMUSG00000030208	Emp1	0.903	0.018
ENSMUSG00000105285	Gm43238	0.903	0.000521
ENSMUSG00000005124	Wisp1	0.901	0.000521
ENSMUSG00000079494	Cml5	0.899	0.0383
ENSMUSG00000036781	Rps27l	0.899	0.000521

Ensembl_ID	Gene	Log2_FC	q_val
ENSMUSG00000066637	Ttc32	0.894	0.013
ENSMUSG00000001707	Eef1e1	0.894	0.000521
ENSMUSG00000078784	1810022K09Rik	0.893	0.000521
ENSMUSG00000063889	Crem	0.893	0.000521
ENSMUSG00000028211	Trp53inp1	0.893	0.000521
ENSMUSG00000067860	Zic3	0.892	0.0374
ENSMUSG00000048758	Rpl29	0.892	0.000521
ENSMUSG00000024766	Lipo1	0.889	0.0112
ENSMUSG00000078861	Zfp931	0.889	0.000521
ENSMUSG00000102854	C130023A14Rik	0.889	0.00339
ENSMUSG00000060636	Rpl35a	0.887	0.000521
ENSMUSG00000090223	Pcp4	0.886	0.000521
ENSMUSG00000020108	Ddit4	0.884	0.000521
ENSMUSG00000027306	Nusap1	0.882	0.00751
ENSMUSG00000072568	Fam84b	0.88	0.00142
ENSMUSG00000047215	Rpl9	0.879	0.000521
ENSMUSG00000074754	Gm561	0.879	0.000521
ENSMUSG00000100750	Gm29084	0.877	0.000521
ENSMUSG00000064356	mt-Atp8	0.875	0.000521
ENSMUSG00000037573	Tob1	0.875	0.000521
ENSMUSG00000002910	Arrdc2	0.872	0.000521
ENSMUSG00000026315	Serpinb8	0.87	0.000521
ENSMUSG00000035595	1600002K03Rik	0.867	0.0183
ENSMUSG00000078862	Gm14326	0.866	0.000521
ENSMUSG00000062691	Cebpzos	0.866	0.0144
ENSMUSG00000029084	Cd38	0.863	0.00339
ENSMUSG00000044155	Lsm8	0.863	0.000521
ENSMUSG00000021520	Uqcrb	0.859	0.000521
ENSMUSG00000063253	Scoc	0.858	0.000521
ENSMUSG00000033186	Mzt1	0.858	0.000521
ENSMUSG00000030188	Magohb	0.856	0.00184
ENSMUSG00000045954	Sdpr	0.851	0.000521
ENSMUSG00000001774	Chordc1	0.849	0.000521
ENSMUSG00000062328	Rpl17	0.847	0.000521
ENSMUSG00000079480	Pin4	0.846	0.000521
ENSMUSG00000055373	Fut9	0.845	0.000521
ENSMUSG00000075266	Cenpw	0.845	0.000521
ENSMUSG00000021676	Iqgap2	0.843	0.000521
ENSMUSG00000065911	Gm24447	0.841	0.000521
ENSMUSG00000106990	Gm42547	0.84	0.000521
ENSMUSG00000073374	C030034I22Rik	0.84	0.0133
ENSMUSG00000062006	Rpl34	0.837	0.000521
ENSMUSG00000010797	Wnt2	0.835	0.00302
ENSMUSG00000090963	Gm17655	0.835	0.0458
ENSMUSG00000048482	Bdnf	0.835	0.000521
ENSMUSG00000068184	Ndufaf2	0.831	0.000521
ENSMUSG00000096349	Gm22513	0.829	0.000521

Ensembl_ID	Gene	Log2_FC	q_val
ENSMUSG00000032373	Car12	0.826	0.00263
ENSMUSG00000048222	Mfap1b	0.825	0.000521
ENSMUSG00000090110	Cmc4	0.825	0.013
ENSMUSG00000094377	Gm24407	0.823	0.000521
ENSMUSG00000030413	Pglyrp1	0.823	0.00783
ENSMUSG00000048355	Arxes1	0.821	0.000521
ENSMUSG00000078427	Sarnp	0.82	0.000521
ENSMUSG00000065145	Vaultrc5	0.817	0.0188
ENSMUSG00000032807	Alox12b	0.814	0.000521
ENSMUSG00000049751	Rpl36al	0.81	0.000521
ENSMUSG00000020738	Sumo2	0.809	0.000521
ENSMUSG00000028179	Cth	0.808	0.00339
ENSMUSG00000032487	Ptgs2	0.807	0.000521
ENSMUSG00000041841	Rpl37	0.803	0.000521
ENSMUSG00000049511	Htr1b	0.803	0.000521
ENSMUSG00000021025	Nfkbia	0.801	0.000521
ENSMUSG00000029817	Tra2a	0.801	0.000521
ENSMUSG00000048616	Nog	0.799	0.000521
ENSMUSG00000033316	Galnt9	0.798	0.000521
ENSMUSG00000018239	Zcchc10	0.797	0.00376
ENSMUSG00000051671	Coa6	0.796	0.000521
ENSMUSG00000028676	Srsf10	0.794	0.000521
ENSMUSG00000060935	Tmem263	0.791	0.000521
ENSMUSG00000028480	Glipr2	0.79	0.0106
ENSMUSG00000007682	Dio2	0.787	0.000521
ENSMUSG00000031758	Cdyl2	0.786	0.000521
ENSMUSG00000015672	Mrpl32	0.786	0.000521
ENSMUSG00000102504	Gm21955	0.785	0.000521
ENSMUSG00000024521	Pmaip1	0.785	0.000985
ENSMUSG00000074715	Ccl28	0.784	0.000985
ENSMUSG00000051451	Crebzf	0.78	0.000521
ENSMUSG00000048251	Bcl11b	0.778	0.000521
ENSMUSG00000008682	Rpl10	0.775	0.000521
ENSMUSG00000097695	Gm26905	0.775	0.000521
ENSMUSG00000034701	Neurod1	0.773	0.00552
ENSMUSG00000051185	Fam174a	0.772	0.000521
ENSMUSG00000025290	Rps24	0.772	0.000521
ENSMUSG00000026072	Il1r1	0.771	0.0144
ENSMUSG00000020460	Rps27a	0.77	0.000521
ENSMUSG00000021732	Fgf10	0.769	0.0199
ENSMUSG00000030047	Arhgap25	0.767	0.00142
ENSMUSG00000105549	Gm43540	0.765	0.000521
ENSMUSG00000019997	Ctgf	0.765	0.000521
ENSMUSG00000027765	P2ry1	0.765	0.0328
ENSMUSG00000024883	Rin1	0.764	0.000521
ENSMUSG00000046516	Cox17	0.763	0.000521
ENSMUSG00000025362	Rps26	0.762	0.000521

Ensembl_ID	Gene	Log2_FC	q_val
ENSMUSG00000017009	Sdc4	0.76	0.000521
ENSMUSG00000029265	Dr1	0.76	0.000521
ENSMUSG00000012405	Rpl15	0.759	0.000521
ENSMUSG00000021098	4930447C04Rik	0.757	0.00142
ENSMUSG00000093909	Gm3883	0.756	0.00783
ENSMUSG00000028410	Dnaja1	0.756	0.000521
ENSMUSG00000020397	Med7	0.755	0.0139
ENSMUSG00000028655	Mfsd2a	0.753	0.000521
ENSMUSG00000020427	Igfbp3	0.753	0.000521
ENSMUSG00000022820	Ndufb4	0.753	0.000521
ENSMUSG00000031530	Dusp4	0.753	0.000521
ENSMUSG00000050029	Rap2c	0.752	0.000521
ENSMUSG00000074519	Etohi1	0.751	0.0115
ENSMUSG00000028495	Rps6	0.751	0.000521
ENSMUSG00000016179	Camk1g	0.75	0.000521
ENSMUSG00000105353	Gm42428	0.75	0.000521
ENSMUSG00000078864	Gm14322	0.75	0.0127
ENSMUSG00000024317	Rnf138	0.749	0.000521
ENSMUSG00000044224	Dnajc21	0.749	0.000521
ENSMUSG00000104960	Snhg8	0.748	0.000521
ENSMUSG00000043991	Pura	0.747	0.000521
ENSMUSG00000060402	Chst8	0.746	0.0118
ENSMUSG00000049744	Arhgap15	0.742	0.000521
ENSMUSG00000034765	Dusp5	0.742	0.000521
ENSMUSG00000088835	Gm23547	0.741	0.0351
ENSMUSG00000021903	Galnt15	0.74	0.00376
ENSMUSG00000046330	Rpl37a	0.739	0.000521
ENSMUSG00000052305	Hbb-bs	0.738	0.000521
ENSMUSG00000054766	Set	0.736	0.000521
ENSMUSG00000102753	Gm37056	0.735	0.0172
ENSMUSG00000042216	Sgsm1	0.73	0.000521
ENSMUSG00000032757	Bet1	0.73	0.000521
ENSMUSG00000089417	Gm22009	0.73	0.000521
ENSMUSG00000030218	Mgp	0.729	0.000521
ENSMUSG00000073295	Nudt11	0.728	0.000521
ENSMUSG00000049517	Rps23	0.728	0.000521
ENSMUSG00000031327	Chic1	0.727	0.000521
ENSMUSG00000021203	Otub2	0.727	0.000521
ENSMUSG00000063457	Rps15	0.726	0.000521
ENSMUSG00000057322	Rpl38	0.726	0.000521
ENSMUSG00000090125	Pou3f1	0.724	0.000521
ENSMUSG00000017404	Rpl19	0.722	0.000521
ENSMUSG00000073293	Nudt10	0.722	0.000521
ENSMUSG00000041592	Sdk2	0.72	0.0136
ENSMUSG00000066798	Zbtb6	0.719	0.000521
ENSMUSG00000026361	Cdc73	0.718	0.0209
ENSMUSG00000063364	3300002I08Rik	0.717	0.0207

Ensembl_ID	Gene	Log2_FC	q_val
ENSMUSG00000098274	Rpl24	0.717	0.000985
ENSMUSG00000062184	Hs6st2	0.715	0.000521
ENSMUSG00000024614	Tmx3	0.713	0.000521
ENSMUSG00000021765	Fst	0.713	0.00184
ENSMUSG00000022021	Diaph3	0.712	0.00518
ENSMUSG00000040693	Slco4c1	0.711	0.0112
ENSMUSG00000042682	Selk	0.71	0.000521
ENSMUSG00000025790	Slco3a1	0.71	0.000521
ENSMUSG00000006360	Crip1	0.709	0.0062
ENSMUSG00000061132	Blnk	0.708	0.000521
ENSMUSG00000048706	Lurap1l	0.707	0.000521
ENSMUSG00000031202	Rab39b	0.706	0.000521
ENSMUSG00000042505	Sdhaf3	0.703	0.000521
ENSMUSG00000047216	Cdh19	0.701	0.00483
ENSMUSG00000028221	Tmem55a	0.701	0.000521
ENSMUSG00000063632	Sox11	0.7	0.000521
ENSMUSG00000024608	Rps14	0.7	0.000521
ENSMUSG00000035686	Thrsp	0.698	0.000521
ENSMUSG00000056260	Lrif1	0.697	0.000521
ENSMUSG00000021556	Golm1	0.697	0.000521
ENSMUSG00000063787	Chchd1	0.695	0.000521
ENSMUSG00000090862	Rps13	0.695	0.000521
ENSMUSG00000079283	2310009B15Rik	0.695	0.0109
ENSMUSG00000039234	Sec24d	0.695	0.0412
ENSMUSG00000037984	Neurod6	0.695	0.000521
ENSMUSG00000071748	Gm14698	0.694	0.000521
ENSMUSG00000104806	Gm42566	0.694	0.00302
ENSMUSG00000044408	Sptssa	0.693	0.000521
ENSMUSG00000074527	Gm14296	0.693	0.000521
ENSMUSG00000001627	Ifrd1	0.693	0.000521
ENSMUSG00000047675	Rps8	0.693	0.000521
ENSMUSG00000016427	Ndufa1	0.691	0.000521
ENSMUSG00000078866	Gm14420	0.69	0.000521
ENSMUSG00000054717	Hmgb2	0.69	0.0201
ENSMUSG00000042842	Serpinb6b	0.688	0.0318
ENSMUSG00000048007	Timm8a1	0.688	0.0158
ENSMUSG00000036777	Anln	0.687	0.000521
ENSMUSG00000064345	mt-Nd2	0.687	0.000521
ENSMUSG00000035104	Eva1a	0.686	0.000521
ENSMUSG00000042595	Fam199x	0.686	0.000521
ENSMUSG00000033849	B3galt2	0.686	0.000521
ENSMUSG00000038007	Acer2	0.686	0.00552
ENSMUSG00000071862	Lrrtm2	0.683	0.000521
ENSMUSG00000087267	4933427J07Rik	0.683	0.000521
ENSMUSG00000063531	Sema3e	0.682	0.000521
ENSMUSG00000031609	Sap30	0.677	0.00686
ENSMUSG00000047714	Ppp1r2	0.677	0.000521

Ensembl_ID	Gene	Log2_FC	q_val
ENSMUSG00000062101	Zfp119b	0.675	0.00184
ENSMUSG00000079083	Jrkl	0.675	0.000521
ENSMUSG00000056116	H2-T22	0.674	0.00184
ENSMUSG00000046318	Ccbe1	0.673	0.00971
ENSMUSG00000046999	1110032F04Rik	0.672	0.000521
ENSMUSG00000095362	Gm14325	0.672	0.0314
ENSMUSG00000033685	Ucp2	0.671	0.0458
ENSMUSG00000061787	Rps17	0.671	0.000521
ENSMUSG00000060594	Layn	0.669	0.00448
ENSMUSG00000029551	Psmg3	0.668	0.0207
ENSMUSG00000029304	Spp1	0.668	0.000521
ENSMUSG00000019772	Vip	0.668	0.000521
ENSMUSG00000105942	Gm43175	0.667	0.000985
ENSMUSG00000068523	Gng5	0.667	0.000521
ENSMUSG00000075271	Ttc30a1	0.665	0.00376
ENSMUSG00000087260	Lamtor5	0.665	0.000521
ENSMUSG00000090553	Snrpe	0.664	0.000521
ENSMUSG00000078868	Gm14412	0.663	0.000521
ENSMUSG00000051579	Tceal8	0.663	0.000521
ENSMUSG00000042670	Immp1l	0.662	0.000521
ENSMUSG00000044017	Adgrd1	0.659	0.00483
ENSMUSG00000031246	Sh3bgrl	0.659	0.00686
ENSMUSG00000018199	Trove2	0.658	0.000521
ENSMUSG00000039208	Metrnl	0.658	0.0062
ENSMUSG00000085328	Gm17131	0.657	0.000985
ENSMUSG00000078974	Sec61g	0.657	0.000521
ENSMUSG00000029838	Ptn	0.657	0.000521
ENSMUSG00000044674	Fzd1	0.656	0.000521
ENSMUSG00000022193	Psmb5	0.655	0.000521
ENSMUSG00000066613	Zfp932	0.655	0.000521
ENSMUSG00000047344	Lancl3	0.653	0.000521
ENSMUSG00000085492	Trmt61b	0.653	0.00686
ENSMUSG00000091625	Lsm5	0.653	0.0139
ENSMUSG00000021091	Serpina3n	0.652	0.000521
ENSMUSG00000042540	Acot5	0.65	0.0194
ENSMUSG00000014813	Stc1	0.648	0.0115
ENSMUSG00000021730	Hcn1	0.645	0.000521
ENSMUSG00000023025	Larp4	0.644	0.000521
ENSMUSG00000046567	4930430F08Rik	0.644	0.0141
ENSMUSG00000066687	Zbtb16	0.641	0.000521
ENSMUSG00000060708	Bloc1s4	0.641	0.000985
ENSMUSG00000048040	Arxes2	0.64	0.000521
ENSMUSG00000025894	Aasdhppt	0.639	0.000521
ENSMUSG00000021290	2010107E04Rik	0.638	0.000521
ENSMUSG00000022012	Enox1	0.638	0.000521
ENSMUSG00000046215	Rprml	0.637	0.00518
ENSMUSG00000038412	Higd1a	0.636	0.000521

Ensembl_ID	Gene	Log2_FC	q_val
ENSMUSG00000026864	Hspa5	0.636	0.000521
ENSMUSG00000019146	Cacng2	0.636	0.000521
ENSMUSG00000027351	Spred1	0.636	0.000521
ENSMUSG00000035273	Hpse	0.634	0.025
ENSMUSG00000038323	1700066M21Rik	0.634	0.000521
ENSMUSG00000031245	Hmgn5	0.633	0.0186
ENSMUSG00000029279	Brdt	0.633	0.000985
ENSMUSG00000071014	Ndufb6	0.633	0.000521
ENSMUSG00000014177	Tvp23b	0.632	0.000521
ENSMUSG00000072761	Gm6712	0.631	0.0421
ENSMUSG00000096025	Gm38400	0.631	0.000521
ENSMUSG00000003031	Cdkn1b	0.63	0.000521
ENSMUSG00000042541	Shfm1	0.629	0.000521
ENSMUSG00000028165	Cisd2	0.628	0.000521
ENSMUSG00000036902	Neto2	0.628	0.000521
ENSMUSG00000050786	Ccdc126	0.627	0.000521
ENSMUSG00000106918	Mrpl33	0.627	0.0147
ENSMUSG00000019961	Tmpo	0.627	0.000521
ENSMUSG00000028645	Slc2a1	0.626	0.000521
ENSMUSG00000067336	Bmpr2	0.625	0.000521
ENSMUSG00000034653	Ythdc2	0.625	0.000521
ENSMUSG00000031765	Mt1	0.625	0.000521
ENSMUSG00000033342	Plppr5	0.622	0.000521
ENSMUSG00000066324	Impad1	0.622	0.000521
ENSMUSG00000047415	Gpr68	0.621	0.00971
ENSMUSG00000019851	Perp	0.62	0.00483
ENSMUSG00000024072	Yipf4	0.619	0.000521
ENSMUSG00000032328	Tmem30a	0.619	0.000521
ENSMUSG00000032551	1110059G10Rik	0.618	0.00263
ENSMUSG00000054162	Spock3	0.616	0.000521
ENSMUSG00000050783	Htr1f	0.616	0.00142
ENSMUSG00000098234	Snhg6	0.615	0.00518
ENSMUSG00000042396	Rbm7	0.615	0.000521
ENSMUSG00000060938	Rpl26	0.615	0.000521
ENSMUSG00000071172	Srsf3	0.615	0.000521
ENSMUSG00000026773	Pfkfb3	0.613	0.00142
ENSMUSG00000073879	Gm5859	0.613	0.000985
ENSMUSG00000020607	Fam84a	0.613	0.000521
ENSMUSG00000048379	Socs4	0.612	0.000521
ENSMUSG00000063406	Tmed5	0.612	0.00909
ENSMUSG00000051920	Rspo2	0.612	0.00224
ENSMUSG00000067925	Cxx1a	0.611	0.000521
ENSMUSG00000031885	Cbfb	0.611	0.00586
ENSMUSG00000024097	Srsf7	0.611	0.000521
ENSMUSG00000000838	Fmr1	0.611	0.000521
ENSMUSG00000028773	Fabp3	0.61	0.000985
ENSMUSG00000060803	Gstp1	0.609	0.000521

Ensembl_ID	Gene	Log2_FC	q_val
ENSMUSG00000074892	B3galt5	0.608	0.0103
ENSMUSG00000034738	Nostrin	0.608	0.0094
ENSMUSG00000035840	Lysmd3	0.608	0.000521
ENSMUSG00000032679	Cd59a	0.608	0.022
ENSMUSG00000054477	Kcnn2	0.607	0.000521
ENSMUSG00000053769	Lysmd1	0.606	0.00263
ENSMUSG00000025324	Atp10a	0.606	0.000521
ENSMUSG00000028936	Rpl22	0.606	0.000521
ENSMUSG00000042742	B630005N14Rik	0.606	0.000521
ENSMUSG00000019689	1110001J03Rik	0.605	0.00184
ENSMUSG00000020224	Llph	0.605	0.000521
ENSMUSG00000049420	Tmem200a	0.605	0.000521
ENSMUSG00000029131	Dnajb6	0.604	0.000521
ENSMUSG00000072949	Acot1	0.604	0.0204
ENSMUSG00000031875	Cmtm3	0.603	0.0109
ENSMUSG00000033307	Mif	0.602	0.000521
ENSMUSG00000093674	Rpl41	0.601	0.000521
ENSMUSG00000102917	Gm37724	0.601	0.00719
ENSMUSG00000036934	4921524J17Rik	0.601	0.000521
ENSMUSG00000026568	Mpc2	0.6	0.000521
ENSMUSG00000057766	Ankrd29	0.599	0.00142
ENSMUSG00000097392	D930016D06Rik	0.599	0.0351
ENSMUSG00000067928	Zfp760	0.598	0.000521
ENSMUSG00000051705	Senp8	0.598	0.000521
ENSMUSG00000020163	Uqcr11	0.598	0.000521
ENSMUSG00000020189	Osbpl8	0.597	0.000521
ENSMUSG00000079317	Trappc2	0.596	0.000521
ENSMUSG00000021930	Spryd7	0.596	0.000521
ENSMUSG00000021226	Acot2	0.595	0.00751
ENSMUSG00000020601	Trib2	0.595	0.000521
ENSMUSG00000018102	Hist1h2bc	0.595	0.000521
ENSMUSG00000021774	Ube2e1	0.595	0.0273
ENSMUSG00000007836	Hnrnpa0	0.594	0.000521
ENSMUSG00000020561	Twistnb	0.594	0.000521
ENSMUSG00000045034	Ankrd34b	0.594	0.000521
ENSMUSG00000028243	Ubxn2b	0.594	0.000521
ENSMUSG00000053070	9230110C19Rik	0.592	0.00339
ENSMUSG00000032381	Fam96a	0.591	0.000521
ENSMUSG00000030869	Ndufab1	0.59	0.000521
ENSMUSG00000050288	Fzd2	0.59	0.0109
ENSMUSG00000038607	Gng10	0.589	0.000521
ENSMUSG00000006333	Rps9	0.588	0.000521
ENSMUSG00000031333	Abcb7	0.588	0.000521
ENSMUSG00000075700	Selt	0.587	0.000521
ENSMUSG00000050711	Scg2	0.586	0.000521
ENSMUSG00000059291	Rpl11	0.586	0.000521
ENSMUSG00000029836	Cbx3	0.585	0.000521

Ensembl_ID	Gene	Log2_FC	q_val
ENSMUSG00000042804	Gpr153	-0.585	0.000985
ENSMUSG00000031853	BC021891	-0.587	0.0124
ENSMUSG00000032540	Abhd5	-0.588	0.0299
ENSMUSG00000026360	Rgs2	-0.59	0.00224
ENSMUSG00000059540	Tcea2	-0.59	0.00184
ENSMUSG00000020435	Osbp2	-0.59	0.0147
ENSMUSG00000049907	Rasl11b	-0.591	0.000521
ENSMUSG00000058454	Dhcr7	-0.594	0.00878
ENSMUSG00000023008	Fmnl3	-0.594	0.00719
ENSMUSG00000009376	Met	-0.595	0.000521
ENSMUSG00000084416	Rpl10a-ps1	-0.595	0.047
ENSMUSG00000068151	A230006K03Rik	-0.596	0.0263
ENSMUSG00000046352	Gjb2	-0.596	0.00184
ENSMUSG00000050721	Plekho2	-0.598	0.000521
ENSMUSG00000024186	Rgs11	-0.599	0.0316
ENSMUSG00000062960	Kdr	-0.6	0.000521
ENSMUSG00000033809	Alg3	-0.601	0.0144
ENSMUSG00000026925	Inpp5e	-0.603	0.047
ENSMUSG00000026344	Lypd1	-0.604	0.0169
ENSMUSG00000061119	Prcp	-0.606	0.000521
ENSMUSG00000071477	Zfp777	-0.606	0.0342
ENSMUSG00000036529	Sbf1	-0.607	0.0318
ENSMUSG00000028766	Alpl	-0.607	0.0238
ENSMUSG00000042115	Klhdc8a	-0.609	0.000985
ENSMUSG00000020836	Coro6	-0.609	0.00142
ENSMUSG00000052331	Ankrd44	-0.61	0.0112
ENSMUSG00000020802	Ube2o	-0.613	0.0304
ENSMUSG00000036196	Slc26a8	-0.615	0.0112
ENSMUSG00000060279	Ap2a1	-0.616	0.013
ENSMUSG00000024948	Map4k2	-0.616	0.0212
ENSMUSG00000055725	Paqr3	-0.622	0.0294
ENSMUSG00000029073	Cptp	-0.622	0.0304
ENSMUSG00000029428	Stx2	-0.623	0.0201
ENSMUSG00000002221	Paxip1	-0.623	0.0275
ENSMUSG00000029594	Rbm19	-0.623	0.0451
ENSMUSG00000055407	Map6	-0.625	0.000521
ENSMUSG00000020067	Mypn	-0.629	0.0346
ENSMUSG00000028969	Cdk5	-0.641	0.000521
ENSMUSG00000017724	Etv4	-0.641	0.0473
ENSMUSG00000030315	Vgll4	-0.642	0.000521
ENSMUSG00000029513	Prkab1	-0.642	0.00184
ENSMUSG00000100153	Gm5601	-0.644	0.0447
ENSMUSG00000030096	Slc6a6	-0.646	0.00815
ENSMUSG00000086905	Gm13716	-0.647	0.00483
ENSMUSG00000087396	4933407K13Rik	-0.648	0.036
ENSMUSG00000063446	Plppr1	-0.648	0.00653
ENSMUSG00000006728	Cdk4	-0.654	0.0372

Ensembl_ID	Gene	Log2_FC	q_val
ENSMUSG00000078624	Olfr613	-0.658	0.000521
ENSMUSG00000002845	Tmem39a	-0.659	0.0399
ENSMUSG00000017764	Zswim1	-0.661	0.000521
ENSMUSG00000051627	Hist1h1e	-0.665	0.000521
ENSMUSG00000033857	Engase	-0.666	0.0458
ENSMUSG00000029298	Gbp9	-0.666	0.0278
ENSMUSG00000037649	H2-DMa	-0.667	0.00518
ENSMUSG00000030269	Mtmr14	-0.668	0.0207
ENSMUSG00000020473	Aebp1	-0.669	0.000985
ENSMUSG00000079139	Gm4204	-0.67	0.00483
ENSMUSG00000032033	Barx2	-0.671	0.000521
ENSMUSG00000058076	Sdhc	-0.673	0.00142
ENSMUSG00000060166	Zdhhc8	-0.674	0.000521
ENSMUSG00000034432	Cops8	-0.674	0.000521
ENSMUSG00000008036	Ap2s1	-0.674	0.00339
ENSMUSG00000023030	Slc11a2	-0.674	0.015
ENSMUSG00000064037	Gpn1	-0.676	0.0136
ENSMUSG00000039176	Polg	-0.679	0.0109
ENSMUSG00000027890	Gstm4	-0.68	0.0191
ENSMUSG00000053414	Hunk	-0.681	0.000521
ENSMUSG00000039057	Myo16	-0.684	0.000521
ENSMUSG00000040165	Cd209c	-0.685	0.0212
ENSMUSG00000033453	Adamts15	-0.686	0.000985
ENSMUSG00000063972	Nr6a1	-0.687	0.0248
ENSMUSG00000040495	Chrm4	-0.688	0.000985
ENSMUSG00000020805	Slc13a5	-0.69	0.00142
ENSMUSG00000031392	Irak1	-0.691	0.00184
ENSMUSG00000022216	Psme1	-0.694	0.00971
ENSMUSG00000046463	5930403N24Rik	-0.694	0.05
ENSMUSG00000031170	Slc38a5	-0.695	0.0243
ENSMUSG00000049470	Aff4	-0.7	0.0282
ENSMUSG00000001930	Vwf	-0.706	0.00586
ENSMUSG00000006498	Ptbp1	-0.711	0.0263
ENSMUSG00000026965	Anapc2	-0.712	0.000521
ENSMUSG00000002007	Srpk3	-0.715	0.0344
ENSMUSG00000025384	Faap100	-0.716	0.0133
ENSMUSG00000107306	Gm42577	-0.716	0.000521
ENSMUSG00000021009	Ptpn21	-0.718	0.000521
ENSMUSG00000043587	Pxylp1	-0.718	0.00224
ENSMUSG00000106948	Gm42785	-0.721	0.000521
ENSMUSG00000005148	Klf5	-0.722	0.0238
ENSMUSG00000100801	Gm15459	-0.724	0.000521
ENSMUSG00000019370	Calm3	-0.731	0.00448
ENSMUSG00000048826	Dact2	-0.733	0.000521
ENSMUSG00000026814	Eng	-0.736	0.00518
ENSMUSG00000010122	Slc47a1	-0.737	0.00719
ENSMUSG00000029090	Adgra3	-0.739	0.0141

Ensembl_ID	Gene	Log2_FC	q_val
ENSMUSG00000020792	Exoc7	-0.74	0.000521
ENSMUSG00000037791	Phf12	-0.74	0.0196
ENSMUSG00000020101	Vsir	-0.741	0.000521
ENSMUSG00000041468	Gpr12	-0.744	0.000521
ENSMUSG00000085811	Cep112it	-0.745	0.000985
ENSMUSG00000042857	Gm9776	-0.751	0.0153
ENSMUSG00000089901	Gm8113	-0.753	0.00142
ENSMUSG00000100725	Gm28062	-0.754	0.0412
ENSMUSG00000027318	Adam33	-0.757	0.00971
ENSMUSG00000014791	Elmo3	-0.757	0.05
ENSMUSG00000103560	Gm38070	-0.758	0.05
ENSMUSG00000020374	Rasgef1c	-0.761	0.000521
ENSMUSG00000020363	Gfpt2	-0.764	0.000521
ENSMUSG00000107495	Gm44215	-0.769	0.000521
ENSMUSG00000020330	Hmmr	-0.771	0.0292
ENSMUSG00000074863	Platr25	-0.773	0.0164
ENSMUSG00000047155	Cyp4x1	-0.776	0.000521
ENSMUSG00000027288	Zfp106	-0.776	0.0175
ENSMUSG00000067276	Capn6	-0.776	0.0285
ENSMUSG00000040524	Zfp609	-0.777	0.0139
ENSMUSG00000092395	Gm20463	-0.777	0.0438
ENSMUSG00000044364	Tmem74b	-0.783	0.00815
ENSMUSG00000060860	Ube2s	-0.788	0.0144
ENSMUSG00000026566	Mpzl1	-0.789	0.00552
ENSMUSG00000040857	Erf	-0.789	0.0094
ENSMUSG00000035835	Plppr3	-0.792	0.00586
ENSMUSG00000042807	Hecw2	-0.792	0.00376
ENSMUSG00000035890	Rnf126	-0.795	0.000521
ENSMUSG00000001870	Ltbp1	-0.795	0.024
ENSMUSG00000091549	Gm6548	-0.798	0.0227
ENSMUSG00000063730	Hsd3b2	-0.808	0.0299
ENSMUSG00000029599	Ddx54	-0.811	0.00142
ENSMUSG00000040938	Slc16a11	-0.812	0.015
ENSMUSG00000032400	Zwilch	-0.812	0.0421
ENSMUSG00000002885	Adgre5	-0.812	0.00483
ENSMUSG00000026383	Epb41l5	-0.814	0.0158
ENSMUSG00000032590	Apeh	-0.82	0.00224
ENSMUSG00000066760	Psg16	-0.831	0.000521
ENSMUSG00000028294	Cfap206	-0.842	0.0292
ENSMUSG00000019876	Pkib	-0.845	0.00586
ENSMUSG00000043993	2900052L18Rik	-0.845	0.0204
ENSMUSG00000102813	Gm37795	-0.85	0.0191
ENSMUSG00000028661	Epha8	-0.856	0.00686
ENSMUSG00000097163	BC051077	-0.859	0.029
ENSMUSG00000032431	Crtap	-0.864	0.0209
ENSMUSG00000074210	E130208F15Rik	-0.866	0.0164
ENSMUSG00000041731	Pgm5	-0.869	0.00142

Ensembl_ID	Gene	Log2_FC	q_val
ENSMUSG00000035486	Plk5	-0.872	0.000521
ENSMUSG00000086130	Gm16211	-0.872	0.000521
ENSMUSG00000051354	Samd3	-0.872	0.00224
ENSMUSG00000093910	Zfp853	-0.873	0.0183
ENSMUSG00000053783	1700016K19Rik	-0.874	0.0385
ENSMUSG00000032122	Slc37a2	-0.878	0.00184
ENSMUSG00000025795	Rassf3	-0.878	0.000521
ENSMUSG00000034685	Fam171a2	-0.88	0.0381
ENSMUSG00000104682	Gm42636	-0.883	0.028
ENSMUSG00000020052	Ascl1	-0.888	0.0243
ENSMUSG00000066797	Zfp648	-0.893	0.0356
ENSMUSG00000050211	Pla2g4e	-0.896	0.000521
ENSMUSG00000043843	Tmem145	-0.896	0.000521
ENSMUSG00000029505	Ep400	-0.901	0.0248
ENSMUSG00000004415	Col26a1	-0.903	0.0273
ENSMUSG00000102700	Gm38312	-0.903	0.000521
ENSMUSG00000037321	Tap1	-0.905	0.0335
ENSMUSG00000044254	Pcsk9	-0.907	0.00653
ENSMUSG00000026970	Rbms1	-0.911	0.00263
ENSMUSG00000081752	Gm14680	-0.917	0.0199
ENSMUSG00000027004	Frzb	-0.921	0.000521
ENSMUSG00000035142	Nubpl	-0.921	0.0225
ENSMUSG00000015947	Fcgr1	-0.922	0.015
ENSMUSG00000107383	Gm4366	-0.925	0.00224
ENSMUSG00000030123	Plxnd1	-0.933	0.00847
ENSMUSG00000054135	A430110L20Rik	-0.939	0.0235
ENSMUSG00000078139	AK157302	-0.94	0.0255
ENSMUSG00000101188	Eif4a-ps4	-0.943	0.000521
ENSMUSG00000050505	Pcdh20	-0.946	0.000521
ENSMUSG00000038058	Nod1	-0.952	0.024
ENSMUSG00000038742	Angptl6	-0.958	0.0217
ENSMUSG00000027188	Pamr1	-0.959	0.000521
ENSMUSG00000101906	Mrgprc2-ps	-0.961	0.000521
ENSMUSG00000000317	Bcl6b	-0.962	0.015
ENSMUSG00000041674	BC006965	-0.97	0.0191
ENSMUSG00000090353	Gm17555	-0.977	0.000521
ENSMUSG00000040605	Bace2	-0.987	0.000521
ENSMUSG00000030735	Gm9755	-1.01	0.0191
ENSMUSG00000106053	Gm20752	-1.01	0.0207
ENSMUSG00000107881	Gm44250	-1.01	0.00142
ENSMUSG00000034121	Mks1	-1.01	0.00412
ENSMUSG00000029370	Rassf6	-1.01	0.0421
ENSMUSG00000032010	Usp2	-1.01	0.000521
ENSMUSG00000045238	A730035I17Rik	-1.01	0.0183
ENSMUSG00000105134	Gm42923	-1.02	0.0339
ENSMUSG00000006931	P3h4	-1.02	0.033
ENSMUSG00000069682	Gm10275	-1.02	0.000521

Ensembl_ID	Gene	Log2_FC	q_val
ENSMUSG00000102705	4632432E15Rik	-1.03	0.015
ENSMUSG00000032565	Nudt16	-1.03	0.000521
ENSMUSG00000035775	Krt20	-1.03	0.0153
ENSMUSG00000028458	Tesk1	-1.03	0.00878
ENSMUSG00000097657	Gm7389	-1.05	0.00783
ENSMUSG00000001750	Tcirg1	-1.05	0.000521
ENSMUSG00000081683	Fzd10	-1.06	0.00302
ENSMUSG00000043671	Dpy19l3	-1.07	0.00518
ENSMUSG00000023192	Grm2	-1.07	0.000521
ENSMUSG00000074507	Gm14340	-1.08	0.0109
ENSMUSG00000075514	Gm13375	-1.09	0.0248
ENSMUSG00000062611	Rps3a2	-1.09	0.00815
ENSMUSG00000103182	Gm37091	-1.09	0.0158
ENSMUSG00000031558	Slit2	-1.09	0.000521
ENSMUSG00000020131	Pcsk4	-1.09	0.0217
ENSMUSG00000026956	Uap1l1	-1.1	0.00783
ENSMUSG00000045251	Zfp688	-1.1	0.00483
ENSMUSG00000005493	Msh4	-1.1	0.00142
ENSMUSG00000031489	Adrb3	-1.1	0.00302
ENSMUSG00000069892	9930111J21Rik2	-1.11	0.000521
ENSMUSG00000048949	Gm6206	-1.11	0.000521
ENSMUSG00000105476	Gm43740	-1.12	0.000521
ENSMUSG00000019214	Chtf18	-1.13	0.000521
ENSMUSG00000032572	Col6a4	-1.13	0.0275
ENSMUSG00000049001	Ndnf	-1.14	0.0447
ENSMUSG00000104103	Gm9517	-1.14	0.00483
ENSMUSG00000027613	Eif6	-1.15	0.000521
ENSMUSG00000107215	Gm43197	-1.15	0.000985
ENSMUSG00000108779	RP24-269A16.7	-1.16	0.0115
ENSMUSG00000102685	Gm37373	-1.16	0.00847
ENSMUSG00000066842	Hmcn1	-1.17	0.00719
ENSMUSG00000109196	RP24-291N22.1	-1.18	0.000521
ENSMUSG00000040296	Ddx58	-1.2	0.000521
ENSMUSG00000104159	Gm38099	-1.2	0.00518
ENSMUSG00000016756	Cmah	-1.2	0.000521
ENSMUSG00000086179	Gm14317	-1.21	0.0479
ENSMUSG00000043801	Oaz1-ps	-1.22	0.00224
ENSMUSG00000073164	2410018L13Rik	-1.22	0.000521
ENSMUSG00000085881	Gm15912	-1.22	0.0204
ENSMUSG00000102591	Gm38383	-1.23	0.000521
ENSMUSG00000100837	1700063D05Rik	-1.24	0.0449
ENSMUSG00000097148	Gm3839	-1.24	0.000521
ENSMUSG00000097797	Gm26901	-1.26	0.0419
ENSMUSG00000075511	1700001L05Rik	-1.26	0.00412
ENSMUSG00000104060	Gm37954	-1.27	0.00483
ENSMUSG00000097275	Gm26648	-1.27	0.0235
ENSMUSG00000085828	Gm15612	-1.27	0.018

Ensembl_ID	Gene	Log2_FC	q_val
ENSMUSG00000082519	Vamp7-ps	-1.28	0.000521
ENSMUSG00000101523	Gm10031	-1.28	0.000521
ENSMUSG00000097327	E030030I06Rik	-1.28	0.00552
ENSMUSG00000019945	1700040L02Rik	-1.29	0.0062
ENSMUSG00000050621	Rps27rt	-1.29	0.0396
ENSMUSG00000002324	Rec8	-1.29	0.0155
ENSMUSG00000098404	Mrip-ps	-1.3	0.000521
ENSMUSG00000049233	Apoo-ps	-1.32	0.00552
ENSMUSG00000091478	Gm10039	-1.33	0.0118
ENSMUSG00000080242	Gm15487	-1.33	0.00184
ENSMUSG00000105065	Gm42513	-1.33	0.000521
ENSMUSG00000091102	5830462I19Rik	-1.33	0.0115
ENSMUSG00000004842	Pou1f1	-1.35	0.00224
ENSMUSG00000002083	Bbc3	-1.35	0.0238
ENSMUSG00000106001	Gm42826	-1.36	0.000521
ENSMUSG00000086922	Gm13835	-1.37	0.0304
ENSMUSG00000106860	1700008H02Rik	-1.38	0.000521
ENSMUSG00000103625	Gm37357	-1.39	0.000521
ENSMUSG00000078808	Vmn1r58	-1.41	0.000521
ENSMUSG00000052142	Rasal3	-1.41	0.0263
ENSMUSG00000074219	Gm10644	-1.41	0.0238
ENSMUSG00000087028	Gm13387	-1.43	0.0144
ENSMUSG00000047773	Ankfn1	-1.43	0.000521
ENSMUSG00000060019	Gm10073	-1.44	0.00448
ENSMUSG00000071041	Gm15210	-1.45	0.00412
ENSMUSG00000097445	Gm26631	-1.46	0.0287
ENSMUSG00000035506	Slc12a8	-1.47	0.00263
ENSMUSG00000108446	RP23-367H8.4	-1.48	0.01
ENSMUSG00000070343	Gm10288	-1.49	0.00184
ENSMUSG00000085783	Gm9816	-1.51	0.000521
ENSMUSG00000080935	Got2-ps1	-1.52	0.000521
ENSMUSG00000103630	Gm37242	-1.54	0.000521
ENSMUSG00000097502	4930528D03Rik	-1.57	0.0227
ENSMUSG00000096528	G430049J08Rik	-1.57	0.00376
ENSMUSG00000081400	Gm13680	-1.57	0.00686
ENSMUSG00000085830	Grin1os	-1.58	0.00224
ENSMUSG00000099608	4933411E06Rik	-1.58	0.000521
ENSMUSG00000028461	Ccdc107	-1.58	0.000521
ENSMUSG00000015850	Adamtsl4	-1.58	0.0175
ENSMUSG00000097979	Gm4691	-1.6	0.0311
ENSMUSG00000023393	Slc17a9	-1.6	0.0332
ENSMUSG00000026331	Slco6c1	-1.64	0.00263
ENSMUSG00000103475	Gm37697	-1.66	0.000521
ENSMUSG00000093385	A330044P14Rik	-1.66	0.000521
ENSMUSG00000102858	Gm37086	-1.68	0.000521
ENSMUSG00000105255	Gm42413	-1.69	0.047
ENSMUSG00000098183	Gm27010	-1.72	0.0121

Ensembl_ID	Gene	Log2_FC	q_val
ENSMUSG00000062456	Rpl9-ps6	-1.73	0.000521
ENSMUSG00000099764	Rps10-ps2	-1.74	0.00847
ENSMUSG00000030048	Gkn3	-1.76	0.000521
ENSMUSG00000042501	Cpa6	-1.77	0.000521
ENSMUSG00000053740	Gm6457	-1.78	0.0278
ENSMUSG00000050490	Gm8394	-1.79	0.0358
ENSMUSG00000051650	B3gnt2	-1.79	0.0243
ENSMUSG00000070610	Gm13127	-1.8	0.00586
ENSMUSG00000062168	Ppef1	-1.81	0.0153
ENSMUSG00000072692	Rpl37rt	-1.81	0.000521
ENSMUSG00000099615	Gm28362	-1.86	0.000521
ENSMUSG00000097961	Gm27000	-1.86	0.00263
ENSMUSG00000060419	Rps16-ps2	-1.87	0.0494
ENSMUSG00000046341	Gm11223	-1.89	0.000521
ENSMUSG00000023140	Reg2	-1.93	0.00448
ENSMUSG00000058625	Gm17383	-1.93	0.00376
ENSMUSG00000092702	Gm24514	-1.93	0.000521
ENSMUSG00000078636	Gm7336	-1.94	0.000521
ENSMUSG00000085950	Gm13589	-1.95	0.00448
ENSMUSG00000075053	Vdac3-ps1	-1.96	0.000521
ENSMUSG00000101316	Gm12663	-1.96	0.0186
ENSMUSG00000063522	2010109I03Rik	-1.97	0.000521
ENSMUSG00000103539	Gm37834	-1.97	0.0133
ENSMUSG00000058126	Tpm3-rs7	-1.98	0.000521
ENSMUSG00000105440	Gm43673	-1.98	0.00878
ENSMUSG00000109335	RP23-287I20.1	-2	0.000521
ENSMUSG00000071035	Gm5499	-2.01	0.000521
ENSMUSG00000103053	Gm38271	-2.02	0.00448
ENSMUSG00000082809	Gm14150	-2.03	0.000521
ENSMUSG00000068706	Gm10250	-2.08	0.000521
ENSMUSG00000104837	Gm42520	-2.09	0.0299
ENSMUSG00000093798	Gm8355	-2.1	0.000521
ENSMUSG00000078134	Gm12355	-2.12	0.00586
ENSMUSG00000082896	Gm5844	-2.12	0.000521
ENSMUSG00000079311	Gm3222	-2.13	0.015
ENSMUSG00000104051	Gm38128	-2.14	0.000521
ENSMUSG00000105370	Gm42718	-2.15	0.000521
ENSMUSG00000050122	Vwa3b	-2.16	0.00751
ENSMUSG00000089647	Gm2245	-2.2	0.00142
ENSMUSG00000083621	Gm14586	-2.21	0.00184
ENSMUSG00000079407	1700110I01Rik	-2.23	0.000985
ENSMUSG00000084817	Gm5526	-2.24	0.00376
ENSMUSG00000081305	Gm12879	-2.26	0.033
ENSMUSG00000108314	RP23-73F23.5	-2.27	0.000521
ENSMUSG00000104496	Gm5837	-2.3	0.0311
ENSMUSG00000097609	Gm26659	-2.31	0.000521
ENSMUSG00000106988	Tsg101-ps	-2.32	0.0209

Ensembl_ID	Gene	Log2_FC	q_val
ENSMUSG00000058809	Hspd1-ps3	-2.32	0.000521
ENSMUSG00000107176	Gm9794	-2.33	0.000521
ENSMUSG00000095690	Rab11b-ps2	-2.34	0.00142
ENSMUSG00000049124	Gm8186	-2.36	0.0466
ENSMUSG00000100580	4933436I20Rik	-2.36	0.00339
ENSMUSG00000105471	A430073D23Rik	-2.37	0.000521
ENSMUSG00000063902	Gm7964	-2.39	0.000521
ENSMUSG00000108500	RP23-335G1.5	-2.42	0.0248
ENSMUSG00000037096	Gm9762	-2.43	0.00142
ENSMUSG00000064193	Gm4735	-2.44	0.000521
ENSMUSG00000104046	Gm37567	-2.44	0.000521
ENSMUSG00000102972	Gm37348	-2.52	0.00847
ENSMUSG00000074292	Gm10660	-2.59	0.000521
ENSMUSG00000079941	Gm11273	-2.59	0.0445
ENSMUSG00000066362	Rps13-ps1	-2.6	0.00751
ENSMUSG00000102289	Gm31258	-2.61	0.0253
ENSMUSG00000102470	Gm37244	-2.63	0.000985
ENSMUSG00000105931	Gm43014	-2.63	0.000521
ENSMUSG00000100033	Gm8337	-2.64	0.0124
ENSMUSG00000083097	Gm14494	-2.67	0.0477
ENSMUSG00000082274	Gm14026	-2.7	0.00909
ENSMUSG00000050097	Ces2b	-2.7	0.000521
ENSMUSG00000082536	Gm13456	-2.73	0.000521
ENSMUSG00000043889	Gm8399	-2.75	0.00412
ENSMUSG00000083325	Gm14121	-2.78	0.000521
ENSMUSG00000103922	Gm6123	-2.78	0.00302
ENSMUSG00000093064	Gm23153	-2.8	0.000521
ENSMUSG00000083563	Gm13340	-2.83	0.000521
ENSMUSG00000098222	Gm8318	-2.85	0.0209
ENSMUSG00000082894	Gm6480	-2.9	0.000521
ENSMUSG00000059040	Eno1b	-2.93	0.00184
ENSMUSG00000083391	Gm14148	-2.99	0.000521
ENSMUSG00000070729	Gm12966	-3	0.00142
ENSMUSG00000052825	Gm9892	-3.02	0.01
ENSMUSG00000108249	Gm43960	-3.02	0.000521
ENSMUSG00000104913	Gm6560	-3.03	0.0121
ENSMUSG00000046440	Gm5564	-3.11	0.000521
ENSMUSG00000067869	Tcea1-ps1	-3.13	0.0161
ENSMUSG00000098113	Gm2445	-3.22	0.0248
ENSMUSG00000083863	Gm13341	-3.27	0.00184
ENSMUSG00000041872	Il17f	-3.28	0.0124
ENSMUSG00000053038	Gm6180	-3.36	0.0332
ENSMUSG00000064694	Gm24146	-3.38	0.000521
ENSMUSG00000082454	Gm12183	-3.42	0.000521
ENSMUSG00000046952	Gm5815	-3.44	0.0106
ENSMUSG00000102718	Gm37761	-3.45	0.000521
ENSMUSG00000071343	Gm10327	-3.5	0.00518

Ensembl_ID	Gene	Log2_FC	q_val
ENSMUSG00000080776	Gm12174	-3.51	0.00224
ENSMUSG00000107951	Gm6210	-3.52	0.000521
ENSMUSG00000083679	Gm12892	-3.61	0.000521
ENSMUSG00000091045	Vmn2r55	-3.62	0.00376
ENSMUSG00000078599	Skint8	-3.65	0.000521
ENSMUSG00000044751	Gm12231	-3.66	0.000521
ENSMUSG00000108857	RP24-297G19.6	-3.75	0.000521
ENSMUSG00000108884	RP23-306P12.3	-3.77	0.000521
ENSMUSG00000070443	Gm10291	-3.78	0.0273
ENSMUSG00000104802	Gm5869	-3.79	0.00263
ENSMUSG00000104095	Gm37315	-3.93	0.00909
ENSMUSG00000092674	Gm24105	-4.05	0.000521
ENSMUSG00000098111	Gm4654	-4.09	0.000521
ENSMUSG00000032899	Styk1	-4.13	0.00339
ENSMUSG00000082319	Gm8822	-4.24	0.00184
ENSMUSG00000082035	Rpl17-ps8	-4.28	0.000521
ENSMUSG00000085180	AI838599	-4.62	0.000521
ENSMUSG00000100863	Gm12669	-4.69	0.0447
ENSMUSG00000065254	Gm23973	-4.78	0.000521
ENSMUSG00000064999	Gm26035	-4.84	0.000521
ENSMUSG00000108255	Gm16499	-10.7	0.000521

App.2. Genes Modulated by 12 Hour Sleep Deprivation

Genes immediately modulated by 12-hour sleep deprivation by at least 1.5 fold compared to mice sleep deprived for 3 hours with 9 hour recovery opportunity. Data presented is the Gene ID and name, the Log2 fold change, and the Benjamini adjusted q-value for significance. Data derived from cuffdiff command.

Ensembl_ID	Gene	Log2_FC	q_val
ENSMUSG00000092137	Gcom1	12.5	0.015
ENSMUSG00000006574	Slc4a1	4.7	0.000521
ENSMUSG00000026822	Lcn2	3.64	0.000521
ENSMUSG00000099907	Gm10421	2.97	0.0453
ENSMUSG00000102059	Gm20257	2.91	0.000521
ENSMUSG00000037095	Lrg1	2.29	0.000521
ENSMUSG00000043556	Fbxl7	1.98	0.0282
ENSMUSG00000051367	Six1	1.97	0.0136
ENSMUSG00000056054	S100a8	1.93	0.0204
ENSMUSG00000033386	Frrs1	1.9	0.0144
ENSMUSG00000098306	Gm28040	1.85	0.0169
ENSMUSG00000054582	Pabpc1l	1.83	0.0278
ENSMUSG00000091956	C2cd4b	1.81	0.0356
ENSMUSG00000023083	H2-M10.2	1.75	0.044
ENSMUSG00000019773	Fbxo5	1.73	0.029
ENSMUSG00000002289	Angptl4	1.7	0.000521
ENSMUSG00000039476	Prrx2	1.68	0.00552
ENSMUSG00000057378	Ryr3	1.68	0.000521
ENSMUSG00000108569	RP23-44H21.1	1.67	0.0103
ENSMUSG00000002831	Plin4	1.64	0.000521
ENSMUSG00000086539	Gm16759	1.61	0.0183
ENSMUSG00000041193	Pla2g5	1.6	0.000521
ENSMUSG00000069265	Hist1h3a	1.58	0.015
ENSMUSG00000093672	Gm20655	1.56	0.0414
ENSMUSG00000068855	Hist2h2ac	1.53	0.00302
ENSMUSG00000035692	Isg15	1.53	0.00878
ENSMUSG00000104195	B230377A18Rik	1.49	0.0479
ENSMUSG00000030431	Tmem238	1.47	0.0412
ENSMUSG00000095098	Ccdc85b	1.46	0.000521
ENSMUSG00000071637	Cebpd	1.45	0.000521
ENSMUSG00000109447	RP24-75N6.1	1.45	0.0487
ENSMUSG00000027555	Car13	1.43	0.000521
ENSMUSG00000033227	Wnt6	1.4	0.0268
ENSMUSG00000006219	Fblim1	1.39	0.0094
ENSMUSG00000107747	Gm5881	1.38	0.0191
ENSMUSG00000085022	Gm5860	1.34	0.0285
ENSMUSG00000005268	Prlr	1.33	0.0282

Ensembl_ID	Gene	Log2_FC	q_val
ENSMUSG00000047907	Tshz2	1.33	0.000521
ENSMUSG00000027868	Tbx15	1.32	0.0496
ENSMUSG00000024175	Tekt4	1.32	0.0427
ENSMUSG00000016024	Lbp	1.3	0.00653
ENSMUSG00000100929	Gm28064	1.29	0.0153
ENSMUSG00000103662	Gm34294	1.29	0.000985
ENSMUSG00000027875	Hmgcs2	1.27	0.000521
ENSMUSG00000049796	Crh	1.26	0.000521
ENSMUSG00000066637	Ttc32	1.24	0.00483
ENSMUSG00000093803	Ppp2r3d	1.24	0.00653
ENSMUSG00000017897	Eya2	1.23	0.0167
ENSMUSG00000033177	Tmprss7	1.23	0.0201
ENSMUSG00000096768	Erdr1	1.21	0.000521
ENSMUSG00000037166	Ppp1r14a	1.21	0.000521
ENSMUSG00000090356	Teddm3	1.2	0.00815
ENSMUSG00000039278	Pcsk1n	1.19	0.000521
ENSMUSG00000083261	Gm7816	1.18	0.0405
ENSMUSG00000061535	C1qtnf7	1.18	0.0304
ENSMUSG00000044103	Il1f9	1.18	0.041
ENSMUSG00000041012	Cmtm8	1.16	0.025
ENSMUSG00000102578	Gm10576	1.13	0.0346
ENSMUSG00000023067	Cdkn1a	1.11	0.000521
ENSMUSG00000097312	Gm26870	1.1	0.00686
ENSMUSG00000034686	Prr7	1.09	0.000521
ENSMUSG00000096972	Gm26883	1.09	0.000521
ENSMUSG00000102579	Gm37965	1.07	0.0094
ENSMUSG00000030111	A2m	1.07	0.0155
ENSMUSG00000063021	Hist1h2ak	1.07	0.0144
ENSMUSG00000107173	Gm43266	1.07	0.024
ENSMUSG00000030711	Sult1a1	1.05	0.000521
ENSMUSG00000049892	Rasd1	1.04	0.000521
ENSMUSG00000023140	Reg2	1.03	0.000521
ENSMUSG00000022146	Osmr	1.02	0.000521
ENSMUSG00000067578	Cbln4	1.01	0.000521
ENSMUSG00000043659	Npsr1	0.992	0.0436
ENSMUSG00000032487	Ptgs2	0.99	0.000521
ENSMUSG00000038775	Vill	0.98	0.0419
ENSMUSG00000036907	C1ql2	0.976	0.0304
ENSMUSG00000008845	Cd163	0.976	0.000521
ENSMUSG00000029343	Crybb1	0.966	0.0136
ENSMUSG00000033730	Egr3	0.959	0.000521
ENSMUSG00000042842	Serpinb6b	0.959	0.00847
ENSMUSG00000044145	1810024B03Rik	0.955	0.0419
ENSMUSG00000071341	Egr4	0.949	0.000521
ENSMUSG00000056313	1810011O10Rik	0.945	0.0118
ENSMUSG00000001948	Spa17	0.944	0.0376
ENSMUSG00000016206	H2-M3	0.935	0.0372

Ensembl_ID	Gene	Log2_FC	q_val
ENSMUSG00000039891	Txlnb	0.934	0.0158
ENSMUSG00000029070	Mxra8	0.931	0.0139
ENSMUSG00000047963	Stbd1	0.93	0.0183
ENSMUSG00000031530	Dusp4	0.923	0.000521
ENSMUSG00000040212	Emp3	0.92	0.0365
ENSMUSG00000051590	Map3k19	0.92	0.000521
ENSMUSG00000050138	Kcnk12	0.909	0.000521
ENSMUSG00000102891	Gm19114	0.907	0.000521
ENSMUSG00000028607	Cpt2	0.907	0.041
ENSMUSG00000036492	Rnf39	0.906	0.000985
ENSMUSG00000026072	Il1r1	0.901	0.000521
ENSMUSG00000048572	Tmem252	0.9	0.00412
ENSMUSG00000040569	Slc26a7	0.895	0.00263
ENSMUSG00000047632	Fgfbp3	0.887	0.000521
ENSMUSG00000024222	Fkbp5	0.882	0.000521
ENSMUSG00000029304	Spp1	0.881	0.000521
ENSMUSG00000084904	Gm14827	0.876	0.000521
ENSMUSG00000105022	Gm43537	0.869	0.0374
ENSMUSG00000042622	Maff	0.868	0.0434
ENSMUSG00000050288	Fzd2	0.865	0.000521
ENSMUSG00000039903	Eva1c	0.865	0.0118
ENSMUSG00000046561	Arsj	0.865	0.00184
ENSMUSG00000032092	Mpzl2	0.86	0.000985
ENSMUSG00000021390	Ogn	0.858	0.00302
ENSMUSG00000034765	Dusp5	0.853	0.000521
ENSMUSG00000032532	Cck	0.848	0.000521
ENSMUSG00000085565	Gm15721	0.847	0.000521
ENSMUSG00000037428	Vgf	0.842	0.000521
ENSMUSG00000058488	Kl	0.841	0.00302
ENSMUSG00000027765	P2ry1	0.838	0.0225
ENSMUSG00000041203	2310036O22Rik	0.838	0.000521
ENSMUSG00000097324	Mir143hg	0.828	0.0498
ENSMUSG00000104586	4921539H07Rik	0.826	0.000521
ENSMUSG00000019232	Etnppl	0.825	0.000521
ENSMUSG00000023882	Zfp54	0.822	0.0475
ENSMUSG00000025776	Crispld1	0.82	0.000521
ENSMUSG00000051048	P4ha3	0.818	0.0172
ENSMUSG00000047420	Fam180a	0.816	0.0136
ENSMUSG00000100210	Hist1h3f	0.809	0.00815
ENSMUSG00000043993	2900052L18Rik	0.809	0.00483
ENSMUSG00000032265	Fam46a	0.808	0.000521
ENSMUSG00000024134	Six2	0.798	0.000985
ENSMUSG00000021702	Thbs4	0.796	0.0139
ENSMUSG00000070858	Gm1673	0.777	0.0155
ENSMUSG00000026062	Slc9a2	0.776	0.00719
ENSMUSG00000040152	Thbs1	0.77	0.00142
ENSMUSG00000016179	Camk1g	0.768	0.000521

Ensembl_ID	Gene	Log2_FC	q_val
ENSMUSG00000061524	Zic2	0.765	0.000521
ENSMUSG00000038059	Smim3	0.765	0.000521
ENSMUSG00000029718	Pcolce	0.764	0.00686
ENSMUSG00000078640	Gm11627	0.764	0.0255
ENSMUSG00000026315	Serpinb8	0.764	0.000521
ENSMUSG00000024014	Pim1	0.76	0.0115
ENSMUSG00000028655	Mfsd2a	0.76	0.000521
ENSMUSG00000046470	Sox18	0.758	0.00224
ENSMUSG00000063727	Tnfrsf11b	0.757	0.00224
ENSMUSG00000017692	Rhbdl3	0.749	0.000521
ENSMUSG00000026167	Wnt10a	0.749	0.000521
ENSMUSG00000073418	C4b	0.748	0.0188
ENSMUSG00000037239	Spred3	0.745	0.000521
ENSMUSG00000105366	Gm43719	0.741	0.0225
ENSMUSG00000102900	Gm37811	0.741	0.000985
ENSMUSG00000067297	Ifit1bl2	0.737	0.0282
ENSMUSG00000031762	Mt2	0.73	0.000521
ENSMUSG00000035299	Mid1	0.73	0.000521
ENSMUSG00000003032	Klf4	0.723	0.00339
ENSMUSG00000022678	Nde1	0.721	0.000521
ENSMUSG00000032289	Thsd4	0.712	0.0147
ENSMUSG00000055148	Klf2	0.709	0.000521
ENSMUSG00000028971	Cort	0.708	0.00686
ENSMUSG00000056999	Ide	0.708	0.000521
ENSMUSG00000022602	Arc	0.706	0.000521
ENSMUSG00000060402	Chst8	0.705	0.0325
ENSMUSG00000028487	Bnc2	0.7	0.0273
ENSMUSG00000104919	Gm42617	0.695	0.00783
ENSMUSG00000040565	Btaf1	0.69	0.000521
ENSMUSG00000099583	Hist1h3d	0.687	0.0496
ENSMUSG00000021379	Id4	0.686	0.000521
ENSMUSG00000020614	Fam20a	0.683	0.00719
ENSMUSG00000048482	Bdnf	0.682	0.000521
ENSMUSG00000001943	Vsig2	0.679	0.0494
ENSMUSG00000046618	Olfml2a	0.677	0.00224
ENSMUSG00000097578	Gm26798	0.672	0.00376
ENSMUSG00000073388	A330017A19Rik	0.671	0.0278
ENSMUSG00000029135	Fosl2	0.668	0.000521
ENSMUSG00000086040	Wipf3	0.666	0.0115
ENSMUSG00000010122	Slc47a1	0.663	0.0155
ENSMUSG00000060591	Ifitm2	0.66	0.0109
ENSMUSG00000108137	Gm44053	0.655	0.0332
ENSMUSG00000024039	Cbs	0.655	0.0285
ENSMUSG00000039208	Metrnl	0.645	0.0183
ENSMUSG00000024087	Cyp1b1	0.645	0.00339
ENSMUSG00000041559	Fmod	0.639	0.000521
ENSMUSG00000088185	Scarna2	0.637	0.000521

Ensembl_ID	Gene	Log2_FC	q_val
ENSMUSG00000032128	Robo3	0.634	0.000521
ENSMUSG00000040740	Slc25a34	0.633	0.0118
ENSMUSG00000064264	Zfp428	0.632	0.000521
ENSMUSG00000044674	Fzd1	0.623	0.000521
ENSMUSG00000098202	B830012L14Rik	0.62	0.000521
ENSMUSG00000031765	Mt1	0.61	0.000521
ENSMUSG00000043445	Pgp	0.61	0.000985
ENSMUSG00000028128	F3	0.609	0.000521
ENSMUSG00000019772	Vip	0.608	0.000521
ENSMUSG00000033633	Clec18a	0.603	0.0196
ENSMUSG00000021835	Bmp4	0.598	0.0299
ENSMUSG00000029822	Osbpl3	0.597	0.00184
ENSMUSG00000086320	Gm12840	0.595	0.0335
ENSMUSG00000029695	Aass	0.592	0.0358
ENSMUSG00000032807	Alox12b	0.591	0.00971
ENSMUSG00000022150	Dab2	0.589	0.0141
ENSMUSG00000009687	Fxyd5	0.588	0.0365
ENSMUSG00000039109	F13a1	0.585	0.0161
ENSMUSG00000063260	Syt10	-0.585	0.00751
ENSMUSG00000031775	Pllp	-0.586	0.000521
ENSMUSG00000027577	Chrna4	-0.587	0.00339
ENSMUSG00000032564	Cpne4	-0.591	0.0109
ENSMUSG00000024670	Cd6	-0.591	0.0344
ENSMUSG00000027004	Frzb	-0.592	0.0139
ENSMUSG00000025370	Cdh9	-0.598	0.000521
ENSMUSG00000054931	Zkscan4	-0.601	0.0294
ENSMUSG00000027188	Pamr1	-0.603	0.00518
ENSMUSG00000067377	Tspan6	-0.605	0.0183
ENSMUSG00000028654	Mycl	-0.606	0.0401
ENSMUSG00000021647	Cartpt	-0.612	0.0481
ENSMUSG00000062760	1810041L15Rik	-0.612	0.0121
ENSMUSG00000025171	Ubtd1	-0.613	0.023
ENSMUSG00000040767	Snrnp25	-0.616	0.0243
ENSMUSG00000003070	Efna2	-0.628	0.00653
ENSMUSG00000035713	Usp35	-0.636	0.0496
ENSMUSG00000026278	Bok	-0.637	0.000521
ENSMUSG00000035202	Lars2	-0.637	0.000521
ENSMUSG00000026765	Lypd6b	-0.641	0.00971
ENSMUSG00000090223	Pcp4	-0.646	0.000521
ENSMUSG00000047773	Ankfn1	-0.649	0.00412
ENSMUSG00000025795	Rassf3	-0.651	0.000521
ENSMUSG00000038550	Ciart	-0.654	0.00878
ENSMUSG00000034810	Scn7a	-0.662	0.000521
ENSMUSG00000018923	Med11	-0.671	0.00909
ENSMUSG00000076617	Ighm	-0.686	0.000521
ENSMUSG00000044254	Pcsk9	-0.693	0.024
ENSMUSG00000027849	Syt6	-0.702	0.000521

Ensembl_ID	Gene	Log2_FC	q_val
ENSMUSG00000037977	6430571L13Rik	-0.708	0.0209
ENSMUSG00000064360	mt-Nd3	-0.718	0.00224
ENSMUSG00000040557	Wbscr27	-0.73	0.0144
ENSMUSG00000042328	Hps4	-0.733	0.0396
ENSMUSG00000000093	Tbx2	-0.738	0.0353
ENSMUSG00000028950	Tas1r1	-0.744	0.0199
ENSMUSG00000021223	Papln	-0.745	0.0385
ENSMUSG00000009376	Met	-0.764	0.000521
ENSMUSG00000039316	Rftn1	-0.783	0.0188
ENSMUSG00000022468	Endou	-0.795	0.00483
ENSMUSG00000027669	Gnb4	-0.798	0.000521
ENSMUSG00000097383	1500026H17Rik	-0.799	0.00971
ENSMUSG00000094655	Gm25360	-0.804	0.0235
ENSMUSG00000044461	Shisa2	-0.815	0.0438
ENSMUSG00000020374	Rasgef1c	-0.823	0.000521
ENSMUSG00000025905	Oprk1	-0.829	0.000521
ENSMUSG00000061086	Myl4	-0.847	0.000521
ENSMUSG00000028174	Rpe65	-0.864	0.044
ENSMUSG00000002043	Trappc6a	-0.871	0.0449
ENSMUSG00000022061	Nkx3-1	-0.877	0.00719
ENSMUSG00000044499	Hs3st5	-0.888	0.00142
ENSMUSG00000044813	Shb	-0.901	0.0199
ENSMUSG00000025188	Hps1	-0.906	0.0372
ENSMUSG00000007080	Pole	-0.94	0.0432
ENSMUSG00000106321	Gm43674	-0.941	0.0314
ENSMUSG00000038173	Enpp6	-0.969	0.00142
ENSMUSG00000062382	Gm10116	-0.971	0.0282
ENSMUSG00000032400	Zwilch	-0.986	0.0436
ENSMUSG00000075511	1700001L05Rik	-0.989	0.0302
ENSMUSG00000042514	Klhl14	-0.991	0.0106
ENSMUSG00000053216	Btn2a2	-0.995	0.027
ENSMUSG00000044734	Serpinb1a	-1	0.00263
ENSMUSG00000035258	Abi3bp	-1.01	0.000521
ENSMUSG00000027496	Aurka	-1.01	0.0356
ENSMUSG00000020131	Pcsk4	-1.01	0.00224
ENSMUSG00000042631	Xkr7	-1.04	0.00376
ENSMUSG00000041674	BC006965	-1.04	0.00483
ENSMUSG00000055602	Tcp10b	-1.05	0.028
ENSMUSG00000021541	Trpc7	-1.05	0.0062
ENSMUSG00000078695	Cisd3	-1.07	0.000521
ENSMUSG00000075334	Rprm	-1.08	0.000521
ENSMUSG00000048351	Coa7	-1.12	0.0109
ENSMUSG00000040605	Bace2	-1.12	0.000521
ENSMUSG00000039552	Rsph4a	-1.12	0.00376
ENSMUSG00000020908	Myh3	-1.13	0.000521
ENSMUSG00000026826	Nr4a2	-1.19	0.000521
ENSMUSG00000050121	Opalin	-1.19	0.000521

Ensembl_ID	Gene	Log2_FC	q_val
ENSMUSG00000021281	Tnfaip2	-1.21	0.033
ENSMUSG00000040258	Nxph4	-1.27	0.0282
ENSMUSG00000076612	Ighg2c	-1.28	0.000521
ENSMUSG00000035486	Plk5	-1.31	0.000521
ENSMUSG00000006269	Atp6v1b1	-1.37	0.0109
ENSMUSG00000025946	Pth2r	-1.41	0.0158
ENSMUSG00000029134	Plb1	-1.43	0.00339
ENSMUSG00000046491	C1qtnf2	-1.49	0.0177
ENSMUSG00000039563	2210406O10Rik	-1.53	0.000521
ENSMUSG00000085783	Gm9816	-1.6	0.0144
ENSMUSG00000039748	Exo1	-1.64	0.0201
ENSMUSG00000020679	Hnf1b	-1.66	0.00586
ENSMUSG00000087107	AI662270	-1.77	0.0263
ENSMUSG00000030048	Gkn3	-1.83	0.00376
ENSMUSG00000010080	Epn3	-2.03	0.0337
ENSMUSG00000070780	Rbm47	-2.07	0.0158
ENSMUSG00000073530	Pappa2	-2.36	0.000521
ENSMUSG00000070687	Htr1d	-2.85	0.000985
ENSMUSG00000063659	Zbtb18	-3.72	0.000521

App.3. Diurnal Genes in Mouse Cortex

Genes identified as diurnal by JTK algorithm. Data presented is the Benjamini adjusted p-value for 24-hour gene expression pattern for mice subjected to 0,3,6 or 12 hour sleep deprivation (C,SD3,SD6 or SD12, respectively). Also included is the timing of the peak expression in control animals (C_phase), where 0 is defined as 6pm (lights off) and 12 is defined as 6am (lights on). Amplitude is normalised to gene expression value. Ordered by genes that remain rhythmic through progressively increasing duration of sleep deprivation, followed by phase, followed by amplitude of oscillation.

Ensembl_ ID	Gene	q_C	q_SD3	q_SD6	q_SD12	C_Phase	Amp
ENSMUSG00000055560	Zfp459	7.00E-04	0.00018	0.00064	0.038	0	0.31
ENSMUSG00000004328	Hif3a	0.0095	0.00018	0.0041	0.028	0	0.26
ENSMUSG00000034858	Fam214a	6.30E-05	1.30E-07	0.0023	0.0077	0	0.22
ENSMUSG00000051351	Zfp46	4.30E-05	0.00015	5.40E-05	0.027	0	0.21
ENSMUSG00000021215	Net1	8.40E-05	7.10E-06	0.00022	0.027	0	0.2
ENSMUSG00000038214	Bend3	0.029	0.067	0.35	0.027	0	0.12
ENSMUSG00000047414	Flrt2	0.00047	0.16	0.046	0.038	0	0.11
ENSMUSG00000035024	Ncapd3	0.047	0.0013	0.091	0.028	0	0.077
ENSMUSG00000070565	Rasal2	0.011	0.00062	0.029	0.038	0	0.057
ENSMUSG00000073761	4933427I04Rik	0.0032	0.007	0.3	0.043	3	0.31
ENSMUSG00000021775	Nr1d2	5.70E-06	0.00011	0.071	0.047	3	0.18
ENSMUSG00000036106	Prr5	0.047	0.015	0.11	0.038	3	0.18
ENSMUSG00000020044	Timp3	0.0048	0.023	0.067	0.036	3	0.1
ENSMUSG00000078117	Gm16485	0.026	0.58	0.75	0.027	3	0.084
ENSMUSG00000004951	Hspb1	0.0044	0.0012	0.0029	0.027	9	0.46
ENSMUSG00000090877	Hspa1b	0.011	0.0013	0.058	0.027	9	0.33
ENSMUSG00000025823	Pdia4	0.0016	0.0023	0.00064	0.038	9	0.31
ENSMUSG00000042116	Vwa1	0.0048	0.00017	0.26	0.03	9	0.23
ENSMUSG00000036915	Kirrel2	0.015	0.086	0.097	0.027	9	0.17
ENSMUSG00000056962	Jmjd6	0.022	0.98	0.04	0.038	9	0.13
ENSMUSG00000022075	Rhobtb2	0.00015	0.0048	0.00043	0.027	9	0.1
ENSMUSG00000045312	Lhfpl2	0.019	0.25	0.058	0.036	9	0.09
ENSMUSG00000028634	Hivep3	0.043	0.0012	0.12	0.047	9	0.088
ENSMUSG00000029648	Flt1	0.04	8.50E-05	0.062	0.0077	9	0.072
ENSMUSG00000021250	Fos	0.0029	0.00082	0.00073	0.028	12	0.49
ENSMUSG00000019916	P4ha1	7.00E-04	1.20E-05	1.80E-05	0.038	12	0.37
ENSMUSG00000028341	Nr4a3	0.0018	2.90E-06	9.30E-05	0.027	12	0.33
ENSMUSG00000056708	Ier5	0.0072	0.00012	4.60E-05	0.036	12	0.32
ENSMUSG00000041378	Cldn5	0.02	0.00022	0.062	0.0076	12	0.29
ENSMUSG00000030093	Wnt7a	0.0058	0.026	0.0095	0.027	12	0.27
ENSMUSG00000062960	Kdr	1.90E-05	2.60E-08	1.80E-05	0.047	12	0.24
ENSMUSG00000043415	Otud1	0.0048	0.00017	0.026	0.0077	12	0.19
ENSMUSG00000027435	Cd93	0.0016	0.00017	6.30E-05	0.027	12	0.18
ENSMUSG00000021224	Numb	0.001	0.0034	0.002	0.038	12	0.16

Ensembl_ ID	Gene	q_C	q_SD3	q_SD6	q_SD12	C_Phase	Amp
ENSMUSG00000029312	Klhl8	0.0072	0.46	0.091	0.016	12	0.1
ENSMUSG00000034575	Papd7	0.017	4.70E-05	4.30E-05	0.038	12	0.079
ENSMUSG00000055116	Arntl	1.10E-06	4.70E-05	2.10E-06	0.027	15	0.25
ENSMUSG00000066829	Zfp810	0.004	6.70E-05	0.00073	0.036	21	0.26
ENSMUSG00000052496	Pkdrej	0.0014	0.0019	0.015	0.027	21	0.25
ENSMUSG00000060314	Zfp941	8.40E-05	0.0019	0.054	0.036	21	0.19
ENSMUSG00000021010	Npas3	0.0018	0.19	0.015	0.027	21	0.073
ENSMUSG00000031483	Erlin2	0.04	0.067	0.33	0.0077	21	0.062
ENSMUSG00000050211	Pla2g4e	0.0044	0.00018	0.00058	0.3	0	0.45
ENSMUSG00000021903	Galnt15	0.00035	7.10E-06	0.00043	0.3	0	0.44
ENSMUSG00000038550	Ciart	5.20E-05	0.00022	0.00058	0.17	0	0.38
ENSMUSG00000031853	BC021891	0.0044	0.0095	0.0033	0.34	0	0.36
ENSMUSG00000098221	Gm27030	0.0065	0.3	0.012	1	0	0.33
ENSMUSG00000032010	Usp2	0.014	0.25	0.0037	0.58	0	0.32
ENSMUSG00000045414	1190002N15Rik	5.20E-05	2.50E-06	0.0095	0.17	0	0.3
ENSMUSG00000096936	Gm3510	0.014	3.00E-04	0.026	0.48	0	0.3
ENSMUSG00000097454	Gm26892	0.00047	0.00018	0.001	0.31	0	0.3
ENSMUSG00000089737	Gm15688	0.0048	0.62	0.018	1	0	0.3
ENSMUSG00000047606	Ankrd34c	7.00E-04	0.003	0.00019	0.44	0	0.29
ENSMUSG00000074766	Ism1	0.0011	0.063	0.0023	0.25	0	0.26
ENSMUSG00000074001	Klhl40	0.00035	1.30E-05	0.0079	0.079	0	0.26
ENSMUSG00000019970	Sgk1	2.20E-05	0.018	0.015	0.26	0	0.25
ENSMUSG00000025511	Tspan4	7.70E-05	0.37	0.022	1	0	0.24
ENSMUSG00000045193	Cirbp	0.0053	4.10E-06	0.026	0.066	0	0.24
ENSMUSG00000034161	Scx	0.024	0.04	0.024	1	0	0.23
ENSMUSG00000031382	Asb11	0.0014	5.00E-04	0.024	0.5	0	0.22
ENSMUSG00000025450	Gm9752	0.0053	1	0.043	0.48	0	0.2
ENSMUSG00000071691	Gm960	0.024	0.33	0.031	0.88	0	0.2
ENSMUSG00000034320	Slc26a2	0.0029	0.07	0.049	0.37	0	0.2
ENSMUSG00000086555	Gm13446	0.0048	0.011	0.049	0.78	0	0.2
ENSMUSG00000039629	Strip2	8.40E-05	0.00091	0.012	0.88	0	0.19
ENSMUSG00000067872	Ccdc87	0.0072	0.5	0.043	1	0	0.19
ENSMUSG00000097820	E530011L22Rik	0.011	0.033	0.026	1	0	0.19
ENSMUSG00000020889	Nr1d1	0.0058	0.053	0.04	0.44	0	0.18
ENSMUSG00000023206	Il15ra	0.019	0.51	0.046	0.6	0	0.18
ENSMUSG00000042686	Jph1	0.0048	0.17	0.026	0.41	0	0.17
ENSMUSG00000037355	Uvssa	0.00027	1	0.0018	1	0	0.17
ENSMUSG00000039096	Rsad1	0.012	0.00032	0.00054	0.76	0	0.16
ENSMUSG00000027796	Smad9	0.0048	0.026	0.002	1	0	0.16
ENSMUSG00000030087	Klf15	0.013	0.00018	0.02	0.64	0	0.15
ENSMUSG00000085084	4930570G19Rik	0.0013	1	0.031	1	0	0.15
ENSMUSG00000055884	Fancm	0.0032	0.024	0.02	1	0	0.14
ENSMUSG00000037224	Zfyve28	0.022	0.0025	0.024	1	0	0.14
ENSMUSG00000036817	Sun1	0.0053	0.029	0.046	0.91	0	0.14
ENSMUSG00000053914	Kdm4d	0.0058	0.17	0.00043	0.83	0	0.13
ENSMUSG00000008305	Tle1	0.013	1	0.015	0.29	0	0.13
ENSMUSG00000099478	Gm28370	0.0053	0.17	0.026	0.39	0	0.13

Ensembl_ ID	Gene	q_C	q_SD3	q_SD6	q_SD12	C_Phase	Amp
ENSMUSG00000020280	Pus10	0.022	0.93	0.049	1	0	0.13
ENSMUSG00000038068	Rnf144b	0.014	0.042	0.0033	0.78	0	0.13
ENSMUSG00000026843	Fubp3	0.017	0.71	0.026	1	0	0.13
ENSMUSG00000034614	Pik3ip1	0.0095	1	0.00043	1	0	0.12
ENSMUSG00000059149	Mfsd4	0.0036	2.00E-05	0.0079	1	0	0.12
ENSMUSG00000095930	Nim1k	7.70E-05	0.045	0.0041	1	0	0.11
ENSMUSG00000084947	Gm15594	0.014	0.13	0.037	0.39	0	0.11
ENSMUSG00000042997	Nhlrc3	0.02	0.6	0.0041	1	0	0.11
ENSMUSG00000059772	Slx1b	0.0087	0.0088	0.0033	0.83	0	0.11
ENSMUSG00000097023	AI854517	0.0032	1	0.018	1	0	0.1
ENSMUSG00000055296	Tmem245	0.043	0.32	0.043	0.95	0	0.1
ENSMUSG00000026489	Adck3	0.031	0.063	0.037	1	0	0.1
ENSMUSG00000030255	Sspn	0.0029	0.004	0.0029	1	0	0.1
ENSMUSG00000010307	Tmem86a	0.047	6.00E-05	0.0047	0.74	0	0.1
ENSMUSG00000026096	Osgepl1	0.047	1	0.015	1	0	0.099
ENSMUSG00000040648	Ppip5k2	0.0065	0.0023	0.017	1	0	0.094
ENSMUSG00000038215	Cep44	0.0065	0.15	0.031	1	0	0.093
ENSMUSG00000069631	Strada	0.004	0.13	0.037	0.5	0	0.088
ENSMUSG00000039307	Hexdc	0.031	0.096	0.043	1	0	0.085
ENSMUSG00000030880	Polr3e	0.047	0.00032	0.0047	0.58	0	0.081
ENSMUSG00000027242	Wdr76	0.014	0.06	0.043	0.29	0	0.073
ENSMUSG00000058761	Rnf169	0.0036	1	0.037	1	0	0.072
ENSMUSG00000029804	Herc3	0.043	0.39	0.049	1	0	0.051
ENSMUSG00000003477	Inmt	4.30E-05	0.015	0.00085	0.68	3	0.39
ENSMUSG00000040170	Fmo2	0.012	0.0015	0.00058	0.14	3	0.36
ENSMUSG00000096257	Ccer2	0.00031	0.021	0.015	0.68	3	0.33
ENSMUSG00000051777	Iqcj	0.013	0.24	0.018	0.88	3	0.29
ENSMUSG00000020131	Pcsk4	0.0087	0.027	0.037	1	3	0.28
ENSMUSG00000059824	Dbp	1.30E-05	0.00044	2.10E-06	0.76	3	0.27
ENSMUSG00000020424	Gatsl3	0.0016	0.063	0.022	0.095	3	0.27
ENSMUSG00000028957	Per3	8.20E-06	8.50E-05	0.0013	0.07	3	0.26
ENSMUSG00000040675	Mthfd1l	1.90E-05	0.057	0.0087	0.56	3	0.25
ENSMUSG00000070601	Vmn2r84	0.004	0.0027	0.04	1	3	0.23
ENSMUSG00000074449	Gm15319	0.0013	0.026	0.0079	0.83	3	0.23
ENSMUSG00000009378	Slc16a12	0.00047	0.0082	0.00064	0.13	3	0.23
ENSMUSG00000046808	Atp10d	0.013	0.096	0.026	0.25	3	0.23
ENSMUSG00000028661	Epha8	0.012	0.001	0.0015	0.39	3	0.22
ENSMUSG00000028645	Slc2a1	0.00035	0.00066	0.046	0.075	3	0.22
ENSMUSG00000038304	Cd160	0.00041	0.086	0.00043	0.78	3	0.22
ENSMUSG00000039059	Hrh3	0.0013	6.70E-05	0.026	0.56	3	0.2
ENSMUSG00000022389	Tef	0.00078	3.00E-04	0.043	0.5	3	0.16
ENSMUSG00000049791	Fzd4	0.00052	0.0012	0.013	0.58	3	0.16
ENSMUSG00000030256	Bhlhe41	8.40E-05	0.68	0.022	1	3	0.14
ENSMUSG00000059602	Syn3	0.031	1	0.017	0.6	3	0.12
ENSMUSG00000086544	Chn1os3	0.037	1	0.0095	1	3	0.12
ENSMUSG00000048347	Pcdhb18	0.022	1	0.049	1	3	0.075
ENSMUSG00000048756	Foxo3	0.024	0.02	0.034	1	3	0.074

Ensembl_ ID	Gene	q_C	q_SD3	q_SD6	q_SD12	C_Phase	Amp
ENSMUSG00000061751	Kalrn	0.022	0.0034	0.0047	1	3	0.072
ENSMUSG00000026790	Odf2	0.034	0.6	0.037	0.76	3	0.068
ENSMUSG00000018001	Cyth3	0.029	1	0.049	1	3	0.059
ENSMUSG00000002847	Pla1a	0.0053	0.22	0.0095	0.52	6	0.33
ENSMUSG00000025491	Ifitm1	0.0044	0.042	0.02	0.91	6	0.31
ENSMUSG00000055866	Per2	2.20E-05	0.00032	0.0026	0.36	6	0.28
ENSMUSG00000072572	Slc39a2	0.031	0.53	0.00073	1	6	0.17
ENSMUSG00000070461	9230112E08Rik	0.0021	1	0.0071	0.86	6	0.11
ENSMUSG00000004568	Arhgef18	0.0021	1	0.002	1	6	0.092
ENSMUSG00000038026	Kcnj9	0.04	1	0.022	1	6	0.09
ENSMUSG00000031770	Herpud1	0.043	0.5	0.046	1	6	0.086
ENSMUSG00000041168	Lonp1	0.047	0.77	0.031	0.91	6	0.078
ENSMUSG00000034807	Colgalt1	0.019	0.85	0.02	1	6	0.071
ENSMUSG00000022602	Arc	0.0095	0.0016	0.0018	0.14	9	0.69
ENSMUSG00000023232	Serinc2	0.00015	0.00028	0.00073	0.095	9	0.65
ENSMUSG00000031530	Dusp4	1.90E-05	4.40E-08	0.00058	1	9	0.46
ENSMUSG00000022769	Sdf2l1	1.90E-05	0.0038	0.0054	0.56	9	0.42
ENSMUSG00000062563	Cys1	8.20E-06	0.00056	0.0015	0.3	9	0.42
ENSMUSG00000087249	Gm16062	0.0095	0.37	0.0047	0.66	9	0.4
ENSMUSG00000026864	Hspa5	0.0013	0.0016	0.00054	0.075	9	0.38
ENSMUSG00000025316	Banp	0.001	0.01	0.013	0.2	9	0.37
ENSMUSG00000024793	Tnfrsf25	0.014	1	0.018	1	9	0.37
ENSMUSG00000072919	Noxred1	0.0032	0.17	0.02	0.52	9	0.35
ENSMUSG00000032501	Trib1	0.022	0.00066	0.00054	0.3	9	0.34
ENSMUSG00000060862	Zbtb40	7.80E-06	0.00032	0.00048	0.3	9	0.33
ENSMUSG00000023272	Creld2	7.80E-06	0.04	0.0033	0.83	9	0.32
ENSMUSG00000042978	Sbk1	0.00011	0.0027	0.0087	0.78	9	0.3
ENSMUSG00000024042	Sik1	0.0014	2.00E-04	0.0087	0.46	9	0.3
ENSMUSG00000021203	Otub2	0.0011	0.0025	0.0047	0.46	9	0.3
ENSMUSG00000009092	Derl3	0.0018	1	0.034	1	9	0.3
ENSMUSG00000049511	Htr1b	0.00023	0.0032	0.037	0.11	9	0.28
ENSMUSG00000040183	Ankrd6	8.20E-06	0.017	0.037	0.2	9	0.27
ENSMUSG00000051335	Gfod1	3.50E-05	3.30E-08	0.002	0.29	9	0.26
ENSMUSG00000031758	Cdyl2	7.80E-06	0.0016	0.013	0.95	9	0.26
ENSMUSG00000038418	Egr1	0.0029	2.30E-07	0.00064	0.23	9	0.26
ENSMUSG00000026773	Pfkfb3	0.0011	0.0027	0.043	0.26	9	0.25
ENSMUSG00000052229	Gpr17	1.00E-05	0.045	0.0087	0.059	9	0.24
ENSMUSG00000063415	Cyp26b1	0.037	0.05	0.0023	0.31	9	0.24
ENSMUSG00000096847	Tmem151b	2.60E-05	0.00015	0.037	0.6	9	0.23
ENSMUSG00000041773	Enc1	0.00031	2.50E-06	0.024	1	9	0.22
ENSMUSG00000021277	Traf3	7.80E-06	0.00066	0.012	1	9	0.22
ENSMUSG00000046667	Rbm12b1	0.00041	1	0.0029	0.76	9	0.21
ENSMUSG00000021587	Pcsk1	0.00061	0.13	0.015	1	9	0.21
ENSMUSG00000025810	Nrp1	0.0036	0.001	0.0012	0.83	9	0.21
ENSMUSG00000021990	Spata13	0.034	0.34	0.02	1	9	0.21
ENSMUSG00000073838	Tufm	0.019	1	0.043	1	9	0.21
ENSMUSG00000053004	Hrh1	0.00052	0.68	0.002	1	9	0.2

Ensembl_ ID	Gene	q_C	q_SD3	q_SD6	q_SD12	C_Phase	Amp
ENSMUSG00000017386	Traf4	0.04	1	0.037	0.22	9	0.2
ENSMUSG00000037035	Inhbb	0.0011	0.43	0.0079	0.83	9	0.2
ENSMUSG00000057329	Bcl2	1.80E-05	0.0014	0.018	0.44	9	0.2
ENSMUSG00000013089	Etv5	0.00052	0.00066	0.0037	0.81	9	0.2
ENSMUSG00000094626	Cecr6	0.00015	0.00091	2.10E-06	0.066	9	0.19
ENSMUSG00000020038	Cry1	9.50E-05	0.13	0.0095	0.52	9	0.19
ENSMUSG00000005483	Dnajb1	0.0016	0.98	0.0013	0.37	9	0.19
ENSMUSG00000035007	Rundc1	9.50E-05	3.00E-04	0.0026	0.36	9	0.19
ENSMUSG00000029817	Tra2a	0.0065	0.0048	0.043	0.14	9	0.19
ENSMUSG00000020032	Nuak1	9.50E-05	2.10E-05	0.00011	0.087	9	0.19
ENSMUSG00000030584	Dpf1	0.0018	0.015	0.0095	1	9	0.18
ENSMUSG00000028527	Ak4	0.0016	0.074	0.00019	0.26	9	0.18
ENSMUSG00000010554	Mettl16	0.0026	0.012	0.0013	0.25	9	0.18
ENSMUSG00000033377	Palmd	0.0016	0.01	0.043	1	9	0.17
ENSMUSG00000068114	Ccdc134	0.00052	0.24	0.0029	1	9	0.17
ENSMUSG00000033594	Spata2l	0.011	0.074	0.043	0.13	9	0.17
ENSMUSG00000032115	Hyou1	0.00031	0.029	0.017	0.88	9	0.17
ENSMUSG00000051726	Kcnf1	9.50E-05	1	0.0029	1	9	0.16
ENSMUSG00000023827	Agpat4	0.0053	1	0.0087	1	9	0.16
ENSMUSG00000000184	Ccnd2	7.00E-04	0.074	0.017	0.83	9	0.16
ENSMUSG00000061079	Zfp143	4.30E-05	0.011	0.04	0.34	9	0.16
ENSMUSG00000049420	Tmem200a	0.0087	0.0013	0.04	1	9	0.16
ENSMUSG00000071719	Tmem28	0.001	0.0015	0.0054	0.68	9	0.16
ENSMUSG00000031168	Ebp	0.043	1	0.037	1	9	0.16
ENSMUSG00000034265	Zdhhc14	0.0048	0.011	0.024	1	9	0.16
ENSMUSG00000032290	Ptpn9	0.0048	0.004	0.00048	0.39	9	0.16
ENSMUSG00000055652	Klhl25	0.0018	0.5	0.012	1	9	0.16
ENSMUSG00000019055	Plod1	0.0048	0.37	0.049	1	9	0.15
ENSMUSG00000024219	Anks1	0.001	1	0.043	0.46	9	0.15
ENSMUSG00000038132	Rbm24	0.012	0.006	0.0033	0.62	9	0.15
ENSMUSG00000073139	BC023829	0.0058	0.0027	0.0095	0.5	9	0.15
ENSMUSG00000040711	Sh3pxd2b	0.0048	3.00E-04	0.013	0.76	9	0.15
ENSMUSG00000030103	Bhlhe40	0.02	0.045	0.049	0.46	9	0.14
ENSMUSG00000048578	Mlec	7.80E-06	0.1	0.00019	0.26	9	0.14
ENSMUSG00000022556	Hsf1	0.0013	0.0027	0.043	1	9	0.14
ENSMUSG00000025408	Ddit3	0.013	0.11	0.012	0.1	9	0.14
ENSMUSG00000037239	Spred3	0.00061	2.00E-04	0.037	1	9	0.14
ENSMUSG00000050530	Fam171a1	0.00047	0.026	0.012	1	9	0.14
ENSMUSG00000042846	Lrrtm3	0.011	0.16	0.034	0.68	9	0.14
ENSMUSG00000071757	Zhx2	0.0018	0.0052	0.015	0.22	9	0.14
ENSMUSG00000097736	9530059O14Rik	0.026	0.078	0.031	0.41	9	0.14
ENSMUSG00000036158	Prickle1	0.0011	0.048	0.0012	0.23	9	0.14
ENSMUSG00000023915	Tnfrsf21	0.001	0.14	0.0041	1	9	0.13
ENSMUSG00000072082	Ccnf	0.024	0.36	0.046	0.95	9	0.13
ENSMUSG00000036964	Trim17	0.0072	0.23	0.04	0.97	9	0.13
ENSMUSG00000001098	Kctd10	0.0029	1	0.049	1	9	0.13
ENSMUSG00000042210	Abhd14a	0.02	0.96	5.40E-05	1	9	0.13

Ensembl_ ID	Gene	q_C	q_SD3	q_SD6	q_SD12	C_Phase	Amp
ENSMUSG00000045282	Tmem86b	0.024	0.029	0.022	1	9	0.13
ENSMUSG00000019487	Trip10	0.024	0.014	0.037	1	9	0.12
ENSMUSG00000051495	Irf2bp2	0.0036	3.80E-05	0.0087	0.18	9	0.12
ENSMUSG00000046269	Usp27x	0.0048	0.0016	0.00064	0.48	9	0.12
ENSMUSG00000020522	Mfap3	0.019	0.029	0.022	0.86	9	0.12
ENSMUSG00000034958	Atcay	0.0044	1	0.026	0.5	9	0.12
ENSMUSG00000021484	Lman2	7.80E-06	1	0.018	1	9	0.12
ENSMUSG00000059796	Eif4a1	0.034	0.75	0.031	1	9	0.12
ENSMUSG00000024781	Lipa	0.013	0.029	0.0033	0.6	9	0.12
ENSMUSG00000040822	1700123O20Rik	0.024	0.37	0.022	1	9	0.12
ENSMUSG00000031523	Dlc1	0.0087	0.83	0.043	0.66	9	0.12
ENSMUSG00000020654	Adcy3	0.0014	1	0.034	1	9	0.12
ENSMUSG00000073805	Fam196a	0.0087	0.015	0.00058	0.13	9	0.11
ENSMUSG00000022814	Umps	0.0032	0.77	0.0087	1	9	0.11
ENSMUSG00000042331	Specc1	3.00E-05	0.18	0.0012	0.71	9	0.11
ENSMUSG00000038855	Itpkb	0.0014	0.0032	0.02	0.48	9	0.11
ENSMUSG00000027940	Tpm3	0.029	0.31	0.034	1	9	0.11
ENSMUSG00000037112	Sik2	0.0011	0.00062	0.0087	0.051	9	0.11
ENSMUSG00000047824	Pygo2	0.0053	1	0.046	1	9	0.11
ENSMUSG00000038485	Socs7	1.90E-05	0.033	0.0047	1	9	0.11
ENSMUSG00000033658	Ddx19b	8.40E-05	0.45	0.02	1	9	0.11
ENSMUSG00000052406	Rexo4	0.0032	0.027	0.04	0.39	9	0.11
ENSMUSG00000052713	Zfp608	0.00035	0.00025	0.043	0.17	9	0.11
ENSMUSG00000020250	Txnrd1	8.20E-06	0.004	0.013	0.13	9	0.11
ENSMUSG00000050511	Oprd1	0.004	0.0044	0.049	0.66	9	0.1
ENSMUSG00000017667	Zfp334	3.00E-05	0.00082	0.0015	0.44	9	0.1
ENSMUSG00000039633	Lonrf1	7.00E-04	0.0076	0.002	0.21	9	0.1
ENSMUSG00000019947	Arid5b	0.0048	0.0088	0.017	0.11	9	0.1
ENSMUSG00000018209	Stk4	0.0029	0.51	0.00022	1	9	0.1
ENSMUSG00000034075	Zdhhc5	0.029	0.023	0.043	1	9	0.1
ENSMUSG00000021071	Trim9	9.50E-05	0.013	0.046	1	9	0.1
ENSMUSG00000035226	Rims4	0.022	0.53	0.029	1	9	0.1
ENSMUSG00000025871	4833439L19Rik	0.0036	0.31	0.02	1	9	0.096
ENSMUSG00000003153	Slc2a3	0.00078	1	0.02	1	9	0.096
ENSMUSG00000032064	Dixdc1	0.0087	0.057	0.049	0.48	9	0.095
ENSMUSG00000070056	Mfhas1	0.0016	1	0.043	1	9	0.094
ENSMUSG00000051510	Mafg	0.00031	1	0.049	1	9	0.094
ENSMUSG00000039804	Ncoa5	0.0095	0.34	0.0041	1	9	0.093
ENSMUSG00000036450	Hif1an	0.0048	0.22	0.0062	1	9	0.092
ENSMUSG00000046562	Unc119b	0.0079	1	0.00085	0.14	9	0.091
ENSMUSG00000034563	Ccpg1	0.001	0.045	0.029	0.14	9	0.088
ENSMUSG00000014547	Wdfy2	0.0016	1	0.022	1	9	0.088
ENSMUSG00000022185	Acin1	0.00013	0.082	0.00064	0.17	9	0.088
ENSMUSG00000036006	Fam65b	0.0079	0.53	0.0033	1	9	0.087
ENSMUSG00000041313	Slc7a1	0.0053	0.14	0.049	1	9	0.086
ENSMUSG00000003585	Sec14l2	0.04	0.68	0.022	1	9	0.085
ENSMUSG00000037896	Rcor1	0.026	0.096	0.011	0.68	9	0.085

Ensembl_ ID	Gene	q_C	q_SD3	q_SD6	q_SD12	C_Phase	Amp
ENSMUSG00000020780	Srp68	0.004	0.013	0.017	1	9	0.083
ENSMUSG00000042426	Dhx29	0.024	0.063	0.046	0.5	9	0.08
ENSMUSG00000017802	Fam134c	0.00017	1	0.04	1	9	0.078
ENSMUSG00000029063	Nadk	0.0065	1	0.018	1	9	0.078
ENSMUSG00000069227	Gprin1	0.0087	1	0.0012	0.78	9	0.078
ENSMUSG00000031774	Fam192a	0.024	0.13	0.046	1	9	0.077
ENSMUSG00000025209	Peo1	0.02	0.4	0.029	0.44	9	0.071
ENSMUSG00000042650	Alkbh5	0.00047	0.93	0.015	1	9	0.07
ENSMUSG00000031155	Pim2	0.0044	0.12	0.026	0.41	9	0.069
ENSMUSG00000039936	Pik3cd	0.047	0.21	0.049	1	9	0.068
ENSMUSG00000031078	Cttn	0.019	0.51	0.024	1	9	0.067
ENSMUSG00000026024	Als2	0.022	1	0.017	1	9	0.066
ENSMUSG00000001036	Epn2	0.043	0.4	0.037	0.37	9	0.065
ENSMUSG00000025085	Ablim1	0.00013	0.029	0.022	1	9	0.063
ENSMUSG00000032624	Eml4	0.0072	0.0023	0.049	0.52	9	0.062
ENSMUSG00000055065	Ddx17	0.0023	1	0.0037	1	9	0.06
ENSMUSG00000039982	Dtx4	0.04	0.021	0.049	0.31	9	0.057
ENSMUSG00000018547	Pip4k2b	0.0087	0.06	0.015	1	9	0.056
ENSMUSG00000022412	Mief1	0.012	1	0.024	1	9	0.055
ENSMUSG00000068742	Cry2	0.026	1	0.043	0.54	9	0.052
ENSMUSG00000004099	Dnmt1	0.0044	0.58	0.031	1	9	0.051
ENSMUSG00000019969	Psen1	0.024	1	0.00054	1	9	0.051
ENSMUSG00000034413	Neurl1b	0.0044	0.9	0.034	1	9	0.049
ENSMUSG00000035629	Rubcn	0.019	1	0.024	1	9	0.048
ENSMUSG00000029922	Mkrn1	0.034	0.8	0.034	0.42	9	0.042
ENSMUSG00000031545	Gpat4	0.015	1	0.034	1	9	0.037
ENSMUSG00000037868	Egr2	0.00078	4.20E-05	2.10E-05	0.22	12	0.68
ENSMUSG00000036390	Gadd45a	0.0053	0.11	0.00048	1	12	0.44
ENSMUSG00000054944	5330416C01Rik	0.019	0.36	0.0087	1	12	0.42
ENSMUSG00000060962	Dmkn	0.0053	0.053	0.0062	1	12	0.4
ENSMUSG00000023034	Nr4a1	0.0087	0.00018	0.00064	0.28	12	0.38
ENSMUSG00000036052	Dnajb5	7.80E-06	2.60E-08	0.00019	0.14	12	0.38
ENSMUSG00000029641	Rasl11a	0.031	0.053	0.034	0.5	12	0.38
ENSMUSG00000037465	Klf10	0.0026	6.30E-06	1.80E-05	0.34	12	0.37
ENSMUSG00000005124	Wisp1	0.00031	0.006	0.0062	1	12	0.35
ENSMUSG00000023067	Cdkn1a	7.80E-06	0.00022	0.022	1	12	0.33
ENSMUSG00000020601	Trib2	2.60E-05	0.00032	6.30E-05	0.26	12	0.32
ENSMUSG00000023905	Tnfrsf12a	0.0072	0.3	0.0029	0.91	12	0.31
ENSMUSG00000020571	Pdia6	0.0021	3.80E-05	5.40E-05	0.14	12	0.29
ENSMUSG00000019960	Dusp6	0.0053	0.00022	0.00027	0.26	12	0.29
ENSMUSG00000070348	Ccnd1	0.0016	0.0019	0.0041	1	12	0.29
ENSMUSG00000059991	Nptx2	7.70E-05	0.0019	0.0087	0.97	12	0.28
ENSMUSG00000002983	Relb	0.0032	0.45	0.029	1	12	0.28
ENSMUSG00000030047	Arhgap25	0.017	0.11	0.018	0.64	12	0.28
ENSMUSG00000025402	Nab2	0.0018	0.00022	0.0041	0.13	12	0.28
ENSMUSG00000024427	Spry4	0.0032	0.00015	0.00014	0.41	12	0.27
ENSMUSG00000019850	Tnfaip3	0.0036	0.029	0.018	0.21	12	0.27

Ensembl_ ID	Gene	q_C	q_SD3	q_SD6	q_SD12	C_Phase	Amp
ENSMUSG00000007617	Homer1	9.50E-05	4.20E-05	0.0013	0.26	12	0.26
ENSMUSG00000089774	Slc5a3	0.0013	0.004	0.024	0.059	12	0.26
ENSMUSG00000040363	Bcor	0.00052	6.60E-10	4.60E-05	0.1	12	0.25
ENSMUSG00000049649	Gpr3	0.004	0.0014	0.011	0.31	12	0.25
ENSMUSG00000032575	Manf	0.0014	0.0027	0.001	0.46	12	0.25
ENSMUSG00000048482	Bdnf	0.00027	1.00E-05	0.00041	1	12	0.25
ENSMUSG00000028680	Plk3	0.0053	0.0032	0.00073	0.91	12	0.24
ENSMUSG00000023805	Synj2	3.50E-05	8.80E-06	0.0026	0.5	12	0.24
ENSMUSG00000037984	Neurod6	0.013	0.0021	0.0087	0.41	12	0.24
ENSMUSG00000032060	Cryab	0.015	1	0.037	1	12	0.23
ENSMUSG00000002897	Il17ra	9.50E-05	0.1	0.00043	1	12	0.22
ENSMUSG00000003814	Calr	1.60E-05	0.0088	9.30E-05	1	12	0.22
ENSMUSG00000049225	Pdp1	1.60E-05	4.40E-08	0.0023	0.39	12	0.22
ENSMUSG00000020484	Xbp1	0.00031	0.0056	0.0026	0.14	12	0.22
ENSMUSG00000063889	Crem	0.0087	0.091	0.022	0.74	12	0.22
ENSMUSG00000041324	Inhba	2.20E-05	0.0048	0.029	1	12	0.21
ENSMUSG00000032487	Ptgs2	0.0029	0.006	0.0054	1	12	0.21
ENSMUSG00000032058	Ppp2r1b	0.0044	0.22	0.0033	0.66	12	0.21
ENSMUSG00000020513	Tubd1	0.0023	0.07	0.018	0.62	12	0.21
ENSMUSG00000037010	Apln	0.00047	0.0088	0.0047	1	12	0.2
ENSMUSG00000038244	Mical2	3.00E-05	0.0016	0.046	1	12	0.2
ENSMUSG00000011256	Adam19	8.40E-05	0.027	0.02	1	12	0.2
ENSMUSG00000042540	Acot5	0.04	0.067	0.04	1	12	0.2
ENSMUSG00000053137	Mapk11	0.00013	0.00062	0.037	1	12	0.19
ENSMUSG00000029135	Fosl2	0.00019	0.00056	0.00085	0.44	12	0.19
ENSMUSG00000022269	Mar-11	0.015	0.18	0.034	0.56	12	0.18
ENSMUSG00000078235	Fam43b	0.00078	5.50E-05	5.00E-05	0.11	12	0.18
ENSMUSG00000055805	Fmnl1	0.0053	2.50E-06	0.0041	0.13	12	0.18
ENSMUSG00000022893	Adamts1	0.0036	0.006	0.00043	0.14	12	0.18
ENSMUSG00000037169	Mycn	0.011	0.17	0.0095	0.1	12	0.18
ENSMUSG00000045314	Sowahb	0.00092	0.013	0.00048	0.2	12	0.18
ENSMUSG00000004460	Dnajb11	0.00017	0.074	0.011	0.42	12	0.17
ENSMUSG00000031217	Efnb1	0.037	0.13	0.024	1	12	0.17
ENSMUSG00000021253	Tgfb3	0.0011	7.90E-06	0.0012	1	12	0.17
ENSMUSG00000044548	Dact1	0.014	0.13	0.001	0.21	12	0.17
ENSMUSG00000030748	Il4ra	0.0032	2.10E-05	0.043	0.78	12	0.17
ENSMUSG00000004891	Nes	0.0026	0.17	0.00019	1	12	0.16
ENSMUSG00000035898	Uba6	0.0044	2.10E-05	0.0062	0.11	12	0.16
ENSMUSG00000024966	Stip1	1.80E-05	0.0021	5.40E-05	0.5	12	0.16
ENSMUSG00000029657	Hsph1	6.30E-05	0.003	0.0037	0.095	12	0.15
ENSMUSG00000006705	Pknox1	0.00019	0.37	0.031	1	12	0.15
ENSMUSG00000041220	Elovl6	0.0058	0.023	0.012	0.46	12	0.15
ENSMUSG00000030357	Fkbp4	0.0014	0.082	0.022	0.74	12	0.15
ENSMUSG00000086118	Gm14169	0.015	0.06	0.043	1	12	0.15
ENSMUSG00000057101	Zfp180	1.90E-05	0.035	0.00085	1	12	0.15
ENSMUSG00000017144	Rnd3	0.00015	4.70E-05	0.0033	0.42	12	0.15
ENSMUSG00000025232	Hexa	0.00052	0.024	5.40E-05	0.54	12	0.15

Ensembl_ ID	Gene	q_C	q_SD3	q_SD6	q_SD12	C_Phase	Amp
ENSMUSG00000069763	Tmem100	0.0021	0.067	0.0095	0.81	12	0.14
ENSMUSG00000031068	Glrx3	0.031	0.3	0.026	1	12	0.14
ENSMUSG00000063229	Ldha	0.031	1	0.00073	0.58	12	0.14
ENSMUSG00000021037	Ahsa1	3.00E-05	0.0056	0.00064	0.16	12	0.14
ENSMUSG00000027540	Ptpn1	0.0072	0.024	0.00058	1	12	0.14
ENSMUSG00000021728	Emb	0.0058	0.006	0.012	0.48	12	0.14
ENSMUSG00000035900	Gramd4	0.0053	0.07	0.013	0.26	12	0.14
ENSMUSG00000029701	Rbm28	0.0018	0.045	0.049	0.37	12	0.14
ENSMUSG00000021951	N6amt2	0.0048	1	0.029	1	12	0.14
ENSMUSG00000026227	2810459M11Rik	0.04	0.042	0.046	0.71	12	0.14
ENSMUSG00000024691	Fam111a	0.02	0.045	0.049	1	12	0.14
ENSMUSG00000030898	Cckbr	0.022	1.40E-06	0.018	0.22	12	0.14
ENSMUSG00000030956	Fam53b	0.0065	0.029	0.0037	0.13	12	0.14
ENSMUSG00000079043	Fastkd5	0.014	0.063	0.013	0.41	12	0.14
ENSMUSG00000044847	Lsm11	0.00013	1	0.0018	1	12	0.13
ENSMUSG00000022765	Snap29	0.024	0.031	0.0037	0.13	12	0.13
ENSMUSG00000067279	Ppp1r3c	0.00035	0.01	0.018	1	12	0.13
ENSMUSG00000018648	Dusp14	0.0079	2.00E-05	0.046	0.83	12	0.13
ENSMUSG00000025277	Abhd6	0.0079	0.00014	0.0062	0.5	12	0.13
ENSMUSG00000022114	Spry2	0.004	0.18	5.40E-05	0.41	12	0.13
ENSMUSG00000021365	Nedd9	0.0044	0.078	0.017	1	12	0.13
ENSMUSG00000054893	Zfp667	0.043	0.02	0.0026	0.6	12	0.12
ENSMUSG00000032316	Clk3	0.0021	0.0082	0.0079	0.58	12	0.12
ENSMUSG00000006736	Tspan31	0.0016	0.46	0.017	1	12	0.12
ENSMUSG00000003348	Mob3a	0.024	1	0.049	0.68	12	0.12
ENSMUSG00000027286	Lrrc57	0.0032	0.1	0.037	0.54	12	0.12
ENSMUSG00000018572	Phf23	0.0072	0.0082	0.0095	0.42	12	0.12
ENSMUSG00000097417	Gm26669	0.0029	2.10E-05	0.02	0.1	12	0.12
ENSMUSG00000030272	Camk1	0.001	0.07	0.0015	0.71	12	0.12
ENSMUSG00000075327	Zbtb2	0.0095	0.15	0.017	0.39	12	0.11
ENSMUSG00000049327	Setd8	0.034	0.037	0.02	0.81	12	0.11
ENSMUSG00000027583	Zbtb46	0.026	0.25	0.046	1	12	0.11
ENSMUSG00000019806	Aig1	0.001	0.074	0.029	1	12	0.11
ENSMUSG00000046417	Lrrc75a	0.011	0.18	0.002	0.14	12	0.11
ENSMUSG00000049532	Sall2	0.0032	0.0088	0.0054	0.31	12	0.11
ENSMUSG00000001143	Lman2l	0.02	0.8	0.049	1	12	0.11
ENSMUSG00000021890	Eaf1	0.029	1	0.034	1	12	0.1
ENSMUSG00000044715	Gskip	0.024	0.14	0.0041	0.95	12	0.1
ENSMUSG00000032285	Dnaja4	0.047	0.082	0.046	1	12	0.1
ENSMUSG00000032437	Stt3b	0.0014	0.55	0.0037	1	12	0.1
ENSMUSG00000020923	Ubtf	0.00047	0.0088	0.0054	1	12	0.1
ENSMUSG00000026626	Ppp2r5a	0.02	0.0095	0.037	0.17	12	0.1
ENSMUSG00000045969	Ing1	0.0087	0.063	5.40E-05	0.12	12	0.099
ENSMUSG00000030521	Mphosph10	0.0014	0.23	0.022	0.29	12	0.097
ENSMUSG00000046093	Hpcal4	0.013	1	0.0023	1	12	0.096
ENSMUSG00000057469	E2f6	0.034	0.026	0.026	1	12	0.095
ENSMUSG00000027562	Car2	0.043	1	0.046	1	12	0.094

Ensembl_ ID	Gene	q_C	q_SD3	q_SD6	q_SD12	C_Phase	Amp
ENSMUSG00000019804	Snx3	0.0023	0.013	0.012	1	12	0.093
ENSMUSG00000035105	Egln3	0.04	0.93	0.0062	1	12	0.092
ENSMUSG00000022607	Ptk2	0.0026	0.36	0.046	1	12	0.092
ENSMUSG00000004056	Akt2	0.0058	0.0088	0.049	1	12	0.091
ENSMUSG00000022505	Emp2	0.037	0.2	0.018	1	12	0.091
ENSMUSG00000030134	Rasgef1a	0.0079	0.0021	0.0023	1	12	0.089
ENSMUSG00000067586	S1pr3	0.024	1	0.022	0.54	12	0.087
ENSMUSG00000035620	Ric8b	0.0079	0.013	0.013	0.066	12	0.085
ENSMUSG00000043388	Tmem130	0.00019	0.14	0.034	0.62	12	0.085
ENSMUSG00000044864	Ankrd50	0.0021	0.1	0.015	1	12	0.078
ENSMUSG00000005936	Kctd20	0.031	1	0.0041	1	12	0.078
ENSMUSG00000052214	Opa3	0.0058	0.11	0.0025	0.62	12	0.077
ENSMUSG00000032249	Anp32a	0.034	0.62	0.026	1	12	0.075
ENSMUSG00000028656	Cap1	0.00035	0.033	0.00019	1	12	0.073
ENSMUSG00000023944	Hsp90ab1	0.001	0.16	0.00054	0.86	12	0.073
ENSMUSG00000021360	Gcnt2	0.014	0.0014	0.024	1	12	0.071
ENSMUSG00000020246	Hcfc2	0.029	0.56	0.022	1	12	0.07
ENSMUSG00000030870	Ubfd1	0.0048	1	0.024	1	12	0.069
ENSMUSG00000030286	Emc3	0.0044	0.43	0.026	1	12	0.069
ENSMUSG00000022587	Ly6e	0.02	0.029	0.02	1	12	0.066
ENSMUSG00000026080	Chst10	0.043	0.46	0.0026	0.36	12	0.065
ENSMUSG00000032026	Rexo2	0.0018	0.13	0.0018	1	12	0.064
ENSMUSG00000033732	Sf3b3	0.0095	0.05	0.022	0.95	12	0.06
ENSMUSG00000025190	Got1	0.031	0.29	0.046	0.91	12	0.056
ENSMUSG00000006763	Saal1	0.0095	1	0.022	1	12	0.054
ENSMUSG00000052833	Sae1	0.029	1	0.034	1	12	0.053
ENSMUSG00000043259	Fam13c	0.017	0.0018	0.031	1	12	0.053
ENSMUSG00000031948	Kars	0.0029	0.42	0.046	1	12	0.053
ENSMUSG00000020864	Ankrd40	0.0065	0.34	0.017	1	12	0.048
ENSMUSG00000027184	Caprin1	0.029	0.11	0.04	0.6	12	0.047
ENSMUSG00000020142	Slc1a4	0.037	1	0.043	1	12	0.025
ENSMUSG00000056749	Nfil3	2.20E-05	7.90E-06	5.00E-05	0.087	15	0.35
ENSMUSG00000027861	Casq2	3.50E-05	0.13	0.046	0.34	15	0.31
ENSMUSG00000032373	Car12	0.047	0.24	0.024	0.52	15	0.25
ENSMUSG00000037474	Dtl	0.0013	0.21	0.0087	0.34	15	0.24
ENSMUSG00000039114	Nrn1	0.0011	0.46	0.018	1	15	0.17
ENSMUSG00000020000	Moxd1	0.0095	0.078	0.026	0.81	15	0.16
ENSMUSG00000070532	Ccdc190	0.0095	0.045	0.0029	0.83	15	0.16
ENSMUSG00000041193	Pla2g5	0.0044	0.23	0.015	1	15	0.15
ENSMUSG00000041959	S100a10	0.017	0.53	0.046	1	15	0.14
ENSMUSG00000001700	Gramd3	0.00061	0.14	9.30E-05	1	15	0.12
ENSMUSG00000042369	Rbm45	0.001	0.24	0.013	1	15	0.1
ENSMUSG00000050711	Scg2	0.022	0.067	0.049	1	15	0.098
ENSMUSG00000075012	Fjx1	0.013	0.64	0.043	0.26	15	0.091
ENSMUSG00000029659	Medag	0.04	0.36	0.018	0.83	15	0.09
ENSMUSG00000021373	Cap2	7.70E-05	0.00062	0.013	1	15	0.084
ENSMUSG00000037712	Fermt2	0.00092	0.074	0.0026	1	15	0.083

Ensembl_ ID	Gene	q_C	q_SD3	q_SD6	q_SD12	C_Phase	Amp
ENSMUSG00000045092	S1pr1	0.031	0.048	0.046	1	15	0.05
ENSMUSG00000019874	Fabp7	0.0032	0.0088	0.0079	0.055	18	0.3
ENSMUSG00000027875	Hmgcs2	0.00013	0.0032	0.001	1	18	0.3
ENSMUSG00000024256	Adcyap1	0.0087	0.88	0.029	0.91	18	0.15
ENSMUSG00000038879	Nipal2	0.04	0.016	0.0095	1	18	0.092
ENSMUSG00000021065	Fut8	0.02	0.39	0.049	0.91	18	0.09
ENSMUSG00000079477	Rab7	0.014	0.75	0.012	1	18	0.043
ENSMUSG00000051354	Samd3	0.00031	0.027	0.04	1	21	0.43
ENSMUSG00000047363	Cstad	0.00017	0.057	0.034	0.1	21	0.34
ENSMUSG00000052525	Spdya	0.034	0.37	0.018	1	21	0.33
ENSMUSG00000042857	Gm9776	0.00023	0.12	0.0095	0.86	21	0.32
ENSMUSG00000097321	1700028E10Rik	0.0079	0.33	0.026	1	21	0.29
ENSMUSG00000053414	Hunk	0.00019	1.70E-05	0.0015	0.18	21	0.28
ENSMUSG00000089889	0610040B10Rik	0.001	1	0.04	1	21	0.27
ENSMUSG00000020363	Gfpt2	0.0029	0.0018	0.0023	1	21	0.27
ENSMUSG00000032940	Rbm11	0.00019	0.027	0.002	0.26	21	0.26
ENSMUSG00000100017	2410022M11Rik	1.80E-05	0.04	0.046	0.13	21	0.26
ENSMUSG00000030089	Slc41a3	0.00041	0.33	0.0054	0.25	21	0.23
ENSMUSG00000097675	1700101I11Rik	0.0048	0.033	0.022	1	21	0.23
ENSMUSG00000097164	Cep83os	0.00035	0.0014	0.0095	0.087	21	0.23
ENSMUSG00000087479	Gm16835	0.022	0.39	0.012	1	21	0.22
ENSMUSG00000020653	Klf11	0.004	0.017	0.0029	0.26	21	0.22
ENSMUSG00000000811	Txnrd3	0.0014	0.0023	0.0029	0.23	21	0.22
ENSMUSG00000042851	Zc3h6	0.0011	0.17	0.034	0.079	21	0.21
ENSMUSG00000006411	Pvrl4	0.0087	0.33	0.046	1	21	0.2
ENSMUSG00000021902	Phf7	0.012	0.029	0.0062	1	21	0.19
ENSMUSG00000073565	Prr16	0.0065	0.045	0.049	0.42	21	0.19
ENSMUSG00000000126	Wnt9a	0.0053	0.0019	0.049	1	21	0.19
ENSMUSG00000028133	Rwdd3	8.20E-06	0.19	0.026	0.6	21	0.18
ENSMUSG00000097638	Carlr	0.015	0.06	0.0026	0.28	21	0.17
ENSMUSG00000042213	Zfand4	0.0021	0.5	0.0087	0.39	21	0.17
ENSMUSG00000050312	Nsun3	0.029	0.42	0.0033	0.71	21	0.17
ENSMUSG00000028636	Ppcs	0.043	0.057	0.046	0.37	21	0.17
ENSMUSG00000020930	Ccdc103	0.019	0.07	0.043	0.68	21	0.17
ENSMUSG00000052395	Rft1	0.0029	0.05	0.0095	0.25	21	0.17
ENSMUSG00000047446	Arl4a	0.00078	0.0082	0.037	0.3	21	0.16
ENSMUSG00000020639	Pfn4	0.00015	5.00E-04	0.029	0.34	21	0.16
ENSMUSG00000032397	Tipin	8.20E-06	0.0038	0.0079	0.11	21	0.16
ENSMUSG00000022833	Ccdc14	0.00011	0.71	0.02	0.52	21	0.15
ENSMUSG00000028653	Trit1	0.0053	0.45	0.0071	0.66	21	0.15
ENSMUSG00000048920	Fkrp	0.017	0.0082	0.024	0.12	21	0.14
ENSMUSG00000050796	B3galt6	0.00027	0.11	0.043	0.39	21	0.13
ENSMUSG00000054723	Vmac	0.022	1	0.029	1	21	0.13
ENSMUSG00000054770	Kctd18	0.015	1	0.029	1	21	0.13
ENSMUSG00000034173	Zbed5	0.00092	0.096	0.026	0.74	21	0.13
ENSMUSG00000041471	Fam35a	0.02	0.12	0.024	1	21	0.12
ENSMUSG00000029802	Abcg2	0.0095	0.013	0.024	0.34	21	0.12

Ensembl_ ID	Gene	q_C	q_SD3	q_SD6	q_SD12	C_Phase	Amp
ENSMUSG00000052616	Ccdc79	0.026	1	0.046	1	21	0.11
ENSMUSG00000072946	Ptgr2	0.00017	0.031	0.029	0.66	21	0.11
ENSMUSG00000021646	Mccc2	0.00052	0.048	0.013	0.56	21	0.11
ENSMUSG00000045140	Pigw	0.0048	0.37	0.0095	0.33	21	0.11
ENSMUSG00000020311	Erlec1	0.0044	1	0.04	0.83	21	0.11
ENSMUSG00000025086	Trub1	0.0011	0.18	0.04	1	21	0.1
ENSMUSG00000024172	St6gal2	0.011	0.24	0.017	1	21	0.1
ENSMUSG00000057147	Dph6	0.00041	1	0.04	1	21	0.095
ENSMUSG00000033439	Trmt13	0.031	0.11	0.026	1	21	0.092
ENSMUSG00000063200	Nol7	0.00047	1	0.046	1	21	0.091
ENSMUSG00000046079	Lrrc8d	0.022	0.34	0.018	1	21	0.089
ENSMUSG00000055553	Kxd1	0.012	0.091	0.0087	0.25	21	0.081
ENSMUSG00000021007	Spata7	0.0029	1	0.043	1	21	0.077
ENSMUSG00000060890	Arr3	0.0018	0.023	0.42	1	0	0.37
ENSMUSG00000097797	Gm26901	0.043	0.013	0.15	0.76	0	0.3
ENSMUSG00000076612	Ighg2c	0.019	0.0019	0.75	1	0	0.25
ENSMUSG00000049580	Tsku	0.04	0.0019	0.067	0.52	0	0.23
ENSMUSG00000031285	Dcx	0.0044	0.021	0.084	1	0	0.22
ENSMUSG00000091272	Gm17641	0.014	0.014	0.071	1	0	0.21
ENSMUSG00000031167	Rbm3	3.50E-05	0.00011	0.067	0.31	0	0.2
ENSMUSG00000032245	Cln6	0.014	0.0016	0.11	1	0	0.18
ENSMUSG00000038393	Txnip	0.00078	0.0018	0.1	0.13	0	0.17
ENSMUSG00000015882	Lcorl	0.0013	0.039	0.33	1	0	0.17
ENSMUSG00000042804	Gpr153	0.031	0.037	0.22	1	0	0.15
ENSMUSG00000029208	Guf1	0.0065	0.006	0.17	0.66	0	0.15
ENSMUSG00000035064	Eef2k	0.0032	3.00E-04	0.097	0.52	0	0.15
ENSMUSG00000040044	Orc3	0.0032	0.004	0.067	0.12	0	0.14
ENSMUSG00000035967	Ddx26b	0.0079	0.013	0.17	0.36	0	0.14
ENSMUSG00000033060	Lmo7	0.0087	0.0038	0.44	1	0	0.13
ENSMUSG00000042032	Mat2b	0.00092	0.006	0.55	1	0	0.13
ENSMUSG00000035944	Ttc38	0.022	0.021	0.59	0.5	0	0.13
ENSMUSG00000037890	Wdr19	0.014	2.10E-05	0.62	0.16	0	0.13
ENSMUSG00000026484	Rnf2	0.0021	0.013	0.12	0.86	0	0.13
ENSMUSG00000027346	Gpcpd1	0.00092	0.00035	0.17	0.64	0	0.13
ENSMUSG00000028211	Trp53inp1	0.037	0.00062	0.097	0.14	0	0.13
ENSMUSG00000036192	Rorb	0.026	0.04	0.32	1	0	0.12
ENSMUSG00000022797	Tfrc	0.0044	0.048	0.29	1	0	0.11
ENSMUSG00000000223	Drp2	0.043	0.006	0.19	1	0	0.11
ENSMUSG00000037434	Slc30a1	0.00078	0.0038	0.11	0.11	0	0.11
ENSMUSG00000055493	Epm2a	0.0011	0.0082	0.12	0.71	0	0.1
ENSMUSG00000024835	Coro1b	0.034	0.018	0.9	0.95	0	0.095
ENSMUSG00000074892	B3galt5	0.034	3.00E-04	0.14	0.18	0	0.093
ENSMUSG00000066357	Wdr6	0.037	0.027	0.078	0.64	0	0.093
ENSMUSG00000078161	Erich3	0.026	0.015	1	1	0	0.09
ENSMUSG00000044308	Ubr3	0.00027	0.012	0.067	0.54	0	0.089
ENSMUSG00000062373	Tmem65	0.024	0.014	0.9	1	0	0.088
ENSMUSG00000078490	Cfap74	0.0065	0.027	0.071	0.74	0	0.087

Ensembl_ ID	Gene	q_C	q_SD3	q_SD6	q_SD12	C_Phase	Amp
ENSMUSG00000042272	Sestd1	0.047	0.029	0.26	0.66	0	0.086
ENSMUSG00000015879	Fam184b	0.0072	0.031	1	1	0	0.084
ENSMUSG00000045174	Amer3	0.047	0.0065	0.12	0.78	0	0.084
ENSMUSG00000040850	Psme4	0.024	0.029	0.26	1	0	0.081
ENSMUSG00000038332	Sesn1	0.013	0.0065	0.067	0.78	0	0.075
ENSMUSG00000034295	Fhod3	0.012	3.00E-04	0.29	0.95	0	0.071
ENSMUSG00000047037	Nipa1	0.0087	0.00035	0.29	1	0	0.067
ENSMUSG00000044022	Pcdhb21	0.0013	0.0023	0.42	1	0	0.066
ENSMUSG00000056367	Actr3b	0.019	0.00056	0.33	0.34	0	0.064
ENSMUSG00000028098	Rnf115	0.0087	0.0095	0.27	0.059	0	0.06
ENSMUSG00000005262	Ufd1l	0.04	0.0034	1	0.54	0	0.057
ENSMUSG00000041483	Zfp281	0.017	0.0044	0.64	0.5	0	0.054
ENSMUSG00000000276	Dgke	0.043	0.0048	0.62	1	0	0.052
ENSMUSG00000020628	Trappc12	0.02	0.031	0.19	0.88	0	0.051
ENSMUSG00000062190	Lancl2	0.04	0.0027	0.67	1	0	0.05
ENSMUSG00000022010	Tsc22d1	0.011	0.048	0.054	1	0	0.046
ENSMUSG00000002831	Plin4	8.40E-05	0.00062	0.078	0.26	3	0.6
ENSMUSG00000007877	Tcap	0.017	0.0056	0.15	1	3	0.32
ENSMUSG00000030711	Sult1a1	0.037	0.00012	0.1	0.97	3	0.27
ENSMUSG00000025324	Atp10a	0.004	0.00066	0.067	0.079	3	0.26
ENSMUSG00000024066	Xdh	0.0095	3.30E-05	0.13	0.07	3	0.26
ENSMUSG00000032278	Paqr5	0.0044	0.00073	0.1	0.13	3	0.25
ENSMUSG00000008845	Cd163	0.017	0.0088	0.071	1	3	0.24
ENSMUSG00000021025	Nfkbia	0.029	1.50E-05	0.23	0.095	3	0.2
ENSMUSG00000041957	Pkp2	0.031	0.014	0.26	0.83	3	0.2
ENSMUSG00000033083	Tbc1d4	0.001	0.042	0.13	0.52	3	0.16
ENSMUSG00000022610	Mapk12	0.00019	0.017	0.44	0.86	3	0.16
ENSMUSG00000036856	Wnt4	0.031	0.00015	1	1	3	0.16
ENSMUSG00000002910	Arrdc2	0.0095	0.016	0.24	1	3	0.15
ENSMUSG00000039634	Zfp189	0.022	0.0015	0.42	0.42	3	0.14
ENSMUSG00000045954	Sdpr	0.00031	0.0027	0.15	0.56	3	0.14
ENSMUSG00000048706	Lurap1l	0.043	0.018	1	0.39	3	0.11
ENSMUSG00000037235	Mxd4	0.037	0.021	0.11	1	3	0.1
ENSMUSG00000005951	Shpk	0.02	0.0034	0.078	0.86	3	0.096
ENSMUSG00000040010	Slc7a5	0.014	0.0019	0.21	0.23	3	0.095
ENSMUSG00000030747	Dgat2	0.022	0.007	0.067	0.3	3	0.09
ENSMUSG00000046999	1110032F04Rik	0.014	0.0082	0.22	1	3	0.086
ENSMUSG00000020823	Sec14l1	0.012	0.007	0.1	0.5	3	0.083
ENSMUSG00000030168	Adipor2	0.019	1.30E-05	0.071	0.21	3	0.079
ENSMUSG00000019894	Slc6a15	0.022	0.029	0.87	1	3	0.058
ENSMUSG00000030048	Gkn3	0.0023	0.00032	0.062	0.66	6	0.33
ENSMUSG00000038059	Smim3	0.024	0.015	0.17	0.41	6	0.2
ENSMUSG00000031431	Tsc22d3	0.0032	4.10E-07	0.062	0.075	6	0.2
ENSMUSG00000069833	Ahnak	0.0014	0.0048	0.38	0.44	6	0.18
ENSMUSG00000054280	Prr14l	0.0018	0.0095	0.75	1	6	0.13
ENSMUSG00000034000	Neu4	0.012	0.048	0.48	0.56	6	0.12
ENSMUSG00000019726	Lyst	0.0065	0.0021	0.2	0.31	6	0.12

Ensembl_ ID	Gene	q_C	q_SD3	q_SD6	q_SD12	C_Phase	Amp
ENSMUSG00000035067	Xkr6	0.047	0.0065	0.55	1	6	0.11
ENSMUSG00000040584	Abcb1a	0.011	0.031	0.071	0.29	6	0.1
ENSMUSG00000028452	Vcp	0.043	0.026	0.46	0.81	6	0.073
ENSMUSG00000035851	Ythdc1	0.0014	0.011	1	1	6	0.064
ENSMUSG00000033316	Galnt9	0.00013	0.004	0.097	1	9	0.4
ENSMUSG00000042216	Sgsm1	8.20E-06	0.0044	0.15	1	9	0.33
ENSMUSG00000067578	Cbln4	0.0023	0.0088	0.22	1	9	0.3
ENSMUSG00000091971	Hspa1a	0.012	0.018	0.15	0.11	9	0.26
ENSMUSG00000074575	Kcng1	0.013	0.0076	0.2	0.079	9	0.26
ENSMUSG00000078684	5830417I10Rik	0.00011	0.006	0.37	0.41	9	0.24
ENSMUSG00000003545	Fosb	0.013	3.30E-08	0.067	0.18	9	0.23
ENSMUSG00000035711	Dok3	0.04	0.029	0.091	0.14	9	0.23
ENSMUSG00000015656	Hspa8	0.015	0.0065	0.23	0.62	9	0.23
ENSMUSG00000016179	Camk1g	2.20E-05	0.04	0.57	1	9	0.22
ENSMUSG00000021676	Iqgap2	2.20E-05	0.0095	0.21	1	9	0.22
ENSMUSG00000035671	Zswim4	0.0032	0.004	0.084	0.28	9	0.21
ENSMUSG00000038894	Irs2	8.40E-05	1.00E-05	0.38	1	9	0.21
ENSMUSG00000025372	Baiap2	0.0053	0.0014	0.16	0.5	9	0.2
ENSMUSG00000001247	Lsr	0.015	0.004	0.27	0.5	9	0.19
ENSMUSG00000061132	Blnk	0.026	0.015	0.15	1	9	0.19
ENSMUSG00000027520	Zdbf2	0.02	0.012	0.81	0.3	9	0.19
ENSMUSG00000034275	Igsf9b	0.00017	0.00011	0.62	0.48	9	0.19
ENSMUSG00000039813	Tbc1d2	0.0032	0.0038	0.27	0.25	9	0.19
ENSMUSG00000037014	Sstr4	0.02	0.048	0.48	1	9	0.18
ENSMUSG00000048878	Hexim1	0.0065	5.50E-06	0.058	0.14	9	0.18
ENSMUSG00000022012	Enox1	9.50E-05	0.011	0.38	1	9	0.18
ENSMUSG00000005958	Ephb3	0.022	0.033	0.058	0.6	9	0.17
ENSMUSG00000089762	Ier5l	0.031	0.024	0.4	0.42	9	0.17
ENSMUSG00000015605	Srf	0.0058	3.30E-05	0.091	0.33	9	0.17
ENSMUSG00000030782	Tgfb1i1	0.0079	0.045	0.26	1	9	0.17
ENSMUSG00000022136	Dnajc3	0.00052	0.0015	0.23	0.22	9	0.16
ENSMUSG00000006362	Cbfa2t3	0.0013	4.40E-08	0.15	0.075	9	0.16
ENSMUSG00000031821	Gins2	0.0044	0.00032	0.24	0.81	9	0.16
ENSMUSG00000035621	Midn	0.024	2.50E-06	0.2	0.31	9	0.16
ENSMUSG00000045613	Chrm2	0.013	0.04	0.058	0.64	9	0.15
ENSMUSG00000020387	Jade2	0.0013	0.007	0.3	0.81	9	0.15
ENSMUSG00000021366	Hivep1	0.0029	3.00E-04	0.097	0.71	9	0.15
ENSMUSG00000015944	Gatsl2	7.00E-04	0.0032	0.084	0.079	9	0.14
ENSMUSG00000031608	Galnt7	0.0018	0.01	0.13	0.3	9	0.14
ENSMUSG00000032012	Pvrl1	0.012	0.0015	0.81	1	9	0.14
ENSMUSG00000044352	Sowaha	0.0053	0.00011	0.14	0.41	9	0.14
ENSMUSG00000028402	Mpdz	0.031	0.045	0.19	0.41	9	0.13
ENSMUSG00000022799	Arhgap31	0.00015	0.029	0.52	1	9	0.13
ENSMUSG00000022951	Rcan1	0.00027	0.0082	0.13	0.29	9	0.13
ENSMUSG00000027351	Spred1	0.00035	0.00015	0.084	1	9	0.13
ENSMUSG00000025582	Nptx1	0.0013	0.033	0.22	0.91	9	0.13
ENSMUSG00000061143	Maml3	0.00041	0.027	0.84	1	9	0.13

Ensembl_ ID	Gene	q_C	q_SD3	q_SD6	q_SD12	C_Phase	Amp
ENSMUSG00000033618	Map3k13	0.0021	0.0015	0.1	0.33	9	0.13
ENSMUSG00000071862	Lrrtm2	0.013	0.0052	0.62	0.28	9	0.13
ENSMUSG00000041130	Zfp598	0.031	0.004	0.29	0.76	9	0.13
ENSMUSG00000030199	Etv6	0.017	0.007	0.19	0.34	9	0.13
ENSMUSG00000033730	Egr3	0.0087	4.20E-05	1	1	9	0.12
ENSMUSG00000016757	Ttll12	0.0048	0.011	0.78	0.97	9	0.12
ENSMUSG00000039735	Fnbp1l	0.0079	0.0056	0.29	0.29	9	0.12
ENSMUSG00000035275	Raver2	0.0032	0.0019	0.054	0.36	9	0.11
ENSMUSG00000061353	Cxcl12	0.0072	0.015	0.2	0.16	9	0.11
ENSMUSG00000054196	Cthrc1	0.029	0.037	0.57	0.42	9	0.11
ENSMUSG00000038496	Slc19a3	0.034	0.033	1	1	9	0.11
ENSMUSG00000091474	2610021A01Rik	0.0026	0.0082	1	0.48	9	0.11
ENSMUSG00000024789	Jak2	0.0023	0.0032	0.2	0.86	9	0.11
ENSMUSG00000039449	Prpf18	0.004	0.0065	0.26	0.66	9	0.11
ENSMUSG00000039372	Mar-04	0.0029	0.0034	0.23	1	9	0.1
ENSMUSG00000033565	Rbfox2	8.20E-06	0.0076	0.48	1	9	0.1
ENSMUSG00000029822	Osbpl3	0.0036	0.026	0.16	1	9	0.1
ENSMUSG00000024817	Uhrf2	0.0014	0.013	0.38	0.14	9	0.1
ENSMUSG00000020882	Cacnb1	0.02	0.0027	0.27	1	9	0.1
ENSMUSG00000028385	Snx30	0.0044	0.0065	0.054	0.64	9	0.1
ENSMUSG00000058881	Zfp516	0.037	0.02	0.44	0.26	9	0.1
ENSMUSG00000022419	Deptor	0.013	0.00066	1	0.54	9	0.1
ENSMUSG00000035566	Pcdh17	0.0011	0.018	0.81	0.58	9	0.1
ENSMUSG00000040896	Kcnd3	0.0016	0.0019	1	1	9	0.1
ENSMUSG00000034613	Ppm1h	0.0087	0.018	0.4	1	9	0.099
ENSMUSG00000020074	Ccar1	0.00017	0.027	0.16	0.46	9	0.099
ENSMUSG00000047466	8030462N17Rik	0.019	0.0034	0.9	0.86	9	0.095
ENSMUSG00000050600	Zfp831	0.0065	0.0065	0.15	0.34	9	0.095
ENSMUSG00000063455	D630045J12Rik	0.0018	0.00025	1	0.54	9	0.094
ENSMUSG00000036698	Ago2	0.0053	0.007	1	1	9	0.093
ENSMUSG00000006456	Rbm14	0.0048	0.0082	0.33	0.44	9	0.092
ENSMUSG00000054808	Actn4	0.0032	0.042	0.38	1	9	0.092
ENSMUSG00000042599	Kdm7a	0.043	8.50E-05	0.27	0.07	9	0.09
ENSMUSG00000030854	Ptpn5	0.04	0.0088	0.14	1	9	0.089
ENSMUSG00000037541	Shank2	0.0016	0.0095	0.78	1	9	0.086
ENSMUSG00000028804	Csmd2	0.02	0.015	1	1	9	0.084
ENSMUSG00000065954	Tacc1	0.0087	0.00035	0.071	0.17	9	0.081
ENSMUSG00000015501	Hivep2	0.017	0.0013	1	1	9	0.081
ENSMUSG00000034832	Tet3	0.011	0.004	0.84	0.62	9	0.08
ENSMUSG00000097545	Mir124a-1hg	0.04	0.026	0.062	0.52	9	0.079
ENSMUSG00000036225	Kctd1	0.043	0.027	0.084	1	9	0.078
ENSMUSG00000037815	Ctnna1	0.00047	0.045	0.058	0.46	9	0.076
ENSMUSG00000039671	Zmynd8	0.004	0.0095	0.81	1	9	0.074
ENSMUSG00000072875	Gpr27	0.034	0.017	0.2	0.42	9	0.073
ENSMUSG00000022494	Shisa9	0.029	0.04	0.57	0.71	9	0.072
ENSMUSG00000057637	Prdm2	0.0032	0.00043	1	0.26	9	0.072
ENSMUSG00000021039	Snw1	0.00061	0.027	0.5	1	9	0.071

Ensembl_ ID	Gene	q_C	q_SD3	q_SD6	q_SD12	C_Phase	Amp
ENSMUSG00000042508	Dmtf1	0.0032	0.024	0.23	1	9	0.071
ENSMUSG00000019188	H13	0.0058	0.004	0.21	0.68	9	0.068
ENSMUSG00000021779	Thrb	0.011	0.011	0.84	1	9	0.067
ENSMUSG00000032187	Smarca4	0.043	0.045	0.42	1	9	0.066
ENSMUSG00000022237	Ankrd33b	0.0058	0.0044	0.52	0.91	9	0.066
ENSMUSG00000037933	Bicd2	0.031	0.037	1	0.62	9	0.065
ENSMUSG00000009569	Mkl2	0.0018	0.0088	1	0.64	9	0.063
ENSMUSG00000004360	9330159F19Rik	0.012	0.00044	1	0.23	9	0.063
ENSMUSG00000062232	Rapgef2	0.00052	0.0056	0.19	0.95	9	0.06
ENSMUSG00000044968	Napepld	0.047	0.018	1	0.3	9	0.055
ENSMUSG00000010797	Wnt2	0.00078	0.021	0.22	1	12	0.37
ENSMUSG00000024014	Pim1	0.011	6.00E-05	0.13	0.81	12	0.25
ENSMUSG00000028214	Gem	0.0058	0.035	0.058	1	12	0.23
ENSMUSG00000060594	Layn	0.0021	0.0019	0.1	0.97	12	0.23
ENSMUSG00000001774	Chordc1	0.0048	0.0032	0.19	0.18	12	0.22
ENSMUSG00000037992	Rara	0.004	0.0082	0.16	1	12	0.22
ENSMUSG00000051590	Map3k19	7.00E-04	0.0019	0.12	1	12	0.21
ENSMUSG00000030110	Ret	0.0011	0.0023	0.27	1	12	0.21
ENSMUSG00000032265	Fam46a	0.0018	0.0065	0.062	1	12	0.19
ENSMUSG00000044224	Dnajc21	0.0048	0.00062	0.084	0.23	12	0.18
ENSMUSG00000031538	Plat	0.00061	0.0018	0.084	0.62	12	0.18
ENSMUSG00000021675	F2rl2	0.031	0.048	0.071	1	12	0.17
ENSMUSG00000020048	Hsp90b1	0.00031	0.012	0.097	1	12	0.17
ENSMUSG00000000531	Grasp	0.0053	0.0023	0.11	0.25	12	0.15
ENSMUSG00000021866	Anxa11	0.04	0.005	1	1	12	0.15
ENSMUSG00000061517	Sox21	0.012	0.00015	0.38	0.13	12	0.14
ENSMUSG00000021743	Fezf2	0.012	0.016	0.38	1	12	0.13
ENSMUSG00000051515	Fam181b	0.04	0.00073	0.33	0.28	12	0.13
ENSMUSG00000027248	Pdia3	7.00E-04	0.045	0.058	0.29	12	0.13
ENSMUSG00000044017	Adgrd1	0.034	0.0032	0.15	1	12	0.13
ENSMUSG00000034403	Pja1	0.017	0.0048	0.15	0.91	12	0.13
ENSMUSG00000040738	Ints8	0.0079	0.018	0.084	0.11	12	0.12
ENSMUSG00000035126	Wdr78	0.047	0.014	0.16	0.33	12	0.12
ENSMUSG00000031673	Cdh11	0.019	0.00014	0.19	1	12	0.12
ENSMUSG00000028243	Ubxn2b	0.0036	0.0021	0.3	0.86	12	0.12
ENSMUSG00000045034	Ankrd34b	0.0029	0.04	0.4	0.66	12	0.11
ENSMUSG00000022332	Khdrbs3	7.00E-04	0.0019	0.12	1	12	0.11
ENSMUSG00000068566	Myadm	0.0018	0.00022	0.38	1	12	0.11
ENSMUSG00000038074	Fkbp14	0.0087	0.01	0.93	0.97	12	0.11
ENSMUSG00000039037	St6galnac5	0.047	0.0034	0.12	1	12	0.11
ENSMUSG00000026482	Rgl1	0.0029	0.031	0.15	1	12	0.11
ENSMUSG00000064065	Ipcef1	0.0072	0.017	0.19	1	12	0.1
ENSMUSG00000057060	Slc35f3	0.031	0.035	0.4	1	12	0.1
ENSMUSG00000020275	Rel	0.0053	0.00035	0.084	0.21	12	0.1
ENSMUSG00000032846	Zswim6	0.0065	0.037	0.15	0.25	12	0.1
ENSMUSG00000034145	Tmem63c	0.022	0.018	0.1	1	12	0.099
ENSMUSG00000023951	Vegfa	0.0095	0.0025	0.14	0.29	12	0.099

Ensembl_ ID	Gene	q_C	q_SD3	q_SD6	q_SD12	C_Phase	Amp
ENSMUSG00000028613	Lrp8	0.037	0.0038	0.87	1	12	0.095
ENSMUSG00000044949	Ubtd2	0.0044	0.0018	0.058	1	12	0.091
ENSMUSG00000026077	Npas2	0.0079	0.004	1	1	12	0.087
ENSMUSG00000021113	Snapc1	0.026	0.004	0.23	1	12	0.085
ENSMUSG00000042109	Csdc2	0.0044	0.0095	1	1	12	0.082
ENSMUSG00000028771	Ptpn12	0.0018	0.023	0.15	0.17	12	0.082
ENSMUSG00000000560	Gabra2	0.0095	0.0056	0.14	1	12	0.079
ENSMUSG00000025986	Slc39a10	0.019	0.015	0.15	0.64	12	0.076
ENSMUSG00000025404	R3hdm2	0.013	0.013	0.16	1	12	0.076
ENSMUSG00000027803	Wwtr1	0.012	0.0048	0.55	0.66	12	0.075
ENSMUSG00000020580	Rock2	0.034	0.006	0.27	1	12	0.075
ENSMUSG00000040548	Tex2	0.02	0.0082	0.29	1	12	0.073
ENSMUSG00000019775	Rgs17	0.029	0.048	1	1	12	0.067
ENSMUSG00000024096	Ralbp1	0.0044	0.018	1	0.95	12	0.064
ENSMUSG00000015484	Fam163a	0.015	0.007	0.55	1	12	0.062
ENSMUSG00000022601	Zbtb11	0.04	0.042	0.75	0.26	12	0.058
ENSMUSG00000052981	Ube2ql1	0.0014	0.045	0.14	1	12	0.058
ENSMUSG00000057069	Ero1lb	0.04	0.026	0.64	0.36	12	0.056
ENSMUSG00000038145	Snrk	0.029	0.0088	0.37	1	12	0.055
ENSMUSG00000021838	Samd4	0.02	0.00035	0.1	0.56	12	0.047
ENSMUSG00000036167	Pphln1	0.031	0.00011	0.084	0.6	12	0.047
ENSMUSG00000015305	Sash1	0.017	0.00022	0.11	0.44	12	0.031
ENSMUSG00000000957	Mmp14	6.30E-05	0.0015	0.24	0.095	15	0.21
ENSMUSG00000000317	Bcl6b	0.013	0.0032	0.062	0.29	15	0.18
ENSMUSG00000056268	Dennd1b	0.047	0.033	0.5	0.81	15	0.17
ENSMUSG00000047420	Fam180a	0.04	0.042	0.24	1	15	0.17
ENSMUSG00000026558	Uck2	0.004	0.029	0.23	1	15	0.16
ENSMUSG00000060373	Hnrnpc	0.015	0.048	0.3	0.95	15	0.1
ENSMUSG00000076431	Sox4	0.0026	0.006	0.23	0.17	15	0.092
ENSMUSG00000021991	Cacna2d3	0.0095	0.02	0.75	1	15	0.086
ENSMUSG00000023175	Bsg	0.0079	0.007	0.17	0.56	15	0.081
ENSMUSG00000004631	Sgce	0.0044	0.027	0.4	0.3	15	0.08
ENSMUSG00000030235	Slco1c1	0.0013	0.029	0.078	0.74	15	0.072
ENSMUSG00000026740	Dnajc1	0.012	0.042	1	0.95	15	0.072
ENSMUSG00000033009	Ogfod1	0.0058	0.015	0.27	0.3	15	0.072
ENSMUSG00000037735	2810032G03Rik	0.031	0.013	0.38	1	15	0.067
ENSMUSG00000024867	Pip5k1b	0.022	0.006	0.67	0.97	15	0.063
ENSMUSG00000040774	Cept1	0.031	0.017	0.52	1	15	0.062
ENSMUSG00000020392	Cdkn2aipnl	0.029	0.0048	1	1	15	0.061
ENSMUSG00000060548	Tnfrsf19	0.011	0.035	0.46	0.91	15	0.055
ENSMUSG00000027200	Sema6d	0.022	0.024	0.38	1	15	0.044
ENSMUSG00000076609	Igkc	0.05	0.0064	1	1	18	0.4
ENSMUSG00000083261	Gm7816	0.0072	0.027	1	1	18	0.32
ENSMUSG00000020846	Fam101b	1.30E-05	0.0076	0.2	0.46	18	0.18
ENSMUSG00000041986	Elmod1	0.02	0.018	0.2	0.39	18	0.11
ENSMUSG00000054277	Arfgap3	0.00035	0.013	0.3	1	18	0.1
ENSMUSG00000037846	Rtkn2	0.017	0.037	0.071	0.44	18	0.09

Ensembl_ ID	Gene	q_C	q_SD3	q_SD6	q_SD12	C_Phase	Amp
ENSMUSG00000039852	Rere	0.026	0.027	1	1	18	0.08
ENSMUSG00000037656	Slc20a2	0.0026	6.70E-05	1	0.83	18	0.061
ENSMUSG00000056091	St3gal5	0.037	0.02	1	1	18	0.05
ENSMUSG00000007656	Arpp19	0.034	0.035	1	1	18	0.049
ENSMUSG00000040605	Bace2	0.00052	0.00041	0.14	1	21	0.44
ENSMUSG00000035142	Nubpl	0.0023	0.024	0.81	1	21	0.36
ENSMUSG00000023935	Spats1	0.00023	0.0065	0.091	1	21	0.35
ENSMUSG00000097343	9030407P20Rik	3.00E-05	0.00066	0.12	0.58	21	0.26
ENSMUSG00000038685	Rtel1	0.02	0.01	0.52	0.62	21	0.25
ENSMUSG00000092448	Gm20387	0.00011	0.027	0.067	1	21	0.23
ENSMUSG00000031558	Slit2	0.0058	0.0034	0.42	1	21	0.22
ENSMUSG00000033590	Myo5c	0.012	0.0088	0.26	0.83	21	0.21
ENSMUSG00000047155	Cyp4x1	0.00015	0.0088	0.52	1	21	0.21
ENSMUSG00000031534	Smim19	2.20E-06	0.037	0.15	0.62	21	0.21
ENSMUSG00000050505	Pcdh20	0.00092	0.0056	0.52	1	21	0.21
ENSMUSG00000048905	4930539E08Rik	0.00023	0.00018	0.1	0.39	21	0.2
ENSMUSG00000018417	Myo1b	0.0095	0.0052	0.3	1	21	0.2
ENSMUSG00000040410	Fbxl4	4.30E-05	0.0065	0.22	0.3	21	0.2
ENSMUSG00000079434	Neu2	3.50E-05	0.006	0.24	1	21	0.19
ENSMUSG00000037266	Rsrp1	0.022	0.026	0.24	1	21	0.19
ENSMUSG00000042807	Hecw2	0.0048	0.017	0.42	1	21	0.19
ENSMUSG00000025795	Rassf3	0.013	0.006	0.3	1	21	0.19
ENSMUSG00000086013	Gm15706	0.00019	0.00066	0.13	1	21	0.18
ENSMUSG00000027188	Pamr1	0.00027	0.00018	1	1	21	0.18
ENSMUSG00000097842	9330104G04Rik	0.00027	0.027	0.38	1	21	0.18
ENSMUSG00000041840	Haus1	0.00019	0.042	0.27	0.13	21	0.17
ENSMUSG00000038982	Bloc1s5	7.80E-06	0.015	0.1	1	21	0.17
ENSMUSG00000038630	Zkscan16	0.0048	0.0082	0.29	1	21	0.17
ENSMUSG00000026153	Fam135a	3.50E-05	0.045	0.27	0.36	21	0.16
ENSMUSG00000032261	Sh3bgrl2	0.0029	0.006	0.084	1	21	0.16
ENSMUSG00000096687	AA474331	0.0016	0.02	0.091	0.41	21	0.15
ENSMUSG00000037400	Atp11b	0.0087	4.60E-07	0.32	0.44	21	0.15
ENSMUSG00000063179	Pstk	0.00017	0.031	0.15	1	21	0.15
ENSMUSG00000050963	Kcns2	0.001	0.0027	0.11	0.12	21	0.15
ENSMUSG00000049907	Rasl11b	1.80E-05	6.00E-05	0.42	0.95	21	0.15
ENSMUSG00000057858	Fam204a	0.00052	0.016	0.13	0.58	21	0.15
ENSMUSG00000037279	Ovol2	0.026	0.0052	0.67	0.17	21	0.14
ENSMUSG00000068391	Chrac1	0.0013	0.0065	0.29	1	21	0.14
ENSMUSG00000039461	Tcta	9.50E-05	0.004	0.24	0.26	21	0.14
ENSMUSG00000091735	Gpr62	0.0011	0.0015	0.62	1	21	0.14
ENSMUSG00000055723	Rras2	0.0036	0.0095	0.15	0.52	21	0.13
ENSMUSG00000060380	C030014I23Rik	0.00078	0.042	0.19	1	21	0.13
ENSMUSG00000043061	Tmem18	0.00052	0.0015	0.091	0.11	21	0.13
ENSMUSG00000022685	Parn	0.0048	0.015	0.67	0.48	21	0.13
ENSMUSG00000091994	E130317F20Rik	0.026	0.033	0.26	1	21	0.13
ENSMUSG00000050730	Arhgap42	0.00035	0.00066	0.37	1	21	0.13
ENSMUSG00000045294	Insig1	1.80E-05	0.013	0.17	0.71	21	0.13

Ensembl_ ID	Gene	q_C	q_SD3	q_SD6	q_SD12	C_Phase	Amp
ENSMUSG00000100147	1700047M11Rik	0.04	0.033	1	1	21	0.13
ENSMUSG00000050967	Creg2	0.0058	0.042	0.3	1	21	0.12
ENSMUSG00000087143	A830082K12Rik	0.004	0.007	0.59	0.91	21	0.12
ENSMUSG00000013495	Tmem175	0.02	0.033	0.2	0.46	21	0.12
ENSMUSG00000022022	Mtrf1	0.00092	0.0018	0.69	1	21	0.12
ENSMUSG00000020287	Mpg	0.0053	0.0014	0.091	0.48	21	0.12
ENSMUSG00000024993	Fam45a	0.012	0.04	0.062	0.36	21	0.12
ENSMUSG00000058298	Mcm9	0.019	0.011	0.2	0.23	21	0.12
ENSMUSG00000045691	Thtpa	0.029	0.01	0.15	1	21	0.11
ENSMUSG00000042208	0610010F05Rik	0.0048	0.031	0.37	0.58	21	0.11
ENSMUSG00000025512	Chid1	0.00035	0.04	0.17	0.97	21	0.11
ENSMUSG00000024750	Zfand5	0.012	0.0048	0.67	1	21	0.11
ENSMUSG00000028173	Wls	0.00092	0.035	1	1	21	0.11
ENSMUSG00000021028	Mbip	0.0011	0.023	0.13	0.66	21	0.11
ENSMUSG00000035824	Tk2	0.013	0.023	0.24	0.37	21	0.11
ENSMUSG00000021710	Nln	0.014	0.0082	0.69	1	21	0.11
ENSMUSG00000039270	Megf9	0.0048	0.017	0.22	0.26	21	0.11
ENSMUSG00000061455	Stx17	0.0053	0.00082	0.062	0.86	21	0.1
ENSMUSG00000022338	Eny2	0.00017	0.013	0.38	0.17	21	0.1
ENSMUSG00000046699	Slitrk4	0.0016	0.0016	0.52	1	21	0.1
ENSMUSG00000001018	Snapin	0.0032	0.021	0.23	0.6	21	0.1
ENSMUSG00000073481	Mar-02	0.0016	0.031	1	1	21	0.1
ENSMUSG00000020642	Rnf144a	0.0026	0.035	0.15	1	21	0.096
ENSMUSG00000045211	Nudt18	0.0032	0.0056	1	1	21	0.09
ENSMUSG00000074461	Gm10699	0.0053	0.0082	0.14	0.91	21	0.09
ENSMUSG00000052298	Cdc42se2	0.0011	0.017	0.2	0.78	21	0.089
ENSMUSG00000097061	9330151L19Rik	0.0023	0.021	0.33	0.78	21	0.088
ENSMUSG00000029211	Gabra4	0.014	0.01	0.97	1	21	0.087
ENSMUSG00000039478	Micu3	0.013	0.011	0.55	1	21	0.087
ENSMUSG00000085148	Mir22hg	0.0072	0.027	0.5	0.88	21	0.086
ENSMUSG00000020436	Gabrg2	0.014	0.031	1	1	21	0.085
ENSMUSG00000028525	Pde4b	0.00027	0.0032	0.46	0.29	21	0.084
ENSMUSG00000037949	Ano10	0.004	0.014	1	1	21	0.082
ENSMUSG00000025742	Prps2	0.0029	0.042	0.84	0.91	21	0.081
ENSMUSG00000014075	Tctex1d2	0.02	0.00044	0.33	1	21	0.08
ENSMUSG00000025037	Maoa	0.031	0.0034	0.26	1	21	0.075
ENSMUSG00000044768	D1Ertd622e	0.034	0.021	0.38	1	21	0.073
ENSMUSG00000037972	Snn	3.00E-05	0.004	0.44	1	21	0.073
ENSMUSG00000032952	Ap4b1	0.0036	0.029	0.12	0.48	21	0.072
ENSMUSG00000039770	Ypel5	0.0011	0.016	0.32	1	21	0.067
ENSMUSG00000022044	Stmn4	0.0014	0.00066	0.26	0.95	21	0.067
ENSMUSG00000024493	Lars	0.031	0.006	0.32	0.066	21	0.045
ENSMUSG00000029617	Ccz1	0.037	0.016	0.87	0.055	21	0.04
ENSMUSG00000079614	Seh1l	0.015	0.037	0.29	0.64	21	0.038
ENSMUSG00000090300	Gm17119	0.029	0.41	0.57	1	0	0.69
ENSMUSG00000100274	1700006F04Rik	0.046	0.96	0.22	1	0	0.41
ENSMUSG00000026736	4930426L09Rik	0.00061	1	0.57	0.97	0	0.39

Ensembl_ ID	Gene	q_C	q_SD3	q_SD6	q_SD12	C_Phase	Amp
ENSMUSG00000083080	Gm11484	0.0032	0.66	1	1	0	0.38
ENSMUSG00000044254	Pcsk9	0.0053	0.086	0.13	0.74	0	0.38
ENSMUSG00000099039	Gm27928	0.04	0.93	1	1	0	0.37
ENSMUSG00000055188	Rbm3os	0.0048	1	0.84	1	0	0.35
ENSMUSG00000073485	H3f3aos	0.0079	0.58	0.21	0.91	0	0.34
ENSMUSG00000086121	Gm16068	0.043	0.12	1	0.6	0	0.34
ENSMUSG00000078906	Gm14444	0.00031	1	0.64	0.62	0	0.33
ENSMUSG00000022357	Klhl38	0.00019	0.096	0.14	0.64	0	0.33
ENSMUSG00000082072	Gm15785	0.029	1	1	1	0	0.3
ENSMUSG00000041809	Efhc1	0.0032	0.45	1	1	0	0.3
ENSMUSG00000101006	Gm28299	0.014	1	0.97	1	0	0.28
ENSMUSG00000037313	Tacc3	0.0026	0.51	0.22	1	0	0.27
ENSMUSG00000041674	BC006965	0.0023	0.17	1	1	0	0.26
ENSMUSG00000078984	Gm11027	0.024	0.68	0.097	1	0	0.26
ENSMUSG00000028307	Aldob	0.0087	1	0.14	0.97	0	0.26
ENSMUSG00000072980	Oip5	0.034	0.83	1	0.66	0	0.25
ENSMUSG00000081974	Gm11960	0.04	1	1	1	0	0.25
ENSMUSG00000082765	Gm14411	0.019	0.71	0.93	1	0	0.25
ENSMUSG00000096943	Gm26721	0.04	0.4	0.23	0.25	0	0.25
ENSMUSG00000083587	Gm14741	0.0095	1	0.078	0.71	0	0.24
ENSMUSG00000040350	Trim7	0.022	1	0.12	0.81	0	0.24
ENSMUSG00000097327	E030030I06Rik	0.037	1	0.97	1	0	0.24
ENSMUSG00000089901	Gm8113	0.013	0.096	0.14	1	0	0.23
ENSMUSG00000044534	Ackr2	0.0023	0.43	0.23	0.88	0	0.23
ENSMUSG00000027635	Dsn1	0.0079	1	0.2	1	0	0.23
ENSMUSG00000092412	Gm20507	0.004	1	0.44	1	0	0.22
ENSMUSG00000101587	Gm29036	0.043	1	0.1	1	0	0.22
ENSMUSG00000097335	Gm26563	0.004	1	0.48	1	0	0.21
ENSMUSG00000021255	Esrrb	0.015	0.62	1	1	0	0.21
ENSMUSG00000004105	Angptl2	0.00052	0.14	0.33	1	0	0.21
ENSMUSG00000074467	Gm10702	7.00E-04	1	1	1	0	0.2
ENSMUSG00000083877	Gm14740	0.0079	0.3	0.054	1	0	0.2
ENSMUSG00000001751	Naglu	0.029	0.082	0.24	0.66	0	0.2
ENSMUSG00000032092	Mpzl2	0.0013	0.23	0.054	0.66	0	0.2
ENSMUSG00000091577	Gm6211	0.0095	1	0.72	1	0	0.2
ENSMUSG00000084087	Gm13650	0.029	1	0.67	1	0	0.2
ENSMUSG00000086291	Gm15513	0.017	0.27	0.17	1	0	0.2
ENSMUSG00000032374	Plod2	0.037	1	0.62	1	0	0.19
ENSMUSG00000042895	Abra	0.0065	1	1	1	0	0.19
ENSMUSG00000094707	A830019P07Rik	0.0079	0.11	0.23	1	0	0.19
ENSMUSG00000085440	Sorbs2os	0.0072	1	0.29	1	0	0.18
ENSMUSG00000026779	Mastl	0.0053	0.36	0.084	1	0	0.18
ENSMUSG00000090353	Gm17555	0.0044	1	1	1	0	0.18
ENSMUSG00000017550	Atad5	0.031	1	0.17	1	0	0.18
ENSMUSG00000040174	Alkbh3	0.004	0.23	0.058	0.23	0	0.17
ENSMUSG00000090284	Gm17613	0.029	1	0.81	1	0	0.17
ENSMUSG00000025255	Zfhx4	0.029	1	1	1	0	0.17

Ensembl_ ID	Gene	q_C	q_SD3	q_SD6	q_SD12	C_Phase	Amp
ENSMUSG00000027353	Mcm8	0.0032	0.23	0.15	1	0	0.17
ENSMUSG00000056394	Lig1	0.014	1	1	1	0	0.17
ENSMUSG00000097876	Gm16892	0.04	1	1	1	0	0.16
ENSMUSG00000060985	Tdrd5	0.019	0.31	0.22	1	0	0.16
ENSMUSG00000052384	Nrros	0.04	0.063	0.57	1	0	0.16
ENSMUSG00000031628	Casp3	0.0018	1	1	0.86	0	0.16
ENSMUSG00000093490	Gm19932	0.0065	0.26	0.37	1	0	0.16
ENSMUSG00000097911	Gm26691	0.00015	1	0.071	1	0	0.16
ENSMUSG00000082593	Gm11331	0.047	1	0.67	1	0	0.16
ENSMUSG00000092335	Gm7221	0.0095	1	1	1	0	0.16
ENSMUSG00000097410	Gm26668	0.015	1	0.24	1	0	0.16
ENSMUSG00000086753	Gm15751	0.022	1	0.5	1	0	0.16
ENSMUSG00000020014	Cfap54	0.0095	1	0.78	1	0	0.16
ENSMUSG00000031730	Dhodh	0.0065	0.053	0.1	1	0	0.15
ENSMUSG00000020709	Adap2	0.037	1	0.5	0.88	0	0.15
ENSMUSG00000020289	Nprl3	0.019	0.12	0.57	0.76	0	0.15
ENSMUSG00000031323	Dmrtc1a	0.00078	0.88	0.15	0.64	0	0.15
ENSMUSG00000094030	Gm21833	0.0026	1	0.72	1	0	0.14
ENSMUSG00000030528	Blm	0.012	1	0.11	1	0	0.14
ENSMUSG00000015217	Hmgb3	0.00023	1	0.27	1	0	0.14
ENSMUSG00000085586	Gm11613	0.019	0.057	0.21	1	0	0.14
ENSMUSG00000039202	Abhd2	0.017	0.11	0.062	0.36	0	0.14
ENSMUSG00000032679	Cd59a	0.043	0.66	0.067	0.28	0	0.14
ENSMUSG00000083849	Gm13477	0.014	0.62	0.16	0.54	0	0.13
ENSMUSG00000042476	Abcb4	0.04	1	1	1	0	0.13
ENSMUSG00000039480	Nt5dc1	0.031	0.1	0.48	1	0	0.13
ENSMUSG00000028637	Ccdc30	0.043	1	0.59	1	0	0.13
ENSMUSG00000093677	Gm20712	0.037	0.34	1	1	0	0.13
ENSMUSG00000078624	Olfr613	0.0021	0.26	1	1	0	0.13
ENSMUSG00000099784	Dalir	0.029	0.11	0.32	1	0	0.13
ENSMUSG00000084897	Gm14226	0.031	1	0.37	1	0	0.13
ENSMUSG00000025766	D3Ertd751e	0.0065	1	0.067	1	0	0.13
ENSMUSG00000017969	Ptgis	0.04	0.078	0.46	1	0	0.13
ENSMUSG00000042104	Uggt2	0.0044	1	0.15	1	0	0.13
ENSMUSG00000030316	Tamm41	0.037	0.27	0.84	0.46	0	0.12
ENSMUSG00000064294	Aox3	0.047	1	0.3	1	0	0.12
ENSMUSG00000089842	Pitpnm2os2	0.047	1	0.81	1	0	0.12
ENSMUSG00000015027	Galns	0.043	0.1	0.57	0.5	0	0.12
ENSMUSG00000093383	Gm20642	0.02	1	1	1	0	0.12
ENSMUSG00000039795	Zfand1	0.00052	0.05	0.078	0.91	0	0.12
ENSMUSG00000085125	Gm16070	0.037	0.3	1	1	0	0.12
ENSMUSG00000059540	Tcea2	0.0053	0.12	0.46	1	0	0.12
ENSMUSG00000018068	Ints2	0.001	0.063	0.15	0.58	0	0.12
ENSMUSG00000039929	Urb1	0.047	0.26	1	1	0	0.12
ENSMUSG00000019846	Lama4	0.014	0.11	0.1	0.76	0	0.11
ENSMUSG00000020176	Grb10	0.014	0.082	0.067	0.81	0	0.11
ENSMUSG00000041477	Dcp1b	0.011	0.62	0.5	1	0	0.11

Ensembl_ ID	Gene	q_C	q_SD3	q_SD6	q_SD12	C_Phase	Amp
ENSMUSG00000089940	Gm4117	0.011	0.88	1	1	0	0.11
ENSMUSG00000038347	Tcte2	0.024	1	0.55	0.78	0	0.11
ENSMUSG00000097879	Gm26869	0.031	1	0.15	1	0	0.11
ENSMUSG00000059820	AU019823	0.0095	1	0.071	1	0	0.11
ENSMUSG00000040557	Wbscr27	0.043	1	1	1	0	0.11
ENSMUSG00000027509	Rae1	0.04	0.11	0.9	0.14	0	0.11
ENSMUSG00000090965	Gm17203	0.019	1	0.4	1	0	0.11
ENSMUSG00000050808	Muc15	0.011	1	0.097	1	0	0.11
ENSMUSG00000030616	Sytl2	0.0044	0.06	0.29	1	0	0.11
ENSMUSG00000025762	Larp1b	0.0026	0.23	0.084	1	0	0.11
ENSMUSG00000078546	2210404O09Rik	0.019	0.33	0.62	0.88	0	0.11
ENSMUSG00000097431	Gm26782	0.017	0.96	0.24	1	0	0.11
ENSMUSG00000038776	Ephx1	0.031	1	0.38	1	0	0.11
ENSMUSG00000029782	Tmem209	0.047	0.56	0.29	1	0	0.11
ENSMUSG00000028572	Hook1	0.014	1	0.38	1	0	0.11
ENSMUSG00000041219	Arhgap11a	0.0072	0.23	1	1	0	0.11
ENSMUSG00000078495	Gm13157	0.034	0.88	0.084	0.31	0	0.1
ENSMUSG00000052676	Zmat1	0.0087	1	0.29	0.68	0	0.1
ENSMUSG00000091509	Gm17066	0.024	0.29	0.23	1	0	0.1
ENSMUSG00000046111	Cep295	0.0058	1	0.2	1	0	0.1
ENSMUSG00000034206	Polq	0.029	1	0.48	1	0	0.1
ENSMUSG00000039349	C130074G19Rik	0.011	0.067	0.33	1	0	0.1
ENSMUSG00000054976	Nyap2	0.00078	1	0.17	0.68	0	0.1
ENSMUSG00000036863	Syde2	0.029	0.32	0.22	0.26	0	0.1
ENSMUSG00000086725	A630052C17Rik	0.037	1	0.38	1	0	0.1
ENSMUSG00000072769	Gm10419	0.04	1	0.27	1	0	0.1
ENSMUSG00000033446	Lpar6	0.0048	0.71	0.52	1	0	0.1
ENSMUSG00000021047	Nova1	0.019	1	0.054	0.74	0	0.099
ENSMUSG00000026672	Optn	0.022	1	0.93	1	0	0.098
ENSMUSG00000039765	Cc2d2a	0.031	0.85	0.23	0.58	0	0.097
ENSMUSG00000036894	Rap2b	0.011	1	0.84	0.46	0	0.096
ENSMUSG00000044791	Setd2	0.024	0.13	0.42	0.64	0	0.093
ENSMUSG00000032925	Itgbl1	0.015	0.37	0.55	0.62	0	0.092
ENSMUSG00000032420	Nt5e	0.00061	0.68	0.32	0.81	0	0.092
ENSMUSG00000039716	Dock3	0.012	1	0.22	1	0	0.091
ENSMUSG00000041014	Nrg3	0.0087	1	0.55	1	0	0.091
ENSMUSG00000028331	Trmo	0.02	0.62	0.44	0.64	0	0.091
ENSMUSG00000097379	Gm26873	0.029	0.55	1	1	0	0.09
ENSMUSG00000071337	Tia1	0.017	1	0.64	1	0	0.089
ENSMUSG00000028207	Asph	0.0023	0.17	0.46	1	0	0.088
ENSMUSG00000039985	Fam60a	0.034	0.66	0.21	1	0	0.088
ENSMUSG00000028550	Atg4c	0.0018	0.15	0.44	1	0	0.088
ENSMUSG00000031938	4931406C07Rik	0.0095	1	0.2	1	0	0.088
ENSMUSG00000039375	Wdr17	0.0048	0.64	1	1	0	0.088
ENSMUSG00000000948	Gm38393	0.0036	0.66	0.69	1	0	0.087
ENSMUSG00000045975	C2cd2	0.043	0.45	0.52	1	0	0.087
ENSMUSG00000039539	Sgcz	0.04	1	1	1	0	0.086

Ensembl_ ID	Gene	q_C	q_SD3	q_SD6	q_SD12	C_Phase	Amp
ENSMUSG00000031337	Mtm1	0.0021	0.34	0.23	0.88	0	0.086
ENSMUSG00000038446	Cdc40	0.013	1	0.12	0.6	0	0.085
ENSMUSG00000020453	Patz1	0.029	0.66	0.22	1	0	0.084
ENSMUSG00000022223	Sdr39u1	0.017	0.12	0.078	1	0	0.084
ENSMUSG00000040118	Cacna2d1	0.026	0.1	0.75	1	0	0.083
ENSMUSG00000063558	Aox1	0.047	1	0.26	0.76	0	0.081
ENSMUSG00000097785	B230217O12Rik	0.0058	0.9	0.11	1	0	0.078
ENSMUSG00000037572	Wdhd1	0.043	0.078	1	0.97	0	0.078
ENSMUSG00000032409	Atr	0.015	0.77	0.27	0.33	0	0.076
ENSMUSG00000027132	Katnbl1	0.037	0.23	0.62	1	0	0.076
ENSMUSG00000026141	Col19a1	0.012	0.18	0.72	0.48	0	0.075
ENSMUSG00000000787	Ddx3x	0.0072	1	0.5	1	0	0.075
ENSMUSG00000055541	Lair1	0.024	0.24	0.058	0.58	0	0.074
ENSMUSG00000034601	2700049A03Rik	0.043	1	0.23	0.81	0	0.074
ENSMUSG00000025551	Fgf14	0.043	0.5	0.84	0.64	0	0.072
ENSMUSG00000025964	Adam23	0.029	1	0.24	1	0	0.071
ENSMUSG00000029246	Ppat	0.04	1	0.64	0.76	0	0.07
ENSMUSG00000017561	Crlf3	0.047	0.68	0.55	0.58	0	0.069
ENSMUSG00000026603	Smyd2	0.0044	0.053	0.87	1	0	0.069
ENSMUSG00000021712	Trim23	0.037	0.07	0.78	0.62	0	0.069
ENSMUSG00000030779	Rbbp6	0.047	0.83	1	0.54	0	0.068
ENSMUSG00000027419	Pcsk2	0.026	0.42	0.38	0.68	0	0.065
ENSMUSG00000036941	Elac1	0.0036	0.45	0.1	1	0	0.065
ENSMUSG00000040037	Negr1	0.029	1	1	1	0	0.065
ENSMUSG00000037369	Kdm6a	0.0048	1	0.62	0.23	0	0.064
ENSMUSG00000033900	Map9	0.043	1	0.67	0.36	0	0.064
ENSMUSG00000030094	Xpc	0.024	1	0.15	1	0	0.061
ENSMUSG00000097605	9430098F02Rik	0.0095	1	0.59	0.28	0	0.061
ENSMUSG00000056771	Gm10010	0.024	0.25	1	1	0	0.061
ENSMUSG00000013878	Rnf170	0.02	0.17	0.5	1	0	0.06
ENSMUSG00000028809	Srrm1	0.031	1	1	1	0	0.057
ENSMUSG00000028878	Fam76a	0.043	1	1	0.22	0	0.057
ENSMUSG00000029088	Kcnip4	0.0058	0.45	1	1	0	0.056
ENSMUSG00000006262	Mob1b	0.024	0.4	0.37	1	0	0.056
ENSMUSG00000055436	Srsf11	0.034	1	1	1	0	0.055
ENSMUSG00000025764	Jade1	0.031	0.26	0.091	1	0	0.054
ENSMUSG00000067942	Zfp160	0.047	0.51	0.78	1	0	0.049
ENSMUSG00000013663	Pten	0.0087	0.086	0.78	0.37	0	0.045
ENSMUSG00000026234	Ncl	0.037	1	0.93	1	0	0.043
ENSMUSG00000100382	Gm28924	0.018	0.33	1	1	3	1.4
ENSMUSG00000084859	1700080N15Rik	0.017	0.85	0.72	1	3	0.4
ENSMUSG00000087625	4930419G24Rik	0.014	0.77	1	1	3	0.38
ENSMUSG00000084994	Gm16352	0.0053	1	1	1	3	0.36
ENSMUSG00000081608	Gm16210	0.019	0.85	1	1	3	0.35
ENSMUSG00000082902	Ccl19-ps1	0.033	1	0.11	1	3	0.34
ENSMUSG00000081656	Gm11246	0.015	0.87	1	1	3	0.3
ENSMUSG00000086458	Gm2639	0.022	1	1	1	3	0.3

Ensembl_ ID	Gene	q_C	q_SD3	q_SD6	q_SD12	C_Phase	Amp
ENSMUSG00000086027	Gm11250	0.047	1	1	1	3	0.3
ENSMUSG00000085449	Gm15520	0.031	0.62	0.37	1	3	0.3
ENSMUSG00000089934	4930473D10Rik	0.031	1	0.9	0.68	3	0.29
ENSMUSG00000082786	Gm14489	0.024	0.43	0.054	1	3	0.28
ENSMUSG00000083745	Gm13543	0.019	0.71	1	0.91	3	0.28
ENSMUSG00000101135	Gm17981	0.029	1	0.93	1	3	0.27
ENSMUSG00000081551	Gm14654	0.014	1	1	0.76	3	0.27
ENSMUSG00000001930	Vwf	0.019	0.77	0.062	1	3	0.26
ENSMUSG00000074529	C330013J21Rik	0.037	1	1	1	3	0.26
ENSMUSG00000081805	Gm14335	0.043	1	1	1	3	0.26
ENSMUSG00000042320	Prox2	9.50E-05	1	0.12	1	3	0.26
ENSMUSG00000082315	Gm16523	0.037	0.24	0.11	1	3	0.24
ENSMUSG00000078880	Gm14308	0.039	0.88	1	0.81	3	0.24
ENSMUSG00000097308	Gm6410	0.02	0.83	1	1	3	0.24
ENSMUSG00000084240	Gm15383	0.015	1	0.97	1	3	0.23
ENSMUSG00000043541	Casc1	0.026	0.73	1	0.81	3	0.23
ENSMUSG00000063447	Ube2d2b	0.0048	0.98	0.59	0.68	3	0.22
ENSMUSG00000093721	Gm3896	0.0053	0.2	0.4	0.29	3	0.22
ENSMUSG00000096870	Gm21816	0.043	0.43	0.78	1	3	0.22
ENSMUSG00000053980	Gm9930	0.0016	1	1	1	3	0.21
ENSMUSG00000091784	Gm17022	0.015	1	1	1	3	0.21
ENSMUSG00000100833	Gm28988	0.0053	0.27	0.23	1	3	0.21
ENSMUSG00000087202	Gm15813	0.0026	1	1	1	3	0.21
ENSMUSG00000093561	Gm20699	0.043	0.53	0.75	0.74	3	0.2
ENSMUSG00000083050	Gm11242	0.0036	0.39	0.11	0.91	3	0.2
ENSMUSG00000057342	Sphk2	0.017	0.42	0.084	1	3	0.2
ENSMUSG00000090263	D730045A05Rik	0.031	0.11	0.4	1	3	0.2
ENSMUSG00000043366	Olfr78	0.00047	0.34	0.69	1	3	0.2
ENSMUSG00000085276	Gm15812	0.034	0.85	0.3	0.86	3	0.2
ENSMUSG00000026228	Htr2b	0.024	1	0.69	1	3	0.2
ENSMUSG00000001918	Slc1a5	0.017	0.29	0.38	0.66	3	0.2
ENSMUSG00000063730	Hsd3b2	0.0095	0.66	1	1	3	0.19
ENSMUSG00000097385	Gm26814	0.011	1	0.32	1	3	0.19
ENSMUSG00000085247	4930545L23Rik	0.011	1	1	1	3	0.19
ENSMUSG00000084010	Gm13302	0.04	0.73	1	0.37	3	0.19
ENSMUSG00000099625	Gm29325	0.0095	1	0.78	1	3	0.19
ENSMUSG00000074252	Gm10654	0.043	1	0.5	1	3	0.19
ENSMUSG00000096553	Gm10097	0.026	1	0.1	1	3	0.18
ENSMUSG00000020633	Dcdc2c	0.02	1	0.62	1	3	0.18
ENSMUSG00000074569	Gcnt7	0.029	0.62	1	1	3	0.18
ENSMUSG00000078157	4931440F15Rik	0.043	0.24	0.084	1	3	0.18
ENSMUSG00000085386	Gm13630	0.004	0.53	0.14	1	3	0.18
ENSMUSG00000024053	Emilin2	0.0013	0.16	0.64	0.78	3	0.17
ENSMUSG00000100768	Gm29055	0.013	0.6	0.81	1	3	0.17
ENSMUSG00000080780	Gm11252	0.0058	1	0.93	1	3	0.17
ENSMUSG00000028438	Kif24	0.0036	1	0.48	1	3	0.17
ENSMUSG00000085118	Gm15774	0.02	0.25	0.87	1	3	0.16

Ensembl_ ID	Gene	q_C	q_SD3	q_SD6	q_SD12	C_Phase	Amp
ENSMUSG00000079177	Fam228a	0.034	0.68	1	0.66	3	0.16
ENSMUSG00000054702	Ap1s3	0.013	0.77	1	1	3	0.16
ENSMUSG00000024912	Fosl1	0.0079	0.85	0.062	1	3	0.16
ENSMUSG00000038225	Primpol	0.011	0.48	1	1	3	0.16
ENSMUSG00000082057	Gm15789	0.0026	1	0.5	0.97	3	0.16
ENSMUSG00000050503	Fbxl22	0.015	0.34	1	1	3	0.16
ENSMUSG00000067081	Asb18	0.0048	1	0.93	1	3	0.16
ENSMUSG00000041147	Brca2	0.0079	0.73	0.12	1	3	0.15
ENSMUSG00000096991	Gm26789	0.013	0.93	1	1	3	0.15
ENSMUSG00000097051	Gm26836	0.026	0.27	1	0.5	3	0.15
ENSMUSG00000090286	Gm17615	0.012	1	0.071	1	3	0.15
ENSMUSG00000084970	1700060J05Rik	0.029	1	0.78	1	3	0.15
ENSMUSG00000048612	Myof	0.024	0.17	0.26	1	3	0.15
ENSMUSG00000029675	Eln	0.037	0.37	0.22	0.42	3	0.15
ENSMUSG00000089707	Slain1os	0.0065	1	1	1	3	0.15
ENSMUSG00000044519	Zfp488	0.0058	1	1	1	3	0.14
ENSMUSG00000089719	Gm15758	0.031	0.43	0.97	0.86	3	0.14
ENSMUSG00000062488	Ifit3b	0.012	0.26	0.37	0.95	3	0.13
ENSMUSG00000027536	Chmp4c	0.017	0.17	0.52	1	3	0.13
ENSMUSG00000101609	Kcnq1ot1	0.043	0.13	1	0.14	3	0.13
ENSMUSG00000089818	Gm15950	0.0036	1	1	1	3	0.13
ENSMUSG00000051427	Ccdc157	0.0029	0.11	0.12	1	3	0.12
ENSMUSG00000024831	Ighmbp2	0.04	0.063	0.52	1	3	0.11
ENSMUSG00000042606	Hirip3	0.00092	1	0.57	1	3	0.11
ENSMUSG00000101599	Gm20342	0.034	0.4	0.52	1	3	0.11
ENSMUSG00000075028	Prdm11	0.047	1	0.81	1	3	0.11
ENSMUSG00000034371	Tkfc	0.034	0.053	0.38	1	3	0.11
ENSMUSG00000027185	Nat10	0.034	0.93	1	1	3	0.11
ENSMUSG00000084241	Gm13416	0.031	0.53	0.72	1	3	0.11
ENSMUSG00000100826	Snhg14	0.0048	0.36	0.59	1	3	0.1
ENSMUSG00000032849	Abcc4	0.043	1	0.62	1	3	0.1
ENSMUSG00000044033	Ccdc141	0.0029	1	0.22	1	3	0.1
ENSMUSG00000014668	Chfr	0.012	1	0.084	1	3	0.099
ENSMUSG00000096967	Gm26621	0.04	0.53	1	1	3	0.098
ENSMUSG00000048721	Fndc9	0.0095	1	1	1	3	0.094
ENSMUSG00000060924	Csmd1	0.017	0.16	0.27	1	3	0.09
ENSMUSG00000060798	Intu	0.022	0.8	0.1	1	3	0.09
ENSMUSG00000056952	Tatdn2	0.0048	0.2	0.64	1	3	0.09
ENSMUSG00000072847	A530017D24Rik	0.043	1	0.67	1	3	0.088
ENSMUSG00000063810	Alms1	0.04	1	0.78	1	3	0.087
ENSMUSG00000097877	Gm26703	0.022	1	0.44	1	3	0.085
ENSMUSG00000097392	D930016D06Rik	0.047	0.98	1	1	3	0.083
ENSMUSG00000029823	Luc7l2	0.004	1	0.35	0.71	3	0.082
ENSMUSG00000097258	Gm26767	0.012	0.51	0.054	1	3	0.08
ENSMUSG00000035456	Prdm8	0.04	0.83	0.75	0.71	3	0.08
ENSMUSG00000038495	Otud7b	0.0079	0.43	0.84	1	3	0.079
ENSMUSG00000039191	Rbpj	0.026	1	0.72	0.81	3	0.079

Ensembl_ ID	Gene	q_C	q_SD3	q_SD6	q_SD12	C_Phase	Amp
ENSMUSG00000028497	Hacd4	0.017	1	0.37	0.97	3	0.073
ENSMUSG00000021244	Ylpm1	0.0048	0.32	1	0.21	3	0.067
ENSMUSG00000026361	Cdc73	0.011	0.5	0.59	1	3	0.067
ENSMUSG00000027425	Csrp2bp	0.037	0.074	0.062	1	3	0.067
ENSMUSG00000020623	Map2k6	0.034	0.32	0.57	0.56	3	0.065
ENSMUSG00000026496	Parp1	0.034	0.17	1	1	3	0.062
ENSMUSG00000097801	Gm26777	0.04	1	0.15	1	3	0.061
ENSMUSG00000036334	Igsf10	0.012	1	1	1	3	0.061
ENSMUSG00000034973	Dopey1	0.022	0.1	0.35	1	3	0.06
ENSMUSG00000057421	Las1l	0.04	1	0.38	1	3	0.06
ENSMUSG00000036591	Arhgap21	0.024	0.16	0.29	0.68	3	0.057
ENSMUSG00000028518	Prkaa2	0.0087	0.086	0.69	0.76	3	0.057
ENSMUSG00000019880	Rspo3	0.0048	0.9	0.44	0.14	3	0.057
ENSMUSG00000034158	Lrrc58	0.047	0.091	1	1	3	0.054
ENSMUSG00000027692	Tnik	0.022	1	0.084	0.58	3	0.05
ENSMUSG00000026618	Iars2	0.04	1	0.37	1	3	0.047
ENSMUSG00000024104	Fam21	0.013	1	0.24	1	3	0.047
ENSMUSG00000005506	Celf1	0.037	0.71	0.75	1	3	0.046
ENSMUSG00000048109	Rbm15	0.04	1	1	1	3	0.043
ENSMUSG00000028399	Ptprd	0.04	0.11	0.5	1	3	0.04
ENSMUSG00000032410	Xrn1	0.037	0.88	0.071	1	3	0.039
ENSMUSG00000064941	Gm23238	0.031	1	0.38	0.86	6	0.54
ENSMUSG00000077611	Gm23946	0.0029	1	1	1	6	0.5
ENSMUSG00000085035	Gm12031	0.0087	1	0.67	1	6	0.43
ENSMUSG00000065251	Gm23971	0.0032	0.93	0.46	1	6	0.39
ENSMUSG00000077709	Snora64	0.043	1	1	1	6	0.38
ENSMUSG00000100555	Gm8173	0.037	1	0.22	1	6	0.37
ENSMUSG00000079076	Gm3086	0.047	1	1	0.66	6	0.36
ENSMUSG00000023968	Crip3	0.022	0.32	0.42	1	6	0.35
ENSMUSG00000079173	Zan	0.02	0.56	1	0.76	6	0.33
ENSMUSG00000100890	1700085C21Rik	0.037	1	0.81	1	6	0.32
ENSMUSG00000093489	Gm20625	0.001	0.23	1	1	6	0.31
ENSMUSG00000085008	Dbhos	0.00052	0.34	1	1	6	0.27
ENSMUSG00000064513	Gm22457	0.022	1	1	1	6	0.26
ENSMUSG00000092549	Gm20491	0.026	1	1	1	6	0.26
ENSMUSG00000098143	Gm26937	0.014	1	0.35	1	6	0.26
ENSMUSG00000089798	1700028K03Rik	0.012	1	0.17	0.76	6	0.25
ENSMUSG00000080888	Gm14387	0.0095	1	1	1	6	0.25
ENSMUSG00000019756	Prl8a1	0.02	1	1	0.5	6	0.25
ENSMUSG00000083606	Gm15916	0.014	1	0.72	1	6	0.25
ENSMUSG00000020703	5530401A14Rik	0.0021	0.12	0.44	0.95	6	0.24
ENSMUSG00000070354	Gm21975	0.04	0.4	1	1	6	0.24
ENSMUSG00000083594	Gm13722	0.0023	1	0.97	1	6	0.23
ENSMUSG00000049871	Nlrc3	0.047	0.23	1	1	6	0.23
ENSMUSG00000094891	Olfr55	0.043	1	1	0.6	6	0.23
ENSMUSG00000097642	Gm26866	0.034	1	0.27	1	6	0.23
ENSMUSG00000081583	Gm14769	0.024	1	0.84	1	6	0.22

Ensembl_ ID	Gene	q_C	q_SD3	q_SD6	q_SD12	C_Phase	Amp
ENSMUSG00000078898	Gm4723	0.024	1	0.32	1	6	0.22
ENSMUSG00000099924	Gm28320	0.0044	1	1	1	6	0.22
ENSMUSG00000031450	Grk1	0.012	1	1	1	6	0.22
ENSMUSG00000097884	Gm26543	0.0095	1	0.78	1	6	0.22
ENSMUSG00000089542	Gm25835	0.0053	0.32	1	0.52	6	0.21
ENSMUSG00000064966	Snord15b	0.015	1	1	0.78	6	0.21
ENSMUSG00000010751	Tnfrsf22	0.043	1	1	1	6	0.21
ENSMUSG00000071036	Gm10309	0.034	0.56	1	1	6	0.21
ENSMUSG00000094856	Gm21962	0.004	1	0.67	1	6	0.21
ENSMUSG00000086580	Gm15280	0.013	0.46	1	1	6	0.2
ENSMUSG00000096243	Gm24265	0.047	1	1	1	6	0.2
ENSMUSG00000045776	Lrtm1	0.019	0.98	1	1	6	0.2
ENSMUSG00000025747	Tyms	0.0036	1	1	1	6	0.19
ENSMUSG00000030148	Clec4a2	0.024	0.73	0.97	1	6	0.19
ENSMUSG00000028655	Mfsd2a	7.00E-04	0.25	0.33	1	6	0.19
ENSMUSG00000096463	Gm21750	0.0053	0.88	0.75	0.88	6	0.18
ENSMUSG00000079489	C030013D06Rik	0.012	1	0.69	1	6	0.18
ENSMUSG00000097695	Gm26905	0.0029	0.85	0.4	0.78	6	0.18
ENSMUSG00000091318	Gm5415	0.022	0.51	0.44	0.54	6	0.18
ENSMUSG00000074896	Ifit3	0.0016	0.66	0.15	0.88	6	0.18
ENSMUSG00000097283	Gm26686	0.0053	0.53	1	1	6	0.18
ENSMUSG00000090338	Gm17081	0.029	1	0.52	1	6	0.17
ENSMUSG00000078864	Gm14322	0.0095	0.32	1	0.54	6	0.17
ENSMUSG00000073609	D2hgdh	0.04	0.37	1	1	6	0.17
ENSMUSG00000097859	Gm26601	0.047	0.9	0.87	1	6	0.17
ENSMUSG00000078902	Gm14443	0.0026	0.45	0.48	1	6	0.17
ENSMUSG00000014813	Stc1	0.00078	0.39	1	0.11	6	0.17
ENSMUSG00000090691	Gm3667	0.026	0.93	0.87	1	6	0.17
ENSMUSG00000008348	Ubc	0.029	0.66	0.37	1	6	0.17
ENSMUSG00000028776	Tinagl1	0.037	0.75	1	1	6	0.16
ENSMUSG00000079018	Ly6c1	0.0048	1	0.42	1	6	0.16
ENSMUSG00000090255	4921534H16Rik	0.029	1	1	1	6	0.16
ENSMUSG00000078190	Dnm3os	0.0053	0.11	1	0.58	6	0.16
ENSMUSG00000043279	Trim56	0.047	1	1	1	6	0.15
ENSMUSG00000019232	Etnppl	0.0065	0.62	0.21	0.64	6	0.15
ENSMUSG00000087458	Gm13999	0.047	1	0.64	1	6	0.15
ENSMUSG00000072972	Adam4	0.022	1	1	1	6	0.15
ENSMUSG00000053769	Lysmd1	0.0029	0.6	0.32	1	6	0.15
ENSMUSG00000084824	Gm16344	0.004	1	1	1	6	0.15
ENSMUSG00000028840	Zfp593	0.015	1	1	1	6	0.15
ENSMUSG00000048108	Tmem72	0.029	1	1	1	6	0.15
ENSMUSG00000087267	4933427J07Rik	0.0072	1	0.12	0.74	6	0.15
ENSMUSG00000085328	Gm17131	0.004	0.77	0.59	0.68	6	0.15
ENSMUSG00000016239	Lonrf3	0.0021	0.13	0.87	1	6	0.14
ENSMUSG00000056947	Mab21l1	0.012	1	1	1	6	0.14
ENSMUSG00000086040	Wipf3	0.043	0.13	0.24	0.07	6	0.14
ENSMUSG00000058360	Gm10040	0.0087	0.55	1	1	6	0.14

Ensembl_ ID	Gene	q_C	q_SD3	q_SD6	q_SD12	C_Phase	Amp
ENSMUSG00000086320	Gm12840	0.031	1	1	1	6	0.14
ENSMUSG00000097551	Gm7976	0.017	0.46	0.97	1	6	0.14
ENSMUSG00000084904	Gm14827	0.029	0.36	1	1	6	0.13
ENSMUSG00000044674	Fzd1	0.015	0.93	1	1	6	0.13
ENSMUSG00000100750	Gm29084	0.0032	0.51	1	1	6	0.13
ENSMUSG00000054499	Dedd2	0.034	1	0.071	0.97	6	0.13
ENSMUSG00000094472	Gm21897	0.013	0.43	0.5	0.83	6	0.13
ENSMUSG00000061331	Gm17132	0.017	0.71	0.5	1	6	0.13
ENSMUSG00000031445	Proz	0.029	0.31	0.67	1	6	0.13
ENSMUSG00000083111	Gm14421	0.04	0.93	1	1	6	0.13
ENSMUSG00000032773	Chrm1	0.026	0.15	0.19	0.64	6	0.13
ENSMUSG00000042903	Foxo4	0.0048	0.62	0.097	1	6	0.13
ENSMUSG00000048218	Amigo2	0.034	1	1	0.42	6	0.12
ENSMUSG00000040447	Spns2	0.004	0.68	0.57	1	6	0.12
ENSMUSG00000029307	Dmp1	0.029	0.45	1	0.41	6	0.12
ENSMUSG00000091542	Gm17167	0.04	1	0.97	1	6	0.12
ENSMUSG00000017009	Sdc4	0.00061	0.2	0.67	0.46	6	0.12
ENSMUSG00000037653	Kctd8	0.037	1	0.44	0.26	6	0.11
ENSMUSG00000066640	Fbxl18	0.043	1	0.59	1	6	0.11
ENSMUSG00000026494	Kif26b	0.0058	1	1	1	6	0.11
ENSMUSG00000071793	2610005L07Rik	0.017	0.53	0.57	1	6	0.11
ENSMUSG00000028019	Pdgfc	0.02	1	0.097	1	6	0.11
ENSMUSG00000090125	Pou3f1	0.047	1	1	1	6	0.11
ENSMUSG00000027306	Nusap1	0.047	1	1	0.83	6	0.11
ENSMUSG00000085894	Gm15832	0.022	0.64	1	1	6	0.11
ENSMUSG00000089756	Gm8898	0.047	1	0.64	1	6	0.1
ENSMUSG00000051331	Cacna1c	0.04	0.082	1	1	6	0.1
ENSMUSG00000022508	Bcl6	0.015	0.1	0.93	1	6	0.1
ENSMUSG00000031028	Tub	0.0048	0.13	0.12	0.95	6	0.1
ENSMUSG00000034235	Usp54	0.0079	0.17	0.27	0.3	6	0.1
ENSMUSG00000006641	Slc5a6	0.04	0.58	1	1	6	0.1
ENSMUSG00000026504	Sdccag8	0.0058	0.16	0.067	0.68	6	0.1
ENSMUSG00000022462	Slc38a2	0.00052	0.13	0.81	1	6	0.098
ENSMUSG00000047216	Cdh19	0.0072	0.2	1	0.88	6	0.098
ENSMUSG00000098243	Gm4258	0.04	1	0.69	1	6	0.097
ENSMUSG00000040852	Plekhh2	0.0044	0.62	0.75	1	6	0.097
ENSMUSG00000044712	Slc38a6	0.0026	0.32	1	0.76	6	0.096
ENSMUSG00000020627	Klhl29	0.0065	0.17	0.75	1	6	0.094
ENSMUSG00000097583	6430590A07Rik	0.026	0.074	0.81	0.81	6	0.093
ENSMUSG00000032525	Nktr	0.0058	0.29	1	1	6	0.092
ENSMUSG00000005580	Adcy9	0.02	0.16	0.24	0.48	6	0.091
ENSMUSG00000095403	Gm21092	0.037	0.43	1	1	6	0.09
ENSMUSG00000041229	Phf8	0.0072	0.43	0.84	1	6	0.089
ENSMUSG00000018500	Adora2b	0.04	0.85	1	0.88	6	0.088
ENSMUSG00000015522	Arnt	0.0053	0.22	0.87	0.74	6	0.088
ENSMUSG00000018707	Dync1h1	0.029	0.96	0.33	1	6	0.086
ENSMUSG00000023959	Clic5	0.043	1	0.69	1	6	0.082

Ensembl_ ID	Gene	q_C	q_SD3	q_SD6	q_SD12	C_Phase	Amp
ENSMUSG00000032602	Slc25a20	0.043	0.26	1	1	6	0.081
ENSMUSG00000048078	Tenm4	0.026	0.62	1	0.91	6	0.081
ENSMUSG00000005533	Igf1r	0.031	0.05	0.62	0.71	6	0.081
ENSMUSG00000054728	Phactr1	0.0048	1	0.38	1	6	0.079
ENSMUSG00000013275	Slc41a1	0.037	0.11	0.93	1	6	0.079
ENSMUSG00000096929	A330023F24Rik	0.043	0.32	0.23	1	6	0.078
ENSMUSG00000042688	Mapk6	0.037	0.13	0.67	1	6	0.078
ENSMUSG00000034055	Phka1	0.034	0.96	0.87	1	6	0.078
ENSMUSG00000011257	Pabpc4	0.026	0.39	1	1	6	0.077
ENSMUSG00000023087	Noct	0.014	0.93	1	0.95	6	0.077
ENSMUSG00000056763	Cspp1	0.02	0.71	0.69	0.66	6	0.076
ENSMUSG00000039210	Gpatch2	0.019	1	1	1	6	0.075
ENSMUSG00000002748	Baz1b	0.037	0.11	0.8	0.86	6	0.075
ENSMUSG00000074519	Etohi1	0.024	0.27	1	0.56	6	0.074
ENSMUSG00000016493	Cd46	0.04	0.58	1	1	6	0.074
ENSMUSG00000034066	Farp2	0.031	1	0.67	1	6	0.074
ENSMUSG00000073557	Ppp1r12b	0.029	1	0.48	1	6	0.074
ENSMUSG00000025931	Paqr8	0.0032	0.25	1	0.97	6	0.073
ENSMUSG00000041341	Atg2b	0.031	1	0.4	1	6	0.073
ENSMUSG00000038170	Pde4dip	0.001	0.45	0.64	0.86	6	0.073
ENSMUSG00000022992	Kansl2	0.037	0.13	1	1	6	0.072
ENSMUSG00000026349	Ccnt2	0.0072	1	0.72	1	6	0.071
ENSMUSG00000057914	Cacnb2	0.037	0.8	0.33	0.34	6	0.071
ENSMUSG00000048960	Prex2	0.047	0.074	1	1	6	0.07
ENSMUSG00000028309	Rnf20	0.037	0.057	0.72	0.91	6	0.069
ENSMUSG00000003500	Impdh1	0.043	1	0.78	0.52	6	0.067
ENSMUSG00000054051	Ercc6	0.0095	0.66	0.9	1	6	0.062
ENSMUSG00000021666	Gfm2	0.04	0.77	1	0.74	6	0.062
ENSMUSG00000001054	Rmnd5b	0.0087	1	0.29	1	6	0.06
ENSMUSG00000031691	Tnpo2	0.0087	0.62	1	0.48	6	0.059
ENSMUSG00000038708	Golga4	0.04	1	0.87	1	6	0.056
ENSMUSG00000021514	Zfp369	0.013	0.4	0.67	1	6	0.055
ENSMUSG00000047789	Slc38a9	0.02	0.71	1	1	6	0.055
ENSMUSG00000029634	Rnf6	0.00019	0.11	1	1	6	0.054
ENSMUSG00000039473	Ubn1	0.012	0.53	0.38	0.6	6	0.054
ENSMUSG00000036104	Rab3gap1	0.0013	0.73	0.9	1	6	0.054
ENSMUSG00000022591	Gm9747	0.047	0.12	1	0.86	6	0.053
ENSMUSG00000027201	Myef2	0.0048	1	1	1	6	0.052
ENSMUSG00000031715	Smarca5	0.047	0.51	1	1	6	0.052
ENSMUSG00000031066	Usp11	0.014	1	0.44	1	6	0.048
ENSMUSG00000033863	Klf9	0.034	1	0.75	0.39	6	0.048
ENSMUSG00000038014	Fam120a	0.0036	0.16	0.67	1	6	0.048
ENSMUSG00000048271	Rbm33	0.02	0.11	0.78	1	6	0.047
ENSMUSG00000060181	Slc35e3	0.015	0.37	0.52	1	6	0.047
ENSMUSG00000021311	Mtr	0.014	0.75	1	1	6	0.045
ENSMUSG00000036323	Srp72	0.0087	1	0.26	0.52	6	0.043
ENSMUSG00000055204	Ankrd17	0.04	0.27	1	1	6	0.042

Ensembl_ ID	Gene	q_C	q_SD3	q_SD6	q_SD12	C_Phase	Amp
ENSMUSG00000021962	Dcp1a	0.0053	1	0.26	1	6	0.042
ENSMUSG00000041720	Pi4ka	0.026	1	1	1	6	0.041
ENSMUSG00000033526	Ppip5k1	0.0095	1	0.058	0.76	6	0.039
ENSMUSG00000021188	Trip11	0.015	0.3	1	1	6	0.036
ENSMUSG00000025139	Tollip	0.031	0.057	0.93	0.74	6	0.034
ENSMUSG00000040242	Fgfr1op2	0.047	0.13	1	0.14	6	0.033
ENSMUSG00000038506	Dcun1d2	0.022	0.83	0.55	1	6	0.03
ENSMUSG00000032556	Bfsp2	0.00011	0.98	0.32	1	9	0.42
ENSMUSG00000036151	Tm6sf2	0.0058	1	0.59	1	9	0.37
ENSMUSG00000051246	Msantd1	0.019	1	1	1	9	0.36
ENSMUSG00000047415	Gpr68	9.50E-05	0.12	0.1	0.64	9	0.34
ENSMUSG00000065145	Vaultrc5	0.015	1	1	1	9	0.32
ENSMUSG00000008384	Sertad1	0.037	0.14	0.11	0.17	9	0.3
ENSMUSG00000083386	Gm15426	0.04	0.55	0.57	1	9	0.29
ENSMUSG00000024136	Dnase1l2	0.0048	1	0.071	0.44	9	0.28
ENSMUSG00000018166	Erbb3	0.0026	0.31	0.1	0.76	9	0.25
ENSMUSG00000028909	Ptpru	0.0072	0.17	1	1	9	0.25
ENSMUSG00000053178	Mterf1b	0.019	0.77	0.64	1	9	0.25
ENSMUSG00000026796	Fam129b	0.0095	0.39	0.067	0.76	9	0.24
ENSMUSG00000034209	Rasl10a	0.0087	0.12	0.097	0.41	9	0.24
ENSMUSG00000063623	C230062I16Rik	0.0018	1	0.59	1	9	0.23
ENSMUSG00000003541	Ier3	0.022	0.14	0.22	0.62	9	0.23
ENSMUSG00000022220	Adcy4	0.0036	0.75	0.42	0.23	9	0.22
ENSMUSG00000024856	Cdk2ap2	0.0036	1	0.17	0.66	9	0.22
ENSMUSG00000054619	Mettl7a1	0.0058	0.082	0.071	0.18	9	0.22
ENSMUSG00000034936	Arl4d	0.047	1	0.64	1	9	0.21
ENSMUSG00000092074	Dynlt1a	0.031	1	0.23	1	9	0.21
ENSMUSG00000040113	Mettl11b	0.0079	0.34	0.64	1	9	0.2
ENSMUSG00000042529	Kcnj12	0.00035	0.19	0.37	1	9	0.2
ENSMUSG00000090210	Itga10	0.019	0.73	0.72	1	9	0.19
ENSMUSG00000028410	Dnaja1	0.013	0.23	0.058	0.76	9	0.19
ENSMUSG00000084088	Gm12941	0.043	0.75	0.62	1	9	0.19
ENSMUSG00000074743	Thbd	0.0044	0.082	0.55	1	9	0.19
ENSMUSG00000035109	Shc4	0.00023	0.3	0.52	1	9	0.19
ENSMUSG00000056116	H2-T22	0.0072	1	0.32	0.74	9	0.18
ENSMUSG00000050248	Evc2	0.0048	0.057	0.15	1	9	0.18
ENSMUSG00000070372	Capza1	0.047	1	0.11	1	9	0.18
ENSMUSG00000028978	Nos3	0.0065	0.9	0.72	1	9	0.18
ENSMUSG00000032323	Cyp11a1	0.0065	1	1	1	9	0.18
ENSMUSG00000022324	Matn2	0.0087	0.17	0.97	1	9	0.17
ENSMUSG00000067352	Gm14149	0.037	0.46	1	1	9	0.17
ENSMUSG00000048897	Zfp710	0.047	0.64	0.97	0.95	9	0.17
ENSMUSG00000044139	Prss53	0.04	1	1	1	9	0.17
ENSMUSG00000018906	P4ha2	0.04	0.21	0.44	0.41	9	0.16
ENSMUSG00000025790	Slco3a1	0.00019	0.17	1	1	9	0.16
ENSMUSG00000079048	4933413L06Rik	0.04	1	1	1	9	0.16
ENSMUSG00000045318	Adra2c	0.022	0.2	0.5	0.58	9	0.16

Ensembl_ ID	Gene	q_C	q_SD3	q_SD6	q_SD12	C_Phase	Amp
ENSMUSG00000034006	Pqlc1	0.02	1	0.59	1	9	0.16
ENSMUSG00000026475	Rgs16	0.02	1	0.48	0.39	9	0.16
ENSMUSG00000018604	Tbx3	0.0058	0.06	1	0.83	9	0.16
ENSMUSG00000037703	Lzts3	0.0013	0.074	0.12	1	9	0.16
ENSMUSG00000032192	Gnb5	0.015	1	0.38	1	9	0.15
ENSMUSG00000042079	Hnrnpf	0.0058	0.43	0.38	0.81	9	0.15
ENSMUSG00000051107	Gm15440	0.0058	0.73	0.35	1	9	0.15
ENSMUSG00000031778	Cx3cl1	0.004	0.086	0.26	1	9	0.15
ENSMUSG00000079737	3110001I22Rik	0.04	1	0.17	0.37	9	0.15
ENSMUSG00000026173	Plcd4	0.014	0.053	0.48	1	9	0.15
ENSMUSG00000039065	Fam173b	0.0032	1	0.5	0.33	9	0.15
ENSMUSG00000023809	Rps6ka2	0.001	0.85	0.12	1	9	0.15
ENSMUSG00000031060	Rbm10	0.024	0.36	0.78	1	9	0.15
ENSMUSG00000097239	Gm27029	0.037	1	0.2	1	9	0.15
ENSMUSG00000025047	Pdcd11	8.20E-06	0.73	0.12	1	9	0.15
ENSMUSG00000067653	Ankrd23	0.024	0.68	0.59	1	9	0.15
ENSMUSG00000022861	Dgkg	0.012	0.14	0.46	1	9	0.15
ENSMUSG00000032702	Kank1	0.0018	0.25	0.33	1	9	0.15
ENSMUSG00000030413	Pglyrp1	0.0053	1	1	1	9	0.15
ENSMUSG00000029436	Mmp17	0.034	1	0.5	1	9	0.15
ENSMUSG00000003200	Sh3gl1	0.0029	1	0.3	1	9	0.14
ENSMUSG00000018849	Wwc1	0.004	0.64	0.18	0.56	9	0.14
ENSMUSG00000014164	Klhl3	0.014	0.15	0.57	1	9	0.14
ENSMUSG00000039976	Tbc1d16	0.019	0.16	0.42	1	9	0.14
ENSMUSG00000025020	Slit1	0.026	0.4	1	1	9	0.14
ENSMUSG00000024451	Arap3	0.019	1	0.097	0.76	9	0.14
ENSMUSG00000054006	D630008O14Rik	0.014	1	0.72	1	9	0.14
ENSMUSG00000041592	Sdk2	0.017	0.34	1	1	9	0.14
ENSMUSG00000040490	Lrfn2	0.0065	0.75	0.24	0.41	9	0.14
ENSMUSG00000018167	Stard3	0.0023	1	0.11	0.78	9	0.14
ENSMUSG00000074247	Dda1	0.012	1	0.2	0.42	9	0.14
ENSMUSG00000054855	Rnd1	0.014	0.51	0.071	1	9	0.14
ENSMUSG00000078651	Aoc2	0.037	1	0.21	1	9	0.14
ENSMUSG00000029875	Ccdc184	0.034	1	0.12	0.21	9	0.14
ENSMUSG00000045349	Sh2d5	0.0072	0.12	1	1	9	0.14
ENSMUSG00000001552	Jup	0.043	1	0.11	0.26	9	0.14
ENSMUSG00000020212	Mdm1	0.001	0.078	0.69	1	9	0.14
ENSMUSG00000031488	Rab11fip1	0.047	0.096	1	0.13	9	0.13
ENSMUSG00000054675	Tmem119	0.043	0.62	0.52	1	9	0.13
ENSMUSG00000066406	Akap13	0.013	0.13	0.97	1	9	0.13
ENSMUSG00000097604	Gm17322	0.0048	1	1	1	9	0.13
ENSMUSG00000056234	Ncoa4	0.047	1	0.69	1	9	0.13
ENSMUSG00000052031	Tagap1	0.04	0.62	0.62	1	9	0.13
ENSMUSG00000000325	Arvcf	0.034	0.36	0.2	0.22	9	0.13
ENSMUSG00000031833	Mast3	0.04	0.057	0.87	1	9	0.13
ENSMUSG00000017692	Rhbdl3	0.0058	1	1	1	9	0.13
ENSMUSG00000040836	Gpr161	0.02	0.067	0.21	1	9	0.13

Ensembl_ ID	Gene	q_C	q_SD3	q_SD6	q_SD12	C_Phase	Amp
ENSMUSG00000030079	Ruvbl1	0.024	1	0.23	1	9	0.13
ENSMUSG00000022054	Nefm	0.019	0.77	0.38	0.86	9	0.13
ENSMUSG00000037622	Wdtc1	0.004	1	0.44	1	9	0.12
ENSMUSG00000003762	Adck4	0.02	0.39	1	1	9	0.12
ENSMUSG00000001985	Grik3	0.024	0.77	1	1	9	0.12
ENSMUSG00000096910	Zfp955b	0.022	0.58	0.9	1	9	0.12
ENSMUSG00000052137	Rbm12b2	0.0036	1	0.4	0.74	9	0.12
ENSMUSG00000020261	Slc36a1	0.0021	0.96	0.4	1	9	0.12
ENSMUSG00000036545	Adamts2	0.026	0.58	1	1	9	0.12
ENSMUSG00000024883	Rin1	0.00015	1	0.97	0.22	9	0.12
ENSMUSG00000064254	Ethe1	0.026	0.48	0.15	1	9	0.12
ENSMUSG00000029053	Prkcz	0.04	1	0.22	1	9	0.12
ENSMUSG00000036206	Sh3bp4	0.017	1	0.071	1	9	0.12
ENSMUSG00000013646	Sh3bp5l	0.037	0.73	0.27	0.76	9	0.12
ENSMUSG00000071645	Tut1	0.0087	0.11	0.054	0.31	9	0.12
ENSMUSG00000020224	Llph	0.02	0.24	0.3	0.68	9	0.12
ENSMUSG00000020422	Tns3	0.0029	0.13	0.091	1	9	0.12
ENSMUSG00000040606	Kazn	0.04	0.053	1	1	9	0.12
ENSMUSG00000024137	E4f1	0.043	0.73	0.22	1	9	0.12
ENSMUSG00000091512	Lamtor3	0.034	1	0.69	1	9	0.11
ENSMUSG00000055128	Cgrrf1	0.029	0.074	0.11	1	9	0.11
ENSMUSG00000052632	Asap2	0.0072	0.063	0.2	1	9	0.11
ENSMUSG00000002393	Nr2f6	0.031	0.55	1	1	9	0.11
ENSMUSG00000008855	Hdac5	0.013	1	0.35	1	9	0.11
ENSMUSG00000067928	Zfp760	0.026	0.096	1	1	9	0.11
ENSMUSG00000041609	Ccdc64	0.0053	0.29	0.091	0.76	9	0.11
ENSMUSG00000007682	Dio2	0.0079	0.091	0.64	1	9	0.11
ENSMUSG00000032840	2410131K14Rik	0.0023	1	1	1	9	0.11
ENSMUSG00000046997	Spsb4	0.031	1	0.062	1	9	0.11
ENSMUSG00000030871	Ears2	0.0079	1	1	1	9	0.11
ENSMUSG00000017314	Mpp2	0.026	0.42	0.24	0.18	9	0.11
ENSMUSG00000036975	Tmem177	0.0058	1	0.071	0.14	9	0.11
ENSMUSG00000031511	Arhgef7	8.20E-06	0.31	0.23	1	9	0.11
ENSMUSG00000031700	Gpt2	0.0013	0.46	0.67	1	9	0.11
ENSMUSG00000022197	Pdzd2	0.012	0.27	1	1	9	0.11
ENSMUSG00000035047	Kri1	0.0095	1	0.062	1	9	0.11
ENSMUSG00000032402	Smad3	0.0079	0.096	0.75	1	9	0.11
ENSMUSG00000052397	Ezr	0.034	0.42	0.87	0.33	9	0.11
ENSMUSG00000034617	Mtrr	0.00078	0.15	0.37	1	9	0.11
ENSMUSG00000043460	Elfn2	0.029	0.057	1	1	9	0.11
ENSMUSG00000070576	Mn1	0.011	0.091	0.4	0.17	9	0.11
ENSMUSG00000030811	Fbxl19	0.047	0.4	0.26	0.58	9	0.11
ENSMUSG00000025980	Hspd1	0.037	0.27	0.48	0.66	9	0.1
ENSMUSG00000019828	Grm1	0.0021	0.1	0.26	1	9	0.1
ENSMUSG00000037172	E330009J07Rik	0.0072	1	0.067	1	9	0.1
ENSMUSG00000062202	Btbd9	2.60E-05	1	0.87	1	9	0.1
ENSMUSG00000002504	Slc9a3r2	0.037	0.93	1	1	9	0.1

Ensembl_ ID	Gene	q_C	q_SD3	q_SD6	q_SD12	C_Phase	Amp
ENSMUSG00000028933	Xrcc2	0.0036	1	0.67	0.91	9	0.1
ENSMUSG00000022641	Bbx	0.013	0.05	0.078	0.25	9	0.1
ENSMUSG00000032232	Cgnl1	0.00078	0.07	0.14	1	9	0.1
ENSMUSG00000003402	Prkcsh	0.037	0.6	0.17	1	9	0.1
ENSMUSG00000029130	Rnf32	0.019	0.091	0.17	1	9	0.1
ENSMUSG00000043439	E130012A19Rik	0.0048	0.14	0.1	0.16	9	0.1
ENSMUSG00000036061	Smug1	0.02	1	0.59	1	9	0.1
ENSMUSG00000020086	H2afy2	0.047	1	0.15	1	9	0.1
ENSMUSG00000046280	She	0.04	0.46	0.4	0.88	9	0.1
ENSMUSG00000030060	Hmces	0.019	0.75	0.29	0.95	9	0.1
ENSMUSG00000021448	Shc3	0.014	0.082	1	1	9	0.099
ENSMUSG00000034674	Tdg	0.037	0.34	0.14	0.68	9	0.099
ENSMUSG00000037013	Ss18	1.90E-05	0.45	0.078	1	9	0.098
ENSMUSG00000027221	Chst1	0.029	0.057	1	1	9	0.098
ENSMUSG00000030805	Stx4a	0.00047	1	0.15	1	9	0.098
ENSMUSG00000040387	Klhl32	0.0044	1	0.14	0.81	9	0.098
ENSMUSG00000021692	Dimt1	0.04	0.1	1	1	9	0.097
ENSMUSG00000038497	Tmco3	0.001	1	0.17	1	9	0.097
ENSMUSG00000023118	Sympk	0.0032	1	0.37	0.5	9	0.097
ENSMUSG00000022263	Trio	8.40E-05	0.29	0.17	1	9	0.096
ENSMUSG00000097596	Gm26673	0.047	1	1	1	9	0.096
ENSMUSG00000002365	Snx9	0.029	0.057	0.72	0.58	9	0.096
ENSMUSG00000041688	Amot	0.0011	0.53	0.78	1	9	0.095
ENSMUSG00000028436	Dcaf12	0.0011	1	0.071	1	9	0.095
ENSMUSG00000025648	Pfkfb4	0.026	1	0.13	0.46	9	0.095
ENSMUSG00000031990	Jam3	0.022	0.83	0.75	1	9	0.094
ENSMUSG00000032536	Trak1	0.011	0.091	0.35	0.56	9	0.094
ENSMUSG00000089857	Zfp882	0.031	1	1	1	9	0.093
ENSMUSG00000021750	Fam107a	0.014	0.15	1	0.21	9	0.093
ENSMUSG00000047959	Kcna3	0.019	1	0.37	1	9	0.093
ENSMUSG00000054792	Klhl18	0.026	0.58	0.37	1	9	0.092
ENSMUSG00000029283	Cdc7	0.022	0.85	0.13	1	9	0.092
ENSMUSG00000025332	Kdm5c	0.00023	0.11	0.062	1	9	0.092
ENSMUSG00000046312	AI464131	0.0014	0.6	0.38	1	9	0.091
ENSMUSG00000027580	Helz2	0.026	1	0.69	1	9	0.091
ENSMUSG00000030098	Grip2	0.016	1	0.17	1	9	0.091
ENSMUSG00000040009	Gnaz	0.012	0.24	0.64	0.48	9	0.091
ENSMUSG00000036377	C530008M17Rik	0.0095	1	1	0.88	9	0.091
ENSMUSG00000018401	Mtmr4	0.0065	1	0.23	0.78	9	0.09
ENSMUSG00000054715	Zscan22	0.034	0.17	0.27	0.52	9	0.089
ENSMUSG00000049807	Arhgap23	0.0026	0.17	0.27	0.97	9	0.089
ENSMUSG00000034271	Jdp2	0.047	0.2	1	1	9	0.088
ENSMUSG00000063888	Rpl7l1	0.024	1	0.091	1	9	0.088
ENSMUSG00000030653	Pde2a	0.013	1	0.46	0.76	9	0.088
ENSMUSG00000016346	Kcnq2	0.0072	1	0.5	1	9	0.088
ENSMUSG00000031442	Mcf2l	0.001	0.17	0.071	1	9	0.088
ENSMUSG00000015214	Mtmr1	0.037	0.17	0.4	1	9	0.088

Ensembl_ ID	Gene	q_C	q_SD3	q_SD6	q_SD12	C_Phase	Amp
ENSMUSG00000028974	Dffa	0.013	1	0.14	0.86	9	0.087
ENSMUSG00000025134	Alyref	0.043	0.26	0.26	1	9	0.087
ENSMUSG00000042078	Svop	0.022	1	0.21	1	9	0.087
ENSMUSG00000042406	Atf4	0.0087	0.24	0.24	1	9	0.087
ENSMUSG00000039879	Heca	0.011	0.75	0.32	0.76	9	0.087
ENSMUSG00000040723	Rcsd1	0.047	1	1	1	9	0.087
ENSMUSG00000039533	Mmd2	0.043	0.88	0.17	0.81	9	0.086
ENSMUSG00000033545	Znrf1	0.043	1	0.22	1	9	0.085
ENSMUSG00000015829	Tnr	0.037	0.29	1	1	9	0.085
ENSMUSG00000037022	Mmaa	0.0036	0.83	0.11	1	9	0.085
ENSMUSG00000039159	Ube2h	0.0044	0.29	0.26	1	9	0.084
ENSMUSG00000022160	Mettl3	0.043	0.11	0.37	1	9	0.083
ENSMUSG00000031527	Eri1	0.013	0.1	0.9	0.1	9	0.082
ENSMUSG00000002279	Lmf1	0.04	0.26	1	1	9	0.082
ENSMUSG00000067889	Sptbn2	0.037	0.48	1	1	9	0.082
ENSMUSG00000021068	Nin	0.026	1	0.44	1	9	0.082
ENSMUSG00000018909	Arrb1	7.00E-04	1	0.21	1	9	0.082
ENSMUSG00000047719	Ubiad1	0.043	1	1	1	9	0.082
ENSMUSG00000038208	Pgap3	0.047	1	0.97	1	9	0.081
ENSMUSG00000033998	Kcnk1	0.014	1	1	1	9	0.079
ENSMUSG00000040111	Gramd1b	0.0058	0.68	0.4	0.97	9	0.079
ENSMUSG00000026889	Rbm18	0.047	0.4	0.46	1	9	0.079
ENSMUSG00000022426	Josd1	0.037	1	1	1	9	0.078
ENSMUSG00000028330	Ncbp1	0.00052	0.53	0.097	1	9	0.077
ENSMUSG00000020964	Sel1l	0.0014	0.23	0.17	0.14	9	0.077
ENSMUSG00000020231	Dip2a	0.0065	0.46	0.78	1	9	0.077
ENSMUSG00000022604	Cep97	0.037	1	0.84	0.83	9	0.077
ENSMUSG00000024935	Slc1a1	0.013	0.14	0.5	1	9	0.076
ENSMUSG00000028039	Efna3	0.047	0.96	1	1	9	0.076
ENSMUSG00000029420	Rimbp2	0.0023	1	0.64	0.34	9	0.076
ENSMUSG00000031864	Ints10	0.0023	0.37	0.13	1	9	0.076
ENSMUSG00000069072	Slc7a14	0.031	0.48	0.69	1	9	0.076
ENSMUSG00000039662	Icmt	0.0014	0.88	0.22	1	9	0.075
ENSMUSG00000068394	Cep152	0.029	0.62	0.59	1	9	0.075
ENSMUSG00000079056	Kcnip3	0.0065	0.77	1	1	9	0.074
ENSMUSG00000055003	Lrtm2	0.015	1	0.48	1	9	0.074
ENSMUSG00000024772	Ehd1	0.024	1	0.32	1	9	0.074
ENSMUSG00000021901	Bap1	0.0053	0.3	0.38	0.91	9	0.073
ENSMUSG00000024245	Tmem178	0.031	0.77	0.2	1	9	0.073
ENSMUSG00000037957	Wdr20	0.017	0.48	0.55	0.76	9	0.073
ENSMUSG00000018474	Chd3	0.0087	1	0.48	1	9	0.073
ENSMUSG00000006464	Bbs1	0.00035	1	0.14	1	9	0.073
ENSMUSG00000043079	Synpo	0.031	0.053	0.24	0.26	9	0.073
ENSMUSG00000021458	2010111I01Rik	0.029	1	0.19	1	9	0.072
ENSMUSG00000003410	Elavl3	0.0029	0.1	0.17	1	9	0.072
ENSMUSG00000026442	Nfasc	0.0072	0.53	1	1	9	0.072
ENSMUSG00000041258	Zfp236	0.0044	0.15	0.22	0.78	9	0.071

Ensembl_ ID	Gene	q_C	q_SD3	q_SD6	q_SD12	C_Phase	Amp
ENSMUSG00000028803	Nipal3	0.047	0.6	0.062	1	9	0.071
ENSMUSG00000055980	Irs1	0.014	0.21	0.14	0.74	9	0.071
ENSMUSG00000048486	Fitm2	0.00011	1	0.12	1	9	0.071
ENSMUSG00000036800	Fam135b	0.019	1	1	1	9	0.071
ENSMUSG00000020451	Limk2	0.0065	1	0.16	1	9	0.07
ENSMUSG00000042429	Adora1	0.019	0.96	0.48	1	9	0.07
ENSMUSG00000035181	Heatr5a	0.04	0.24	0.4	1	9	0.07
ENSMUSG00000027612	Mmp24	0.0087	1	0.3	1	9	0.07
ENSMUSG00000020785	Camkk1	0.0032	1	1	1	9	0.07
ENSMUSG00000023988	Bysl	0.024	0.17	0.64	0.97	9	0.069
ENSMUSG00000078234	Klhdc7a	0.0053	1	1	0.68	9	0.069
ENSMUSG00000020607	Fam84a	0.022	0.83	1	0.97	9	0.069
ENSMUSG00000032897	Nfyc	0.043	1	1	1	9	0.069
ENSMUSG00000026608	Kctd3	0.00061	1	0.27	1	9	0.069
ENSMUSG00000001156	Mxd1	0.014	0.2	0.3	0.26	9	0.069
ENSMUSG00000002346	Slc25a42	0.017	0.83	1	1	9	0.068
ENSMUSG00000022994	Adcy6	0.04	0.11	0.19	0.41	9	0.068
ENSMUSG00000021177	Tdp1	0.026	0.98	1	1	9	0.068
ENSMUSG00000041794	Myrip	0.0087	0.73	0.72	1	9	0.068
ENSMUSG00000047731	Wbp1l	0.047	0.96	1	1	9	0.068
ENSMUSG00000025314	Ptprj	0.043	0.057	0.62	1	9	0.068
ENSMUSG00000022228	Zscan26	0.0072	0.12	1	1	9	0.067
ENSMUSG00000054252	Fgfr3	0.011	0.9	0.11	1	9	0.066
ENSMUSG00000096188	Cmtm4	0.0013	1	0.29	1	9	0.066
ENSMUSG00000034105	Tldc1	0.04	1	1	1	9	0.066
ENSMUSG00000021451	Sema4d	0.019	0.18	0.3	1	9	0.066
ENSMUSG00000078515	Ddi2	0.022	0.43	0.23	0.95	9	0.066
ENSMUSG00000038762	Abcf1	0.0072	0.37	0.11	1	9	0.065
ENSMUSG00000058297	Spock2	0.015	0.71	0.57	1	9	0.064
ENSMUSG00000027457	Snph	0.024	1	0.57	0.58	9	0.064
ENSMUSG00000009681	Bcr	0.011	1	0.48	0.88	9	0.064
ENSMUSG00000024188	Luc7l	0.0087	0.32	0.38	0.3	9	0.064
ENSMUSG00000034853	Acot11	0.022	1	1	0.91	9	0.064
ENSMUSG00000027329	Spef1	0.047	1	0.3	1	9	0.064
ENSMUSG00000052353	Cemip	0.022	0.07	0.52	1	9	0.064
ENSMUSG00000089682	Bcl2l2	0.001	0.27	0.062	0.42	9	0.063
ENSMUSG00000020198	Ap3d1	0.0053	0.64	0.091	1	9	0.062
ENSMUSG00000001150	Mcm3ap	0.0018	0.55	0.46	1	9	0.062
ENSMUSG00000020412	Ascc2	0.017	0.44	0.071	0.39	9	0.062
ENSMUSG00000032009	Sesn3	0.034	0.06	1	1	9	0.061
ENSMUSG00000031513	Leprotl1	0.0023	1	0.78	1	9	0.061
ENSMUSG00000048148	Nwd1	0.019	1	1	1	9	0.061
ENSMUSG00000054920	Klhl5	0.026	1	0.27	1	9	0.061
ENSMUSG00000039697	Ncoa7	0.037	0.15	1	0.44	9	0.061
ENSMUSG00000006998	Psmd2	0.0087	0.43	0.058	0.46	9	0.061
ENSMUSG00000025821	Zfp282	0.02	0.68	0.75	1	9	0.06
ENSMUSG00000032652	Crebl2	0.022	0.13	0.55	1	9	0.06

Ensembl_ ID	Gene	q_C	q_SD3	q_SD6	q_SD12	C_Phase	Amp
ENSMUSG00000072647	Adam1a	0.0058	0.25	0.72	1	9	0.06
ENSMUSG00000079469	Pigb	0.013	1	0.32	1	9	0.06
ENSMUSG00000038366	Lasp1	0.029	0.62	0.097	0.44	9	0.06
ENSMUSG00000024621	Csf1r	0.037	1	0.062	0.64	9	0.06
ENSMUSG00000031537	Ikbkb	0.024	1	0.26	1	9	0.06
ENSMUSG00000001482	Def8	0.017	1	1	1	9	0.06
ENSMUSG00000002006	Pdzd4	0.034	0.19	0.4	1	9	0.059
ENSMUSG00000048118	Arid4a	0.012	0.14	0.27	0.56	9	0.059
ENSMUSG00000029068	Ccnl2	0.047	1	1	1	9	0.059
ENSMUSG00000021681	Aggf1	0.022	0.24	0.38	0.54	9	0.058
ENSMUSG00000048458	Fam212b	0.037	0.12	0.33	1	9	0.058
ENSMUSG00000055319	Sec23ip	0.0023	0.2	0.48	0.78	9	0.058
ENSMUSG00000039738	Slx4	0.017	0.45	0.32	1	9	0.058
ENSMUSG00000040383	Aqr	0.043	1	0.59	1	9	0.058
ENSMUSG00000032788	Pdxk	0.0072	0.98	1	1	9	0.058
ENSMUSG00000004677	Myo9b	0.015	1	0.062	1	9	0.058
ENSMUSG00000041037	Irgq	0.011	1	0.32	0.64	9	0.057
ENSMUSG00000031791	Tmem38a	0.0013	0.73	0.44	1	9	0.056
ENSMUSG00000004394	Tmed4	0.034	0.71	0.72	1	9	0.056
ENSMUSG00000029120	Ppp2r2c	0.0079	1	0.15	1	9	0.056
ENSMUSG00000026305	Lrrfip1	0.014	0.27	0.32	1	9	0.056
ENSMUSG00000017421	Zfp207	0.0079	0.078	0.16	0.26	9	0.054
ENSMUSG00000028911	Srsf4	0.029	1	0.84	1	9	0.054
ENSMUSG00000026848	Tor1b	0.043	0.18	0.062	1	9	0.054
ENSMUSG00000026918	Brd3	0.011	0.23	0.52	0.76	9	0.054
ENSMUSG00000040260	Daam2	0.004	0.66	0.84	1	9	0.054
ENSMUSG00000034931	Dhx8	0.047	1	0.29	0.97	9	0.054
ENSMUSG00000020661	Dnmt3a	0.024	1	1	0.88	9	0.053
ENSMUSG00000027236	Eif3j1	0.043	1	0.37	1	9	0.053
ENSMUSG00000027519	Rab22a	0.013	0.17	1	1	9	0.052
ENSMUSG00000021573	Tppp	0.0036	0.36	0.75	1	9	0.052
ENSMUSG00000052698	Tln2	0.029	0.66	1	0.62	9	0.052
ENSMUSG00000025217	Btrc	0.001	0.58	0.29	1	9	0.051
ENSMUSG00000030207	Fam234b	0.034	1	0.16	1	9	0.051
ENSMUSG00000034602	Mon2	0.0079	1	0.15	1	9	0.051
ENSMUSG00000014763	Fam120b	0.02	0.05	0.084	1	9	0.05
ENSMUSG00000029502	Golga3	0.00078	1	0.1	1	9	0.05
ENSMUSG00000028953	Abcf2	0.019	1	0.38	1	9	0.05
ENSMUSG00000030000	Add2	0.00092	1	0.19	0.66	9	0.05
ENSMUSG00000027339	Rassf2	0.017	1	0.57	1	9	0.05
ENSMUSG00000002428	Hltf	0.013	0.96	1	1	9	0.049
ENSMUSG00000037851	Iars	0.043	0.56	0.81	1	9	0.049
ENSMUSG00000002455	Prpf6	0.022	1	0.33	1	9	0.049
ENSMUSG00000045216	Hs6st1	0.043	1	0.37	1	9	0.049
ENSMUSG00000058979	Cecr5	0.04	0.4	0.097	1	9	0.048
ENSMUSG00000038013	Wipf2	0.0095	0.074	0.5	0.76	9	0.048
ENSMUSG00000055013	Agap1	0.019	1	0.87	1	9	0.048

Ensembl_ ID	Gene	q_C	q_SD3	q_SD6	q_SD12	C_Phase	Amp
ENSMUSG00000017639	Rab11fip4	0.004	0.75	0.67	1	9	0.048
ENSMUSG00000002341	Ncan	0.029	0.62	1	1	9	0.047
ENSMUSG00000032607	Amt	0.024	1	0.22	1	9	0.046
ENSMUSG00000049739	Zfp646	0.043	0.58	0.26	1	9	0.046
ENSMUSG00000049288	Lix1l	0.04	1	0.15	1	9	0.045
ENSMUSG00000022415	Syngr1	0.043	0.58	0.97	1	9	0.045
ENSMUSG00000039367	Sec24c	0.0013	1	0.062	1	9	0.045
ENSMUSG00000034300	Fam53c	0.024	0.77	0.23	1	9	0.045
ENSMUSG00000057230	Aak1	0.029	1	1	1	9	0.045
ENSMUSG00000026596	Abl2	0.0095	0.85	1	1	9	0.044
ENSMUSG00000005615	Pcyt1a	0.013	1	0.23	1	9	0.044
ENSMUSG00000038615	Nfe2l1	0.022	0.31	0.44	1	9	0.043
ENSMUSG00000021559	Dapk1	0.012	0.75	0.16	0.54	9	0.043
ENSMUSG00000022594	Lynx1	0.04	1	1	1	9	0.042
ENSMUSG00000025417	Pip4k2c	0.02	0.5	1	1	9	0.041
ENSMUSG00000024743	Syt7	0.012	1	1	1	9	0.041
ENSMUSG00000037526	Atg14	0.034	0.33	0.2	1	9	0.041
ENSMUSG00000032086	Bace1	0.02	1	0.21	1	9	0.041
ENSMUSG00000062519	Zfp398	0.026	0.23	1	0.3	9	0.04
ENSMUSG00000061911	Myt1l	0.037	0.15	1	1	9	0.039
ENSMUSG00000031302	Nlgn3	0.034	1	1	1	9	0.039
ENSMUSG00000064145	Arih2	0.031	0.77	0.93	1	9	0.038
ENSMUSG00000031153	Gripap1	0.0065	0.68	0.81	1	9	0.038
ENSMUSG00000071856	Mcc	0.037	0.85	1	0.95	9	0.036
ENSMUSG00000031824	6430548M08Rik	0.04	1	1	1	9	0.036
ENSMUSG00000034088	Hdlbp	0.043	0.29	0.78	1	9	0.035
ENSMUSG00000038486	Sv2a	0.034	1	0.054	1	9	0.034
ENSMUSG00000022000	Zc3h13	0.022	1	1	1	9	0.031
ENSMUSG00000040481	Bptf	0.037	0.11	1	0.41	9	0.03
ENSMUSG00000029106	Add1	0.014	0.51	0.14	1	9	0.029
ENSMUSG00000002052	Supt6	0.034	1	0.3	1	9	0.019
ENSMUSG00000099440	Gm29593	0.00061	0.9	0.3	0.86	12	0.66
ENSMUSG00000037405	Icam1	0.024	0.56	0.46	0.58	12	0.3
ENSMUSG00000097183	Gm17501	0.004	0.063	0.23	1	12	0.28
ENSMUSG00000075297	H60b	0.043	0.58	0.23	0.88	12	0.28
ENSMUSG00000072620	Slfn2	0.0036	1	0.67	1	12	0.27
ENSMUSG00000097466	D430036J16Rik	0.0087	0.34	0.44	0.6	12	0.26
ENSMUSG00000055200	Sertad3	0.02	0.26	0.22	0.18	12	0.25
ENSMUSG00000084899	Gm15344	0.047	1	1	1	12	0.24
ENSMUSG00000043557	Mdga1	0.015	0.12	0.38	0.81	12	0.23
ENSMUSG00000046470	Sox18	0.043	0.057	0.084	0.81	12	0.23
ENSMUSG00000000489	Pdgfb	0.015	0.13	0.11	0.6	12	0.2
ENSMUSG00000039208	Metrnl	0.017	0.23	0.091	1	12	0.19
ENSMUSG00000054958	Nt5c1a	0.022	1	0.93	1	12	0.19
ENSMUSG00000040842	Szrd1	0.024	1	0.67	1	12	0.17
ENSMUSG00000070583	Fv1	0.001	0.12	0.067	0.26	12	0.17
ENSMUSG00000020848	Doc2b	0.0032	0.53	0.097	0.88	12	0.16

Ensembl_ ID	Gene	q_C	q_SD3	q_SD6	q_SD12	C_Phase	Amp
ENSMUSG00000097929	Tunar	0.0058	0.3	0.59	1	12	0.16
ENSMUSG00000027776	Il12a	0.031	0.25	0.33	1	12	0.16
ENSMUSG00000025425	St8sia5	0.00078	1	0.062	0.95	12	0.16
ENSMUSG00000024647	Cbln2	0.00015	1	0.16	1	12	0.15
ENSMUSG00000050002	Idnk	0.00041	1	0.067	0.52	12	0.15
ENSMUSG00000026563	Tada1	0.0087	1	0.22	1	12	0.15
ENSMUSG00000026655	Fam107b	0.031	0.21	0.78	1	12	0.14
ENSMUSG00000005447	Pafah1b3	0.034	0.77	0.93	0.83	12	0.14
ENSMUSG00000021457	Syk	0.02	0.096	0.15	1	12	0.14
ENSMUSG00000036968	Cnpy4	0.00047	1	0.054	0.64	12	0.14
ENSMUSG00000033792	Atp7a	0.0013	0.14	0.091	1	12	0.14
ENSMUSG00000019853	Hebp2	0.022	0.62	0.078	1	12	0.14
ENSMUSG00000025817	Nudt5	0.011	0.45	0.69	0.62	12	0.14
ENSMUSG00000006403	Adamts4	0.015	0.082	0.52	0.97	12	0.14
ENSMUSG00000021062	Rab15	0.00047	0.12	0.15	1	12	0.14
ENSMUSG00000017418	Arl5b	0.047	0.074	0.14	1	12	0.14
ENSMUSG00000073468	Sft2d1	0.011	1	0.9	1	12	0.14
ENSMUSG00000035237	Lcat	0.014	0.07	0.37	1	12	0.13
ENSMUSG00000068299	1700019G17Rik	0.04	0.8	0.27	1	12	0.13
ENSMUSG00000027220	Syt13	7.80E-06	1	0.084	1	12	0.13
ENSMUSG00000049303	Syt12	0.0036	1	0.27	1	12	0.13
ENSMUSG00000041308	Sntb2	0.031	0.48	0.27	1	12	0.13
ENSMUSG00000084159	Gm12696	0.0044	0.091	0.52	1	12	0.13
ENSMUSG00000038780	Smurf1	0.011	0.32	0.38	1	12	0.13
ENSMUSG00000030494	Rhpn2	0.043	0.3	0.81	1	12	0.13
ENSMUSG00000021948	Prkcd	0.02	1	1	0.42	12	0.12
ENSMUSG00000097102	2310069G16Rik	0.019	0.37	0.4	0.29	12	0.12
ENSMUSG00000022443	Myh9	8.40E-05	0.64	0.071	0.52	12	0.12
ENSMUSG00000031799	Tpm4	0.0065	0.14	0.19	1	12	0.12
ENSMUSG00000032297	Celf6	0.0029	0.33	0.15	0.56	12	0.12
ENSMUSG00000027649	Ctnnbl1	0.013	0.14	0.21	0.78	12	0.12
ENSMUSG00000047635	2810006K23Rik	0.0087	0.078	0.11	1	12	0.11
ENSMUSG00000085069	Gm13111	0.004	0.36	1	1	12	0.11
ENSMUSG00000004268	Emg1	0.022	1	0.5	0.62	12	0.11
ENSMUSG00000020577	Tspan13	0.019	1	0.3	1	12	0.11
ENSMUSG00000036273	Lrrk2	0.0095	0.13	0.14	0.64	12	0.11
ENSMUSG00000031783	Polr2c	0.024	0.17	0.44	0.6	12	0.11
ENSMUSG00000057130	Txnl4a	0.034	0.067	0.058	0.36	12	0.11
ENSMUSG00000024150	Mcfd2	0.0087	1	0.67	1	12	0.11
ENSMUSG00000066877	Nck2	0.047	0.07	1	1	12	0.11
ENSMUSG00000025049	Taf5	0.012	0.15	0.062	0.74	12	0.11
ENSMUSG00000028035	Dnajb4	0.029	0.05	0.72	0.26	12	0.11
ENSMUSG00000026617	Bpnt1	0.024	0.19	0.27	1	12	0.1
ENSMUSG00000091002	Tcerg1l	0.031	0.83	0.87	1	12	0.1
ENSMUSG00000029581	Fscn1	0.014	0.27	0.9	1	12	0.1
ENSMUSG00000038705	Gmeb2	0.024	0.15	0.1	1	12	0.1
ENSMUSG00000019039	Dalrd3	0.026	1	0.4	0.68	12	0.1

Ensembl_ ID	Gene	q_C	q_SD3	q_SD6	q_SD12	C_Phase	Amp
ENSMUSG00000029447	Cct6a	0.011	0.6	0.11	1	12	0.099
ENSMUSG00000051316	Taf7	0.043	0.33	0.87	1	12	0.099
ENSMUSG00000024999	Noc3l	0.0044	0.17	0.24	1	12	0.098
ENSMUSG00000020834	Dhrs13	0.015	1	0.48	0.14	12	0.098
ENSMUSG00000027424	Mgme1	0.0065	0.23	0.3	1	12	0.097
ENSMUSG00000029334	Prkg2	0.024	0.73	0.23	1	12	0.095
ENSMUSG00000096979	Gm26880	0.031	0.77	1	1	12	0.095
ENSMUSG00000032905	Atg12	0.0021	0.11	0.054	1	12	0.094
ENSMUSG00000020251	Glt8d2	0.019	0.07	0.38	0.97	12	0.093
ENSMUSG00000075467	Dnlz	0.0044	0.77	0.52	0.86	12	0.092
ENSMUSG00000030062	Rpn1	0.026	0.29	0.17	1	12	0.091
ENSMUSG00000042496	Prdm10	0.017	0.25	0.2	1	12	0.091
ENSMUSG00000031536	Polb	0.017	1	1	0.83	12	0.09
ENSMUSG00000006289	Osgep	0.022	1	0.67	1	12	0.085
ENSMUSG00000028698	Pik3r3	0.0044	0.16	0.52	1	12	0.084
ENSMUSG00000026036	Nif3l1	0.0058	1	0.9	1	12	0.083
ENSMUSG00000021276	Cinp	0.014	1	0.15	1	12	0.083
ENSMUSG00000034659	Tmem109	0.022	1	0.15	0.39	12	0.083
ENSMUSG00000021057	Akap5	0.04	0.2	0.071	1	12	0.082
ENSMUSG00000032264	Zw10	0.037	0.43	0.058	1	12	0.082
ENSMUSG00000013076	Amotl1	0.0026	0.55	0.078	0.83	12	0.082
ENSMUSG00000046691	Chtf8	0.019	0.12	0.11	1	12	0.082
ENSMUSG00000032867	Fbxw8	0.04	1	0.9	1	12	0.081
ENSMUSG00000036943	Rab8b	0.0079	0.082	1	0.31	12	0.081
ENSMUSG00000027642	Rpn2	0.029	1	0.37	0.17	12	0.079
ENSMUSG00000008398	Elk3	0.047	0.17	0.27	1	12	0.079
ENSMUSG00000019432	Ddx39b	0.012	0.13	0.4	1	12	0.078
ENSMUSG00000032118	Fez1	0.0065	1	0.29	1	12	0.078
ENSMUSG00000042729	Wdr74	0.022	1	0.9	1	12	0.077
ENSMUSG00000067713	Prkag1	0.012	0.96	0.29	1	12	0.077
ENSMUSG00000037253	Mex3c	0.043	0.078	1	1	12	0.077
ENSMUSG00000024668	Sdhaf2	0.037	0.23	0.4	1	12	0.077
ENSMUSG00000034336	Ina	0.0036	0.053	0.37	0.6	12	0.077
ENSMUSG00000021810	Ecd	0.026	1	0.9	1	12	0.077
ENSMUSG00000026202	Tuba4a	0.02	0.11	0.5	1	12	0.077
ENSMUSG00000027797	Dclk1	0.0058	0.21	0.22	1	12	0.076
ENSMUSG00000038291	Snx25	0.019	1	0.67	1	12	0.076
ENSMUSG00000037788	Vopp1	0.0048	0.053	0.058	0.68	12	0.076
ENSMUSG00000019977	Hbs1l	0.024	1	0.15	0.62	12	0.075
ENSMUSG00000005823	Gpr108	0.013	1	0.37	1	12	0.074
ENSMUSG00000034361	Cpne2	0.026	0.15	0.13	1	12	0.074
ENSMUSG00000031105	Slc25a14	0.04	0.6	0.55	1	12	0.074
ENSMUSG00000028907	Utp11l	0.029	0.33	1	0.56	12	0.073
ENSMUSG00000027350	Chgb	0.00047	0.51	0.15	1	12	0.073
ENSMUSG00000032470	Mras	0.043	0.082	0.17	1	12	0.073
ENSMUSG00000022964	Tmem50b	0.0058	0.14	0.72	0.74	12	0.073
ENSMUSG00000029538	Srsf9	0.0095	0.62	0.27	1	12	0.073

Ensembl_ ID	Gene	q_C	q_SD3	q_SD6	q_SD12	C_Phase	Amp
ENSMUSG00000006205	Htra1	0.024	0.1	1	0.76	12	0.072
ENSMUSG00000037824	Tspan14	0.0095	1	0.27	1	12	0.071
ENSMUSG00000028883	Sema3a	0.0095	0.54	0.3	1	12	0.071
ENSMUSG00000018736	Ndel1	0.022	0.45	0.38	1	12	0.071
ENSMUSG00000044952	Kctd21	0.037	0.11	0.078	1	12	0.069
ENSMUSG00000085007	Gm11549	0.017	0.43	0.78	1	12	0.068
ENSMUSG00000022391	Rangap1	0.02	1	0.35	1	12	0.068
ENSMUSG00000034343	Ube2f	0.04	1	0.37	1	12	0.068
ENSMUSG00000023932	Cdc5l	0.017	1	0.62	1	12	0.067
ENSMUSG00000028863	Meaf6	0.037	1	0.35	1	12	0.067
ENSMUSG00000035776	Cd99l2	0.0013	0.66	0.062	0.66	12	0.067
ENSMUSG00000030007	Cct7	0.0095	1	0.078	1	12	0.067
ENSMUSG00000024812	Tjp2	0.0079	1	0.17	1	12	0.066
ENSMUSG00000058587	Tmod3	0.034	0.22	0.52	0.36	12	0.065
ENSMUSG00000044117	2900011O08Rik	0.0058	0.43	0.59	1	12	0.065
ENSMUSG00000013160	Atp6v0d1	0.02	0.71	0.23	1	12	0.065
ENSMUSG00000001576	Ergic1	0.012	0.25	0.097	1	12	0.064
ENSMUSG00000013539	Tango2	0.026	1	0.38	1	12	0.063
ENSMUSG00000039983	Ccdc32	0.047	0.51	1	0.29	12	0.063
ENSMUSG00000024065	Ehd3	0.04	0.68	0.59	0.68	12	0.062
ENSMUSG00000015087	Rabl6	0.024	0.2	0.091	1	12	0.062
ENSMUSG00000020869	Lrrc59	0.0029	0.66	0.15	1	12	0.061
ENSMUSG00000049792	Bag5	0.043	0.43	0.11	1	12	0.061
ENSMUSG00000046791	2410016O06Rik	0.0048	0.83	0.16	1	12	0.06
ENSMUSG00000009575	Cbx5	0.043	0.19	0.72	1	12	0.06
ENSMUSG00000007815	Rhoa	0.037	1	0.084	0.52	12	0.06
ENSMUSG00000041438	Cirh1a	0.031	0.51	0.12	1	12	0.06
ENSMUSG00000029263	Pigg	0.011	0.26	1	1	12	0.059
ENSMUSG00000041078	Grid1	0.019	0.07	1	1	12	0.058
ENSMUSG00000028793	Rnf19b	0.00047	0.11	0.29	1	12	0.058
ENSMUSG00000027680	Fxr1	0.017	0.27	0.78	0.34	12	0.057
ENSMUSG00000040385	Ppp1ca	0.0087	0.31	0.15	0.36	12	0.057
ENSMUSG00000017776	Crk	0.047	0.12	0.84	1	12	0.055
ENSMUSG00000036667	Tcaf1	0.0044	0.31	0.46	0.81	12	0.053
ENSMUSG00000066900	Suds3	0.026	0.13	0.97	0.5	12	0.052
ENSMUSG00000021196	Pfkp	0.022	1	0.21	0.56	12	0.051
ENSMUSG00000026457	Adipor1	0.0095	1	1	1	12	0.049
ENSMUSG00000004500	Zfp324	0.026	1	0.37	1	12	0.049
ENSMUSG00000036333	Kidins220	0.019	0.057	0.4	1	12	0.048
ENSMUSG00000032802	Srxn1	0.04	1	0.5	1	12	0.047
ENSMUSG00000026104	Stat1	0.024	0.096	0.44	1	12	0.046
ENSMUSG00000032366	Tpm1	0.04	0.73	0.24	1	12	0.044
ENSMUSG00000020917	Acly	0.034	0.58	0.23	1	12	0.044
ENSMUSG00000026851	BC005624	0.043	1	0.46	1	12	0.043
ENSMUSG00000040446	Rprd1a	0.026	1	0.69	1	12	0.043
ENSMUSG00000021190	Lgmn	0.0079	1	0.67	0.6	12	0.042
ENSMUSG00000018398	Sep-08	0.026	0.23	0.3	1	12	0.028

Ensembl_ ID	Gene	q_C	q_SD3	q_SD6	q_SD12	C_Phase	Amp
ENSMUSG00000021476	Habp4	0.013	1	0.84	1	12	0.028
ENSMUSG00000031410	Nxf7	0.00041	0.15	0.19	0.86	15	0.33
ENSMUSG00000054488	Gm9946	0.015	1	1	1	15	0.32
ENSMUSG00000001029	Icam2	0.011	0.33	0.52	0.56	15	0.21
ENSMUSG00000030865	Chp2	0.043	0.33	1	1	15	0.19
ENSMUSG00000078773	Rad54b	0.031	1	0.33	1	15	0.18
ENSMUSG00000032436	Cmtm7	0.024	1	0.23	1	15	0.18
ENSMUSG00000100801	Gm15459	0.013	0.51	0.062	1	15	0.18
ENSMUSG00000050666	Vstm4	0.02	0.5	0.21	1	15	0.17
ENSMUSG00000026946	Nmi	0.047	1	0.93	1	15	0.16
ENSMUSG00000042439	Zfp532	0.0065	1	0.44	0.66	15	0.16
ENSMUSG00000024670	Cd6	0.0079	1	1	0.34	15	0.16
ENSMUSG00000032902	Slc16a1	0.0053	0.33	0.26	0.26	15	0.16
ENSMUSG00000027954	Efna1	0.047	0.55	0.15	0.5	15	0.16
ENSMUSG00000049796	Crh	0.0095	0.12	0.4	0.86	15	0.16
ENSMUSG00000085457	1110046J04Rik	0.026	0.71	0.26	0.86	15	0.15
ENSMUSG00000022132	Cldn10	0.0053	0.75	0.12	1	15	0.15
ENSMUSG00000097039	Pvt1	0.013	0.1	1	1	15	0.15
ENSMUSG00000019577	Pdk4	0.011	1	0.24	1	15	0.14
ENSMUSG00000051355	Commd1	0.02	1	0.52	1	15	0.14
ENSMUSG00000083674	Zfp133-ps	0.019	1	1	1	15	0.14
ENSMUSG00000021696	Elovl7	0.043	0.078	0.81	1	15	0.13
ENSMUSG00000084946	Dlx1as	0.0044	1	0.067	1	15	0.13
ENSMUSG00000037286	Stag1	0.034	0.66	1	1	15	0.13
ENSMUSG00000029649	Pomp	0.019	0.66	0.62	1	15	0.13
ENSMUSG00000052962	Mrpl35	0.037	1	1	1	15	0.13
ENSMUSG00000059187	Fam19a1	0.0029	0.93	0.22	1	15	0.13
ENSMUSG00000023913	Pla2g7	0.014	1	0.42	1	15	0.12
ENSMUSG00000024889	Rce1	0.013	1	0.52	1	15	0.12
ENSMUSG00000049489	Fam58b	0.04	0.3	0.67	0.88	15	0.12
ENSMUSG00000027673	Ndufb5	0.0072	0.85	0.81	1	15	0.12
ENSMUSG00000074457	S100a16	0.0079	0.13	0.42	1	15	0.12
ENSMUSG00000032135	Mcam	0.031	0.12	0.27	1	15	0.12
ENSMUSG00000058318	Phf21a	0.022	0.6	1	1	15	0.12
ENSMUSG00000002233	Rhoc	0.043	0.086	1	1	15	0.11
ENSMUSG00000025920	Stau2	0.0036	0.05	0.59	1	15	0.11
ENSMUSG00000050069	Grem2	0.043	0.15	0.81	1	15	0.11
ENSMUSG00000037514	Pank2	0.0029	1	1	1	15	0.11
ENSMUSG00000024844	Banf1	0.037	0.8	0.64	1	15	0.11
ENSMUSG00000001891	Ugp2	0.0065	1	0.17	1	15	0.11
ENSMUSG00000054226	Tprkb	0.0087	1	0.11	1	15	0.1
ENSMUSG00000042487	Leo1	0.013	0.078	0.38	0.44	15	0.1
ENSMUSG00000028383	Hsdl2	0.0048	0.057	0.3	0.97	15	0.1
ENSMUSG00000032667	Pon2	0.034	0.39	0.62	0.95	15	0.1
ENSMUSG00000062797	l7Rn6	0.043	1	1	1	15	0.1
ENSMUSG00000020717	Pecam1	0.0079	0.26	0.21	0.095	15	0.1
ENSMUSG00000075486	Commd6	0.019	1	0.81	0.62	15	0.1

Ensembl_ ID	Gene	q_C	q_SD3	q_SD6	q_SD12	C_Phase	Amp
ENSMUSG00000063434	Sorcs3	0.0036	0.21	0.24	0.78	15	0.1
ENSMUSG00000030638	Sh3gl3	0.022	1	0.62	1	15	0.1
ENSMUSG00000075701	Vimp	0.024	0.96	0.15	1	15	0.1
ENSMUSG00000024387	Csnk2b	0.0072	1	0.14	1	15	0.099
ENSMUSG00000052428	Tmco1	0.037	1	0.16	1	15	0.098
ENSMUSG00000020415	Pttg1	0.026	0.07	1	1	15	0.098
ENSMUSG00000047044	D030056L22Rik	0.02	0.14	1	1	15	0.098
ENSMUSG00000029534	St7	0.0079	1	0.22	0.78	15	0.097
ENSMUSG00000038402	Foxf2	0.017	0.082	0.15	1	15	0.094
ENSMUSG00000040128	Pnrc1	0.0079	0.37	0.69	0.62	15	0.092
ENSMUSG00000022969	Il10rb	0.0058	0.21	0.13	0.64	15	0.092
ENSMUSG00000025260	Hsd17b10	0.034	0.53	0.2	1	15	0.09
ENSMUSG00000033216	Eefsec	0.012	1	0.5	1	15	0.09
ENSMUSG00000041911	Dlx1	0.0048	0.057	0.22	0.71	15	0.09
ENSMUSG00000096916	Zfp850	0.026	0.23	1	1	15	0.089
ENSMUSG00000063480	Nhp2l1	0.013	0.62	0.11	1	15	0.088
ENSMUSG00000027195	Hsd17b12	0.014	0.32	0.16	1	15	0.085
ENSMUSG00000002015	Bcap31	0.026	1	0.93	0.26	15	0.084
ENSMUSG00000032507	Fbxl2	0.034	0.55	1	1	15	0.083
ENSMUSG00000035199	Arl6ip5	0.0053	0.39	1	1	15	0.083
ENSMUSG00000039682	Lap3	0.037	0.73	0.17	1	15	0.082
ENSMUSG00000021891	Mettl6	0.022	1	1	0.95	15	0.081
ENSMUSG00000027384	Ndufaf5	0.037	1	0.46	0.83	15	0.081
ENSMUSG00000027259	Adal	0.029	0.4	0.14	1	15	0.081
ENSMUSG00000028822	Tmem50a	0.043	0.55	1	1	15	0.08
ENSMUSG00000039717	Ralyl	0.015	0.23	0.93	1	15	0.08
ENSMUSG00000053768	Chchd3	0.02	0.4	0.32	1	15	0.079
ENSMUSG00000031939	Taf1d	0.024	1	1	1	15	0.077
ENSMUSG00000028618	Tmem59	0.00078	1	0.26	1	15	0.077
ENSMUSG00000032199	Polr2m	0.022	1	0.29	1	15	0.076
ENSMUSG00000051537	Gm5124	0.029	0.85	1	1	15	0.076
ENSMUSG00000043463	Rab9b	0.04	1	0.59	1	15	0.076
ENSMUSG00000019810	Fuca2	0.02	1	0.23	1	15	0.075
ENSMUSG00000022257	Laptm4b	0.0072	1	0.5	1	15	0.074
ENSMUSG00000019897	Ccdc59	0.029	0.48	0.81	1	15	0.074
ENSMUSG00000009030	Pdcl	0.037	1	0.84	0.68	15	0.073
ENSMUSG00000100455	Gm29170	0.037	0.96	0.22	1	15	0.072
ENSMUSG00000031950	Gabarapl2	0.043	1	0.46	1	15	0.072
ENSMUSG00000025353	Ormdl2	0.0036	0.29	0.64	1	15	0.071
ENSMUSG00000017176	Nt5c3b	0.0029	0.17	0.32	1	15	0.07
ENSMUSG00000028403	Zdhhc21	0.04	1	0.84	1	15	0.07
ENSMUSG00000032181	Scg3	0.0072	1	0.15	1	15	0.069
ENSMUSG00000040990	Sh3kbp1	0.02	0.88	0.67	1	15	0.067
ENSMUSG00000051444	Bbs12	0.04	1	0.81	0.83	15	0.066
ENSMUSG00000022108	Itm2b	0.015	1	1	1	15	0.066
ENSMUSG00000055239	Kcmf1	0.011	0.26	0.75	1	15	0.066
ENSMUSG00000003948	Mmd	0.047	0.17	0.19	1	15	0.064

Ensembl_ ID	Gene	q_C	q_SD3	q_SD6	q_SD12	C_Phase	Amp
ENSMUSG00000058589	Anks1b	0.0013	0.11	0.55	1	15	0.064
ENSMUSG00000032434	Cmtm6	0.034	1	0.1	1	15	0.062
ENSMUSG00000008301	Phax	0.047	0.42	0.64	1	15	0.062
ENSMUSG00000001847	Rac1	0.029	0.71	0.46	1	15	0.059
ENSMUSG00000028567	Txndc12	0.0095	1	0.097	1	15	0.057
ENSMUSG00000021219	Rgs6	0.043	1	1	1	15	0.057
ENSMUSG00000030591	Psmd8	0.047	0.93	0.17	1	15	0.057
ENSMUSG00000031901	Dus2	0.029	0.68	1	0.54	15	0.055
ENSMUSG00000021792	Fam213a	0.0087	1	1	0.68	15	0.054
ENSMUSG00000029405	G3bp2	0.019	0.77	0.38	1	15	0.054
ENSMUSG00000022403	St13	0.04	1	0.11	1	15	0.054
ENSMUSG00000074748	Atxn7l3b	0.014	0.14	0.29	1	15	0.053
ENSMUSG00000026755	Arpc5l	0.014	0.98	0.12	0.5	15	0.053
ENSMUSG00000032570	Atp2c1	0.037	0.053	0.46	1	15	0.053
ENSMUSG00000031578	Mak16	0.026	1	0.52	1	15	0.052
ENSMUSG00000047514	Tspyl1	0.015	1	0.9	1	15	0.051
ENSMUSG00000013698	Pea15a	0.034	0.14	0.058	1	15	0.049
ENSMUSG00000020166	Cnot2	0.047	0.29	0.4	0.91	15	0.048
ENSMUSG00000019843	Fyn	0.011	0.71	0.4	1	15	0.037
ENSMUSG00000020358	Hnrnpab	0.034	0.51	0.13	0.68	15	0.035
ENSMUSG00000036275	9530068E07Rik	0.026	1	0.59	1	15	0.026
ENSMUSG00000055795	Gm5160	0.031	1	1	1	18	0.91
ENSMUSG00000081043	Gm11512	0.015	0.24	1	1	18	0.76
ENSMUSG00000080921	Rpl38-ps2	0.046	1	1	1	18	0.74
ENSMUSG00000065254	Gm23973	0.017	1	1	1	18	0.67
ENSMUSG00000044751	Gm12231	0.013	0.82	1	1	18	0.63
ENSMUSG00000098111	Gm4654	0.0058	0.46	1	1	18	0.61
ENSMUSG00000082908	Gm13736	0.0013	1	1	1	18	0.58
ENSMUSG00000082120	Gm15720	0.046	1	1	1	18	0.58
ENSMUSG00000101445	Gm28932	0.0095	1	1	1	18	0.57
ENSMUSG00000064694	Gm24146	0.047	1	1	1	18	0.57
ENSMUSG00000067189	Gm7335	0.011	1	1	1	18	0.53
ENSMUSG00000081603	Gm14681	0.012	1	1	1	18	0.51
ENSMUSG00000044211	Gm7887	0.019	1	1	1	18	0.5
ENSMUSG00000083563	Gm13340	0.0036	1	1	1	18	0.48
ENSMUSG00000081824	BC002163	0.04	1	1	1	18	0.48
ENSMUSG00000093183	Gm25687	0.036	1	1	1	18	0.48
ENSMUSG00000084835	Gm12352	0.034	1	0.57	1	18	0.47
ENSMUSG00000083621	Gm14586	0.0029	1	1	1	18	0.47
ENSMUSG00000082536	Gm13456	0.0044	0.98	1	1	18	0.46
ENSMUSG00000089782	Gm3531	0.047	0.32	1	1	18	0.46
ENSMUSG00000094437	Gm9830	0.026	0.37	1	1	18	0.46
ENSMUSG00000061684	Rpl21-ps8	0.026	1	1	1	18	0.44
ENSMUSG00000092072	Gm4540	0.031	1	0.32	1	18	0.43
ENSMUSG00000064281	Rpl19-ps1	0.015	0.85	1	1	18	0.41
ENSMUSG00000081400	Gm13680	0.013	0.37	1	1	18	0.41
ENSMUSG00000066553	Gm6969	0.004	0.5	0.83	1	18	0.41

Ensembl_ ID	Gene	q_C	q_SD3	q_SD6	q_SD12	C_Phase	Amp
ENSMUSG00000050621	Rps27rt	0.022	1	1	0.78	18	0.4
ENSMUSG00000060787	Olfr464	0.0011	0.13	1	1	18	0.4
ENSMUSG00000044424	Gm9493	0.00052	0.25	1	1	18	0.4
ENSMUSG00000092599	1700010K23Rik	0.029	1	1	1	18	0.39
ENSMUSG00000070343	Gm10288	0.0065	1	1	1	18	0.39
ENSMUSG00000046721	Rpl14-ps1	0.024	1	1	1	18	0.38
ENSMUSG00000080848	Gm9385	0.0058	1	0.72	1	18	0.38
ENSMUSG00000046440	Gm5564	0.013	1	1	1	18	0.37
ENSMUSG00000083097	Gm14494	0.037	1	1	1	18	0.37
ENSMUSG00000063902	Gm7964	0.0065	1	1	1	18	0.37
ENSMUSG00000078193	Gm2000	0.0021	1	1	1	18	0.37
ENSMUSG00000093006	Gm24157	0.031	1	1	1	18	0.37
ENSMUSG00000000901	Mmp11	0.02	1	1	1	18	0.35
ENSMUSG00000055093	Gm8430	0.022	1	1	0.76	18	0.35
ENSMUSG00000060419	Rps16-ps2	0.0058	1	1	0.76	18	0.35
ENSMUSG00000083380	Gm3244	0.0087	0.53	1	1	18	0.35
ENSMUSG00000037096	Gm9762	0.031	1	1	1	18	0.34
ENSMUSG00000083899	Gm12346	0.0044	1	1	1	18	0.34
ENSMUSG00000079225	Gm9531	0.013	1	1	1	18	0.34
ENSMUSG00000095597	Gm6472	0.0018	1	1	1	18	0.33
ENSMUSG00000040078	Gm9769	0.02	1	1	1	18	0.33
ENSMUSG00000063656	Gm10135	0.024	1	0.96	1	18	0.32
ENSMUSG00000046341	Gm11223	0.034	0.93	1	1	18	0.32
ENSMUSG00000083679	Gm12892	0.019	1	1	1	18	0.32
ENSMUSG00000071035	Gm5499	0.047	1	1	1	18	0.32
ENSMUSG00000082896	Gm5844	0.0079	0.56	1	1	18	0.31
ENSMUSG00000084235	Gm15421	0.0095	1	1	1	18	0.31
ENSMUSG00000079139	Gm4204	0.004	0.17	1	1	18	0.31
ENSMUSG00000039617	Gm7488	0.00078	1	1	1	18	0.3
ENSMUSG00000084319	Tpt1-ps3	0.0044	0.71	1	1	18	0.3
ENSMUSG00000048949	Gm6206	0.013	1	1	1	18	0.3
ENSMUSG00000043889	Gm8399	0.043	1	1	1	18	0.29
ENSMUSG00000081752	Gm14680	0.017	0.17	1	1	18	0.29
ENSMUSG00000101523	Gm10031	0.0058	0.75	1	1	18	0.29
ENSMUSG00000085262	Gm11574	0.04	1	1	1	18	0.29
ENSMUSG00000075053	Vdac3-ps1	0.0048	0.58	1	1	18	0.29
ENSMUSG00000100153	Gm5601	0.022	0.48	0.69	1	18	0.28
ENSMUSG00000062611	Rps3a2	0.026	0.53	1	0.81	18	0.27
ENSMUSG00000091421	Gm4202	0.0058	0.46	1	1	18	0.26
ENSMUSG00000082762	Gm12366	0.0058	0.46	1	1	18	0.25
ENSMUSG00000086922	Gm13835	0.0072	0.5	1	1	18	0.25
ENSMUSG00000100618	Gm29595	0.004	1	0.19	1	18	0.24
ENSMUSG00000085783	Gm9816	0.043	1	1	1	18	0.24
ENSMUSG00000081272	Gm13509	0.0087	1	1	1	18	0.23
ENSMUSG00000063684	Gm13910	0.047	0.98	1	1	18	0.23
ENSMUSG00000073236	2500004C02Rik	5.20E-05	1	1	1	18	0.22
ENSMUSG00000040296	Ddx58	0.047	1	1	1	18	0.21

Ensembl_ ID	Gene	q_C	q_SD3	q_SD6	q_SD12	C_Phase	Amp
ENSMUSG00000085881	Gm15912	0.047	1	1	0.37	18	0.21
ENSMUSG00000043483	Gm6863	0.0058	1	1	1	18	0.2
ENSMUSG00000101188	Eif4a-ps4	0.022	0.32	1	1	18	0.2
ENSMUSG00000084416	Rpl10a-ps1	0.04	1	1	1	18	0.2
ENSMUSG00000032413	Rasa2	0.0079	1	0.48	1	18	0.2
ENSMUSG00000079297	Gm2223	0.0087	1	1	1	18	0.19
ENSMUSG00000083327	Vcp-rs	0.0036	1	1	1	18	0.19
ENSMUSG00000030876	Mettl9	0.004	1	0.57	0.42	18	0.18
ENSMUSG00000078919	Dpm1	0.0072	1	1	1	18	0.18
ENSMUSG00000031170	Slc38a5	0.029	0.4	0.64	0.3	18	0.18
ENSMUSG00000034532	Fbxo16	0.00052	0.21	0.81	1	18	0.18
ENSMUSG00000073164	2410018L13Rik	0.047	0.29	1	1	18	0.18
ENSMUSG00000097148	Gm3839	0.04	1	0.64	1	18	0.17
ENSMUSG00000013584	Aldh1a2	0.012	1	1	0.97	18	0.17
ENSMUSG00000081051	Gm15427	0.0029	1	1	1	18	0.17
ENSMUSG00000097745	AI115009	0.012	0.25	0.72	1	18	0.16
ENSMUSG00000030498	Gas2	0.02	1	1	1	18	0.16
ENSMUSG00000042793	Lgr6	0.014	1	1	0.33	18	0.16
ENSMUSG00000089957	A830011K09Rik	0.026	1	1	1	18	0.16
ENSMUSG00000026384	Ptpn4	0.0053	0.6	1	1	18	0.16
ENSMUSG00000049539	Hist1h1a	0.031	1	1	1	18	0.15
ENSMUSG00000032942	Ucp3	0.014	0.58	0.4	0.76	18	0.15
ENSMUSG00000015568	Lpl	0.022	0.33	0.078	0.42	18	0.15
ENSMUSG00000006931	P3h4	0.0095	0.12	0.84	0.88	18	0.15
ENSMUSG00000027746	Ufm1	0.047	1	1	1	18	0.14
ENSMUSG00000050545	Fam228b	0.024	1	0.5	1	18	0.14
ENSMUSG00000005886	Ncoa2	0.011	1	1	1	18	0.14
ENSMUSG00000097649	Gm10561	0.015	0.14	0.46	1	18	0.14
ENSMUSG00000052544	St6galnac3	0.029	1	0.27	0.36	18	0.14
ENSMUSG00000022329	Stk3	0.012	0.39	1	1	18	0.13
ENSMUSG00000044350	Lacc1	0.0065	1	0.062	1	18	0.13
ENSMUSG00000097515	1700040D17Rik	0.047	1	1	1	18	0.13
ENSMUSG00000031029	Eif3f	0.043	0.2	0.81	1	18	0.13
ENSMUSG00000033423	Eri3	0.043	0.73	0.84	1	18	0.13
ENSMUSG00000022677	Fopnl	0.0021	0.36	0.38	1	18	0.12
ENSMUSG00000059182	Skap2	0.015	1	0.071	0.58	18	0.12
ENSMUSG00000031639	Tlr3	0.0065	0.063	0.058	0.83	18	0.12
ENSMUSG00000048000	Gigyf2	0.0065	0.58	1	0.78	18	0.12
ENSMUSG00000066233	Tmem42	0.0021	0.091	1	1	18	0.12
ENSMUSG00000036086	Zranb3	0.034	0.75	1	1	18	0.12
ENSMUSG00000057406	Whsc1	0.0029	0.98	1	1	18	0.12
ENSMUSG00000074922	Fam122a	0.013	0.85	1	1	18	0.12
ENSMUSG00000052712	BC004004	0.00041	0.063	0.59	0.66	18	0.11
ENSMUSG00000024425	Ndfip1	0.02	0.46	1	1	18	0.11
ENSMUSG00000037148	Arhgap10	0.0029	1	1	1	18	0.11
ENSMUSG00000026471	Mr1	0.034	1	0.44	1	18	0.11
ENSMUSG00000041468	Gpr12	0.04	0.71	1	0.39	18	0.11

Ensembl_ ID	Gene	q_C	q_SD3	q_SD6	q_SD12	C_Phase	Amp
ENSMUSG00000050587	Lrrc4c	0.00047	0.4	1	1	18	0.11
ENSMUSG00000015289	Lage3	0.0021	0.46	0.2	1	18	0.11
ENSMUSG00000038240	Pdss2	0.0048	1	1	0.64	18	0.11
ENSMUSG00000092486	2610524H06Rik	0.00013	1	0.24	0.91	18	0.11
ENSMUSG00000045160	Bola3	0.043	0.75	1	1	18	0.11
ENSMUSG00000024099	Ndufv2	0.015	1	0.48	1	18	0.11
ENSMUSG00000068115	Ninl	0.024	0.42	1	1	18	0.1
ENSMUSG00000055633	Zfp580	0.0087	0.19	1	1	18	0.1
ENSMUSG00000007987	Ift22	0.031	0.51	1	0.88	18	0.1
ENSMUSG00000021767	Kat6b	0.013	1	1	1	18	0.099
ENSMUSG00000091890	A830073O21Rik	0.014	0.66	0.64	0.48	18	0.099
ENSMUSG00000024592	C330018D20Rik	0.0021	0.18	0.3	1	18	0.099
ENSMUSG00000037072	Sep-15	0.024	0.9	0.78	1	18	0.098
ENSMUSG00000020831	0610010K14Rik	0.047	1	0.9	1	18	0.097
ENSMUSG00000030525	Chrna7	0.043	1	1	1	18	0.095
ENSMUSG00000052726	Kcnt2	0.019	1	1	0.52	18	0.095
ENSMUSG00000099681	1700052K11Rik	0.011	0.66	0.44	1	18	0.093
ENSMUSG00000041769	Ppp2r2d	0.00078	1	0.52	1	18	0.092
ENSMUSG00000018446	C1qbp	0.0072	0.24	0.35	1	18	0.091
ENSMUSG00000019872	Smpdl3a	0.037	0.086	0.2	1	18	0.091
ENSMUSG00000033102	Cdc14b	0.011	1	1	1	18	0.09
ENSMUSG00000035239	Neu3	0.043	0.98	0.19	1	18	0.089
ENSMUSG00000029474	Rnf34	0.024	1	1	0.58	18	0.086
ENSMUSG00000039831	Arhgap29	0.017	1	1	1	18	0.085
ENSMUSG00000046688	Tifa	0.029	0.46	1	1	18	0.085
ENSMUSG00000055313	Pgbd1	0.034	1	0.75	0.97	18	0.085
ENSMUSG00000027030	Stk39	0.02	1	1	1	18	0.085
ENSMUSG00000032067	Pts	0.047	1	0.3	0.81	18	0.084
ENSMUSG00000001289	Pfdn5	0.037	0.73	0.97	1	18	0.083
ENSMUSG00000007613	Tgfbr1	0.029	0.55	0.078	0.81	18	0.083
ENSMUSG00000020457	Drg1	0.014	1	1	1	18	0.081
ENSMUSG00000025198	Erlin1	0.0023	1	1	0.88	18	0.081
ENSMUSG00000019699	Akt3	0.0058	0.6	1	1	18	0.081
ENSMUSG00000042705	Commd10	0.024	0.29	0.48	1	18	0.081
ENSMUSG00000005687	Bcas2	0.0079	1	1	0.48	18	0.08
ENSMUSG00000022248	Rad1	0.043	1	1	1	18	0.08
ENSMUSG00000020903	Stx8	0.034	1	1	1	18	0.079
ENSMUSG00000025040	Fundc1	0.031	1	1	1	18	0.078
ENSMUSG00000048058	Ldlrad3	0.024	0.55	0.97	1	18	0.077
ENSMUSG00000026527	Rgs7	0.0044	1	1	1	18	0.077
ENSMUSG00000021610	Clptm1l	0.0053	0.14	0.067	1	18	0.077
ENSMUSG00000031997	Trpc6	0.04	0.8	1	1	18	0.076
ENSMUSG00000021752	Kctd6	0.029	1	0.22	1	18	0.076
ENSMUSG00000002058	Unc119	0.04	0.58	1	1	18	0.075
ENSMUSG00000064037	Gpn1	0.043	1	1	1	18	0.075
ENSMUSG00000058240	Cryzl1	7.00E-04	1	0.67	1	18	0.073
ENSMUSG00000029518	Rab35	0.022	0.18	0.59	1	18	0.073

Ensembl_ ID	Gene	q_C	q_SD3	q_SD6	q_SD12	C_Phase	Amp
ENSMUSG00000041417	Pik3r1	0.014	1	0.3	0.76	18	0.073
ENSMUSG00000018042	Cyb5r3	0.031	0.3	1	1	18	0.073
ENSMUSG00000048249	Crebrf	0.0065	1	1	0.83	18	0.072
ENSMUSG00000038286	Bphl	0.034	0.9	0.72	1	18	0.072
ENSMUSG00000068882	Ssb	0.026	0.6	1	1	18	0.072
ENSMUSG00000026709	Dars2	0.0079	0.5	1	1	18	0.071
ENSMUSG00000015668	Pdzd11	0.022	1	1	1	18	0.07
ENSMUSG00000085151	1110018N20Rik	0.019	1	0.4	1	18	0.069
ENSMUSG00000039530	Tusc3	0.047	0.26	0.93	1	18	0.068
ENSMUSG00000022635	Zcrb1	0.04	0.93	0.23	1	18	0.068
ENSMUSG00000051154	Commd3	0.024	0.73	1	1	18	0.068
ENSMUSG00000027011	Ube2e3	0.0014	1	0.57	1	18	0.065
ENSMUSG00000029146	Snx17	0.0048	0.14	0.87	1	18	0.065
ENSMUSG00000022297	Fzd6	0.0095	1	0.42	1	18	0.062
ENSMUSG00000044600	Smim7	0.031	0.68	0.44	1	18	0.062
ENSMUSG00000070520	Ndnl2	0.00015	0.096	0.19	0.21	18	0.062
ENSMUSG00000036766	Dner	0.043	0.32	0.48	1	18	0.062
ENSMUSG00000021665	Hexb	0.0065	0.6	1	1	18	0.061
ENSMUSG00000036371	Serbp1	0.022	1	0.59	1	18	0.061
ENSMUSG00000017286	Glod4	0.013	1	0.55	1	18	0.059
ENSMUSG00000025451	Paip1	0.034	1	0.69	1	18	0.058
ENSMUSG00000001127	Araf	0.043	0.39	0.57	1	18	0.055
ENSMUSG00000021432	Slc35b3	0.017	1	1	1	18	0.054
ENSMUSG00000048644	Ctxn1	0.0079	0.9	1	1	18	0.051
ENSMUSG00000054405	Dnajc8	0.015	1	1	1	18	0.047
ENSMUSG00000040151	Hs2st1	0.0053	1	1	1	18	0.046
ENSMUSG00000099881	2810013P06Rik	0.037	0.96	0.9	1	18	0.046
ENSMUSG00000032563	Mrpl3	0.04	0.074	1	0.6	18	0.043
ENSMUSG00000032046	Abhd12	0.043	1	1	1	18	0.042
ENSMUSG00000062461	Gm5453	0.013	1	1	1	21	0.78
ENSMUSG00000082454	Gm12183	0.047	0.5	1	1	21	0.62
ENSMUSG00000093056	Gm24812	0.026	1	1	1	21	0.59
ENSMUSG00000093497	Gm20713	0.029	0.9	1	1	21	0.52
ENSMUSG00000083863	Gm13341	0.029	1	1	1	21	0.48
ENSMUSG00000097445	Gm26631	0.014	1	1	1	21	0.48
ENSMUSG00000083992	Gm11478	0.013	1	1	1	21	0.43
ENSMUSG00000087115	Pcsk2os2	0.043	1	1	1	21	0.38
ENSMUSG00000097527	1700112J16Rik	0.014	0.25	0.97	1	21	0.34
ENSMUSG00000055134	9130017K11Rik	0.00035	0.23	0.21	1	21	0.34
ENSMUSG00000085612	Gm15868	0.04	0.83	1	1	21	0.34
ENSMUSG00000087114	Gm16099	0.029	1	1	1	21	0.33
ENSMUSG00000087700	Gm15283	0.031	0.096	1	1	21	0.32
ENSMUSG00000032400	Zwilch	0.026	1	0.62	1	21	0.32
ENSMUSG00000085631	9630028H03Rik	0.037	1	1	1	21	0.32
ENSMUSG00000032565	Nudt16	0.019	1	0.15	0.26	21	0.31
ENSMUSG00000086728	Man2c1os	0.0087	0.56	0.2	0.66	21	0.31
ENSMUSG00000086022	Rad51ap2	5.20E-05	0.12	0.13	1	21	0.3

Ensembl_ ID	Gene	q_C	q_SD3	q_SD6	q_SD12	C_Phase	Amp
ENSMUSG00000062588	Gm6104	0.012	1	0.33	1	21	0.29
ENSMUSG00000085517	Gm12963	0.047	1	1	1	21	0.28
ENSMUSG00000002007	Srpk3	0.0072	0.14	0.16	1	21	0.28
ENSMUSG00000085738	Gm12335	0.028	0.9	1	1	21	0.28
ENSMUSG00000051224	Tceanc	0.004	0.11	0.091	1	21	0.28
ENSMUSG00000024352	Spata24	0.0026	0.36	0.15	1	21	0.28
ENSMUSG00000047773	Ankfn1	0.0095	0.43	1	1	21	0.28
ENSMUSG00000097574	C920006O11Rik	0.00061	1	0.27	1	21	0.27
ENSMUSG00000025038	Efhc2	0.0065	0.17	0.3	1	21	0.27
ENSMUSG00000039496	Cdnf	0.034	1	0.19	1	21	0.27
ENSMUSG00000097123	Gm6297	0.0018	0.34	0.33	0.74	21	0.26
ENSMUSG00000079330	Lemd1	0.00017	0.26	0.062	1	21	0.25
ENSMUSG00000038403	Hfe2	0.004	0.77	0.67	1	21	0.25
ENSMUSG00000044364	Tmem74b	0.0044	0.05	0.26	1	21	0.24
ENSMUSG00000030757	Zkscan2	0.012	0.13	0.15	0.71	21	0.24
ENSMUSG00000002059	Rab34	0.0058	0.13	0.071	0.6	21	0.23
ENSMUSG00000009566	Fpgs	0.0095	1	0.87	1	21	0.23
ENSMUSG00000032558	Nphp3	0.0013	1	0.32	0.33	21	0.23
ENSMUSG00000097350	4732491K20Rik	0.0053	1	0.14	0.26	21	0.23
ENSMUSG00000085436	Zfp335os	0.0095	1	0.72	0.68	21	0.23
ENSMUSG00000020330	Hmmr	0.0053	1	0.52	1	21	0.23
ENSMUSG00000074771	Ankef1	0.0021	1	0.48	1	21	0.22
ENSMUSG00000084898	Gm12371	0.00092	0.14	0.44	0.95	21	0.22
ENSMUSG00000097166	9330179D12Rik	0.00011	0.17	0.33	1	21	0.22
ENSMUSG00000027550	Lrrcc1	0.00035	0.31	0.16	1	21	0.22
ENSMUSG00000084985	Gm16135	0.043	1	1	1	21	0.22
ENSMUSG00000034842	Art3	0.0018	0.26	0.69	0.64	21	0.22
ENSMUSG00000086487	Gm11638	0.017	1	0.2	0.3	21	0.21
ENSMUSG00000097838	C530050E15Rik	0.017	0.6	0.13	0.29	21	0.21
ENSMUSG00000085408	C530005A16Rik	0.014	1	0.24	1	21	0.21
ENSMUSG00000027955	Fam198b	0.0044	0.62	0.55	1	21	0.2
ENSMUSG00000032062	2310030G06Rik	0.011	1	0.26	1	21	0.2
ENSMUSG00000029513	Prkab1	0.014	0.23	0.12	1	21	0.2
ENSMUSG00000028654	Mycl	0.043	0.05	0.23	1	21	0.2
ENSMUSG00000035125	Gcfc2	0.0053	0.93	0.097	1	21	0.2
ENSMUSG00000034035	Ccdc17	0.004	1	1	0.5	21	0.2
ENSMUSG00000036196	Slc26a8	0.0029	0.13	0.11	1	21	0.19
ENSMUSG00000020912	Krt12	0.00023	0.078	0.33	1	21	0.19
ENSMUSG00000042616	Oscp1	0.029	0.83	0.22	1	21	0.19
ENSMUSG00000069835	Sat2	0.00015	0.19	0.48	0.39	21	0.18
ENSMUSG00000079450	Cldn34c1	0.0087	0.13	0.091	1	21	0.18
ENSMUSG00000045322	Tlr9	0.031	0.13	0.16	0.26	21	0.18
ENSMUSG00000042834	Nrep	0.0018	0.21	0.87	1	21	0.18
ENSMUSG00000084803	5830444B04Rik	0.011	0.3	1	1	21	0.17
ENSMUSG00000070632	Btbd8	0.0026	0.12	0.21	0.71	21	0.17
ENSMUSG00000032498	Mlh1	0.037	0.46	0.26	1	21	0.17
ENSMUSG00000052331	Ankrd44	0.017	0.25	0.59	1	21	0.17

Ensembl_ ID	Gene	q_C	q_SD3	q_SD6	q_SD12	C_Phase	Amp
ENSMUSG00000097787	2700046G09Rik	0.0036	0.34	0.3	0.66	21	0.17
ENSMUSG00000021319	Sfrp4	0.02	1	0.17	0.46	21	0.17
ENSMUSG00000094595	Fsbp	0.0079	0.64	0.17	1	21	0.17
ENSMUSG00000032298	Neil1	0.043	0.063	0.29	1	21	0.17
ENSMUSG00000022375	Lrrc6	0.0023	0.37	0.52	0.41	21	0.17
ENSMUSG00000026383	Epb41l5	0.0044	0.51	0.16	1	21	0.17
ENSMUSG00000074863	Platr25	0.012	1	1	1	21	0.17
ENSMUSG00000073427	Gm4924	0.013	1	0.24	1	21	0.16
ENSMUSG00000020374	Rasgef1c	0.011	0.23	0.44	1	21	0.16
ENSMUSG00000072969	Armcx5	2.60E-05	0.96	0.11	0.71	21	0.16
ENSMUSG00000097456	Gm16958	0.031	0.27	0.38	1	21	0.16
ENSMUSG00000035032	Nek11	0.047	0.5	0.15	1	21	0.16
ENSMUSG00000090667	Gm765	0.043	1	0.23	0.91	21	0.16
ENSMUSG00000055612	Cdca7	0.043	1	0.59	1	21	0.16
ENSMUSG00000093553	Gm20633	0.001	0.11	1	1	21	0.16
ENSMUSG00000046287	Pnma3	0.011	0.11	0.72	0.2	21	0.16
ENSMUSG00000085829	Gm4285	0.0058	1	0.11	1	21	0.15
ENSMUSG00000028007	Snx7	0.00019	0.19	1	0.86	21	0.15
ENSMUSG00000099473	Gm18775	0.04	1	1	1	21	0.15
ENSMUSG00000068117	Mei1	0.013	0.5	0.091	1	21	0.15
ENSMUSG00000029333	Rasgef1b	0.0029	0.074	0.22	1	21	0.15
ENSMUSG00000097571	Jpx	0.0065	0.43	0.97	1	21	0.15
ENSMUSG00000039913	Pak7	0.00052	0.27	0.81	1	21	0.15
ENSMUSG00000045930	Clec14a	0.0072	1	1	0.88	21	0.15
ENSMUSG00000099966	2810402E24Rik	0.022	1	0.17	1	21	0.15
ENSMUSG00000063446	Plppr1	0.013	0.2	0.67	1	21	0.14
ENSMUSG00000072809	9330160F10Rik	0.0023	0.19	0.87	1	21	0.14
ENSMUSG00000093606	B130034C11Rik	0.0016	0.074	1	1	21	0.14
ENSMUSG00000029798	Herc6	0.00013	1	0.37	1	21	0.14
ENSMUSG00000063626	Unc5d	0.029	0.23	0.44	1	21	0.14
ENSMUSG00000038147	Cd84	0.034	0.71	1	1	21	0.14
ENSMUSG00000097062	Gm17586	0.0087	0.11	0.19	1	21	0.14
ENSMUSG00000042155	Klhl23	0.0023	0.6	0.16	1	21	0.14
ENSMUSG00000032718	Mansc1	7.00E-04	0.27	0.054	1	21	0.14
ENSMUSG00000037808	Fam76b	0.015	0.43	0.11	0.91	21	0.14
ENSMUSG00000004446	Bid	0.029	0.62	0.3	0.58	21	0.14
ENSMUSG00000032122	Slc37a2	0.0087	0.75	1	1	21	0.13
ENSMUSG00000047989	Ino80c	0.00019	0.51	0.23	1	21	0.13
ENSMUSG00000073073	Gm8098	0.012	0.29	0.2	0.56	21	0.13
ENSMUSG00000079109	Pms2	0.024	0.93	0.12	1	21	0.13
ENSMUSG00000078307	AI593442	0.02	0.091	0.054	0.68	21	0.13
ENSMUSG00000056459	Zbtb25	0.0058	1	0.058	1	21	0.13
ENSMUSG00000099760	Gm28800	0.031	1	0.22	1	21	0.13
ENSMUSG00000013622	Atraid	0.00035	0.12	0.16	1	21	0.13
ENSMUSG00000036916	Zfp280c	0.0095	1	0.59	1	21	0.13
ENSMUSG00000031548	Sfrp1	0.0087	1	0.24	1	21	0.13
ENSMUSG00000040016	Ptger3	0.019	1	0.15	1	21	0.13

Ensembl_ ID	Gene	q_C	q_SD3	q_SD6	q_SD12	C_Phase	Amp
ENSMUSG00000040370	Lyrm5	0.0011	1	0.12	1	21	0.12
ENSMUSG00000026189	Pecr	0.022	0.06	0.071	1	21	0.12
ENSMUSG00000074227	Spint2	0.0053	1	1	0.29	21	0.12
ENSMUSG00000032415	Ube2cbp	0.015	1	1	1	21	0.12
ENSMUSG00000030802	Bckdk	0.00047	0.39	0.78	1	21	0.12
ENSMUSG00000026896	Ifih1	0.014	1	0.72	1	21	0.12
ENSMUSG00000000392	Fap	0.024	0.19	0.27	0.78	21	0.12
ENSMUSG00000096995	2810029C07Rik	0.037	1	0.071	0.91	21	0.12
ENSMUSG00000025888	Casp1	0.017	1	1	1	21	0.12
ENSMUSG00000022360	Atad2	0.0032	1	1	0.83	21	0.12
ENSMUSG00000049612	Omg	8.40E-05	1	0.59	1	21	0.12
ENSMUSG00000039630	Hnrnpu	0.024	0.25	0.5	1	21	0.12
ENSMUSG00000042097	Zfp239	0.034	0.32	1	1	21	0.12
ENSMUSG00000019917	Sep-10	0.013	1	0.35	1	21	0.12
ENSMUSG00000074211	Sdhaf1	0.022	0.26	1	1	21	0.12
ENSMUSG00000040586	Ofd1	0.017	0.14	0.058	1	21	0.12
ENSMUSG00000037376	Trmt6	0.0023	1	0.1	1	21	0.12
ENSMUSG00000042225	Ammecr1	0.013	1	0.97	0.48	21	0.12
ENSMUSG00000026017	Carf	0.043	0.48	1	1	21	0.12
ENSMUSG00000034401	Spata6	0.0013	1	0.55	1	21	0.12
ENSMUSG00000031129	Slc9a9	0.00052	0.13	0.19	1	21	0.12
ENSMUSG00000029186	Pi4k2b	0.031	0.77	0.26	1	21	0.12
ENSMUSG00000015405	Ace2	0.047	1	0.46	0.76	21	0.11
ENSMUSG00000030031	Kbtbd8	0.0029	0.31	0.054	1	21	0.11
ENSMUSG00000027167	Elp4	0.015	0.77	0.59	1	21	0.11
ENSMUSG00000025321	Itgb8	0.0065	0.12	0.33	0.97	21	0.11
ENSMUSG00000029469	Ift81	0.00035	1	0.37	1	21	0.11
ENSMUSG00000022656	Pvrl3	0.014	1	1	1	21	0.11
ENSMUSG00000027615	Hps3	0.029	0.68	0.46	0.83	21	0.11
ENSMUSG00000024818	Slc25a45	0.0052	1	1	1	21	0.11
ENSMUSG00000037089	Slc35b2	0.031	0.078	0.81	0.34	21	0.11
ENSMUSG00000002109	Ddb2	0.011	0.063	0.062	1	21	0.11
ENSMUSG00000026977	Mar-07	0.0023	0.96	0.78	1	21	0.11
ENSMUSG00000071252	2210408I21Rik	0.001	0.091	0.48	0.95	21	0.11
ENSMUSG00000068615	Gjd2	0.013	0.15	0.15	1	21	0.11
ENSMUSG00000026037	Orc2	0.0014	1	0.62	1	21	0.11
ENSMUSG00000021326	Trim27	0.047	0.51	1	0.95	21	0.11
ENSMUSG00000022358	Fbxo32	0.047	0.18	0.21	1	21	0.11
ENSMUSG00000047022	Mipol1	0.0032	0.37	0.11	1	21	0.11
ENSMUSG00000028329	Xpa	0.0095	1	0.37	1	21	0.1
ENSMUSG00000020263	Appl2	0.043	1	1	1	21	0.1
ENSMUSG00000043154	Ppp2r3a	0.02	0.53	0.64	0.71	21	0.1
ENSMUSG00000057895	Zfp105	0.047	1	0.1	0.079	21	0.1
ENSMUSG00000035509	Fbxl21	0.04	0.98	0.19	1	21	0.1
ENSMUSG00000047669	Msl3l2	0.013	1	0.2	1	21	0.1
ENSMUSG00000021209	Ppp4r4	0.034	0.13	0.5	0.2	21	0.1
ENSMUSG00000007589	Tinf2	0.029	0.18	0.48	1	21	0.1

Ensembl_ ID	Gene	q_C	q_SD3	q_SD6	q_SD12	C_Phase	Amp
ENSMUSG00000017677	Wsb1	0.012	0.23	0.33	1	21	0.1
ENSMUSG00000022827	Rabl3	0.043	0.11	0.078	1	21	0.1
ENSMUSG00000018796	Acsl1	0.012	1	0.62	1	21	0.1
ENSMUSG00000044566	Cage1	0.022	1	1	1	21	0.1
ENSMUSG00000055401	Fbxo6	0.013	0.063	0.69	1	21	0.1
ENSMUSG00000033632	AW554918	0.00078	1	1	1	21	0.1
ENSMUSG00000021282	Eif5	0.0011	1	0.19	1	21	0.1
ENSMUSG00000055963	Triqk	0.0095	0.17	0.59	1	21	0.099
ENSMUSG00000028295	Smim8	0.02	1	0.35	1	21	0.099
ENSMUSG00000049122	Frmd3	0.015	0.62	0.12	1	21	0.099
ENSMUSG00000028683	Eif2b3	0.0095	0.45	0.4	0.64	21	0.099
ENSMUSG00000022881	Rfc4	0.014	1	0.5	1	21	0.099
ENSMUSG00000026495	Efcab2	0.022	1	1	1	21	0.099
ENSMUSG00000040771	Oard1	0.0032	1	0.29	1	21	0.099
ENSMUSG00000030254	Rad18	0.031	0.6	0.19	1	21	0.098
ENSMUSG00000002068	Ccne1	0.013	1	1	1	21	0.098
ENSMUSG00000031198	Fundc2	0.014	1	0.59	1	21	0.098
ENSMUSG00000051022	Hs3st1	0.02	0.71	0.067	0.56	21	0.097
ENSMUSG00000022255	Mtdh	0.029	1	0.75	0.68	21	0.097
ENSMUSG00000044229	Nxpe4	0.047	0.11	0.24	0.1	21	0.097
ENSMUSG00000021115	Vrk1	0.037	0.11	0.46	0.37	21	0.097
ENSMUSG00000028222	Calb1	0.024	0.14	1	1	21	0.096
ENSMUSG00000024498	Tcerg1	0.014	1	0.11	1	21	0.096
ENSMUSG00000029328	Hnrnpdl	0.0014	1	0.5	1	21	0.095
ENSMUSG00000030042	Pole4	0.0058	0.53	0.78	1	21	0.095
ENSMUSG00000038507	Parp12	0.0095	1	0.48	1	21	0.095
ENSMUSG00000032355	Mlip	7.80E-06	0.8	0.48	1	21	0.094
ENSMUSG00000021619	Atg10	0.022	0.77	0.59	1	21	0.094
ENSMUSG00000036890	Gtdc1	0.0048	1	0.81	0.48	21	0.094
ENSMUSG00000033931	Rbm34	0.0072	1	0.13	1	21	0.093
ENSMUSG00000079659	Tmem243	0.0013	1	1	1	21	0.093
ENSMUSG00000087674	4930447M23Rik	0.034	0.77	1	1	21	0.092
ENSMUSG00000039043	Arpin	0.014	1	1	1	21	0.092
ENSMUSG00000036632	Alg5	0.0095	0.078	0.27	1	21	0.09
ENSMUSG00000022707	Gbe1	0.0032	0.091	0.48	1	21	0.09
ENSMUSG00000026035	Ppil3	0.017	1	0.3	0.29	21	0.09
ENSMUSG00000024253	Dync2li1	0.011	0.32	0.57	0.97	21	0.09
ENSMUSG00000034321	Exosc1	0.00017	0.77	0.78	1	21	0.089
ENSMUSG00000028568	Btf3l4	0.037	1	0.93	1	21	0.089
ENSMUSG00000029270	Fam69a	0.0018	0.12	0.67	0.97	21	0.089
ENSMUSG00000019792	Trmt11	0.0058	1	0.13	1	21	0.089
ENSMUSG00000022864	D16Ertd472e	0.034	1	1	1	21	0.089
ENSMUSG00000038047	Haus6	0.0048	0.64	0.48	0.62	21	0.089
ENSMUSG00000037492	Zmat4	0.04	0.3	0.062	1	21	0.089
ENSMUSG00000008136	Fhl2	0.013	0.12	0.058	0.13	21	0.088
ENSMUSG00000008333	Snrpb2	0.013	0.17	0.4	0.68	21	0.088
ENSMUSG00000021537	Cetn3	0.017	1	0.37	1	21	0.088

Ensembl_ ID	Gene	q_C	q_SD3	q_SD6	q_SD12	C_Phase	Amp
ENSMUSG00000022837	Iqcb1	0.0053	1	0.37	1	21	0.088
ENSMUSG00000025658	Cnksr2	0.022	1	0.37	0.3	21	0.088
ENSMUSG00000031671	Setd6	0.0058	1	1	1	21	0.087
ENSMUSG00000021033	Gstz1	0.0079	0.1	1	1	21	0.086
ENSMUSG00000053012	Krcc1	0.019	1	0.3	0.97	21	0.086
ENSMUSG00000029234	Tmem165	0.00041	0.96	1	1	21	0.085
ENSMUSG00000055835	Zfp1	0.034	1	0.29	1	21	0.085
ENSMUSG00000055900	Tmem69	0.022	1	0.38	1	21	0.085
ENSMUSG00000039242	B3galnt2	0.047	0.46	0.48	1	21	0.085
ENSMUSG00000041488	Stx3	0.013	0.33	0.16	0.97	21	0.085
ENSMUSG00000035958	Tdp2	0.0023	1	0.33	1	21	0.085
ENSMUSG00000039529	Atp8b1	0.04	1	1	1	21	0.084
ENSMUSG00000022092	Ppp3cc	0.0026	0.68	0.27	1	21	0.084
ENSMUSG00000020956	Dtd2	0.0072	0.45	0.27	1	21	0.084
ENSMUSG00000027499	Pkia	0.011	1	1	1	21	0.084
ENSMUSG00000055409	Nell1	0.015	0.17	0.17	1	21	0.083
ENSMUSG00000069844	Sco1	0.0065	1	0.64	0.66	21	0.083
ENSMUSG00000059142	Zfp945	0.029	0.73	1	1	21	0.082
ENSMUSG00000020840	Blmh	0.043	1	0.33	1	21	0.082
ENSMUSG00000056004	9330182L06Rik	0.037	0.31	0.35	1	21	0.081
ENSMUSG00000025170	Rab40b	0.04	0.074	1	1	21	0.081
ENSMUSG00000027667	Zfp639	0.031	1	0.3	1	21	0.08
ENSMUSG00000028292	Rars2	0.02	0.85	1	0.83	21	0.079
ENSMUSG00000016494	Cd34	0.0053	0.68	0.3	1	21	0.079
ENSMUSG00000031591	Asah1	0.026	0.71	0.48	1	21	0.079
ENSMUSG00000050697	Prkaa1	0.022	1	0.24	0.42	21	0.078
ENSMUSG00000036598	Ccdc113	0.04	1	1	1	21	0.078
ENSMUSG00000021852	Slc35f4	0.02	0.24	0.75	1	21	0.077
ENSMUSG00000030967	Zranb1	0.024	1	0.75	1	21	0.077
ENSMUSG00000016487	Ppfibp1	0.037	0.5	0.84	1	21	0.077
ENSMUSG00000033319	Fem1c	0.014	0.48	0.24	1	21	0.077
ENSMUSG00000038622	Med30	0.0018	0.98	0.42	1	21	0.077
ENSMUSG00000057497	Fam136a	0.00031	0.091	0.097	0.11	21	0.077
ENSMUSG00000032468	Armc8	0.0087	0.13	0.33	0.62	21	0.077
ENSMUSG00000061665	Cd2ap	0.015	1	0.29	1	21	0.076
ENSMUSG00000034480	Diaph2	0.0072	1	0.67	0.58	21	0.076
ENSMUSG00000061119	Prcp	0.0087	0.85	0.17	0.6	21	0.076
ENSMUSG00000033910	Gucy1a3	0.037	1	0.44	1	21	0.076
ENSMUSG00000022523	Fgf12	0.0072	1	0.52	1	21	0.075
ENSMUSG00000038844	Kif16b	0.0095	0.091	0.23	1	21	0.075
ENSMUSG00000078771	Evi2a	0.037	0.58	1	1	21	0.075
ENSMUSG00000034442	Trmt5	0.031	0.85	0.44	1	21	0.074
ENSMUSG00000097823	Gm16701	0.0095	1	0.5	1	21	0.074
ENSMUSG00000031583	Wrn	0.024	0.14	0.52	0.76	21	0.074
ENSMUSG00000065979	Cpped1	0.0079	0.34	1	0.83	21	0.074
ENSMUSG00000071253	Slc25a16	0.029	0.56	0.35	0.29	21	0.074
ENSMUSG00000030423	Pop4	0.014	1	0.78	1	21	0.073

Ensembl_ ID	Gene	q_C	q_SD3	q_SD6	q_SD12	C_Phase	Amp
ENSMUSG00000046603	Tcaim	0.043	0.43	0.78	1	21	0.073
ENSMUSG00000045259	Klhdc9	0.034	1	1	1	21	0.073
ENSMUSG00000039166	Akap7	0.0036	1	1	1	21	0.073
ENSMUSG00000038991	Txndc5	0.015	0.06	1	1	21	0.072
ENSMUSG00000021368	Tbc1d7	0.031	0.64	0.81	1	21	0.071
ENSMUSG00000004642	Slbp	0.026	0.85	0.57	1	21	0.07
ENSMUSG00000075478	Slitrk1	0.024	0.05	0.17	1	21	0.07
ENSMUSG00000028646	Rragc	0.012	1	0.69	1	21	0.07
ENSMUSG00000072623	Zfp9	0.0087	1	0.21	1	21	0.07
ENSMUSG00000051730	Mettl5	0.02	0.23	0.15	1	21	0.07
ENSMUSG00000031292	Cdkl5	0.034	1	0.42	0.81	21	0.07
ENSMUSG00000027080	Med19	0.04	1	1	1	21	0.069
ENSMUSG00000019818	Cd164	0.0072	1	0.19	0.28	21	0.069
ENSMUSG00000074165	Zfp788	0.017	0.16	0.2	1	21	0.069
ENSMUSG00000023106	Denr	0.012	1	0.24	1	21	0.069
ENSMUSG00000028869	Gnl2	0.0044	1	0.93	1	21	0.068
ENSMUSG00000026187	Xrcc5	0.04	0.25	0.93	0.95	21	0.068
ENSMUSG00000033781	Asb13	0.015	0.091	0.21	1	21	0.068
ENSMUSG00000046314	Stxbp6	0.0065	0.68	0.81	1	21	0.067
ENSMUSG00000020691	Mettl2	0.024	0.6	0.87	1	21	0.067
ENSMUSG00000097718	Gm26896	0.017	0.93	0.42	0.5	21	0.067
ENSMUSG00000021377	Dek	0.014	0.71	1	1	21	0.067
ENSMUSG00000042447	Mios	0.011	0.53	0.46	1	21	0.066
ENSMUSG00000020459	Mtif2	0.037	1	0.72	0.86	21	0.066
ENSMUSG00000027810	Eif2a	0.015	1	1	1	21	0.066
ENSMUSG00000032417	Rwdd2a	0.037	0.77	0.59	1	21	0.065
ENSMUSG00000021357	Exoc2	0.0087	0.078	0.13	0.64	21	0.064
ENSMUSG00000026634	Angel2	0.047	0.23	0.42	1	21	0.064
ENSMUSG00000042579	4632404H12Rik	0.02	1	0.19	1	21	0.064
ENSMUSG00000070705	Eid2b	0.047	0.25	0.57	0.64	21	0.064
ENSMUSG00000018651	Tada2a	0.031	1	0.52	1	21	0.063
ENSMUSG00000042446	Zmym4	0.031	0.34	0.15	1	21	0.063
ENSMUSG00000033918	Parl	0.0044	0.42	0.57	0.97	21	0.063
ENSMUSG00000063296	Tmem117	0.047	1	0.59	1	21	0.063
ENSMUSG00000033166	Dis3	0.043	0.98	0.35	0.95	21	0.062
ENSMUSG00000022339	Ebag9	0.034	1	0.35	1	21	0.061
ENSMUSG00000039047	Pigk	0.0013	0.83	0.55	0.68	21	0.06
ENSMUSG00000021684	Pde8b	0.022	0.34	0.72	1	21	0.059
ENSMUSG00000028223	Decr1	0.043	1	0.16	1	21	0.059
ENSMUSG00000049092	Gpr137c	0.047	0.64	0.11	1	21	0.059
ENSMUSG00000005583	Mef2c	0.024	1	0.93	1	21	0.059
ENSMUSG00000062995	Ica1	0.014	1	1	1	21	0.058
ENSMUSG00000046311	Zfp62	0.02	0.1	1	1	21	0.058
ENSMUSG00000038070	Cntln	0.029	1	0.62	1	21	0.058
ENSMUSG00000027834	Serpini1	0.04	0.71	1	1	21	0.058
ENSMUSG00000015733	Capza2	0.011	1	0.5	1	21	0.057
ENSMUSG00000044442	N6amt1	0.031	0.8	0.078	1	21	0.056

Ensembl_ ID	Gene	q_C	q_SD3	q_SD6	q_SD12	C_Phase	Amp
ENSMUSG00000043190	Rfesd	0.012	0.19	0.097	1	21	0.055
ENSMUSG00000020952	Scfd1	0.029	0.057	0.26	0.25	21	0.054
ENSMUSG00000028015	Ctso	0.015	0.39	0.11	0.76	21	0.053
ENSMUSG00000041935	AW549877	0.019	1	0.35	1	21	0.053
ENSMUSG00000059669	Taf1b	0.024	0.21	0.57	0.88	21	0.052
ENSMUSG00000025898	Cwf19l2	0.031	1	0.57	1	21	0.052
ENSMUSG00000037573	Tob1	0.015	0.057	0.13	1	21	0.052
ENSMUSG00000066456	Hmgn3	0.015	1	0.9	1	21	0.052
ENSMUSG00000096210	H1f0	0.0018	0.93	0.33	1	21	0.052
ENSMUSG00000050379	Sep-06	0.034	1	1	1	21	0.052
ENSMUSG00000020794	Ube2g1	0.034	1	0.69	1	21	0.051
ENSMUSG00000028790	Khdrbs1	0.026	1	0.38	1	21	0.05
ENSMUSG00000022808	Snx4	0.029	1	0.87	1	21	0.05
ENSMUSG00000035762	Tmem161b	0.047	1	0.62	0.62	21	0.049
ENSMUSG00000020677	Ddx52	0.015	0.53	1	0.54	21	0.048
ENSMUSG00000064138	Fam172a	0.019	0.75	0.62	1	21	0.048
ENSMUSG00000021929	Kpna3	0.022	1	0.3	1	21	0.047
ENSMUSG00000032252	Glce	0.024	1	1	1	21	0.047
ENSMUSG00000030978	Rrm1	0.047	0.46	1	1	21	0.047
ENSMUSG00000033111	3830406C13Rik	0.026	0.8	0.75	1	21	0.047
ENSMUSG00000029833	Trim24	0.031	1	0.32	1	21	0.047
ENSMUSG00000014353	Tmem87b	0.047	0.45	0.81	1	21	0.047
ENSMUSG00000026771	Spopl	0.034	1	1	0.56	21	0.046
ENSMUSG00000006599	Gtf2h1	0.022	1	1	1	21	0.046
ENSMUSG00000034007	Scaper	0.04	1	0.87	1	21	0.046
ENSMUSG00000033653	Vps8	0.029	1	1	1	21	0.045
ENSMUSG00000037787	Apopt1	0.014	0.66	0.97	1	21	0.045
ENSMUSG00000023307	Mar-05	0.034	0.22	1	1	21	0.045
ENSMUSG00000023460	Rab12	0.0079	0.31	0.55	1	21	0.044
ENSMUSG00000049536	Tceal1	0.024	0.27	0.52	0.78	21	0.042
ENSMUSG00000026098	Pms1	0.034	0.8	1	1	21	0.042
ENSMUSG00000028397	Kdm4c	0.0072	1	0.37	1	21	0.042
ENSMUSG00000025609	Mkln1	0.047	1	1	1	21	0.04
ENSMUSG00000046671	Mtfr1l	0.019	0.27	0.57	1	21	0.038
ENSMUSG00000024234	Mtpap	0.024	1	0.75	1	21	0.038
ENSMUSG00000028086	Fbxw7	0.029	1	1	1	21	0.035
ENSMUSG00000019795	Pcmt1	0.022	0.36	1	1	21	0.034
ENSMUSG00000025264	Tsr2	0.037	0.88	1	1	21	0.034
ENSMUSG00000027108	Ola1	0.043	1	0.93	1	21	0.033

App.4. Diurnal Genes Affected by Sleep Deprivation

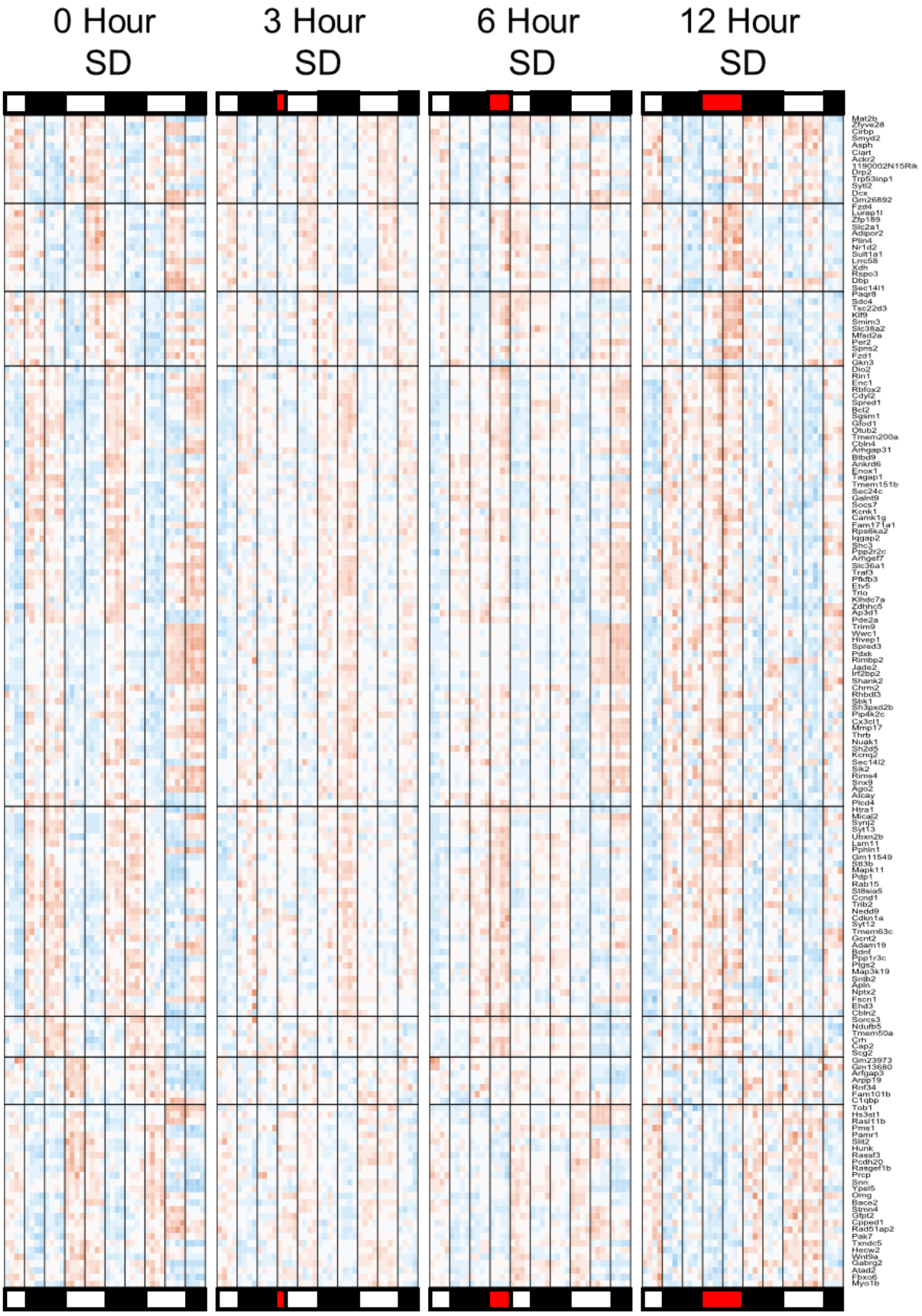

App.5. Non-Diurnal Genes Affected by Sleep Deprivation

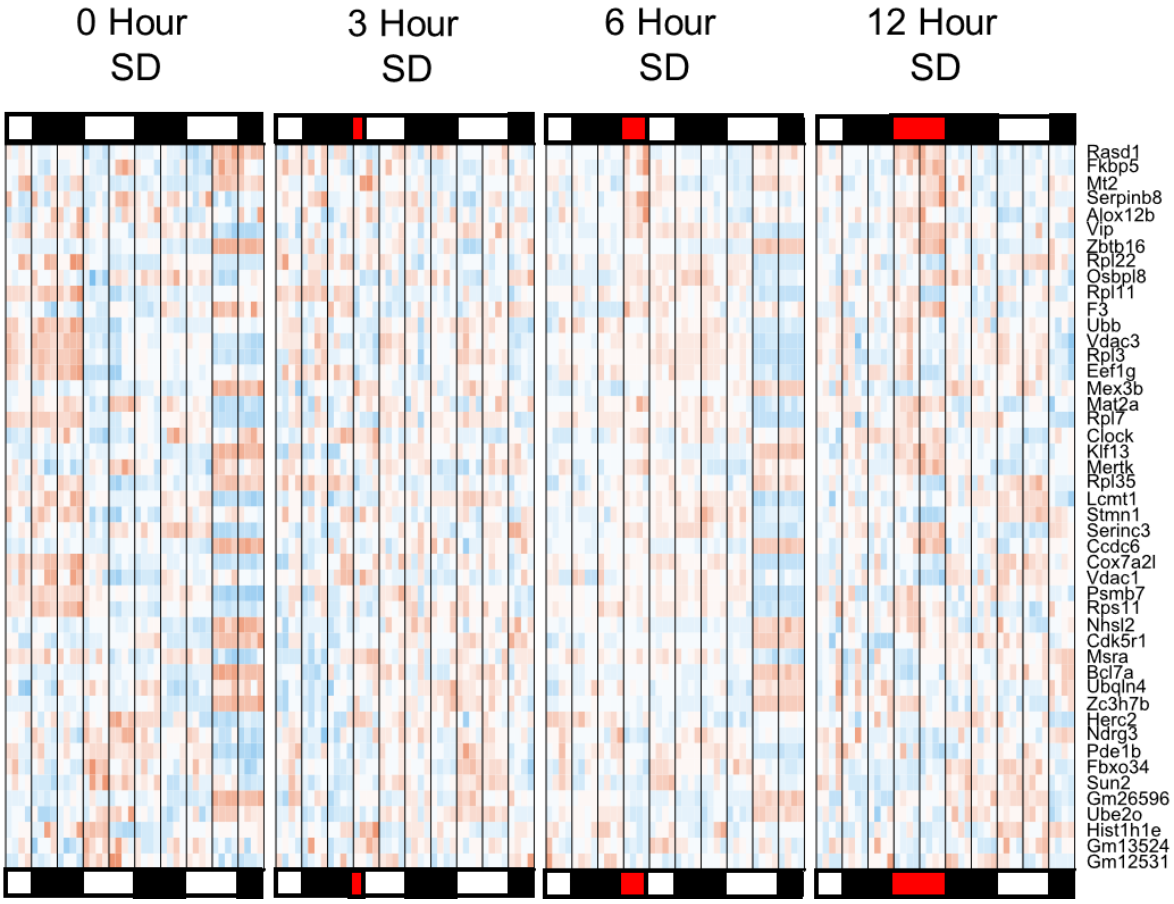

App.6. Genes showing a Homeostatic Expression Profile

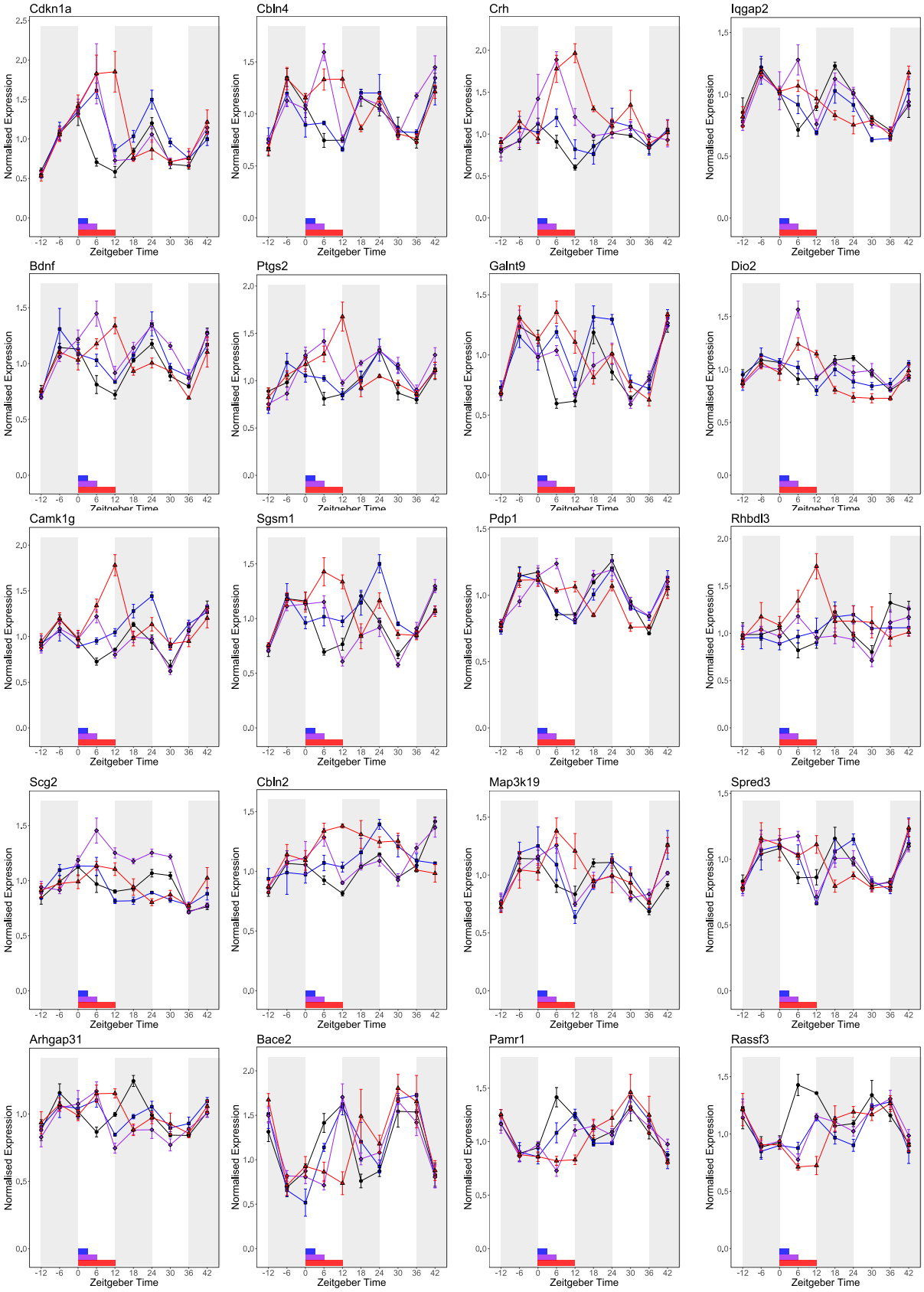

App.7. Genes showing a Stress Expression Profile

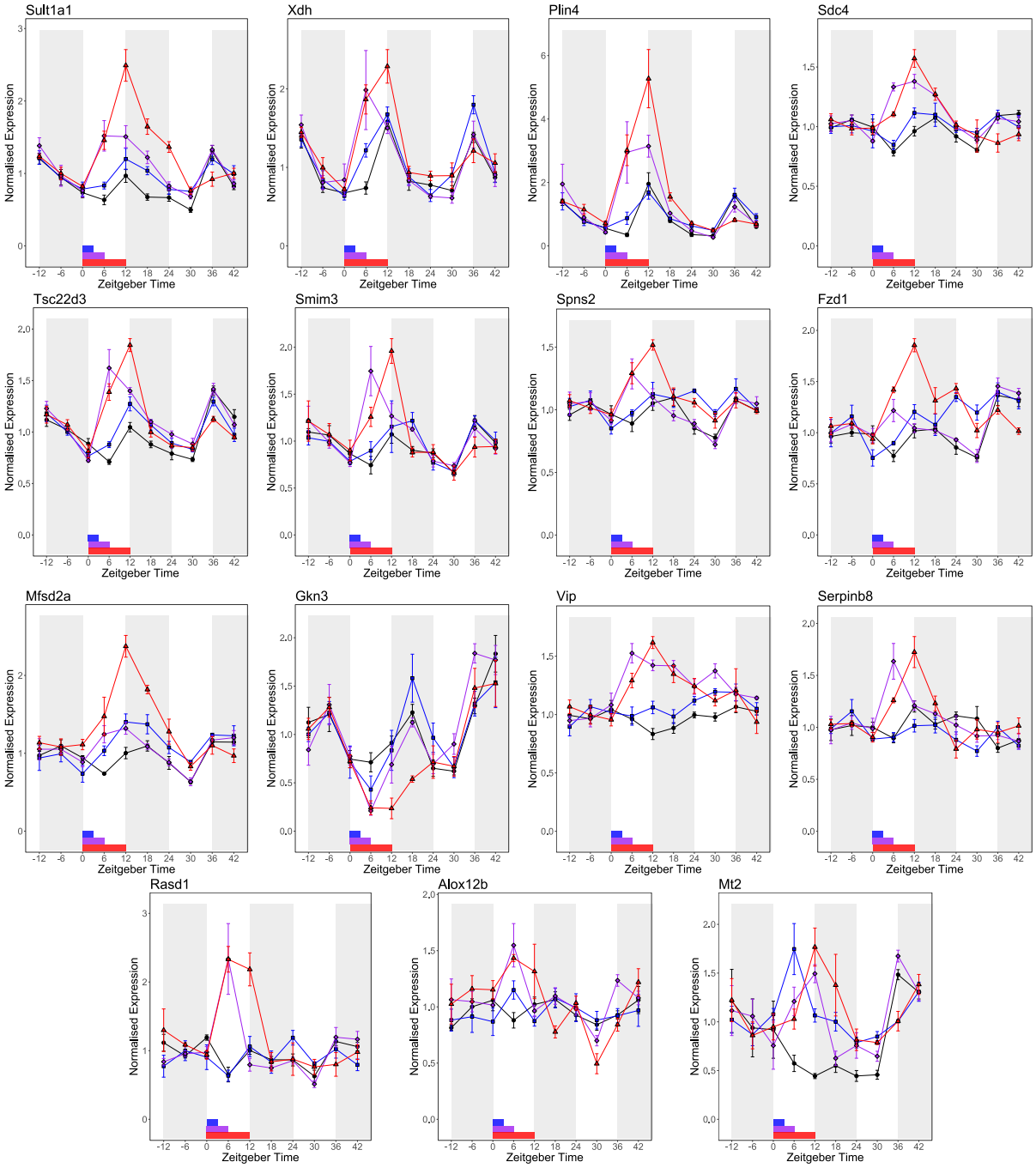

App.8. Diurnal Transcripts Affected by Sleep Deprivation

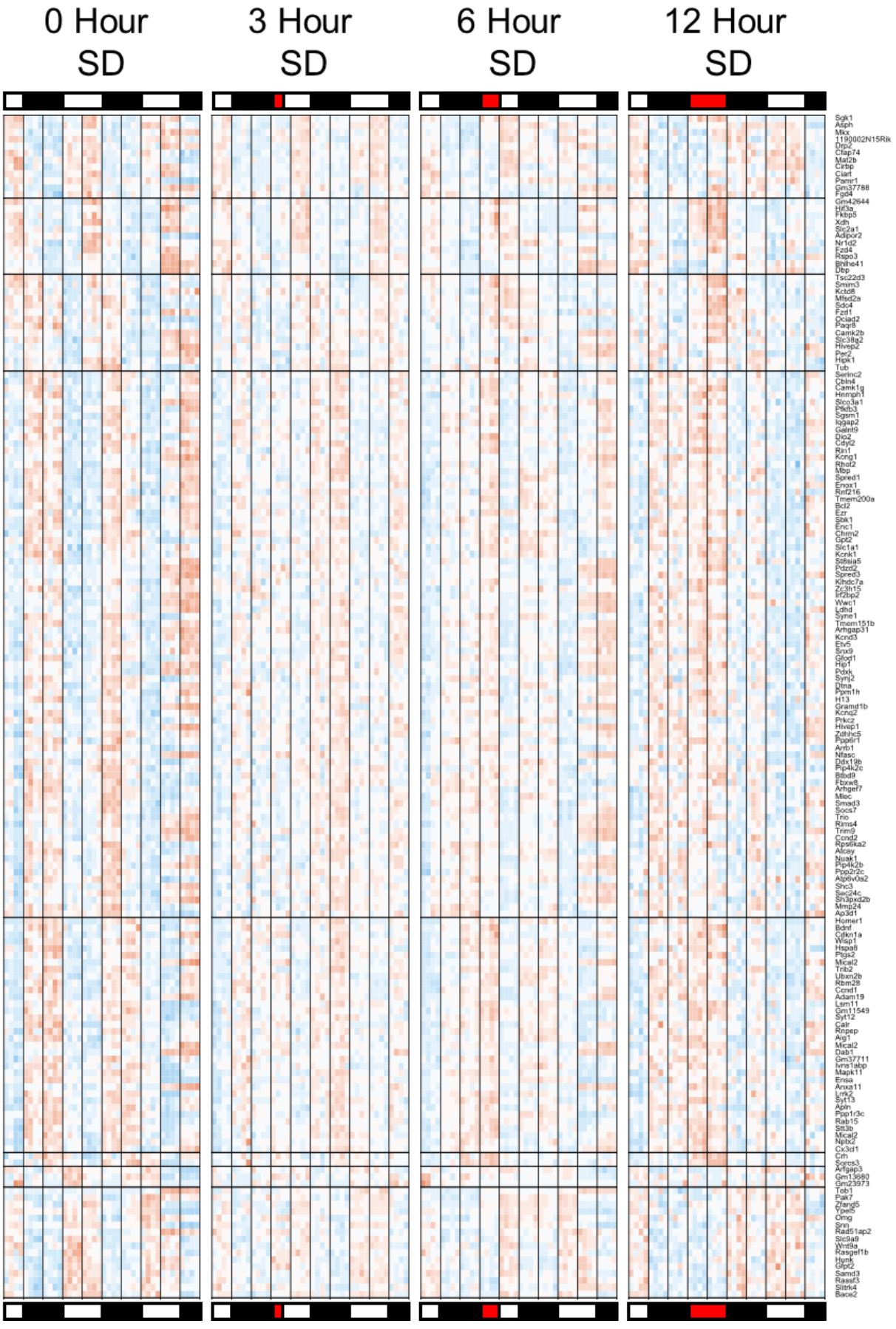

App.9. Non-Diurnal Transcripts Affected by Sleep Deprivation

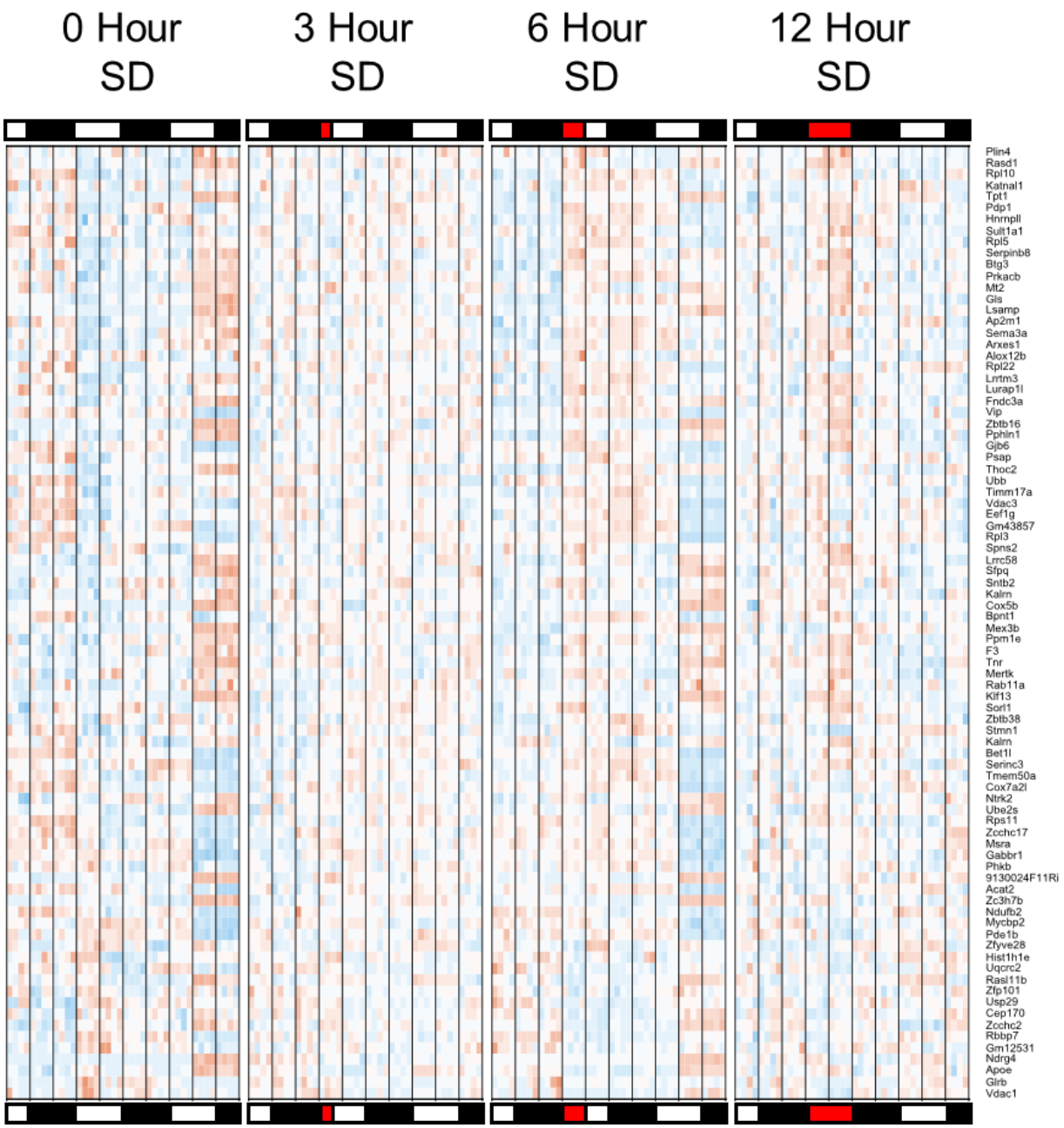

App.10. Isoforms showing a Homeostatic Expression Profile

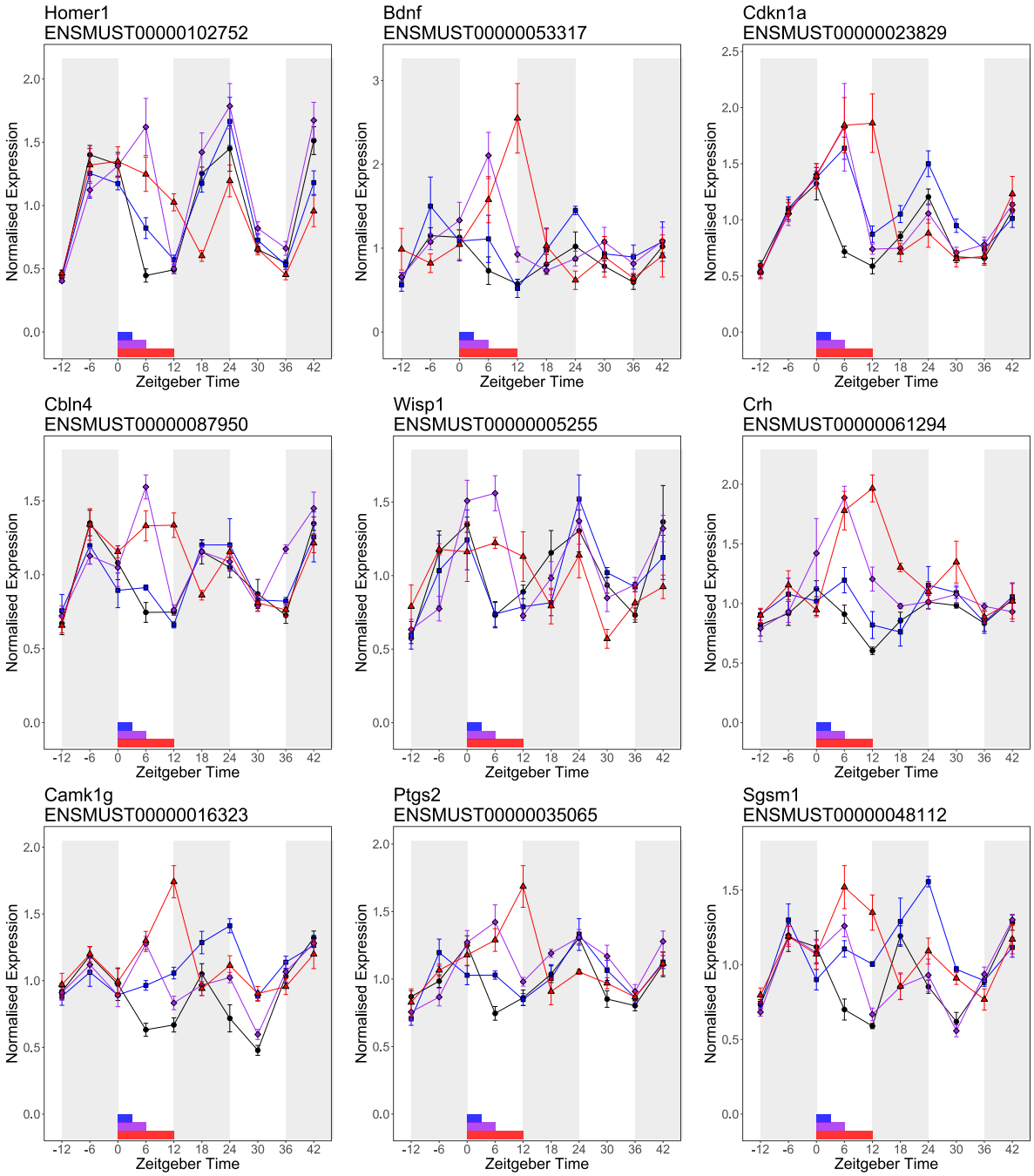

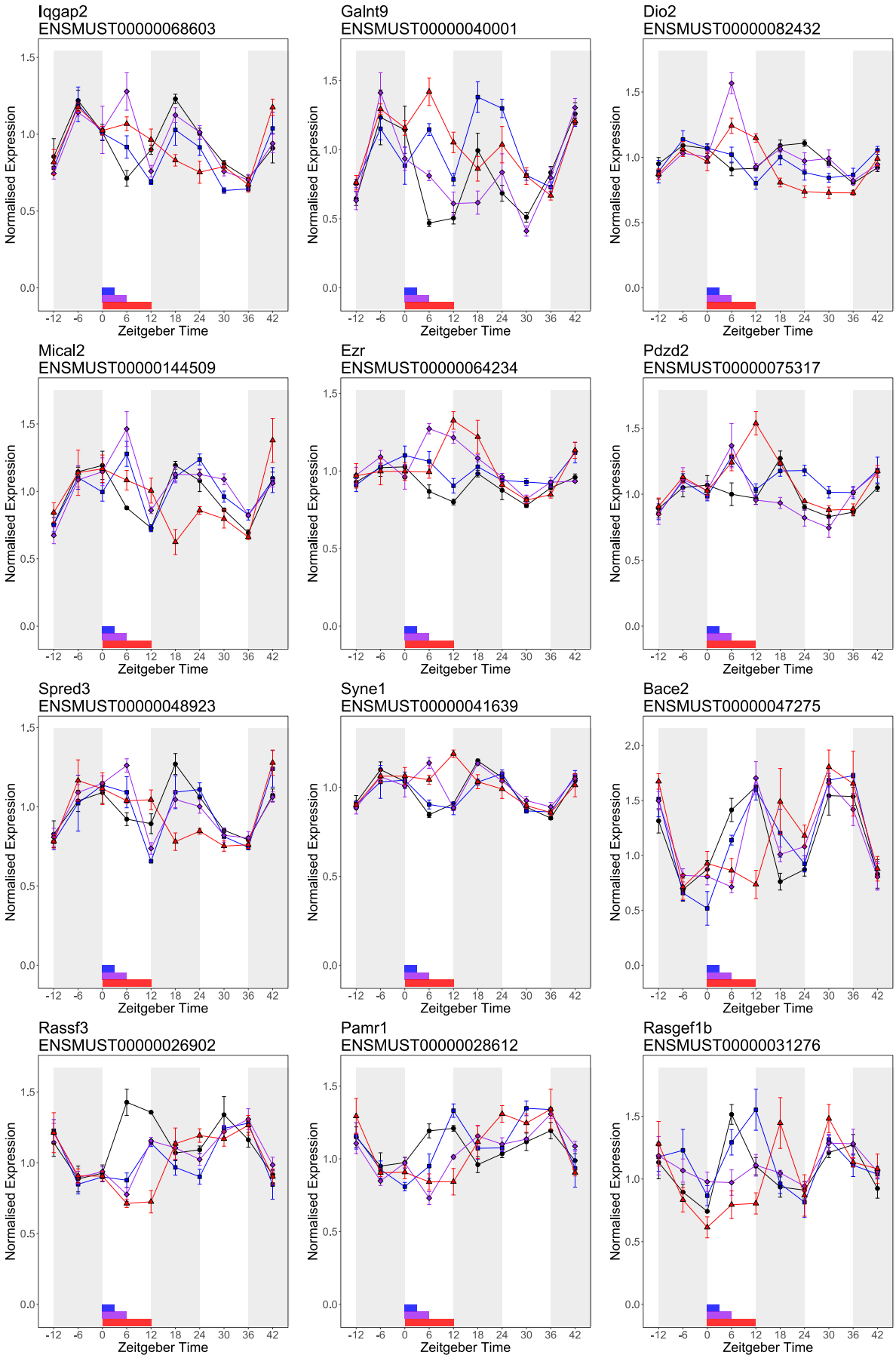
Iqgap2
ENSMUST00000068603
Galnt9
ENSMUST00000040001
Dio2
ENSMUST00000082432
Mical2
ENSMUST00000144509
Ezr
ENSMUST00000064234
Pdzd2
ENSMUST00000075317
Spred3
ENSMUST00000048923
Syne1
ENSMUST00000041639
Bace2
ENSMUST00000047275
Rassf3
ENSMUST00000026902
Pamr1
ENSMUST00000028612
Rasgef1b
ENSMUST00000031276
Normalised Expression
Zeitgeber Time

App.11. Isoform showing a Stress Expression Profiles

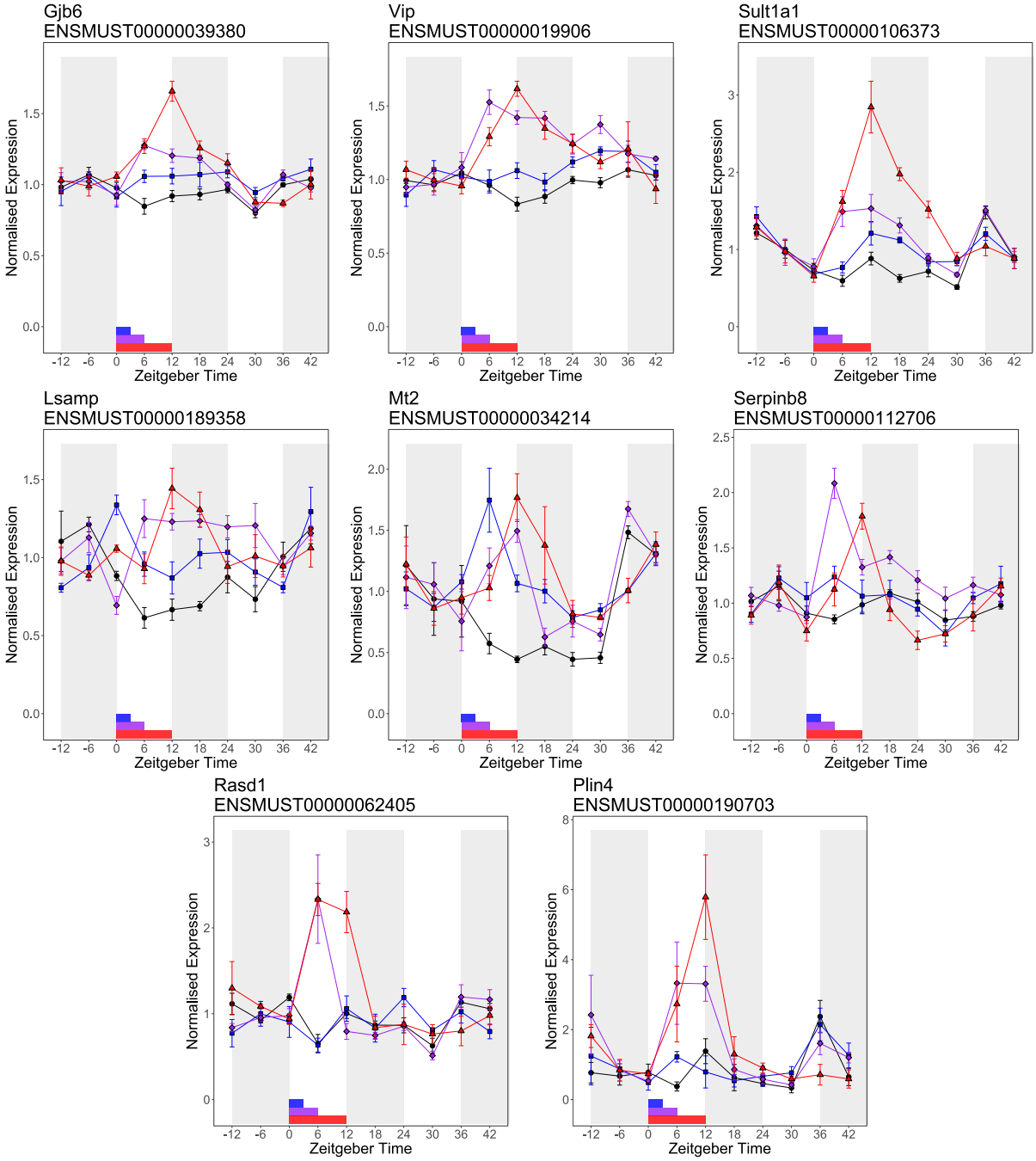

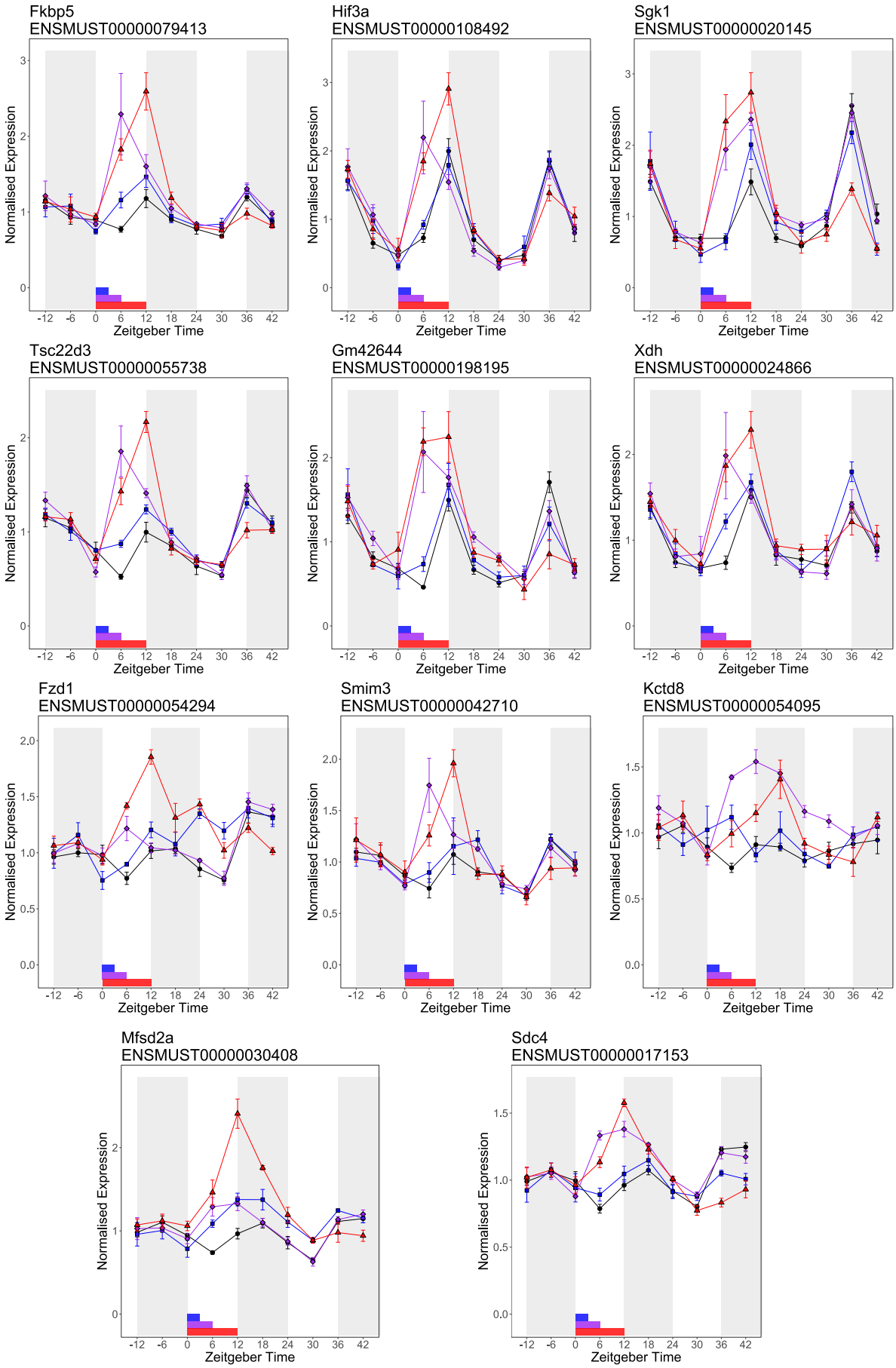
Fkbp5
ENSMUST00000079413
Hif3a
ENSMUST00000108492
Sgk1
ENSMUST00000020145
Tsc22d3
ENSMUST00000055738
Gm42644
ENSMUST00000198195
Xdh
ENSMUST00000024866
Fzd1
ENSMUST00000054294
Smim3
ENSMUST00000042710
Kctd8
ENSMUST00000054095
Mfsd2a
ENSMUST00000030408
Sdc4
ENSMUST00000017153
Normalised Expression
Zeitgeber Time
-12 -6 0 6 12 18 24 30 36 42

App.12. Protein whose Abundance is Modulated by Sleep Deprivation

Abundance of proteins modulated by sleep deprivation, normalised to the abundance in non-sleep deprived animals. T_00 represents 6pm Day0 (0hrs SD), T_24 represents 6pm Day1 (12hrs SD, 0hrs Recovery), whilst T_48 represents 6pm Day2 (12hrs SD, 24hrs Recovery). Also included are the fdr adjusted p-values for the pairwise comparisons.

Protein	T_00	T_24	T_48	q_00_24	q_00_48	q_24_48
GNAL	1	1.73	1.5	0.00364	0.0272	0.0269
PC4L1	1	1.47	1.79	0.00474	0.0226	0.0165
F6RT34	1	1.28	1.2	0.0112	0.0272	0.0268
CRYM	1	1.27	1.18	0.00273	0.0449	0.0198
AINX	1	1.19	1.11	0.00474	0.0309	0.0362
LRC57	1	0.962	0.891	0.0288	0.0172	0.0131
RP3A	1	0.955	0.905	0.0414	0.0172	0.0197
S4A10	1	0.92	0.96	0.00494	0.0272	0.0172
GFAP	1	0.894	1.14	0.0135	0.0307	0.00329
RL21	1	0.894	0.812	0.0309	0.0493	0.0472
HMGN2	1	0.892	1.41	0.0195	0.0272	0.00568
CO3	1	0.888	1.14	0.00378	0.0172	7.00E-04
RL8	1	0.877	0.755	0.0175	0.0272	0.0204
VIME	1	0.87	1.3	0.039	0.0299	0.0149
H4	1	0.808	0.671	0.0112	0.0172	0.0169
H31	1	0.793	0.652	0.0101	0.0469	0.0299
HPT	1	0.654	1.73	0.0297	0.0172	0.00787
TY3H	1	2.02	1.49	0.0122	0.0493	0.0554
MOG	1	1.33	1.32	0.00788	0.0272	0.85
CN37	1	1.31	1.23	0.00294	0.0449	0.149
GLTP	1	1.31	1.31	0.00273	0.0172	0.928
SIR2	1	1.21	1.16	0.0122	0.0429	0.103
NFM	1	1.2	1.13	0.00761	0.0469	0.0716
ENPP6	1	1.2	1.24	0.0487	0.0335	0.525
CRYAB	1	1.18	1.13	0.0165	0.0352	0.185
ACY2	1	1.16	1.17	0.00762	0.0299	0.499
NDRG4	1	1.06	1.07	0.0406	0.0469	0.562
SYGP1	1	0.972	0.945	0.0484	0.0384	0.0717
PLEC	1	0.96	0.932	0.0309	0.0299	0.0531
NED4L	1	0.956	0.952	0.00378	0.0272	0.48
CTRO	1	0.944	0.924	0.0297	0.0272	0.188
NMDZ1	1	0.938	0.914	0.0404	0.0272	0.188
KPCD	1	0.937	0.905	0.0372	0.0335	0.143
ARPC3	1	0.931	0.894	0.0402	0.0316	0.108
KALRN	1	0.928	0.925	0.039	0.0469	0.871
SRBS2	1	0.92	0.903	0.0163	0.0335	0.223
S12A5	1	0.913	0.877	0.0131	0.0272	0.107

Protein	T_00	T_24	T_48	q_00_24	q_00_48	q_24_48
GRM2	1	0.903	0.925	0.00273	0.0243	0.0824
KCD16	1	0.891	0.9	0.0135	0.0401	0.649
AT1A1	1	0.88	0.852	0.0406	0.0386	0.329
RL36A	1	0.877	0.836	0.0165	0.0352	0.203
RL13A	1	0.876	0.826	0.0195	0.0385	0.185
H12	1	0.808	0.688	0.0323	0.0425	0.0821
RL34	1	0.794	0.711	0.00396	0.0385	0.135
H13	1	0.776	0.695	0.0297	0.0272	0.169
H14	1	0.694	0.615	0.0178	0.0402	0.0888
S10A9	1	2.91	0.955	0.0135	0.736	0.00329
CO1A1	1	1.96	0.863	0.00378	0.0884	0.00371
PDE10	1	1.94	1.09	0.00364	0.317	0.00371
CO1A2	1	1.79	0.84	0.00273	0.0561	7.00E-04
GBG7	1	1.69	1.1	0.00273	0.137	0.00329
NTCP4	1	1.65	1.08	0.00474	0.353	0.0117
ADCY5	1	1.62	1.04	0.00364	0.452	0.00329
PDE1B	1	1.54	1.04	0.00827	0.193	0.00329
PPR1B	1	1.53	1	0.00474	0.999	0.00781
ANR63	1	1.48	1.07	0.0112	0.327	0.0165
ARP21	1	1.26	0.99	0.0234	0.843	0.0117
PCP4	1	1.25	1.1	0.0178	0.0975	0.00329
SCN4B	1	1.21	0.924	0.0414	0.235	0.0197
AL1A1	1	1.2	0.942	0.00783	0.234	0.0246
IPP2	1	1.19	1.05	0.0112	0.107	0.0251
ACTN2	1	1.18	1	0.0178	0.854	0.00493
RCN1	1	1.16	1.02	0.0122	0.546	0.0208
MAOM	1	1.15	1.03	0.0452	0.21	0.0301
PHAR1	1	1.11	0.958	0.0406	0.133	0.023
CATA	1	0.941	1.03	0.00273	0.0974	0.0169
E9Q8N8	1	0.924	1.01	0.0476	0.538	0.0459
IDE	1	0.918	0.994	0.0122	0.572	0.0147
STXB6	1	0.91	1.03	0.0417	0.249	0.0169
PVRL1	1	0.908	0.962	0.00396	0.112	0.0357
FIBG	1	0.899	0.969	0.0178	0.193	0.024
FIBA	1	0.892	0.977	0.0309	0.383	0.0371
S6A11	1	0.89	1.21	0.0452	0.104	0.0268
BLVRB	1	0.888	1.02	0.00898	0.297	0.00371
A2AP	1	0.878	1.02	0.0127	0.394	0.0362
E9Q035	1	0.869	1.01	0.00635	0.659	0.00329
H2AW	1	0.867	1.1	0.0215	0.0836	0.00732
SPTA1	1	0.866	1.04	0.0262	0.188	0.0147
HEMO	1	0.859	1.08	0.0373	0.112	0.00761
PLMN	1	0.842	1	0.0177	0.94	0.0343
ALBU	1	0.836	0.979	0.0293	0.468	0.00782
PZP	1	0.822	1.02	0.00762	0.308	0.00271
A1AT4	1	0.82	0.994	0.00474	0.74	0.0049
SPA3K	1	0.815	0.966	0.00776	0.214	0.00755

Protein	T_00	T_24	T_48	q_00_24	q_00_48	q_24_48
APOC1	1	0.787	0.92	0.00378	0.104	0.0251
A8DUK4	1	0.742	0.973	0.00399	0.476	0.0197
HBA	1	0.709	0.974	0.0177	0.513	0.00568
SEGN	1	0.588	3.62	0.0405	0.0833	0.0468
PENK	1	1.41	1.11	0.037	0.386	0.126
MOBP	1	1.32	1.27	0.00474	0.0678	0.283
GRP2	1	1.28	1.03	0.00913	0.638	0.0631
ANLN	1	1.27	1.26	0.0297	0.113	0.948
MYPR	1	1.27	1.29	0.00474	0.0795	0.799
F7A0B0	1	1.24	1.1	0.0269	0.323	0.239
CD82	1	1.22	1.21	0.00679	0.107	0.84
MAG	1	1.21	1.16	0.014	0.0545	0.135
MYO1D	1	1.21	1.22	0.0234	0.0706	0.785
BCAS1	1	1.2	1.14	0.0309	0.0985	0.326
NFL	1	1.2	1.12	0.00679	0.0572	0.0752
ILEUA	1	1.2	1.22	0.00378	0.12	0.769
MK03	1	1.15	1.14	0.0484	0.0671	0.89
CDK18	1	1.14	1.1	0.0309	0.0935	0.337
NECA2	1	1.13	1.11	0.0052	0.139	0.504
HPCL1	1	1.13	1.14	0.0372	0.134	0.926
AGAP2	1	1.13	1.05	0.0464	0.223	0.122
NUCB2	1	1.11	1.14	0.0482	0.222	0.75
DC1I1	1	1.1	1.12	0.0404	0.115	0.533
BCR	1	1.1	1.02	0.0135	0.633	0.182
CAD13	1	1.09	1.05	0.0406	0.123	0.157
AMPL	1	1.09	1.07	0.0406	0.107	0.164
CTL1	1	1.09	1.11	0.0241	0.0649	0.318
FMN2	1	1.08	0.992	0.035	0.865	0.184
CRAC1	1	1.07	1.1	0.0409	0.201	0.624
LACE1	1	1.06	1.05	0.0178	0.363	0.834
DDAH1	1	1.06	1.05	0.0452	0.179	0.745
PLCL1	1	1.06	1.06	0.0417	0.13	0.789
AOFB	1	1.05	1.01	0.0405	0.638	0.358
PDE1A	1	1.05	1.02	0.0297	0.325	0.176
PLXA2	1	1.04	0.998	0.035	0.896	0.116
NSF1C	1	1.04	1.05	0.0059	0.189	0.709
PEX19	1	1.03	1.07	0.0297	0.267	0.431
IQEC1	1	0.973	0.953	0.0135	0.147	0.328
ERC2	1	0.968	0.939	0.0309	0.0857	0.177
KIF5C	1	0.965	0.994	0.015	0.625	0.162
VP13A	1	0.965	0.96	0.0297	0.0698	0.602
RB33A	1	0.963	0.97	0.0297	0.157	0.696
WDR7	1	0.963	0.951	0.0297	0.132	0.475
CAD10	1	0.961	0.942	0.0452	0.128	0.419
AL1L1	1	0.961	0.96	0.0181	0.155	0.977
NRX1A	1	0.958	0.952	0.033	0.117	0.72
SHRM2	1	0.958	0.972	0.0297	0.12	0.253

Protein	T_00	T_24	T_48	q_00_24	q_00_48	q_24_48
ANK1	1	0.956	0.983	0.0309	0.411	0.259
Q68FG2	1	0.955	0.915	0.0317	0.0705	0.129
BIEA	1	0.954	0.948	0.045	0.0852	0.693
AP2S1	1	0.954	0.928	0.0297	0.105	0.314
PPCEL	1	0.951	0.969	0.00273	0.277	0.481
CADM2	1	0.948	0.901	0.0405	0.0795	0.119
TCPR1	1	0.947	0.946	0.0406	0.0625	0.978
AUP1	1	0.945	0.956	0.0405	0.413	0.855
LRRT4	1	0.944	0.956	0.0321	0.0747	0.381
CTNB1	1	0.944	0.953	0.0161	0.0501	0.453
GRIA2	1	0.943	0.934	0.0309	0.0997	0.68
KLC2	1	0.942	0.98	0.0317	0.223	0.0741
RAB14	1	0.939	0.938	0.0405	0.203	0.987
A2APX7	1	0.938	0.906	0.0298	0.0977	0.322
DHE3	1	0.934	0.936	0.0321	0.132	0.964
DLGP2	1	0.934	0.906	0.0135	0.0975	0.332
CTND1	1	0.931	0.936	0.039	0.0706	0.828
MPP2	1	0.931	0.932	0.037	0.0675	0.957
PYGM	1	0.931	0.932	0.0297	0.0692	0.956
ANXA2	1	0.928	0.966	0.00273	0.324	0.319
SHAN1	1	0.922	0.941	0.0444	0.0871	0.201
CBR2	1	0.92	1.05	0.0441	0.227	0.0821
ANXA5	1	0.919	1	0.0135	0.836	0.0565
TMM65	1	0.914	0.918	0.0415	0.227	0.949
B2RUS7	1	0.911	0.904	0.0405	0.49	0.972
GBG2	1	0.902	0.88	0.0452	0.206	0.765
EPHB3	1	0.902	0.91	0.0309	0.0673	0.748
RL36	1	0.9	0.823	0.0452	0.0779	0.147
PMGE	1	0.9	1.02	0.0223	0.621	0.14
KCC2G	1	0.899	0.881	0.0475	0.0977	0.501
COCA1	1	0.895	1	0.0297	0.967	0.366
VGLU2	1	0.895	0.926	0.0117	0.151	0.404
UBTD1	1	0.892	0.931	0.0297	0.209	0.392
SC6A1	1	0.891	0.939	0.0174	0.248	0.342
TAGL	1	0.883	0.943	0.0444	0.143	0.135
CAH1	1	0.88	1.02	0.0244	0.712	0.0737
SYT2	1	0.872	0.852	0.0101	0.0706	0.559
MUG1	1	0.865	0.993	0.00827	0.873	0.152
RL13	1	0.86	0.77	0.00364	0.0881	0.17
MOT1	1	0.858	0.93	0.0444	0.354	0.378
RL28	1	0.835	0.754	0.0452	0.078	0.0564
RL4	1	0.802	0.759	0.00152	0.0643	0.25
B3AT	1	0.8	1.02	0.0309	0.65	0.0678
H15	1	0.775	0.738	0.0291	0.0647	0.392
CEP95	1	0.775	0.81	0.0415	0.0706	0.49
WDR33	1	0.765	0.971	0.0372	0.662	0.0739
J3QMC5	1	1.1	1.92	0.244	0.0272	0.00325

Protein	T_00	T_24	T_48	q_00_24	q_00_48	q_24_48
PSIP1	1	1.08	1.18	0.126	0.0402	0.0498
CMGA	1	1.07	1.43	0.368	0.0272	0.0493
AKAP5	1	1.04	0.893	0.0863	0.0272	0.00329
ITIH4	1	1.04	1.34	0.478	0.0172	0.023
D19L1	1	1.02	1.52	0.827	0.0485	0.0298
KCC4	1	1.01	0.883	0.556	0.0386	0.0396
SAE1	1	1.01	1.1	0.71	0.0352	0.0177
TMEDA	1	1	1.14	0.932	0.0272	0.0266
XRP2	1	1	1.3	0.964	0.0243	0.0321
ROCK2	1	1	0.96	0.841	0.0383	0.0139
MYO6	1	1	1.26	0.981	0.0478	0.0169
NOE1	1	0.997	0.931	0.841	0.0352	0.0115
GPSM1	1	0.995	1.26	0.841	0.0243	0.00454
KINH	1	0.988	1.13	0.349	0.0172	0.00329
PCBP3	1	0.988	1.32	0.797	0.0272	0.00329
CDC42	1	0.986	1.18	0.573	0.0405	0.0478
LMNB1	1	0.982	1.15	0.145	0.0157	0.000976
Sep-05	1	0.979	0.922	0.139	0.0272	0.0157
NDUA2	1	0.976	0.866	0.444	0.0352	0.0242
RL14	1	0.975	0.767	0.465	0.0499	0.0169
E9QK48	1	0.963	1.19	0.411	0.0272	0.0169
AMPD2	1	0.963	1.16	0.288	0.0493	0.00271
RL7A	1	0.96	0.768	0.279	0.0307	0.00493
RL18	1	0.952	0.797	0.359	0.0488	0.048
FABP7	1	0.944	1.44	0.383	0.0384	0.00761
RS8	1	0.936	0.806	0.161	0.0386	0.0222
RL18A	1	0.935	0.829	0.0884	0.0243	0.024
CALB2	1	0.93	1.9	0.125	0.0384	0.00477
ACBD7	1	0.908	1.83	0.247	0.0352	0.0153
S10A5	1	0.83	11.3	0.302	0.0469	0.0266
A1AG1	1	0.817	1.11	0.0835	0.0299	0.0299
OMP	1	0.773	7.08	0.0945	0.0307	0.00731
RL6	1	0.745	0.645	0.0687	0.0469	0.0251
MVP	1	1.15	1.29	0.147	0.0272	0.153
NMRL1	1	1.13	1.16	0.0687	0.0172	0.358
RGS14	1	1.09	1.07	0.097	0.0402	0.488
E9Q7G0	1	1.08	1.14	0.224	0.0352	0.374
CALU	1	1.07	1.1	0.144	0.0352	0.394
NOP56	1	1.07	1.12	0.0784	0.0449	0.107
SAFB1	1	1.05	1.1	0.184	0.0272	0.172
E9Q5C9	1	1.05	1.09	0.142	0.0272	0.101
Q3UJB0	1	1.04	1.08	0.244	0.0469	0.225
EIF3A	1	1.04	1.05	0.0915	0.0469	0.297
SYAC	1	1.01	1.03	0.234	0.0386	0.154
RMD3	1	1.01	1.04	0.696	0.0402	0.108
GLRX3	1	1	0.963	0.846	0.0335	0.0716
ADHX	1	0.999	1.07	0.935	0.0385	0.0659

Protein	T_00	T_24	T_48	q_00_24	q_00_48	q_24_48
SHAN3	1	0.997	0.918	0.848	0.0469	0.0591
SNX3	1	0.988	0.942	0.601	0.0405	0.12
ACSL1	1	0.986	0.951	0.449	0.0449	0.103
OGT1	1	0.985	0.96	0.303	0.0385	0.12
KAD1	1	0.98	1.06	0.499	0.0402	0.0785
TBAL3	1	0.98	1.14	0.76	0.0172	0.101
RS9	1	0.979	0.854	0.381	0.0384	0.0752
F8VPN4	1	0.976	0.966	0.0808	0.0383	0.233
AGRL1	1	0.974	0.951	0.134	0.0494	0.112
AGAP3	1	0.973	0.951	0.307	0.0452	0.328
PITM2	1	0.971	0.958	0.114	0.0469	0.268
ACYP1	1	0.969	0.93	0.166	0.0413	0.0821
PREP	1	0.968	0.939	0.0749	0.0493	0.0583
ARP2	1	0.966	0.922	0.0687	0.0494	0.0748
BSN	1	0.964	0.928	0.179	0.0494	0.0785
UN13A	1	0.962	0.931	0.0808	0.0384	0.0695
AT2B1	1	0.962	0.911	0.142	0.0352	0.0693
DGLA	1	0.96	0.93	0.118	0.0498	0.177
COR1A	1	0.954	0.895	0.193	0.0469	0.101
NPTN	1	0.947	0.905	0.0946	0.0384	0.116
SYN1	1	0.946	0.93	0.0649	0.0386	0.369
MAGI2	1	0.943	0.933	0.0808	0.0243	0.602
BRNP1	1	0.941	0.933	0.0865	0.0499	0.737
SYT1	1	0.937	0.913	0.132	0.0412	0.426
TAGL3	1	0.937	0.889	0.0515	0.0449	0.113
HOME1	1	0.925	0.876	0.0693	0.0469	0.139
GBB5	1	0.919	0.907	0.1	0.0493	0.493
AKA7G	1	0.912	0.854	0.0613	0.0385	0.107
NU5M	1	0.911	0.846	0.166	0.0469	0.224
RL31	1	0.91	0.88	0.0835	0.0352	0.333
RL3	1	0.902	0.867	0.0687	0.0487	0.203
RGS6	1	0.892	0.864	0.103	0.0494	0.328
RL19	1	0.862	0.77	0.0808	0.0402	0.138
RL24	1	0.835	0.693	0.114	0.0386	0.105
RL29	1	0.818	0.68	0.108	0.0352	0.0571
CPNE9	1	0.803	0.723	0.0535	0.0307	0.224
DDC	1	1.35	1.06	0.101	0.518	0.023
PTN5	1	1.19	0.935	0.0915	0.23	7.00E-04
NETO2	1	1.16	0.971	0.242	0.735	0.0445
E9Q6Y8	1	1.15	1	0.123	0.939	0.0205
GRIN3	1	1.14	0.879	0.31	0.276	0.0169
CYB5B	1	1.13	0.956	0.0808	0.327	0.0169
TOP1	1	1.11	0.955	0.271	0.52	0.0269
SYT10	1	1.11	1.59	0.433	0.0583	0.00787
CBR3	1	1.1	0.996	0.192	0.937	0.0162
PTMA	1	1.09	1.22	0.179	0.0663	0.0468
HTRA1	1	1.08	0.962	0.335	0.525	0.00577

Protein	T_00	T_24	T_48	q_00_24	q_00_48	q_24_48
CPNE5	1	1.08	0.974	0.114	0.316	0.0179
NSMA2	1	1.08	0.937	0.13	0.128	0.0315
ISLR2	1	1.08	0.957	0.296	0.434	0.0493
MAP1B	1	1.07	1.13	0.0687	0.0728	0.0365
RT07	1	1.07	0.902	0.257	0.137	0.0407
RIFK	1	1.07	1.14	0.537	0.252	0.0459
STRN	1	1.07	0.992	0.0535	0.585	0.00454
DGKB	1	1.06	0.944	0.149	0.165	0.0049
HP1B3	1	1.06	0.853	0.394	0.12	0.0418
SLK	1	1.06	1.01	0.0781	0.387	0.00493
RPGP1	1	1.06	0.976	0.11	0.327	0.0407
MAON	1	1.05	0.984	0.157	0.43	0.00329
KPCB	1	1.05	0.962	0.194	0.213	0.0285
NIPS1	1	1.05	0.88	0.104	0.0721	0.0169
LMNB2	1	1.05	1.13	0.342	0.106	0.0363
TOM70	1	1.05	0.935	0.128	0.132	0.0334
GABT	1	1.04	0.984	0.361	0.66	0.0445
F136A	1	1.04	0.977	0.274	0.45	0.0459
GRP78	1	1.04	0.963	0.247	0.251	0.0407
SRSF2	1	1.04	1.11	0.197	0.0556	0.0407
ITPR1	1	1.04	0.945	0.0535	0.0648	0.00727
UCHL1	1	1.04	0.981	0.48	0.645	0.0246
BAIP2	1	1.04	0.938	0.244	0.106	0.0197
HNRPC	1	1.03	1.1	0.131	0.0678	0.0495
PP2AA	1	1.03	0.982	0.468	0.625	0.0396
DAPK3	1	1.03	0.95	0.468	0.26	0.0301
FUS	1	1.03	1.11	0.303	0.0586	0.0413
CYLD	1	1.03	0.938	0.0835	0.051	0.00974
ENSA	1	1.03	0.955	0.506	0.321	0.0169
HPCA	1	1.03	0.945	0.34	0.166	0.00544
NDUA5	1	1.03	0.925	0.155	0.0728	0.0268
RLBP1	1	1.03	1.14	0.553	0.121	0.00329
MLF2	1	1.03	0.961	0.61	0.417	0.0127
CPLX2	1	1.03	0.957	0.265	0.135	0.00371
ATP5H	1	1.02	0.952	0.547	0.259	0.0169
NDUA6	1	1.02	0.835	0.658	0.084	0.0169
AKA12	1	1.02	1.15	0.639	0.102	0.0169
IST1	1	1.02	1.11	0.535	0.105	0.0072
RHG44	1	1.02	0.973	0.507	0.291	0.0334
TCPA	1	1.02	0.998	0.476	0.93	0.0139
E9PV14	1	1.02	1.13	0.617	0.0649	0.0495
SCN2B	1	1.02	0.957	0.594	0.198	0.0246
MLP3B	1	1.01	1.08	0.573	0.0836	0.0488
ATPO	1	1.01	0.929	0.729	0.149	0.046
CD166	1	1.01	0.95	0.677	0.197	0.0365
NGEF	1	1.01	0.905	0.726	0.104	0.0169
OSCP1	1	1.01	1.12	0.354	0.0706	0.0429

Protein	T_00	T_24	T_48	q_00_24	q_00_48	q_24_48
RGS20	1	1.01	0.914	0.815	0.159	0.0198
CX6B1	1	1.01	0.936	0.793	0.183	0.0459
RS2	1	1.01	0.94	0.759	0.165	0.0268
SKP1	1	1.01	0.943	0.787	0.182	0.0415
PUF60	1	1.01	1.07	0.766	0.113	0.027
CAH2	1	1.01	1.08	0.762	0.108	0.0472
NDUB4	1	1.01	0.941	0.818	0.164	0.0486
AK1A1	1	1.01	0.969	0.468	0.0833	0.0325
GDN	1	1.01	1.14	0.854	0.0556	0.0407
BCS1	1	1.01	0.965	0.868	0.378	0.0478
SFPQ	1	1.01	1.07	0.776	0.0779	0.0347
F177A	1	1.01	1.09	0.793	0.0795	0.00454
RS10	1	1.01	0.954	0.854	0.184	0.0486
HPLN1	1	1.01	0.97	0.822	0.256	0.0165
PDE2A	1	1.01	0.953	0.586	0.0975	0.0232
PFKAP	1	1	0.967	0.89	0.343	0.012
NBEA	1	1	0.974	0.926	0.341	0.0407
CA2D3	1	1	0.897	0.952	0.1	0.0358
COQ9	1	1	0.954	0.943	0.189	0.0346
KAP3	1	1	0.896	0.961	0.0795	0.041
PPM1E	1	1	1.09	0.975	0.121	0.0197
SUCB1	1	1	0.948	0.976	0.145	0.048
LRRC7	1	1	0.95	0.985	0.227	0.041
BPHL	1	0.999	0.912	0.995	0.171	0.0174
A3KGU7	1	0.999	0.961	0.94	0.0583	0.0484
CCZ1	1	0.999	1.09	0.986	0.171	0.0407
PHB	1	0.999	0.938	0.967	0.124	0.0408
CPNE6	1	0.997	1.15	0.866	0.0643	0.00605
TCOF	1	0.996	1.09	0.934	0.157	0.0408
INPP	1	0.995	1.02	0.874	0.36	0.0493
UBP4	1	0.995	1.05	0.814	0.137	0.00493
LDHA	1	0.995	0.94	0.898	0.177	0.0478
MYH10	1	0.995	0.952	0.746	0.084	0.0246
QCR7	1	0.994	0.914	0.806	0.084	0.0049
GLSK	1	0.994	0.935	0.874	0.182	0.0266
ABLM2	1	0.994	0.917	0.908	0.175	0.0495
MIF	1	0.993	0.85	0.945	0.196	0.045
CNRP1	1	0.993	0.893	0.882	0.165	0.0169
U5S1	1	0.993	1.04	0.567	0.0779	0.0315
PLCB1	1	0.992	0.952	0.807	0.213	0.0396
GMFB	1	0.991	0.932	0.818	0.157	0.0454
RUFY1	1	0.991	1.1	0.894	0.208	0.0169
F169A	1	0.991	1.04	0.793	0.237	0.0459
RAB6A	1	0.99	0.937	0.621	0.071	0.0277
KAP1	1	0.99	0.934	0.606	0.0747	0.0266
PGM2L	1	0.99	0.941	0.714	0.135	0.0424
LAP2A	1	0.99	1.13	0.743	0.0742	0.0328

Protein	T_00	T_24	T_48	q_00_24	q_00_48	q_24_48
S4R1W8	1	0.99	1.43	0.955	0.0955	0.0268
ATPB	1	0.989	0.934	0.617	0.128	0.0486
NANP	1	0.987	0.897	0.667	0.0974	0.00974
HECD1	1	0.987	1.03	0.726	0.375	0.0199
MYO1B	1	0.985	0.927	0.444	0.0664	0.0169
KIF2A	1	0.985	1.04	0.553	0.192	0.0334
Q14BI1	1	0.983	0.933	0.782	0.288	0.0472
NDUAA	1	0.983	0.903	0.653	0.114	0.0424
XPO1	1	0.982	1.04	0.42	0.137	0.0208
VAC14	1	0.981	1.04	0.687	0.376	0.0494
PHB2	1	0.979	0.918	0.476	0.107	0.0195
HCFC1	1	0.979	1.03	0.518	0.308	0.0347
KBTBB	1	0.979	1.04	0.309	0.115	0.0325
E9Q616	1	0.978	1.03	0.531	0.358	0.0268
GTR3	1	0.978	0.921	0.411	0.0795	0.0493
HS12A	1	0.978	0.921	0.384	0.084	0.0493
ROA3	1	0.975	1.07	0.657	0.255	0.0298
E9PZ43	1	0.974	1.07	0.496	0.19	0.00341
LMNA	1	0.973	1.03	0.0946	0.168	0.048
41	1	0.972	1.05	0.57	0.286	0.023
KKCC2	1	0.972	0.918	0.343	0.0837	0.048
PCLO	1	0.972	0.942	0.29	0.12	0.0266
APC	1	0.972	1.03	0.163	0.137	0.0208
PRDX6	1	0.969	0.909	0.328	0.108	0.0358
LSAMP	1	0.968	0.937	0.696	0.414	0.0293
LYSM1	1	0.967	1.01	0.586	0.916	0.0268
A1BN54	1	0.967	0.905	0.297	0.102	0.0101
PREX1	1	0.966	0.995	0.13	0.701	0.0445
GRIN1	1	0.965	1.02	0.255	0.315	0.0334
NDUB7	1	0.965	0.899	0.355	0.112	0.0276
GPM6B	1	0.96	0.858	0.475	0.112	0.0486
NRX3A	1	0.958	1.02	0.0852	0.291	0.0208
RS25	1	0.957	0.863	0.149	0.061	0.0459
ACSF2	1	0.957	0.996	0.159	0.822	0.041
HCDH	1	0.956	1.02	0.142	0.383	0.0387
B1AQX9	1	0.954	0.919	0.0852	0.0676	0.0341
RL27	1	0.951	0.835	0.359	0.0833	0.0226
SO1C1	1	0.944	2	0.761	0.0705	0.0169
RB27B	1	0.941	0.891	0.246	0.12	0.0385
CXA1	1	0.939	1.01	0.351	0.853	0.024
DLGP3	1	0.937	0.883	0.44	0.209	0.0424
CIRBP	1	0.935	1.06	0.136	0.176	0.0197
CLGN	1	0.933	1.51	0.695	0.086	0.023
EST1C	1	0.924	1.04	0.0586	0.259	0.0409
KCJ10	1	0.921	1.15	0.224	0.0934	0.015
ADCY8	1	0.91	1.05	0.103	0.207	0.0268
CO4A2	1	0.908	0.764	0.199	0.0721	0.0408

Protein	T_00	T_24	T_48	q_00_24	q_00_48	q_24_48
RL7	1	0.904	0.722	0.293	0.105	0.00329
TBA8	1	0.903	1.06	0.144	0.216	0.00371
NQO1	1	0.901	1.48	0.114	0.084	0.0454
RL35	1	0.885	0.738	0.224	0.084	0.0177
UT1	1	0.879	1.02	0.151	0.734	0.0161
KNG1	1	0.871	1.03	0.114	0.446	0.0169
CFAH	1	0.868	0.996	0.108	0.925	0.041
VTDB	1	0.86	1.02	0.0884	0.583	0.00325
CENPE	1	0.859	0.954	0.11	0.366	0.0472
ENOB	1	0.852	1.09	0.142	0.207	0.0478
SYNPR	1	0.848	0.99	0.108	0.849	0.0179
A1AT2	1	0.832	1.04	0.116	0.353	0.0169
A1AT3	1	0.831	0.978	0.0649	0.654	0.0402
APOA1	1	0.823	0.913	0.103	0.195	0.0115
E9QAF8	1	0.799	0.956	0.108	0.514	0.0459

App.13. Genes Affected by 6 hour Illumination in SH-SY5Y Cells

Data are presented that show the genes identified by Cuffdiff as being modulated by at least twofold immediately following 6 hour illumination in opsin expressing SH-SY5Y cells, compared to dark maintained cells collected at the same timepoint. The FPKM value of expression is listed for Control and Illuminated cells, and the log2 fold change, together with the Benjamini adjusted p-value for this comparison.

Ensembl_Gene_ID	Gene_name	Control	Illuminated	Log2_FC	q_val
ENSG00000279047	CTC-270D5.1	6.66E-07	0.504	19.5	0.0329
ENSG00000232656	IDI2-AS1	0.0104	0.481	5.53	0.0477
ENSG00000231728	LL0XNC01-116E7.2	0.224	6.26	4.8	0.00255
ENSG00000230615	RP5-1198O20.4	0.733	12.7	4.11	0.00138
ENSG00000183715	OPCML	0.0367	0.618	4.07	0.00138
ENSG00000119508	NR4A3	0.182	2.71	3.89	0.00138
ENSG00000232176	RP11-146N23.1	0.345	4.26	3.63	0.0123
ENSG00000170345	FOS	0.841	9.78	3.54	0.00138
ENSG00000123700	KCNJ2	0.382	4.08	3.42	0.00138
ENSG00000225358	MIPEPP1	0.102	0.79	2.95	0.0181
ENSG00000223414	LINC00473	9.72	70.4	2.86	0.00138
ENSG00000130513	GDF15	13	91.4	2.81	0.00138
ENSG00000130164	LDLR	7.13	50	2.81	0.00138
ENSG00000176058	TPRN	6.06	40.7	2.75	0.00138
ENSG00000230333	AC004538.3	0.216	1.36	2.66	0.0276
ENSG00000186480	INSIG1	12.9	80.6	2.64	0.00138
ENSG00000277813	ACEA_U3	8070	49300	2.61	0.00138
ENSG00000213626	LBH	15.3	91	2.57	0.00138
ENSG00000123358	NR4A1	12.8	72.1	2.49	0.00138
ENSG00000266289	RP11-1C8.6	0.38	2.06	2.44	0.00739
ENSG00000204584	RP11-304F15.3	0.181	0.972	2.43	0.00138
ENSG00000160870	CYP3A7	0.138	0.728	2.4	0.0323
ENSG00000052802	MSMO1	15.8	81.5	2.37	0.00138
ENSG00000172339	ALG14	2.05	10.3	2.33	0.00462
ENSG00000131471	AOC3	0.167	0.83	2.32	0.00138
ENSG00000273674	CTD-2378E12.1	0.177	0.867	2.29	0.0264
ENSG00000015520	NPC1L1	0.116	0.565	2.28	0.00138
ENSG00000112773	FAM46A	5.2	25	2.27	0.00138
ENSG00000144655	CSRNP1	1.15	5.43	2.24	0.00138
ENSG00000134007	ADAM20	0.166	0.765	2.21	0.00138
ENSG00000128564	VGF	247	1070	2.11	0.00138
ENSG00000095794	CREM	19.2	82.5	2.11	0.00138
ENSG00000274588	DGKK	0.404	1.72	2.09	0.00138
ENSG00000163406	SLC15A2	0.274	1.16	2.08	0.00255
ENSG00000164442	CITED2	0.284	1.19	2.06	0.00255
ENSG00000215458	AP001053.11	0.4	1.67	2.06	0.00138
ENSG00000103257	SLC7A5	19.8	82.2	2.05	0.00138
ENSG00000259326	RP11-102L12.2	0.151	0.615	2.02	0.0427

Ensembl_Gene_ID	Gene_name	Control	Illuminated	Log2_FC	q_val
ENSG00000166762	CATSPER2	0.65	2.6	2	0.0091
ENSG00000112972	HMGCS1	23.2	92.7	2	0.00138
ENSG00000116741	RGS2	15.8	62.3	1.98	0.00138
ENSG00000179094	PER1	14.2	55.8	1.97	0.00138
ENSG00000181773	GPR3	2.15	8.29	1.95	0.00138
ENSG00000166401	SERPINB8	0.133	0.511	1.95	0.0091
ENSG00000112541	PDE10A	12.2	46.7	1.94	0.00138
ENSG00000162616	DNAJB4	10.8	41.3	1.94	0.00138
ENSG00000166546	BEAN1	0.286	1.09	1.93	0.0239
ENSG00000272468	RP1-86C11.7	0.674	2.55	1.92	0.0145
ENSG00000124762	CDKN1A	142	537	1.92	0.00138
ENSG00000277352	KB-68A7.2	2.99	11.2	1.91	0.00138
ENSG00000149201	CCDC81	0.385	1.44	1.91	0.00138
ENSG00000067064	IDI1	11.7	44	1.91	0.00138
ENSG00000105825	TFPI2	64.3	236	1.87	0.00138
ENSG00000132002	DNAJB1	35.8	128	1.84	0.00138
ENSG00000106366	SERPINE1	0.269	0.953	1.83	0.00138
ENSG00000075426	FOSL2	6.77	23.4	1.79	0.00138
ENSG00000179528	LBX2	2.46	8.44	1.78	0.0447
ENSG00000278959	RP11-455I9.1	1.03	3.43	1.74	0.00138
ENSG00000236453	AC003092.1	0.601	2.01	1.74	0.0264
ENSG00000085465	OVGP1	0.57	1.9	1.74	0.00138
ENSG00000257017	HP	0.207	0.691	1.74	0.04
ENSG00000253490	AC145110.1	0.204	0.664	1.71	0.00138
ENSG00000237854	LINC00674	3.18	10.3	1.7	0.00138
ENSG00000242265	PEG10	40.3	131	1.7	0.00138
ENSG00000162772	ATF3	8.07	25.8	1.67	0.00138
ENSG00000100625	SIX4	1.18	3.7	1.66	0.00138
ENSG00000167210	LOXHD1	0.186	0.582	1.65	0.0318
ENSG00000013375	PGM3	17.7	55.3	1.64	0.00138
ENSG00000280287	RP13-554M15.7	1.08	3.33	1.63	0.00462
ENSG00000272512	RP11-54O7.17	0.565	1.73	1.62	0.00138
ENSG00000177508	IRX3	0.413	1.27	1.62	0.00558
ENSG00000177710	SLC35G5	0.225	0.688	1.61	0.0357
ENSG00000044574	HSPA5	55.6	170	1.61	0.00138
ENSG00000010818	HIVEP2	8.85	27.1	1.61	0.0406
ENSG00000145632	PLK2	6.31	19.1	1.6	0.00138
ENSG00000232872	CTAGE3P	0.233	0.698	1.58	0.00138
ENSG00000229091	HSPA8P8	0.361	1.07	1.56	0.00992
ENSG00000197019	SERTAD1	1.21	3.59	1.56	0.00138
ENSG00000182308	DCAF4L1	0.226	0.666	1.56	0.00138
ENSG00000140743	CDR2	5.59	16.3	1.54	0.00138
ENSG00000120694	HSPH1	40.1	116	1.53	0.00138
ENSG00000165181	C9orf84	0.167	0.484	1.53	0.00138
ENSG00000197978	GOLGA6L9	0.615	1.78	1.53	0.0208
ENSG00000099251	HSD17B7P2	0.878	2.53	1.53	0.00138
ENSG00000164326	CARTPT	5.34	15.4	1.53	0.00138

Ensembl_Gene_ID	Gene_name	Control	Illuminated	Log2_FC	q_val
ENSG00000167508	MVD	10.5	29.7	1.5	0.00138
ENSG00000154734	ADAMTS1	42.4	119	1.49	0.00138
ENSG00000120875	DUSP4	66.7	186	1.48	0.00138
ENSG00000224411	RP11-1033A18.1	19.4	53.9	1.47	0.00138
ENSG00000152457	DCLRE1C	4.72	13.1	1.47	0.00138
ENSG00000196689	TRPV1	0.543	1.49	1.46	0.0447
ENSG00000104549	SQLE	16.1	44.4	1.46	0.00138
ENSG00000233974	RP11-823P9.3	0.603	1.66	1.46	0.0167
ENSG00000198857	HSD3BP5	0.549	1.48	1.43	0.0065
ENSG00000276445	LLNLR-268E12.1	1.04	2.8	1.42	0.0208
ENSG00000116717	GADD45A	14	37.4	1.42	0.00138
ENSG00000218208	RP11-367G18.2	1.54	4.1	1.41	0.0335
ENSG00000268654	MIMT1	0.29	0.769	1.41	0.0341
ENSG00000105321	CCDC9	4.72	12.3	1.39	0.00138
ENSG00000280219	RP11-752L20.3	0.465	1.21	1.38	0.00739
ENSG00000021826	CPS1	0.779	2.03	1.38	0.00558
ENSG00000070495	JMJD6	17.3	44.8	1.37	0.00138
ENSG00000100219	XBP1	42.4	109	1.36	0.00138
ENSG00000113161	HMGCR	26.2	67.3	1.36	0.00138
ENSG00000176142	TMEM39A	11.2	28.6	1.36	0.00138
ENSG00000080824	HSP90AA1	280	715	1.35	0.00138
ENSG00000006327	TNFRSF12A	10.5	26.6	1.34	0.00138
ENSG00000273356	RP11-804H8.6	0.749	1.9	1.34	0.0239
ENSG00000203589	RP5-886K2.1	0.474	1.19	1.33	0.0201
ENSG00000268234	FKBP4P6	0.334	0.835	1.32	0.0323
ENSG00000126368	NR1D1	2.6	6.49	1.32	0.0437
ENSG00000261087	KB-1460A1.5	1.3	3.23	1.31	0.00138
ENSG00000139278	GLIPR1	1.16	2.87	1.31	0.00462
ENSG00000131480	AOC2	1.48	3.66	1.3	0.00138
ENSG00000171790	SLFNL1	0.63	1.55	1.3	0.00138
ENSG00000280385	AP000648.5	2.98	7.29	1.29	0.00138
ENSG00000130522	JUND	81.9	200	1.29	0.00138
ENSG00000111664	GNB3	2.36	5.71	1.28	0.016
ENSG00000147059	SPIN2A	0.279	0.668	1.26	0.0201
ENSG00000115232	ITGA4	1.99	4.73	1.25	0.00138
ENSG00000184205	TSPYL2	6.34	15	1.24	0.00138
ENSG00000083857	FAT1	50.7	120	1.24	0.00138
ENSG00000170458	CD14	0.515	1.22	1.24	0.00138
ENSG00000172071	EIF2AK3	8.48	20	1.24	0.00138
ENSG00000164675	IQUB	0.386	0.905	1.23	0.0214
ENSG00000204950	LRRC10B	1.3	3.03	1.23	0.00138
ENSG00000228709	AP001065.15	28.1	65.7	1.22	0.00138
ENSG00000128590	DNAJB9	9.92	23.1	1.22	0.0264
ENSG00000105327	BBC3	16	37.1	1.22	0.00138
ENSG00000110172	CHORDC1	14.1	32.6	1.21	0.00138
ENSG00000160570	DEDD2	12.6	29.1	1.2	0.00138
ENSG00000273319	RP11-138A9.2	0.515	1.18	1.2	0.00138

Ensembl_Gene_ID	Gene_name	Control	Illuminated	Log2_FC	q_val
ENSG00000104856	RELB	1.67	3.85	1.2	0.00138
ENSG00000276112	AL353644.6	7760	17700	1.19	0.00138
ENSG00000261646	RP11-489G11.3	0.34	0.776	1.19	0.0091
ENSG00000173846	PLK3	7.03	16	1.19	0.00138
ENSG00000213599	SLX1A-SULT1A3	0.487	1.1	1.17	0.00826
ENSG00000279602	CTD-3014M21.1	3.08	6.94	1.17	0.00138
ENSG00000248905	FMN1	5.43	12.2	1.17	0.00138
ENSG00000106211	HSPB1	249	560	1.17	0.00138
ENSG00000260518	BMS1P8	3.54	7.87	1.15	0.00138
ENSG00000280347	AC000123.2	3.91	8.7	1.15	0.00138
ENSG00000059728	MXD1	3.93	8.65	1.14	0.00138
ENSG00000215007	DNAJA1P3	0.482	1.06	1.13	0.0341
ENSG00000109089	CDR2L	23.5	51.5	1.13	0.00138
ENSG00000129993	CBFA2T3	2.78	6.08	1.13	0.00138
ENSG00000275993	CH507-42P11.8	0.588	1.29	1.13	0.00138
ENSG00000260645	RP11-250B2.5	0.926	2.03	1.13	0.00138
ENSG00000268089	GABRQ	0.331	0.722	1.13	0.00138
ENSG00000203685	C1orf95	0.369	0.802	1.12	0.0467
ENSG00000233967	RP11-250B2.3	1.36	2.96	1.12	0.0341
ENSG00000236255	AC009404.2	3.32	7.2	1.12	0.00138
ENSG00000130766	SESN2	6.44	13.9	1.11	0.00138
ENSG00000280111	CTA-292E10.9	0.493	1.06	1.1	0.0346
ENSG00000228502	EEF1A1P11	0.62	1.33	1.1	0.00826
ENSG00000260034	LCMT1-AS2	1.49	3.18	1.1	0.00255
ENSG00000135362	PRR5L	0.551	1.18	1.1	0.0487
ENSG00000141441	GAREM	23.7	50.7	1.1	0.00138
ENSG00000181450	ZNF678	8.03	16.9	1.08	0.00138
ENSG00000233588	CYP51A1P2	3.34	7.04	1.08	0.00138
ENSG00000131016	AKAP12	12.2	25.4	1.06	0.00138
ENSG00000137094	DNAJB5	15.1	31.5	1.06	0.00138
ENSG00000241095	CYP51A1P1	2.74	5.73	1.06	0.00138
ENSG00000272106	RP11-345P4.9	7.64	15.9	1.06	0.00138
ENSG00000117479	SLC19A2	5.91	12.3	1.06	0.00138
ENSG00000223345	HIST2H2BA	7.23	15	1.05	0.00255
ENSG00000215156	RP11-1023L17.2	1.57	3.24	1.05	0.00255
ENSG00000181026	AEN	25.6	52.9	1.05	0.00138
ENSG00000269955	LUC7L2	7.17	14.8	1.05	0.0421
ENSG00000130254	SAFB2	19.9	41.1	1.04	0.0138
ENSG00000128683	GAD1	5.91	12.2	1.04	0.00138
ENSG00000185304	RGPD2	0.259	0.533	1.04	0.00739
ENSG00000149257	SERPINH1	40.7	83.6	1.04	0.00138
ENSG00000272947	RP11-71H17.9	1.57	3.21	1.03	0.016
ENSG00000234857	HNRNPUL2-BSCL2	7.13	14.6	1.03	0.0167
ENSG00000133874	RNF122	13.9	28.3	1.03	0.00138
ENSG00000277007	RP11-392O17.2	0.329	0.673	1.03	0.0174
ENSG00000279792	RP11-893F2.18	2.15	4.4	1.03	0.0432
ENSG00000120306	CYSTM1	4.85	9.82	1.02	0.00255

Ensembl_Gene_ID	Gene_name	Control	Illuminated	Log2_FC	q_val
ENSG00000176641	RNF152	27.3	55.4	1.02	0.00362
ENSG00000271204	RP11-138A9.1	0.549	1.11	1.02	0.0091
ENSG00000173276	ZBTB21	8.73	17.6	1.01	0.00138
ENSG00000168003	SLC3A2	32.3	65.1	1.01	0.00138
ENSG00000166455	C16orf46	2.36	4.74	1.01	0.00138
ENSG00000280047	CTC-463A16.1	0.407	0.817	1.01	0.00362
ENSG00000263931	RP11-180P8.1	11.8	23.7	1	0.00138
ENSG00000112599	GUCA1B	0.8	1.6	1	0.0239
ENSG00000134070	IRAK2	0.369	0.739	1	0.00255
ENSG00000265763	ZNF488	0.61	0.304	-1	0.00255
ENSG00000151657	KIN	9.35	4.65	-1.01	0.0312
ENSG00000187952	HS6ST1P1	3.66	1.81	-1.02	0.00138
ENSG00000204947	ZNF425	2.4	1.19	-1.02	0.0346
ENSG00000214654	RP11-27I1.4	8.85	4.34	-1.03	0.00138
ENSG00000160111	CPAMD8	1.01	0.493	-1.03	0.0442
ENSG00000224383	PRR29	1.42	0.698	-1.03	0.0379
ENSG00000128394	APOBEC3F	2.38	1.16	-1.03	0.0145
ENSG00000136531	SCN2A	5.54	2.7	-1.04	0.00138
ENSG00000113196	HAND1	28.2	13.7	-1.04	0.00138
ENSG00000277287	RP4-794I6.4	0.912	0.442	-1.04	0.00138
ENSG00000148225	WDR31	1.71	0.829	-1.04	0.00462
ENSG00000008283	CYB561	181	87.5	-1.05	0.00138
ENSG00000182747	SLC35D3	6.65	3.22	-1.05	0.00138
ENSG00000205634	LINC00898	0.628	0.304	-1.05	0.0174
ENSG00000179921	GPBAR1	2.07	1	-1.05	0.00138
ENSG00000066926	FECH	19.1	9.22	-1.05	0.00138
ENSG00000255690	TRIL	12.6	6.06	-1.06	0.00138
ENSG00000198246	SLC29A3	6.1	2.93	-1.06	0.00138
ENSG00000214248	CTD-3193O13.12	0.744	0.355	-1.07	0.00138
ENSG00000007237	GAS7	2.81	1.34	-1.07	0.0487
ENSG00000143365	RORC	0.735	0.349	-1.08	0.0065
ENSG00000176381	PRR18	1.4	0.659	-1.08	0.0294
ENSG00000277831	RP11-269C23.5	3.72	1.75	-1.09	0.0447
ENSG00000270964	RP11-502I4.3	1.48	0.699	-1.09	0.00138
ENSG00000228903	RASA4CP	1.3	0.611	-1.09	0.0346
ENSG00000230658	KLHL7-AS1	1.04	0.487	-1.09	0.00138
ENSG00000119938	PPP1R3C	4.7	2.21	-1.09	0.00138
ENSG00000130518	KIAA1683	4.43	2.08	-1.09	0.00138
ENSG00000071794	HLTF	26	12.2	-1.09	0.00138
ENSG00000181004	BBS12	3.26	1.53	-1.09	0.00138
ENSG00000130700	GATA5	2	0.934	-1.1	0.00138
ENSG00000171729	TMEM51	25.1	11.7	-1.1	0.00138
ENSG00000172086	KRCC1	13.7	6.36	-1.11	0.00138
ENSG00000225391	NHEG1	0.848	0.391	-1.12	0.0427
ENSG00000272425	RP11-363E6.4	0.693	0.319	-1.12	0.0227
ENSG00000141540	TTYH2	5.62	2.59	-1.12	0.00138
ENSG00000187624	C17orf97	2.67	1.23	-1.12	0.00138

Ensembl_Gene_ID	Gene_name	Control	Illuminated	Log2_FC	q_val
ENSG00000265692	RP13-516M14.4	0.826	0.379	-1.12	0.0188
ENSG00000258701	LINC00638	1.5	0.689	-1.13	0.00138
ENSG00000176909	MAMSTR	2.07	0.942	-1.13	0.00138
ENSG00000205683	DPF3	2.65	1.2	-1.14	0.0195
ENSG00000178403	NEUROG2	23.2	10.5	-1.15	0.00138
ENSG00000165555	NOXRED1	0.641	0.288	-1.15	0.0312
ENSG00000158008	EXTL1	2.35	1.05	-1.15	0.0427
ENSG00000008196	TFAP2B	103	46.2	-1.16	0.00138
ENSG00000175279	APITD1	10.9	4.87	-1.16	0.00138
ENSG00000156253	RWDD2B	15.9	7.06	-1.17	0.00138
ENSG00000184828	ZBTB7C	3.63	1.61	-1.18	0.00138
ENSG00000152582	SPEF2	1.8	0.796	-1.18	0.0452
ENSG00000172159	FRMD3	11.3	4.99	-1.18	0.00138
ENSG00000157978	LDLRAP1	1.44	0.637	-1.18	0.0221
ENSG00000261251	RP3-388M5.9	1.16	0.509	-1.18	0.0312
ENSG00000251408	RP11-586D19.2	0.691	0.304	-1.19	0.0294
ENSG00000180938	ZNF572	2.96	1.3	-1.19	0.00138
ENSG00000168874	ATOH8	0.894	0.392	-1.19	0.0167
ENSG00000262075	DKFZP434A062	0.539	0.236	-1.19	0.00138
ENSG00000260400	RP11-119F7.5	4.32	1.89	-1.19	0.00138
ENSG00000180787	ZFP3	5.39	2.35	-1.2	0.00138
ENSG00000197557	TTC30A	6.37	2.76	-1.21	0.00138
ENSG00000179240	RP11-111M22.2	5.45	2.36	-1.21	0.00138
ENSG00000121075	TBX4	2.96	1.28	-1.21	0.00138
ENSG00000163827	LRRC2	0.697	0.301	-1.21	0.0174
ENSG00000106018	VIPR2	1.33	0.573	-1.21	0.00138
ENSG00000159674	SPON2	3.25	1.4	-1.22	0.0065
ENSG00000231345	RP11-564C4.6	2.64	1.13	-1.22	0.00138
ENSG00000213171	LINGO4	0.901	0.386	-1.22	0.00138
ENSG00000266405	CBX3P2	2.23	0.956	-1.22	0.0252
ENSG00000004799	PDK4	1.28	0.547	-1.23	0.0091
ENSG00000260589	STAM-AS1	1.05	0.443	-1.24	0.00362
ENSG00000160172	FAM86C2P	3.78	1.6	-1.24	0.00138
ENSG00000227087	RBMX2P5	1.36	0.574	-1.25	0.0395
ENSG00000170915	PAQR8	27.1	11.2	-1.27	0.00138
ENSG00000164743	C8orf48	0.863	0.355	-1.28	0.0174
ENSG00000141668	CBLN2	6.76	2.78	-1.28	0.00138
ENSG00000171388	APLN	1.79	0.732	-1.29	0.00138
ENSG00000278002	RP11-596C23.2	1.45	0.592	-1.29	0.00138
ENSG00000135835	KIAA1614	6.02	2.46	-1.29	0.0138
ENSG00000047621	C12orf4	6.15	2.5	-1.3	0.00138
ENSG00000197180	CH17-340M24.3	3.26	1.32	-1.3	0.0123
ENSG00000127903	ZNF835	2.38	0.959	-1.31	0.00138
ENSG00000157429	ZNF19	3.64	1.46	-1.32	0.0174
ENSG00000161544	CYGB	83.4	33.3	-1.32	0.00138
ENSG00000163449	TMEM169	14	5.59	-1.32	0.00138
ENSG00000074416	MGLL	3.56	1.41	-1.34	0.00739

Ensembl_Gene_ID	Gene_name	Control	Illuminated	Log2_FC	q_val
ENSG00000119714	GPR68	2.33	0.915	-1.35	0.00138
ENSG00000117971	CHRNB4	18.5	7.18	-1.36	0.00138
ENSG00000186280	KDM4D	1.58	0.608	-1.38	0.00138
ENSG00000139832	RAB20	2.28	0.873	-1.38	0.00138
ENSG00000171631	P2RY6	1.54	0.588	-1.39	0.00138
ENSG00000026508	CD44	0.544	0.207	-1.39	0.00255
ENSG00000280187	CTC-351M12.1	2.52	0.958	-1.4	0.00138
ENSG00000251484	RP5-1065J22.4	2.04	0.771	-1.4	0.0452
ENSG00000269051	CTD-2245F17.3	3.04	1.15	-1.4	0.0341
ENSG00000275329	RP11-83N9.6	0.69	0.259	-1.41	0.0131
ENSG00000204815	TTC25	3.13	1.17	-1.42	0.00362
ENSG00000140986	RPL3L	0.672	0.247	-1.44	0.0138
ENSG00000108622	ICAM2	2.74	0.995	-1.46	0.00138
ENSG00000267355	RPL9P29	2.58	0.924	-1.48	0.0233
ENSG00000110324	IL10RA	1.33	0.473	-1.49	0.0437
ENSG00000212916	MAP10	2.3	0.816	-1.49	0.00138
ENSG00000111859	NEDD9	9.05	3.18	-1.51	0.00138
ENSG00000260063	RP5-968P14.2	0.789	0.277	-1.51	0.00462
ENSG00000247317	RP11-273G15.2	2.46	0.86	-1.51	0.00138
ENSG00000236437	AP001891.1	1.94	0.675	-1.52	0.00138
ENSG00000234996	RP11-480I12.7	0.845	0.294	-1.52	0.00138
ENSG00000198416	ZNF658B	0.49	0.17	-1.53	0.00255
ENSG00000229921	KIF25-AS1	0.66	0.228	-1.53	0.00138
ENSG00000251661	RP11-326C3.11	2.03	0.702	-1.53	0.0195
ENSG00000166510	CCDC68	0.583	0.2	-1.55	0.00462
ENSG00000224090	AC097468.4	1.45	0.483	-1.58	0.00462
ENSG00000121966	CXCR4	219	71.7	-1.61	0.00138
ENSG00000247796	CTD-2366F13.1	1.75	0.57	-1.62	0.027
ENSG00000162407	PPAP2B	6.09	1.98	-1.62	0.00138
ENSG00000249669	MIR143HG	4.6	1.48	-1.63	0.00138
ENSG00000234944	RP11-124O11.1	1.32	0.422	-1.65	0.00138
ENSG00000100336	APOL4	0.98	0.311	-1.66	0.0115
ENSG00000269936	MIR145	3.55	1.11	-1.68	0.00138
ENSG00000100060	MFNG	1.23	0.384	-1.68	0.0174
ENSG00000279137	RP11-205K6.3	1.03	0.322	-1.68	0.00138
ENSG00000273218	LLNLR-246C6.1	0.562	0.175	-1.69	0.0195
ENSG00000272960	RP11-339B21.15	6.03	1.87	-1.69	0.0406
ENSG00000113578	FGF1	2.21	0.679	-1.7	0.0123
ENSG00000237954	RP11-14O19.2	3.34	1.01	-1.73	0.00138
ENSG00000253669	KB-1732A1.1	0.524	0.154	-1.77	0.0497
ENSG00000041353	RAB27B	4.86	1.42	-1.78	0.00138
ENSG00000130222	GADD45G	1.18	0.332	-1.83	0.00826
ENSG00000168404	MLKL	0.621	0.174	-1.83	0.0312
ENSG00000172554	SNTG2	0.606	0.167	-1.86	0.03
ENSG00000169302	STK32A	0.96	0.258	-1.89	0.0188
ENSG00000139352	ASCL1	6.61	1.73	-1.93	0.00138
ENSG00000224008	LINC01441	0.93	0.241	-1.95	0.00138

Ensembl_Gene_ID	Gene_name	Control	Illuminated	Log2_FC	q_val
ENSG00000187800	PEAR1	6.15	1.5	-2.04	0.00138
ENSG00000134323	MYCN	5.82	1.39	-2.07	0.00138
ENSG00000165695	AK8	1.18	0.279	-2.08	0.0447
ENSG00000112769	LAMA4	1.11	0.258	-2.1	0.00138
ENSG00000100302	RASD2	0.855	0.194	-2.14	0.00138
ENSG00000101292	PROKR2	1.78	0.393	-2.18	0.00138
ENSG00000108771	DHX58	0.92	0.198	-2.22	0.0167
ENSG00000231473	LINC00441	1.39	0.285	-2.29	0.0115
ENSG00000170983	LINC00208	0.594	0.116	-2.35	0.00558
ENSG00000148950	IMMP1L	247	47.1	-2.39	0.00138
ENSG00000189350	FAM179A	0.543	0.0978	-2.47	0.0258
ENSG00000266524	GDF10	3.13	0.555	-2.49	0.00138
ENSG00000145975	FAM217A	1.09	0.0348	-4.97	0.0201

App.14. Genes affected by 12 hour illumination

Data are presented that show the genes identified by Cuffdiff as being modulated by at least twofold immediately following 12 hour illumination in opsin expressing SH-SY5Y cells, compared to dark maintained cells collected at the same timepoint. The FPKM value of expression is listed for Control and Illuminated cells, and the log2 fold change, together with the Benjamini adjusted p-value for this comparison.

Ensembl_Gene_ID	Gene_name	Control	Illuminated	Log2 FC	q_val
ENSG00000225358	MIPEPP1	0.0265	0.467	4.14	0.0368
ENSG00000167210	LOXHD1	0.0964	1.28	3.73	0.00138
ENSG00000172901	AQPEP	0.0552	0.726	3.72	0.0115
ENSG00000170345	FOS	1.13	14.8	3.71	0.00138
ENSG00000152818	UTRN	0.204	2.22	3.45	0.00138
ENSG00000130513	GDF15	22.6	210	3.22	0.00138
ENSG00000204584	RP11-304F15.3	0.143	1.16	3.02	0.00138
ENSG00000179950	PUF60	0.181	1.44	2.99	0.00138
ENSG00000186480	INSIG1	12.7	96.1	2.92	0.00138
ENSG00000123700	KCNJ2	0.29	2.16	2.9	0.00138
ENSG00000130675	MNX1	0.117	0.864	2.88	0.0416
ENSG00000044574	HSPA5	50.8	365	2.84	0.00138
ENSG00000052802	MSMO1	16.6	118	2.83	0.00138
ENSG00000130164	LDLR	7.39	51.5	2.8	0.00138
ENSG00000172927	MYEOV	0.158	1.1	2.8	0.00558
ENSG00000176358	TAC4	0.198	1.33	2.74	0.00826
ENSG00000204055	RP11-247A12.2	0.246	1.61	2.71	0.0107
ENSG00000176761	ZNF285B	0.139	0.897	2.69	0.00138
ENSG00000119508	NR4A3	0.265	1.69	2.67	0.00138
ENSG00000227676	LINC01068	0.431	2.48	2.52	0.0153
ENSG00000105219	CNTD2	0.164	0.907	2.47	0.00462
ENSG00000112972	HMGCS1	22.6	124	2.46	0.00138
ENSG00000004776	HSPB6	0.124	0.681	2.46	0.0294
ENSG00000270011	ZNF559-ZNF177	0.836	4.44	2.41	0.00138
ENSG00000124762	CDKN1A	192	1010	2.4	0.00138
ENSG00000237854	LINC00674	3.35	17.6	2.39	0.00138
ENSG00000105825	TFPI2	67.2	349	2.38	0.00138
ENSG00000253955	CTB-33O18.3	0.167	0.853	2.36	0.00362
ENSG00000270948	RP11-460N20.7	0.259	1.3	2.33	0.0288
ENSG00000131471	AOC3	0.31	1.52	2.3	0.00138
ENSG00000015520	NPC1L1	0.196	0.937	2.26	0.00138
ENSG00000226803	RP11-203B9.4	1.59	7.43	2.22	0.0131
ENSG00000274588	DGKK	0.394	1.83	2.22	0.00138
ENSG00000160471	COX6B2	2.09	9.64	2.21	0.00138
ENSG00000278959	RP11-455I9.1	0.9	4.13	2.2	0.00138
ENSG00000165457	FOLR2	0.147	0.672	2.19	0.0123

Ensembl_Gene_ID	Gene_name	Control	Illuminated	Log2 FC	q_val
ENSG00000162772	ATF3	8.01	36.5	2.19	0.00138
ENSG00000171786	NHLH1	0.109	0.494	2.18	0.00739
ENSG00000179094	PER1	12.7	57.6	2.18	0.00138
ENSG00000132002	DNAJB1	35.8	160	2.17	0.00138
ENSG00000175197	DDIT3	10.9	48.7	2.16	0.0167
ENSG00000181773	GPR3	2.06	8.91	2.11	0.00138
ENSG00000128564	VGF	247	1060	2.1	0.00138
ENSG00000242265	PEG10	39.6	165	2.06	0.00138
ENSG00000182308	DCAF4L1	0.25	1.04	2.05	0.00138
ENSG00000072858	SIDT1	0.169	0.696	2.04	0.0131
ENSG00000140961	OSGIN1	1.55	6.34	2.03	0.00138
ENSG00000144655	CSRNP1	1.22	4.94	2.02	0.00138
ENSG00000102524	TNFSF13B	0.427	1.74	2.02	0.0174
ENSG00000145050	MANF	26.9	109	2.02	0.00138
ENSG00000131480	AOC2	1.55	6.24	2.01	0.00138
ENSG00000165181	C9orf84	0.119	0.476	2	0.00138
ENSG00000279602	CTD-3014M21.1	2.8	11.2	2	0.00138
ENSG00000164442	CITED2	0.145	0.582	2	0.0065
ENSG00000175592	FOSL1	0.22	0.873	1.99	0.00138
ENSG00000067064	IDI1	11.4	44.6	1.97	0.00138
ENSG00000213626	LBH	18.3	71.6	1.97	0.00138
ENSG00000147724	FAM135B	0.179	0.695	1.95	0.00138
ENSG00000118985	ELL2	0.567	2.18	1.95	0.0201
ENSG00000250337	LINC01021	1.87	7.16	1.94	0.00138
ENSG00000145632	PLK2	7.32	27.7	1.92	0.00138
ENSG00000162631	NTNG1	0.278	1.05	1.92	0.00138
ENSG00000260640	KB-1000E4.2	0.812	3.06	1.91	0.0442
ENSG00000189292	FAM150B	0.371	1.39	1.9	0.0138
ENSG00000186395	KRT10	1.06	3.94	1.9	0.00138
ENSG00000111711	GOLT1B	14.5	53.7	1.89	0.00138
ENSG00000123358	NR4A1	14	51.4	1.88	0.00138
ENSG00000210082	MT-RNR2	161	576	1.84	0.00138
ENSG00000197019	SERTAD1	1.26	4.44	1.82	0.00138
ENSG00000275066	SYNRG	0.363	1.27	1.81	0.0406
ENSG00000100625	SIX4	1.19	4.12	1.79	0.00138
ENSG00000211459	MT-RNR1	155	534	1.78	0.00138
ENSG00000115232	ITGA4	1.96	6.72	1.78	0.00138
ENSG00000112773	FAM46A	5.12	17.4	1.77	0.00138
ENSG00000104549	SQLE	16.3	55.3	1.76	0.00138
ENSG00000105321	CCDC9	4.9	16.6	1.76	0.00138
ENSG00000162616	DNAJB4	13.4	45.4	1.76	0.00138
ENSG00000126368	NR1D1	3.09	10.4	1.75	0.00138
ENSG00000276445	LLNLR-268E12.1	1.59	5.27	1.73	0.00138
ENSG00000236453	AC003092.1	1.07	3.55	1.73	0.00138
ENSG00000125657	TNFSF9	0.199	0.656	1.72	0.0131
ENSG00000175356	SCUBE2	0.333	1.1	1.72	0.0335
ENSG00000116717	GADD45A	16.2	53.3	1.72	0.00138

Ensembl_Gene_ID	Gene_name	Control	Illuminated	Log2 FC	q_val
ENSG00000259326	RP11-102L12.2	0.226	0.742	1.72	0.0346
ENSG00000116741	RGS2	15.3	50.1	1.71	0.00138
ENSG00000163141	BNIPL	0.989	3.21	1.7	0.00362
ENSG00000266289	RP11-1C8.6	0.649	2.09	1.69	0.00826
ENSG00000182223	ZAR1	0.25	0.802	1.68	0.0123
ENSG00000074416	MGLL	2.54	8.13	1.68	0.0201
ENSG00000114315	HES1	1.23	3.9	1.67	0.00138
ENSG00000106211	HSPB1	241	762	1.66	0.00138
ENSG00000128590	DNAJB9	9.99	31.1	1.64	0.00138
ENSG00000102580	DNAJC3	4.34	13.5	1.64	0.00138
ENSG00000272716	RP11-563N4.1	0.929	2.89	1.64	0.00362
ENSG00000104856	RELB	1.59	4.92	1.64	0.00138
ENSG00000100219	XBP1	39.8	122	1.62	0.00138
ENSG00000070495	JMJD6	16.8	51.4	1.62	0.00138
ENSG00000177337	DLGAP1-AS1	2	6.12	1.61	0.0323
ENSG00000167508	MVD	13.8	41.5	1.59	0.00138
ENSG00000271840	RP1-224A6.9	0.864	2.59	1.59	0.00255
ENSG00000166592	RRAD	0.26	0.779	1.58	0.0201
ENSG00000262772	RP11-353N14.2	0.198	0.592	1.58	0.0239
ENSG00000240132	ETF1P2	1.13	3.38	1.58	0.0306
ENSG00000168003	SLC3A2	31.9	95.1	1.58	0.00138
ENSG00000149257	SERPINH1	44	131	1.58	0.00138
ENSG00000248905	FMN1	6.18	18.3	1.57	0.00138
ENSG00000234857	HNRNPUL2-BSCL2	4.12	12.2	1.56	0.0357
ENSG00000103257	SLC7A5	21.8	64.2	1.56	0.00138
ENSG00000106366	SERPINE1	0.373	1.1	1.56	0.00138
ENSG00000087074	PPP1R15A	6.97	20.5	1.56	0.00138
ENSG00000108551	RASD1	0.584	1.72	1.56	0.00138
ENSG00000095794	CREM	18.4	53.7	1.55	0.00138
ENSG00000260708	CTA-29F11.1	13.8	40.2	1.54	0.00138
ENSG00000130066	SAT1	7.18	20.9	1.54	0.00138
ENSG00000140743	CDR2	6.33	18.3	1.53	0.00138
ENSG00000095303	PTGS1	2.62	7.59	1.53	0.00138
ENSG00000177710	SLC35G5	0.242	0.699	1.53	0.0432
ENSG00000280184	AL023806.1	0.52	1.49	1.52	0.00138
ENSG00000143217	PVRL4	0.678	1.94	1.52	0.00138
ENSG00000149201	CCDC81	0.548	1.56	1.51	0.00138
ENSG00000273356	RP11-804H8.6	1.05	2.96	1.5	0.00138
ENSG00000170458	CD14	0.658	1.86	1.5	0.00138
ENSG00000139278	GLIPR1	1.26	3.55	1.49	0.00138
ENSG00000120875	DUSP4	80.3	226	1.49	0.00138
ENSG00000166455	C16orf46	2.7	7.52	1.48	0.0201
ENSG00000120437	ACAT2	7.54	21	1.48	0.0201
ENSG00000166598	HSP90B1	174	483	1.47	0.00138
ENSG00000181450	ZNF678	8.04	22.2	1.46	0.00138
ENSG00000121068	TBX2	69.1	190	1.46	0.00138
ENSG00000080824	HSP90AA1	266	730	1.46	0.00138

Ensembl_Gene_ID	Gene_name	Control	Illuminated	Log2 FC	q_val
ENSG00000118194	TNNT2	0.313	0.859	1.46	0.0174
ENSG00000136235	GPNMB	0.413	1.13	1.45	0.0091
ENSG00000196139	AKR1C3	0.704	1.92	1.45	0.00462
ENSG00000125844	RRBP1	6	16.4	1.45	0.00138
ENSG00000223414	LINC00473	10.7	29.1	1.45	0.00138
ENSG00000106258	CYP3A5	0.947	2.57	1.44	0.00138
ENSG00000085465	OVGP1	0.865	2.34	1.44	0.00362
ENSG00000148600	CDHR1	0.295	0.797	1.43	0.0115
ENSG00000267280	TBX2-AS1	92.6	250	1.43	0.0416
ENSG00000113161	HMGCR	25.8	69.6	1.43	0.00138
ENSG00000182827	ACBD3	25.1	67.6	1.43	0.00138
ENSG00000108256	NUFIP2	15.6	41.9	1.43	0.00138
ENSG00000173846	PLK3	7.63	20.5	1.43	0.00138
ENSG00000135842	FAM129A	0.276	0.742	1.43	0.00362
ENSG00000147604	RPL7	8.59	23	1.42	0.00362
ENSG00000167074	TEF	2.2	5.91	1.42	0.00138
ENSG00000119777	TMEM214	26.8	71.8	1.42	0.00138
ENSG00000059728	MXD1	4.07	10.8	1.42	0.00138
ENSG00000198300	PEG3	6.13	16.4	1.42	0.00138
ENSG00000185684	EP400NL	3.36	8.94	1.41	0.00138
ENSG00000234704	BRD2	1.83	4.85	1.41	0.00138
ENSG00000262074	SNORD3B-2	1.27	3.36	1.41	0.00362
ENSG00000111664	GNB3	2.91	7.71	1.4	0.00255
ENSG00000079459	FDFT1	49.8	131	1.4	0.00138
ENSG00000155660	PDIA4	74.6	196	1.4	0.00138
ENSG00000144674	GOLGA4	17.1	45	1.4	0.00138
ENSG00000168389	MFSD2A	1.82	4.76	1.39	0.00138
ENSG00000241095	CYP51A1P1	2.94	7.68	1.38	0.00138
ENSG00000176142	TMEM39A	11.9	31	1.38	0.00138
ENSG00000229670	PKP4P1	0.269	0.698	1.38	0.00462
ENSG00000176641	RNF152	27.4	70.7	1.36	0.00138
ENSG00000151135	TMEM263	17.5	44.8	1.36	0.00138
ENSG00000130766	SESN2	6.15	15.7	1.36	0.00138
ENSG00000099251	HSD17B7P2	1.08	2.77	1.35	0.00138
ENSG00000224411	RP11-1033A18.1	19	48.3	1.35	0.00138
ENSG00000189129	PLAC9	0.588	1.5	1.35	0.0323
ENSG00000008405	CRY1	8.72	22.2	1.35	0.00138
ENSG00000164211	STARD4	32.2	81.8	1.35	0.00138
ENSG00000146676	PURB	12.9	32.8	1.35	0.00138
ENSG00000279541	CTC-444N24.7	10.2	26	1.35	0.00138
ENSG00000276112	AL353644.6	7190	18300	1.34	0.00138
ENSG00000267731	RP11-147L13.8	0.449	1.14	1.34	0.00138
ENSG00000279254	RP11-536C12.1	0.725	1.84	1.34	0.00138
ENSG00000128342	LIF	0.697	1.77	1.34	0.0115
ENSG00000130254	SAFB2	17.9	45.2	1.34	0.00138
ENSG00000047634	SCML1	1.83	4.64	1.34	0.00138
ENSG00000163644	PPM1K	7.06	17.8	1.34	0.00138

Ensembl_Gene_ID	Gene_name	Control	Illuminated	Log2 FC	q_val
ENSG00000105327	BBC3	18.9	47.7	1.34	0.00138
ENSG00000205213	LGR4	3.52	8.88	1.34	0.00138
ENSG00000051108	HERPUD1	22.2	55.9	1.33	0.00138
ENSG00000170385	SLC30A1	7.97	20.1	1.33	0.00138
ENSG00000225536	STIP1P3	0.748	1.88	1.33	0.00138
ENSG00000280385	AP000648.5	3.07	7.7	1.33	0.00138
ENSG00000117318	ID3	42.5	106	1.32	0.00138
ENSG00000113811	SELK	33.2	82.6	1.32	0.00138
ENSG00000231340	ACTG1P10	1.46	3.64	1.31	0.0258
ENSG00000236255	AC009404.2	3.85	9.55	1.31	0.00138
ENSG00000152932	RAB3C	32.6	80.8	1.31	0.00138
ENSG00000001630	CYP51A1	23.2	57.5	1.31	0.00138
ENSG00000041982	TNC	0.419	1.03	1.3	0.0107
ENSG00000137558	PI15	1.29	3.18	1.3	0.00138
ENSG00000167797	CDK2AP2	16	39.5	1.3	0.00138
ENSG00000133816	MICAL2	0.389	0.959	1.3	0.0195
ENSG00000272106	RP11-345P4.9	8.01	19.7	1.3	0.00138
ENSG00000102100	SLC35A2	12.4	30.5	1.3	0.00138
ENSG00000188816	HMX2	0.279	0.684	1.29	0.039
ENSG00000006327	TNFRSF12A	11.2	27.4	1.29	0.00138
ENSG00000172733	PURG	7.47	18.2	1.29	0.00138
ENSG00000280328	RP11-972P1.7	1.06	2.58	1.29	0.00462
ENSG00000184205	TSPYL2	6.47	15.8	1.28	0.00138
ENSG00000166856	GPR182	0.363	0.884	1.28	0.0208
ENSG00000179119	SPTY2D1	9.29	22.6	1.28	0.00138
ENSG00000083857	FAT1	59	144	1.28	0.00138
ENSG00000260034	LCMT1-AS2	1.37	3.32	1.28	0.00138
ENSG00000154734	ADAMTS1	39.8	96.5	1.28	0.00138
ENSG00000158887	MPZ	4.19	10.1	1.27	0.00138
ENSG00000232872	CTAGE3P	0.272	0.656	1.27	0.0091
ENSG00000233588	CYP51A1P2	3.44	8.3	1.27	0.00138
ENSG00000271755	RP1-153G14.4	0.361	0.872	1.27	0.00138
ENSG00000133424	LARGE	1.83	4.41	1.27	0.00255
ENSG00000105499	PLA2G4C	1.37	3.31	1.27	0.0174
ENSG00000180667	YOD1	6.38	15.3	1.26	0.00138
ENSG00000113615	SEC24A	7.73	18.5	1.26	0.00138
ENSG00000280047	CTC-463A16.1	0.399	0.956	1.26	0.00138
ENSG00000225880	LINC00115	2.04	4.86	1.26	0.0195
ENSG00000197063	MAFG	13	31.1	1.25	0.00138
ENSG00000134070	IRAK2	0.343	0.816	1.25	0.00138
ENSG00000147526	TACC1	2.43	5.78	1.25	0.00138
ENSG00000117360	PRPF3	33.9	80.5	1.25	0.00138
ENSG00000120694	HSPH1	40	95	1.25	0.00138
ENSG00000004478	FKBP4	65.2	154	1.25	0.00138
ENSG00000172893	DHCR7	18.2	43.2	1.25	0.00138
ENSG00000217801	RP11-465B22.3	1.95	4.61	1.24	0.00138
ENSG00000173334	TRIB1	4.14	9.8	1.24	0.00138

Ensembl_Gene_ID	Gene_name	Control	Illuminated	Log2 FC	q_val
ENSG00000166012	TAF1D	112	266	1.24	0.00138
ENSG00000164326	CARTPT	4.24	10	1.24	0.00138
ENSG00000163697	APBB2	13.2	31.2	1.24	0.00138
ENSG00000213599	SLX1A-SULT1A3	0.395	0.932	1.24	0.00462
ENSG00000160570	DEDD2	12.5	29.5	1.24	0.00138
ENSG00000261087	KB-1460A1.5	1.64	3.87	1.24	0.00138
ENSG00000156232	WHAMM	1.44	3.4	1.24	0.00138
ENSG00000163660	CCNL1	59.9	141	1.23	0.00138
ENSG00000184226	PCDH9	4.37	10.3	1.23	0.00138
ENSG00000132326	PER2	1.06	2.49	1.23	0.00739
ENSG00000128228	SDF2L1	7.52	17.5	1.22	0.00138
ENSG00000232442	CTD-3184A7.4	7.05	16.4	1.22	0.00138
ENSG00000154359	LONRF1	5.56	12.9	1.21	0.00138
ENSG00000203930	LINC00632	6.98	16.2	1.21	0.00138
ENSG00000164236	ANKRD33B	0.332	0.768	1.21	0.0312
ENSG00000197780	TAF13	20.6	47.8	1.21	0.00138
ENSG00000108829	LRRC59	44.3	102	1.21	0.00138
ENSG00000224945	RP11-82L18.2	5.32	12.3	1.2	0.0091
ENSG00000165997	ARL5B	12.4	28.5	1.2	0.00138
ENSG00000099194	SCD	57.2	132	1.2	0.00138
ENSG00000162783	IER5	13.6	31.3	1.2	0.00138
ENSG00000011007	TCEB3	19	43.7	1.2	0.00138
ENSG00000229091	HSPA8P8	0.421	0.964	1.2	0.0318
ENSG00000179218	CALR	200	457	1.2	0.00138
ENSG00000181026	AEN	27.9	63.8	1.19	0.00138
ENSG00000279145	RP11-547D13.1	0.244	0.557	1.19	0.00138
ENSG00000204524	ZNF805	7.36	16.8	1.19	0.00138
ENSG00000168374	ARF4	65.5	149	1.18	0.00138
ENSG00000126947	ARMCX1	8.35	18.9	1.18	0.00138
ENSG00000115289	PCGF1	31.7	71.5	1.17	0.00138
ENSG00000164136	IL15	0.64	1.44	1.17	0.027
ENSG00000119547	ONECUT2	3.6	8.1	1.17	0.00138
ENSG00000138434	SSFA2	16.6	37.3	1.17	0.00138
ENSG00000261505	LA16c-358B7.3	2.15	4.83	1.17	0.0432
ENSG00000256223	ZNF10	4.06	9.11	1.17	0.00558
ENSG00000280347	AC000123.2	3.98	8.92	1.16	0.00138
ENSG00000260941	LINC00622	0.741	1.66	1.16	0.00255
ENSG00000119973	PRLHR	0.472	1.06	1.16	0.00138
ENSG00000112541	PDE10A	13.3	29.6	1.16	0.00255
ENSG00000158615	PPP1R15B	30	66.6	1.15	0.00138
ENSG00000144749	LRIG1	0.649	1.44	1.15	0.0363
ENSG00000117479	SLC19A2	6.33	14	1.15	0.00138
ENSG00000130522	JUND	86.5	192	1.15	0.00138
ENSG00000078804	TP53INP2	16.6	36.9	1.15	0.00138
ENSG00000268089	GABRQ	0.346	0.763	1.14	0.00138
ENSG00000104722	NEFM	20.2	44.5	1.14	0.00138
ENSG00000120149	MSX2	3.74	8.24	1.14	0.00138

Ensembl_Gene_ID	Gene_name	Control	Illuminated	Log2 FC	q_val
ENSG00000121671	CRY2	6.16	13.6	1.14	0.00138
ENSG00000120742	SERP1	36.2	79.8	1.14	0.00138
ENSG00000242125	SNHG3	47.5	104	1.14	0.0264
ENSG00000168439	STIP1	74.4	164	1.14	0.00138
ENSG00000095574	IKZF5	4.97	10.9	1.14	0.0107
ENSG00000232531	AC027612.1	0.822	1.81	1.14	0.0123
ENSG00000250910	AC097467.2	0.455	1	1.14	0.04
ENSG00000136240	KDELR2	53.4	117	1.13	0.00138
ENSG00000164244	PRRC1	19.3	42.3	1.13	0.00138
ENSG00000078237	C12orf5	5.39	11.7	1.12	0.00138
ENSG00000187601	MAGEH1	9.65	21	1.12	0.00138
ENSG00000102401	ARMCX3	12	26	1.12	0.00138
ENSG00000112218	GPR63	1.41	3.06	1.12	0.00138
ENSG00000111641	NOP2	33.1	71.8	1.12	0.00138
ENSG00000206082	LINC01002	1.16	2.5	1.11	0.00138
ENSG00000162775	RBM15	10.7	23	1.11	0.00138
ENSG00000273448	RP11-166O4.6	0.969	2.09	1.11	0.00138
ENSG00000268713	CTC-444N24.8	3.92	8.46	1.11	0.00138
ENSG00000181472	ZBTB2	4.74	10.2	1.11	0.00138
ENSG00000228653	HNRNPCP7	1.02	2.2	1.11	0.0107
ENSG00000026508	CD44	0.449	0.966	1.11	0.0123
ENSG00000116604	MEF2D	15.7	33.8	1.1	0.00138
ENSG00000127920	GNG11	16.3	35.1	1.1	0.00138
ENSG00000133398	MED10	26.9	57.8	1.1	0.00138
ENSG00000131016	AKAP12	11.4	24.5	1.1	0.00138
ENSG00000160888	IER2	17	36.4	1.1	0.00138
ENSG00000219665	CTD-2006C1.2	7.4	15.8	1.1	0.00739
ENSG00000152332	UHMK1	13.9	29.8	1.1	0.00138
ENSG00000111860	CEP85L	4.91	10.5	1.09	0.00255
ENSG00000129493	HEATR5A	14.2	30.3	1.09	0.0233
ENSG00000157020	SEC13	45.5	96.9	1.09	0.00138
ENSG00000272512	RP11-54O7.17	0.568	1.21	1.09	0.00138
ENSG00000115520	COQ10B	8.5	18.1	1.09	0.00138
ENSG00000226549	SCDP1	1.15	2.44	1.09	0.00362
ENSG00000168994	PXDC1	0.839	1.78	1.09	0.00138
ENSG00000110172	CHORDC1	13.7	29	1.09	0.00138
ENSG00000150991	UBC	375	797	1.08	0.00138
ENSG00000280111	CTA-292E10.9	0.513	1.09	1.08	0.0264
ENSG00000139112	GABARAPL1	13.7	29	1.08	0.00138
ENSG00000128016	ZFP36	5.18	11	1.08	0.00138
ENSG00000182700	IGIP	1.96	4.15	1.08	0.00138
ENSG00000059769	DNAJC25	3.61	7.63	1.08	0.00138
ENSG00000136159	NUDT15	8.09	17.1	1.08	0.00138
ENSG00000167110	GOLGA2	23.4	49.2	1.08	0.00138
ENSG00000066405	CLDN18	0.495	1.04	1.07	0.00138
ENSG00000123485	HJURP	6.61	13.9	1.07	0.00138
ENSG00000280138	RP11-463O12.5	0.484	1.02	1.07	0.00138

Ensembl_Gene_ID	Gene_name	Control	Illuminated	Log2 FC	q_val
ENSG00000112893	MAN2A1	5.42	11.3	1.07	0.00138
ENSG00000122420	PTGFR	0.909	1.9	1.06	0.00138
ENSG00000198912	C1orf174	8.89	18.5	1.06	0.00138
ENSG00000198380	GFPT1	8	16.6	1.06	0.00255
ENSG00000257315	ZBED6	34.9	72.4	1.05	0.00138
ENSG00000170889	RPS9	1.09	2.25	1.05	0.00138
ENSG00000229222	KRT18P4	0.466	0.965	1.05	0.0437
ENSG00000143384	MCL1	60.6	126	1.05	0.00138
ENSG00000006194	ZNF263	24.7	51.2	1.05	0.00138
ENSG00000184432	COPB2	50.6	105	1.05	0.00138
ENSG00000110048	OSBP	14.1	29.2	1.04	0.00138
ENSG00000172667	ZMAT3	29.5	60.7	1.04	0.00138
ENSG00000224773	HSPA8P7	1.09	2.24	1.04	0.00138
ENSG00000261609	GAN	3.21	6.6	1.04	0.00138
ENSG00000135045	C9orf40	3.23	6.62	1.04	0.00138
ENSG00000251201	TMED7-TICAM2	5.72	11.7	1.03	0.00558
ENSG00000185222	WBP5	18	36.9	1.03	0.00138
ENSG00000070444	MNT	11	22.4	1.03	0.00138
ENSG00000255387	RP11-23F23.3	0.367	0.751	1.03	0.0406
ENSG00000109089	CDR2L	24.4	49.9	1.03	0.00138
ENSG00000118298	CA14	2.74	5.58	1.02	0.00138
ENSG00000075702	WDR62	2.21	4.49	1.02	0.00138
ENSG00000112599	GUCA1B	1.1	2.22	1.02	0.00826
ENSG00000169057	MECP2	12.6	25.6	1.02	0.00138
ENSG00000124370	MCEE	5.18	10.5	1.02	0.00138
ENSG00000162734	PEA15	55.7	112	1.01	0.00138
ENSG00000120129	DUSP1	9.96	20.1	1.01	0.00138
ENSG00000105472	CLEC11A	4.15	8.38	1.01	0.00138
ENSG00000169239	CA5B	4.32	8.72	1.01	0.0318
ENSG00000234176	HSPA8P1	0.895	1.8	1.01	0.00138
ENSG00000279821	RP11-1334A24.5	0.334	0.672	1.01	0.00826
ENSG00000049130	KITLG	2.49	5.01	1.01	0.00138
ENSG00000174010	KLHL15	3.96	7.98	1.01	0.00138
ENSG00000151247	EIF4E	5.04	10.1	1.01	0.0472
ENSG00000153487	ING1	7.06	14.2	1.01	0.00138
ENSG00000151929	BAG3	4.39	8.82	1	0.00138
ENSG00000185245	GP1BA	0.486	0.974	1	0.00255
ENSG00000139354	GAS2L3	6.55	13.1	1	0.0065
ENSG00000196850	PPTC7	6.8	13.6	1	0.00138
ENSG00000104228	TRIM35	7.63	15.3	1	0.0115
ENSG00000139163	ETNK1	19.1	38.2	1	0.0201
ENSG00000101445	PPP1R16B	7.12	3.55	-1	0.0335
ENSG00000241345	RP4-630C24.3	1.35	0.672	-1	0.00558
ENSG00000132334	PTPRE	2.72	1.36	-1	0.0131
ENSG00000135472	FAIM2	4.86	2.42	-1.01	0.00138
ENSG00000248540	RP11-247C2.2	7.29	3.63	-1.01	0.00138
ENSG00000006756	ARSD	2.46	1.23	-1.01	0.0442

Ensembl_Gene_ID	Gene_name	Control	Illuminated	Log2 FC	q_val
ENSG00000172159	FRMD3	9.38	4.66	-1.01	0.00138
ENSG00000080166	DCT	0.646	0.321	-1.01	0.0174
ENSG00000255248	RP11-166D19.1	1.44	0.715	-1.01	0.0395
ENSG00000197191	CYSRT1	1.48	0.734	-1.01	0.0188
ENSG00000087008	ACOX3	7.83	3.88	-1.01	0.0091
ENSG00000183160	TMEM119	32.3	16	-1.02	0.00138
ENSG00000226384	GTF2H4	4.19	2.07	-1.02	0.0437
ENSG00000108175	ZMIZ1	75.1	37.1	-1.02	0.00138
ENSG00000166145	SPINT1	1.64	0.806	-1.02	0.0214
ENSG00000137124	ALDH1B1	17.4	8.52	-1.03	0.00138
ENSG00000159399	HK2	29.3	14.4	-1.03	0.00138
ENSG00000178802	MPI	47	23.1	-1.03	0.00138
ENSG00000136213	CHST12	15	7.38	-1.03	0.00138
ENSG00000280057	RP1-168L15.6	0.846	0.415	-1.03	0.0323
ENSG00000163364	LINC01116	31.6	15.5	-1.03	0.00138
ENSG00000276855	CTD-3157E16.2	3.38	1.66	-1.03	0.0123
ENSG00000266411	RP11-180P8.3	6.35	3.11	-1.03	0.00138
ENSG00000204934	ATP6V0E2-AS1	3.97	1.94	-1.03	0.0138
ENSG00000137860	SLC28A2	0.96	0.47	-1.03	0.0195
ENSG00000136870	ZNF189	11.6	5.66	-1.03	0.00138
ENSG00000114520	SNX4	20.6	10.1	-1.03	0.00138
ENSG00000141736	ERBB2	7.7	3.76	-1.03	0.0276
ENSG00000134333	LDHA	350	171	-1.04	0.00138
ENSG00000119888	EPCAM	2.46	1.2	-1.04	0.0091
ENSG00000162407	PPAP2B	4.7	2.29	-1.04	0.00138
ENSG00000173281	PPP1R3B	20.8	10.1	-1.04	0.00138
ENSG00000177674	AGTRAP	12.8	6.2	-1.04	0.00138
ENSG00000115866	DARS	81	39.3	-1.04	0.00138
ENSG00000064225	ST3GAL6	40.8	19.8	-1.04	0.00138
ENSG00000204947	ZNF425	3.14	1.52	-1.04	0.027
ENSG00000005882	PDK2	22.3	10.8	-1.04	0.00362
ENSG00000102466	FGF14	21.2	10.3	-1.05	0.0138
ENSG00000162552	WNT4	1.11	0.536	-1.05	0.0432
ENSG00000112320	SOBP	24.7	12	-1.05	0.00138
ENSG00000130475	FCHO1	3.4	1.64	-1.05	0.00255
ENSG00000203943	SAMD13	2.12	1.02	-1.05	0.00739
ENSG00000137872	SEMA6D	3.28	1.58	-1.05	0.027
ENSG00000128581	IFT22	25.6	12.4	-1.05	0.00138
ENSG00000164967	RPP25L	10.6	5.1	-1.05	0.00138
ENSG00000185669	SNAI3	1.17	0.566	-1.05	0.0411
ENSG00000124279	FASTKD3	6.25	3.02	-1.05	0.0123
ENSG00000206559	ZCWPW2	1.28	0.62	-1.05	0.0416
ENSG00000120860	CCDC53	23	11.1	-1.05	0.00138
ENSG00000158483	FAM86C1	4.31	2.08	-1.05	0.00739
ENSG00000198185	ZNF334	6.52	3.14	-1.05	0.00138
ENSG00000152969	JAKMIP1	10.1	4.83	-1.06	0.00138
ENSG00000141540	TTYH2	5.26	2.53	-1.06	0.00138

Ensembl_Gene_ID	Gene_name	Control	Illuminated	Log2 FC	q_val
ENSG00000272365	RP11-389C8.3	2.48	1.19	-1.06	0.0208
ENSG00000124688	MAD2L1BP	41.6	19.9	-1.06	0.00138
ENSG00000268996	MAN1B1-AS1	1.54	0.74	-1.06	0.0065
ENSG00000069712	KIAA1107	4.38	2.09	-1.06	0.00138
ENSG00000229186	ADAM1A	1.99	0.954	-1.06	0.00138
ENSG00000103852	TTC23	4.16	1.99	-1.06	0.0115
ENSG00000260400	RP11-119F7.5	4.21	2.01	-1.06	0.00138
ENSG00000228889	UBAC2-AS1	2.06	0.986	-1.06	0.00138
ENSG00000151552	QDPR	31	14.8	-1.06	0.00138
ENSG00000165698	C9orf9	4.51	2.15	-1.07	0.00138
ENSG00000110400	PVRL1	40	19	-1.07	0.00138
ENSG00000157927	RADIL	8.03	3.82	-1.07	0.00138
ENSG00000159307	SCUBE1	3.52	1.67	-1.07	0.0306
ENSG00000179627	ZBTB42	1.25	0.594	-1.08	0.0115
ENSG00000134954	ETS1	6.08	2.89	-1.08	0.00138
ENSG00000074370	ATP2A3	5.29	2.51	-1.08	0.00138
ENSG00000273081	RP4-813F11.4	0.968	0.458	-1.08	0.00362
ENSG00000080644	CHRNA3	141	66.6	-1.08	0.00138
ENSG00000162849	KIF26B	1.8	0.849	-1.08	0.00138
ENSG00000223658	AC011242.6	8.64	4.08	-1.08	0.00138
ENSG00000136279	DBNL	32.9	15.5	-1.09	0.00138
ENSG00000181754	AMIGO1	1.86	0.874	-1.09	0.00138
ENSG00000276550	HERC2P2	2.73	1.28	-1.09	0.00138
ENSG00000133256	PDE6B	12.6	5.89	-1.09	0.00138
ENSG00000274225	KB-68A7.1	2.5	1.17	-1.09	0.0487
ENSG00000204624	PTCHD2	3.45	1.62	-1.09	0.00138
ENSG00000027001	MIPEP	3.39	1.59	-1.09	0.00739
ENSG00000168398	BDKRB2	2.53	1.19	-1.09	0.00138
ENSG00000278266	RP11-575F12.3	2.18	1.02	-1.1	0.00138
ENSG00000225791	TRAM2-AS1	8.99	4.2	-1.1	0.00138
ENSG00000060642	PIGV	11.1	5.2	-1.1	0.00138
ENSG00000224596	ZMIZ1-AS1	0.555	0.258	-1.1	0.0335
ENSG00000122971	ACADS	4.78	2.22	-1.1	0.00138
ENSG00000008196	TFAP2B	92.7	43.1	-1.1	0.00138
ENSG00000100234	TIMP3	3.81	1.77	-1.1	0.00138
ENSG00000184828	ZBTB7C	3.25	1.51	-1.11	0.00138
ENSG00000158445	KCNB1	2.83	1.32	-1.11	0.00138
ENSG00000138642	HERC6	1.82	0.842	-1.11	0.0312
ENSG00000259877	RP11-46C24.7	4.59	2.12	-1.11	0.00138
ENSG00000264247	LINC00909	8.98	4.16	-1.11	0.0091
ENSG00000271151	RP11-394I13.2	2.02	0.936	-1.11	0.00826
ENSG00000280187	CTC-351M12.1	2.6	1.2	-1.11	0.00138
ENSG00000155085	AK9	4.94	2.28	-1.11	0.00138
ENSG00000226137	BAIAP2-AS1	6.44	2.97	-1.12	0.00138
ENSG00000165912	PACSIN3	16.7	7.69	-1.12	0.00138
ENSG00000273456	RP11-686O6.2	2.17	1	-1.12	0.0482
ENSG00000146966	DENND2A	8.94	4.11	-1.12	0.027

Ensembl_Gene_ID	Gene_name	Control	Illuminated	Log2 FC	q_val
ENSG00000234882	EIF3EP1	2.24	1.03	-1.12	0.0472
ENSG00000197748	CFAP43	1.91	0.876	-1.12	0.00362
ENSG00000231584	FAHD2CP	8.18	3.75	-1.12	0.00138
ENSG00000143355	LHX9	1.74	0.795	-1.12	0.00558
ENSG00000186280	KDM4D	1.67	0.765	-1.13	0.00138
ENSG00000170629	DPY19L2P2	1.3	0.594	-1.13	0.00138
ENSG00000170382	LRRN2	3.51	1.61	-1.13	0.00138
ENSG00000145911	N4BP3	2.17	0.992	-1.13	0.00138
ENSG00000188859	FAM78B	5.67	2.59	-1.13	0.00138
ENSG00000188549	C15orf52	5.55	2.53	-1.13	0.00138
ENSG00000136859	ANGPTL2	4.05	1.85	-1.14	0.0487
ENSG00000162755	KLHDC9	5.09	2.32	-1.14	0.0264
ENSG00000186301	MST1P2	0.472	0.214	-1.14	0.0406
ENSG00000118965	WDR35	20.6	9.38	-1.14	0.00138
ENSG00000089041	P2RX7	2.57	1.17	-1.14	0.00138
ENSG00000178171	AMER3	5.43	2.46	-1.14	0.00138
ENSG00000174807	CD248	8.84	3.99	-1.15	0.00138
ENSG00000262075	DKFZP434A062	0.497	0.224	-1.15	0.00138
ENSG00000165171	WBSCR27	4.4	1.98	-1.15	0.00138
ENSG00000264548	RP13-516M14.2	0.507	0.228	-1.15	0.0346
ENSG00000157557	ETS2	17.2	7.71	-1.15	0.00138
ENSG00000261754	CTC-523E23.1	1.53	0.685	-1.16	0.00255
ENSG00000124212	PTGIS	1.03	0.46	-1.16	0.00138
ENSG00000258701	LINC00638	1.22	0.547	-1.16	0.00138
ENSG00000205502	C2CD4B	2.72	1.22	-1.16	0.00138
ENSG00000135245	HILPDA	24.4	10.9	-1.16	0.00362
ENSG00000128805	ARHGAP22	5.5	2.45	-1.17	0.00138
ENSG00000168806	LCMT2	8.89	3.95	-1.17	0.00138
ENSG00000168899	VAMP5	2.29	1.02	-1.17	0.027
ENSG00000084453	SLCO1A2	3.84	1.7	-1.17	0.0352
ENSG00000107807	TLX1	6.55	2.91	-1.17	0.00362
ENSG00000082684	SEMA5B	12	5.31	-1.17	0.00138
ENSG00000066926	FECH	19	8.41	-1.17	0.00138
ENSG00000198890	PRMT6	14.7	6.5	-1.17	0.00138
ENSG00000235169	SMIM1	12.6	5.59	-1.18	0.00138
ENSG00000185614	FAM212A	2.38	1.05	-1.18	0.00558
ENSG00000041353	RAB27B	2.7	1.19	-1.18	0.00138
ENSG00000138496	PARP9	2	0.881	-1.18	0.00255
ENSG00000120899	PTK2B	6.64	2.93	-1.18	0.00558
ENSG00000241852	C8orf58	16.7	7.35	-1.18	0.00138
ENSG00000138316	ADAMTS14	1.73	0.762	-1.18	0.00138
ENSG00000279205	RP11-632P5.1	0.726	0.319	-1.19	0.0282
ENSG00000186918	ZNF395	41.9	18.4	-1.19	0.00138
ENSG00000171729	TMEM51	23.3	10.2	-1.19	0.00138
ENSG00000174460	ZCCHC12	2.09	0.918	-1.19	0.00138
ENSG00000181652	ATG9B	3.88	1.7	-1.19	0.0282
ENSG00000150672	DLG2	11.5	5.05	-1.19	0.00138

Ensembl_Gene_ID	Gene_name	Control	Illuminated	Log2 FC	q_val
ENSG00000233198	RNF224	1.12	0.492	-1.19	0.00462
ENSG00000176349	AC110781.3	1.51	0.659	-1.2	0.0195
ENSG00000072163	LIMS2	0.8	0.349	-1.2	0.0146
ENSG00000111490	TBC1D30	1.63	0.711	-1.2	0.016
ENSG00000136720	HS6ST1	19.9	8.68	-1.2	0.00138
ENSG00000230444	TFAMP1	2.84	1.24	-1.2	0.0107
ENSG00000150977	RILPL2	0.788	0.343	-1.2	0.00138
ENSG00000141668	CBLN2	5.8	2.52	-1.2	0.00138
ENSG00000140876	NUDT7	8.41	3.66	-1.2	0.00138
ENSG00000144452	ABCA12	1.49	0.646	-1.2	0.00138
ENSG00000110031	LPXN	1.72	0.747	-1.21	0.0138
ENSG00000249307	LINC01088	2.26	0.978	-1.21	0.0195
ENSG00000248927	CTD-2334D19.1	1.22	0.527	-1.21	0.0188
ENSG00000176381	PRR18	1.47	0.636	-1.21	0.0195
ENSG00000267194	RP1-193H18.2	3.19	1.38	-1.21	0.00138
ENSG00000214273	AGGF1P1	0.864	0.373	-1.21	0.00362
ENSG00000228612	HK2P1	1.42	0.611	-1.21	0.00138
ENSG00000214654	RP11-27I1.4	8.91	3.84	-1.21	0.00138
ENSG00000156384	SFR1	6.49	2.8	-1.21	0.00138
ENSG00000197872	FAM49A	5.76	2.48	-1.21	0.0123
ENSG00000173826	KCNH6	5.54	2.38	-1.22	0.00138
ENSG00000196155	PLEKHG4	15.1	6.5	-1.22	0.00138
ENSG00000243819	RN7SL832P	1.23	0.527	-1.22	0.00255
ENSG00000149292	TTC12	12.7	5.42	-1.22	0.00138
ENSG00000063761	ADCK1	2.6	1.11	-1.22	0.00138
ENSG00000273297	RP11-38M8.1	6.96	2.98	-1.23	0.00138
ENSG00000184986	TMEM121	3.16	1.35	-1.23	0.00138
ENSG00000186231	KLHL32	0.56	0.239	-1.23	0.0174
ENSG00000130518	KIAA1683	5.08	2.16	-1.23	0.00138
ENSG00000154102	C16orf74	4.22	1.8	-1.23	0.00138
ENSG00000158008	EXTL1	1.95	0.83	-1.24	0.0426
ENSG00000255036	RP11-23J9.4	0.723	0.307	-1.24	0.0091
ENSG00000132437	DDC	146	62	-1.24	0.00138
ENSG00000205037	RP11-863P13.4	6.33	2.68	-1.24	0.0368
ENSG00000119714	GPR68	2.29	0.968	-1.24	0.00138
ENSG00000185112	FAM43A	6.46	2.73	-1.25	0.00138
ENSG00000187952	HS6ST1P1	2.4	1.01	-1.25	0.00138
ENSG00000160172	FAM86C2P	3.98	1.67	-1.26	0.00138
ENSG00000166073	GPR176	20.1	8.42	-1.26	0.00138
ENSG00000278928	RP11-481F24.3	33.4	14	-1.26	0.00138
ENSG00000082458	DLG3	1.75	0.734	-1.26	0.0323
ENSG00000233922	AL133493.2	4.02	1.68	-1.26	0.00138
ENSG00000218510	LINC00339	16.2	6.75	-1.26	0.00138
ENSG00000182957	SPATA13	2.01	0.835	-1.27	0.027
ENSG00000165061	ZMAT4	11.7	4.83	-1.27	0.00138
ENSG00000116574	RHOU	16.4	6.77	-1.28	0.00138
ENSG00000141665	FBXO15	1.31	0.538	-1.28	0.00739

Ensembl_Gene_ID	Gene_name	Control	Illuminated	Log2 FC	q_val
ENSG00000181004	BBS12	3.32	1.36	-1.28	0.00138
ENSG00000219891	ZSCAN12P1	14.7	6.06	-1.28	0.00138
ENSG00000175279	APITD1	9.66	3.96	-1.29	0.00138
ENSG00000279518	AC083843.4	0.479	0.196	-1.29	0.0282
ENSG00000101347	SAMHD1	2.96	1.21	-1.29	0.00138
ENSG00000157429	ZNF19	3.26	1.33	-1.29	0.0487
ENSG00000164649	CDCA7L	19.3	7.87	-1.29	0.00138
ENSG00000138380	CARF	7.83	3.19	-1.3	0.0091
ENSG00000174327	SLC16A13	3.87	1.57	-1.3	0.00138
ENSG00000172086	KRCC1	14.5	5.88	-1.3	0.00138
ENSG00000176720	BOK	4.66	1.89	-1.3	0.00138
ENSG00000163082	SGPP2	0.756	0.306	-1.3	0.00138
ENSG00000095203	EPB41L4B	10	4.06	-1.31	0.00138
ENSG00000213171	LINGO4	0.76	0.307	-1.31	0.00138
ENSG00000171811	CFAP46	1.39	0.559	-1.32	0.0167
ENSG00000139187	KLRG1	7.15	2.86	-1.32	0.00138
ENSG00000008283	CYB561	160	64	-1.32	0.00138
ENSG00000253426	RP11-10A14.4	4.59	1.84	-1.32	0.00826
ENSG00000186496	ZNF396	2.33	0.933	-1.32	0.00138
ENSG00000071794	HLTF	26.6	10.6	-1.33	0.00138
ENSG00000251216	RP11-161D15.3	31.4	12.4	-1.34	0.00138
ENSG00000229481	CTD-2554C21.3	0.718	0.284	-1.34	0.0065
ENSG00000224090	AC097468.4	1.43	0.564	-1.34	0.0065
ENSG00000196660	SLC30A10	0.862	0.34	-1.34	0.00138
ENSG00000260000	RP3-467N11.1	2.1	0.827	-1.34	0.00138
ENSG00000156253	RWDD2B	14.8	5.83	-1.35	0.00138
ENSG00000140368	PSTPIP1	0.925	0.363	-1.35	0.0306
ENSG00000006071	ABCC8	4.99	1.95	-1.36	0.0487
ENSG00000004799	PDK4	1.05	0.41	-1.36	0.00138
ENSG00000071282	LMCD1	11.6	4.54	-1.36	0.00138
ENSG00000107014	RLN2	1.72	0.671	-1.36	0.0346
ENSG00000104953	TLE6	9.04	3.52	-1.36	0.00138
ENSG00000235750	KIAA0040	1.46	0.569	-1.36	0.0115
ENSG00000168491	CCDC110	2.12	0.824	-1.36	0.00255
ENSG00000240204	SMKR1	5.29	2.06	-1.36	0.00138
ENSG00000183798	EMILIN3	3.35	1.3	-1.37	0.00138
ENSG00000170743	SYT9	7.42	2.87	-1.37	0.00138
ENSG00000100336	APOL4	1	0.387	-1.37	0.0174
ENSG00000164086	DUSP7	32	12.3	-1.37	0.00138
ENSG00000126562	WNK4	3.19	1.23	-1.37	0.0221
ENSG00000230438	SERPINB9P1	0.993	0.383	-1.38	0.0437
ENSG00000154319	FAM167A	49.7	19.2	-1.38	0.00138
ENSG00000026559	KCNG1	3.13	1.2	-1.38	0.00138
ENSG00000135835	KIAA1614	4.63	1.78	-1.38	0.0065
ENSG00000204815	TTC25	3.38	1.3	-1.38	0.00138
ENSG00000271270	TMCC1-AS1	8.25	3.17	-1.38	0.00138
ENSG00000198865	CCDC152	0.836	0.32	-1.38	0.00362

Ensembl_Gene_ID	Gene_name	Control	Illuminated	Log2 FC	q_val
ENSG00000166407	LMO1	52.2	20	-1.39	0.00138
ENSG00000213888	LINC01521	7.58	2.9	-1.39	0.00138
ENSG00000092850	TEKT2	1.13	0.432	-1.39	0.00558
ENSG00000007402	CACNA2D2	94.5	36	-1.39	0.00138
ENSG00000223486	AC092198.1	0.738	0.281	-1.39	0.00138
ENSG00000030419	IKZF2	1.56	0.592	-1.4	0.0306
ENSG00000271122	RP11-379H18.1	12.9	4.89	-1.4	0.00138
ENSG00000171992	SYNPO	38.2	14.4	-1.41	0.00138
ENSG00000255121	RP11-110I1.12	1.73	0.652	-1.41	0.00255
ENSG00000168874	ATOH8	0.928	0.349	-1.41	0.0107
ENSG00000198075	SULT1C4	28.9	10.8	-1.41	0.00138
ENSG00000170915	PAQR8	26.7	10	-1.42	0.00138
ENSG00000156564	LRFN2	4.66	1.74	-1.42	0.00138
ENSG00000129910	CDH15	0.604	0.225	-1.43	0.00362
ENSG00000272097	RP11-421M1.8	3.55	1.32	-1.43	0.00138
ENSG00000254656	RTL1	402	149	-1.43	0.00138
ENSG00000275917	CHRFAM7A	0.792	0.294	-1.43	0.00362
ENSG00000226508	AC104655.3	3.83	1.42	-1.43	0.0131
ENSG00000134107	BHLHE40	8	2.96	-1.43	0.00138
ENSG00000183831	ANKRD45	1.85	0.682	-1.44	0.00138
ENSG00000198520	C1orf228	4.54	1.67	-1.44	0.00362
ENSG00000269837	IPO5P1	3.64	1.34	-1.44	0.0065
ENSG00000114541	FRMD4B	2.96	1.09	-1.44	0.00138
ENSG00000196659	TTC30B	5.25	1.93	-1.44	0.00138
ENSG00000198570	RD3	16.4	5.98	-1.45	0.00138
ENSG00000179431	FJX1	1.02	0.371	-1.45	0.00138
ENSG00000179921	GPBAR1	1.66	0.603	-1.46	0.00138
ENSG00000265096	C1QTNF1-AS1	5.04	1.84	-1.46	0.0195
ENSG00000177106	EPS8L2	4.45	1.62	-1.46	0.0065
ENSG00000181072	CHRM2	5.66	2.05	-1.46	0.00138
ENSG00000108984	MAP2K6	8.06	2.92	-1.46	0.00138
ENSG00000180787	ZFP3	5.17	1.87	-1.47	0.00138
ENSG00000089127	OAS1	1.3	0.47	-1.47	0.0276
ENSG00000133805	AMPD3	4.14	1.5	-1.47	0.00138
ENSG00000112357	PEX7	10.1	3.65	-1.47	0.00138
ENSG00000078114	NEBL	2.52	0.903	-1.48	0.00138
ENSG00000106003	LFNG	5.19	1.85	-1.49	0.00138
ENSG00000149050	ZNF214	1.68	0.599	-1.49	0.00362
ENSG00000091409	ITGA6	0.905	0.322	-1.49	0.0368
ENSG00000245848	CEBPA	3.25	1.16	-1.49	0.00138
ENSG00000108771	DHX58	0.98	0.349	-1.49	0.0318
ENSG00000232859	LYRM9	3.19	1.13	-1.49	0.00826
ENSG00000117394	SLC2A1	51.7	18.2	-1.51	0.00138
ENSG00000228903	RASA4CP	1.15	0.404	-1.51	0.0107
ENSG00000138061	CYP1B1	0.712	0.249	-1.52	0.0437
ENSG00000267355	RPL9P29	2.4	0.841	-1.52	0.0282
ENSG00000214376	VSTM5	0.526	0.184	-1.52	0.0492

Ensembl_Gene_ID	Gene_name	Control	Illuminated	Log2 FC	q_val
ENSG00000169218	RSPO1	0.663	0.232	-1.52	0.00255
ENSG00000136205	TNS3	8.37	2.92	-1.52	0.00138
ENSG00000114268	PFKFB4	15.2	5.28	-1.52	0.00138
ENSG00000183111	ARHGEF37	3.63	1.26	-1.52	0.00138
ENSG00000279368	RP1-80N2.4	1.12	0.39	-1.52	0.00138
ENSG00000251408	RP11-586D19.2	0.829	0.288	-1.53	0.0288
ENSG00000169129	AFAP1L2	0.959	0.332	-1.53	0.00255
ENSG00000112715	VEGFA	246	85.1	-1.53	0.00138
ENSG00000072952	MRVI1	3.49	1.21	-1.53	0.00138
ENSG00000224008	LINC01441	0.751	0.26	-1.53	0.00138
ENSG00000168481	LGI3	1.38	0.473	-1.54	0.00138
ENSG00000171608	PIK3CD	5.48	1.87	-1.55	0.0384
ENSG00000197557	TTC30A	6.14	2.1	-1.55	0.00138
ENSG00000251011	TMEM108-AS1	4.6	1.56	-1.56	0.0437
ENSG00000272667	RP11-395A13.2	3.44	1.16	-1.57	0.00462
ENSG00000166432	ZMAT1	2.5	0.838	-1.58	0.00138
ENSG00000171084	FAM86JP	3.74	1.25	-1.58	0.00138
ENSG00000117152	RGS4	1130	379	-1.58	0.00138
ENSG00000227028	SLC8A1-AS1	1.45	0.483	-1.58	0.0432
ENSG00000198939	ZFP2	0.969	0.323	-1.59	0.00362
ENSG00000007062	PROM1	0.629	0.209	-1.59	0.0146
ENSG00000158050	DUSP2	0.878	0.291	-1.59	0.00138
ENSG00000152256	PDK1	25.6	8.43	-1.6	0.00138
ENSG00000254202	RP11-120I21.2	3.15	1.04	-1.61	0.00255
ENSG00000131095	GFAP	0.824	0.269	-1.61	0.039
ENSG00000204175	GPRIN2	0.958	0.313	-1.61	0.00138
ENSG00000173727	CMB9-22P13.1	1.95	0.635	-1.62	0.00739
ENSG00000161544	CYGB	79.4	25.8	-1.62	0.00138
ENSG00000142621	FHAD1	1.7	0.551	-1.62	0.00462
ENSG00000235597	LINC01102	5.57	1.8	-1.63	0.00138
ENSG00000224383	PRR29	1.63	0.527	-1.63	0.00462
ENSG00000214140	PRCD	99.8	32.2	-1.63	0.00138
ENSG00000182389	CACNB4	3.52	1.13	-1.64	0.00138
ENSG00000175147	TMEM51-AS1	4.82	1.55	-1.64	0.00138
ENSG00000137198	GMPR	1.01	0.323	-1.64	0.0146
ENSG00000196668	LINC00173	2.6	0.826	-1.65	0.0123
ENSG00000182489	XKRX	1.56	0.496	-1.65	0.00138
ENSG00000273145	CITF22-92A6.1	0.885	0.278	-1.67	0.0227
ENSG00000105880	DLX5	0.76	0.238	-1.68	0.0239
ENSG00000196542	SPTSSB	1.14	0.357	-1.68	0.00826
ENSG00000254162	RP11-48B3.3	0.702	0.219	-1.68	0.00138
ENSG00000278291	RP11-172H24.4	1.06	0.33	-1.68	0.00138
ENSG00000258555	SPECC1L-ADORA2A	16.6	5.17	-1.68	0.00138
ENSG00000133121	STARD13	5.06	1.57	-1.68	0.00138
ENSG00000275763	FLJ44313	0.546	0.17	-1.68	0.0146
ENSG00000224843	LINC00240	1.12	0.349	-1.69	0.039
ENSG00000247796	CTD-2366F13.1	2.57	0.798	-1.69	0.0146

Ensembl_Gene_ID	Gene_name	Control	Illuminated	Log2 FC	q_val
ENSG00000110665	C11orf21	1.16	0.361	-1.69	0.0258
ENSG00000101292	PROKR2	1.25	0.387	-1.69	0.00138
ENSG00000117971	CHRNB4	18.2	5.59	-1.7	0.00138
ENSG00000212916	MAP10	2.33	0.715	-1.71	0.00138
ENSG00000075290	WNT8B	0.496	0.152	-1.71	0.016
ENSG00000165633	VSTM4	2.78	0.85	-1.71	0.00138
ENSG00000148225	WDR31	1.61	0.492	-1.71	0.00138
ENSG00000279673	RP11-185E8.2	0.726	0.222	-1.71	0.0138
ENSG00000117148	ACTL8	2.76	0.84	-1.72	0.00138
ENSG00000132669	RIN2	3.13	0.95	-1.72	0.00462
ENSG00000165025	SYK	1.13	0.341	-1.72	0.00138
ENSG00000178403	NEUROG2	25.7	7.76	-1.73	0.00138
ENSG00000255690	TRIL	13.2	3.98	-1.73	0.00138
ENSG00000196990	FAM163B	38.3	11.5	-1.73	0.00138
ENSG00000180938	ZNF572	3.09	0.923	-1.74	0.00138
ENSG00000259583	RP11-66B24.4	2.95	0.881	-1.74	0.00138
ENSG00000016402	IL20RA	0.575	0.171	-1.75	0.0264
ENSG00000184254	ALDH1A3	7.13	2.09	-1.77	0.00138
ENSG00000156097	GPR61	1.91	0.559	-1.77	0.00138
ENSG00000113578	FGF1	2.11	0.618	-1.77	0.0346
ENSG00000278709	RP5-1059L7.1	2.59	0.744	-1.8	0.016
ENSG00000251669	FAM86EP	4.04	1.16	-1.8	0.00138
ENSG00000183873	SCN5A	5.98	1.69	-1.82	0.00138
ENSG00000129757	CDKN1C	3.67	1.02	-1.84	0.00138
ENSG00000269998	RP11-272L13.3	1.58	0.44	-1.84	0.0115
ENSG00000163827	LRRC2	0.731	0.203	-1.85	0.00362
ENSG00000183208	GDPGP1	3.4	0.944	-1.85	0.027
ENSG00000260317	RP11-48B3.4	0.832	0.229	-1.86	0.00138
ENSG00000139352	ASCL1	5.55	1.49	-1.9	0.00138
ENSG00000248866	USP46-AS1	2.28	0.607	-1.91	0.00138
ENSG00000183250	C21orf67	2.76	0.734	-1.91	0.00138
ENSG00000182747	SLC35D3	6.85	1.79	-1.94	0.00138
ENSG00000123146	CD97	0.81	0.212	-1.94	0.00138
ENSG00000205634	LINC00898	0.574	0.149	-1.94	0.00138
ENSG00000073464	CLCN4	3.62	0.942	-1.94	0.00138
ENSG00000139832	RAB20	2.56	0.657	-1.96	0.00138
ENSG00000136944	LMX1B	0.67	0.171	-1.97	0.00138
ENSG00000167191	GPRC5B	14.4	3.6	-2	0.00138
ENSG00000185567	AHNAK2	2.37	0.595	-2	0.00138
ENSG00000168830	HTR1E	14.1	3.52	-2.01	0.00138
ENSG00000267296	CEBPA-AS1	0.575	0.14	-2.04	0.00826
ENSG00000224699	LAMTOR5-AS1	7.55	1.83	-2.04	0.00362
ENSG00000232160	RAP2C-AS1	2.4	0.57	-2.07	0.0091
ENSG00000147082	CCNB3	2.15	0.512	-2.07	0.0288
ENSG00000186523	FAM86B1	1.99	0.469	-2.09	0.00138
ENSG00000167767	KRT80	1.61	0.373	-2.11	0.00138
ENSG00000229921	KIF25-AS1	0.772	0.176	-2.13	0.00558

Ensembl_Gene_ID	Gene_name	Control	Illuminated	Log2 FC	q_val
ENSG00000147571	CRH	0.97	0.22	-2.14	0.00362
ENSG00000272425	RP11-363E6.4	0.775	0.176	-2.14	0.00138
ENSG00000237989	AP001046.5	0.603	0.131	-2.2	0.00138
ENSG00000279137	RP11-205K6.3	0.803	0.173	-2.22	0.00138
ENSG00000111186	WNT5B	2.07	0.437	-2.24	0.00255
ENSG00000172339	ALG14	9.34	1.94	-2.26	0.0174
ENSG00000196581	AJAP1	2.84	0.581	-2.29	0.00138
ENSG00000223749	MIR503HG	1.28	0.262	-2.29	0.0329
ENSG00000129521	EGLN3	63.1	12.8	-2.3	0.00138
ENSG00000198416	ZNF658B	0.606	0.122	-2.32	0.00138
ENSG00000133665	DYDC2	0.659	0.132	-2.32	0.0233
ENSG00000137699	TRIM29	37.5	7.49	-2.32	0.00138
ENSG00000100302	RASD2	1.34	0.267	-2.33	0.00138
ENSG00000247095	MIR210HG	3.73	0.728	-2.36	0.016
ENSG00000100060	MFNG	1.66	0.311	-2.42	0.00138
ENSG00000119938	PPP1R3C	4.33	0.786	-2.46	0.00138
ENSG00000077713	SLC25A43	0.676	0.116	-2.55	0.00992
ENSG00000166394	CYB5R2	0.776	0.133	-2.55	0.00138
ENSG00000231881	RP5-1120P11.3	1.23	0.204	-2.59	0.0329
ENSG00000214548	MEG3	0.646	0.107	-2.59	0.00138
ENSG00000121966	CXCR4	228	37.7	-2.6	0.00138
ENSG00000234944	RP11-124O11.1	1.5	0.242	-2.63	0.00138
ENSG00000134323	MYCN	5.98	0.954	-2.65	0.00138
ENSG00000160013	PTGIR	2.98	0.466	-2.68	0.00138
ENSG00000225968	ELFN1	10.3	1.6	-2.69	0.00138
ENSG00000187800	PEAR1	5.76	0.894	-2.69	0.00138
ENSG00000152582	SPEF2	1.29	0.198	-2.7	0.00138
ENSG00000170983	LINC00208	0.589	0.0894	-2.72	0.0258
ENSG00000253669	KB-1732A1.1	0.692	0.104	-2.73	0.0115
ENSG00000170161	GLIDR	6.81	1	-2.76	0.00462
ENSG00000183690	EFHC2	0.731	0.106	-2.79	0.00138
ENSG00000056998	GYG2	0.604	0.0867	-2.8	0.00138
ENSG00000163485	ADORA1	0.761	0.108	-2.81	0.00138
ENSG00000251661	RP11-326C3.11	2.42	0.325	-2.9	0.00138
ENSG00000164303	ENPP6	1.42	0.188	-2.92	0.00138
ENSG00000236437	AP001891.1	2.22	0.286	-2.95	0.00362
ENSG00000171388	APLN	1.83	0.236	-2.95	0.00138
ENSG00000034239	EFCAB1	0.819	0.1	-3.03	0.00362
ENSG00000108622	ICAM2	3.4	0.415	-3.03	0.00138
ENSG00000249669	MIR143HG	5.48	0.669	-3.04	0.00138
ENSG00000231890	DARS-AS1	2.68	0.325	-3.04	0.00138
ENSG00000236204	LINC01376	0.547	0.0614	-3.15	0.0123
ENSG00000269936	MIR145	4.79	0.426	-3.49	0.00138
ENSG00000237954	RP11-14O19.2	3.49	0.304	-3.52	0.00138
ENSG00000172995	ARPP21	1.24	0.1	-3.62	0.00138
ENSG00000225373	WASH5P	1.23	0.089	-3.78	0.00138
ENSG00000111859	NEDD9	8.48	0.506	-4.07	0.00138

Ensembl_Gene_ID	Gene_name	Control	Illuminated	Log2 FC	q_val
ENSG00000261143	ADAMTS7P3	2.24	0.132	-4.08	0.0384
ENSG00000155974	GRIP1	0.907	0.0351	-4.69	0.00138